WCAP-14293

AP600
LOW-PRESSURE INTEGRAL SYSTEMS TEST AT OREGON STATE UNIVERSITY TEST ANALYSIS REPORT

SEPTEMBER 1995

WESTINGHOUSE ELECTRIC CORPORATION
Energy Systems Business Unit
Advanced Technology Business Area
P.O. Box 355
Pittsburgh, Pennsylvania 15230-0355

COPYRIGHT NOTICE

The reports transmitted herewith each bear a Westinghouse copyright notice. The NRC is permitted to make the number of copies of the information contained in these reports which are necessary for its internal use in connection with generic and plant-specific reviews and approvals as well as the issuance, denial, amendment, transfer, renewal, modification, suspension, revocation, or violation of a license, permit, order, or regulation subject to the requirements of 10 CFR 2.790 regarding restrictions on public disclosure to the extent such information has been identified as proprietary by Westinghouse, copyright protection notwithstanding. With respect to the non-proprietary versions of these reports, the NRC is permitted to make the number of copies beyond those necessary for its internal use which are necessary in order to have one copy available for public viewing in the appropriate docket files in the public document room in Washington, D.C. and in local public document rooms as may be required by NRC regulations if the number of copies submitted is insufficient for this purpose. Copies made by the NRC must include the copyright notice in all instances and the proprietary notice if the original was identified as proprietary.

TABLE OF CONTENTS

TABLE OF CONTENTS (Continued)

TABLE OF CONTENTS (Continued)

TABLE OF CONTENTS (Continued)

TABLE OF CONTENTS (Continued)

TABLE OF CONTENTS (Continued)

TABLE OF CONTENTS (Continued)

LIST OF TABLES

LIST OF TABLES (Continued)

LIST OF TABLES (Continued)

LIST OF TABLES (Continued)

LIST OF TABLES (Continued)

LIST OF FIGURES

ACRONYMS

ADS	automatic depressurization system
APEX	advanced plant test facility at OSU
ASME	American Society of Mechanical Engineers
BAMS	break and ADS measurement system
CCT	condensate collection tank
CD ROM	compact disk read-only memory
CMT	core makeup tank
CL	cold leg
CLBL	cold-leg balance line
CRP	condensate return pump
CVS	chemical and volume control system
DAS	data acquisition system
DBE	design basis event
DEG	double-ended guillotine
DP	differential pressure transmitter
DVI	direct vessel injection
FMM	magnetic flow meter
GSM	general scaling methodology
H2TS	hierarchical two-tiered scaling analysis
HFM	heat flux meters
HPS	heated phase switch
HX	heat exchanger
HL	hot leg
IRWST	in-containment refueling water storage tank
LAN	local area network
LCS	lower containment sump
LDP	level differential pressure
LOCA	loss-of-coolant accident
LRGMS	large main steam
LTC	long-term cooling
MSS	main steam system
NSS	nonsafety systems
OSU	Oregon State University
PC	personal computer
PIRT	phenomena identification ranking table
PPIRT	plausible phenomena identification ranking table
PQP	project quality plan
PRHR	passive residual heat removal
PT	pressure transducer
PWR	pressurized water reactor
PXS	passive core cooling system
QLR	quick look report
RCP	reactor coolant pump
RCS	reactor coolant system
RNS	normal residual heat removal system
RPV	reactor pressure vessel
S signal	safety signal

ACRONYMS (Continued)

SASM	severe accident scaling methodology
SBLOCA	small-break loss-of-coolant accident
SCR	silicon-controlled rectifier
SG	steam generator
SGS	steam generator system
VI	virtual instrumentation

ACKNOWLEDGMENTS

The authors express their appreciation for the extensive discussions and inputs obtained from Mr. L. K. (Louis) Lau, lead designer of the OSU test facility, and Mr. C. L. (Carl) Dumsday, Manager of Test Operations for Westinghouse at the OSU test facility.

To W. (Bill) Brown, who performed the technical review of the equations developed for analysis of the data, and to M. (Michael) Parks, team leader, I. (Igor) Halijasmaa, R. (Rain) Veinjarv and P. (Peter) Ward, who performed the verification and validation check calculations for the coding of those equations, the authors extend their thanks and appreciation for an arduous task that was done well.

We also gratefully acknowledge M. H. (Mike) Mankowski for his efforts in generating composite figures of safety system flows included in the transient descriptions included in Section 5 of this report and D. J. (Don) Longo for his efforts in preparing and performing heat transfer calculations with the CMT data.

The thorough and insightful review of the report performed by E. H. (Earl) Novendstern, Manager, Plant Safety Analysis, E. J. (Gene) Piplica, Manager, Test Engineering, and B. A. (Brian) McIntyre, Manager, Advanced Plant Safety and Licensing, is gratefully acknowledged; their comments significantly improved the final report.

Our thanks to the technical editors, Marlane Cox, Leslie McSwain, and Tom Hendrick for the efforts and understanding they put forth to transform the report from the initial drafts written in phrases and jargon to its current form and format.

To the Word Processing team members, a special thanks is extended, not only for their skill, patience and cooperation in working with the large volume of material that formed the basis of this report, but also for their willing cooperation to work with the editors and authors, the long hours they put in, and the enthusiasm they displayed through it all.

Finally, but not in the least, the authors express their gratitude to R. B. (Bob) Tupper and P. (Paul) Wardman for the assistance in initially scheduling and tracking the tasks necessary to complete this report, and especially to B. E. (Bruce) Rarig for his diligence and determination in tracking tasks, attention to detail, and promoting communications among the following up with the authors, reviewers, technical editors, word processing team, and reproduction office during the critical final stages of the report generation effort.

SUMMARY

The Oregon State University (OSU) test facility is a 1/4-height, reduced-pressure simulation of the AP600 nuclear steam supply system and the AP600 passive safety features. A series of design-basis events were simulated at OSU to obtain data for verification and validation of the computer models used for the safety analysis of AP600.

The purpose of this report is to describe the analysis of the test data and the thermal-hydraulic behavior of the test facility, to identify the phenomena observed in the tests and the relationship to the phenomena identification ranking table (PIRT), and to show the applicability of the OSU tests for computer model verification and validation through mass and energy balances.

1.0 INTRODUCTION

This report describes the analysis of the Oregon State University (OSU) test data used to validate certain AP600 safety analysis computer codes. The test data report for the OSU tests is given in the OSU Final Data Report,[1] which describes the test facility, the valid instrumentation, and the test facility performance for the different tests. This report will examine, in additional detail, the thermal-hydraulic behavior of the test facility and the phenomenon observed in the tests, as identified in the phenomena identification ranking table (PIRT), Table 1.3-1. This analysis will aid computer code validation activities.

The OSU test facility is a 1/4-height, reduced-pressure model of the AP600 and its passive emergency core cooling systems. The test facility located at the Radiation Center at the University in Corvallis, Oregon includes the reactor coolant system (RCS), steam generators (SGs), passive core cooling system (PXS), automatic depressurization system (ADS), and nonsafety-related injection systems, such as the normal residual heat removal system (RNS) and the chemical and volume control system (CVS). The test facility, fabricated from austenitic stainless steel designed for normal operation at 450°F and 400 psig, was scaled using the hierarchical, two-tiered scaling analysis (H2TS) method developed by the U.S. Nuclear Regulatory Commission (NRC). Simulated piping breaks were tested in the hot leg (HL), cold leg (CL), pressure balance line between the cold leg and the core makeup tank (CMT), and the direct vessel injection (DVI) line. Decay heat that scaled to 3 percent of the full power (about 2 minutes after shutdown) was supplied by electrically heated rods in the reactor vessel. Simulated transients were programmed by the control system to proceed automatically. About 850 data channels were recorded by the data acquisition system (DAS) and downloaded to compact disks for subsequent data reduction and plotting. The OSU test facility was specifically designed to examine the small-break loss-of-coolant transient (SBLOCA) periods as well as the long-term-cooling (LTC) aspects of the AP600 passive safety systems.

1.1 Background

AP600 is a 600-MWe Westinghouse advanced reactor designed to enhance plant safety with accident mitigation features that, once actuated, depend only on natural forces, such as gravity and natural circulation, to perform all required safety functions.

The AP600 primary system is a two-loop design. Each loop contains one hot leg, two cold legs, and one SG with two canned motor reactor coolant pumps (RCPs) attached directly to the SG outlet channel head. The passive safety systems comprise the following:

- Two full-pressure CMTs that provide borated makeup water to the primary system at full system pressure.
- Two accumulators (ACCs) that provide borated water to the reactor vessel if the primary pressure $\leq$ 700 psia.
- A passive residual heat removal (PRHR) heat exchanger (HX), comprised of a C-shaped tube bundle submerged in the in-containment refueling water storage tank (IRWST), that can remove heat from the primary system at full system pressure.
- The ADS, which is comprised of a set of valves connected to the RCS at the pressurizer steam space and the two hot legs. The valves connected to the pressurizer vent to the IRWST through a sparger. The valves connected to the hot leg vent to the containment. These valves are opened sequentially to provide controlled depressurization of the primary system.
- An IRWST that provides a large source of core cooling water, which drains by gravity after the ADS has actuated.
- A passive containment cooling system (PCS) that utilizes the AP600 steel containment shell to transfer heat to the environment (ultimate heat sink). The PCS was not directly included in the OSU tests, however, the containment circulation of condensed liquid back to the IRWST or sump was simulated for selective tests.

In reviews of the AP600, the U.S. NRC identified several concerns regarding the performance of the AP600 passive safety systems. Those concerns include the following:

- Possible high-pressure passive safety system interactions that could retard cooling of the core.
- Possible active system/passive system interaction that could retard cooling of the core.
- The dependence on small temperature differences resulting in small density differences, which then are responsible for driving heads for recirculating flows.

- The effects of code accuracy in predicting long transients in which the driving heads for flow in the system are small.

- The behavior of the primary system and the containment during the LTC phase of the transient; specifically, the reduced driving heads for flow from the sump and the resulting pressure drops in the primary system that could reduce venting and increase steam binding of the system at low pressure.

The OSU test facility was specifically designed to obtain experimental thermal hydraulic data that would address NRC concerns.

The OSU test facility was constructed specifically to investigate the AP600 passive system characteristics. The facility design models the detail of the AP600 geometry, including the primary system, pipe routings, and layout for the passive safety systems. The primary system consists of one hot leg and two cold legs, with two active pumps and an SG for each of the two loops. There are two CMTs, each connected to a cold leg of one primary loop. The pressurizer is connected to the other primary loop, as in the AP600 plant design. Gas-driven accumulators are connected to the DVI lines. The discharge lines from a CMT and one of the two IRWST and reactor sump lines are connected to each DVI line. The two independent lines of each stage of ADS 1, 2, and 3 are modeled by one line containing an orifice. Two-phase flow from ADS 1-3 is separated in a swirl-vane separator, and liquid and vapor flows are measured to obtain the total flow rate. The separated flow streams are then recombined and discharged into the IRWST through a sparger. Thus, mass and energy flow from the ADS into the IRWST are preserved.

The period for simulation included not only IRWST injection, but also IRWST draining and sump injection to simulate the LTC mode of the AP600. The time scale for the OSU test facility is about one-half; that is, the sequence of events occurred about twice as fast in the test facility as in the AP600.

To model the LTC aspects of the transients, two-phase flow from the break was separated in a swirl-vane separator, and the liquid and vapor portions of the total flow were measured. The liquid fraction of the flow was discharged to the reactor sump, as in the AP600 plant. The vapor was discharged to the atmosphere, and the equivalent liquid flow was capable of being added to the IRWST and sump to simulate the condensate return from passive containment. A similar approach was also used for the two ADS-4 valves on the hot legs. The two-phase flow was separated in a swirl-vane separator, the two stream flows were measured, the liquid phase was discharged into the reactor sump while the vapor phase was discharged to the atmosphere, and the liquid equivalent was capable of being added to the IRWST and sump. The IRWST, reactor sump, and separators could be pressurized to simulate containment pressurization following a postulated loss-of-coolant accident (LOCA).

Prior to the performance of matrix tests, a series of cold, low-pressure and hot, high-pressure pre-operational tests were performed to characterize the OSU facility to show proper operation of the

facility and to verify that piping/component parameters properly matched the AP600 plant, and to provide benchmark data on facility behavior for the computer code analysis. The tests that were analyzed in Sections 5, 6, and 7 were selected to examine the AP600 passive safety system performance in mitigating the effects of design-basis events (DBEs). Events that were evaluated include LOCAs ranging from 0.5-in. diameter equivalent to the double-ended guillotine (DEG) break of an 8-in. DVI line. A larger break was also simulated for LTC performance via 4-in. equivalent diameter breaks on both the top and bottom of a cold leg.

1.2 Test Objectives

The OSU facility was designed and constructed to specifically examine the LTC performance of the AP600 passive safety-related systems and their interaction with the nonsafety-related active systems. The range and types of tests investigated in the OSU test facility covered the ranges and phenomena expected for the SBLOCA and LTC transients. Tests were performed to examine the different break sizes and locations to cover the range of phenomena of interest. The data from the tests are used to validate the safety analysis computer codes used to analyze the AP600.

To cover the range of conditions for the LTC transient, various tests were performed. One test modeled as large a break as possible to rapidly depressurize the facility so that decay power would be at a high value when LTC began. Other tests were performed with conditions that would result in a hot IRWST and sump when the primary system transitioned into LTC. Both conditions maximized the production of core steam to be vented through the ADS-4 valves to maintain sump injection.

A detailed scaling analysis was developed for the OSU tests to relate the scaled-pressure and reduced-height facility to the AP600 plant. The OSU Facility Scaling Report[2] specified the facility dimensions, resulting flow areas for the breaks, and pressure drops needed to preserve the phenomena expected for the AP600 SBLOCA and LTC transients. The scaling study provides the bridge to relate the AP600 SPES-2 Test Analysis Report[3] to the similar OSU tests, and to relate the OSU tests to the AP600 design.

The following are the specific test objectives of the OSU program:

- To provide data to establish the pedigree of the passive safety-related systems for LTC.
- To provide overlap with the full-pressure, full-height SPES-2 tests[3] so that an assessment of the scaling effects of the OSU tests could be made. Therefore, similar break locations and sizes (scaled) were examined in both facilities and comparisons were made.
- To cover the range of phenomena expected for the AP600 LOCA in addition to the LTC period.

1.3 Important Small-Break Loss-of-Coolant Accident and Long-Term Cooling Phenomena Identification and Ranking Table

The OSU test matrix was developed to simulate the thermal-hydraulic phenomena expected during SBLOCA and LTC transients.

1.3.1 Small-Break Loss-of-Coolant Accident

The SBLOCA can be divided into the following four periods that characterize thermal-hydraulic phenomena:

- Blowdown - Initial depressurization from plant operating pressure to the SG secondary-side pressure, after which pressure stabilizes.

- Natural Circulation - The period from the stabilization of primary pressure with secondary-side pressure until ADS-1 is activated. The primary reactor system is cooled by different modes of heat transfer. Each cooling mode is dependent on the system mass inventory. As the mass is lost through the break, cooling proceeds from single-phase natural circulation, to two-phase natural circulation, to reflux condensation cooling.

- ADS 1-4 Blowdown - Once the CMTs drain to their setpoint, the ADS-1 valve opens and the reactor system is depressurized through the ADS flow path in addition to the break. As the CMT continues to drain into the reactor vessel, additional valves are opened on the pressurizer and RCS hot legs to enhance blowdown of the system.

- IRWST Injection - Stable injection from the IRWST indicates the complete depressurization of the primary system down to containment pressure. Also, injection from the IRWST indicates the end of the small-break transient and the beginning of the LTC transient.

Using these different periods, the important thermal-hydraulic phenomena have been identified and ranked in a PIRT (Table 1.3-1). This PIRT has been updated from that which was provided in the *Applicability of the NOTRUMP Computer Code to the AP600 SSAR Small-Break LOCA Analysis*[4] and reflects small changes from the WCOBRA/TRAC LTC Preliminary Validation Report.[21] The only changes other than footnotes were, 1) ADS subsonic flow was increased in importance to "M" since this contributes to the system depressurization and the mass redistribution and the mass redistribution into the pressurizer and 2) in the natural circulation phase, the wall stored energy to "L" from "N/A" due to the heat transfer to the CMT walls. Individual phenomena were emphasized for the ADS, and other components have been added to the PIRT. The phenomena for each identified phase of the small-break transient relative to the AP600 small-break performance is discussed in the following paragraphs.

The reactor is assumed to be operating at normal full-power, steady-state conditions at the start of the blowdown. The break opens at time zero, and pressurizer pressure begins to fall as mass is lost out the break. This depressurization is largely defined by critical flow through the break. With the break located at the bottom of the cold leg, a mixture flow exits the break for the majority of the transient, since the mixture level stays high in the reactor vessel. Pressurizer pressure falls below the safety signal setpoint, causing the reactor to trip. The safety systems actuation signal (S) follows and results in the opening of the CMT isolation valves. Once the residual fissions decrease, core power is defined by the decay heat model. The RCPs trip after a short delay. Pump performance, both before and after the trip, is modeled according to the pump characteristic curves. After the pumps coast down, the primary RCS is cooled by natural circulation, with energy removed from the primary system by the SGs via their safety valves and the break. Stored energy from the metal in the reactor vessel and pressurizer is transferred to the coolant. These phenomena are essentially the same for AP600 as for conventional pressurized water reactors (PWRs). Liquid in the upper plenum and upper head (depending on the temperature) will flash, and the upper head will start to drain.

Blowdown phase phenomena unique to AP600 are those associated with CMT delivery. Once the CMT isolation valves open, the CMT injects borated water by gravity-driven recirculation into the RCS through the DVI lines. The CMT injected volume is replaced with hot liquid via the cold-leg balance line (CLBL); this hot liquid collects at the top of the CMT. The downcomer fluid stays subcooled through the initial blowdown phase.

For the natural circulation phase of the transient, the primary system exists in a quasi-steady-state condition with the secondary side, with decay energy being removed by the SG secondary side as the primary system drains. The SG in the AP600 plays a more limited role in the natural circulation cooling phase than for conventional plants because the SGs drain relatively early in the transient. Since PRHR is activated on an S signal during a SBLOCA, the IRWST becomes the primary heat sink for the RCS early in the transient. The PRHR will remove energy from the primary system, causing it to depressurize. The SG secondary side becomes a potential heat source once PRHR reduces primary pressure to that of the secondary side. PRHR is ranked high in the PIRT since it becomes a significant heat removal path, particularly after primary pressure is less than SG pressure. Therefore, condensation in the SG tubes during a SBLOCA ceases early. The requirements for detailed models for condensation heat transfer in the SG tubes are not as significant for AP600 as for a conventional plant. The importance shifts to the PRHR performance and the IRWST heat-sink behavior. The reverse heat transfer path due to secondary heating of the RCS primary system continues until the SGs drain. The CMT continues to deliver in the recirculation mode, but eventually a vapor region forms at the top of the CMT volume, and CMT draindown begins. As the CMT drains while injecting, its level falls to the ADS actuation setpoint, initiating the third phase of the AP600 SBLOCA transient, ADS blowdown. The downcomer and lower plenum are ranked as medium importance in the PIRT since they provide the driving head for natural circulation.

The ADS blowdown phase continues through the actuation of ADS-1, ADS-2, ADS-3, and ADS-4 as the primary system depressurizes to approximately the containment pressure. The PIRT relates

AP600-specific components, events, and phenomena that occur during automatic depressurization of the RCS to achieve water injection by gravity from the IRWST. Since ADS-1 creates an opening at the top of the pressurizer, the pressurizer two-phase fluid level increases markedly. Pressurizer tank level and surge-line phenomena are significant factors in the depressurization behavior following ADS actuation. Flashing of fluid in the RCS occurs due to the depressurization caused by the ADS.

Following actuation of ADS-1, the next two stages of ADS, ADS-2 and ADS-3, activate via timers. Once the pressure drops below 700 psia, accumulator injection begins, reducing flow delivered from the CMT. CMT flow may even be stopped temporarily due to pressurization of the DVI line by the accumulator. The CMT drain rate, and DVI line and cold-leg balance line flow characteristics are significant because ADS-4 actuation is based on the CMT liquid level decreasing below a low-low setpoint value. Condensation of vapor on the CMT walls is of somewhat less importance since recirculation results in heating of the CMT.

Critical flow through the ADS stages is the major factor in determining when the RCS has depressurized to the extent that the gravity injection of water from the IRWST can begin. ADS-4 performance is affected by the nature of flow in the hot legs. Successful operation of the ADS leads to the IRWST injection cooling phase of the AP600 SBLOCA event.

The final stage of the SBLOCA is IRWST injection. At this point, the primary system is depressurized, and the transient continues into the LTC phase of the accident. By the time of IRWST injection, the CMT is either completely or very nearly empty. CMT phenomena have, therefore, become relatively unimportant, whereas the IRWST gravity-drain rate through the DVI line is important. The hot-leg flow phenomena, together with ADS-4 flow, is also important. Moreover, the break critical flow behavior is now less important than before because all ADS flow paths are open, providing a large area through which to vent steam. Keeping the core covered with liquid or a two-phase mixture becomes a function of the decay heat level and IRWST flow.

The impact of noncondensable gas released when the accumulators empty of liquid during AP600 SBLOCAs is shown to be of low importance in the SBLOCA PIRT because of the large number of vent paths for the gas.

1.3.2 Long-Term Cooling Transient

LTC is a post-accident phase defined as the period after IRWST injection begins until the plant is recovered. The AP600 passive safety systems are designed to provide post-accident core cooling indefinitely. Steam generated in the core is vented to containment. The steam condenses on the containment shell, and the condensate is directed into the IRWST and sump where it flows into the core through the DVI line. The closed-circuit reflux condensation process ensures adequate cooling inventory to maintain the core in a coolable state indefinitely.

When the reactor system is in the LTC mode, the primary system is drained to the hot-leg level. With the SG primary side being filled with stagnant steam, the pressurizer and upper head of the reactor vessel are empty. The CMTs and accumulators have already injected, and the PRHR may or may not be active, depending on whether the IRWST level covers the HX and noncondensable gas is present in the PRHR tubes. Initial injection flow to the vessel comes from the IRWST as long as the IRWST head is larger than the containment sump. If the IRWST has drained to the sump level, there could be injection from both the sump and the IRWST until the IRWST has drained. Flow from the sump or IRWST is directed to the reactor vessel through the DVI line into the downcomer. The delivery of injection flow is gravity-driven from the elevated sump water level into the reactor vessel. The driving force for core cooling is the level in the reactor downcomer, which provides the elevation head to drive flow through the core and out the hot leg. This gravity-flooding behavior of the core is no different than that in operating plants with the exception that injection flow is driven by a pump and not gravity as in the AP600. The inclusion of a large vent path on the top of the hot leg through the ADS-4 valves provides a low-pressure drop vent path so that ample flow through the core can occur. In operating plant cold-leg breaks, the downcomer must drive core flow through the SG primary side, superheating the primary fluid, and creating a backpressure that reduces core inlet flow (steam binding). This situation is avoided in the AP600 by using the large vent areas on the top of the hot legs so that very little, if any, flow goes through the SGs. Also, once the IRWST drains, the ADS 1-3 vent path is also available to vent core-generated steam.

Since the primary system is at containment pressure, only the driving heads in the downcomer and the two-phase pressure drop in the core, hot leg, and ADS-4 determine the resulting core flow. If the PIRT is examined, only those items related to the core, downcomer, upper plenum, hot leg, and ADS-4 are highly ranked. While most items indicated on the PIRT for LTC are directly measured in the tests, the hot-leg flow regime must be inferred from the data. Using the OSU data, the importance of these phenomena can be assessed and used for guidance in validating the AP600 safety analysis computer codes for the LTC period.

TABLE 1.3-1

PHENOMENA IDENTIFICATION RANKING TABLE FOR AP600 SBLOCA AND LTC TRANSIENT

Component Phenomenon	SBLOCA TRANSIENT				LTC Transient
	Initial Blowdown	Natural Circulation	ADS Blowdown	IRWST Injection	Sump Injection
Break					
Critical flow	H	H	H	M	L
Subsonic flow	N/A	N/A	M	M	L
ADS Stages 1 to 3 Critical flow	H* (inadvertent ADS)	H* (inadvertent ADS)	H	M	L
Two-phase pressure drop	H*	H*	H	M	L
Valve loss coefficients	H*	H*	H	M	L
Single-phase pressure drop	H*	H*	N/A	L	L
Vessel/Core					
Decay heat	H	H	H	H	H
Forced convection	M	N/A	N/A	N/A	N/A
Flashing	M	N/A	M	L	N/A
Wall stored energy	M	L	M	M	M
Natural circulation flow and heat transfer	M	M	M	M	M
Mixture level mass inventory	H	H	H	H	H
RCP					
RCP performance	M	N/A	N/A	N/A	N/A
Pressurizer					
Pressurizer fluid level	M	M	M	L	L
Wall stored heat	M	M	M	L	L
Pressurizer Surge Line					
Pressure drop/flow regime	L	L	M	L	L
Downcomer/Lower Plenum	L	M	M	M	M
Upper Head/Upper Plenum	L	M	M	M	H
Cold Legs	L	M	M	M	L

* The ADS is not normally opened during these phases unless the transient is an inadvertent ADS; for that case, the ADS phenomena would be ranked as high (H).

TABLE 1.3-1 (Cont.)
PHENOMENA IDENTIFICATION RANKING TABLE FOR AP600 SBLOCA AND LTC TRANSIENT

Component Phenomenon	SBLOCA TRANSIENT				LTC Transient
	Initial Blowdown	Natural Circulation	ADS Blowdown	IRWST Injection	Sump Injection
Steam Generator					
2ϕ - natural circulation	L	M	L	L	L
Steam generator heat transfer	L	M	L	L	L
Secondary conditions	L	M	L	L	L
Hot Leg					
Flow pattern transition	L	H	H	H	H
ADS-4					
Critical flow	N/A	N/A	H	H	L
Subsonic flow	N/A	N/A	L	H	H
CMT					
Recirculation injection	M	M	L	L	L
Gravity draining injection	N/A	M	H	L	L
Vapor condensation rate	N/A	M	M	L	L
CMT Balance Lines					
Pressure drop	M	H	H	L	L
Flow composition	M	H	H	L	L
Accumulators					
Injection flow rate	N/A	M	H	N/A	N/A
Noncondensible gas entrainment	N/A	N/A	L	L	L
IRWST					
Gravity draining injection	N/A	N/A	N/A	H	M
Vapor condensation rate	N/A	N/A	M	L	L
DVI Line					
Pressure drop	M	M	M	M	M
PRHR					
Natural circulation flow and heat transfer	L	H	M	L	L
Sump					
Gravity draining injection	N/A	N/A	N/A	N/A	H
Level	N/A	N/A	N/A	N/A	H
Temperature	N/A	N/A	N/A	N/A	H

1.4 Test Facility Scaling

A detailed component and system scaling analysis was performed for the OSU test facility and is given in the OSU Facility Scaling Report.[2] The results of the scaling analysis were used to specify the design of the facility. The primary objective of the scaling analysis was to design a working scale model capable of producing the same types of flow behavior encountered in the AP600 during the SBLOCA transient, and LTC.

Various scaling techniques can be applied to the design of a small-scale thermal-hydraulic test facility. The traditional approach has been to use power-to-fluid-volume (P/V) scaling. This scaling approach has been successfully applied in various studies such as the *FLECHT SEASET Program Final Report*.[5] The optimum condition for this scaling approach occurs when the scale model implements the same working fluid as the full-scale system, is built at full height using similar materials, and is operated at full pressure. This generally results in constructing a very tall and thin scale model. Unfortunately, the hydrodynamic behavior in the plenum regions may not be fully represented in the full-height model. A reduced-height, power-to-volume scaled model gives a better representation of multidimensional effects in the plenum and downcomer regions.[6]

The hierarchical two-tiered scaling analysis (H2TS) method has been used to develop the similarity criteria necessary to scale the systems and processes of importance to AP600 integral system and LTC. The H2TS method, developed by the NRC, is fully described in Appendix D of *An Integrated Structure and Scaling Methodology for Severe Accident Technical Issue Resolution*[7] and is referred to as the SASM methodology. There are four basic elements of the H2TS analysis method. The first element consists of system decomposition. Each system can be subdivided into interacting subsystems (or modules), further subdivided into interacting constituents (materials), and further subdivided into interacting phases (liquid, vapor, or solid). Each phase can be characterized by one or more geometric configurations, and each geometric configuration can be described by three field equations (mass, energy, and momentum conservation). Each field equation can be characterized by several processes. This is depicted in Figure 1.4-1.

After identifying the system of interest and decomposing it as in Figure 1.4-1, the next step is to identify the scaling level at which the similarity criteria should be developed. This is determined by the phenomena being considered.

For example, if the phenomenon being considered involves mass, momentum, or energy transport between materials such as water and solid particles, then the scaling analysis should be performed at the constituent level. If the phenomenon of interest involves mass, momentum, or energy transport between vapor and liquid, then the scaling analysis should be performed at the phase level. Therefore, identifying the scaling level will depend on the phenomenon being addressed. Table 1.4-1 presents the system hierarchy implemented in the OSU Facility Scaling Report.[2]

Thermal-hydraulic phenomena involving integral system interactions, such as primary system depressurization or loop natural circulation, are examined at the "system" level. Thermal-hydraulic phenomena—such as PRHR decay heat removal, CMT, accumulator, and IRWST passive safety injection, automatic depressurization and LCS recirculation cooling—are examined at the subsystem level. Thermal-hydraulic phenomena important to individual components—such as the reactor core, pressurizer, SGs, hot legs, cold legs, coolant pumps, and interconnecting piping—are examined at the module level. Specific interaction between the steam-liquid mixture and the stainless steel structure are examined at the constituent level.

The OSU scaling study presents scaling analysis performed at different levels. The thermal-hydraulic phenomena of interest, the system level at which the analysis was performed, the control volume for the analysis (i.e., the geometric configuration), the applicable balance equations, and the processes important to the thermal-hydraulic phenomena of interest are discussed and analyzed for the simulated reactor system as well as the major components in the system.

The third element of the H2TS method requires the performance of a top-down (system) scaling analysis. The top-down scaling analysis examined the synergistic effects on the system caused by complex interactions between the constituents deemed important by the plausible phenomena identification ranking table (PPIRT). This has been modified as discussed in Section 1.3, and a revised PIRT is presented in Table 1.3-1. The top-down scaling approach used the conservation equations at a given scaling level to obtain characteristic time ratios and similarity criteria, and identified important processes to be addressed in the bottom-up scaling analysis.

The fourth element of the H2TS method required the performance of a bottom-up (process) scaling analysis, which developed the similarity criteria for specific processes such as flow-pattern transitions, and geometry- and flow-dependent heat transfer. The focus of the bottom-up scaling analysis was to develop similarity criteria to scale individual processes of importance to system behavior identified by the PIRT and develop the design information for the test facility.

The basic objective of the H2TS method was to develop sets of characteristic time ratios for the transfer processes of interest. This can be done by writing the control volume balance equations for each constituent, k, as follows:

$$\frac{dV_k\Psi_k}{dt} = \Delta[Q_k\Psi_k] \pm \Sigma j_{km}A_{km} \qquad 1.4\text{-}1$$

Defining $\Delta[Q_k\Psi_k]$:

$$\Delta[Q_k\Psi_k] = [Q_k\Psi_k]_{in} - [Q_k\Psi_k]_{out} \qquad 1.4\text{-}2$$

where:

ψ_k	=	Conserved property; ρ, ρu, or $\rho\varepsilon$ (mass, momentum, or energy per unit volume)
V_k	=	Control volume
Q_k	=	Volumetric flow rate
j_{km}	=	Flux of property ψ_k transferred from constituent k to m across the transfer area A_{km}

ψ_k transferred from constituent k to m across the transfer area A_{km}. Hence, $\Delta[Q_k\psi_k]$ represents the usual mass, momentum, or energy convection terms, and $\Sigma j_{km}A_{km}$ represents transport process terms such as condensation.

Equation 1.4-1 can be put in dimensionless form by specifying the following dimensionless groups in terms of the constant initial and boundary conditions:

$$V_k^* = \frac{V_k}{V_{k,0}},\ \psi_k^* = \frac{\psi_k}{\psi_{k,0}},\ Q_k^* = \frac{Q_k}{Q_{k,0}},\ j_{km}^* = \frac{j_{km}}{j_{km,0}},\ A_{km}^* = \frac{A_{km}}{A_{km,0}} \qquad 1.4\text{-}3$$

Substituting these groups into Equation 1.4-1 yields:

$$V_{k,0}\psi_{k,0}\frac{dV_k^*\psi_k^*}{dt} = Q_{k,0}\psi_{k,0}\Delta[Q_k^*\psi_k^*] \pm \Sigma\,(j_{km,0}A_{km,0})j_{km}^*A_{km}^* \qquad 1.4\text{-}4$$

Dividing both sides of this equation by $Q_{k,0}\ \psi_{k,0}$ yields:

$$\tau_k\frac{dV_k^*\psi_k^*}{dt} = \Delta[Q_k^*\psi_k^*] \pm \Sigma\prod_{km} j_{km}^*A_{km}^* \qquad 1.4\text{-}5$$

where the residence time of constituent k is:

$$\tau_k = \frac{V_{k,0}}{Q_{k,0}} \qquad 1.4\text{-}6$$

and the characteristic time ratio for a transfer process between constituents k and m is given by:

$$\Pi_{km} = \frac{j_{km,0}A_{km,0}}{Q_{k,0}\psi_{k,0}} \qquad 1.4\text{-}7$$

It is the Π (pi) ratio of the proposed test facility to the plant that are of interest. Important processes can be replicated in the model by fixing the variables that control the process, such as geometry, so that the following criteria is met:

$$\frac{\Pi m}{\Pi p} = 1 \qquad 1.4\text{-}8$$

A deviation from unity indicates the possible deviation of the proposed test design from the plant.

The transients modeled at the OSU facility were SBLOCA transients that transition into the LTC mode for the AP600 design. Since the operating pressure for the OSU facility was chosen as 400 psia, a scaling approach was needed to develop the test design so that the most important parameters identified in the PIRT would be preserved.

The SBLOCA and LTC scenario shown in Figure 1.4-2 indicates the five periods of interest. After the initial blowdown phase, there are extended periods of single- and two-phase natural circulation as the reactor system drains. Eventually, the ADS valves will open, creating a larger break, which will depressurize the primary system down to containment pressure. This is the ADS operational period. Once IRWST injection begins, there will be a two-phase natural circulation cooling mode with injection from the IRWST and venting from the ADS-4 valves located on the hot legs. This is the IRWST injection period. The LTC period begins as IRWST and sump injection continues for extended times. The LTC mode is with injection from the IRWST or sump and venting through the ADS-4 valves.

A top-down scaling analysis was performed using the SASM methodology for both single- and two-phase natural circulation. The objective of the scaling analysis was to scale the steady-state single- and two-phase natural circulation flow rates and the natural circulation heat transfer. A bottom-up scaling was then performed to develop the similarity criteria to specifically scale the core and SG heat transfer regimes, flow regimes and transitions, frictional and form pressure losses, and critical heat flux. To maintain similarity, the Π values developed from the dimensionless conservation equations should be preserved or the ratio of the groups should be unity.

The scaling study requires the user to choose a length scale and an area or diameter scale for the facility to satisfy the system of equations, power requirements, and geometric representation of the facility relative to the plant. Other scaling considerations such as flow regimes in the loop piping must also be considered. Small diameters distort the flow regime and have different transitions between the flow regime compared with the prototype. Small-diameter pipes also have different two-phase counter-flow behavior compared with the prototype. Reduced size can also cause manufacturing problems for the core heater simulators.

An evaluation determined that a 1/4-length scale was the most appropriate for the OSU facility since it minimized the power requirements while maximizing the height. A 1/4-scaled facility also had

sufficient volume and size to correctly model the plant pressure drop and possible three-dimensional flow behavior that could occur in the simulated reactor vessel, plenums, and downcomer. To chose a consistent diameter scale, a simple relationship was derived from the one-dimensional momentum equation to relate the length ratio to the diameter ratio. The choice of the diameter ratio was further verified with a bottom-up scaling approach in which the two-phase flow regimes and transitions between flow regimes were examined using the work of Taitel and Dukler.[8] The possible distortions in the flow regimes and their transitions was also examined for the horizontal piping following the approach of Schwartzbeck and Kocamustafaogullari.[9] The flooding review by Bankoff and Lee[10] was also used to verify that the chosen diameter ratio would have minimum surface tension effects if flooding occurred. Using this approach, the facility dimensions could be specified with confidence that the key parameters and phenomena identified in the PIRT would be preserved in the OSU facility so that the resulting data could be used for AP600 safety analysis code validation.

The OSU tests were designed to start in an all-liquid recirculation mode with the simulated RCPs operating with system pressure at about 400 psia. When a break is initiated, the system begins to depressurize. To preserve the depressurization behavior of the OSU facility, a reference pressure was selected and a scaling rationale developed to relate the lower pressure OSU tests to the higher-pressure AP600 transient for the depressurization transients. The results of the scaling approach were used to develop the relationships that led to selection of the OSU facility break areas, ADS valve areas, accumulator gas pressure, and SG secondary-side safety pressures to preserve the scaling relationships between the facility at its reduced pressure and the AP600 plant at its higher pressure. The scaling process used is shown in Figure 1.4-3, in which a top-down scaling approach was used to develop the systems scaling analysis for a simplified control volume of the reactor primary system. A bottom-up approach was then used to develop the fluid property relationships for the depressurization transients. The approach, originally developed by Kocamustafaogullari and Ishii[11] and expanded on by Moskal,[12] was extended to relate the OSU fluid property conditions to the AP600 plant conditions. Moskal defines the property relationship:

$$Y = \frac{\Delta\rho}{\rho_g \rho_l h_{fg}} \qquad 1.4\text{-}9$$

as the key property group to be preserved. This particular grouping also appears in the coefficients for the core velocity from the two-phase natural circulation loop scaling analysis previously described. The fluid properties and depressurization approach is to select a reference pressure for both the OSU facility and the AP600 that will capture the important parameters identified in the PIRT. Examining Figure 1.4-2, the AP600 primary system pressure will stabilize, after the initial subcooled blowdown, to a near constant value, slightly above the safety valve setpoint for the SG secondary side. The primary pressure will remain at this value for a relatively long period, depending upon the break size and when the ADS activates, which will depressurize the primary system to the containment pressure. During this time period, the passive safety-related systems of the AP600 will be in operation and the phenomena of importance, which are identified in the PIRT, will be present. Therefore, the

secondary-side SG safety valve setpoint pressure was chosen as the reference pressure for the AP600 plant. Note that this ignores the subcooled depressurization portion of the transient which, for a SBLOCA, is a short period compared with the total transient length.

A similar reference pressure can be chosen for the OSU facility where the primary pressure stabilizes above the SG pressure, so that:

$$\left[\frac{Y}{Yo}\right]_m = \left[\frac{Y}{Yo}\right]_p \qquad 1.4\text{-}10$$

where:

$Yo]_m$ = OSU reference pressure
$Yo]_p$ = AP600 reference pressure

The top-down and bottom-up pressure scaling must also be consistent with the natural circulation scaling, which establishes the facility volume, time, and velocity scaled ratios given the selection of the length and diameter for the facility.

The bottom-up pressure scaling examined the critical flow through the break and the ADS valves, and developed the relationships for the break areas and the valve areas that were consistent with the fluid property scaling given above. Therefore, given a break size in the AP600, a corresponding break size can be calculated for the OSU facility that will maintain the time, velocity, and volume scaling for a selected length and diameter scale which was chosen from the two-phase natural circulation scaling relationships.

TABLE 1.4-1 GENERAL SYSTEM HIERARCHY: OSU/AP600 SCALING ANALYSIS	
SYSTEM:	Primary loop
SUBSYSTEMS:	PRHR, CMT, IRWST, accumulator, ADS, LCS recirc. system
MODULES:	Reactor core, pressurizer, steam generators, hot legs, cold legs, reactor coolant pumps, interconnecting piping
CONSTITUENTS:	Steam-liquid mixture, stainless steel structure

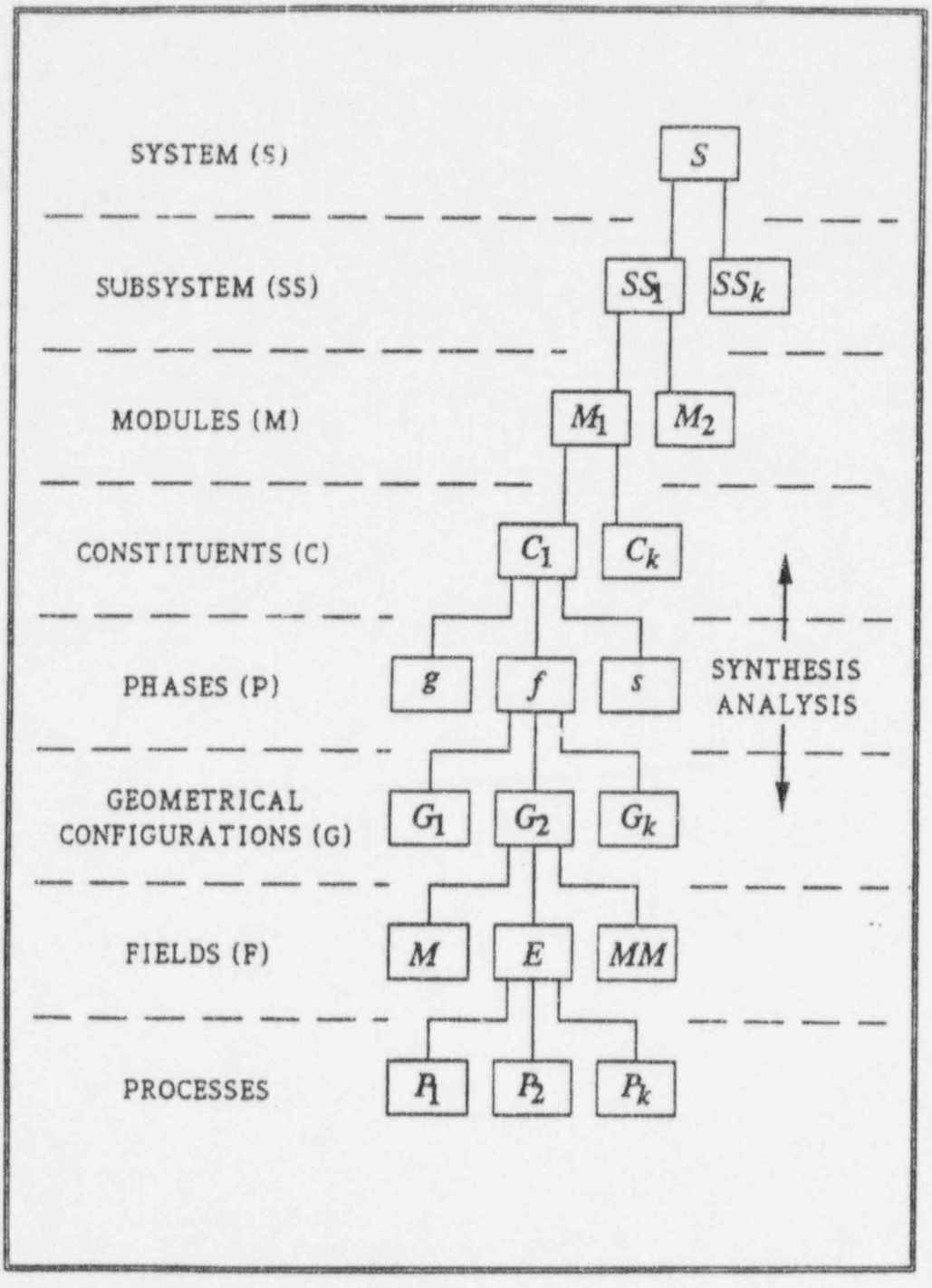

Figure 1.4-1 Decomposition Paradigm and Hierarchy[7]

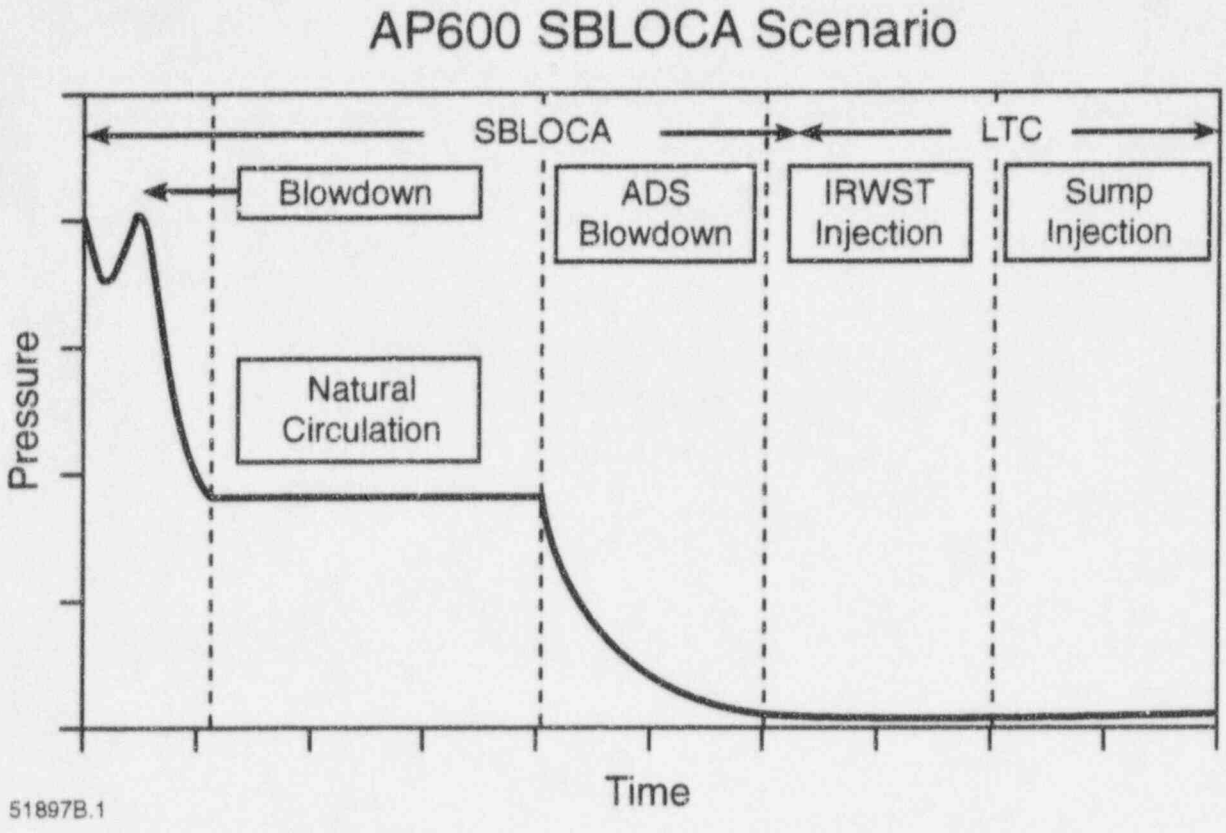

Figure 1.4-2 AP600 SBLOCA Scenario

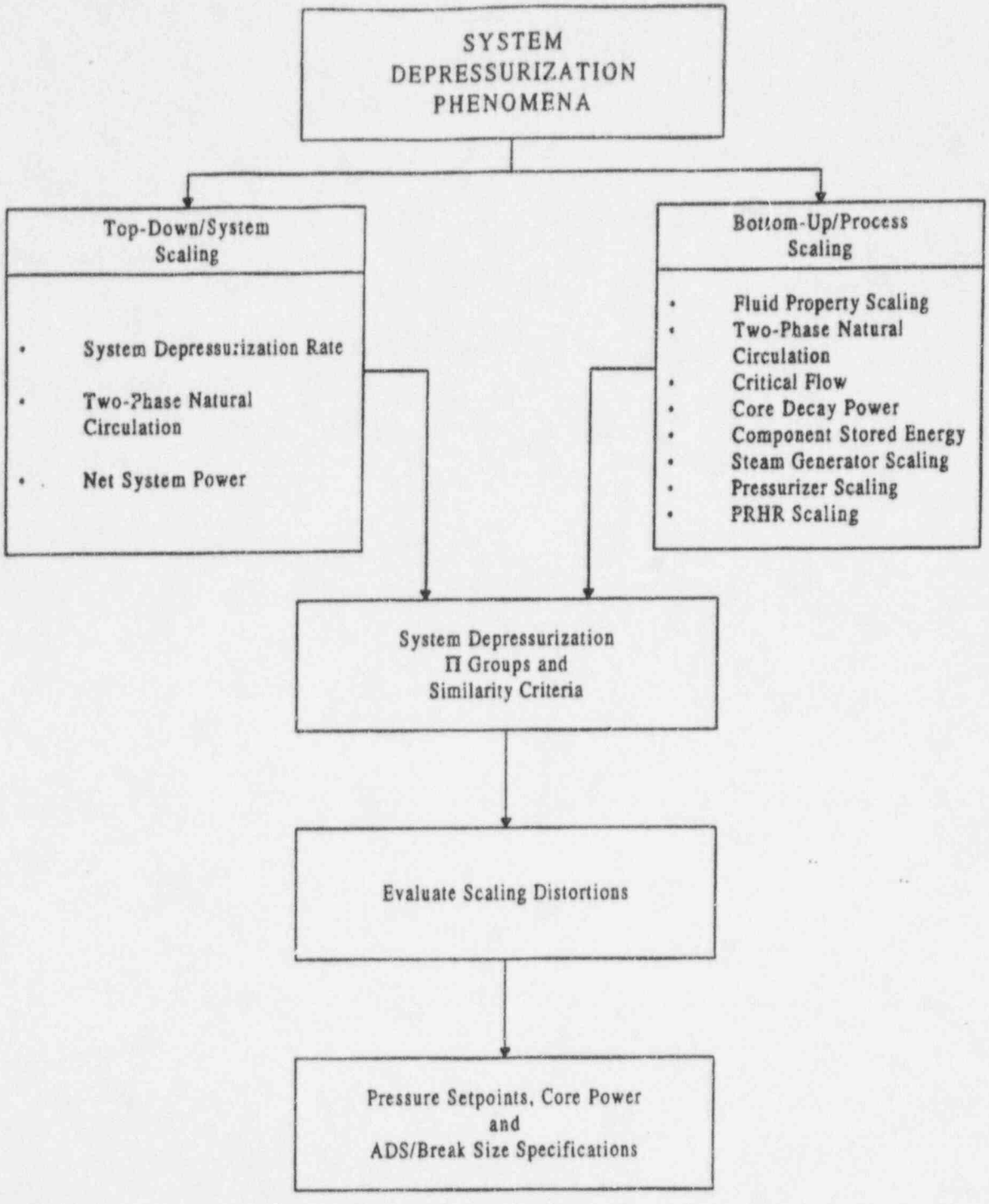

Figure 1.4-3 Scaling Analysis Flow Diagram for System Depressurization

1.5 Test Scaling Assessment and Dimensions

To assess the scaling of the OSU facility, both the proposed scaled facility and the AP600 were modeled using the *NOTRUMP, A Nodal Transient Small-Break and General Network Code.*[13] The objective of this study was to investigate whether the OSU facility response to a small-break transient would be similar to the response of the AP600. A 2-in. cold-leg break on the CMT-side of the plant was selected. The OSU facility initial conditions for this break are shown in Table 1.5-1. Table 1.5-2 shows the scaling relationships between the plant and the OSU facility, which account for the time scale difference (two-to-one for OSU) and the normalization of flow, pressure, two-phase mixture levels, and total system mass.

Figure 1.5-1 compares the normalized pressure transient for the plant and the OSU test facility and indicates that reasonably good agreement was achieved. The reference pressure chosen is based on when the primary pressure stabilizes above the secondary-side pressure at time, t_0. The normalized CMT levels are shown in Figures 1.5-2 and 1.5-3, and the normalized accumulator levels are shown in Figure 1.5-4 and 1.5-5. These figures are in good agreement and indicate that the scaling correctly preserves the timing of the events for the OSU facility compared with the AP600 when the time scaling logic is applied. ADS 1-3 flow is shown in Figure 1.5-6 and is in reasonable agreement between the test facility and the plant. Break flows are compared in Figure 1.5-7, and a difference between the facility and the plant is indicated. One possible explanation for the difference is that, when scaling the critical flow area for the break, a quality of the flow must be assumed. In reality, the quality of the flow at the break is not a constant and will change with time. Furthermore, exact similitude cannot be simultaneously achieved for both the break energy flow rate and the break mass flow rate with a reduced pressure scale. However, the integrated mass inventory similitude can be preserved. Figure 1.5-8 shows the normalized mass inventory for both the test facility and the plant. Again, agreement between the two calculations is very good, indicating that the scaling approach will yield thermal-hydraulic phenomena similar to the AP600.

In addition to the NOTRUMP code calculations that compared the OSU and the AP600 response, the results from the SPES-2 and OSU tests can be compared to investigate the scaling performance of the OSU facility. Comparisons of a 2-in. cold-leg break from SPES-2 Test S00303[3] have been made with OSU Matrix Test SB01.

The derived OSU scaling factors were applied to the SPES-2 results to compare time, pressure, and flow rates. The OSU time scale was multiplied by a factor of 2. The OSU pressure scale was normalized using the reference pressure (maximum pressure on secondary side). Similarly, the SPES-2 pressure scale was normalized using the reference pressure for the test. The flow rate normalization factor in SPES-2 was the maximum flow rate for the process being examined. For purposes of comparison, the flow rate normalization factor in OSU was the maximum flow rate observed for the identical process in SPES-2 multiplied by the ratio 395/96. Thus, the flow rates can be compared on a similar basis.

A 2-in. cold-leg break was simulated in both the OSU and SPES-2 facilities. The break location for these tests was the bottom of a single cold leg. Each system was at its steady-state initial condition at break initiation. Subsequent depressurization behavior was recorded for each facility, and key data plots are presented for the purpose of comparison. The vertical axis of each graph has been normalized as described previously.

Figure 1.5-9 presents a comparison plot of the SPES-2 and OSU reactor vessel pressure histories and Figure 1.5-10 through 1.5-14 present the data comparisons for the key passive safety systems.

In general, the data comparisons for the 2-in. break case indicate good agreement. The timing of key events, such as ADS valve actuation, were preserved. One difference can be identified in Figure 1.5-14, however, where it is observed that the onset of IRWST injection was delayed in the OSU facility relative to SPES-2. The difference in the IRWST injection time is due, in part, to the oversizing used in the SPES-2 facility.

Similar comparisons were performed for the DEG DVI line break, and the agreement between OSU and SPES-2 was very good. These comparisons of a full-height, full-pressure test facility with the OSU reduced-height, reduced-pressure facility support the scaling logic used in the OSU test design.

As with any scaled test, scaling distortions are unavoidable, therefore, the purpose of the PIRT is to identify the most important processes to be scaled so that the system response is most prototypical. In the OSU Facility Scaling Report,[2] Section 10.2 specifically discusses scaling distortion for the facility, and an evaluation is made of the scaling distortions on the primary parameters developed from the PIRT. The results are provided in Table 1.5-3. As the table indicates, all of the important pi ratios are within 20 percent, which is acceptable in terms of the uncertainties for scaling of the tests.

The depressurization ratio given in the table incorporates the use of the revised depressurization scaling, which uses the system energy and volumetric scaling as a basis. This portion of the scaling was revised after the completion of the Westinghouse tests at OSU. The original scaling for the breaks, which was used for the tests in this report, used the break-dominated depressurization process described in Section 5.4.1 of the Facility Scaling Report.[2] This scaling approach was used for all breaks modeled in the OSU tests given in this report as well as the OSU Final Data Report.[1] This scaling process is valid for break sizes of 2 in. or more, but was found to be inaccurate for smaller breaks. Therefore, the 1-in. cold-leg break and the 1/2-in. cold-leg breaks are oversized when considering the system energy and volumetric scaling methodology. The ratio of the break diameter scale factors between the two methods is given in Table 5-6 in the Facility Scaling Report,[2] and is 1.5. The break areas used for the Westinghouse tests were greater than the scaled values; therefore, the timing of the events for these 1-in. and 0.5-in. tests will be distorted from the properly scaled values, and the events and total transient will be shorter than the revised scaling would predict. Revision of the scaled break diameters is the only significant re-scaling for the OSU test facility. This distortion only affects a few tests; the remaining tests have the properly scaled break diameter. Data for the affected tests are still suitable for the purposes of computer code validation, since the break area used in the test can be simulated in the code prediction of the test.

TABLE 1.5-1 INITIAL CONDITIONS FOR OSU TEST FACILITY TO MODEL A 2-IN. COLD-LEG BREAK	
Reactor Cooling System	
Core Power	0.700 MWt
Core Flow	116.7 lb/sec.
Pressurizer Pressure	400 psia
Core Inlet Temperature	410.4°F
Core Outlet Temperature	415.6°F
Secondary	
SG Temperature	407.6°F
Break Size Simulated	2-in. cold-leg break

TABLE 1.5-2 SCALE FACTORS TO RELATE THE AP600 PLANT TO OSU NOTRUMP CALCULATIONS		
	AP600	**OSU**
Time	$t-t_o$ [1]	$2*(t-t_o)$
Pressure	P/1080	P/320
Flow	W/96	W

Note:

[1] t_o is the reference time when the primary pressure stabilizes above the secondary-side pressure.

TABLE 1.5-3
DISTORTION FACTORS FOR THE AP600 DOMINANT PROCESSES IDENTIFIED USING THE H2TS METHODOLOGY

Characteristic Time Ratio	Distortion Factor (DF) (%)	Operational Mode
Π_{Ri}	0	• 1ϕ natural circulation
Π_{F}	0	• 1ϕ/2ϕ natural circulation
Π_{h}	0	• 2ϕ natural circulation with fluid property similitude/LCS recirculation
Π_{h}	(Not scaled)	• 2ϕ natural circulation pressured scaled - core void fraction preserved instead of Π_{h}
Π_{t}/ε_{o}	0	• Depressurization - 1-in. cold-leg break (energy dominated)
$\Pi_{\Gamma,CMT}$	17.4	• CMT draining with hot walls
Π_{cond}	2.8	• CMT draining with cold walls
$\Pi_{HC,Head}$	6.3	• CMT draining with cold walls
$\Pi_{m,IRWST}$	0	• IRWST draining (property similitude)
$\Pi_{h,IRWST}$	0	• IRWST draining (property similitude)
$\Pi_{m,IRWST}$	-9.5	• IRWST heat up (pressure scaled)
$\Pi_{h,IRWST}$	19.1	• IRWST heat up (pressure scaled)
$\Pi_{q,DC}$	-16.7	• Downcomer heat transfer during Accumulator injection
$\Pi_{m,sump}$	TBD*	• Sump filling and recirculation AP600 data not available

*TBD - To be determined

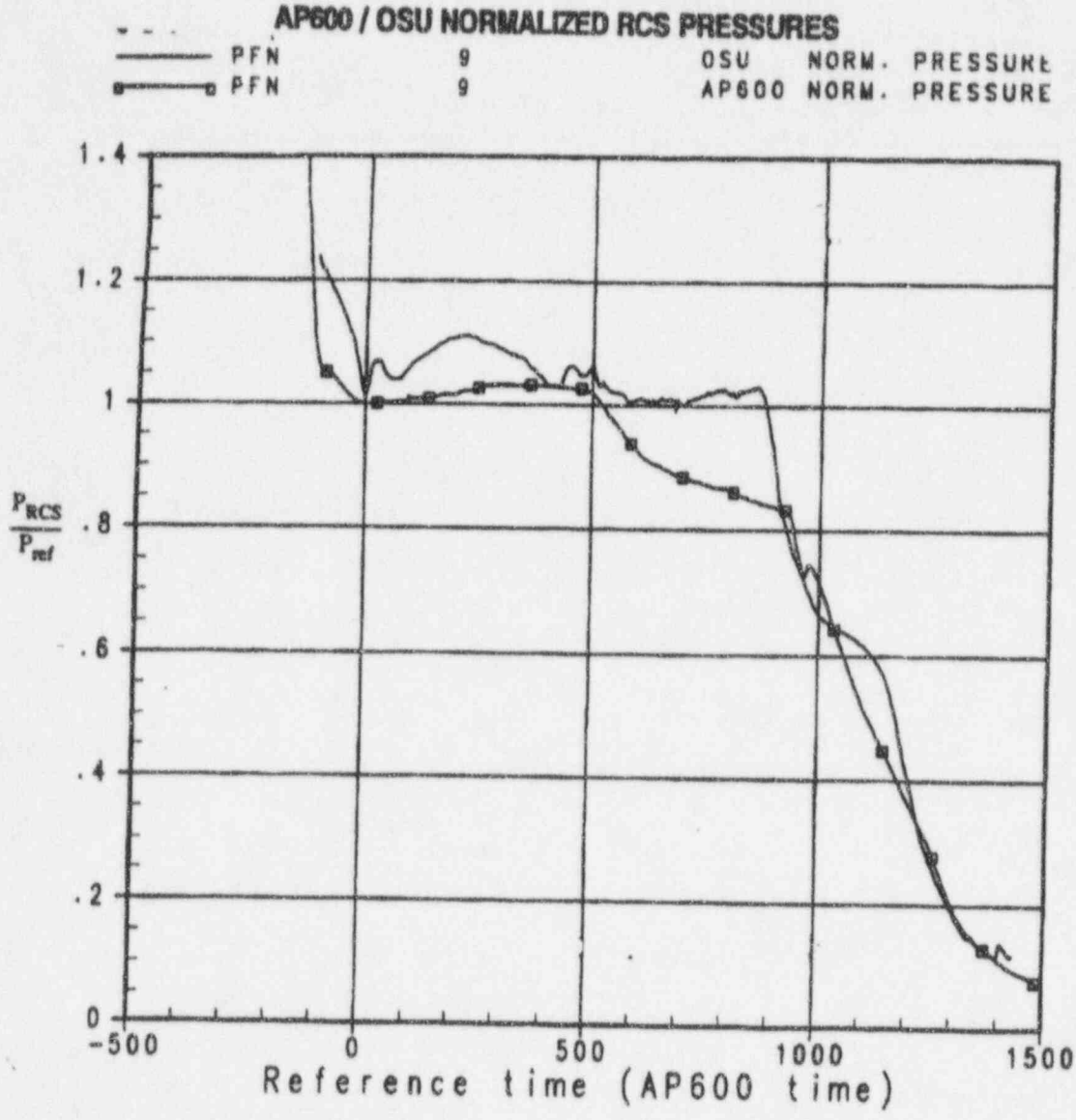

Figure 1.5-1 Normalized Pressure Comparisons between AP600 and OSU Facility

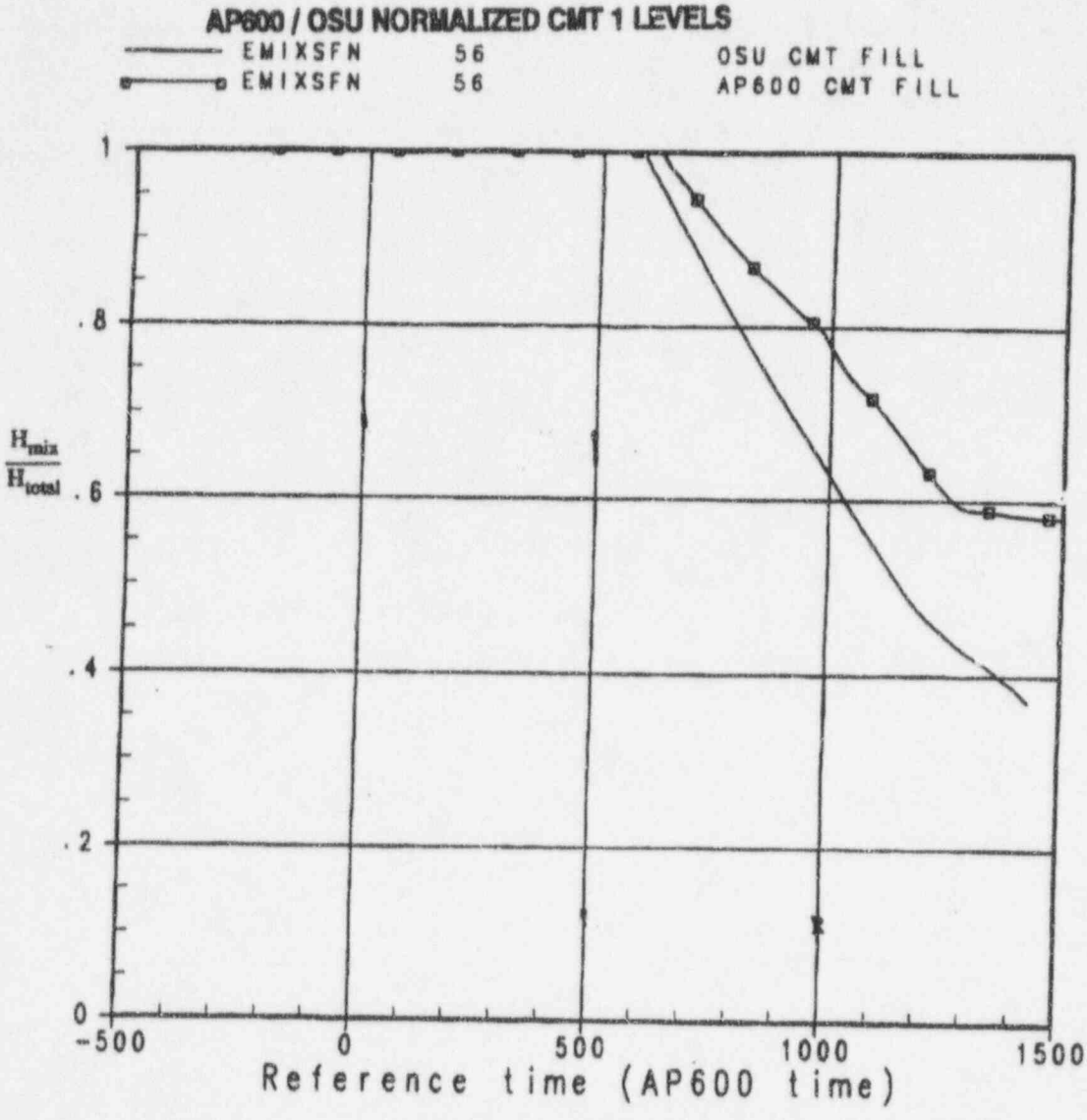

Figure 1.5-2 Normalized CMT-1 Level for AP600 and OSU Facility

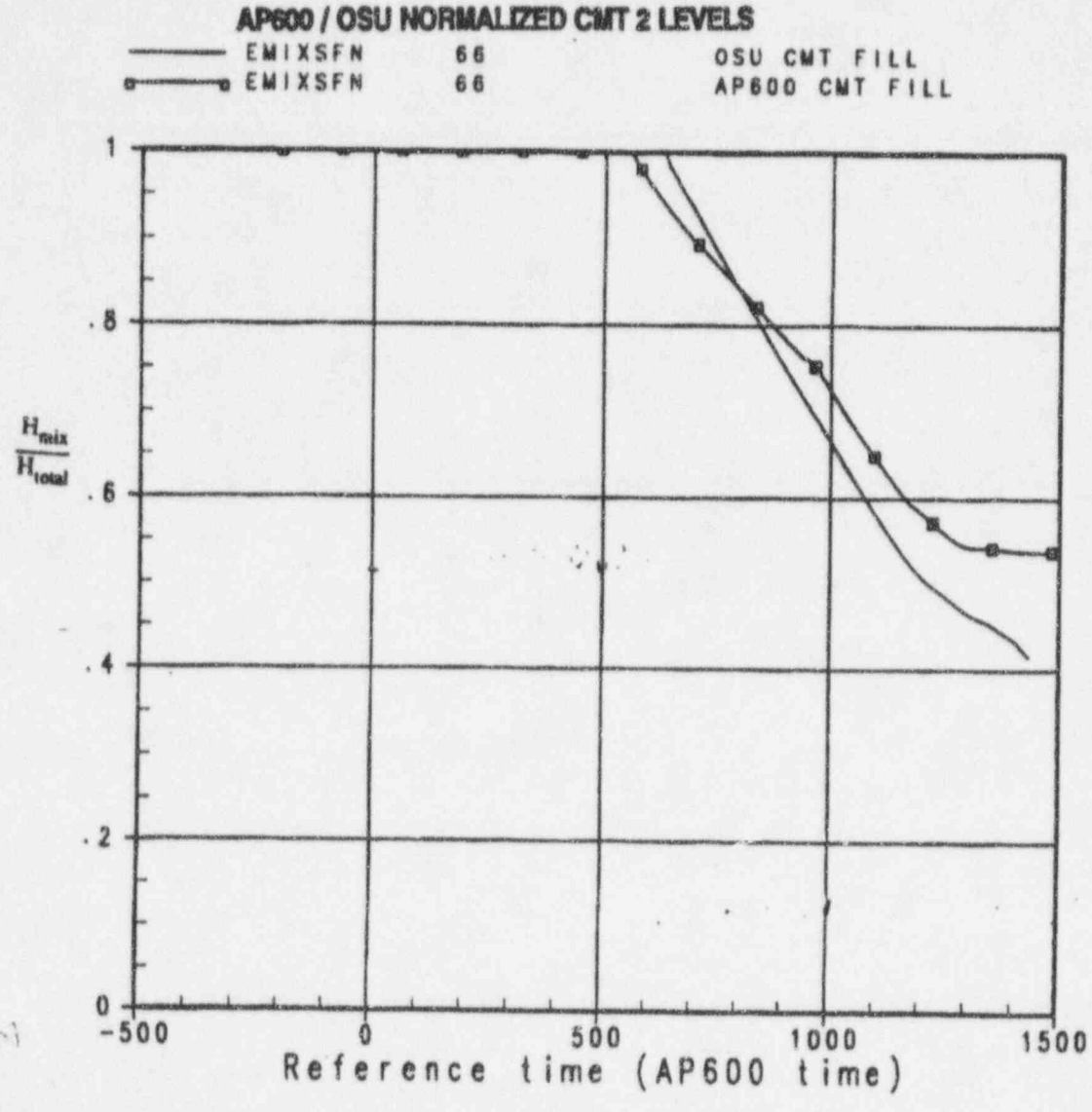

Figure 1.5-3 Normalized CMT-2 Level for AP600 and OSU Facility

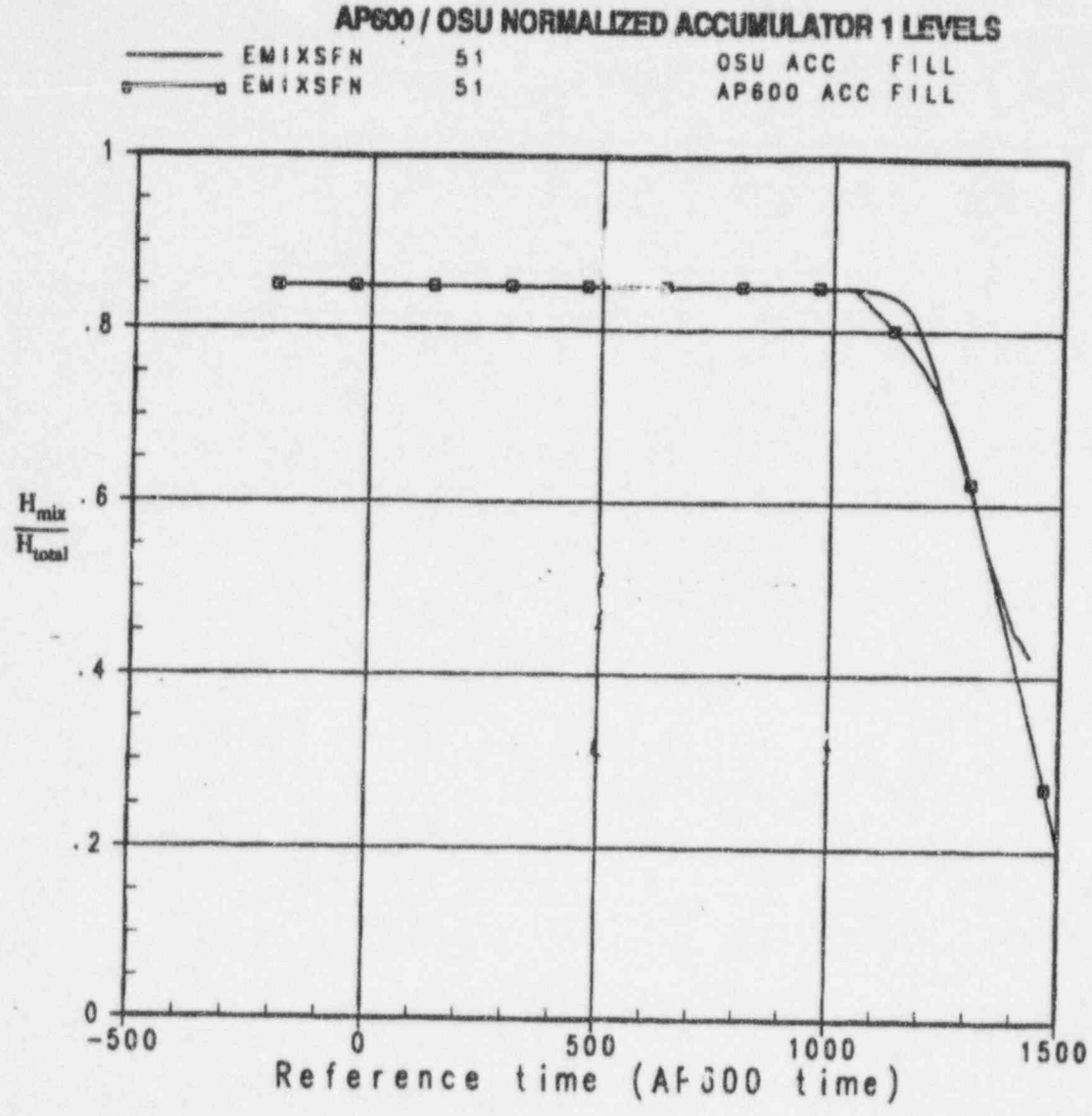

Figure 1.5-4 Normalized ACC-1 Level for AP600 and OSU Facility

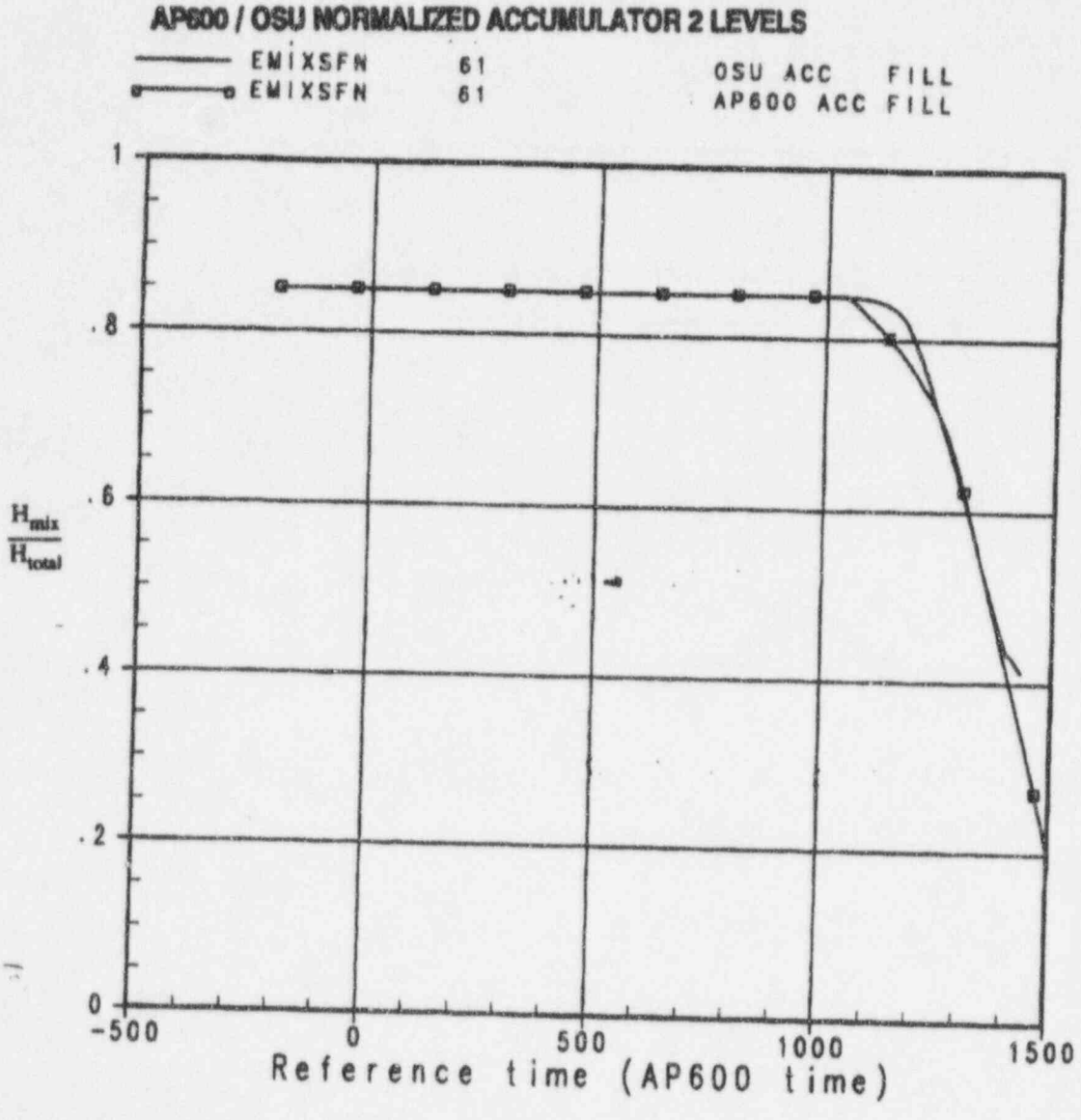

Figure 1.5-5 Normalized ACC-2 Level for AP600 and OSU Facility

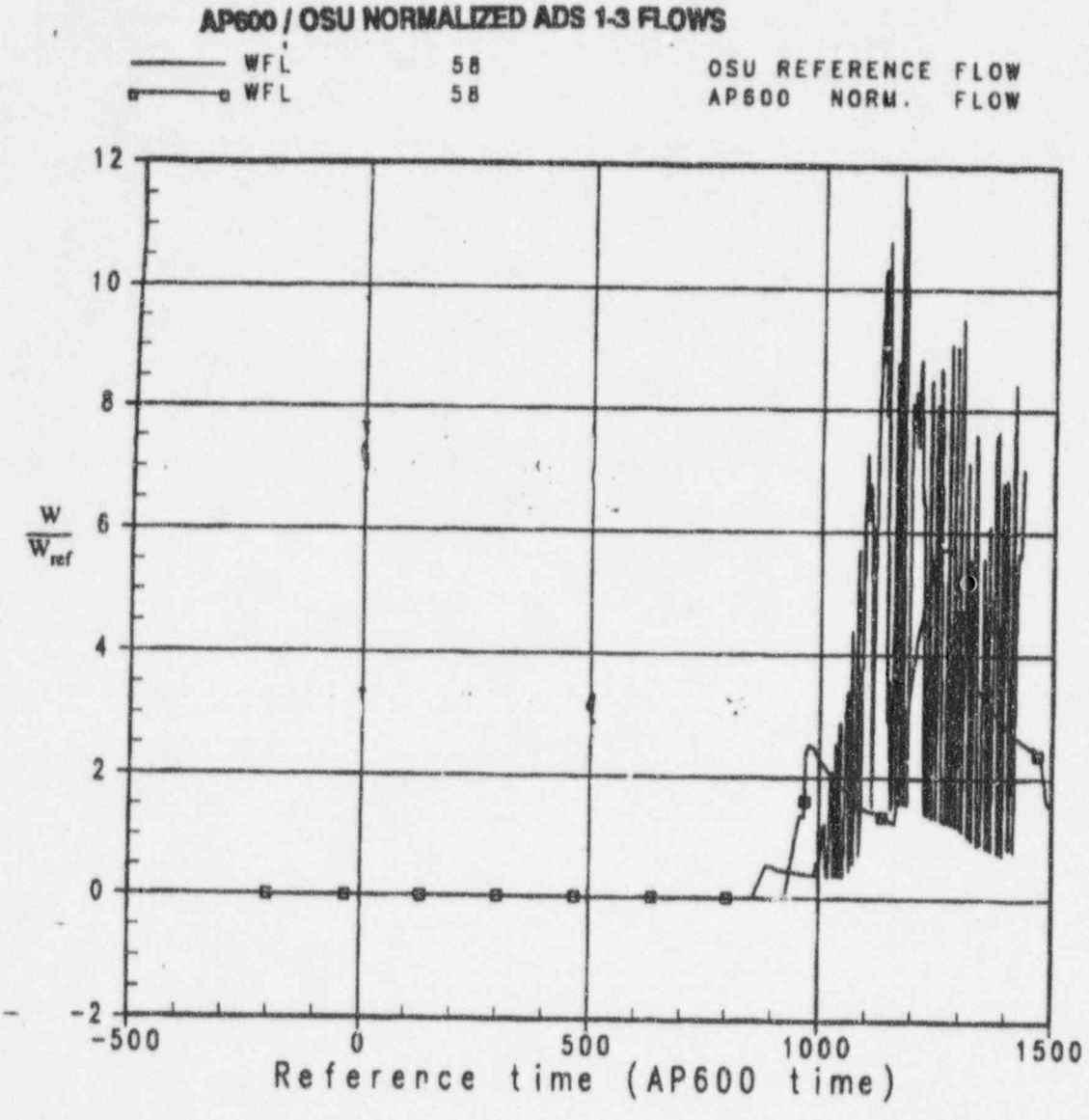

Figure 1.5-6 Normalized ADS 1-3 Flows for AP600 and OSU Facility

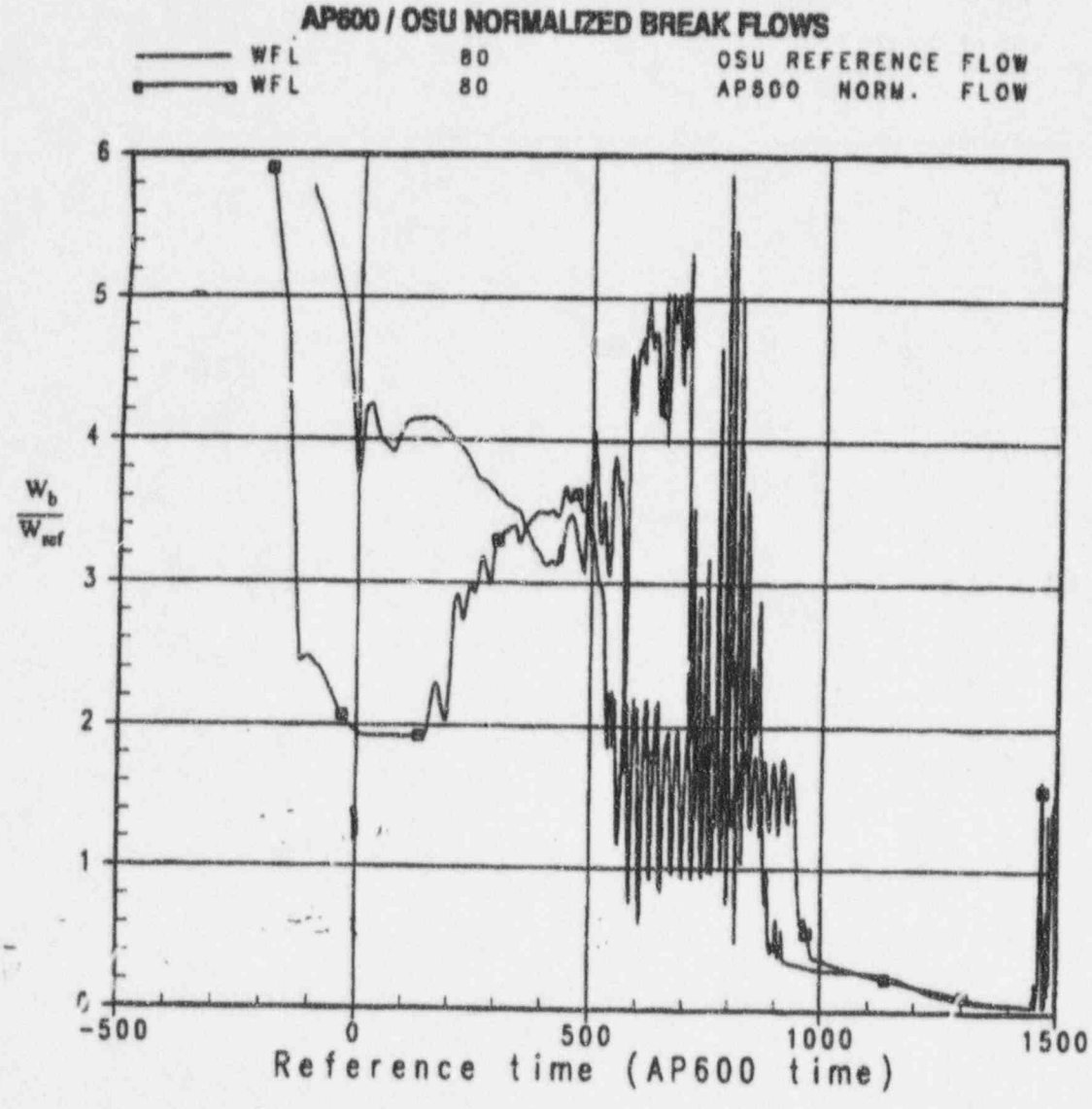

Figure 1.5-7 Normalized Break Flow for AP600 and OSU Facility

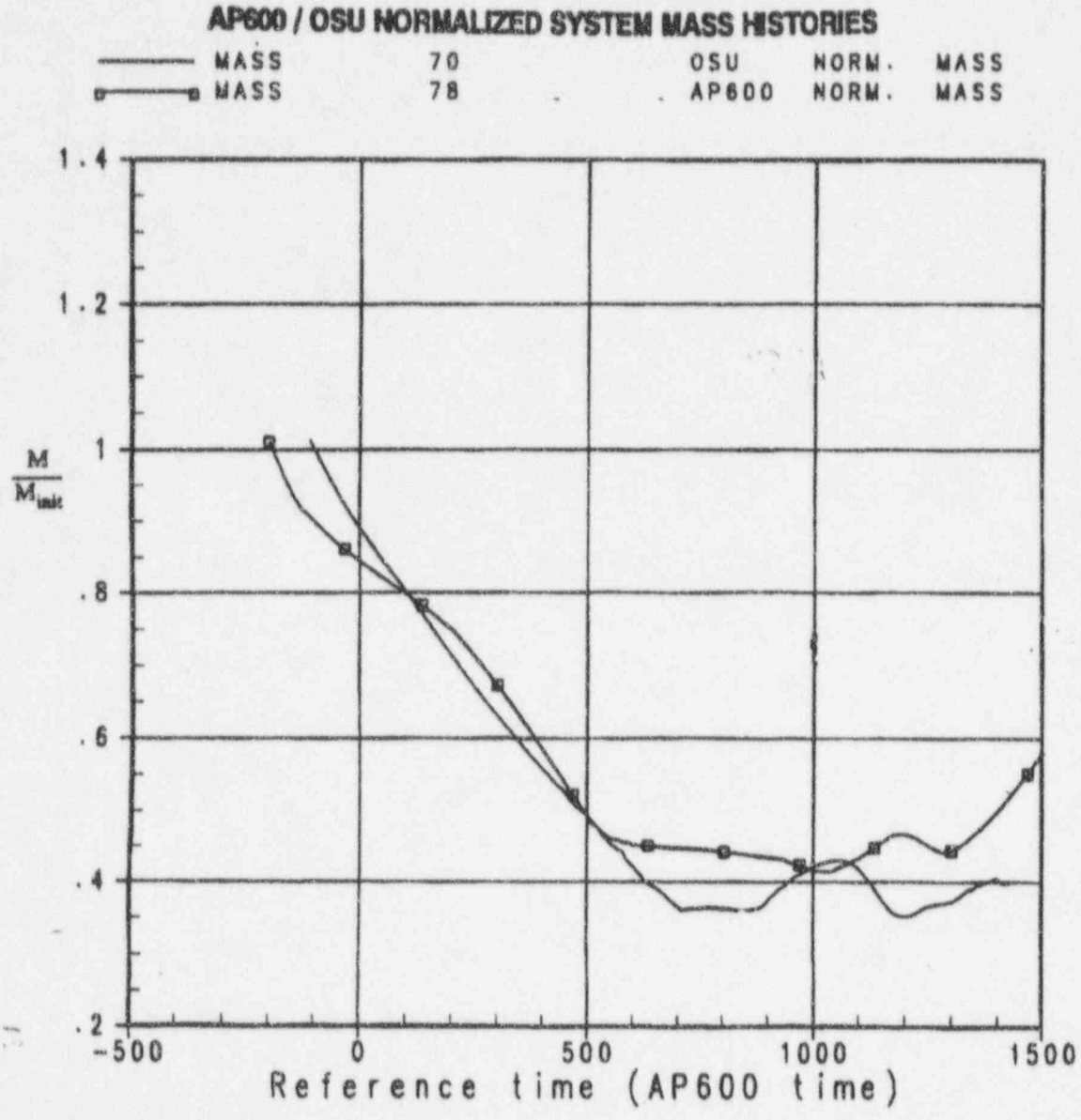

Figure 1.5-8 Normalized System Mass for AP600 and OSU Facility

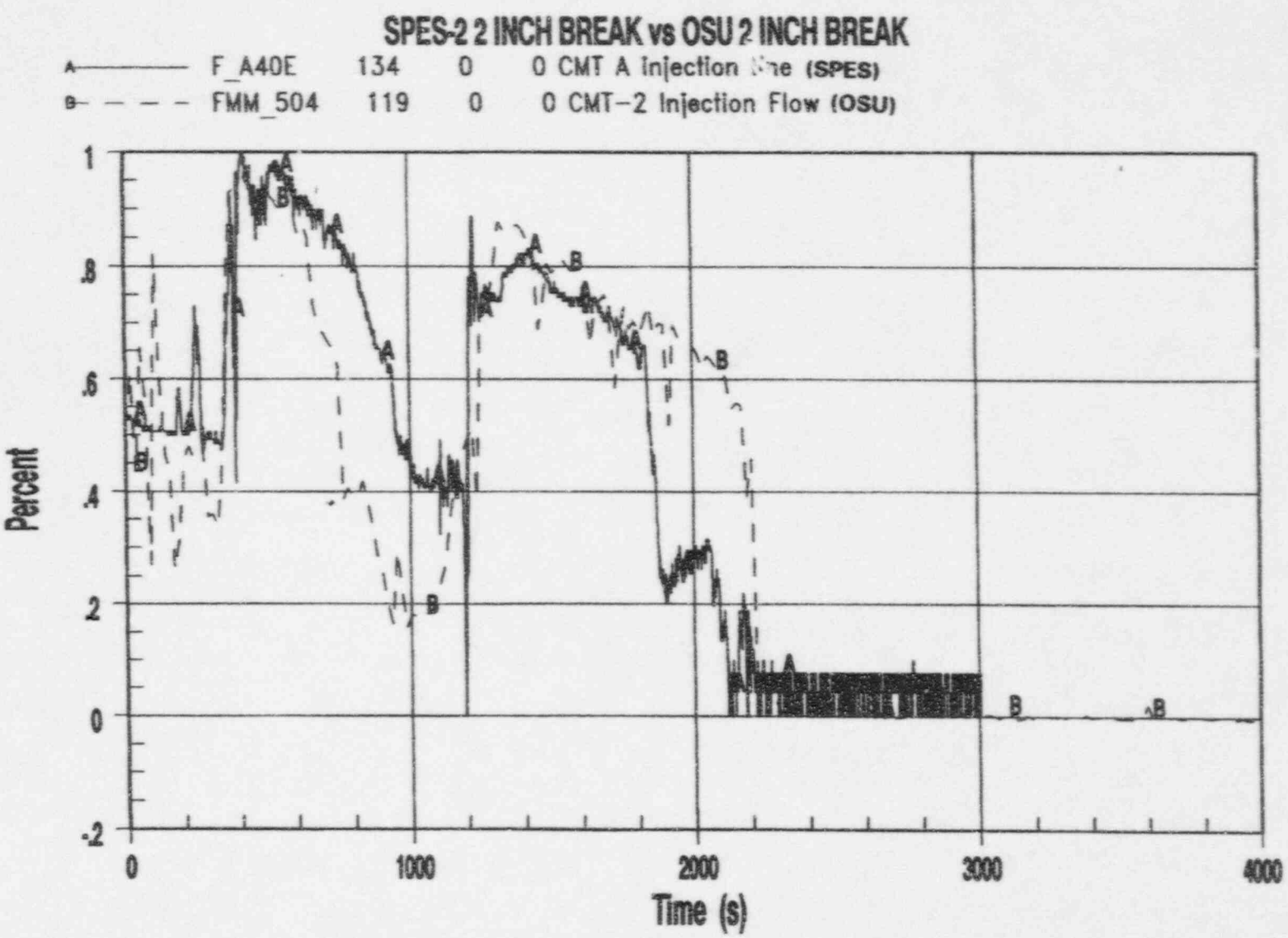

Figure 1.5-9 Comparison of OSU and SPES-2 CMT-1 Injection Flow Rate

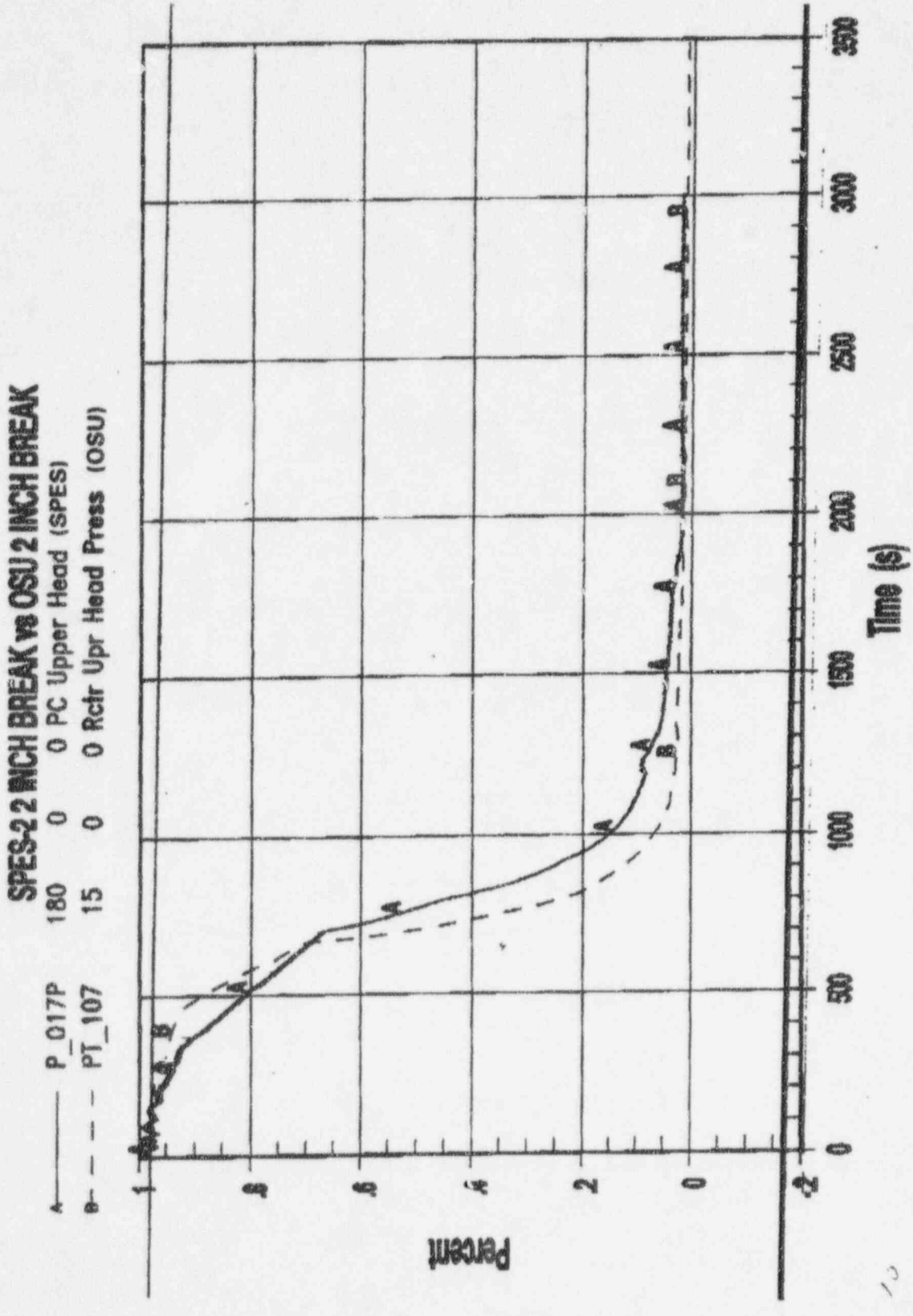

Figure 1.5-10 Comparison of OSU and SPES-2 2-In. Break Pressure Histories

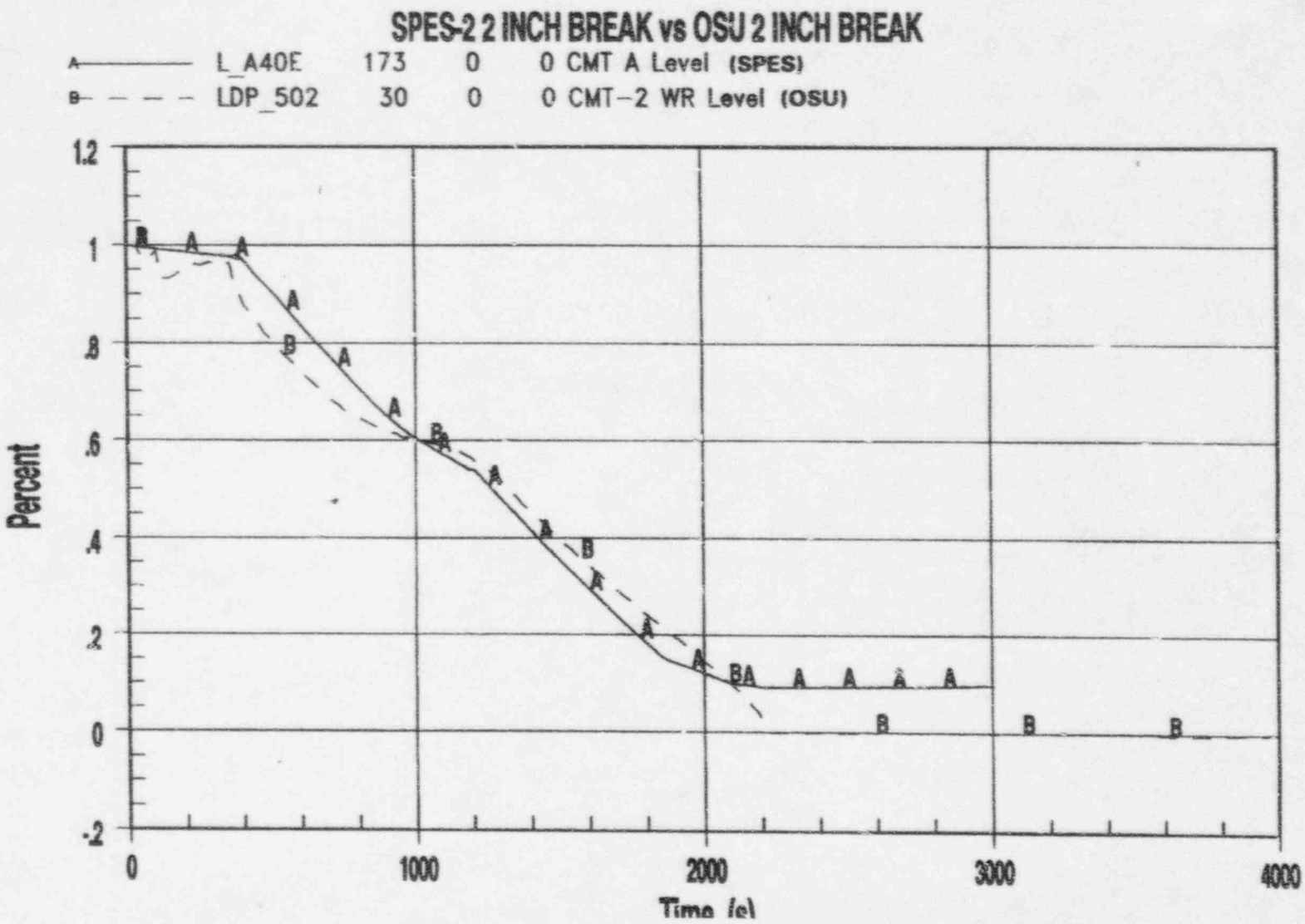

Figure 1.5-11 Comparison of OSU and SPES-2 CMT-1 Liquid Level Histories

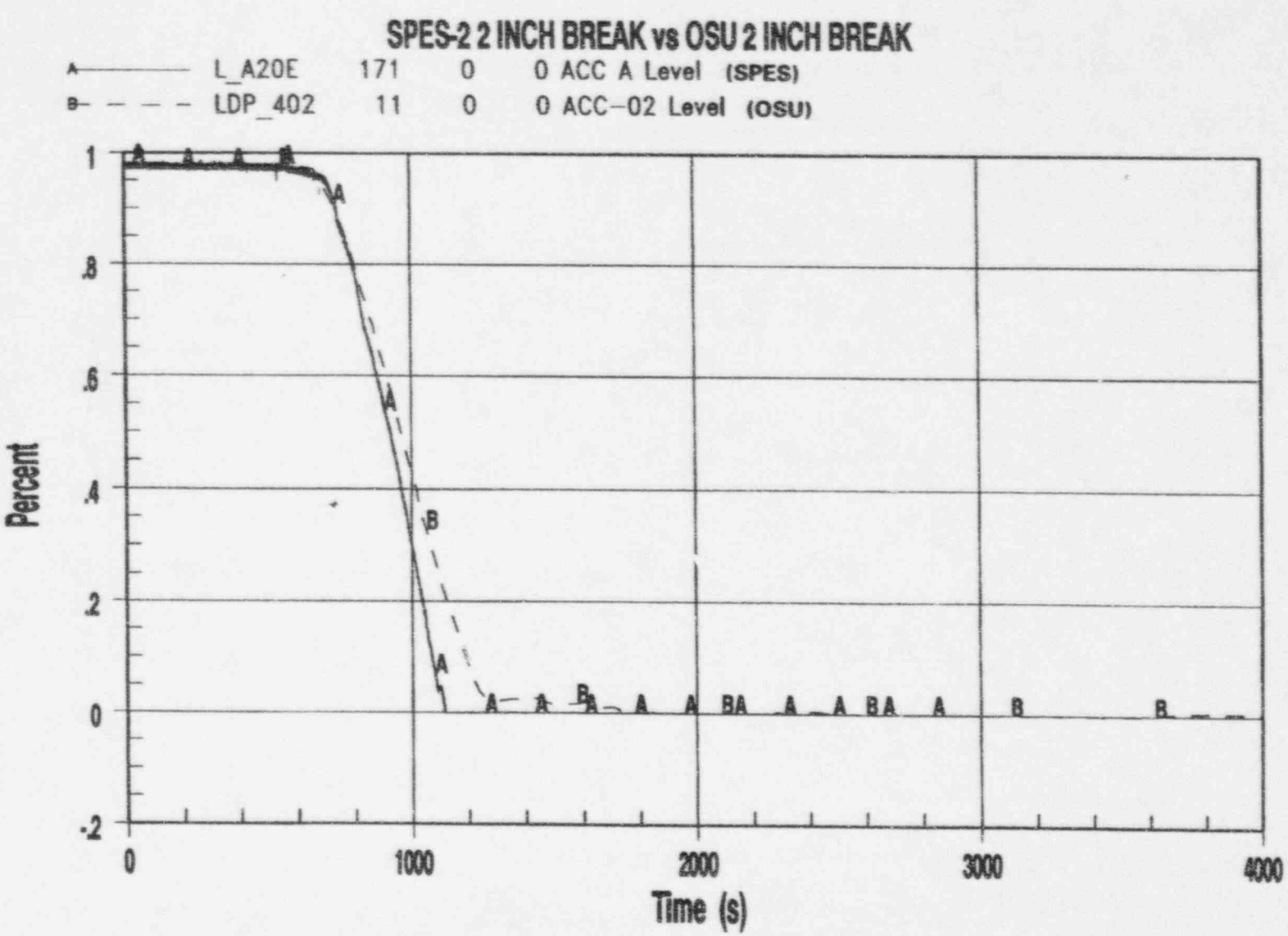

Figure 1.5-12 Comparison of OSU and SPES-2 ACC-1 Liquid Level Histories

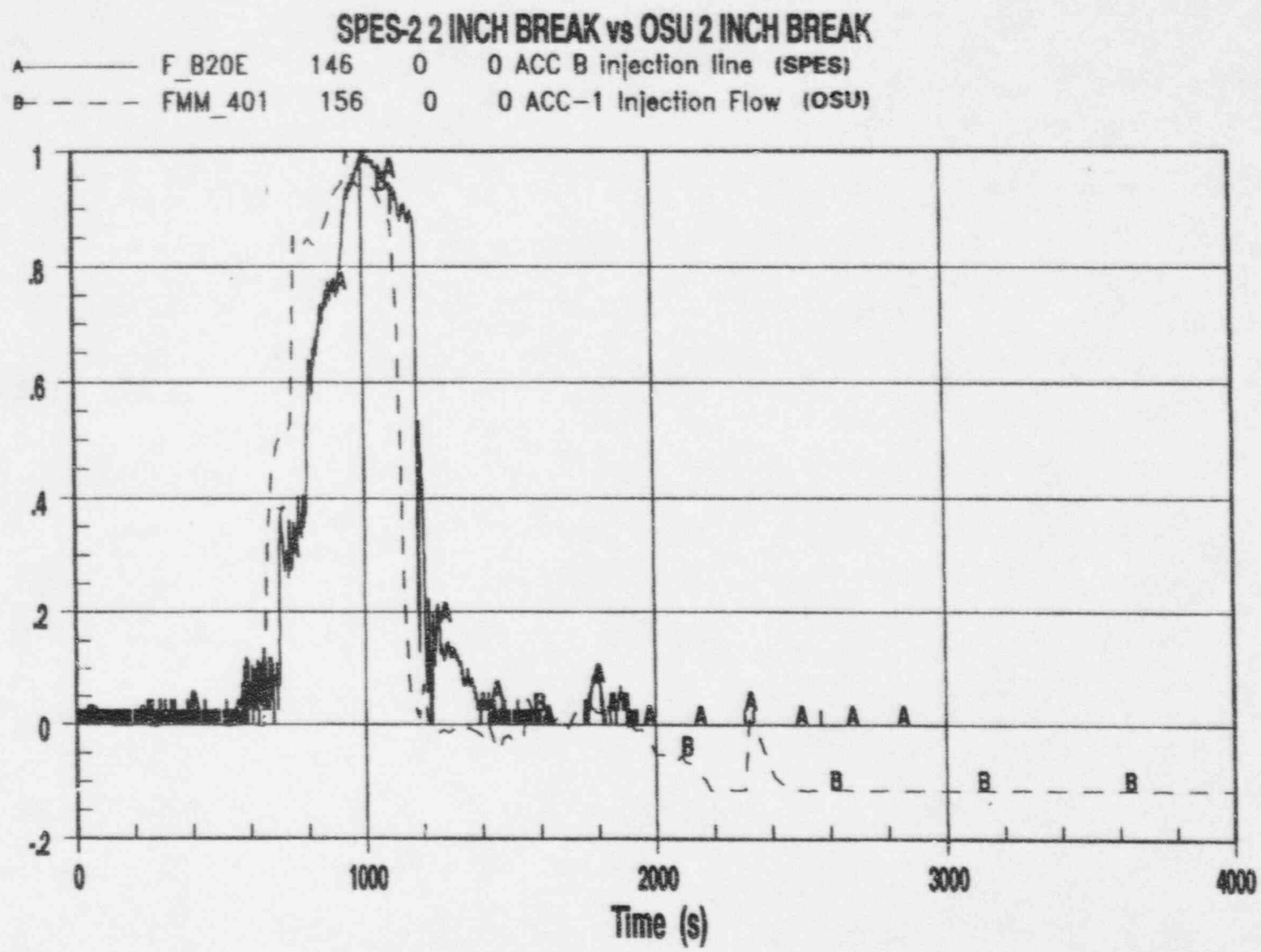

Figure 1.5-13 Comparison of OSU and SPES-2 ACC-1 Injection Flow Rate

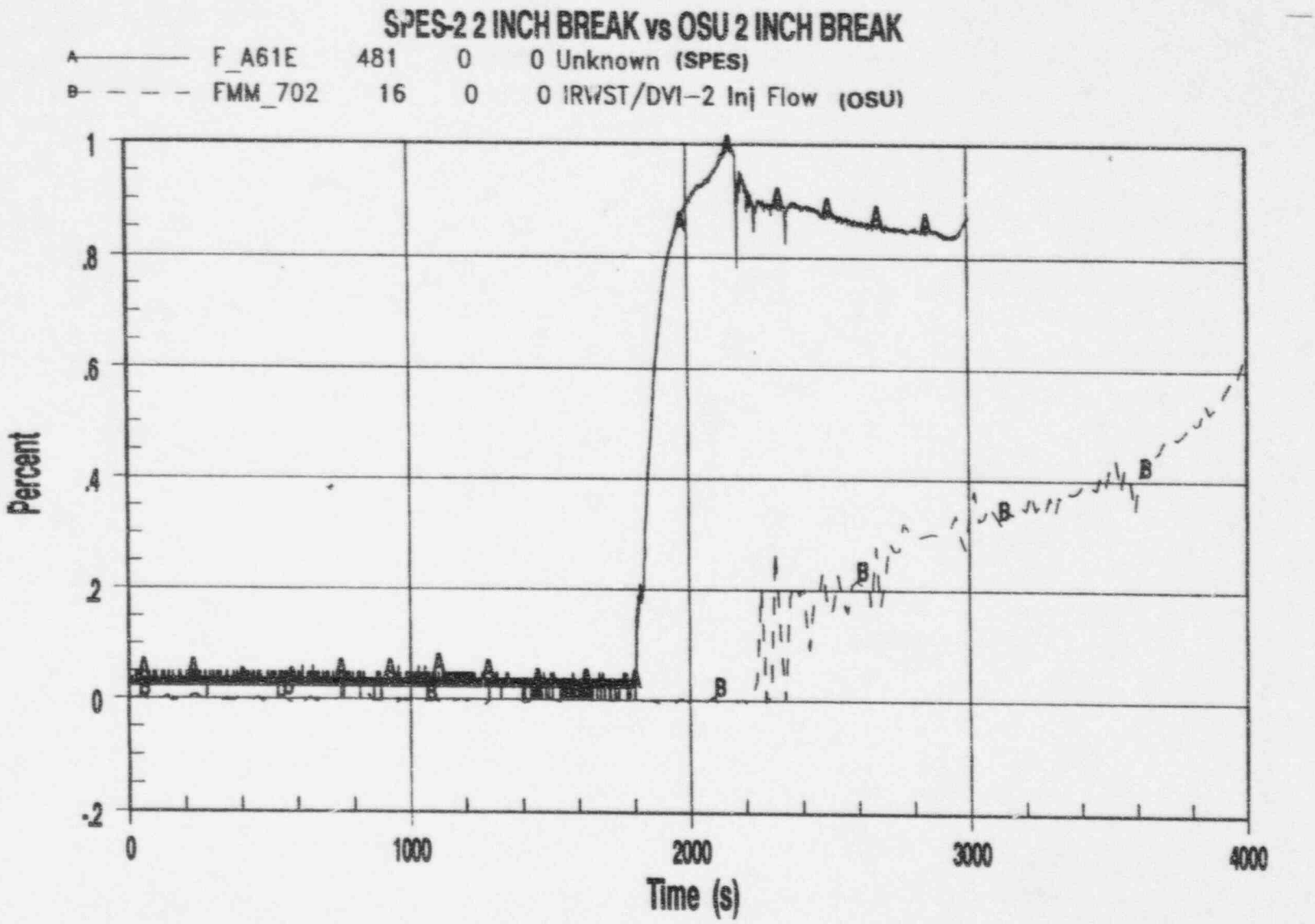

Figure 1.5-14 Comparison of OSU and SPES-2 IRWST-1 Flow Rate

2.0 FACILITY DESCRIPTION SUMMARY

The OSU low-pressure integral systems effect test facility is a scaled representation of the AP600. The design operating conditions for the facility are 400 psig at 450°F. The facility includes all the passive safety-related injection systems that appear in the AP600 design, as well as nonsafety-related injection systems such as the normal residual heat removal system (RNS) and chemical and volume control system (CVS).

The test facility operated in a steady-state fashion with a maximum electrical power of 660 kW, using four primary system recirculation pumps and two SGs. SBLOCAs are simulated using break spool pieces. The break can be located on the hot legs, cold legs, DVI lines, or cold-leg balance line. The test facility is designed to simulate the scaled decay power of AP600.

2.1 Overall Facility Description

The OSU test facility is a scaled model of the AP600 reactor coolant system (RCS), steam generator system (SGS), passive core cooling system (PXS), automatic depressurization system (ADS), lower containment sump (LCS), chemical and volume control system (CVS), and normal residual heat removal system (RNS). In addition, the facility is capable of simulating the AP600 passive containment cooling system (PCS) condensate return process. Figure 2.1-1 is an isometric drawing of the test facility, and Figure 2.1-2 is a simplified flow diagram of the test facility. The facility reflects the scaled AP600 geometry, including the piping routings. All components and piping are fabricated from austenitic stainless steel. The relative locations of all tanks and vessels—such as the IRWST, CMTs, and accumulators were maintained as determined by the scaling approach. The facility uses a unique break and ADS measurement system (BAMS) to measure two-phase break and ADS flow.

The RCS is composed of a reactor vessel, which has electrically heated rods to simulate the decay heat in the reactor core, and two primary loops. Each primary loop consists of two cold-leg pipes and one hot-leg pipe connecting a SG to the reactor vessel. A reactor coolant pump (RCP) on each cold leg takes suction from the SG channel head (downstream of the SG U-tubes) and discharges it into the downcomer region of the reactor vessel. A pressurizer with an electric heater is connected to one of the two hot legs through surge-line piping. The top of the pressurizer is connected to the ADS 1-3 line. An ADS-4 line is connected to each hot leg.

The reactor vessel contains two DVI nozzles that connect to the DVI lines of the PXS. A flow venturi is incorporated in each DVI nozzle to limit the loss of inventory from the reactor vessel in the event of a double-ended DVI line break.

This test facility models the primary and secondary side of the SGs with one generator per primary loop. A simulated feedwater line is used for each loop to maintain proper secondary water level. The steam produced in each generator is measured and exhausted to the atmosphere through a common diffuser and stack.

The test control logic simulates the response of the AP600 by providing an S signal at a fixed time following a break.

The passive safety injection systems consist of two CMTs, two accumulators, one IRWST, and one passive residual heat removal heat exchanger (PRHR HX). The test facility simulates the AP600 IRWST with a cylindrical tank with scaled water volume and height. The IRWST is located above the reactor core; two injection lines connect to the two DVI lines. Each IRWST injection line also connects to the sump tank with interconnecting piping and isolation valves. The PRHR HX is located inside the IRWST, using IRWST water as the heat sink. The inlet of the PRHR HX is connected to the pressurizer-side hot leg via a tee at the ADS-4 line, and the outlet is connected to the SG channel head at the cold-leg side. Since the inlet is hot and the outlet is cold, water is circulated through this system by natural convection. The water volume and elevation of each CMT are scaled and modeled.

They are elevated above the reactor vessel and the DVI lines. A line connecting the top of each CMT to its cold leg provides pressure balance between the RCS and the CMT. Therefore, the CMT injects cooling water by its own elevation head. The accumulators are also modeled with scaled volume and height. However, they are pressurized with nitrogen and, therefore, inject when RCS pressure is below the preselected scaled accumulator pressure.

The AP600 uses four stages of valves to depressurize the RCS. The first three stages of the ADS are provided through connections to the pressurizer. These three stages are arranged in parallel, with each stage containing two lines with each line containing an isolation and control valve. The fourth stage of the ADS contains four separate lines.

The OSU test facility uses only one set of valves to model the ADS 1-3 stages for AP600. This is done using removable flow nozzles to match the scaled flow characteristics of either one or two lines of valves. The lines of ADS 1-3 split into parallel lines from one connection off the pressurizer in the AP600.

The discharge lines from the ADS 1-3 valves are joined into one line connected to the ADS 1-3 separator. This two-phase flow is separated using a swirl-vane separator. The liquid and vapor flows are measured to obtain the ADS total flow for mass and energy balance analysis. The separated flow streams are then recombined and discharged into the IRWST through a sparger.

The OSU test facility uses one ADS-4 line connected to the top of each hot leg. Each line contains a pneumatically operated, full port ball valve acting as the ADS-4 isolation valve and a flow nozzle simulating the flow area in the AP600. Two sets of flow nozzles are used in the test: one simulates 100-percent flow area and the other simulates 50-percent flow area. In the test facility, ADS-4 discharge flows to the ADS-4 separators, where the steam and liquid flows are separated and measured. Steam flow is measured and exhausted to the atmosphere.

The lower containment sump in the AP600 consists of two volumes: normally flooded and normally nonflooded. The normally flooded volume consists of those compartments which collect liquid break flow and ADS flow. The normally flooded volume is modeled in OSU with a cylindrical tank, identified as the primary sump tank. The normally nonflooded volume includes those compartments which do not collect any liquid flow. The normally nonflooded volume is modeled in OSU with a cylindrical tank, identified as the secondary sump tank. These two tanks are connected with a line at a level simulating the curb level in the AP600.

In the AP600, the RNS is used to provide nonsafety-related cooling water injection to the reactor core. The RNS pump takes suction from the IRWST and discharges it into the DVI lines. The test facility RNS pump takes suction from the IRWST at the scaled location and elevation and discharges equal flow to both DVI lines at scaled locations.

BAMS is uniquely designed for the test facility to indirectly measure two-phase flow and energy leaving the break and ADS location. This system separates two-phase flow into single-phase liquid and single-phase steam flows for direct flow rate and temperature measurements. The BAMS consists of steam-liquid separators and the interconnecting pipes and valves to the various break sources, the primary sump tank, the ADS 1-3 lines, and the main steam header.

Two-phase flow (steam and water) from the ADS 1-3 lines enters the ADS 1-3 separator, where the steam is separated from the mixture. Steam flows out of one outlet while liquid drains down the other. These two lines recombine the separated flows downstream and discharge into the IRWST via the sparger located inside the IRWST. Therefore, the mass and energy from ADS 1-3 is transferred to the IRWST as in the AP600.

Two ADS-4 separators are used, one for each ADS-4 line. Each ADS-4 separator separates two-phase flow into single-phase steam and single-phase liquid for flow rate, pressure, and temperature measurements. The steam line connects to a common steam header, and the liquid line connects to the primary sump tank. These connections simulate the ADS-4 operation process in the AP600, where the steam flow rises to the containment wall and liquid drains to the sump.

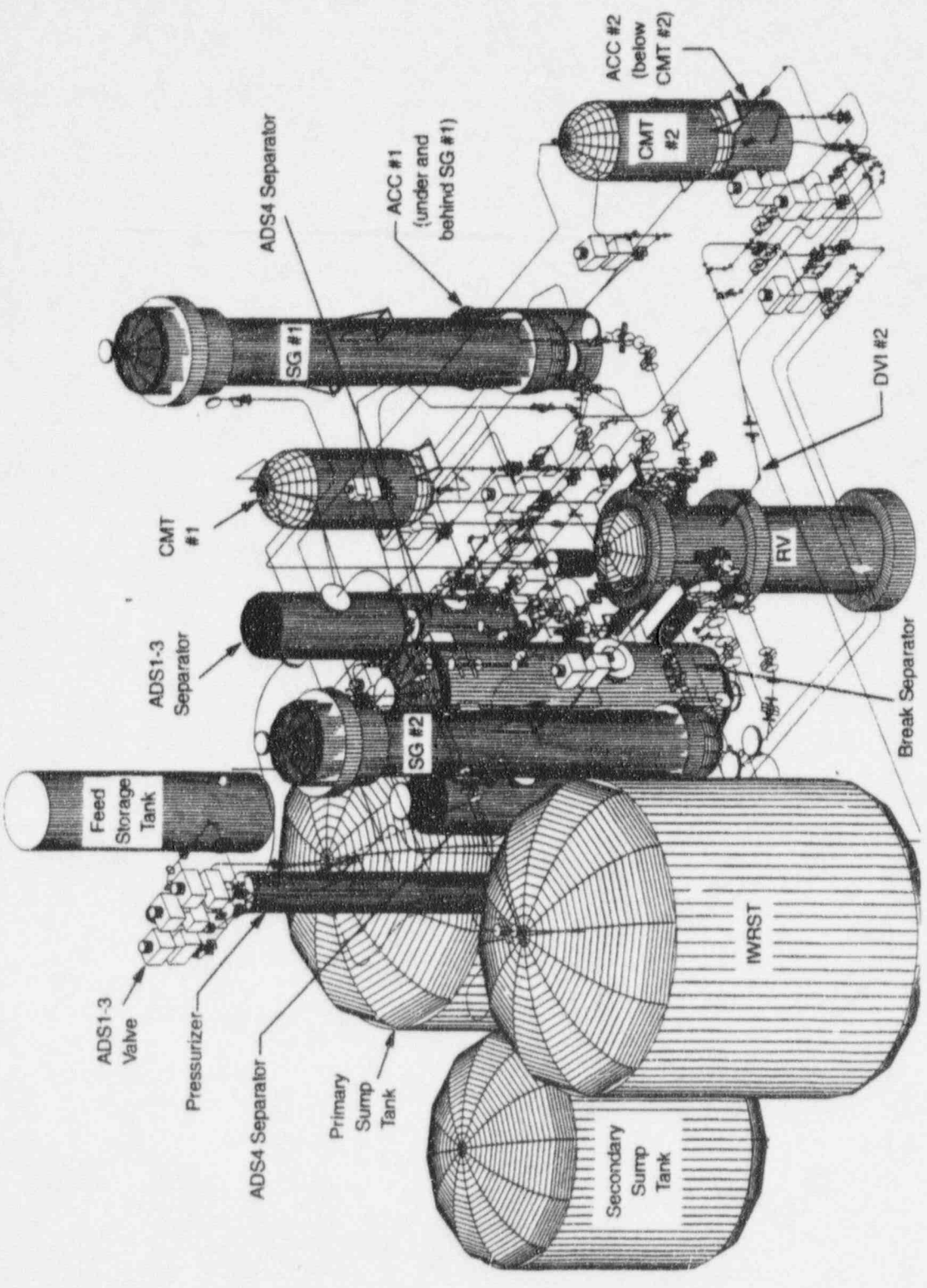

Figure 2.1-1 Isometric Drawing of the OSU Test Facility

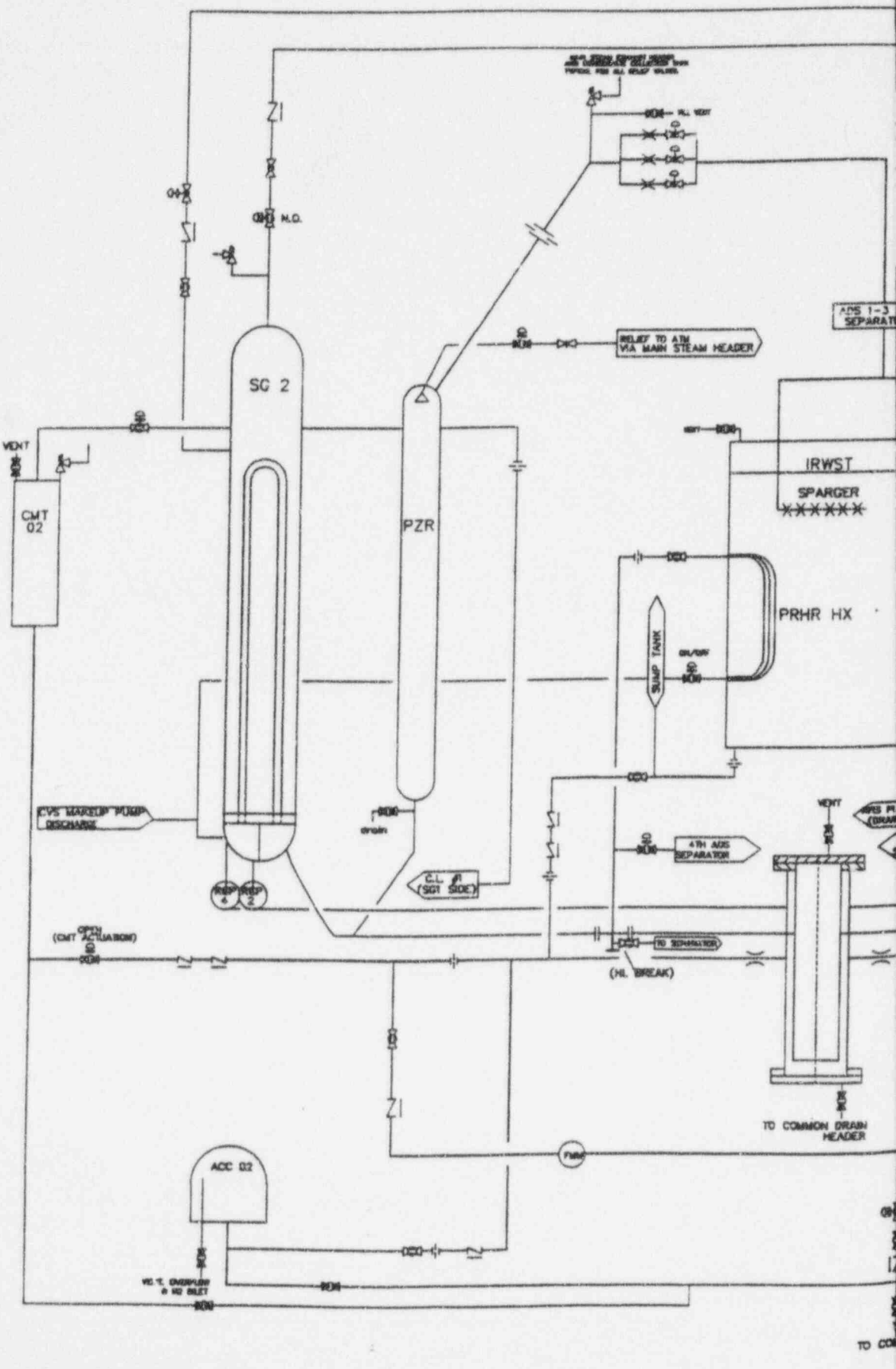
SG 2
PZR
CMT 02
IRWST
SPARGER
PRHR HX
SUMP TANK
VENT
RELIEF TO ATM VIA MAIN STEAM HEADER
CVS MAKEUP PUMP DISCHARGE
4TH ADS SEPARATOR
TO COMMON DRAIN HEADER
ACC 02
(HL BREAK)

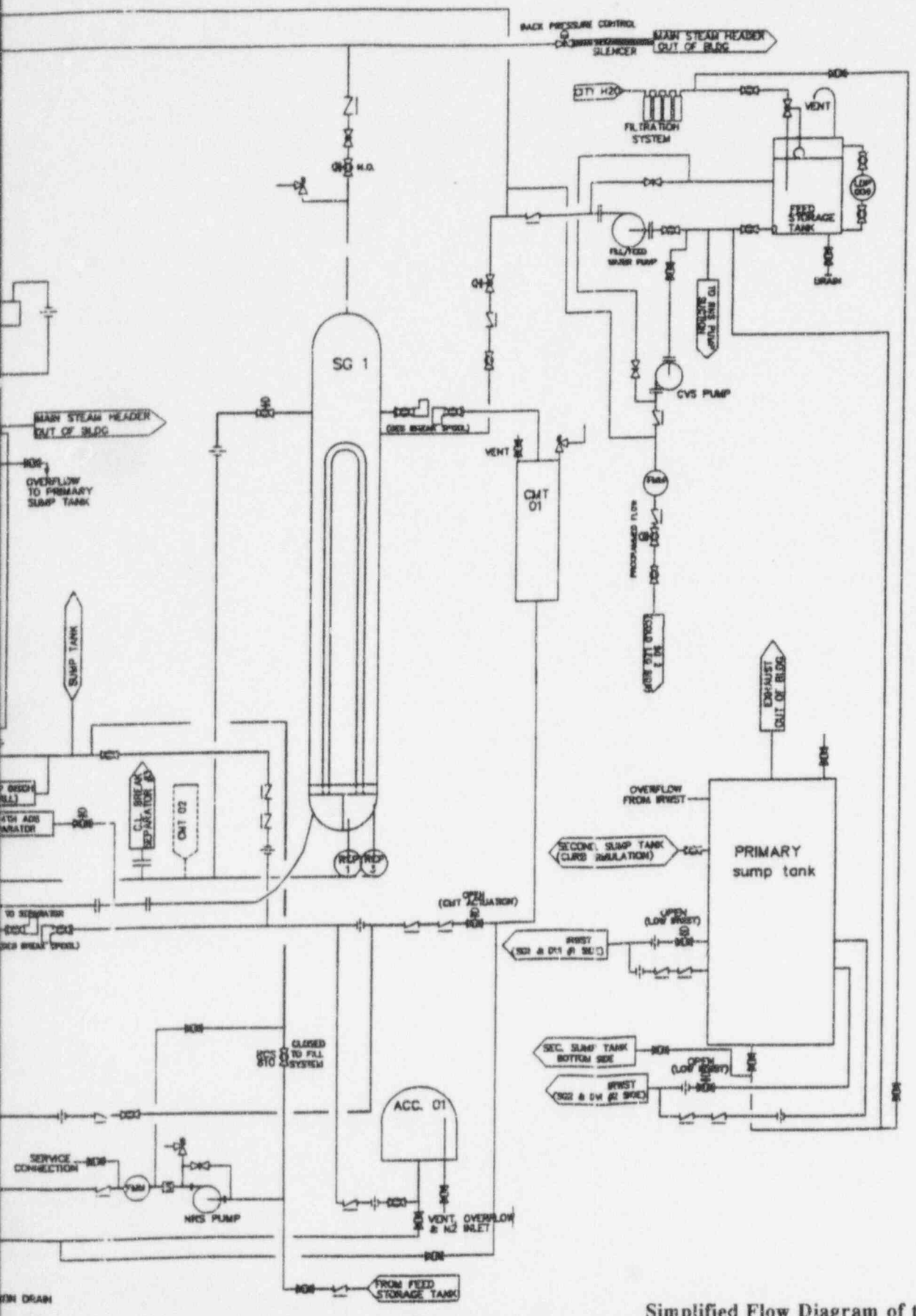

Figure 2.1-2
Simplified Flow Diagram of the OSU Test Facility

9510270126-01

2.2 Facility Instrumentation

OSU used standard instrumentation to indicate mass, flow, temperature, and pressure in the system and components. The instrumentation plan was specifically designed to provide a transient mass and energy balance on the components and for the entire system. Details of the instrumentation and its performance can be found in the OSU Final Data Report.[1] The function of each of the instruments is discussed below. The use of the instruments for the mass and energy balances is provided in Section 4.

2.2.1 Differential Pressure Transmitters (FDP, LDP, DP)

Differential pressure transmitters measure the flow (FDP), or the level (LDP), in the system.

The only application of FDPs is to measure differential pressure across the flow orifices in the ADS-1, ADS-2, and ADS-3 lines (FDP-604, FDP-605, and FDP-606, respectively).

The level (LDP) transmitters measure levels in the facility tanks, the RCS hot-leg and cold-leg pipes, SG tubes, and PRHR HX tubes. The LDPs were designed to measure level (mass) in a component and were calibrated at ambient temperature. The level data recorded by the facility's data acquisition system (DAS) were uncompensated for temperature. The resulting signals were temperature compensated for the mass and energy balance calculations.

2.2.2 Pressure Transmitters

Pressure transmitters (PTs) are identical to differential pressure transmitters except that the low-pressure side of the transmitter senses atmospheric pressure.

2.2.3 Magnetic Flow Meters

Foxboro™ magnetic flow meters (FMMs) were used to measure liquid flow, in the different liquid solid lines. The FMMs are not designed to accurately measure steam or two-phase flow, and the data from the transmitters are invalid when either of these are measured.

Fourteen Foxboro™ vortex flow meters (FVMs) were used to measure steam flow in the test facility. The FVMs measure steam flow from the ADS 1-3, ADS 4-1, ADS 4-2, and break separators. In addition, they measure steam flow from the primary sump, the IRWST, and the BAMS header. These meters are known to have a manufacturer's warranted cutoff of 141 actual cfm (acfm) which means they may not detect flows below 0.088 lbm/sec. at ambient conditions.

2.2.4 Heated Phase Switches

Heated phase switches (HPSs) manufactured by Reotherm™ were used to indicate fluid phase in different components. There are 12 switches: one each on the cold and hot legs, CMT balance lines, PRHR HX inlet, and ADS 1-3 header. In addition, two switches are installed in the pressurizer surge line. The HPSs were usually used in conjunction with an LDP to indicate a separate level in a component.

2.2.5 Heat Flux Meters

Heat flux meters (HFMs) were used to measure heat flux through pipe or tank walls to indicate heat loss. The small, wafer-thin instruments are glued to a pipe or tank surface. Three thermocouples are imbedded into each HFM. Two thermocouples measure temperature on either side of the HFM. The thermocouple signals are measured by the DAS, and their temperature difference is converted to a heat flux using coefficients provided by the vendor. The third thermocouple measures the temperature of the surface.

2.2.6 Load Cells

The mass of water in the IRWST, primary sump, and secondary sump was measured by load cells mounted under the four supports of each tank. After the transmitter load cell was calibrated, it measured only the weight of water in the tank. The transmitter also provided local indication of weight in the tank for use by test personnel. The load cells were found to be sensitive to variations in ambient conditions, and thus, are not used for absolute measurements. Their readings are valid for tracing short time scale variations in mass.

2.2.7 Thermocouples

Thermocouples are assigned one of four instrument designations, depending on the thermocouple's application. A TF thermocouple inserted through the wall of a pipe or tank is mounted on a thermocouple rod. TW thermocouples are mounted on the inside or outside walls of a tank or pipe. TR thermocouples, unique to the reactor vessel, are mounted on vertical thermocouple rods installed in the reactor vessel. TH thermocouples are mounted on the heaters for the reactor vessel and the pressurizer. Thermocouple type and diameter are specified in Appendix C of the OSU Final Data Report.[1]

The reactor vessel contains TH thermocouples to measure temperatures of selected heaters. Selected heater thermocouples are used as inputs to the safety shutdown of the reactor heaters to detect abnormally high temperatures.

Thermocouples mounted in hollow rods (TR thermocouples) are unique to the reactor vessel. Five thermocouple rods are installed in the reactor vessel to provide radial and axial fluid temperature

distributions in the heated section of the reactor vessel. Each rod contains thermocouples mounted along its entire length. Thermocouples protrude from the hollow rod and are sealed from the outside with silver solder.

The CMTs are instrumented with numerous fluid and wall thermocouples to measure the CMT wall heat flux and temperature, as indicated in Appendix G, Dwg. OSU 600501 and 600502 of the Final Data Report.[1] Each CMT contains one long and two short thermocouple rods instrumented with thermocouples along its entire length. In addition, inside and outside wall thermocouples, fluid thermocouples installed 1 in. from the inside wall, and tank centerline thermocouples are installed at the same elevation to measure the temperature of the fluid and walls at that elevation.

The IRWST also contains two thermocouple rods to measure the energy gain in the IRWST as shown in Appendix G, Dwg. OSU 600701 of the Final Data Report.[1]

One long and one short tube of each SG are instrumented with shell-side (secondary-side) wall thermocouples and tube-side (primary or RCS-side) fluid thermocouples as shown in Appendix G, Dwg. OSU 600301 of the Final Data Report.[1]

3.0 TEST SUMMARY

The following sections describe the test matrix and the data validation processes used for the low-pressure integral systems tests performed at OSU. The initial test validation process was based on specific instruments that were required to function or selected backup instruments that were available. The OSU Final Data Report[1] describes the instrumentation from the tests and assesses their performance and reliability. This report utilizes the valid instrumentation to interpret the data.

3.1 Test Validation

As described in the OSU Final Data Report,[1] the OSU test facility data were reviewed and validated using a three-step process. The first step was performed at the OSU test facility. Immediately following each test, the data were recorded on a compact disc as a read-only file, and documented in a Day-of-Test Report. The Day-of-Test Report evaluated the test from a very basic standpoint, including operability of key instruments and deviations from specified initial conditions. The Day-of-Test Report also documented any facility modifications or onsite test observations. The Day-of-Test Report assessed whether the test needed to be rerun because of some significant problem observed during the performance of the test.

The overall test acceptance criteria are shown in Table 3.1-1. The critical instruments were the minimum set of instruments required to perform a transient, component-by-component mass and energy balance.

The second step in the data validation process was performed by the test engineering personnel at the Westinghouse Energy Center in Monroeville, Pennsylvania. This step was performed after receiving the Day-of-Test Report and processing of the data. This data validation was documented in the Quick Look Report (QLR). The QLR provided a preliminary validation of all test data. The key purpose of the QLR was to issue some pedigree of the data, without specifically evaluating the data for code validation purposes (reviewed, but not yet validated, data) shortly after the test was performed.

The third step was a detailed review of the transient progression, facility and component performance, and cross-test comparisons as reported in the Final Data Report.[1]

This report utilizes the insight derived from the instrumentation performance and the transient progression gained in the Final Data Report[1] to determine and understand the thermal-hydraulic behavior of the facility during each test. The objective of the analysis is to provide the explanation of the test facility response.

TABLE 3.1-1
OVERALL ACCEPTANCE CRITERIA

- Test initial conditions shall be achieved in a specified tolerance.
- Setpoints shall be achieved in an acceptable tolerance band.
- Sufficient instrumentation shall be operational before the test (exceptions shall be approved by the Westinghouse test engineer).
- Critical instruments not operating shall be identified to the Westinghouse test engineer before the tests. These instruments must be operational before and during the test, or exceptions should be approved.
- A zero check of LDPs, DPs, and FDPs shall be in acceptable tolerances.

  The zero check was eliminated from the acceptance criteria for Category III tests. The earlier pre-test and post-test checks of zero shift showed acceptable variation in the readings of these instruments. Performing these checks required that each instrument be manually isolated and then returned to service. Based on the consistency of the readings from earlier tests and the large number of manual operations, it was decided that the risk of an instrument remaining isolated after the check was greater than an instrument having a zero shift.

3.2 Test Matrix

Before the test matrix was initiated, a series of pre-operational tests were performed to provide an understanding of facility control and operating characteristics, to confirm design features essential to scaling, and to check that the instruments and the data acquisition system (DAS) were performing as expected. Tests were conducted while the facility was in cold conditions to measure system pressure drops and volume of the components. Pressure drops in the test facility were adjusted to the desired scaled AP600 values by using orifice plates. Pre-operational testing was also performed in the hot condition to characterize system heat losses. Results of the pre-operational tests are presented in Section 4 of the OSU Final Data Report.[1]

System volume determination tests were performed for the accumulators, CMTs, pressurizer, IRWST, sumps, SG secondary sides, and reactor vessel to compare the actual volumes with the calculated volumes for the facility used in the safety analysis computer codes.

Line resistance determination tests were performed to measure line resistance for the accumulator lines, IRWST lines, and sump injection lines for a given flow rate. The pressure drop in CMT injection and ADS 1-3 lines was measured over a range of flows. Resistance of the RNS injection lines was measured to demonstrate that the pressure drops were within 10 percent of each other. The RCP head was measured for full flow and pump coastdown conditions. The line resistances also provided data for the computer models of the test facility.

Three separate hot functional tests were performed. The objectives of the tests were to show proper operation of the equipment prior to the formal matrix test program and to provide data necessary to document temperature characteristics of the system. The first hot functional test measured the steady-state heat loss, natural-circulation flow, and forced-flow characteristics. These tests verified the calculations used to help size the test facility. OSU-HS01 was performed to determine surface heat losses from the system at 100°, 200°, 300°, and 400°F; characterize passive residual heat removal (PRHR) under natural circulation and forced cooling; characterize the primary cooling system at 100, 300, 500, and 600 kW; and characterize the CMT natural-convection characteristics. The objective of the second test (OSU-HS02) was to verify the measuring capability of the break and ADS measurement system (BAMS) and the control of the ADS. The third hot functional test was an inadvertent ADS-1 actuation to assess overall facility performance prior to executing the formal matrix test program.

The formal test matrix summary given in Table 3.2-1 was designed to provide a wide range of test data on the performance of the passive emergency core cooling systems used in the AP600. The tests were intended to provide overlap with the full height, full pressure SPES-2 tests[3] as well as the AP600 plant SSAR calculations. The test parameters investigated were:

- Cold-leg break sizes of 1/2, 1, 2, 4 (bottom of cold leg), and 4 in. (top and bottom of cold leg)

- Break locations of cold leg with CMTs, cold leg without CMTs, top of pipe, bottom of pipe, balance line breaks, DVI line breaks, and no breaks with inadvertent ADS actuation
- Different single failures, one of four ADS-4 valves, ADS-1 valves, and ADS-3 valves
- Beyond design-basis tests with multiple failures
- Spurious S signal (no break)

The break-size range and location, as well as the different assumed single-failure disruptions, provide a thorough and comprehensive set of integral systems data for code validation.

TABLE 3.2-1
OSU MATRIX TEST SUMMARY

Test No.	Break Size and Location	PRHR HX	CVS Pump	RNS Pump	ADS 4-1 (HL-1)	ADS 4-2 (HL-2)	Comments
SB01	2-in. CL-3 bottom of cold leg (CMT side)	On	Off	Off	50-percent flow area in AP600	100-percent flow area in AP600	Failure of one of two lines in ADS 4-1; reference cold-leg break case
SB06	4-in. CL-3 bottom of cold leg (CMT side)	On	Off	Off	50-percent flow area in AP600	100-percent flow area in AP600	Failure of one of two lines in ADS 4-1
SB09	2-in. CL-3 to CMT-1 balance line	On	Off	Off	50-percent flow area in AP600	100-percent flow Area in AP600	Same as SB01 except different break location; asymmetric behavior of CMTs
SB10	DEG CL-3 to CMT-1 balance line	On	Off	Off	50-percent flow area in AP600	100-percent flow area in AP600	Limiting break on balance line; asymmetric behavior of CMTs; failure of one of two lines in ADS 4-1
SB12	DEG DVI-1 line break	On	Off	Off	100-percent flow area in AP600	100-percent flow area in AP600	Limiting break on DVI line; failure of one of two lines of ADS-1 and ADS-3
SB13	2-in. DVI-1 line break	On	Off	Off	50-percent flow area in AP600	100-percent flow area in AP600	Same as SB01 except different break location
SB14	Inadvertent ADS (no break)	On	Off	Off	50-percent flow area in AP600	100-percent flow area in AP600	No-break case with one failure of two lines in ADS 4-1
SB15	2-in. HL-2 bottom of pipe	On	Off	Off	50-percent flow area in AP600	100-percent flow area in AP600	Same as SB01 except break location

TABLE 3.2-1 (Continued)
OSU MATRIX TEST SUMMARY

Test No.	Break Size and Location	PRHR HX	CVS Pump	RNS Pump	ADS 4-1 (HL-1)	ADS 4-2 (HL-2)	Comments
SB18	2-in. CL-3 bottom of cold leg (CMT side)	On	Off	Off	50-percent flow area in AP600	100-percent flow area in AP600	Repeat test of SB01; confirm behavior of system and instrumentation
SB19	2-in. CL-3 bottom of cold leg (CMT side)	On	Off	Off	50-percent flow area in AP600	100-percent flow area in AP600	Same as SB01 except containment backpressure simulated
SB21	4-in. top of and 4-in. bottom of CL-3 (CMT side)	On	Off	Off	50-percent flow area in AP600	100-percent flow area in AP600	Same as SB01 except larger break size; largest break size simulated in matrix tests
SB23	1/2-in. CL-3 bottom of cold leg (CMT side)	On	Off	Off	50-percent flow area in AP600	100-percent flow area in AP600	Same as SB01 except smaller break size

Note:
DSG -- double-ended guillotine
PRA -- probabilistic risk assessment

4.0 DATA REDUCTION METHODOLOGY

The OSU test facility is a scaled model of the AP600 and its passive emergency core cooling systems that were used to perform selected tests to study the thermal-hydraulic behavior of those systems under postulated accident conditions. Data collected from the facility included fluid, metal, and ambient temperatures, pressures, liquid levels, differential pressures, volumetric flow rates and power supplied to the core simulation. These data were used as inputs to calculations of instantaneous and integrated masses, mass flow rates, energy, and energy transfer into and out of facility components.

The AP600 incorporates and takes advantage of passive safety systems features, that is, flow is driven by differences in temperature (natural convection) and elevation heads (gravity). The Oregon State University (OSU) test facility is a scaled model of the systems and components important to the accident mitigation capability of the AP600 design. Data collected from the OSU test program are used to validate the safety analysis codes used to predict the performance of the passive safety system for design-basis accidents.

Computer software has been developed to reduce the experimental data collected from the OSU test facility into engineering parameters against which code predictions may be directly compared. The data analysis software performs calculations and generates plot files that contain these calculated engineering parameters. The calculations performed by this software include mass and energy balances for the system.

Sections 4.1 through 4.22 describe the underlying assumptions, conversions, corrections and compensations made to the data; the formulation of the mass and energy equations for each component included in the OSU test facility; and the formulation of the overall system mass and energy balance equations. Also, the nomenclature used in the development of the mass and energy equations is defined in Subsection 4.0.1. The equations described in this section were coded in FORTRAN to run on workstations. Results obtained from this code were used as the basis of the analyses presented in Sections 5, 6, and 7.

4.0.1 Nomenclature

This section contains the nomenclature utilized throughout Section 4. In certain subsections, specific conversion constants and subscripts are defined, where applicable, within the subsection.

Variable Definitions

ρ	=	Density, lb./ft.^{3}
A	=	Area, in.^{2}
c_p	=	Specific heat, at constant pressure, Btu/(lbm-°F)
c_v	=	Specific heat, at constant volume, Btu/(lbm-°F)
Δz	=	Height of water, ft.
D	=	Diameter, in.

e	=	Emissivity
E	=	Energy, Btu
g	=	Gravitational acceleration, 32.2 ft./sec.^{2}
g_c	=	Conversion constant, 32.2 (lbm-ft./lbf-sec.^{2})
h	=	Enthalpy, Btu/lbm
H	=	Heat transfer coefficient, Btu/hr - ft.^{2} - °F
k	=	Mean thermal conductivity, Btu-in./hr - ft.^{2} - °F
L	=	Elevation, in.
LDP	=	Level transducer reading, in.
M	=	Mass, lbm
$\dot{M}$	=	Mass flow rate, lbm/sec.
P	=	Pressure, psia
Q	=	Rate of energy transfer, Btu/sec.
R	=	Heat transfer resistance, (hr.-°F)/Btu
S	=	Entropy, Btu/lbm - °F
span	=	Water level span within a tank, in.
t	=	Time, sec.
T	=	Temperature, °F
U	=	Stored energy, Btu
v	=	Specific volume, ft.^{3}/lbm
V	=	Volume, in.^{3}
vf	=	Void fraction
W	=	Volumetric flow rate, (ft.^{3}/min. for steam, gpm for liquid)
X	=	Flow quality
x	=	Insulation thickness, in.
Z	=	Compressibility factor

Subscript Definitions

ACC	=	Accumulator
ADS	=	Automatic depressurization system
air	=	Air
AMB	=	Ambient
AVG	=	Average
BRK	=	Break separator tank
CL	=	Cold leg
CLBL	=	Cold-leg balance line
CMT/DVIL	=	Interface of CMT and DVI-line
CMT	=	Core makeup tank
COMP	=	Compensated
corr	=	Corrected value
CVS	=	Simulated nonsafety Chemical and Volume Control System

DC	=	Downcomer
DEF	=	Deficit
DVIL	=	DVI line
f	=	Liquid phase of water
fg	=	Vaporization
FL	=	Fluid in the control volume
flux	=	Flux
flux_conv	=	Convective flux
flux_rad	=	Radiative flux
g	=	Steam
H_2O	=	Water (liquid and steam)
HL	=	Hot leg
initial	=	Initial
inner_metal	=	Inner surface of metal
IRWST INJ	=	IRWST injection
LOCAL	=	Local
LOW	=	Low threshold
mean_metal	=	Average metal surface
metal	=	Metal
mix	=	Mixture of liquid and steam
out	=	Out
outer_conv_metal	=	Convection at outer metal surface
outer_metal	=	Outer surface of metal
outer_rad_metal	=	Radiation at outer metal surface
OVERFLW	=	Overflow
READING	=	Recorded by the data acquisition system
ref	=	Reference
RNS	=	Simulated nonsafety Normal Residual Heat Removal System
RODS	=	Heated rods
SAT	=	Saturation
SG	=	Steam generator
STM VENT	=	Steam vent
STM XHST	=	Steam exhaust
transient	=	Transient
zone	=	Zone

4.0.2 Energy Equation Approximation

Several assumptions were made in calculating the total energy associated with the working fluid in the test, these are:

1. The total energy of the fluid is approximated by the enthalpy of the fluid. Kinetic and potential energy are neglected.

2. The enthalpy of the fluid is approximated by the specific heat of the fluid.

3. The change in physical properties between two consecutive time-steps is negligible.

The equation for calculating the change in fluid energy may be represented as:

$$\frac{dE}{dt} = \frac{dU}{dt} = \frac{d(c_v\ M\ T)}{dt} = \frac{\Delta(c_v\ M\ T)}{\Delta t} \qquad 4.0.2\text{-}1$$

where all terms are for fluid at local conditions. Assumption 3 provides for the specific heat at constant volume to be taken as constant over a time interval:

$$\frac{dE}{dt} \approx c_v \frac{\Delta(M\ T)}{\Delta t} \qquad 4.0.2\text{-}2$$

Assumptions 1 and 2 provide for the specific heat at constant volume to be replaced by the specific heat at constant pressure:

$$\frac{dE}{dt} \approx c_P \frac{\Delta(M\ T)}{\Delta t} \qquad 4.0.2\text{-}3$$

For the liquid phase of water, the specific heat at constant volume is approximately equal to the specific heat at constant pressure:

$$c_v \approx c_p \qquad 4.0.2\text{-}4$$

Thus, equation 4.0.2-3 holds for the liquid phase of water. For vapor, the definition of enthalpy is noted to be:

$$h = U + Pv \qquad 4.0.2\text{-}5$$

where the product of the pressure and specific volume may be significant. However, both the mass of vapor (steam) and the change in vapor mass is small for the OSU tests. Thus, the contribution of the pressure/specific volume term to the total energy associated with a given component, including the reactor vessel simulation, is very small. Thus, the specific heat at constant pressure provides a reasonable approximation of the total energy associated with the steam in the OSU tests.

4.0.3 Ambient Conditions

Ambient pressure and temperature for the test facility environment were monitored during each test. The ambient pressure data channel was used to convert data from units of psig to units of psia for

subsequent calculations, as opposed to using the constant 14.7. Ambient temperatures were used to evaluate heat loss from the test facility to the ambient. The ambient test facility environment was monitored by the following data channels:

Channel ID	Function
PT-003	ambient pressure
TF-005	ambient temperature, lower elevation of test facility; [ ]^{a,b,c} elevation
TF-006	ambient temperature, middle elevation of test facility; [ ]^{a,b,c} elevation
TF-007	ambient temperature, top elevation of test facility; [ ]^{a,b,c} elevation

4.1 LDP Compensation Function

Level transducers measure the variation in density of a vertical span relative to a reference. When the reference and the measured span are not at the same temperature, the effect of density differences needs to be accounted for to obtain a "true" level. The method of applying a compensation to level transducer outputs to account for differences in fluid density between the measured region and the reference leg is described below.

First, an average temperature for the column of water being monitored was calculated:

$$T_{AVG} = \frac{\sum_{i=1}^{n} T_i L_i}{\sum_{i=1}^{n} L_i} \qquad 4.1\text{-}1$$

where:

T	=	Temperature, °F
L	=	Span along the column that a temperature measurement was applied, in.

and the subscripts:

i	=	Index of measurement arrays
n	=	Total number of fluid temperature measurements in a column of water
AVG	=	Span-weighted average fluid temperature in the monitored water column

The fluid density in the monitored water column was then calculated as:

$$\rho_{AVG} = \rho\,(P, \min\,(T_{AVG}, T_{SAT})) \qquad 4.1\text{-}2$$

where:

T_{SAT}	=	Saturation temperature at local pressure

The corrected fluid level of the monitored water column (that is, the compensated LDP reading denoted as LDP_{COMP}) was calculated as:

$$LDP_{COMP} = \frac{62.303}{\rho_{AVG}} LDP_{READING} \qquad 4.1\text{-}3$$

where:

62.303	=	Reference density of water, lbm/ft.^{3}
LDP	=	Reading from a level transducer, in.

and the subscripts:

COMP	=	Density-compensated value
READING	=	Data as recorded by the data acquisition system (DAS)

All level transducer data used in the calculation of mass inventories, energy of fluid volumes, and inferred flows were density-compensated prior to being used in calculations.

4.2 Selected Level Compensations

A number of level transducer (LDP) readings were density-compensated, the majority of which were calculated as part of the normal mass and energy calculations performed to support analysis of the data. However, a number of other compensated LDPs were calculated to support the OSU Final Data Report.[1] The list of these compensated LDPs, together with the pressures and temperatures used to compensate them, are listed in Table 4.2-1. The compensated levels are provided in the OSU Final Data Report.[1]

Note that, since these LDPs are not directly used in the mass and energy calculations performed as part of the analysis, no minimum or maximum range information is applied to the compensated LDP. Also, where more than one temperature data channel is listed for a level transducer, a straight numeric average on all the data channels is used. This is in contrast to the calculation modules, where, typically, only the subset of submerged channels is used.

TABLE 4.2-1 PRESSURES AND TEMPERATURES FOR COMPENSATED LDPs		
Name	**Pressure**	**Temperature(s)**
CLDP-104	PT-102	TF-166, TF-164, TF-165, TF-167, TF-147, TF-148, TF-149, TF-150
CLDP-109	PT-108	TR-001-1, TR-001-2, TR-001-3, TR-303-1, TR-303-2, TR-303-3, TR-313-1, TR-313-2, TR-313-3, TR-308-1
CLDP-110	PT-108	TR-001-4, TR-001-5, TR-001-6, TR-303-4, TR-303-5, TR-303-6, TR-313-4, TR-313-5, TR-313-6, TR-308-2, TR-308-3, TR-318-1, TR-318-2
CLDP-112	PT-107 LDP-115(1) DP-114(1) LDP-113(1)	TF-169
CLDP-113	PT-107 LDP-115(1) DP-114(1)	TF-169
CLDP-115	PT-107	TF-171
CLDP-116	PT-111	TF-126, TF-127, TF-162, TF-163, TF-164, TF-165, TF-155, TF-156, TF-130, TF-131, TF-147, TF-148
CLDP-127	PT-107	TF-126, TF-127, TF-162, TF-163, TF-164, TF-165, TF-155, TF-156, TF-130, TF-131, TF-147, TF-148
CLDP-138	PT-108	TR-001-1, TR-001-2, TR-001-3, TR-303-1, TR-303-2, TR-303-3, TR-313-1, TR-313-2, TR-313-3, TR-308-1, TR-001-4, TR-001-5, TR-001-6, TR-303-4, TR-303-5, TR-303-6, TR-313-4, TR-313-5, TR-313-6, TR-308-2, TR-308-3, TR-318-1, TR-318-2
CLDP-139	PT-107	TF-169
CLDP-140	PT-111	TF-126, TF-127, TF-162, TF-163, TF-164, TF-165, TF-155, TF-156, TF-130, TF-131, TF-147, TF-148
CLDP-801	PT-202	TF-803

Note:

(1) These level values were used to adjust the measured pressure from PT-107.

4.3 Accumulators

Each of the two accumulators consists of a tank with a fluid flow path at the bottom connected to the direct vessel injection line. The accumulator fluid mass conservation equations are described in Subsection 4.3.1, and the fluid energy conservation equations are described in Subsection 4.3.2.

4.3.1 Fluid Mass Conservation Equations

The general fluid (H_2O) mass conservation equation, which relates the change in stored fluid mass with respect to time (the fluid-mass time derivative) to the mass flow rates in and out, reduces to the following for each of the two accumulators, ACC_i, where i = 1,2:

$$\frac{dM_{H_2O,ACC_i}}{dt} = - \dot{M}_{out\ H_2O,ACC_i} \qquad 4.3\text{-}1$$

where the subscript:

H_2O = water (liquid and steam)

Due to the fact that no steam is present in the accumulators, the fluid mass conservation equation further simplifies to:

$$\frac{dM_{f,ACC_i}}{dt} = - \dot{M}_{out\ f,ACC_i} \qquad 4.3\text{-}2$$

where the subscript:

f = liquid phase of water

From this point on in the discussions of the mass conservation calculations, the expressions will be in the liquid-only form.

The left-hand side of the water mass conservation equation is approximated from the value of the water mass at two consecutive time points (denoted by subscripts n-1 and n):

$$\frac{dM_{f,ACC_i}}{dt} \approx \frac{\Delta M_{f,ACC_i}}{\Delta t} = \frac{M_{f,ACC_i,n} - M_{f,ACC_i,n-1}}{t_n - t_{n-1}} \qquad 4.3\text{-}3$$

The water mass calculations are based on measured water level. In general, the water mass may be expressed as follows:

$$M_{f,ACC_i} = \rho_{f,ACC_i} \times V_{f,ACC_i} \times C \qquad 4.3\text{-}4$$

where:

C = Conversion constant, $in.^3$ to $ft.^3$

Due to the cylindrical shape of the accumulator tanks, the water volume is calculated as follows:

$$V_{f,ACC_i} = L_{f,ACC_i} \times A_{ACC_i} \qquad 4.3\text{-}5$$

Thus, the water mass expression becomes:

$$M_{f,ACC_i} = \rho_{f,ACC_i} \times L_{f,ACC_i} \times A_{ACC_i} \times C \qquad 4.3\text{-}6$$

Rather than using the LDP compensation method to calculate the corrected water level from the measured water level as is done for many other OSU test facility components, an equivalent approach was employed for the accumulators. Using the concept of head and recalling that measured water levels (LDPs) are applicable (calibrated) at a reference density, the following is true:

$$\Delta P\ [psi] = \rho_{corr} \times L_{corr} \times \left(\frac{g}{g_c}\right) \times C = \rho_{ref} \times LDP \times \left(\frac{g}{g_c}\right) \times C \qquad 4.3\text{-}7$$

so that, in the case of the accumulators:

$$\rho_{f,ACC_i} \times L_{f,ACC_i} = \rho_{ref,ACC_i} \times LDP\text{-}XXX_{ACC_i} \qquad 4.3\text{-}8$$

where:

LDP-XXX = Level instrument channel measurement, in.

Thus, the water mass expression becomes:

$$M_{f,ACC_i} = \rho_{ref,ACC_i} \times LDP\text{-}XXX_{ACC_i} \times A_{ACC_i} \times C \qquad 4.3\text{-}9$$

In certain OSU tests, the measured water level for the accumulators was adversely impacted by air in the sense line. For those tests, the following correction was developed:

$$LDP_{corr,ACC_i} = Y_{ACC_i} \times F_{ACC_i} \times LDP\text{-}XXX_{ACC_i} \qquad 4.3\text{-}10$$

$Y_{ACC\,i}$ is the following constant based on initial conditions:

$$Y_{ACC_i} = \left[\frac{span_{ACC_i}}{(LDP\text{-}XXX_{ACC_i})_{initial}}\right] \times \left[\frac{(P_{ACC_i} \times v_{air,ACC_i}/Z_{air,ACC_i})_{initial}}{(P_{AMB} \times v_{air,AMB}/Z_{air,AMB})_{initial}}\right] \qquad 4.3\text{-}11$$

$F_{ACC\,i}$ is given by the following:

$$F_{ACC_i} = \left[\frac{(P_{AMB} \times v_{air,AMB}/Z_{air,AMB})_{initial}}{(P_{ACC_i} \times v_{air,ACC_i}/Z_{air,ACC_i})_{transient}}\right] \qquad 4.3\text{-}12$$

In the previous equation, the specific volume ($ft.^3/lbm$) and compressibility factor of air are given by the following functions of pressure (psia), respectively:

$$v_{air} = 301.39 \times P^{1.0788}$$

$$Z_{air} = 1.0\times10^{-8} \times P^2 + 3.0\times10^{-5} \times P + 1.0002 \qquad 4.3\text{-}13$$

In the tests without air in the sense line, the factors $Y_{ACC\,i}$ and $F_{ACC\,i}$ are both set to 1.0 to deactivate the LDP correction.

Thus, the final expression for the water mass is as follows:

$$M_{f,ACC_i} = \rho_{ref,ACC_i} \times LDP_{corr,ACC_i} \times A_{ACC_i} \times C \qquad 4.3\text{-}14$$

This completes the discussion of the calculations related to the left-hand side of the water mass conservation equation.

On the right-hand side of the water mass conservation equation, the calculation of the outlet water mass flow rate is performed directly from the liquid volumetric flow rate (FMM) measurement as follows:

$$\dot{M}_{out\ f,ACC_i} = \max(0.0,\ FMM\text{-}XXX_{ACC_i}) \times \rho_{f,ACC_i} \times C_1 \qquad 4.3\text{-}15$$

where:

$FMM\text{-}XXX_{ACC_i}$	=	Liquid flow rate measurement from flow meter FMM-XXX, gpm
C_1	=	Conversion constant, gpm to $ft.^3/sec.$

The integrated outlet water mass flow is also computed for use in the overall system mass balance.

The water density is simply the reciprocal of the water-specific volume:

$$\rho_{f,ACC_i} = \frac{1}{v_{f,ACC_i}} \qquad 4.3\text{-}16$$

The water-specific volume is calculated as a function of pressure and temperature from the ASME steam table function VCL:

$$v_{f,ACC_i} = VCL(P_{ACC_i},\ T_{f,ACC_i}) \qquad 4.3\text{-}17$$

The water temperature is given by the fluid thermocouple measurement. Care is taken to insure that the water temperature value employed is at or below the saturation temperature. Thus, for i = 1,2:

$$T_{f,ACC_i} = \min(TF\text{-}XXX_{ACC_i},\ T_{sat,ACC_i}) \qquad 4.3\text{-}18$$

where:

$TF\text{-}XXX_{ACC_i}$ = Temperature reading from fluid thermocouple TF-XXX, °F

The saturation temperature is calculated as a function of pressure from the ASME steam table function TSL as follows:

$$T_{sat,ACC_i} = TSL(P_{ACC_i}) \qquad 4.3\text{-}19$$

Accumulator pressure, $P_{ACC\,i}$, is set equal to the value from the corresponding $PT\text{-}XXX_{ACC\,i}$ measurement after conversion from gauge (psig) to absolute (psia) pressure.

This completes the discussion of the calculations related to the right-hand side of the water mass conservation equation.

Note that in the case of the accumulators, it is possible to calculate all quantities on both the left-hand side and right-hand side of the fluid mass conservation equation. This information can then be used to check the fluid mass conservation equation.

Finally, a complete list of the applicable data for both accumulators appears in Table 4.3-1, including the level instrument channel ID ($LDP\text{-}XXX_{ACC\,i}$), the pressure measurement ID ($PT\text{-}XXX_{ACC\,i}$), the fluid thermocouple measurement ID ($TF\text{-}XXX_{ACC\,i}$), the outlet liquid volumetric flow rate measurement ID ($FMM\text{-}XXX_{ACC\,i}$), the water reference density, the water level span, and the tank cylindrical area.

4.3.2 Fluid Energy Conservation Equations

The general fluid (H_2O) energy conservation equation, which relates the change in stored fluid energy with respect to time (the fluid-energy time derivative) to the energy rates in and out (due to the connected flow paths) and the energy addition rate due to other external devices, reduces to the following for each of the two accumulator, ACC_i, where i = 1,2:

$$\frac{d[M \times c_p \times (T - T_{ref})]_{H_2O,ACC_i}}{dt} = - Q_{out\ H_2O,ACC_i} + Q_{[metal \Rightarrow H_2O],ACC_i} \qquad 4.3\text{-}20$$

Due to the fact that no steam is present in the accumulators, the fluid energy conservation equation further simplifies to:

$$\frac{d[M \times c_p \times (T-T_{ref})]_{f,ACC_i}}{dt} = - Q_{out\ f,ACC_i} + Q_{[metal \Rightarrow f],ACC_i} \qquad 4.3\text{-}21$$

From this point on in the discussions of the energy conservation calculations, the expressions will be in their reduced, water-only form.

The left-hand side of the water energy conservation equation is approximated as follows:

$$\frac{d[M \times c_p \times (T-T_{ref})]_{f,ACC_i}}{dt} \approx \frac{\Delta[M \times c_p \times (T-T_{ref})]_{f,ACC_i}}{\Delta t} \qquad 4.3\text{-}22$$

and:

$$\frac{\Delta[M \times c_p \times (T-T_{ref})]_{f,ACC_i}}{\Delta t} \approx c_{p_{f,ACC_i}} \times \left[\frac{\Delta[M \times (T-T_{ref})]_{f,ACC_i}}{\Delta t}\right]$$

$$\approx c_{p_{f,ACC_i}} \times (T_{f,ACC_i}-T_{ref}) \times \left[\frac{M_{f,ACC,n} - M_{f,ACC,n-1}}{t_n - t_{n-1}}\right] \qquad 4.3\text{-}23$$

$$+ c_{p_{f,ACC_i}} \times M_{f,ACC_i} \times \left[\frac{T_{f,ACC,n} - T_{f,ACC,n-1}}{t_n - t_{n-1}}\right]$$

where the subscripts:

n-1, n = Two consecutive time points

The water-specific heat capacity at constant pressure is calculated as a function of pressure and temperature from the ASME steam table function CPL as follows:

$$c_{p_{f,ACC_i}} = CPL(P_{ACC_i}, T_{f,ACC_i}) \qquad 4.3\text{-}24$$

For use in the overall system energy balance calculations, the water stored energy in each accumulator is given by the following:

$$U_{f,ACC_i} = M_{f,ACC_i} \times c_{P,f,ACC_i} \times (T_{f,ACC_i} - T_{ref}) \qquad 4.3\text{-}25$$

This completes the discussion of the calculations related to the left-hand side of the water energy conservation equation.

On the right-hand side of the water energy conservation equation, the calculation of the outlet water energy transport rate is given by the following, where i = 1,2:

$$Q_{out\ f,ACC_i} = \dot{M}_{out\ f,ACC_i} \times h_{f,ACC_i} \qquad 4.3\text{-}26$$

The water-specific enthalpy is calculated as a function of pressure and temperature from the ASME steam table function HCL as follows (note that the water-specific entropy is also an output of HCL):

$$h_{f,ACC_i} = HCL(P_{ACC_i}, T_{f,ACC_i}, S_{f,ACC_i}) \qquad 4.3\text{-}27$$

The heat transfer between the accumulator tank metal and the accumulator fluid inventory during accumulator injection is negligible, for the following reasons:

- The accumulators are pre-filled before initiation of the tests, so that the fluid and tank metal walls are in thermal equilibrium at the beginning of the transients.
- Although the overpressure gas decreases in temperature as it expands to fill the volume left by the injected water, the water temperature remains approximately uniform throughout the injection phase.
- The mass and specific heat of the overpressure gas is small compared to the mass and specific heat of the tank metal, and therefore draws an insignificant amount of energy from the tank metal walls.

Thus, the accumulator metal-to-fluid energy addition rate is neglected, and:

$$Q_{\{metal \Rightarrow f\},ACC_i} \approx 0.0 \qquad 4.3\text{-}28$$

This completes the discussion of the calculations related to the right-hand side of the water energy conservation equation.

Note that, in the case of the accumulators, it is possible to calculate all quantities on both the left-hand side and right-hand side of the fluid energy conservation equation. This information can then be used to check the fluid energy conservation equation.

TABLE 4.3-1 INSTRUMENTATION EMPLOYED FOR ACCUMULATOR FLUID CALCULATIONS		
Description	**ACC-1**	**ACC-2**
Level ID (in.)	LDP-401	LDP-402
Pressure ID (psig)	PT-401	PT-402
Water temp ID (°F)	TF-401	TF-402
Outlet flow ID (gpm)	FMM-401	FMM-402
Ref water ρ ($lbm/ft.^3$)	62.40	62.40
Water level span (in.)	36.75	37.00
Tank area (cylin) ($in.^2$)	416.6208	417.1392

4.4 Core Makeup Tanks and Cold-Leg Balance Lines

Each of the two core makeup tanks (CMTs) consists of a tank with a fluid flow path at the top for the cold-leg balance line (CLBL) connection and a fluid flow path at the bottom for the direct vessel injection line (DVI) connection. Each of the two cold-leg balance lines consists of a series of connected pipes with a fluid flow path at the bottom for the inlet connection from the cold leg and a fluid flow path at the top for the outlet connection to the CMT. The CMT fluid mass, fluid energy, and metal energy conservation equations are described in Subsections 4.4.1, 4.4.2, and 4.4.3, respectively. The cold-leg balance line fluid mass, fluid energy, and metal energy conservation equations are described in Subsections 4.4.4, 4.4.5, and 4.4.6, respectively.

4.4.1 Core Makeup Tank Fluid Mass Conservation Equations

The general fluid (H_2O) mass conservation equation, which relates the change in stored fluid mass with respect to time (the mass time derivative) to the mass flow rates in and out, reduces to the following for each of the two CMTs, CMT_i, where i = 1,2:

$$\frac{dM_{H_2O,CMT_i}}{dt} = \dot{M}_{in\ (from\ CLBL_i)\ H_2O,CMT_i} - \dot{M}_{out\ (to\ DVIL_i)\ H_2O,CMT_i} \qquad 4.4\text{-}1$$

The left-hand side of the fluid mass conservation equation is approximated from the value of the fluid mass at two consecutive time points (denoted by subscripts n-1 and n) as follows:

$$\frac{dM_{H_2O,CMT_i}}{dt} \approx \frac{\Delta M_{H_2O,CMT_i}}{\Delta t} = \frac{M_{H_2O,CMT_i,n} - M_{H_2O,CMT_i,n-1}}{t_n - t_{n-1}} \qquad 4.4\text{-}2$$

The H_2O fluid mass is the sum of the liquid and steam masses:

$$M_{H_2O,CMT_i} = M_{f,CMT_i} + M_{g,CMT_i} \qquad 4.4\text{-}3$$

where the subscripts:

H_2O	=	Water (liquid and steam)
f	=	Liquid phase of water
g	=	Steam

The water and steam mass calculations are based on the measured tank water level. A list of the level (LDP-XXX) instrument channel IDs for both CMTs appears in Table 4.4-1. To span the entire tank, either the main LDP, or a sum of the three alternate LDPs, is employed for the indicated water level, which is then corrected for temperature effects using the LDP compensation method. As is generally assumed for each OSU test facility component, zero quality water is modeled below the compensated water level, and 100 percent quality steam is modeled above the compensated water level. This assumption is appropriate because the fluid below the water level is predominantly water, the fluid above the water level is predominantly steam, and any amount of frothing is indeterminate with the available instrumentation.

To utilize the measurements from the numerous tank fluid thermocouples available, each CMT is divided into a number of axial fluid property zones for the calculation of various fluid conditions. Table 4.4-1 contains a list of the fluid thermocouples employed (ten per tank), along with their elevations. Axial fluid property zone boundaries are taken at the vertical midpoint between consecutive fluid thermocouples, which yields ten zones per tank.

In general, the tank liquid and steam masses are given by:

$$M_{f,CMT_i} = \sum_{j=1}^{N_{zone,CMT_i}} M_{f,CMT_{ij}}$$

$$M_{g,CMT_i} = \sum_{j=1}^{N_{zone,CMT_i}} M_{g,CMT_{ij}} \qquad 4.4\text{-}4$$

where:

N_{zone,CMT_i} = Number of zones in the CMT, (10)

j = Specific zone within the CMT

For zones j below those containing the compensated water level (which contain all water), the zone j water and steam masses are given by, where i = 1,2 and j = 1,...,levzone-1:

$$M_{f,CMT_{ij}} = \rho_{f,CMT_{ij}} \times V_{CMT_{ij}} \times C$$

$$M_{g,CMT_{ij}} = 0 \qquad 4.4\text{-}5$$

where:

C	=	Conversion constant, $in.^3$ to $ft.^3$
levzone	=	Zone containing the compensated water level

For the zone j containing the compensated water level, the zone j water and steam masses are given by, where i = 1,2 and j = levzone:

$$M_{f,CMT_{i,j}} = \rho_{f,CMT_{i,j}} \times V_{f,CMT_{i,j}} \times C$$
$$M_{g,CMT_{i,j}} = \rho_{g,CMT_{i,j}} \times V_{g,CMT_{i,j}} \times C \qquad 4.4\text{-}6$$

For zones j above those containing the compensated water level, which contain all steam, the zone j water and steam masses are given by, where i = 1,2 and j = levzone+1,...,$N_{zone,CMT\ i}$:

$$M_{f,CMT_{i,j}} = 0$$
$$M_{g,CMT_{i,j}} = \rho_{g,CMT_{i,j}} \times V_{CMT_{i,j}} \times C \qquad 4.4\text{-}7$$

The tank fluid volumes are calculated as a function of level from the volume versus height tabular data listed in Table 4.4-2, via linear interpolation within the table. No extrapolation at either end is performed; the first and last table points define the applicable range (the first point is [h_{min} (= 0.), V_{min} (= 0.)], and the last point is [h_{max}, V_{max}]).

During initialization, the volume versus height data/function is employed to calculate the total volume of each zone j as follows:

for j=1:

$$V_{CMT_{i,j}} = V(l)_{CMT_{i,j}} \qquad 4.4\text{-}8$$

for j=2,...,N_{zone,CMT_i}:

$$V_{CMT_{i,j}} = V(l)_{CMT_{i,j}} - \sum_{k=1}^{j-1} V_{CMT_{i,k}}$$

where:

$V(l)_{CMT}$ = Volume as a function of elevation, $in.^3/in.$, and l is the elevation of the top of zone j

The zone j top elevations are determined from the elevations of the fluid thermocouples (or the elevation of the top of the tank in the case of the top zone).

During the transient calculations, the volume versus height data/function is employed to calculate the water volume of the zone containing the compensated water level, j = levzone, as follows:

if j=levzone=1:

$$V_{f,CMT_{i,j}} = V(l_f)_{CMT_i} \qquad 4.4\text{-}9$$

if j=levzone>1:

$$V_{f,CMT_{i,j}} = V(l_f)_{CMT_i} - \sum_{k=1}^{j-1} V_{CMT_{i,k}}$$

where:

$V(l_f)_{CMT_i}$ = Volume as a function of elevation, $in.^3/in.$, and l_f is the elevation of the compensated water level.

The steam volume of the zone containing the compensated water level, j = levzone, is then the following:

$$V_{g,CMT_{i,j}} = V_{CMT_{i,j}} - V_{f,CMT_{i,j}} \qquad 4.4\text{-}10$$

The zone j water and steam densities are the reciprocal of the water- and steam-specific volumes, respectively:

$$\rho_{f,CMT_{i,j}} = \frac{1}{V_{f,CMT_{i,j}}}$$

$$\rho_{g,CMT_{i,j}} = \frac{1}{V_{g,CMT_{i,j}}} \qquad 4.4\text{-}11$$

The zone j water-specific volume is calculated as a function of pressure and temperature from the ASME steam table function VCL as follows, where i = 1,2:

$$v_{f,CMT_{i,j}} = VCL(P_{CMT_{i,j}}, T_{f,CMT_{i,j}}) \qquad 4.4\text{-}12$$

The zone j steam-specific volume is calculated as a function of pressure and temperature from the ASME steam table function HSS as follows, where i = 1,2 (note that the steam-specific enthalpy is the main output of HSS, and the steam-specific entropy is also an output of HSS):

$$h_{g,CMT_{ij}} = HSS(P_{CMT_{ij}}, T_{g,CMT_{ij}}, S_{g,CMT_{ij}}, v_{g,CMT_{ij}}) \qquad 4.4\text{-}13$$

The zone j water and steam temperatures are given by the zone temperatures, which are the fluid thermocouple measurements TF-XXX (see Table 4.4-1). Extra precautions ensure that the water temperature value employed is at or below the saturation temperature, and that the steam temperature value employed is at or above the saturation temperature. Thus:

$$\begin{aligned} T_{f,CMT_{ij}} &= \min(T_{CMT_{ij}}, T_{sat,CMT_{ij}}) \\ T_{g,CMT_{ij}} &= \max(T_{CMT_{ij}}, T_{sat,CMT_{ij}}) \end{aligned} \qquad 4.4\text{-}14$$

where:

$$T_{CMT_{ij}} = TF\text{-}XXX_{CMT_{ij}} \qquad 4.4\text{-}15$$

The zone j saturation temperature is calculated as a function of pressure from the ASME steam table function TSL as follows:

$$T_{sat,CMT_{ij}} = TSL(P_{CMT_{ij}}) \qquad 4.4\text{-}16$$

The pressure of the top zone is set equal to the value from the $PT\text{-}XXX_{CMT\,i}$ measurement (see Table 4.4-1) (after conversion from gauge [psig] to absolute [psia] pressure). For the zones below, the pressure is adjusted for hydrostatic effects to account for the density differences that occur from zone to zone throughout the tank.

This completes the discussion of the calculations related to the left-hand side of the fluid mass conservation equation.

On the right-hand side of the fluid mass conservation equation, the CMT inlet fluid mass flow rate is equal to the cold-leg balance line outlet fluid mass flow rate (which appears on the right-hand side of the cold-leg balance line mass conservation equation):

$$\dot{M}_{\text{in (from CLBL}_i\text{) H}_2\text{O,CMT}_i} = \dot{M}_{\text{out (to CMT}_i\text{) H}_2\text{O,CLBL}_i} \qquad 4.4\text{-}17$$

Although a liquid volumetric flow rate measurement (FMM) is available for this line, it cannot be relied on for accurate mass flow rate calculations because two-phase fluid flow can occur in the line. Thus, the total mass flow rate must be inferred from a combination of the CMT and cold-leg balance line mass conservation equations, once all other terms have been calculated in these equations. The integrated inlet mass flow is also computed for use in the overall system mass balance.

Regarding the CMT outlet fluid mass flow rate to the DVI line, the calculation may be performed directly from the liquid volumetric flow rate measurement (FMM-XXX), since when there is flow, the water flowing in the line is at either subcooled or saturated conditions (see Table 4.4-1 for the instrument channel IDs). Thus:

$$\dot{M}_{\text{out (to DVIL}_i\text{) H}_2\text{O,CMT}_i} = \dot{M}_{\text{out (to DVIL}_i\text{) f,CMT}_i} \qquad 4.4\text{-}18$$

$$= \max(0., \text{FMM-XXX}_{\text{CMT/DVIL}_i}) \times \rho_{\text{f,CMT/DVIL}_i} \times C_1$$

where:

FMM-XXX	=	Liquid volumetric flow rate measurement from flow meter FMMM-XXX, gpm
C_1	=	Conversion constant, gpm to ft.^{3}/sec.

The integrated outlet water mass flow is also computed for use in the overall system mass balance.

The outlet line water density is the reciprocal of the outlet line water-specific volume:

$$\rho_{\text{f,CMT/DVIL}_i} = \frac{1}{v_{\text{f,CMT/DVIL}_i}} \qquad 4.4\text{-}19$$

The outlet line water-specific volume is calculated as a function of pressure and temperature from the ASME steam table function VCL as follows:

$$v_{f,CMT/DVIL_i} = VCL(P_{CMT/DVIL_i}, T_{f,CMT/DVIL_i}) \qquad 4.4\text{-}20$$

The outlet line water temperature is simply given by the outlet line fluid thermocouple measurement TF-XXX (see Table 4.4-1). Care is taken to ensure that the water temperature value employed is at or below the saturation temperature. Thus:

$$T_{f,CMT/DVIL_i} = \min(TF\text{-}XXX_{CMT/DVIL_i}, T_{sat,CMT/DVIL_i}) \qquad 4.4\text{-}21$$

The outlet line saturation temperature is calculated as a function of pressure from the ASME steam table function TSL as follows:

$$T_{sat,CMT/DVIL_i} = TSL(P_{CMT/DVIL_i}) \qquad 4.4\text{-}22$$

The pressure in the outlet line is equal to the pressure at the bottom of the tank.

This completes the discussion of the calculations related to the right-hand side of the fluid mass conservation equation.

4.4.2 Core Makeup Tank Fluid Energy Conservation Equations

The general fluid (H_2O) energy conservation equation, which relates the change in stored fluid energy with respect to time (the energy time derivative) to the energy rates in and out (due to the connected flow paths) and the energy addition rate due to other external devices, reduces to the following for each of the two CMTs, CMT_i, where i = 1,2:

$$\frac{d[M \times c_p \times (T - T_{ref})]_{H_2O,CMT_i}}{dt} = Q_{in\ (from\ CLBL_i)\ H_2O,CMT_i} - Q_{out\ (to\ DVIL_i)\ H_2O,CMT_i} + Q_{[metal \Rightarrow H_2O],CMT_i} \qquad 4.4\text{-}23$$

The left-hand side of the energy conservation equation is approximated as follows:

$$\frac{d[M \times c_p \times (T-T_{ref})]_{H_2O,CMT_i}}{dt} \approx \sum_{j=1}^{N_{sum,CMT_i}} \frac{\Delta[M \times c_p \times (T-T_{ref})]_{f,CMT_{ij}}}{\Delta t} + \sum_{j=1}^{N_{sum,CMT_i}} \frac{\Delta[M \times c_p \times (T-T_{ref})]_{g,CMT_{ij}}}{\Delta t} \quad 4.4\text{-}24$$

where:

$$\frac{\Delta[M \times c_p \times (T-T_{ref})]_{f,CMT_{ij}}}{\Delta t} = c_{p_{f,CMT_{ij}}} \times \left[\frac{\Delta[M \times (T-T_{ref})]_{f,CMT_{ij}}}{\Delta t}\right]$$

$$\approx c_{p_{f,CMT_{ij}}} \times (T_{f,CMT_{ij}} - T_{ref}) \times \left[\frac{M_{f,CMT_{ij}n} - M_{f,CMT_{ij}n-1}}{t_n - t_{n-1}}\right] + c_{p_{f,CMT_{ij}}} \times M_{f,CMT_{ij}} \times \left[\frac{T_{f,CMT_{ij}n} - T_{f,CMT_{ij}n-1}}{t_n - t_{n-1}}\right] \quad 4.4\text{-}25$$

and:

$$\frac{\Delta[M \times c_p \times (T-T_{ref})]_{g,CMT_{ij}}}{\Delta t} = c_{p_{g,CMT_{ij}}} \times \left[\frac{\Delta[M \times (T-T_{ref})]_{g,CMT_{ij}}}{\Delta t}\right]$$

$$\approx c_{p_{g,CMT_{ij}}} \times (T_{g,CMT_{ij}} - T_{ref}) \times \left[\frac{M_{g,CMT_{ij}n} - M_{g,CMT_{ij}n-1}}{t_n - t_{n-1}}\right] + c_{p_{g,CMT_{ij}}} \times M_{g,CMT_{ij}} \times \left[\frac{T_{g,CMT_{ij}n} - T_{g,CMT_{ij}n-1}}{t_n - t_{n-1}}\right] \quad 4.4\text{-}26$$

where the subscripts:

n-1, n = Two consecutive time points

The zone j water-specific heat capacity at constant pressure is calculated as a function of pressure and temperature from the ASME steam table function CPL as follows:

$$c_{p_{f,CMT_{ij}}} = CPL(P_{CMT_{ij}}, T_{f,CMT_{ij}}) \qquad 4.4\text{-}27$$

The zone j steam-specific heat capacity at constant pressure is calculated as a function of pressure and temperature from the ASME steam table function CPV as follows (note that the steam-specific volume is also an output of CPV):

$$c_{p_{g,CMT_{ij}}} = CPV(P_{CMT_{ij}}, T_{g,CMT_{ij}}, v_{g,CMT_{ij}}) \qquad 4.4\text{-}28$$

For use in the overall system energy balance calculations, the fluid stored energy in each of the two CMTs is given by the following:

$$U_{H_2O,CMT_i} = U_{f,CMT_i} + U_{g,CMT_i} \qquad 4.4\text{-}29$$

where:

$$U_{f,CMT_i} = \sum_{j=1}^{N_{zones,CMT_i}} M_{f,CMT_{ij}} \times c_{p,f,CMT_{ij}} \times (T_{f,CMT_{ij}} - T_{ref}) \qquad 4.4\text{-}30$$

and:

$$U_{g,CMT_i} = \sum_{j=1}^{N_{zones,CMT_i}} M_{g,CMT_{ij}} \times c_{p,g,CMT_{ij}} \times (T_{g,CMT_{ij}} - T_{ref}) \qquad 4.4\text{-}31$$

This completes the discussion of the calculations related to the left-hand side of the fluid energy conservation equation.

On the right-hand side of the fluid energy conservation equation, the CMT inlet fluid energy transport rate is equal to the CLBL outlet fluid energy transport rate (which appears in the CLBL energy conservation equation):

$$Q_{in\ (from\ CLBL_i)\ H_2O,CMT_i} = Q_{out\ (to\ CMT_i)\ H_2O,CLBL_i} \qquad 4.4\text{-}32$$

In a manner analogous to that performed for the corresponding term on the right-hand side of the fluid mass conservation equation, the above CMT inlet fluid energy transport rate term must be inferred from a combination of the CMT and CLBL energy conservation equations, due to the two-phase flow which exists, once all other terms have been calculated in these equations.

The CMT outlet fluid energy transport rate to the DVI line is given by the following:

$$Q_{out\ (to\ DVIL_j)\ H_2O,CMT_i} = Q_{out\ (to\ DVIL_j)\ f,CMT_i} = \dot{M}_{out\ (to\ DVIL_j)\ f,CMT_i} \times h_{f,CMT/DVIL_j} \qquad 4.4\text{-}33$$

The outlet line water-specific enthalpy is calculated as a function of pressure and temperature from the ASME steam table function HCL as follows (note that the water-specific entropy is also an output of HCL):

$$h_{f,CMT/DVIL_j} = HCL(P_{CMT/DVIL_j},\ T_{f,CMT/DVIL_j},\ S_{f,CMT/DVIL_j}) \qquad 4.4\text{-}34$$

The energy addition rate to the fluid due to heat transfer from the metal walls is calculated from the CONTRA inverse heat conduction[23] solution, and is discussed in Subsection 4.4.3.

This completes the discussion of the calculations related to the right-hand side of the fluid energy conservation equation.

4.4.3 Core Makeup Tank Metal Energy Conservation Equations

The general metal energy conservation equation, which relates the change in stored metal energy with respect to time (the metal energy time derivative) to the energy rates in and out (due to heat transfer), reduces to the following for each of the two CMTs, CMT_j, where i = 1,2:

$$\frac{d[M \times c_p \times (T-T_{ref})_{metal,CMT_i}}{dt} = - Q_{[metal \Rightarrow H_2O],CMT_i} - Q_{[metal \Rightarrow ambient],CMT_i} \qquad 4.4\text{-}35$$

To utilize the measurements from the numerous wall thermocouples available, the metal of each tank is divided into 13 metal segments which correspond to the axial positions where wall thermocouples are located in the CMTs. Table 4.4-3 lists the wall thermocouple channel IDs used for each metal segment of both CMTs. In addition, Table 4.4-4 lists the mass, inner surface area, and outer surface

area for each metal segment, as well as the ambient temperature channel ID, all of which are required in the metal energy calculations.

The left-hand side of the fluid mass conservation equation is approximated from the value of the fluid mass at two consecutive time points as follows:

$$\frac{d[M \times c_p \times (T-T_{ref})]_{metal,CMT_i}}{dt} = \frac{\Delta[M \times c_p \times (T-T_{ref})]_{metal,CMT_i}}{\Delta t} \qquad 4.4\text{-}36$$

where:

$$\frac{\Delta[M \times c_p \times (T-T_{ref})]_{metal,CMT_i}}{\Delta t} = \sum_{m=1}^{N_{metal,CMT_i}} M_{metal,CMT_{i,m}} \times c_{p_{metal,CMT_{i,m}}} \times \left[\frac{T_{metal,CMT_{i,m}n} - T_{metal,CMT_{i,m}n-1}}{t_n - t_{n-1}}\right] \qquad 4.4\text{-}37$$

where:

N_{metal,CMT_i} = Total number of metal segments in each CMT, (13)

and the subscripts:

m = Specific metal segment of the CMT
n-1, n = Two consecutive time points

In the equation above, the temperature used for each metal segment is an average of the temperatures obtained from the thermocouples listed in Table 4.4-3 for that metal segment.

The metal segment specific heat capacity at constant pressure is calculated as a function of the metal segment average temperature from the metal c_p versus temperature tabular data listed in Table 4.4-5, via linear interpolation within the table. No extrapolation at either end is performed; the first and last table points define the applicable range (the first point is $[T_{min}, c_{p,min}]$, and the last point is $[T_{max}, c_{p,max}]$).

This completes the discussion of the calculations related to the left-hand-side of the metal energy conservation equation.

On the right-hand-side of the metal energy conservation equation, the total metal-to-fluid heat transfer rate is equal to the sum of the individual metal segment metal-to-fluid heat transfer rates:

$$Q_{[metal \Rightarrow H_2O],CMT_i} = \sum_{m=1}^{N_{metal,CMT_i}} Q_{[metal \Rightarrow H_2O],CMT_{i,m}} \qquad 4.4\text{-}38$$

The integrated metal-to-fluid heat transfer is also computed for use in the overall system energy balance.

For the detailed analyses of the heat transfer between the fluid and the metal wall in each of the two CMTs, the CONTRA inverse heat conduction[23] solution is employed to calculate the transient inner surface heat fluxes and temperatures, given the transient temperature data collected from thermocouples imbedded in the walls of the CMTs. The CONTRA inverse heat conduction calculational method models a wall as a one-dimensional cylinder in radial coordinates, and applies to each axial position where wall thermocouples are located in the CMTs (refer to Table 4.4-3). A stand-alone pre-processor code ("osucontra", the OSU CONTRA driver software) employs the CONTRA inverse heat conduction solution on the transient wall thermocouple temperature data for the modeled metal segments of each of the two CMTs and calculates the transient inner surface heat flux and temperature for each of these metal segments.

Therefore, the energy addition rate to the fluid due to heat transfer from the CMT metal is given by the following for each metal segment m:

$$Q_{[metal \Rightarrow H_2O],CMT_{i,m}} = Q_{flux\,[metal \Rightarrow H_2O],CMT_{i,m}} \times A_{inner\_metal,CMT_{i,m}} \times C_2 \qquad 4.4\text{-}39$$

where:

Q_{flux} = Heat flux, Btu/hr.-ft^2
C_2 = Conversion constant, hours to seconds

Also on the right-hand-side of the metal energy conservation equation, the total metal-to-ambient heat transfer rate is equal to the sum of the individual metal segment metal-to-ambient heat transfer rates:

$$Q_{[metal \Rightarrow ambient],CMT_i} = \sum_{m=1}^{N_{metal,CMT_i}} Q_{[metal \Rightarrow ambient],CMT_{i,m}} \qquad 4.4\text{-}40$$

The integrated metal-to-ambient heat transfer is also computed for use in the overall system energy balance.

The metal segment m metal-to-ambient heat transfer rate is given by the following:

$$Q_{\{metal \Rightarrow ambient\},CMT_{i,m}} = Q_{flux\ \{metal \Rightarrow ambient\},CMT_{i,m}} \times A_{outer\_metal,CMT_{i,m}} \times C_2 \qquad 4.4\text{-}41$$

The metal segment m metal-to-ambient heat flux is expressed as the sum of the convective and radiative heat fluxes as follows:

$$Q_{flux\ \{metal \Rightarrow ambient\},CMT_{i,m}} = Q_{flux\_conv\ \{metal \Rightarrow ambient\},CMT_{i,m}} + Q_{flux\_rad\ \{metal \Rightarrow ambient\},CMT_{i,m}} \qquad 4.4\text{-}42$$

Note that for ambient heat transfer considerations, each CMT metal segment is treated as a vertical cylinder (CMTs are not insulated).

The metal segment m outer surface convective heat flux is given by the following, where i = 1,2:

$$Q_{flux\_conv\ \{metal \Rightarrow ambient\},CMT_{i,m}} = H_{outer\_conv\_metal,CMT_{i,m}} \times (T_{outer\_metal,CMT_{i,m}} - T_{AMB}) \qquad 4.4\text{-}43$$

where:

H = Heat transfer coefficient, Btu/hr.-ft.^{2}-°F

A natural convection heat transfer correlation[16] of the following form is employed:

$$Nu = C\ (Gr\ Pr)^m \qquad 4.4\text{-}44$$

where, for vertical cylinders:

$$C = 0.13,\ m = 1/3\ ;\ \text{for } (Gr\ Pr) > 10^9 \quad \text{(turbulent range)}$$
$$C = 0.59,\ m = 1/4\ ;\ \text{for } (Gr\ Pr) > 10^9 \quad \text{(laminar range)} \qquad 4.4\text{-}45$$

For the OSU test facility air at atmospheric pressure and ambient temperature (averaged over the tests), the turbulent range (Gr Pr > 10^9; C = 0.13, m = 1/3) applies at the outer surfaces of the CMTs, and the above correlation simplifies to the following expression for the convective heat transfer coefficient for each metal segment m:

$$H_{outer\_conv\_metal,CMT_{i,n}} = 0.19 \times (|T_{outer\_metal,CMT_{i,n}} - T_{AMB}|)^{1/3} \qquad 4.4\text{-}46$$

Employing the assumption of radiation heat transfer between infinite parallel planes in the limiting case of a convex object completely enclosed by a very large concave surface (typical assumption for the calculation of radiation energy loss from a hot object in a room), with an assumed emissivity of 0.84 for the uninsulated CMTs, the metal segment m outer surface radiative heat flux reduces to:

$$Q_{flux\_rad\ (metal \Rightarrow ambient),CMT_{i,n}} = 1.4389 \times 10^{-9} \times [\ (T_{outer\_metal,CMT_{i,n}} + C_3)^4 - (T_{ambient} + C_3)^4\ ] \qquad 4.4\text{-}47$$

where:

C_3 = Conversion constant, 459.6 (°F to °R)

The coefficient 1.4389 x 10^{-9} is the product of the Stefan-Boltzmann constant (1.713 x 10^{-9} Btu/(hr.-ft.^{2}-°R^4)) and the emissivity (0.84).

This completes the discussion of the calculations related to the right-hand-side of the metal energy conservation equation.

Note that it is possible to calculate all quantities on both the left-hand-side and right-hand-side of the metal energy conservation equation, as shown above. This information can then be used to check the metal energy conservation equation.

4.4.4 Cold-Leg Balance Line Fluid Mass Conservation Equations

The general fluid (H_2O) mass conservation equation, which relates the change in stored fluid mass with respect to time (the fluid mass time derivative) to the mass flow rates in and out, reduces to the following for each of the two cold-leg balance lines, $CLBL_i$ where i = 1,2:

$$\frac{dM_{H_2O,CLBL_i}}{dt} = \dot{M}_{in\ (CL_i)\ H_2O,CLBL_i} - \dot{M}_{out\ (CMT_i)\ H_2O,CLBL_i} \qquad 4.4\text{-}48$$

The left-hand side of the fluid mass conservation equation is approximated from the value of the fluid mass at two consecutive time points (denoted by subscripts n-1 and n) as follows:

$$\frac{dM_{H_2O,CLBL_i}}{dt} \approx \frac{\Delta M_{H_2O,CLBL_i}}{\Delta t} = \frac{M_{H_2O,CLBL_i,n} - M_{H_2O,CLBL_i,n-1}}{t_n - t_{n-1}} \qquad 4.4\text{-}49$$

The H_2O fluid mass is the sum of the water and steam masses:

$$M_{H_2O,CLBL_i} = M_{f,CLBL_i} + M_{g,CLBL_i} \qquad 4.4\text{-}50$$

The water and steam mass calculations are based upon the measured water level. A list of the level (LDP-XXX) instrument channel IDs for both cold-leg balance lines appears in Table 4.4-6. These LDPs are corrected for temperature effects using the LDP compensation method. As is generally assumed for each OSU test facility component, zero quality water is modeled below the compensated water level, and 100 percent quality steam is modeled above the compensated water level. This assumption is appropriate because the fluid below the water level is predominantly water, the fluid above the water level is predominantly steam, and any amount of frothing is indeterminate with the available instrumentation.

For the fluid property calculations, the measurements from the two fluid thermocouples available in each CLBL are utilized. Table 4.4-6 contains a list of these fluid thermocouples; one is located at the bottom of the line and one is located at the top of the line. If the line is completely filled with water (water level at top), an average of the two fluid thermocouple temperatures is employed for the water properties. If the line consists of all steam (water level at bottom), an average of the two fluid thermocouple temperatures is employed for the steam properties. Otherwise (water level in between top and bottom), the bottom fluid thermocouple temperature is employed for the water properties, and the top fluid thermocouple temperature is employed for the steam properties.

In general, the liquid and steam masses are given by:

$$M_{f,CLBL_i} = \rho_{f,CLBL_i} \times V_{f,CLBL_i} \times C$$
$$M_{g,CLBL_i} = \rho_{g,CLBL_i} \times V_{g,CLBL_i} \times C \qquad 4.4\text{-}51$$

where:

C = Conversion constant, $in.^3$ to $ft.^3$

The water volume is calculated as a function of compensated water level from the volume versus height tabular data listed in Table 4.4-7, via linear interpolation within the table. No extrapolation at either end is performed; the first and last table points define the applicable range (the first point is [h_{min} (= 0.), V_{min} (= 0.)], and the last point is [h_{max}, V_{max}]). Thus:

$$V_{f,CLBL_i} = V(l)_{CLBL_i} \qquad 4.4\text{-}52$$

where:

$V(l)_{CLBL_i}$ = Volume as a function of elevation, $in.^3/in.$, and l is the compensated water level

The steam volume is then given by:

$$V_{g,CLBL_i} = V_{CLBL_i} - V_{f,CLBL_i} \qquad 4.4\text{-}53$$

In the above, the cold-leg balance line total volume, V_{CLBL_i}, is given by the last point (V_{max}) in the aforementioned volume versus height table.

The water and steam densities are the reciprocal of the water- and steam-specific volumes, respectively:

$$\rho_{f,CLBL_i} = \frac{1}{V_{f,CLBL_i}}$$

$$\rho_{g,CLBL_i} = \frac{1}{V_{g,CLBL_i}} \qquad 4.4\text{-}54$$

The water-specific volume is calculated as a function of pressure and temperature from the ASME steam table function VCL as follows:

$$v_{f,CLBL_i} = VCL(P_{CLBL_i}, T_{f,CLBL_i}) \qquad 4.4\text{-}55$$

The steam-specific volume is calculated as a function of pressure and temperature from the ASME steam table function HSS as follows (note that the steam-specific enthalpy is the main output of HSS, and the steam-specific entropy is also an output of HSS):

$$h_{g,CLBL_i} = HSS(P_{CLBL_i}, T_{g,CLBL_i}, S_{g,CLBL_i}, v_{g,CLBL_i}) \qquad 4.4\text{-}56$$

As stated above, the water and steam temperatures are given by the fluid thermocouple measurements TF-XXX (see Table 4.4-6). Care is taken to ensure that the water temperature value employed is at or below the saturation temperature, and that the steam temperature value employed is at or above the saturation temperature. Thus:

$$\begin{aligned} T_{f,CLBL_i} &= \min(T_{f,CLBL_i}, T_{sat,CLBL_i}) \\ T_{g,CLBL_i} &= \max(T_{g,CLBL_i}, T_{sat,CLBL_i}) \end{aligned} \qquad 4.4\text{-}57$$

The saturation temperature is calculated as a function of pressure from the ASME steam table function TSL as follows:

$$T_{sat,CLBL_i} = TSL(P_{CLBL_i}) \qquad 4.4\text{-}58$$

In all of the above, the cold-leg balance line pressure, P_{CLBL_i}, is set equal to the value from the corresponding $PT\text{-}XXX_{CMT_i}$ measurement (see Table 4.4-6 for list) (after conversion from gauge [psig] to absolute [psia] pressure).

This completes the discussion of the calculations related to the left-hand side of the fluid mass conservation equation.

Although a liquid volumetric flow rate measurement (FMM) is available for each cold-leg balance line, the measured values cannot be relied on for accurate mass flow rate calculations since two-phase fluid flow can occur in the line. Thus, the total mass flow rates on the right-hand side of the cold-leg balance line fluid mass conservation equation must be inferred from a combination of the CMT and cold-leg balance line fluid mass conservation equations, once all other terms have been calculated in these equations. The integrated cold-leg balance line outlet (to CMT) mass flow is also computed for use in the overall system mass balance.

This completes the discussion of the calculations related to the right-hand side of the fluid mass conservation equation.

4.4.5 Cold-Leg Balance Line Fluid Energy Conservation Equations

The general fluid (H_2O) energy conservation equation, which relates the change in stored fluid energy with respect to time (the fluid-energy time derivative) to the energy rates in and out (due to the connected flow paths) and the energy addition rate due to other external devices, reduces to the following for each of the two cold-leg balance lines, $CLBL_i$, where i = 1,2:

$$\frac{d[M \times c_p \times (T-T_{ref})]_{H_2O,CLBL_i}}{dt} = Q_{in\ (from\ CL_i)\ H_2O,CLBL_i} - Q_{out\ (to\ CMT_i)\ H_2O,CLBL_i} + Q_{[metal \Rightarrow H_2O],CLBL_i} \qquad 4.4\text{-}59$$

The left-hand side of the fluid energy conservation equation is approximated as follows:

$$\frac{d[M \times c_p \times (T-T_{ref})]_{H_2O,CLBL_i}}{dt} \approx \frac{\Delta[M \times c_p \times (T-T_{ref})]_{f,CLBL_i}}{\Delta t} + \frac{\Delta[M \times c_p \times (T-T_{ref})]_{g,CLBL_i}}{\Delta t} \qquad 4.4\text{-}60$$

where (subscripts n-1 and n denote two consecutive time points):

$$\frac{\Delta[M \times c_p \times (T-T_{ref})]_{f,CLBL_i}}{\Delta t} \approx c_{p_{f,CLBL_i}} \times \left[\frac{\Delta[M \times (T-T_{ref})]_{f,CLBL_i}}{\Delta t}\right]$$

$$\approx c_{p_{f,CLBL_i}} \times (T_{f,CLBL_i}-T_{ref}) \times \left[\frac{M_{f,CLBL_i,n} - M_{f,CLBL_i,n-1}}{t_n - t_{n-1}}\right] \qquad 4.4\text{-}61$$

$$+ c_{p_{f,CLBL_i}} \times M_{f,CLBL_i} \times \left[\frac{T_{f,CLBL_i,n} - T_{f,CLBL_i,n-1}}{t_n - t_{n-1}}\right]$$

and:

$$\frac{\Delta[M \times c_p \times (T-T_{ref})]_{g,CLBL_i}}{\Delta t} = c_{P_{g,CLBL_i}} \times \left[\frac{\Delta[M \times (T-T_{ref})]_{g,CLBL_i}}{\Delta t}\right]$$

$$= c_{P_{g,CLBL_i}} \times (T_{g,CLBL_i}-T_{ref}) \times \left[\frac{M_{g,CLBL_i,n} - M_{g,CLBL_i,n-1}}{t_n - t_{n-1}}\right] \quad 4.4\text{-}62$$

$$+ c_{P_{g,CLBL_i}} \times M_{g,CLBL_i} \times \left[\frac{T_{g,CLBL_i,n} - T_{g,CLBL_i,n-1}}{t_n - t_{n-1}}\right]$$

The water-specific heat capacity at constant pressure is calculated as a function of pressure and temperature from the ASME steam table function CPL as follows:

$$c_{P_{f,CLBL_i}} = CPL(P_{CLBL_i}, T_{f,CLBL_i}) \quad 4.4\text{-}63$$

The steam-specific heat capacity at constant pressure is calculated as a function of pressure and temperature from the ASME steam table function CPV as follows (note that the steam-specific volume is also an output of CPV):

$$c_{P_{g,CLBL_i}} = CPV(P_{CLBL_i}, T_{g,CLBL_i}, v_{g,CLBL_i}) \quad 4.4\text{-}64$$

For use in the overall system energy balance calculations, the fluid stored energy in each of the two cold-leg balance lines is given by the following:

$$U_{H_2O,CLBL_i} = U_{f,CLBL_i} + U_{g,CLBL_i} \quad 4.4\text{-}65$$

where:

$$U_{f,CLBL_i} = M_{f,CLBL_i} \times c_{P,f,CLBL_i} \times (T_{f,CLBL_i} - T_{ref}) \quad 4.4\text{-}66$$

and:

$$U_{g,CLBL_i} = M_{g,CLBL_i} \times c_{P,g,CLBL_i} \times (T_{g,CLBL_i} - T_{ref}) \qquad 4.4\text{-}67$$

This completes the discussion of the calculations related to the left-hand side of the fluid energy conservation equation.

On the right-hand side of the cold-leg balance line fluid energy conservation equation, the energy addition rate to the fluid due to heat transfer from the cold-leg balance line metal is calculated from the cold-leg balance line metal energy conservation equation, which is discussed in Subsection 4.4.6.

Once the metal-to-fluid heat transfer rate is known, the fluid energy transport rates on the right-hand side of the cold-leg balance line fluid energy conservation equation are inferred from a combination of the CMT and cold-leg balance line fluid energy conservation equations, in a manner analogous to that performed for the mass flow rates on the right-hand side of the fluid mass conservation equation, once all other terms have been calculated in these equations.

This completes the discussion of the calculations related to the right-hand side of the fluid energy conservation equation.

4.4.6 Cold-Leg Balance Line Metal Energy Conservation Equations

The general metal energy conservation equation, which relates the change in stored metal energy with respect to time (the metal-energy time derivative) to the energy rates in and out (due to heat transfer), reduces to the following for each of the two cold-leg balance lines, $CLBL_i$, where i = 1,2:

$$\frac{d[M \times c_p \times (T - T_{ref})]_{metal,CLBL_i}}{dt} = - Q_{[metal \Rightarrow H_2O],CLBL_i} - Q_{[metal \Rightarrow ambient],CLBL_i} \qquad 4.4\text{-}68$$

Due to the fact that no metal thermocouple instrumentation exists in the cold-leg balance lines, fluid thermocouples are employed to obtain pseudo-metal temperatures. Each cold-leg balance line is divided into two metal segments. Table 4.4-8 lists the following data required in the metal energy calculations for each metal segment: fluid thermocouple channel ID for the pseudo-metal temperature, metal mass, outer surface area, and mean surface area. In addition, Table 4.4-9 lists the following data required in the metal energy calculations (which are not on a segment basis): ambient temperature channel ID, insulation thickness, and insulation mean thermal conductivity.

The left-hand side of the metal energy conservation equation is approximated as follows:

$$\frac{d[M \times c_p \times (T-T_{ref})]_{metal,CLBL_i}}{dt} = \frac{\Delta[M \times c_p \times (T-T_{ref})]_{metal,CLBL_i}}{\Delta t} \quad 4.4\text{-}69$$

where (subscripts n-1 and n denote two consecutive time points):

$$\frac{\Delta[M \times c_p \times (T-T_{ref})]_{metal,CLBL_i}}{\Delta t} = \sum_{m=1}^{N_{metal,CLBL_i}} M_{metal,CLBL_{i,m}} \times c_{P_{metal,CLBL_{i,m}}} \times \left[\frac{T_{metal,CLBL_{i,m}n} - T_{metal,CLBL_{i,m}n-1}}{t_n - t_{n-1}}\right] \quad 4.4\text{-}70$$

where:

$N_{metal,CLBL}$ = Number of metal segments in each cold-leg balance line, (2)

The metal segment specific heat capacity at constant pressure is calculated as a function of the metal segment temperature from the metal c_p versus temperature tabular data listed in Table 4.4-10, via linear interpolation within the table. No extrapolation at either end is performed; the first and last table points define the applicable range (the first point is $[T_{min}, c_{p,min}]$, and the last point is $[T_{max}, c_{p,max}]$).

This completes the discussion of the calculations related to the left-hand side of the metal energy conservation equation.

On the right-hand side of the metal energy conservation equation, the total metal-to-ambient heat transfer rate is equal to the sum of the individual metal segment metal-to-ambient heat transfer rates:

$$Q_{[metal \Rightarrow ambient],CLBL_i} = \sum_{m=1}^{N_{metal,CLBL_i}} Q_{[metal \Rightarrow ambient],CLBL_{i,m}} \quad 4.4\text{-}71$$

The integrated metal-to-ambient heat transfer is also computed for use in the overall system energy balance.

The metal segment m metal-to-ambient heat transfer rate is given by the following:

$$Q_{[metal \Rightarrow ambient],CLBL_{-,m}} = \frac{(T_{metal,CLBL_{-,m}} - T_{ambient})}{(R_{outer\_metal,CLBL_{-,m}} + R_{insul\_metal,CLBL_{-,m}})} \times C_2 \qquad 4.4\text{-}72$$

where:

C_2 = Conversion constant, hours to seconds

The metal segment m outer surface heat transfer resistance is given by the following:

$$R_{outer\_metal,CLBL_{-,m}} = \frac{1.0}{A_{outer\_metal,CLBL_{-,m}} \times (H_{outer\_conv\_metal,CLBL_{-,m}} + H_{outer\_rad\_metal,CLBL_{-,m}})} \qquad 4.4\text{-}73$$

Note that for ambient heat transfer considerations, each cold-leg balance line metal segment is treated as a horizontal cylinder (also recall that the cold-leg balance lines are insulated).

A natural convection heat transfer correlation[16] of the following form is employed:

$$Nu = C\ (Gr\ Pr)^m \qquad 4.4\text{-}74$$

where, for horizonal cylinders:

$$C = 0.13,\ m = 1/3;\ \text{for } (Gr\ Pr) > 10^9 \text{ (turbulent range)}$$

$$C = 0.53,\ m = 1/4;\ \text{for } (Gr\ Pr) < 10^9 \text{ (laminar range)} \qquad 4.4\text{-}75$$

For the OSU test facility air at atmospheric pressure and ambient temperature (averaged over the tests), the laminar range ($Gr\ Pr < 10^9$; $C = 0.53$, $m = 1/4$) applies at the outer surfaces of the cold-leg balance lines, and the above correlation simplifies to the following expression for the convective heat transfer coefficient for each metal segment m:

$$H_{outer\_conv\_metal,CLBL_{-,m}} = 0.28 \times \left(\frac{1.0}{D}\right)^{1/4} \times (|T_{metal,CLBL_{-,m}} - T_{AMB}|)^{1/4} \qquad 4.4\text{-}76$$

Using an outer diameter of 3.25 in. for the cold-leg balance lines, the above correlation further simplifies to the following expression:

$$H_{outer\_conv\_metal,CLBL_{i,m}} = 0.21 \times (|T_{metal,CLBL_{i,m}} - T_{AMB}|)^{1/4} \qquad 4.4\text{-}77$$

Employing the assumption of radiation heat transfer between infinite parallel planes in the limiting case of a convex object completely enclosed by a very large concave surface (typical assumption for the calculation of radiation energy loss from a hot object in a room), with an assumed emissivity of 0.8 for the insulated cold-leg balance lines, the metal segment m outer surface heat transfer coefficient due to radiation reduces to the following:

$$H_{outer\_conv\_metal,CLBL_{i,m}} = 1.3704 \times 10^{-9} \times [T^2_{insul\_metal,CLBL_{i,m}} + (T_{ambient} + C_3)^2] \times [T_{insul\_metal,CLBL_{i,m}} + (T_{ambient} + C_3)] \qquad 4.4\text{-}78$$

where:

C_3 = Conversion constant, 459.6 (°F to °R)

The coefficient 1.3704 x 10^{-9} is the product of the Stefan-Boltzmann constant (1.713 x 10^{-9} Btu/(hr.-ft.^{2}-°R^4)) and the emissivity (0.8).

The insulation temperature for metal segment m is approximated by the following (assumes that the temperature drop in the insulation is 90 percent of the overall temperature drop):

$$T_{insul\_metal,CLBL_{i,m}} = 0.1 \times (T_{metal,CLBL_{i,m}} - T_{ambient}) + T_{ambient} + C_3 \qquad 4.4\text{-}79$$

The metal segment m insulation heat transfer resistance is given by the following:

$$R_{insul\_metal,CLBL_{i,m}} = \frac{\Delta x_{insul\_metal,CLBL_i}}{A_{mean\_metal,CLBL_{i,m}} \times k_{insul\_metal,CLBL_i}} \qquad 4.4\text{-}80$$

where:

Δx = Insulation thickness, in.

k = Mean thermal conductivity of insulation, Btu-in./hr.-ft.^{2}-°F

Finally, having calculated both the change in stored metal energy (from the left-hand side) and the metal-to-ambient heat transfer rate (from the right-hand side), the metal energy conservation equation is rearranged to solve for the metal-to-fluid heat transfer rate. Recall that the latter is used in the fluid energy conservation equation calculations which were described earlier. The integrated metal-to-fluid heat transfer is also computed for use in the overall system energy balance.

This completes the discussion of the calculations related to the right-hand side of the metal energy conservation equation.

TABLE 4.4-1 INSTRUMENTATION EMPLOYED FOR CMT FLUID CALCULATIONS				
Description	**CMT-1**		**CMT-2**	
Levels – main	LDP-507		LDP-502	
– alternate	LDP-501		LDP-504	
	LDP-503		LDP-506	
	LDP-505		LDP-508	
Top pressure	PT-501		PT-502	
Temperatures/elev (in.)	TF-501	0.300	TF-504	0.300
(Bottom to top)	TF-507	21.170	TF-510	21.170
	TF-509	37.191	TF-512	37.191
	TF-513	40.891	TF-516	40.891
	TF-515	43.711	TF-518	43.711
	TF-519	46.531	TF-522	46.531
	TF-523	49.351	TF-526	49.351
	TF-527	52.171	TF-530	52.171
	TF-547	54.541	TF-548	54.541
	TF-529	56.911	TF-532	56.911
DVI line – flow out bottom	FMM-501		FMM-504	
– temperature	TF-549		TF-550	

TABLE 4.4-2 VOLUME VERSUS HEIGHT TABLES FOR CMT FLUID VOLUME CALCULATIONS			
CMT-1		CMT-2	
Height (in.)	**Volume ($in.^3$)**	**Height (in.)**	**Volume ($in.^3$)**
0.00	0.0	0.00	0.0
3.25	122.0	0.50	69.0
6.25	393.0	3.50	294.0
9.25	1103.0	6.50	1080.0
12.25	2009.0	10.50	1956.0
15.25	3006.0	13.50	2942.0
17.00	3599.0	15.00	3455.0
31.50	8888.0	30.00	8957.0
36.75	10786.0	35.00	10763.0
44.25	13484.0	42.50	13451.0
48.75	15105.0	46.625	14961.0
51.75	16130.0	50.00	16050.0
54.75	17036.0	53.00	17061.0
57.75	17704.0	56.00	17706.0
58.90	17945.0	59.00	17911.0

TABLE 4.4-3 CMT METAL WALL THERMOCOUPLE INSTRUMENTATION		
Metal Segment	**CMT-1**	**CMT-2**
1	TW-503, TW-501	TW-504, TW-502
2	TW-507, TW-505	TW-508, TW-506
3	TW-511, TW-509	TW-512, TW-510
4	TW-515, TW-513	TW-516, TW-514
5	TW-521, TW-519, TW-517	TW-522, TW-520, TW-518
6	TW-525, TW-523	TW-526, TW-524
7	TW-529, TW-527	TW-530, TW-528
8	TW-533, TW-531	TW-534, TW-532
9	TW-535, TW-537	TW-538, TW-536
10	TW-541, TW-539	TW-542, TW-540
11	TW-545, TW-543	TW-546, TW-544
12	TW-551, TW-549, TW-547	TW-552, TW-550, TW-548
13	TW-555, TW-553	TW-556, TW-554

Note:
Thermocouples for each metal segment are listed in the following order: inside surface, centerline (if applicable; only if three thermocouples are listed), outside surface.

TABLE 4.4-4 DATA FOR CMT METAL ENERGY CALCULATIONS			
CMT-1 or CMT-2 Metal			
Metal Segment	**Metal Mass (lbm)**	**Inner Surface Area (ft^2)**	**Outer Surface Area (ft^2)**
1	347.4	5.50	6.28
2	91.3	1.70	1.89
3	91.3	1.70	1.89
4	187.1	3.48	3.87
5	77.9	1.45	1.61
6	77.9	1.45	1 61
7	155.7	2.90	3.23
8	72.1	1.34	1.49
9	72.1	1.34	1.49
10	162.9	2.80	3.15
11	123.0	1.83	2.09
12	86.4	1.03	1.57
13	86.4	1.03	1.57
Ambient Temperature ID [°F]		TF-006	

TABLE 4.4-5 SPECIFIC HEAT CAPACITY VERSUS TEMPERATURE TABLE FOR CMT METAL ENERGY CALCULATIONS	
Metal C_p [Btu/(lbm-°F)]	**Metal Temperature [°F]**
0.1085	70.
0.1109	100.
0.1175	200.
0.1223	300.
0.1256	400.
0.1279	500.
0.1297	600.

TABLE 4.4-6 INSTRUMENTATION EMPLOYED FOR COLD-LEG BALANCE LINE FLUID CALCULATIONS		
Description	**CLBL-1**	**CLBL-2**
Level	LDP-509	LDP-510
Temperatures: bottom	TF-533	HPS201-3
top	TF-531	TF-546
Pressure	PT-501	PT-502

TABLE 4.4-7 VOLUME VERSUS HEIGHT TABLES FOR COLD-LEG BALANCE LINE FLUID VOLUME CALCULATIONS			
CLBL-1		CLBL-2	
Height (in.)	Volume ($in.^3$)	Height (in.)	Volume ($in.^3$)
0.000	0.000	0.000	0.000
11.000	16.453	9.000	13.461
44.440	49.398	38.440	42.465
45.560	66.147	39.560	55.765
47.375	85.687	41.500	75.316
50.815	108.477	44.000	90.298
51.935	158.539	48.191	124.537
75.250	181.449	49.309	147.629
78.693	218.059	74.500	172.387
80.000	257.284	77.000	196.405
		78.949	209.478
		80.000	225.046

TABLE 4.4-8 DATA FOR COLD-LEG BALANCE LINE METAL ENERGY CALCULATIONS (PER SEGMENT)				
CLBL-1 Metal Segments				
Metal Segment	Pseudo-Metal Temperature ID (°F)	Metal Mass (lbm)	Outer Surface Area ($ft.^2$)	Mean Surface Area ($ft.^2$)
1	TF-533	42.9	9.03	5.82
2	TF-531	42.9	9.03	5.82
CLBL-2 Metal Segments				
Metal Segment	Pseudo-Metal Temperature ID (°F)	Metal Mass (lbm)	Outer Surface Area ($ft.^2$)	Mean Surface Area ($ft.^2$)
1	HPS201-3	31.9	6.00	5.16
2	TF-546	31.9	6.00	5.16

TABLE 4.4-9 DATA FOR COLD-LEG BALANCE LINE METAL ENERGY CALCULATIONS		
Description	**CLBL-1**	**CLBL-2**
Ambient temperature ID (°F)	TF-006	TF-006
Insulation thickness (in.)	1.0	1.0
Insulation mean thermal conductivity [(Btu-in.)/(hr.-ft.^{2}-°F)]	0.31	0.31

TABLE 4.4-10 SPECIFIC HEAT CAPACITY VERSUS TEMPERATURE TABLE FOR COLD-LEG BALANCE LINE METAL ENERGY CALCULATIONS	
Metal c_p [Btu/(lbm-°F)]	**Metal Temperature (°F)**
0.1085	70
0.1109	100
0.1175	200
0.1223	300
0.1256	400
0.1279	500
0.1297	600

4.5 In-Containment Refueling Water Storage Tank (IRWST)

For the AP600, the IRWST is a reservoir of coolant held inside containment at ambient containment pressure. Once the RCS has been depressurized by actuation of all four stages of the ADS, the IRWST inventory flows to the core by gravity through piping and valves connecting the IRWST to the DVI lines. The IRWST injection phase continues until the IRWST inventory is depleted and recirculation of the containment sump inventory through the RCS is initiated.

The OSU test facility simulated the IRWST with a tank and associated piping. In addition to piping and valves connecting the IRWST to the DVI lines, the IRWST simulation accounted for the following AP600 features:

- A sparger to distribute flow from ADS 1-3 to the IRWST
- A submersed heat exchanger to simulate the operation of PRHR during simulated events
- An overflow line between the IRWST and the containment sump tank to simulate the interaction of the IRWST directly with the sump

The operation of each of these features is accounted for in the mass and energy balance performed for the IRWST simulation.

4.5.1 General Mass and Energy Balance Formulation

The liquid mass inventory in the IRWST is calculated as:

$$M_{f,IRWST} = \rho_f \times V_{f,IRWST} \qquad 4.5\text{-}1$$

The vapor mass inventory of the IRWST is calculated as:

$$M_{g,IRWST} = \rho_g \times V_{g,IRWST} \qquad 4.5\text{-}2$$

where the subscripts:

f = liquid phase of water
g = steam

Flow meter FVM-701 is located in the exhaust line from the IRWST. If the measured flow from FVM-701 is less than an input threshold value, then no steam property calculations are performed. Thus, no steam inventory is modeled in the tank until there is a measured exhaust flow from FVM-701.

The general mass balance equation for the IRWST is expressed as:

$$\frac{dM_{IRWST}}{dt} = \dot{M}_{ADS} - \dot{M}_{STM\ VENT} - \dot{M}_{OVRFLW} - \dot{M}_{IRWST\ INJ} \qquad 4.5\text{-}3$$

where the subscripts:

ADS	=	Mass flow rate, both vapor and liquid, from ADS 1-3 separator
STM VENT	=	Vapor mass flow rate exhausted from IRWST through FVM-701
OVRFLW	=	Liquid mass flow rate through IRWST overflow line measured by FMM-703
IRWST INJ	=	Total mass flow rate injected from IRWST through both injection lines

Minimum flow criteria:

If the mass flow rates injected from the IRWST are less than a threshold value, then the mass flow rates are set to zero. A similar adjustment is made to $\dot{M}_{ADS}$, $\dot{M}_{STM\ VENT}$, and $\dot{M}_{OVRFLW}$.

If $\dot{M}_{IRWST\ INJ} < \dot{M}_{IRWST\ INJ\ LOW}$, then $\dot{M}_{IRWST\ INJ} = 0.$

If $\dot{M}_{ADS} < \dot{M}_{ADS\ LOW}$, then $\dot{M}_{ADS} = 0.$

If $\dot{M}_{OVRFLW} < \dot{M}_{OVRFLW\ LOW}$, then $\dot{M}_{OVRFLW} = 0.$

$\dot{M}_{IRWST\ INJ\ LOW} = \dot{M}_{ADS\ LOW,\ f} = \dot{M}_{OVRFLW\ LOW} = 0.5$ gpm

$\dot{M}_{ADS\ LOW,\ g} = 0.5$ cfm

Similarly, the general energy balance on the IRWST is written as:

$$\frac{\sum M_j c_p dT_j}{dt} = Q_{PRHR} + \dot{M}_{ADS} h_{ADS} - \dot{M}_{STM\ VENT} h_g - \dot{M}_{OVRFLW} h_f - \dot{M}_{IRWST\ INJ} h_{IRWST\ INJ} - Q_{metal} - Q_{AMB} \qquad 4.5\text{-}4$$

Q_{PRHR} is calculated using Equation 4.5-4.

where:

Q_{PRHR} = Heat addition rate from PRHR, Btu/sec.
Q_{metal} = Energy loss to metal
Q_{AMB} = Energy loss to ambient environment

and the subscripts:

j = Control volume within the IRWST associated with axial thermocouple locations

The IRWST simulation may experience four modes of operation:

Case 1: IRWST inventory is subcooled; ADS has not been actuated; there is no overflow of IRWST inventory.

Case 2: At least some portion of the IRWST inventory is saturated (due to actuation of PRHR); ADS has not been actuated; there may be overflow from the IRWST.

Case 3: At least some portion of the IRWST inventory is saturated; ADS has been actuated; both PRHR and ADS energy is added to the IRWST.

Case 4: After ADS actuation, IRWST inventory is injected into the primary system.

The simplification of the general mass and energy balance equations for these four cases are as follows.

4.5.2 Case 1

For this case, there is no liquid or vapor flow out of the IRWST, implying the following:

- No injection flow from the IRWST
- No liquid swell (due to heating) that provides for liquid flow through the overflow lines
- No steam generation and, therefore, the bulk liquid temperature of the IRWST inventory is lower than its saturation temperature ($T_f < T_{SAT}$)

According to the first two items, measured flow from the IRWST is given as:

$$\dot{M}_{FMM-701} = \dot{M}_{FMM-702} = \dot{M}_{FMM-703} = \dot{M}_{FVM-701} = \dot{M}_{FVM-601} = \dot{M}_{FMM-601} = 0 \qquad 4.5\text{-}5$$

where the subscripts:

FMM-701
FMM-702
FMM-703
FVM-701
FVM-601
FMM-601
= Flow meters in lines containing both liquid and vapor flow from the IRWST

With no mass entering or leaving the IRWST, the time rate of change in mass of the IRWST is defined as:

$$\frac{dM_{IRWST}}{dt} = 0 \qquad 4.5\text{-}6$$

Under these conditions, the energy balance on the IRWST is expressed as:

$$\frac{\sum M_j \, c_p \, dT_j}{dt} = Q_{PRHR} \qquad 4.5\text{-}7$$

The fluid thermocouples used in calculating the mass inventory of the IRWST and their respective elevations referenced to the top of the ceramic filler in the IRWST are given in Table 4.5-1. The difference form of the preceding equation is:

$$\sum M_j \, c_p \, \Delta T_j = Q_{PRHR} \, \Delta t \qquad 4.5\text{-}8$$

Liquid mass inventory of the IRWST is then calculated as follows:

Step 1: Calculate a temperature-compensated water level in the IRWST using outputs from level transducer LDP-701 and the thermocouples identified in Table 4.5-1 as input to the subroutine developed to perform this calculation.

If the temperature compensated level is less than the threshold value of 90.5 in., then $\dot{M}_{OVRFLW} = 0$.

Step 2: Calculate a pressure and density gradient for the water inventory in the IRWST using outputs from total pressure transducer PT-701, the compensated level measurement, and the thermocouples identified in Table 4.5-1. This is accomplished as follows:

First, the IRWST is divided into regions. Located in the middle of each region is one of the thermocouples identified in Table 4.5-1. The boundary between adjacent regions is defined as the midpoint between adjacent thermocouples. The bottom boundary of the region at the bottom of the IRWST is the top surface of the ceramic filler. The top boundary of the region at the top of the IRWST is the top of the IRWST.

Next, water column in the IRWST is partitioned into the regions defined above. In the event that the water level resides in a region, but is below the thermocouple in that region, then the height of water in that region is applied to the adjacent region.

Then, the pressure recorded by instrument PT-701 is applied to the top surface of the IRWST inventory and assumed to be representative of the pressure in that region. The liquid density in the first region is calculated as:

$$\rho_1 = \rho(P_1, T_1) \qquad 4.5\text{-}9$$

where P_1 is the pressure measurement of instrument PT-701 and T_1 is the first thermocouple below the surface of the compensated water level. The pressure at the top of the next lowest region is then calculated as:

$$P_j = P_{j-1} + \frac{g}{g_c} \rho_{j-1} \Delta z_{j-1} \qquad 4.5\text{-}10$$

where the subscript:

j = Control volume within the IRWST associated with axial thermocouple locations

The calculations defined in Equations 4.5-9 and 4.5-10 are repeated for each of the regions in the IRWST that are below the compensated level indicated by LDP-701.

Step 3: Liquid mass in the IRWST is then calculated as the sum of the masses of each region:

$$M_{IRWST} = \sum \rho_j V(z) \qquad 4.5\text{-}11$$

where:

V(z) = Volume of the IRWST as a function of height from the top surface of the ceramic fill located in the bottom of the tank

4.5.3 Case 2

In this case, the IRWST liquid inventory is warmed sufficiently due to PRHR so that the liquid volume has swelled above the overflow line. The temperature of the IRWST inventory at or near the top of the IRWST is expected to be at or near saturation. Thus, there may be both liquid and vapor flow out of the IRWST. This situation may be described as:

- There is no injection flow from the IRWST
- Liquid flow may occur through the overflow line, measured by FMM-703, due to volume swelling resulting from heating
- There may be steam generation, measured by FVM-701

From these three conditions, the mass balance on the IRWST given by Equation 4.5-3 is simplified as:

$$\frac{dM_{IRWST}}{dt} = -\dot{M}_{FVM-701} - \dot{M}_{FMM-703} \qquad 4.5\text{-}12$$

Noting that the left-hand side of the previous equation may be approximated as a difference:

$$\frac{dM_{IRWST}}{dt} \approx \frac{M_{IRWST,i} - M_{IRWST,i-1}}{t_i - t_{i-1}} \qquad 4.5\text{-}13$$

where the subscript:

i = Index of data and time arrays

The mass depletion of the IRWST may now be written as:

$$M_{IRWST,\,i} = M_{IRWST,\,i-1} - \dot{M}_{FVM-701,\,i}\,\Delta t - \dot{M}_{FMM-703,\,i}\,\Delta t \qquad 4.5\text{-}14$$

where:

$\Delta t = t_i - t_{i-1}$

Density and enthalpy of vapor and liquid flow are evaluated using the ASME steam table routines and the outputs from the following instruments:

	Pressure	Temperature
Vapor (steam)	PT-701	TF-722
Liquid (overflow)	PT-701	TF-723

The units of measurement for the vapor and liquid flow meters are ft.^{3}/min. and gpm, respectively. The vapor mass flow is calculated as:

$$\dot{M}_{FVM-701} = \rho_{(PT-701,\ TF-722)}\ W_{(FVM-701)} \times C_1 \qquad 4.5\text{-}15$$

Similarly, the liquid mass flow rate is calculated as:

$$\dot{M}_{FMM-703} = \rho_{(PT-701,\ TF-723)}\ W_{(FMM-703)} \times C_2 \qquad 4.5\text{-}16$$

where:

C_1 = Conversion constant, min. to sec.
C_2 = Conversion constant, gpm to ft.^{3}/sec.

The rate of energy transfer associated with the IRWST inventory is simplified from Equation 4.5-4 and expressed as:

$$\frac{\sum M_j\, c_p\, dT_j}{dt} = Q_{PRHR} - \dot{M}_{FVM-701}\, h_g - \dot{M}_{FMM-703}\, h_f \qquad 4.5\text{-}17$$

The difference form of the previous equation is written as:

$$\sum M_j\, c_p\, \Delta T_j = Q_{PRHR}\, \Delta t - \dot{M}_{FVM-701}\, h_g\, \Delta t - \dot{M}_{FMM-703}\, h_f\, \Delta t \qquad 4.5\text{-}18$$

4.5.4 Case 3

In this case, the operation of the ADS increases the mass in the IRWST. Also, operation of PRHR and the ADS may heat up the IRWST inventory. The combination of added mass and inventory heatup may cause the IRWST liquid volume to swell to above the overflow line. The temperature of the IRWST inventory is expected to be at or near saturation, and not all ADS flow may be condensed. Thus, there may be both liquid and vapor flow out of the IRWST, implying the following:

- There is no injection flow from the IRWST to the DVI line
- ADS flow, possibly both steam and water, is being exhausted into the IRWST
- Liquid flow may occur through the overflow line, measured by FMM-703, due to volume swelling resulting from heating and injection of water from ADS 1-3
- There may be steam generation, measured by FVM-701

From these four conditions, the mass balance on the IRWST is given as:

$$\frac{dM_{IRWST}}{dt} = \dot{M}_{ADS} - \dot{M}_{FVM-701} - \dot{M}_{FMM-703} \qquad 4.5\text{-}19$$

The ADS flow may consist of both vapor and liquid components:

$$\dot{M}_{ADS} = \dot{M}_{FVM-601} + \dot{M}_{FMM-601} \qquad 4.5\text{-}20$$

where the subscripts:

FVM-601	=	Vapor flow meter downstream of ADS 1-3 separator
FMM-601	=	Liquid flow meter downstream of ADS 1-3 separator

Expressing the left-hand side of Equation 4.5-20 as a difference and expanding, the liquid mass inventory of the IRWST is calculated as:

$$M_{IRWST,\,i} = M_{IRWST,\,i-1} + \dot{M}_{FVM-601,\,i}\,\Delta t + \dot{M}_{FMM-601,\,i}\,\Delta t - \dot{M}_{FVM-701,\,i}\,\Delta t - \dot{M}_{FMM-703,\,i}\,\Delta t \qquad 4.5\text{-}21$$

Similarly, the energy balance for this case may be written as:

$$\frac{\sum M_j\, c_p\, dT_j}{dt} = \dot{M}_{FVM-601}\, h_g + \dot{M}_{FMM-601}\, h_f - \dot{M}_{FVM-701}\, h_g - \dot{M}_{FMM-703}\, h_f \qquad 4.5\text{-}22$$

The enthalpy of the vapor and liquid components of the ADS flow, measured by FVM-601 and FMM-601, respectively, is evaluated using the ASME steam table routines and data from the following instruments:

	Pressure	Temperature
Vapor phase	PT-605	TF-617
Liquid phase	PT-605	TF-616

The difference form of the energy equation is written as:

$$\sum M_j c_p \Delta T_j = \dot{M}_{FVM-601} h_g \Delta t + \dot{M}_{FMM-601} h_f \Delta t - \dot{M}_{FVM-701} h_g \Delta t - \dot{M}_{FMM-703} h_f \Delta t \qquad 4.5\text{-}23$$

4.5.5 Case 4

This case occurs late in the transient:

- PRHR is no longer active and ADS 1-3, while open, has low flow
- While there may be some steam venting of the IRWST volume, there is most likely no liquid overflow
- At this time, the IRWST may be injecting into the DVI lines

The mass balance on the IRWST is given by Equation 4.5-3 where:

$$\dot{M}_{IRWST\ INJ} = \dot{M}_{FMM-701} + \dot{M}_{FMM-702} \qquad 4.5\text{-}24$$

The mass balance for this case is expressed as:

$$M_{IRWST,\,i} = M_{IRWST,\,i-1} + \dot{M}_{FVM-601,\,i}\Delta t + \dot{M}_{FMM-601,\,i}\Delta t - \dot{M}_{FVM-701,\,i}\Delta t - \dot{M}_{FMM-703,\,i}\Delta t - \dot{M}_{FMM-701,\,i}\Delta t - \dot{M}_{FMM-702,\,i}\Delta t \qquad 4.5\text{-}25$$

Similarly, the energy balance is written as:

$$\frac{\sum M_j c_p dT_j}{dt} = \dot{M}_{FVM-601} h_g + \dot{M}_{FMM-601} h_f - \dot{M}_{FVM-701} h_g - \dot{M}_{FMM-703} h_f - \dot{M}_{FMM-701} h_f - \dot{M}_{FMM-702} h_f \qquad 4.5\text{-}26$$

Expressing the preceding equation in its difference form:

$$\sum M_j c_p \Delta T_j = (\dot{M}_{FVM-601} h_g + \dot{M}_{FMM-601} h_f - \dot{M}_{FVM-701} h_g - \dot{M}_{FMM-703} h_f - \dot{M}_{FMM-701} h_f - \dot{M}_{FMM-702} h_f)\Delta t \qquad 4.5\text{-}27$$

4.5.6 Direct Vessel Injection Line Flow Reversal

Liquid flow reversal can occur in the DVI-1. The total injection flow is calculated as:

$$\dot{M}_{IRWST\ INJ} = \dot{M}_{IRWST\ INJ,\ 1} + \dot{M}_{IRWST\ INJ,\ 2} \qquad 4.5\text{-}28$$

$$\dot{M}_{IRWST\ INJ,\ 1} = \rho W_{(FMM\text{-}701)} \times C_2 \qquad 4.5\text{-}29$$

$$\dot{M}_{IRWST\ INJ,\ 2} = \rho W_{(FMM\text{-}702)} \times C_2 \qquad 4.5\text{-}30$$

where:

ρ = water density of the lowest-most region calculated in Equation 4.5-9
C_2 = Conversion constant, gpm to ft.^{3}/sec.

Flow reversals can occur for injection line number 1. If the measured flow is less than a threshold value,

$$W_{(FMM\text{-}701)} < W_{IRWST\ INJ\ LOW} \qquad 4.5\text{-}31$$

then the reverse DVI flow is calculated as:

$$\dot{M}_{IRWST\ INJ,\ reversed} = \dot{M}_{IRWST\ INJ,\ total} - \dot{M}_{ACC,\ 1} - \dot{M}_{SUMP,\ 1} - \dot{M}_{CMT,\ 1} \qquad 4.5\text{-}32$$

where:

$$\dot{M}_{IRWST\ INJ,\ total} = \rho W_{(FMM\text{-}205)} \times C_2 \qquad 4.5\text{-}33$$

where the density of injection liquid is calculated at pressure and temperature conditions using PT-109 and the minimum temperature from TF-113 and TF-115.

$\dot{M}_{ACC,\ 1}$ is calculated using Equation 4.3-15.

$\dot{M}_{SUMP,\ 1}$ is calculated using Equation 4.9-9.

$\dot{M}_{CMT,\ 1}$ is calculated using Equation 4.4-18.

If $\dot{M}_{IRWST\ INJ,\ reversed} < 0.0$

and if $\dot{M}_{(FMM-701)} < \dot{M}_{IRWST\ INJ\ LOW}$

then

$$\dot{M}_{IRWST\ INJ,\ 1} = \dot{M}_{IRWST\ INJ,\ reversed} \qquad 4.5\text{-}34$$

otherwise,

$$\dot{M}_{IRWST\ INJ,\ 1} = 0.0 \qquad 4.5\text{-}35$$

Note: Flow reversal does not occur for injection line number 2.

If $\dot{M}_{(FMM-702)} \geq \dot{M}_{IRWST\ INJ\ LOW}$

then

$$\dot{M}_{IRWST\ INJ,\ 2} = \rho W_{(FMM-702)} \times C_2 \qquad 4.5\text{-}36$$

otherwise

$$\dot{M}_{IRWST\ INJ,\ 2} = 0.0 \qquad 4.5\text{-}37$$

4.5.7 Energy Loss due to Ambient Heat Transfer Rate

An equivalent heat transfer coefficient, accounting for heat resistance due to any insulation applied to the outside surface of the IRWST volumes and natural convection from the outside surface to the ambient, is used to evaluate the heat loss to ambient from the metal surfaces of the IRWST. The same metal surface temperatures used to evaluate metal heat storage of the IRWST is used to calculate heat loss to the ambient. Surface areas included in this calculation account for IRWST and associated piping.

The metal-to-ambient heat transfer calculation methodology for the IRWST is similar to methodology used for other insulated components of the system. Each IRWST metal segment is treated as an insulated vertical cylinder. The turbulent range form of the natural convection heat transfer correlation from Reference 16 applies, based upon the conditions of the OSU test facility air at atmospheric pressure and ambient temperature (averaged over the tests). In the radiation heat transfer correlation, an emissivity of 0.8 is assumed.

The detailed calculations and equations are identical to those for the metal-to-ambient heat transfer for the cold-leg balance lines in Subsection 4.4.6, the only exception is that in the final expression for the natural convection heat transfer coefficient, the coefficient multiplier 0.21 is replaced with 0.09 and the

exponent 1/4 is replaced with 1/3 (these differences are due to both the vertical orientation and the turbulent range of applicability for the IRWST).

The total energy loss to ambient rate is equal to the sum of the individual metal segment heat transfer rates:

$$Q_{ambient} = \sum_{m=1}^{N_{surf}} Q_m \qquad 4.5\text{-}38$$

$$Q_m = \frac{T_{metal,m} - T_{ambient}}{(R_{surf\_metal,m} + R_{insul\_metal,m})} \qquad 4.5\text{-}39$$

$$R_{surf\_metal,m} = \frac{1.0}{A_{metal,m} \times (H_{conv\_metal,m} + H_{rad\_metal,m})} \qquad 4.5\text{-}40$$

$$H_{conv\_metal,m} = 0.09 \times (|(T_{metal,m} - T_{ambient})|)^{1/3} \qquad 4.5\text{-}41$$

$$H_{rad\_metal,m} = 1.713\times10^{-9} \times e \times [T^2_{insul\_metal,m} + (T_{ambient} + C)^2] \times [T_{insul\_metal,m} + (T_{ambient} + C)] \qquad 4.5\text{-}42$$

The insulation temperature for metal segment, m, is approximated by:

$$T_{insul\_metal,m} = \left(0.1 \times (T_{metal,m} - T_{ambient}) + T_{ambient}\right) + C \qquad 4.5\text{-}43$$

This assumes that the temperature drop in the insulation is 90 percent overall temperature drop:

$$R_{insul\_metal,m} = \frac{\Delta x_{insul\_metal}}{A_{mean\_metal,m} \times k_{insul\_metal}} \qquad 4.5\text{-}44$$

where:

C	=	Conversion constant, °F to °R
Δx_{insul_metal}	=	Insulation thickness
$A_{metal,m}$	=	Segment outer surface area

$A_{mean\_metal,m}$ = Mean segment area
e = Emissivity of insulation layer (0.8)
k_{insul_metal} = Mean thermal conductivity of insulation
$T_{ambient}$ = Ambient temperature
N_{surf} = Number of surface metal segments
$R_{surf\_metal,m}$ = Metal segment outer surface heat transfer resistance
$H_{conv\_metal,m}$ = Metal segment outer surface heat transfer coefficient due to convection
$H_{rad\_metal,m}$ = Metal segment outer surface heat transfer coefficient due to radiation
1.713×10^{-9} = Stefan-Boltzmann constant BTU/hr.-ft.^{2} - °R^4

4.5.8 Energy Loss to Metal

$$Q_{metal} = \sum_{m=1}^{N_{metal}} c_{p\ metal} \times M_{metal,m} \times \left[\frac{T_{n,metal,m} - T_{n-1,metal,m}}{t_n - t_{n-1}} \right] \qquad 4.5\text{-}45$$

where:

$c_{p\ metal}$ = Heat capacity of the metal
$M_{metal,m}$ = Mass of the metal segment
$T_{n,metal,m}$ = Metal temperature at time n
t_n = Time at time-step n
N_{metal} = Number of metal segments

4.5.9 Fluid Stored Energy

For use in the overall system energy balance calculations, the fluid stored energy in the IRWST is given by the following:

$$U_{H_2O,IRWST} = U_{f,IRWST} + U_{g,IRWST} \qquad 4.5\text{-}46$$

where:

$$U_{f,IRWST} = \sum_{j=1}^{N_{zone,IRWST}} M_{f,IRWST} \times c_{p,f,IRWST} \times (T_{f,IRWST} - T_{ref}) \qquad 4.5\text{-}47$$

where:

$N_{zone,\ IRWST}$ = Number of zones in the IRWST (12)

$U_{g,\ IRWST}$ is not considered here. Note that there is a steam inventory in the IRWST during ADS 1-3 actuation. However, the stored energy due to steam is negligible compared to the stored energy due to the large volume of liquid in the IRWST.

TABLE 4.5-1 IRWST MASS AND ENERGY CALCULATIONS IDENTIFICATION OF FLUID THERMOCOUPLES AND ELEVATION		
Index	**Thermocouple ID**	**Elevation[1] (in.)**
1	TF-701	1.00
2	TF-702	8.99
3	TF-703	16.97
4	TF-704	26.85
5	TF-705	36.73
6	TF-706	46.61
7	TF-707	56.49
8	TF-708	66.36
9	TF-709	76.24
10	TF-710	87.36
11	TF-711	98.47
12	TF-712	109.59

Note:
(1) Elevations referenced from top surface of plate in bottom of IRWST and run vertically upwards.

TABLE 4.5-2 VOLUME VERSUS HEIGHT TABLE FOR IRWST FLUID VOLUME CALCULATIONS	
Height (in.)	**Volume ($in.^3$)**
0.0	0.0
10.5	73,391.0
42.0	297,302.0
56.625	403,788.0
74.5	531,187.0
90.0	640,577.0
93.75	666,472.0
115.0	749,140.0

TABLE 4.5-3 DATA FOR IRWST METAL ENERGY CALCULATIONS (PER SEGMENT)		
Metal Segment	**Metal Temperature ID (°F)**	**Metal Mass (lbm)**
1	TFM-701	2148
2	TFM-702	1353
3	TFM-703	2394
4	TF-719	146

TABLE 4.5-4 DATA FOR IRWST METAL ENERGY CALCULATIONS	
Description	**Data**
Ambient Temperature ID (°F)	TF-006
Insulation Thickness (in.)	1.5
Insulation mean thermal conductivity [(Btu-in.)/(hr.-ft.^{2} - °F)]	0.141

TABLE 4.5-5 DATA FOR IRWST ENERGY LOSS DUE TO AMBIENT HEAT TRANSFER			
Surface	**Metal Temperature ID (°F)**	**Outer Surface Area (ft.^{2})**	**Mean Surface Area (ft.^{2})**
1	TFM-701	107.72	53.11
2	TFM-702	89.46	44.10
3	TFM-703	75.32	86.68

4.6 Automatic Depressurization System 1-3 Separator

The ADS provides a means of depressurizing the RCS in a controlled, staged manner through the use of four pairs of valves, with each valve pair sequenced to open at different primary system pressures. The first three pairs of valves, called ADS stages 1, 2, and 3 (ADS 1-3), are located in parallel piping paths running from the top of the pressurizer to the IRWST. This portion of the ADS operates independently of the fourth and final stage of the ADS.

The ADS 1-3 flow path was simulated in the OSU test facility by three valves (one valve each having a scaled stage 1, stage 2, and stage 3 flow area), a steam/water separator tank, a vortex (vapor) flow meter, a magnetic (liquid) flow meter, and associated piping. During testing, flow through the ADS 1-3 flow path was measured by separating the vapor and liquid components of the flow, measuring the flow rate of the component flows, recombining the flows, then directing the total metered flow to a sparger located in the IRWST.

Flow through ADS 1-3 may be calculated as:

$$\dot{M}_{ADS\ 1\text{-}3} = \dot{M}_{ADS\ 1\text{-}3,\ f} + \dot{M}_{ADS\ 1\text{-}3,\ g} + \frac{dM_{ADS\ 1\text{-}3\ SEP}}{dt} \qquad 4.6\text{-}1$$

where the subscripts:

f	=	Liquid phase of water
g	=	Steam
ADS 1-3	=	Stages 1 through 3 of the ADS
SEP	=	Steam water separator tank for ADS 1-3

Energy is transported out of the primary system by both the vapor and liquid flows. Also, the stored energy of the ADS 1-3 separator inventory may change due to changes in the amount of liquid and vapor in the separator, changes in temperature and pressure of the liquid or vapor inventory in the separator, or a change in the temperature of the separator tank metal mass. Accounting for these terms, the energy rate equation for ADS 1-3 flow may be expressed as:

$$Q_{ADS\ 1\text{-}3} = Q_{ADS\ 1\text{-}3,\ f} + Q_{ADS\ 1\text{-}3,\ g} + c_P \frac{d(M_{ADS\ 1\text{-}3\ SEP}\ T)}{dt}$$

$$+ Q_{ADS\ 1\text{-}3,\ METAL} + Q_{ADS\ 1\text{-}3,\ AMB} \qquad 4.6\text{-}2$$

where the subscripts:

METAL = Metal mass of the ADS 1-3 separator tank and associated piping
AMB = Energy loss to ambient environment

4.6.1 Automatic Depressurization System 1-3 Separator Liquid Inventory

The ADS 1-3 separator is, in its simplest form, a tank. Liquid inventory in the ADS 1-3 separator is monitored by a level transducer. The functional steps and associated system of equations for operating on the output from the ADS 1-3 separator level transducers to calculate liquid mass in the ADS 1-3 steam/water separator tank follows:

Step 1: Compensate the readings from the ADS 1-3 separator level transducer listed in Table 4.6-1 to account for temperature differences between fluid in the separator tank and fluid in the reference leg of the instrument line. The local pressure and fluid temperature instruments to be used to accomplish the compensation are also identified in Table 4.6-1.

Step 2: The local pressures and temperatures measured using the instruments identified in Table 4.6-1 are used as inputs to the ASME steam tables to calculate the density of the liquid and vapor in the ADS 1-3 separator:

$$\rho_{ADS\ 1\text{-}3,\ f} = \rho_f\ (PT\text{-}605,\ TF\text{-}616)$$

$$\rho_{ADS\ 1\text{-}3,\ g} = \rho_g\ (PT\text{-}605,\ TF\text{-}617) \qquad 4.6\text{-}3$$

where:

PT-605 = Data channel ID for local pressure measurement in the ADS 1-3 separator tank
TF-616 = Data channel ID for local liquid temperature measurement, °F
TF-617 = Data channel ID for local vapor temperature measurement, °F

As identified previously, both liquid and vapor flow meters have an associated local fluid temperature used to evaluate the thermodynamic properties of the liquid and vapor phases in the ADS 1-3 separator.

Step 3: Using the compensated liquid level and the ADS 1-3 separator volume as a function of height (see Table 4.6-2), determine the volume of liquid in the ADS 1-3 separator as:

$$V_{ADS\ 1\text{-}3\ SEP,\ f} = V(l)_{ADS\ 1\text{-}3\ SEP} \times LDP\text{-}610_{COMP} \qquad 4.6\text{-}4$$

where:

V(l) = Volume of the ADS 1-3 separator as a function of elevation, $in.^3/in.$

$LDP\text{-}610_{COMP}$ = Compensated fluid levels data from level transducer LDP-610, in.

Step 4: Liquid mass inventory in the ADS 1-3 separator is now calculated as:

$$M_{ADS\ 1\text{-}3\ SEP,\ f} = \rho_{ADS\ 1\text{-}3,\ f} \times V_{ADS\ 1\text{-}3\ SEP,\ f} \qquad 4.6\text{-}5$$

Vapor mass in the separator is then calculated as:

$$M_{ADS\ 1\text{-}3\ SEP,\ g} = \rho_{ADS\ 1\text{-}3,\ g} \times (V_{ADS\ 1\text{-}3\ SEP,\ TOT} - V_{ADS\ 1\text{-}3\ SEP,\ f}) \qquad 4.6\text{-}6$$

where the subscript:

TOT = Total volume of ADS 1-3 separator, $ft.^3$

Step 5: The rate of change in mass inventory of the break separator tank may be approximated by differencing two consecutive calculated values of liquid and vapor mass:

$$\frac{dM_{ADS\ 1\text{-}3\ SEP}}{dt} \approx \frac{\Delta M_{ADS\ 1\text{-}3\ SEP}}{\Delta t} = \frac{M_{ADS\ 1\text{-}3\ SEP,\ f,\ i} - M_{ADS\ 1\text{-}3\ SEP,\ f,\ i-1}}{t_i - t_{i-1}}$$

$$+ \frac{M_{ADS\ 1\text{-}3\ SEP,\ g,\ i} - M_{ADS\ 1\text{-}3\ SEP,\ g,\ i-1}}{t_i - t_{i-1}} \qquad 4.6\text{-}7$$

where the subscript:

i = Index of data and time arrays

4.6.2 Steam Flow Rates

The density of steam in the ADS 1-3 exhaust line, evaluated using the pressure and temperature inputs from the data channels identified in Table 4.6-3, is used to calculate the steam mass flow rate through the ADS 1-3 valves as:

$$\dot{M}_{ADS\ 1\text{-}3,\ g} = C_1 \times \rho_{ADS\ 1\text{-}3,\ g} \times W_{FVM\text{-}601} \qquad 4.6\text{-}8$$

where:

W = = Volumetric flow rate of steam, $ft.^3/min$
C_1 = Conversion constant, minutes to seconds

and the subscript:

FVM-601 = Instrument channel ID for steam vapor flow meter in line between ADS 1-3 separator and sparger

4.6.3 Liquid Flow Rates

Liquid from ADS 1-3 is ducted from the separator through a magnetic flow meter into a header where it is mixed with steam flow before passing to the sparger in the IRWST. Mass flow from the ADS 1-3 separator to the sparger is calculated as:

$$\dot{M}_{ADS\ 1\text{-}3,\ f} = C_2 \times \rho_{ADS\ 1\text{-}3,\ f} \times W_{FMM\text{-}601} \qquad 4.6\text{-}9$$

where:

W = Volumetric flow rate of liquid, gpm
C_2 = Conversion constant, gpm to $ft.^3/sec.$

and the subscript:

FMM-601 = Instrument channel ID for liquid flow meter in line between ADS 1-3 separator and sparger

The density of the liquid passing through the flow meter is evaluated using data from the pressure and temperature instruments identified in Table 4.6-3.

4.6.4 Total Flow Rate

The total liquid and vapor flows through ADS 1-3 are then calculated as:

$$\dot{M}_{ADS\ 1\text{-}3,\ f} = \dot{M}_{FMM\text{-}601} + \frac{\Delta M_{ADS\ 1\text{-}3,\ f}}{\Delta t} \qquad 4.6\text{-}10$$

$$\dot{M}_{ADS\ 1\text{-}3,\ g} = \dot{M}_{FVM\text{-}601} + \frac{\Delta M_{ADS\ 1\text{-}3,\ g}}{\Delta t} \qquad 4.6\text{-}11$$

The total flow through the ADS is zero when the three ADS 1-3 valves are closed. Thus, the above total liquid and vapor flows are used only when at least one valve is open.

The total flow through the ADS (for $t \geq$ valve open time) is then calculated as:

$$\dot{M}_{ADS\ 1\text{-}3,\ TOTAL} = \dot{M}_{ADS\ 1\text{-}3,\ f} + \dot{M}_{ADS\ 1\text{-}3,\ g} \qquad 4.6\text{-}12$$

For $t <$ valve open time, $\dot{M}_{ADS\ 1\text{-}3} = 0$.

The total mass flow rate is integrating step-wise over time to calculate the total mass inventory passed by the ADS 1-3:

$$M_{ADS\ 1\text{-}3} = \sum (\dot{M}_{ADS\ 1\text{-}3,\ TOTAL} \times \Delta t) \qquad 4.6\text{-}13$$

The flow quality of the ADS 1-3 flow is also calculated as:

$$X = \frac{\dot{M}_{ADS\ 1\text{-}3,\ g}}{\dot{M}_{ADS\ 1\text{-}3,\ TOTAL}} \qquad 4.6\text{-}14$$

4.6.5 Energy Balance

Energy flow through ADS 1-3 consists of the following:

- Rate of change in stored energy of the ADS 1-3 separator liquid and steam inventory
- Energy transport rate from the ADS 1-3 separator by exiting steam flow
- Energy transport rate from the ADS 1-3 separator by exiting liquid flow
- Rate of change in stored energy of the ADS 1-3 metal components
- Rate of energy loss from the ADS 1-3 components to the environment

The expressions for evaluating these five energy transfer or transport terms are developed in the following sections.

The combination of these five terms results in energy rate equation 4.6-2. Consistent with the influence of valve position on total flow equation 4.6-12, the energy flow rate through the ADS is zero when the three ADS 1-3 valves are closed. Thus:

$Q_{ADS\ 1\text{-}3} = 0$, for the t < valve open time.

4.6.5.1 Rate of Change in Stored Energy of the Automatic Depressurization System 1-3 Separator Liquid and Steam Inventory

The rate of change of energy in the liquid and steam in the ADS 1-3 separator may be expressed as:

$$Q_{ADS\ 1\text{-}3} = c_P \frac{d(M_{ADS\ 1\text{-}3\ SEP}\ T)}{dt}$$

$$= c_{P,f}\,(T_f - T_{ref})\,\frac{d(M_{ADS\ 1\text{-}3\ SEP,\ f})}{dt} + c_{P,f}\,M_{ADS\ 1\text{-}3\ SEP,\ f}\,\frac{d(T_f)}{dt} \qquad 4.6\text{-}15$$

$$+ c_{P,g}\,(T_g - T_{ref})\,\frac{d(M_{ADS\ 1\text{-}3\ SEP,\ g})}{dt} + c_{P,g}\,M_{ADS\ 1\text{-}3\ SEP,\ g}\,\frac{d(T_g)}{dt}$$

where:

$T_{ref} = 32°F$

Expressing the previous equation as a difference and solving for consecutive data, the rate of change of energy of the fluid in the ADS 1-3 separator is calculated:

$$c_p \frac{\Delta(M_{ADS\ 1\text{-}3\ SEP}\ T)}{\Delta t}$$

$$= c_{P,f}\,(T_f - T_{ref})\,\frac{\Delta(M_{ADS\ 1\text{-}3\ SEP,f})}{\Delta t} + c_{P,f}\,M_{ADS\ 1\text{-}3\ SEP,f}\,\frac{\Delta(T_f)}{\Delta t} \qquad 4.6\text{-}16$$

$$+ c_{P,g}\,(T_g - T_{ref})\,\frac{\Delta(M_{ADS\ 1\text{-}3\ SEP,g})}{\Delta t} + c_{P,g}\,M_{ADS\ 1\text{-}3\ SEP,g}\,\frac{\Delta(T_g)}{\Delta t}$$

The specific heats of the liquid and vapor phases, $c_{P,f}$ and $c_{P,g}$ respectively, are evaluated using the output of the data channels identified in Table 4.6-2.

4.6.5.2 Energy Transport Rate from the Automatic Depressurization System 1-3 Separator by Exiting Steam Flow

The enthalpy of the steam exhaust from the ADS 1-3 separator is determined using the output from the pressure and temperature sensors associated with FVM-601 (Table 4.6-2):

$$h_{FVM\text{-}601,g} = h_g\,(PT\text{-}605,\ TF\text{-}617) \qquad 4.6\text{-}17$$

FVM-601 is the data channel ID for the ADS 1-3 vapor flow meter, and PT-605 and TF-617 denote the vapor pressure and temperatures, respectively, associated with that flow meter.

The rate of energy transport of the ADS 1-3 flow due to the steam component, then, is expressed as:

$$Q_{ADS\ 1\text{-}3,g} = \dot{M}_{ADS\ 1\text{-}3,g} \times h_{FVM\text{-}601,g} \qquad 4.6\text{-}18$$

4.6.5.3 Energy Transport Rate from the Automatic Depressurization System 1-3 Separator by Exiting Liquid Flow

The enthalpy of ADS liquid flow is determined using the output from the pressure and temperature sensors associated with FMM-601 (Table 4.6-2):

$$h_{FMM\text{-}601,f} = h_f\,(PT\text{-}605,\ TF\text{-}616) \qquad 4.6\text{-}19$$

FMM-601 is the data channel ID of the ADS 1-3 liquid flow meter, and PT-605 and TF-616 denote the data channel IDs for the liquid pressure and temperatures, respectively, associated with that flow meter.

The rate of energy transport due to ADS 1-3 liquid flow, then, is expressed as:

$$Q_{ADS\ 1\text{-}3,\ f} = \dot{M}_{ADS\ 1\text{-}3,\ f} \times h_{FMM\text{-}601,\ f} \qquad 4.6\text{-}20$$

4.6.5.4 Rate of Change in Stored Energy of the Automatic Depressurization System 1-3 Metal Components

The ADS is heat-traced downstream from the ADS valves. Therefore, the change in stored energy of the ADS piping due to energy loss from the fluid is negligible.

4.6.5.5 Rate of Energy Loss from the Automatic Depressurization System 1-3 Components to the Environment

Piping between the ADS 1-3 valves and the separator, and between the separator and the IRWST were provided with heat-tracing. This had the effect of off-setting any energy loss to the ambient environment. Thus, for the purpose of evaluating the rate of energy loss from the fluid to the ambient environment (through piping):

$$Q_{AMB} \equiv 0.0 \qquad 4.6\text{-}21$$

TABLE 4.6-1 INSTRUMENTATION TO BE USED FOR ADS 1-3 LEVELS INSTRUMENT CORRECTION				
Location	**Function**	**Level Transducer**	**Pressure Transducer**	**Fluid Temperature**
ADS 1-3 Separator	Density compensation of levels data	LDP-610	PT-605	TF-616

TABLE 4.6-2 VOLUME VERSUS HEIGHT FOR ADS 1-3 VOLUME CALCULATIONS	
Height (in.)	**Volume ($in.^3$)**
0.	656.
86.5	2858.
98.72	4436.
121.72	11013.
140.62	16047.
146.87	17725.

TABLE 4.6-3 ADS 1-3 SEPARATOR STEAM AND LIQUID PRESSURE AND TEMPERATURE INSTRUMENT CHANNELS			
Flow Meter Description	**Flow Meter Channel ID**	**Pressure Channel ID**	**Temperature Channel ID**
ADS 1-3 separator steam flow	FVM-601	PT-605	TF-617
ADS 1-3 separator liquid flow	FMM-601	PT-605	TF-616

4.7 Automatic Depressurization System-4 Separators

The ADS provides a means of depressurizing the RCS in a controlled, staged manner through the use of four pairs of valves, with each valve pair sequenced so that they will open at different primary system pressures. Mass, flow, and energy calculations associated with the first three pairs of valves, called ADS 1-3, are described in Section 4.6. A redundant fourth pair of valves, are located on each of the two hot legs and exhaust directly to the containment atmosphere. The ADS-4 valves are used to complete depressurization of the RCS to near containment pressure.

The ADS-4 flow paths were simulated in the OSU test facility by a valve, a steam/water separator tank, a vortex (vapor) flow meter, a magnetic (liquid) flow meter, and associated piping from each of the two hot legs. During testing, flow through the two ADS-4 flow paths was measured by separating the vapor and liquid components of the flow, measuring the flow rate of the component flows, recombining the flows, then directing the total metered flow to a simulation of the containment sump.

Flow through each of the ADS-4 flow paths may be calculated as:

$$\dot{M}_{ADS\ 4\text{-}X} = \dot{M}_{ADS\ 4\text{-}X,\ f} + \dot{M}_{ADS\ 4\text{-}X,\ g} + \frac{dM_{ADS\ 4\text{-}X\ SEP}}{dt} \qquad 4.7\text{-}1$$

where the subscripts:

ADS-4	=	Fourth-stage ADS
X	=	Hot leg to which the flow path is connected where: X = 1, for HL-1 X = 2, for HL-2
f	=	Liquid component of ADS-4 flow
SEP	=	Steam water separator tank for ADS-4
g	=	Vapor (steam) component of ADS-4 flow

The total ADS-4 flow rate is then calculated as:

$$\dot{M}_{ADS\ 4} = \dot{M}_{ADS\ 4\text{-}1} + \dot{M}_{ADS\ 4\text{-}2} \qquad 4.7\text{-}2$$

Energy is transported out of the primary system by the ADS-4 vapor and liquid flows. Also, the stored energy of the ADS-4 separator liquid inventory may change due to a change in the amount of liquid in the separator, a change in temperature of the liquid inventory in the separator, or a change in the temperature of the separator tank metal mass. Accounting for these terms, the energy equation for ADS-4 flow may be expressed as:

$$Q_{ADS\ 4\text{-}X} = Q_{ADS\ 4\text{-}X,\ f} + Q_{ADS\ 4\text{-}X,\ g} + c_P \frac{d\ (\ M_{ADS\ 4\text{-}X\ SEP}\ T_f\ )}{dt} \qquad 4.7\text{-}3$$

$$+ Q_{ADS\ 4\text{-}X,\ METAL} + Q_{ADS\ 4\text{-}X,\ AMB}$$

where the subscripts:

METAL	=	Metal mass of the ADS-4 separator tank and associated piping
AMB	=	Energy loss to ambient environment

The total energy associated with the ADS-4 (accounting for both separators) is calculated by summing the terms in the previous equation for each of the two separators.

4.7.1 Automatic Depressurization System-4 Separator Liquid Inventory

The ADS-4 separator is, in its simplest form, a tank. Liquid inventory in the ADS-4 separators is monitored by level transducers. The functional steps and associated system of equations for operating on the output from the ADS-4 separator level transducers to calculate inventory mass in the separator tanks are:

Step 1: A differential head is calculated to account for the orifice in the liquid line. The inputs to this calculation are: pipe diameter, beta ratio of orifice to pipe restriction (β=1.0 = no orifice), pressure, temperature, and liquid flow. The output differential head is added to the measured LDP value. The readings are compensated (adjusted for orifice effect) from the ADS-4 separator level transducers listed in Table 4.7-1 to account for temperature differences between fluid in the separator tank and fluid in the reference leg of the instrument line. The local pressure and fluid temperature instruments used to accomplish the compensation are also identified in Table 4.7-1.

Step 2: The local pressures and temperatures from the instruments identified in Table 4.7-1 are used to calculate the density of the liquid and vapor in the ADS-4 separator:

$$\rho_{f,\ ADS\ 4\text{-}X} = \rho_f\ (PT\text{-}YYY,\ TF\text{-}ZZL)$$

$$\rho_{g,\ ADS\ 4\text{-}X} = \rho_g\ (PT\text{-}YYY,\ TF\text{-}ZZV) \qquad 4.7\text{-}4$$

where:

PT-YYY	=	Channel ID for local pressure measurement in ADS-4 separator tank
TF-ZZL,	=	Channel ID for local temperature measurement of liquid exiting ADS-4 separator
TF-ZZV	=	Channel ID for local temperature measurement of vapor exiting ADS-4 separator

As noted previously, both liquid and vapor flow meters have an associated local fluid temperature used to evaluate the thermodynamic properties of the liquid and vapor phases in the ADS-4 separator.

Step 3: Using the compensated liquid level and the ADS-4 separator volume as a function of height, determine the volume of liquid in the ADS-4 separator as:

$$V_{\text{ADS 4-X SEP, f}} = V(l)_{\text{ADS 4-X SEP}} \times \text{LDP-XXX}_{\text{COMP}} \qquad 4.7\text{-}5$$

where:

V(l)	=	Volume of ADS-4 separator as a function of elevation, $ft.^3/ft.$ (Tables 4.7-4 and 4.7-5)
$\text{LDP-XXX}_{\text{COMP}}$	=	Compensated fluid level data from level transducer for ADS-4 separator, ft. XXX = 611 for ADS 4-1 separator XXX = 612 for ADS 4-2 separator

Step 4: Liquid mass inventory in the ADS-4 separator is now calculated as:

$$M_{\text{ADS 4-X SEP}} = \rho_{\text{f, ADS 4-X}} \times V_{\text{f, ADS 4-X SEP}} \qquad 4.7\text{-}6$$

The vapor mass inventory of an ADS-4 separator is then calculated as:

$$M_{\text{ADS 4-x SEP, g}} = \rho_g \times (V_{\text{ADS 4-X SEP, TOTAL}} - V_{\text{ADS 4-X SEP, f}}) \qquad 4.7\text{-}7$$

where the subscript:

TOTAL	=	Total volume associated with an ADS-4 separator, $ft.^3$

Step 5: The rate of change in mass inventory of an ADS separator tank may be calculated by differencing two consecutive calculated values of the liquid and vapor masses:

$$\frac{dM_{ADS\ 4\text{-}X\ SEP}}{dt} = \frac{\Delta M_{ADS\ 4\text{-}X\ SEP}}{\Delta t}$$

$$= \frac{M_{ADS\ 4\text{-}X\ SEP,\ f,\ i} - M_{ADS\ 4\text{-}X\ SEP,\ f,\ i\text{-}1}}{t_i - t_{i\text{-}1}} \qquad 4.7\text{-}8$$

$$+ \frac{M_{ADS\ 4\text{-}X\ SEP,\ g,\ i} - M_{ADS\ 4\text{-}X\ SEP,\ g,\ i\text{-}1}}{t_i - t_{i\text{-}1}}$$

where the subscript:

i = Index of data and time arrays

4.7.2 Steam Flow Rates

The density of steam in the exhaust line from the ADS-4 separator is evaluated using the ASME steam table routines with pressure and temperature inputs from the data channels identified in Table 4.7-2. Using this density, the steam portion of flow through the ADS-4 valves is calculated as:

$$\dot{M}_{ADS\ 4\text{-}X,\ g} = C \times \rho_g \times W_{FVM\text{-}XXX} \qquad 4.7\text{-}9$$

where:

W = Volumetric flow rate of steam, $ft.^3$/min.
C = Conversion constant, minutes to seconds

and the subscript:

FVM-XXX = Instrument channel ID for steam vapor flow meter
XXX = 603 for ADS 4-1 separator
XXX = 602 for ADS 4-2 separator

4.7.3 Liquid Flow Rates

Liquid from ADS-4 is directed from the separator through a magnetic flow meter into the primary sump tank. Mass flow from the ADS-4 separator to the primary sump is calculated as:

$$\dot{M}_{ADS\ 4\text{-}X,\ f} = C_1 \times \rho_{ADS\ 4\text{-}X,\ f} \times W_{FMM\text{-}XXX} \qquad 4.7\text{-}10$$

where:

W	=	Volumetric flow rate of liquid, gpm
C_1	=	Conversion constant, gpm to $ft.^3$/sec.

and the subscript:

FMM-XXX	=	Instrument channel ID for liquid flow meter
		XXX = 603 for ADS 4-1 separator
		XXX = 602 for ADS 4-2 separator

The density of the liquid passing through the flow meter is determined using data from the pressure and temperature instruments identified in Table 4.7-2.

Minimum Flow Criteria:

Until the measured level from LDP-502 or LDP-507 is less than an input threshold value, all mass flow rates are set to zero.

4.7.4 Total Flow Rate

Total liquid and vapor flow through ADS-4 are then calculated as:

$$\dot{M}_{ADS\ 4\text{-}X,\ f} = \dot{M}_{FMM\text{-}XXX} + \frac{\Delta M_{ADS\ 4\text{-}X,\ f}}{\Delta t} \qquad 4.7\text{-}11$$

$$\dot{M}_{ADS\ 4\text{-}X,\ g} = \dot{M}_{FVM\text{-}XXX} + \frac{\Delta M_{ADS\ 4\text{-}X,\ g}}{\Delta t} \qquad 4.7\text{-}12$$

Total flow through one ADS-4 flow path is then calculated as:

$$\dot{M}_{ADS\ 4\text{-}X} = \dot{M}_{ADS\ 4\text{-}X,\ f} + \dot{M}_{ADS\ 4\text{-}X,\ g} \qquad 4.7\text{-}13$$

The total ADS-4 flow rate is calculated by summing the total flow rate for each of the two flow paths. The total mass passed by ADS-4 is calculated by integrating step-wise over time:

$$M_{ADS\ 4,\ TOTAL} = \sum \left(\dot{M}_{ADS\ 4\text{-}1,\ TOTAL} + \dot{M}_{ADS\ 4\text{-}2,\ TOTAL} \right) \times \Delta t \qquad 4.7\text{-}14$$

The flow quality of the each of the ADS-4 flow paths is also calculated as:

$$X_{ADS\ 4\text{-}X} = \frac{\dot{M}_{ADS\ 4\text{-}X,\ g}}{\dot{M}_{ADS\ 4\text{-}X,\ TOTAL}} \qquad 4.7\text{-}15$$

Calculation of Local Flow Qualities:

Flow qualities are calculated at several locations to provide results for comparison against code predictions for modeled system boundaries. This is accomplished by calculating the flow quality at a separator for the ADS flows and then calculating the quality at the point of interest in the test facility by assuming the expansion process associated with the exhaust line is isentropic (constant entropy).

The entropy associated with the flow to the separator is:

$$S_{SEP} = (1 - X_{SEP})\ S_{f,SEP} + X_{SEP} S_{g,SEP} \qquad 4.7\text{-}16$$

The entropy at the location of interest is calculated as a function of the local temperature and pressure at that location.

$$S_{g,\ LOCAL} = S\ (P,\ T_g) \qquad 4.7\text{-}17$$

$$S_{f,\ LOCAL} = S\ (P,\ T_f) \qquad 4.7\text{-}18$$

The entropy of vaporization is calculated as:

$$S_{fg,\,LOCAL} = S_{g,\,LOCAL} - S_{f,\,LOCAL} \qquad 4.7\text{-}19$$

The local flow quality at the location of interest is calculated as:

$$X_{LOCAL} = \frac{S_{SEP} - S_{g,\,LOCAL}}{S_{fg}} \qquad 4.7\text{-}20$$

The calculation for X_{LOCAL} is performed at four locations: ADS 1-3 separator, ADS 4-1 separator, ADS 4-2 separator, and the break separator. The instruments used are identified in Table 4.7-3.

4.7.5 Energy Balance

Energy flow through the ADS-4 separator consists of the following:

- Rate of change in stored energy of the ADS-4 separator fluid inventory
- Energy transport rate from the ADS-4 separator by exiting steam flow
- Energy transport rate from the ADS-4 separator by exiting liquid flow
- Rate of change in stored energy of the ADS-4 metal components
- Rate of energy loss from the ADS-4 components to the environment

The expressions for evaluating these five energy transfer or transport terms are developed in the following sections.

4.7.5.1 Rate of Change in Stored Energy of the Automatic Depressurization System-4 Separator Fluid Inventory

The rate of change of energy associated with the fluid (both steam and liquid) inventory of a ADS-4 separator may be expressed as:

$$Q_{ADS\ 4\text{-}X\ SEP} = c_{P,f} \frac{d\left(M_{ADS\ 4\text{-}X\ SEP}\ T_f\right)}{dt}$$

$$= c_{P,f}\left(T_f - T_{REF}\right) \frac{d\left(M_{ADS\ 4\text{-}X\ SEP,f}\right)}{dt}$$

$$+ c_{P,f}\ M_{ADS\ 4\text{-}X\ SEP,f} \frac{d(T_f)}{dt} \qquad 4.7\text{-}21$$

$$+ c_{P,g}\left(T_g - T_{REF}\right) \frac{d\left(M_{ADS\ 4\text{-}X\ SEP,g}\right)}{\Delta t} + c_{P,g}\ M_{ADS\ 4\text{-}X\ SEP,g} \frac{d\left(T_g\right)}{dt}$$

Expressing the previous equation as a difference:

$$c_{P,f} \frac{d(M_{ADS\ 4\text{-}X\ SEP}\ T_f)}{dt} = c_{P,f}\left(T_f - T_{REF}\right) \frac{\Delta M_{ADS\ 4\text{-}X\ SEP,f}}{\Delta t}$$

$$+ c_{P,f}\ M_{ADS\ 4\text{-}X\ SEP,f} \frac{\Delta T_f}{\Delta t} \qquad 4.7\text{-}22$$

$$+ c_{P,g}\left(T_g - T_{REF}\right) \frac{\Delta M_{ADS\ 4\text{-}X\ ,g}}{\Delta t} + c_{P,g}\ M_{ADS\ 4\text{-}X\ SEP,g} \frac{\Delta T_g}{\Delta t}$$

Expanding the terms on the right-hand side of the equation:

$$c_{P,f}\,(T_f - T_{REF})\,\frac{\Delta M_{ADS\ 4\text{-}X\ SEP,\ f}}{\Delta t}$$

$$= c_{P,f}\,(T_{f,i} - T_{REF})\,\frac{M_{ADS\ 4\text{-}X\ SEP,\ f,\ i} - M_{ADS\ 4\text{-}X\ SEP,\ f,\ i-1}}{t_i - t_{i-1}} \qquad 4.7\text{-}23$$

$$c_{P,f}\,M_{ADS\ 4\text{-}X\ SEP,\ f}\,\frac{\Delta T_f}{\Delta t} = c_{P,f}\,M_{ADS\ 4\text{-}X\ SEP,\ f,\ i}\,\frac{T_{f,i} - T_{f,i-1}}{t_i - t_{i-1}}$$

$$c_{P,g}\,(T_g - T_{REF})\,\frac{\Delta M_{ADS\ 4\text{-}X\ SEP,\ g}}{\Delta t}$$

$$= c_{P,g}\,(T_{g,i} - T_{REF})\,\frac{M_{ADS\ 4\text{-}X\ SEP,\ g,\ i} - M_{ADS\ 4\text{-}x\ SEP,\ g,\ i-1}}{t_i - t_{i-1}} \qquad 4.7\text{-}24$$

$$c_{P,g}\,M_{ADS\ 4\text{-}X\ SEP,\ g}\,\frac{\Delta T_g}{\Delta t} = c_{P,g}\,M_{ADS\ 4\text{-}X\ SEP,\ g,\ i}\,\frac{T_{g,i} - T_{g,i-1}}{t_i - t_{i-1}}$$

where:

i = Index of data and time arrays

The specific heat of the liquid, $c_{P,f}$, is evaluated using the pressures and temperatures measured using the instruments identified in Table 4.7-2. The total change in energy associated with the change in inventory of the two ADS-4 separators is then calculated as:

$$Q_{ADS\ 4} = Q_{ADS\ 4\text{-}1} + Q_{ADS\ 4\text{-}2} \qquad 4.7\text{-}25$$

4.7.5.2 Energy Transport Rate from the Automatic Depressurization System-4 Separator by Exiting Steam Flow

The enthalpy of the steam exhaust from the ADS-4 separator is evaluated using the output from the pressure and temperature sensors associated with vapor flow meters (Table 4.7-2):

$$h_{g,\ FVM\text{-}XXX} = h_g(PT\text{-}XXX,\ TF\text{-}XXX) \qquad 4.7\text{-}26$$

FVM-XXX is the data channel ID for the ADS-4 vapor flow meter, and PT-XXX and TF-XXX denote the vapor pressure and temperatures, respectively, associated with that flow meter. The rate of energy transport of the ADS-4 flow due to the steam component, then, is expressed as:

$$Q_{ADS\ 4\text{-}X,\ g} = \dot{M}_{ADS\ 4\text{-}X,\ g} \times h_{g,\ FVM\text{-}XXX} \qquad 4.7\text{-}27$$

The energy transport associated with steam flow from the two ADS-4 separators is then calculated as:

$$Q_{ADS\ 4,\ g} = Q_{ADS\ 4\text{-}1,\ g} + Q_{ADS\ 4\text{-}2,\ g} \qquad 4.7\text{-}28$$

4.7.5.3 Energy Transport Rate from the Automatic Depressurization System-4 Separator by Exiting Liquid Flow

The enthalpy of the ADS liquid flow is determined using the output from the pressure and temperature sensors associated with the liquid flow meters as given in Table 4.7-2:

$$h_{f,\ FMM\text{-}XXX} = h_f\ (PT\text{-}XXX,\ TF\text{-}XXX) \qquad 4.7\text{-}29$$

FMM-XXX is the data channel ID of the ADS-4 liquid flow meter of interest, and PT-XXX and TF-XXX denote the data channel IDs for the liquid pressure and temperatures, respectively, associated with that flow meter. The rate of energy transport due to liquid flow from the ADS-4 separator, then, is expressed as:

$$Q_{ADS\ 4\text{-}X,\ f} = \dot{M}_{ADS\ 4\text{-}X,\ f} \times h_{f,\ FMM\text{-}XXX} \qquad 4.7\text{-}30$$

The total energy transport associated with liquid flow from the two ADS-4 separators is then calculated as:

$$Q_{ADS\ 4,\ f} = Q_{ADS\ 4\text{-}1,\ f} + Q_{ADS\ 4\text{-}2,\ f} \qquad 4.7\text{-}31$$

4.7.5.4 Rate of Change in Stored Energy of the Automatic Depressurization System-4 Metal Components

The ADS system is heat-traced and, therefore, the change in stored energy of the ADS metal components due to energy loss from the fluid is negligible.

4.7.5.5 Rate of Energy Loss from the Automatic Depressurization System-4 Components to the Environment

The rate of energy loss from the ADS-4 separator and its associated piping to the environment is taken to be zero since the separator and steam exhaust line are heat-traced. Thus, the separator and steam lines are treated as an adiabatic boundary.

4.7.5.6 Fluid Stored Energy

For use in the overall system energy balance calculations, the fluid stored energy in each of the two ADS-4 separators is given by the following:

$$U_{ADS\ 4} = U_{f,\ ADS\ 4} + U_{g,\ ADS\ 4} \qquad 4.7\text{-}32$$

where:

$$U_{f,\ ADS\ 4} = M_{f,\ ADS\ 4} \times c_{P,f,\ ADS\ 4} \times (T_{f,\ ADS\ 4} - T_{ref}) \qquad 4.7\text{-}33$$

and:

$$U_{g,\ ADS\ 4} = M_{g,\ ADS\ 4} \times c_{P,g,\ ADS\ 4} \times (T_{g,\ ADS\ 4} - T_{ref}) \qquad 4.7\text{-}34$$

TABLE 4.7-1 INSTRUMENTATION TO BE USED FOR ADS-4 SEPARATOR LEVELS INSTRUMENT CORRECTION				
Location	**Function**	**Level Transducer**	**Pressure Transducer**	**Fluid Temperature**
ADS 4-1 Separator	Density compensation of levels data	LDP-611	PT-611	TF-619
ADS 4-2 Separator	Density compensation of levels data	LDP-612	PT-610	TF-618

TABLE 4.7-2 ADS-4 SEPARATOR STEAM AND LIQUID PRESSURE AND TEMPERATURE INSTRUMENT CHANNELS			
Flow Meter Description	**Flow Meter Channel ID**	**Pressure Channel ID**	**Temperature Channel ID**
ADS Separator 4-1 steam flow	FVM-603	PT-611	TF-623
ADS Separator 4-1 liquid flow	FMM-603	PT-611	TF-619
ADS Separator 4-2 steam flow	FVM-602	PT-610	TF-622
ADS Separator 4-2 liquid flow	FMM-602	PT-610	TF-618

TABLE 4.7-3 INSTRUMENTS TO BE USED IN CALCULATION OF LOCAL FLOW QUALITIES				
Location	Separator		Local Primary Loop Location	
	Pressure	Temperature	Pressure	Temperature
ADS 1-3 Separator ⇒ Pressurizer	PT-605	TF-616 (liquid) TF-617 (vapor)	PT-604	TF-602 (liquid and vapor)
ADS 4-1 Separator ⇒ HL-1	PT-611	TF-619 (liquid) TF-623 (vapor)	PT-205	TF-609 (liquid and vapor)
ADS 4-2 Separator ⇒ HL-2	PT-610	TF-618 (liquid) TF-622 (vapor)	PT-202	TF-610 (liquid and vapor)
Break Separator ⇒ Break Location	PT-905	TF-912 (liquid) TF-613 (vapor)	Define as a Namelist in Input; Dependant upon Break Location	

TABLE 4.7-4 VOLUME VERSUS HEIGHT FOR ADS 4-1 FLUID VOLUME CALCULATIONS	
Height (in.)	**Volume ($in.^3$)**
0	0
2.0	54.9
27.75	234.4
40.25	1792.0
62.25	8076.0
89.75	16,171.0
100.75	17,232.0

TABLE 4.7-5 VOLUME VERSUS HEIGHT FOR ADS 4-2 FLUID VOLUME CALCULATIONS	
Height (in.)	**Volume ($in.^3$)**
0	0
27.75	96.0
41.25	1672.0
62.5	7843.0
90.75	16,183.0
101.25	17,016.0

4.8 Break Separator

The purpose of the break separator is to separate break flow into liquid and vapor components and to measure the flow rates of the single-phase flow components. Once measured, vapor flow is exhausted to the ambient environment, and liquid is directed to the primary sump simulation of the test facility. The break separator consists of a tank (separator); a vortex (vapor) flow meter; a magnetic (liquid) flow meter; and associated valves, piping, and instrumentation.

The total break flow may be calculated as:

$$\dot{M}_{BREAK} = \dot{M}_{BRK\,LIQ} + \dot{M}_{BRK\,STM} + \frac{dM_{BRK\,SEP}}{dt} \qquad 4.8\text{-}1$$

where the subscripts:

BREAK	=	Total break flow
BRK LIQ	=	Liquid flow from break separator
BRK SEP	=	Break separator tank
BRK STM	=	Steam exhaust from break separator

To address possible reverse flow from the sump to the break separator, a condition of reverse flow is determined by evaluating the level from LDP-901.

If LDP-901 ≥ 75.275 in., then:

$$\dot{M}_{f,BRK\,SEP} = \frac{dM_{SUMP}}{dt} - \dot{M}_{f,ADS4\text{-}1\,SEP} - \dot{M}_{f,ADS4\text{-}2\,SEP} - \dot{M}_{OVRFLW} + \dot{M}_{SUMP\,INJ} \qquad 4.8\text{-}2$$

where:

$\dot{M}_{OVRFLW}$ = Liquid mass flow rate through IRWST overflow line measured by FMM-703

This new value for $\dot{M}_{f,BRK\,SEP}$ is then used in Equation 4.9-1 of Section 4.9, to calculate the general mass balance for the sumps.

Energy is transported out of the primary system by both the vapor and liquid components of break flow. Additionally, the following occurrences cause the stored energy level of the break separator to vary: a change in the fluid inventory held within the separator; a change in temperature of the fluid inventory held within the separator; a change in the temperature of the metal mass of the separator tank or a loss of energy to ambient. Thus, the energy balance for the break separator, accounting for the change in stored energy of both the liquid inventory of the separator and the separator tank, may be expressed as:

$$Q_{BREAK} = Q_{BRK\,LIQ} + Q_{BRK\,STM} + c_P \frac{d(M_{BRK\,SEP}\,\Delta T)}{dt} + Q_{BRK\,SEP\,METAL} + Q_{BRK\,SEP\,AMB} \qquad 4.8\text{-}3$$

where the subscripts:

METAL	=	Metal mass of break separator tank and associated piping
AMB	=	Energy loss to ambient environment

4.8.1 Break Separator Liquid Inventory

The break separator is, in its simplest form, a tank. Liquid inventory in the break separator is monitored by a level transducer. For all tests, with the exception of double-ended DVI line breaks, an orifice was in place within the span of the level transducer. Therefore, a correction was made to the level indication to adjust for the pressure drop through the orifice. The functional steps and associated system of equations for operating on the output from the break separator level transducers to calculate liquid mass in the sump tanks follows:

Step 1: Calculate the pressure drop through the orifice and add this value to the readings from the break separator level transducer listed in Table 4.8-1 to account for the pressure drop through the orifice. The instruments used to measure level, local pressure, and fluid temperature are identified in Table 4.8-1. The flow meters used to calculate the pressure drop are identified in Table 4.8-2.

Step 2: Compensate the adjusted level indication for the break separator level to account for temperature differences between fluid in the separator tank and fluid in the reference leg of the instrument line. The local pressure and fluid temperatures used to accomplish the compensation are also identified in Table 4.8-1.

Step 3: The local pressures and temperatures identified in Table 4.8-2 are used to calculate the density of the fluid in the break separator:

$$\rho_{f,\,BRK\,SEP} = \rho_f(PT\text{-}905,\ TF\text{-}912)$$

$$\rho_{g,\,BRK\,SEP} = \rho_g(PT\text{-}905,\ TF\text{-}913) \qquad 4.8\text{-}4$$

where:

PT-905	=	Local pressure in break separator tank
TF-912	=	Local liquid temperature of fluid in break separator tank
TF-913	=	Local vapor temperature of fluid at break separator exhaust

and the subscripts:

f	=	Liquid phase of water
g	=	Vapor phase of water

There is only one liquid temperature measurement instrument for the break separator, located in the drain line to the primary sump just downstream of flow meter FMM-905. This temperature measurement is used to evaluate the thermodynamic properties of liquid in the break separators.

Step 4: Using the compensated liquid level and the break separator volume as a function of height, determine the volume of liquid in the break separator as:

$$V_{f,\,BRK\,SEP} = V(l)_{BRK\,SEP} \times LDP\text{-}905_{COMP} \qquad 4.8\text{-}5$$

where:

V	=	Volume, $ft.^3$
V(l)	=	Tank (steam/water separator) volume as a function of elevation, $ft.^3/ft.$ (See Table 4.8-3)
$LDP\text{-}905_{COMP}$	=	Compensated fluid levels data from level transducer LDP-905, ft.

Step 5: The liquid mass inventory in the break separator is now calculated as:

$$M_{f,\,BRK\,SEP} = \rho_{f,\,BRK\,SEP} \times V_{f,\,BRK\,SEP} \qquad 4.8\text{-}6$$

The vapor mass inventory of the break separator is then calculated as:

$$M_{g,\ BRK\ SEP} = \rho_g \times (V_{BRK\ SEP,\ TOTAL} - V_{f,\ BRK\ SEP}) \qquad 4.8\text{-}7$$

where the subscript:

TOTAL = Total volume associated with the break separator, ft.^{3}

Step 6: The rate of change in mass inventory of the break separator tank may be calculated by differencing two consecutive calculated values of the liquid and vapor masses:

$$\frac{dM_{BRK\ SEP}}{dt} = \frac{\Delta M_{BRK\ SEP}}{\Delta t} = \frac{M_{f,\ BRK\ SEP,\ i} - M_{f,\ BRK\ SEP,\ i-1}}{t_i - t_{i-1}} + \frac{M_{g,\ BRK\ SEP,\ i} - M_{g,\ BRK\ SEP,\ i-1}}{t_i - t_{i-1}} \qquad 4.8\text{-}8$$

where the subscript:

i = Index of data and time arrays

4.8.2 Steam Flow Rates

The density of steam in the exhaust line from the break separator is evaluated using the pressure and temperature values recorded from the data channels identified in Table 4.8-2. Using this density, the steam portion of the break flow vented to ambient is calculated as:

$$\dot{M}_{FVM\text{-}XXX} = C \times \rho_g \times W_{FVM\text{-}XXX} \qquad 4.8\text{-}9$$

where:

W = Volumetric flow rate of steam, ft.^{3}/min.
C = Conversion constant, minutes to seconds

and the subscript:

FVM-XXX = Instrument channel ID where:
XXX = 905 (6-in. line)
906 (8-in. common exhaust line)

Total break steam flow is calculated as:

$$\dot{M}_{g,\ BRK} = \dot{M}_{FVM-905} + \dot{M}_{FVM-906} + \frac{dM_{g,\ BRK\ SEP}}{dt} \qquad 4.8\text{-}10$$

4.8.3 Liquid Flow Rates

A single line directs liquid flow from the break separator into the primary sump tank. The mass flow from the break separator to the primary sump tank is calculated as:

$$\dot{M}_{FMM-905} = C_1 \times \rho_f \times W_{FMM-905} \qquad 4.8\text{-}11$$

where:

W	=	Volumetric flow rate of liquid, gpm
C_1	=	Conversion constant, gpm to $ft.^3/sec.$

and the subscript:

FMM-905	=	Instrument channel ID for liquid flow meter in line between break separator and primary sump

The density of the liquid passing through the flow meters is determined using data from the pressure and temperature instruments identified in Table 4.8-2.

Total liquid break flow rate passed to the sump simulation is calculated as:

$$\dot{M}_{f,\ BRK} = \dot{M}_{FMM-905} + \frac{dM_{f,\ BRK\ SEP}}{dt} \qquad 4.8\text{-}12$$

4.8.4 Total Flow Rate

The total break flow rate is then calculated as:

$$\dot{M}_{BRK,\ TOTAL} = \dot{M}_{f,\ BRK} + \dot{M}_{g,\ BRK} \qquad 4.8\text{-}13$$

The flow quality of the break flow is also calculated as:

$$X_{BRK} = \frac{\dot{M}_{g,\ BRK}}{\dot{M}_{BRK,\ TOTAL}} \qquad 4.8\text{-}14$$

4.8.5 Energy Balance

The energy flow through the break separator consists of the following:

- Rate of change in stored energy of the break separator fluid inventory
- Energy transport rate from the break separator by steam exhaust flow
- Energy transport rate from the break separator by liquid flow to the sump
- Rate of change in stored energy of the metal of the break separator tank
- Rate of energy loss to the environment

The expressions evaluating these energy transfer or transport terms are developed in the following subsections:

4.8.5.1 Rate of Change in Stored Energy of the Break Separator Fluid Inventory

The rate of change of energy in the break separator fluid may be expressed as:

$$Q_{BRK\ SEP} = c_P \frac{d(M_f\ \Delta T_f)}{dt} = c_{P,\,f}\,(T_f - T_{REF}) \frac{d(M_{f,\,BRK\ SEP})}{dt} + c_{P,\,f}\,M_{f,\,BRK\ SEP} \frac{d(T_f)}{dt} \qquad 4.8\text{-}15$$

where:

ΔT_f	=	$T_f - T_{REF}$
T_{REF}	=	Reference temperature, 32°F
T_f	=	Measured liquid temperature, °F

Expressing the previous equation as a difference:

4.8-16

$$c_{P,\,f} \frac{d(\,M_{f,\,BRK\ SEP}\ T_f\,)}{dt} = c_{P,\,f}\,(T_f - T_{REF}) \frac{\Delta M_{f,\,BRK\ SEP}}{\Delta t} + c_{P,\,f}\,M_{f,\,BRK\ SEP} \frac{\Delta T_f}{\Delta t}$$

Expanding the terms on the right-hand side of the equation:

$$c_{P,\,f}\,(T_f - T_{REF}) \frac{\Delta M_{f,\,BRK\ SEP}}{\Delta t} = c_{P,\,f}\,(T_f - T_{REF}) \frac{M_{f,BRK\ SEP,\,i} - M_{f,BRK\ SEP,\,i-1}}{t_i - t_{i-1}}$$

4.8-17

$$c_{P,\,f}\,M_{f,\,BRK\ SEP} \frac{\Delta T_f}{\Delta t} = c_{P,\,f}\,M_{f,\,BRK\ SEP,\,i} \frac{T_{f,\,i} - T_{f,\,i-1}}{t_i - t_{i-1}}$$

where:

i = Index of data and time array

The specific heat of the liquid, $c_{P,f}$, is evaluated using the pressures and temperatures identified in Table 4.8-1.

The rate of change of energy in the steam in the break separator may be expressed as:

$$c_{P,g} \frac{d(M_{g,\,BRK\,SEP}\,T_g)}{dt} = c_{P,g}\,(T_g - T_{REF})\,T_g \frac{d(M_{g,\,BRK\,SEP})}{dt} + c_{P,g}\,M_{g,\,BRK\,SEP} \frac{d(T_g)}{dt} \quad 4.8\text{-}18$$

Expressing the previous equation as a difference:

$$c_{P,g} \frac{d(M_{g,\,BRK\,SEP}\,T_g)}{dt} \approx c_{P,g}\,(T_g - T_{REF})\,T_g \frac{\Delta M_{g,\,BRK\,SEP}}{\Delta t} + c_{P,g}\,M_{g,\,BRK\,SEP} \frac{\Delta(T_g)}{\Delta t} \quad 4.8\text{-}19$$

Expanding the two terms on the right-hand side of the equation:

$$c_{P,g}\,(T_g - T_{REF})\,T_g \frac{\Delta M_{g,\,BRK\,SEP}}{\Delta t} = c_{P,g}\,(T_g - T_{REF}) \frac{M_{g,\,BRK\,SEP,\,i} - M_{g,\,BRK\,SEP,\,i-1}}{t_i - t_{i-1}}$$

$$c_{P,g}\,M_{g,\,BRK\,SEP} \frac{\Delta T_g}{\Delta t} = c_{P,g}\,M_{g,\,BRK\,SEP,\,i} \frac{T_{g,\,i} - T_{g,\,i-1}}{t_i - t_{i-1}} \quad 4.8\text{-}20$$

The specific heat of the steam, $c_{P,f}$, is evaluated using the pressures and temperatures measured by the instruments identified in Table 4.8-1.

4.8.5.2 Energy Transport Rate from the Break Separator by Steam Exhaust Flow

The enthalpy of the steam exhaust from the break separator is calculated using the output from the pressure and temperature sensors associated with FVM-905 and FVM-906 (Table 4.8-2):

$$h_{g,\,FVM\text{-}XXX} = h_g(PT\text{-}YYY,\ TF\text{-}ZZZ) \quad 4.8\text{-}21$$

FVM-XXX denotes a specific flow meter, and PT-YYY and TF-ZZZ denote the vapor pressure and temperatures associated with that flow meter. The rate of energy transport from the break separator due to exhaust steam, then, is expressed as:

$$Q_{FVM-XXX} = \dot{M}_{FVM-XXX} \times h_{g,\ FVM-XXX} \qquad 4.8\text{-}22$$

where:

$Q_{FVM-XXX}$ = Rate of energy transport due to steam flow through flow meter FVM-XXX

The total energy transport rate, then, is calculated as:

$$Q_{BRK,\ g} = Q_{FVM-905} + Q_{FVM-906} \qquad 4.8\text{-}23$$

4.8.5.3 Energy Transport Rate from the Break Separator by Liquid Flow to the Sump

The enthalpy of liquid flow into the break separator is calculated using the output from the pressure and temperature sensors associated with FMM-905 (Table 4.8-2):

$$h_{f,\ FMM-905} = h_f\ (PT\text{-}905,\ TF\text{-}912) \qquad 4.8\text{-}24$$

FMM-905 denotes the flow meter to which the enthalpy is applicable, and PT-905 and TF-912 denote the liquid pressure and temperatures associated with that flow meter. The rate of energy transport from the break separator due to liquid overflow into the sump, then, is expressed as:

$$Q_{BRK,f} = \dot{M}_{BRK,\ f} \times h_{f,\ FMM-905} \qquad 4.8\text{-}25$$

4.8.5.4 Rate of Change in Stored Energy of the Metal of the Break Separator Tank

The break separator tank and associated piping is heat-traced. Therefore the change of stored energy of the metal components due to energy loss from the fluid is negligible.

4.8.5.5 Rate of Energy Loss to the Environment

The rate of energy loss from the break separator and its associated piping to the environment is zero because the separator and the steam exhaust lines are heat-traced. Thus, the separator and steam lines are treated as an adiabatic boundary. Heat loss to the environment from the liquid drain line running from the break separator to the sump is neglected since the run of pipe is small.

TABLE 4.8-1
INSTRUMENTATION TO BE USED FOR BREAK SEPARATOR MASS AND ENERGY BALANCE

Location	Function	Level Transducer	Pressure Transducer	Fluid Temperature
Break separator	Density compensation of levels data	LDP-905	PT-905	TF-912

TABLE 4.8-2
BREAK SEPARATOR STEAM EXHAUST AND LIQUID PRESSURE AND TEMPERATURE INSTRUMENT CHANNELS

Flow Meter Description	Flow Meter Channel ID	Pressure Channel ID	Temperature Channel ID
Break separator steam exhaust flow	FVM-905	PT-905	TF-915
	FVM-906	0.5 × (PT-902 + PT-905)	TF-918
Break separator liquid flow	FMM-905	PT-905	TF-912

TABLE 4.8-3 VOLUME VERSUS HEIGHT FOR BREAK SEPARATOR FLUID VOLUME CALCULATIONS	
Height (in.)	**Volume ($in.^3$)**
0.0	607.4
39.5	1243.5
55.5	6648.1
81.0	26447.0
82.25	28204.6
88.5	32338.0
106.25	46324.7
136.25	69545.3
145.75	76835.0
151.75	81884.1
181.75	104933.0
196.25	107575.2

4.9 Sumps

In the AP600, the sump collects all liquid released from the primary system and serves as the source of post-accident LTC water inventory. In the OSU test facility, the sump is modeled by two tanks: a primary sump tank and a smaller secondary sump tank. These tanks have associated with them piping, vapor and liquid flow meters, and other pressure and temperature measurement instrumentation.

Accounting for all possible flow paths associated with the sump, the general mass balance on that component may be expressed as:

$$\frac{dM_{SUMP}}{dt} = \dot{M}_{BRK\ SEP} + \dot{M}_{ADS\ 4\text{-}1\ SEP} + \dot{M}_{ADS\ 4\text{-}2\ SEP} + \dot{M}_{IRWST} - \dot{M}_{STM\ XHST} - \dot{M}_{SUMP\ INJ} \qquad 4.9.1$$

where the subscripts are defined as:

SUMP	=	Both primary and secondary sump tanks
BRK SEP	=	Liquid flow from break separator through FMM-905
ADS 4-1 SEP	=	Liquid flow from the ADS 4-1 steam/water separator through FMM-603
ADS 4-2 SEP	=	Liquid flow from the ADS 4-2 steam/water separator through FMM-602
IRWST	=	Liquid overflow from IRWST into sump through FMM-703
STM XHST	=	Steam exhaust from sump through FVM-903
SUMP INJ	=	Liquid flow from sump to DVI line through FMM-901 and FMM-902

Energy is transported into and out of the sump by both the vapor and liquid components of flow associated with the sump. In addition, the stored energy associated with the sump may change due to a change in the liquid inventory held within the sump, a change in temperature of the liquid inventory held within the sump, or a change in the temperature of the metal mass of the sump tanks, or heat loss to the ambient. Thus, the energy balance for the sump, accounting for the change in stored energy of both the liquid inventory of the sump and the sump tank(s) may be expressed as:

$$c_p \frac{d(M_{SUMP}\ T_f)}{dt} = Q_{BRK\ SEP} + Q_{ADS\ 4\text{-}1\ SEP} + Q_{ADS\ 4\text{-}2\ SEP} + Q_{IRWST} - Q_{STM\ XHST} - Q_{SUMP\ INJ} - Q_{SUMP\ METAL} - Q_{SUMP\ AMB} \qquad 4.9\text{-}2$$

where the subscripts are defined as:

METAL	=	Metal mass of sump tanks and associated piping
AMB	=	Energy loss to ambient environment

4.9.1 Sump Liquid Inventory

For convenience, liquid mass in the primary and secondary sump tanks are calculated separately, then summed to yield the total liquid mass in the sump. Liquid inventory in the sump tanks are measured by a level transducer. Load cells installed on the two sump tanks are not used for inventory calculations.

After reviewing the primary- and secondary-sump fluid temperatures for all tests (using thermocouples in Table 4.9-1, and including TF-907 which is located at the top of the primary-sump tank), it was determined that the sump temperatures were always less than the saturation temperature evaluated at the total pressure. It was concluded that 1) the water region clearly remained subcooled in the sump tanks, and 2) it was not possible for a steam region to be supported above the water level in the sump tanks (as occurs in some internal system components, such as the CMTs). The region above the water level is a cool mixture of air and some steam, and an accurate calculation of its composition is not possible since the partial pressure of the steam in the mixture is unknown.

Therefore, steam inventory is not modeled in the sump tanks and the region above the water level is not included in sump inventory.

4.9.1.1 Use of Level Measurement for Mass Calculation

The functional steps and associated system of equations for operating on the output of the sump level transducers to calculate liquid mass in the sump tanks follows:

Step 1: Compensate all readings from the primary and secondary sump level transducers to account for temperature differences between fluid in the tanks and fluid in the reference legs of the instrument lines. The two channels of level data to be compensated are identified in Table 4.9-1. The instruments used to measure local pressure and fluid temperatures to be used to accomplish the compensation are also identified in Table 4.9-1.

Step 2: The local pressures and temperatures as recorded from the instrument channels identified in Table 4.9-1 are used to calculate the density of the liquid in the sump tanks:

$$\rho_{f,j} = \rho_{f,j}(P, T) \qquad 4.9\text{-}3$$

where the subscripts are defined as:

f	=	Liquid phase of water
j	=	Either sump tank

The instrument IDs and the elevation of the instruments for the local fluid temperature measurements to be used in the calculation of fluid densities for both the primary and secondary sumps are given in Table 4.9-1.

Step 3: Using the compensated liquid level and the sump volume as a function of height, determine the volume of liquid in the sump:

$$V_{f,\,j} = V(l)_{SUMP_j} \times LDP\text{-}XXX_{COMP} \qquad 4.9\text{-}4$$

where:

V	=	Volume, $in.^3$
V(l)	=	Volume as a function of elevation, $in.^3/in.$
$LDP\text{-}XXX_{COMP}$	=	Compensated fluid levels data from the level transducer (in.) identified as
		XXX = 901 (primary sump LDP transducer)
		XXX = 902 (secondary sump LDP transducer)

Step 4: The liquid mass inventory in the primary and secondary sump is calculated as:

$$M_{f,\,SUMP\,j} = \rho_{f,\,j} \times V_{f,\,j} \times C \qquad 4.9\text{-}5$$

where:

C	=	Conversion constant, $in.^3$ to $ft.^3$

The total liquid mass inventory in the sump is calculated as:

$$M_{f,\,SUMP} = M_{f,\,SUMP\,P} + M_{f,\,SUMP\,S} \qquad 4.9\text{-}6$$

where the subscripts:

P	=	Primary sump
S	=	Secondary sump

Step 5: The rate of change in mass inventory of the sump tanks may be calculated by differencing two consecutive calculated values of the liquid masses:

$$\frac{dM_{SUMP}}{dt} = \frac{\Delta M_{SUMP}}{\Delta t} = \frac{M_{f,\,SUMP,\,i} - M_{f,\,SUMP,\,i-1}}{t_i - t_{i-1}} \qquad 4.9\text{-}7$$

where the subscript:

i = Index of data and time arrays

4.9.2 Sump Steam Exhaust Flow

Although steam inventory is not modeled in the sump tanks (Subsection 4.9.1), steam exhaust flow can be calculated using a vapor flow meter on either of the two exhaust lines (3/4-in. schedule 40 piping containing FVM-903, and the common 8-in. header containing FVM-906). The meters measure flow in standard cubic feet per minute, scfm.

Positive flow was indicated by these two vapor flow meters at various times during the tests. However, after checking the readings of the exhaust line fluid thermocouples (Table 4.9-2), the temperatures were usually less than their corresponding saturation temperatures (evaluated at the total pressures), although some were above their saturation temperatures. As discussed in Subsection 4.9.1, when vapor-space temperatures are less than saturation, an air/steam mixture may exist and there is no way of accurately measuring how much steam is present.

Therefore, steam exhaust flow modeling was limited to positive vapor flow meter readings in conjunction with fluid thermocouple readings indicating temperatures at or above the saturation temperature.

4.9.2.1 Steam Flow Rates

The density of steam in the 3/4-in. and 8-in. common header exhaust lines is evaluated using the ASME steam table routines with pressure and temperature inputs from the data channels identified in Table 4.9-2. Using these densities, the steam mass flow is calculated as:

$$\dot{M}_{FVM\text{-}XXX} = C_1 \times \rho_{g,\ FVM\text{-}XXX} \times W_{FVM\text{-}XXX} \qquad 4.9\text{-}8$$

where:

W	=	Volumetric flow rate of steam, $ft.^3/min.$
C_1	=	Conversion constant, minutes to seconds

and the subscript:

FVM-XXX	=	Instrument channel ID where:
		XXX = 903 (3/4-in. exhaust line)
		XXX = 906 (8-in. common exhaust line)

The total steam mass flow rate exhausted by the primary sump and the break separator is calculated as:

$$\dot{M}_{STM\ XHST} = \dot{M}_{FVM-903} + \dot{M}_{FVM-906} \qquad 4.9\text{-}9$$

The total steam mass flow is calculated by integrating the mass flow rate step-wise over time:

$$M_{STM\ XHST} = \sum (\dot{M}_{STM\ XHST} \times \Delta t) \qquad 4.9\text{-}10$$

4.9.3 Sump Injection

Two lines provide for liquid to flow from the primary sump into the DVI lines and the reactor pressure vessel simulation. Mass flow from the sump through either of the two sump injection lines is calculated as:

$$\dot{M}_{FMM-XXX} = C_2 \times \rho_{FMM-XXX} \times W_{FMM-XXX} \qquad 4.9\text{-}11$$

where:

W	=	Volumetric flow rate of liquid, gpm
C_2	=	Conversion constant gpm to $ft.^3/sec.$

and the subscript:

FMM-XXX	=	Instrument channel ID where:
		XXX = 901 (piping run to DVI-1)
		XXX = 902 (piping run to DVI-2)

The density of the liquid passing through the flow meters is determined using data from the pressure and temperature instruments identified in Table 4.9-2 as input to the ASME steam tables. The total mass flow rate to the DVI lines from the sump is calculated as:

$$\dot{M}_{SUMP\ INJ} = \dot{M}_{FMM-901} + \dot{M}_{FMM-902} \qquad 4.9\text{-}12$$

The total mass injected by each injection line into the DVI line is calculated by integrating the product of the measured mass flow rates and the time interval over which the measurement is taken:

$$M_{FMM-XXX} = \sum (\dot{M}_{FMM-XXX,\,i} \times \Delta t_i) \qquad 4.9\text{-}13$$

The total liquid mass injected from the sump is calculated as:

$$M_{SUMP\ INJ} = M_{FMM-901} + M_{FMM-902} \qquad 4.9\text{-}14$$

4.9.4 Total Flow Rate Out of the Sump

Total mass flow rate out of the sump is then calculated as:

$$\dot{M}_{SUMP} = \dot{M}_{SUMP\ INJ} + \dot{M}_{STM\ XHST} \qquad 4.9\text{-}15$$

Total mass flow out of the sump is calculated by integrating the mass flow rate step-wise over time:

$$M_{SUMP,\ TOTAL} = \sum \dot{M}_{SUMP} \times \Delta t \qquad 4.9\text{-}16$$

4.9.5 Energy Balance

Energy into the sump from the break separator, the two ADS-4 separators, and the IRWST overflow lines are calculated in and obtained from their respective modules. Thus, the calculation of an energy balance on the sump requires that the following parameters be evaluated:

- Rate of change in stored energy of the sump liquid inventory
- Energy removal rate from the sump by steam exhaust flow
- Energy removal rate from the sump by injection flow supplied to the DVI lines
- Rate of change in stored energy of the metal of the sump tanks
- Rate of energy loss to the environment

The expressions for evaluating these five energy transfer or transport terms are developed in the following sections.

4.9.5.1 Rate of Change in Stored Energy of the Sump Liquid Inventory

The rate of change of energy in the liquid in the sump may be expressed as:

$$c_{P,f} \frac{d(M_{f,SUMP}\ T_f)}{dt} = c_{P,f}\ (T_f - T_{REF}) \frac{d(M_{f,SUMP})}{dt} + c_{P,f}\ M_{f,SUMP} \frac{d(T_f)}{dt} \qquad 4.9\text{-}17$$

Expressing the previous equation as a difference:

$$c_{P,f} \frac{d(M_{f,SUMP}\ T_f)}{dt} = c_{P,f}\ (T_f - T_{REF}) \frac{\Delta M_{f,SUMP}}{\Delta t} + c_{P,f}\ M_{f,SUMP} \frac{\Delta T_f}{\Delta t} \qquad 4.9\text{-}18$$

Expanding the two terms on the right-hand side of the equation:

$$c_{P,f}\,(T_f - T_{REF})\,\frac{\Delta M_{f,\,SUMP}}{\Delta t} = c_{P,f}\,(T_{f,i} - T_{REF})\,\frac{M_{f,\,SUMP,\,i} - M_{f,\,SUMP,\,i-1}}{t_i - t_{i-1}} \qquad 4.9\text{-}19$$

$$c_{P,f}\,M_{f,\,SUMP}\,\frac{\Delta T_f}{\Delta t} = c_{P,f}\,M_{f,\,SUMP,\,i}\,\frac{T_{f,i} - T_{f,i-1}}{t_i - t_{i-1}} \qquad 4.9\text{-}20$$

where:

i = Index of data and time arrays

Each of the terms on the right-hand side of the previous equation is to be evaluated for both the primary and secondary sump tank inventories. The specific heat of the liquid, $c_{P,f}$, is evaluated using the pressures and temperatures identified in Table 4.9-1. Note that, for the primary sump, the specific heat of the liquid may be evaluated for more than one zone or region, depending on the water level in the sump.

4.9.5.2 Energy Removal Rate from the Sump by Steam Exhaust Flow

The enthalpy of the steam exhaust from the sump is calculated using the output from the pressure and temperature sensors associated with FVM-903 and FVM-906 (Table 4.9-2):

$$h_{g,\,FVM\text{-}XXX} = h_g(PT\text{-}YYY,\ TF\text{-}ZZZ) \qquad 4.9\text{-}21$$

FVM-XXX denotes a specific flow meter, and PT-YYY and TF-ZZZ denote the vapor pressure and temperatures associated with that flow meter. The rate of energy transport from the sump due to exhaust steam, then, is expressed as:

$$Q_{FVM\text{-}XXX} = \dot{M}_{FVM\text{-}XXX} \times h_{g,\,FVM\text{-}XXX} \qquad 4.9\text{-}22$$

The total energy transport rate, then, is ca-culated as:

$$Q_{STM\ EXHST} = Q_{FVM\text{-}903} + Q_{FVM\text{-}906} \qquad 4.9\text{-}23$$

4.9.5.3 Energy Removal Rate from the Sump by Injection Flow Supplied to the Direct Vessel Injection Lines

The enthalpy of the injected liquid from the sump is determined using the output from the pressure and temperature sensors associated with FMM-901 and FMM-902 (Table 4.9-2) and the ASME steam table routines. Expressed mathematically:

$$h_{f,\ FMM-XXX} = h_f\ (PT-YYY,\ TF-ZZZ) \qquad 4.9\text{-}24$$

FMM-XXX denotes a specific flow meter, and PT-YYY and TF-ZZZ denote the liquid pressure and temperatures associated with that flow meter. The rate of energy transport from the sump due to injected liquid, then, is expressed as:

$$Q_{FMM-XXX} = \dot{M}_{FMM-XXX} \times h_{f,\ FMM-XXX} \qquad 4.9\text{-}25$$

The total energy transport rate, then, is calculated as:

$$Q_{SUMP\ INJ} = Q_{FMM-901} + Q_{FMM-902} \qquad 4.9\text{-}26$$

4.9.5.4 Rate of Change in Stored Energy of the Metal of the Sump Tanks

The change in stored energy of the sump tanks and associated piping may be expressed as:

$$Q_{SUMP\ METAL} = c_{P,\ METAL}\ M_{SUMP\ METAL}\ \frac{d(\ T_{SUMP\ METAL}\ )}{dt} \qquad 4.9\text{-}27$$

where the subscript:

METAL = Metal of the primary and secondary tanks and all associated piping

For each sump tank, the calculations parallel those for the cold-leg balance lines (see Subsection 4.4.6). Each sump tank is divided into a number of metal segments. Fluid thermocouples are employed to obtain pseudo-metal temperatures when necessary. Tables 4.9-3, 4.9-4, and 4.9-5 list the data required for the calculations.

4.9.5.5 Rate of Energy Loss to the Environment

The rate of energy loss from the sump and its associated piping to the environment may be expressed as:

$$Q_{SUMP\ AMB} = H \times A \times \Delta T \qquad 4.9\text{-}28$$

where:

A = Effective external surface area of the sump, $ft.^2$
H = Overall effective heat transfer coefficient, Btu/(sec.-$ft.^2$-°F)
ΔT = Difference between ambient air temperature and bulk metal temperature, °F

An equivalent heat transfer coefficient, accounting for heat resistance due to any insulation applied to the outside surface of the sump volumes and natural convection from the outside surface to the ambient, is used to evaluate the heat loss to ambient from the metal surfaces of the sump tanks. The same metal surface temperatures used to evaluate metal heat storage of the sumps is used to calculate heat loss to the ambient. Surface areas included in this calculation account for sump tanks and associated piping.

The metal-to-ambient heat transfer calculation methodology for the sumps is similar to methodology used for other insulated components of the system. Each sump tank metal segment is treated as an insulated vertical cylinder. The turbulent range form of the natural convection heat transfer correlation from Reference 16 applies, based upon the conditions of the OSU test facility air at atmospheric pressure and ambient temperature (averaged over the tests). In the radiation heat transfer correlation, an emissivity of 0.8 is assumed.

The detailed calculations and equations are identical to those for the metal-to-ambient heat transfer for the cold-leg balance lines in Subsection 4.4.6, the only exception is that in the final expression for the natural convection heat transfer coefficient, the coefficient multiplier 0.21 is replaced with 0.09 and the exponent 1/4 is replaced with 1/3 (these differences are due to both the vertical orientation and the turbulent range of applicability for the sumps).

TABLE 4.9-1 INSTRUMENTATION TO BE USED FOR SUMP MASS AND ENERGY BALANCE				
Function	**Location**	**Level Transducer**	**Pressure Transducer**	**Fluid Temperature**
Density compensation of level data	Primary sump	LDP-901	PT-901	TF-901 SC-903 TF-905
	Secondary sump	LDP-902	PT-901	SC-902

TABLE 4.9-2 SUMP STEAM EXHAUST AND INJECTION PRESSURE AND TEMPERATURE INSTRUMENT CHANNELS			
Flow Meter Description	**Flow Meter Channel ID**	**Pressure Channel ID**	**Temperature Channel ID**
Sump steam exhaust flow	FVM-903	PT-901	TF-906
	FVM-906	0.5 (PT-901 + PT-905)	TF-918
Sump injection flow	FMM-901	PT-901	TF-909
	FMM-902	PT-901	TF-904

TABLE 4.9-3 DATA FOR SUMPS METAL ENERGY CALCULATIONS (PER SEGMENT)				
Primary Sump Metal Segments				
Metal Segment	**Pseudo-Metal Temperature ID (°F)**	**Metal Mass (lbm)**	**Outer Surface Area ($ft.^2$)**	**Mean Surface Area ($ft.^2$)**
1	TF-901	1907.7	84.65	82.25
2	TFM-901	1677.8	115.70	114.18
3	TF-907	2132.4	84.65	82.25
Secondary Sump Metal Segments				
Metal Segment	**Pseudo-Metal Temperature ID (°F)**	**Metal Mass (lbm)**	**Outer Surface Area ($ft.^2$)**	**Mean Surface Area ($ft.^2$)**
1	SC-902	1096.6	43.43	41.71
2	TFM-902	2889.7	152.93	149.15

TABLE 4.9-4 DATA FOR SUMPS METAL ENERGY CALCULATIONS		
Description	**Primary Sump**	**Secondary Sump**
Ambient temperature ID (°F)	TF-005	TF-005
Insulation thickness (in.)	1.5	1.5
Insulation mean thermal conductivity [(Btu-in.)/(hr.-$ft.^2$-°F)]	0.141	0.141

TABLE 4.9-5 SPECIFIC HEAT CAPACITY VERSUS TEMPERATURE TABLE FOR SUMPS METAL ENERGY CALCULATIONS	
Metal c_p [Btu/(lbm-°F)]	**Metal Temperature (°F)**
0.1085	70.
0.1109	100.
0.1175	200.
0.1223	300.
0.1256	400.
0.1279	500.
0.1297	600.

4.10 Passive Residual Heat Removal

The passive residual heat removal heat exchanger (PRHR HX) consists of a number of tubes with a fluid flow path at the top for the inlet connection from hot leg-2 (HL-2) and a fluid flow path at the bottom for the outlet connection to steam generator-2 (SG-2) channel head. The PRHR HX fluid mass, fluid energy, and tube metal energy conservation equations are described in Subsections 4.10.1, 4.10.2, and 4.10.3, respectively.

4.10.1 Fluid Mass Conservation Equation

The general fluid (H_2O) mass conservation equation, which relates the change in stored fluid mass with respect to time (the fluid-mass time derivative) to the mass flow rates in and out, reduces to the following:

$$\frac{dM_{H_2O,PRHR}}{dt} = \dot{M}_{in\ (from\ HL_2)\ H_2O,PRHR} - \dot{M}_{out\ (to\ SG_2)\ H_2O,PRHR} \qquad 4.10\text{-}1$$

The left-hand side of the fluid mass conservation equation is approximated from the value of the fluid mass at two consecutive time points (denoted by subscripts n-1 and n):

$$\frac{dM_{H_2O,PRHR}}{dt} \approx \frac{\Delta M_{H_2O,PRHR}}{\Delta t} = \frac{M_{H_2O,PRHR,n} - M_{H_2O,PRHR,n-1}}{t_n - t_{n-1}} \qquad 4.10\text{-}2$$

The H_2O fluid mass is simply the sum of the water and steam masses:

$$M_{H_2O,PRHR} = M_{f,PRHR} + M_{g,PRHR} \qquad 4.10\text{-}3$$

The water and steam mass calculations are based on the measured water level. The level (LDP) instrument channel ID for PRHR is listed in Table 4.10-1. This LDP is corrected for temperature effects using the LDP compensation method. As is generally assumed for each OSU test facility component, zero quality water is modeled below the compensated water level, and 100 percent quality steam is modeled above the compensated water level. This assumption is appropriate because the fluid below the water level is predominantly water, the fluid above the water level is predominantly steam, and any amount of frothing is indeterminate with the available instrumentation.

To use the available measurements from the fluid thermocouples, the PRHR HX is divided into five axial fluid property zones for the calculation of various fluid conditions. Table 4.10-1 contains a list

of the fluid thermocouples employed for each axial fluid property zone, along with the zone top elevations.

Note that, since LDP-802 (which spans just the tubes) is being employed for the water level of the entire PRHR HX (including the inlet and outlet), instead of the usual method of using the axial fluid property zone temperatures/elevations in the LDP compensation calculations, it is necessary to use an alternate set of temperature channels/elevations for the LDP corrections. Table 4.1 1-1 contains a list of the fluid thermocouples employed for each LDP compensation region, along with their elevations. The LDP compensation region boundaries are taken at the vertical midpoint between consecutive fluid thermocouples.

In general, the water and steam masses are given by:

$$M_{f,PRHR} = \sum_{j=1}^{N_{zone,PRHR}} M_{f,PRHR_j}$$

$$M_{g,PRHR} = \sum_{j=1}^{N_{zone,PRHR}} M_{g,PRHR_j} \qquad 4.10\text{-}4$$

where:

$N_{zone,\ PRHR}$ = Number of zones within the PRHR, (5)

For zones j below those containing the compensated water level (which contain all water), the zone j water and steam masses are given by the following. where j = 1,...,levzone-1:

$$M_{f,PRHR_j} = \rho_{f,PRHR_j} \times V_{PRHR_j} \times C$$

$$M_{g,PRHR_j} = 0. \qquad 4.10\text{-}5$$

where:

levzone = The zone containing the compensated water level
C = Conversion constant, $in.^3$ to $ft.^3$

For the zone j containing the compensated water level, the zone j water and steam masses are given by the following, where j = levzone:

$$M_{f,PRHR_j} = \rho_{f,PRHR_j} \times V_{f,PRHR_j} \times C$$

$$M_{g,PRHR_j} = \rho_{g,PRHR_j} \times V_{g,PRHR_j} \times C \qquad 4.10\text{-}6$$

For zones j above those containing the compensated water level (which contain all steam) the zone j water and steam masses are given by the following, where j = levzone+1,...,$N_{zone,PRHR}$:

$$M_{f,PRHR_j} = 0.$$

$$M_{g,PRHR_j} = \rho_{g,PRHR_j} \times V_{PRHR_j} \times C \qquad 4.10\text{-}7$$

The fluid volumes are calculated as a function of level from the volume-versus-height tabular data listed in Table 4.10-2, via linear interpolation within the table. No extrapolation at either end is performed; the first and last table points define the applicable range. The first point is [h_{min} (= 0.), V_{min} (= 0.)], and the last point is [h_{max}, V_{max}].

During initialization, the volume-versus-height data/function is employed to calculate the total volume of each zone j as follows:

for j = 1:

$$V_{PRHR_j} = V(1)_{PRHR_j}$$

for j = 2,...,$N_{zone,PRHR}$:

$$V_{PRHR_j} = V(1)_{PRHR_j} - \sum_{k=1}^{j-1} V_{PRHR_k} \qquad 4.10\text{-}8$$

where:

$V(1)_{PRHR}$ = Volume as a function of elevation, $in.^3/in.$, and 1 is the elevation of the top of zone;

During the transient calculations, the volume-versus-height data/function is employed to calculate the water volume of the zone containing the compensated water level, j = levzone, as follows:

if j=levzone=1:

$$V_{f,PRHR_j} = V(l_f)_{PRHR}$$

if j=levzone>1:

$$V_{f,PRHR_j} = V(l_f)_{PRHR} - \sum_{k=1}^{j-1} V_{PRHR_k} \qquad 4.10\text{-}9$$

where:

$V(l_f)$ = Volume as a function of elevation, $in.^3/in.$, and l_f is the elevation of the compensated water level

The steam volume of the zone containing the compensated water level, j = levzone, is then the following:

$$V_{g,PRHR_j} = V_{PRHR_j} - V_{f,PRHR_j} \qquad 4.10\text{-}10$$

The zone j water and steam densities are the reciprocal of the water- and steam-specific volumes, respectively:

$$\rho_{f,PRHR_j} = \frac{1}{V_{f,PRHR_j}}$$

$$\rho_{g,PRHR_j} = \frac{1}{V_{g,PRHR_j}} \qquad 4.10\text{-}11$$

The zone j water-specific volume is calculated as a function of pressure and temperature from the ASME steam table function VCL as follows:

$$v_{f,PRHR_j} = VCL(P_{PRHR}, T_{f,PRHR_j}) \qquad 4.10\text{-}12$$

The zone j steam-specific volume is calculated as a function of pressure and temperature from the ASME steam table function HSS as follows (note that the steam-specific enthalpy is the main output of HSS, and the steam-specific entropy is also an output of HSS):

$$h_{g,PRHR_j} = HSS(P_{PRHR}, T_{g,PRHR_j}, S_{g,PRHR_j}, v_{g,PRHR_j}) \qquad 4.10\text{-}13$$

The zone j water and steam temperatures are simply given by the zone temperatures, which are the fluid thermocouple measurements TF-XXX (Table 4.10-1). Care is taken to ensure that the water temperature value employed is at or below the saturation temperature and that the steam temperature value employed is at or above the saturation temperature:

$$T_{f,PRHR_j} = \min(T_{PRHR_j}, T_{sat,PRHR})$$

$$T_{g,PRHR_j} = \max(T_{PRHR_j}, T_{sat,PRHR}) \qquad 4.10\text{-}14$$

where:

$$T_{PRHR_j} = TF\text{-}XXX_{PRHR_j} \qquad 4.10\text{-}15$$

The saturation temperature is calculated as a function of pressure from the ASME steam table function TSL as follows:

$$T_{sat,PRHR} = TSL(P_{PRHR}) \qquad 4.10\text{-}16$$

The pressure is set equal to the value from the $PT\text{-}XXX_{PRHR}$ measurement (Table 4.10-1) after conversion from gauge (psig) to absolute (psia) pressure.

This completes the discussion of the calculations related to the left-hand side of the fluid mass conservation equation.

On the right-hand side of the fluid mass conservation equation, the calculation of the outlet fluid mass flow rate (to the SG-2 outlet) is performed directly from the liquid volumetric flow rate measurement ($FMM\text{-}XXX_{PRHR\_outlet}$), due to the fact that the water flowing in the line remains subcooled (Table 4.10-1 for the instrument channel ID). Thus:

$$\dot{M}_{out\ (to\ SG_2)\ H_2O,PRHR} = \dot{M}_{out\ (to\ SG_2)\ f,PRHR}$$

$$= \max(0, FMM\text{-}XXX_{PRHR\_outlet}) \times \rho_{f,PRHR_1} \times C_1 \qquad 4.10\text{-}17$$

where:

C_1 = Conversion constant, gpm to $ft.^3/sec.$

The integrated outlet water mass flow is also computed for use in the overall system mass balance. The water density is given by that from axial fluid property zone 1 (at the bottom).

Although a liquid volumetric flow rate measurement (FMM) is available for the inlet line, it cannot be relied on for accurate mass flow rate calculations due to two-phase flow. Thus, having calculated both the change in stored fluid mass (from the left-hand side) and the outlet fluid mass flow rate (from the right-hand side), the fluid mass conservation equation is rearranged to solve for (infer) the inlet fluid mass flow rate (from the HL-2).

This completes the discussion of the calculations related to the right-hand side of the fluid mass conservation equation.

4.10.2 Fluid Energy Conservation Equation

The general fluid (H_2O) energy conservation equation, which relates the change in stored energy with respect to time (the fluid-energy time derivative) to the energy rates in and out (due to the connected flow paths) and the energy addition rate due to other external devices, reduces to the following:

$$\frac{d[M \times c_p \times (T - T_{ref})]_{H_2O,PRHR}}{dt} = Q_{in\ (from\ HL_2)\ H_2O,PRHR} - Q_{out\ (to\ SG_2)\ H_2O,PRHR} + Q_{[metal \Rightarrow H_2O],PRHR} \qquad 4.10\text{-}18$$

The left-hand side of the energy conservation equation is approximated:

$$\frac{d[M \times c_p \times (T-T_{ref})]_{H_2O,PRHR}}{dt} \approx \sum_{j=1}^{N_{tube,PRHR}} \frac{\Delta[M \times c_p \times (T-T_{ref})]_{f,PRHR_j}}{\Delta t} + \sum_{j=1}^{N_{tube,PRHR}} \frac{\Delta[M \times c_p \times (T-T_{ref})]_{g,PRHR_j}}{\Delta t} \qquad 4.10\text{-}19$$

where:

$$\frac{\Delta[M \times c_p \times (T-T_{ref})]_{f,PRHR_j}}{\Delta t} \approx c_{p_{f,PRHR_j}} \times \left[\frac{\Delta[M \times (T-T_{ref})]_{f,PRHR_j}}{\Delta t}\right]$$

$$\approx c_{p_{f,PRHR_j}} \times (T_{f,PRHR_j}-T_{ref}) \times \left[\frac{M_{f,PRHR_j,n} - M_{f,PRHR_j,n-1}}{t_n - t_{n-1}}\right] + c_{p_{f,PRHR_j}} \times M_{f,PRHR_j} \times \left[\frac{T_{f,PRHR_j,n} - T_{f,PRHR_j,n-1}}{t_n - t_{n-1}}\right] \qquad 4.10\text{-}20$$

and:

$$\frac{\Delta[M \times c_p \times (T-T_{ref})]_{g,PRHR_j}}{\Delta t} \approx c_{p_{g,PRHR_j}} \times \left[\frac{\Delta[M \times (T-T_{ref})]_{g,PRHR_j}}{\Delta t}\right]$$

$$\approx c_{p_{g,PRHR_j}} \times (T_{g,PRHR_j}-T_{ref}) \times \left[\frac{M_{g,PRHR_j,n} - M_{g,PRHR_j,n-1}}{t_n - t_{n-1}}\right] + c_{p_{g,PRHR_j}} \times M_{g,PRHR_j} \times \left[\frac{T_{g,PRHR_j,n} - T_{g,PRHR_j,n-1}}{t_n - t_{n-1}}\right] \qquad 4.10\text{-}21$$

The zone j water-specific heat capacity at constant pressure is calculated as a function of pressure and temperature from the ASME steam table function CPL as follows:

$$c_{p_{f,PRHR_j}} = CPL(P_{PRHR}, T_{f,PRHR_j}) \qquad 4.10\text{-}22$$

The zone j steam-specific heat capacity at constant pressure is calculated as a function of pressure and temperature from the ASME steam table function CPV as follows (note that the steam-specific volume is also an output of CPV):

$$c_{p_{g,PRHR_j}} = CPV(P_{PRHR}, T_{g,PRHR_j}, v_{g,PRHR_j}) \qquad 4.10\text{-}23$$

For use in the overall system energy balance calculations, the fluid stored energy in the PRHR is given by the following:

$$U_{H_2O,PRHR} = U_{f,PRHR} + U_{g,PRHR} \qquad 4.9\text{-}24$$

where:

$$U_{f,PRHR} = \sum_{j=1}^{N_{\text{nodes PRHR}}} M_{f,PRHR_j} \times c_{p_{f,PRHR_j}} \times (T_{f,PRHR_j} - T_{ref}) \qquad 4.9\text{-}25$$

and:

$$U_{g,PRHR} = \sum_{j=1}^{N_{\text{nodes PRHR}}} M_{g,PRHR_j} \times c_{p_{g,PRHR_j}} \times (T_{g,PRHR_j} - T_{ref}) \qquad 4.9\text{-}26$$

This completes the discussion of the calculations related to the left-hand side of the fluid energy conservation equation.

On the right-hand side of the fluid energy conservation equation, the calculation of the outlet fluid energy transport rate (to the SG-2 outlet) is given by the following:

$$Q_{out\ (to\ SG_2)\ H_2O,PRHR} = Q_{out\ (to\ SG_2)\ f,PRHR}$$

$$= \dot{M}_{out\ (to\ SG_2)\ f,PRHR} \times h_{f,PRHR\_outlet} \qquad 4.10\text{-}27$$

The outlet line water-specific enthalpy is calculated as a function of pressure and temperature from the ASME steam table function HCL as follows (note that the water-specific entropy is also an output of HCL):

$$h_{f,PRHR\_outlet} = HCL(P_{PRHR},\ T_{f,PRHR},\ S_{f,PRHR\_outlet}) \qquad 4.10\text{-}28$$

The water temperature is given by that from axial fluid property zone 1 (at the bottom).

The energy addition rate to the fluid due to heat transfer from the metal is given by:

$$Q_{[metal \Rightarrow H_2O],PRHR} = Q_{[tube\ metal \Rightarrow H_2O],PRHR} + Q_{[inlet\ line\ metal \Rightarrow H_2O],PRHR} + Q_{[outlet\ line\ metal \Rightarrow H_2O],PRHR} \qquad 4.10\text{-}29$$

Due to the small size of the inlet and outlet lines, their contributions in the previous equation are ignored, i.e.:

$$Q_{[inlet\ line\ metal \Rightarrow H_2O],PRHR} \approx 0.0$$

$$Q_{[outlet\ line\ metal \Rightarrow H_2O],PRHR} \approx 0.0 \qquad 4.10\text{-}30$$

The contribution from the tube metal-to-fluid heat transfer rate is calculated from the tube metal energy conservation equation, which is discussed in Subsection 4.10.3.

Finally, having calculated the change in stored fluid energy (from the left-hand side) and the outlet fluid energy transport rate and metal-to-fluid heat transfer rate (from the right-hand side), the fluid energy conservation equation is rearranged to solve for (infer) the inlet fluid energy transport rate (from the HL-2).

This completes the discussion of the calculations related to the right-hand side of the fluid energy conservation equation.

4.10.3 Tube Metal Energy Conservation Equation

The general metal energy conservation equation, which relates the change in stored metal energy with respect to time (the metal-energy time derivative) to the energy rates in and out (due to heat transfer), reduces to the following for the PRHR HX tube metal (note that here, the "ambient" is the IRWST fluid in which the tubes reside):

$$\frac{d[M \times c_p \times (T - T_{ref})]_{tube\ metal,PRHR}}{dt} = - Q_{[tube\ metal \Rightarrow H_2O],PRHR} - Q_{[tube\ metal \Rightarrow IRWST],PRHR} \qquad 4.10\text{-}31$$

Due to the location of the thermocouple instrumentation, the tube metal is divided into fou metal segments. Table 4.10-3 lists the tube metal thermocouple channel ID and tube metal mass data for each tube metal segment, which are required in the tube metal energy calculations.

The left-hand side of the tube metal energy conservation equation is approximated:

$$\frac{d[M \times c_p \times (T - T_{ref})]_{tube\ metal,PRHR}}{dt} \approx \frac{\Delta[M \times c_p \times (T - T_{ref})]_{tube\ metal,PRHR}}{\Delta t} \qquad 4.10\text{-}32$$

where:

$$\frac{\Delta[M \times c_p \times (T - T_{ref})]_{tube\ metal,PRHR}}{\Delta t} \approx \sum_{m=1}^{N_{tube\ metal,PRHR}} M_{tube\ metal,PRHR_m} \times cp_{tube\ metal,PRHR_m} \times \left[\frac{T_{tube\ metal,PRHR_m,n} - T_{tube\ metal,PRHR_m,n-1}}{t_n - t_{n-1}} \right] \qquad 4.10\text{-}33$$

where:

$N_{tube\ metal,\ PRHR}$	=	Number of PRHR tube metal segments, (4)
n, n-1	=	Two consecutive time points

The integrated tube metal stored energy is also computed for use in the overall system energy balance. The tube metal segment specific heat capacity at constant pressure is calculated as a function of the

tube metal segment temperature from the metal c_p versus temperature tabular data listed in Table 4.10-4, via linear interpolation within the table. No extrapolation at either end is performed; the first and last table points define the applicable range. The first point is (T_{min}, $c_{p,min}$), and the last point is (T_{max}, $c_{p,max}$).

This completes the discussion of the calculations related to the left-hand side of the tube metal energy conservation equation.

On the right-hand side of the tube metal energy conservation equation, the tube metal-to-IRWST heat transfer rate is inferred from the IRWST fluid energy conservation equation. Subsection 6.1.2 shows that the inferred PRHR heat transfer is consistent with the external tube wall-to-IRWST water heat transfer rate.

Finally, having calculated both the change in stored tube metal energy (from the left-hand side) and the tube metal-to-IRWST heat transfer rate (from the right-hand side), the tube metal energy conservation equation is rearranged to solve for (infer) the tube metal-to-fluid heat transfer rate.

This completes the discussion of the calculations related to the right-hand side of the tube metal energy conservation equation.

TABLE 4.10-1 INSTRUMENTATION EMPLOYED FOR PRHR FLUID CALCULATIONS	
Description	**Item**
Level (in.)	LDP-802
Pressure (psig)	PT-107
Outlet Line Liquid Flow Rate (gpm)	FMM-804
Zone Temperature [°F]/Top Elev (in.)	TF-804 4.375
[Bottom (outlet) to Top (inlet)]	TF-805 7.000
	TF-809 50.000
	TF-811 52.875
	TF-803 57.000
LDP Comp Region Temp (°F)/Elev (in.)	TF-805 0.000
Bottom (outlet) to Top (inlet)	TF-809 29.625
	TF-811 57.000

TABLE 4.10-2 VOLUME VERSUS HEIGHT TABLES FOR PRHR FLUID VOLUME CALCULATIONS	
Height (in.)	**Volume* ($in.^3$)**
0.00	0.0
1.75	0.0
7.00	871.3
50.00	1076.7
55.75	1513.4
57.00	1513.4

*A deadband was included for the volume at the top (inlet) and bottom (outlet) to accommodate level instrument fluctuations that were observed in the tests.

TABLE 4.10-3 DATA FOR PRHR TUBE METAL ENERGY CALCULATIONS (PER SEGMENT)		
Metal Segment	**Temperature ID (°F)**	**Mass (lbm)**
1 (Bottom horizontal)	TW-801	37.0
2 (Bot 1/2 vertical)	TW-803	40.0
3 (Top 1/2 vertical)	TW-806	40.0
4 (Top horizontal)	TW-808	37.0

TABLE 4.10-4 SPECIFIC HEAT CAPACITY VERSUS TEMPERATURE TABLE FOR PRHR TUBE METAL ENERGY CALCULATIONS	
Metal c_p [Btu/(lbm-°F)]	**Metal Temperature (°F)**
0.1085	70.0
0.1109	100.0
0.1175	200.0
0.1223	300.0
0.1256	400.0
0.1279	500.0
0.1297	600.0

4.11 Reactor Pressure Vessel

The reactor pressure vessel (RPV) model includes the lower plenum, core, upper plenum, and upper head. The vessel analysis includes liquid level and mass, core power, steam production due to core power, and flow quality at the core exit.

The core vessel is shown in Figure 4.11-1. A total of eight regions are modeled. The actual spans and elevations of the lower plenum, core, upper plenum, and upper head are used. Elevations are relative to the inside bottom of the vessel. Volumes for supporting structures are also included so as to support the use of actual elevations and simplify coding algorithms.

Figure 4.11-1 also shows the six axial core heater power steps. Total heater power was varied during the tests; power history data is provided for each test. A top-skewed power distribution was used for all tests.

Fluid thermocouple elevations in the core are shown in Figure 4.11-1. The fifteen locations include all elevations outside of the core region. Where multiple thermocouples are provided at a given elevation, the average was used in all analyses. Two issues were identified with the core fluid thermocouples:

- The core fluid thermocouples are located in instrumented rods, with one rod at the core center and the remainder at the core perimeter. Fluid temperature histories for core center and perimeter thermocouples were found to differ. This was attributed to smaller power-to-flow ratios for the perimeter heater rods than for the center rod due to larger flow areas. In order to best represent the average core temperature associated with the average flow area, the center-rod temperatures were used exclusively.

- The core fluid thermocouple histories were noisy. The noise was investigated and found to be unrelated to core thermal-hydraulic phenomena. A time-history smoothing method was selected to minimize the noise. This smoothing was applied to all core fluid thermocouples. The smoothing algorithm is provided in Section 4.20.

LDPs available to determine liquid levels are shown in Figure 4.11-2. Level instrumentation issues common to all tests were identified and are summarized below.

Values for LDPs spanning the supporting structures tend to be influenced by flow through the supporting structures. The flow effect tends to bias the LDPs toward higher readings and may cause an LDP to read full during an entire test. Since the bias is a function of flow quality and flow rate, the effect varies during the tests. As a result, DP-111 and DP-114 were not useful; they read either full scale or clearly overstated the liquid levels. These LDPs were not used in any analyses.

LDP-112 generally read full scale. Figure 4.11-3 provides an uncorrected plot of LDP-112 and the adjacent LDP-113 data. LDP-113 is directly above LDP-112. During the period around

[ ]^{a,b,c} seconds, LDP-113 clearly indicated that the level had dropped into the span of LDP-112, yet LDP-112 failed to respond. LDP-112 was not used in any analyses.

The pressure taps used in the vessel analysis are also shown in Figure 4.11-2. Since the pressure taps (PT-107 and PT-108) are located at the top and bottom of the vessel, the pressures should differ due to the effects of water column density. Figure 4.11-4 shows the pressure gradient (P_{PT-108} - P_{PT-107}) for Matrix Tests SB01 and SB18. The gradients are similar for about the first [ ]^{a,b,c} seconds, after which the gradient for Matrix Test SB01 deviates to a value inconsistent with the height of the water column. This was found to be due to an error in PT-108 for Matrix Test SB01. To minimize the impact of pressure irregularities, RPV analyses are based on one of the pressure taps, which is selected on a test-by-test basis. PT-107 was used for Matrix Test SB01 and PT-108 was used for Matrix Test SB18.

The pressure tap irregularities were found to be on the order of two psi for Matrix Test SB01. The potential impact of a two psi error is related to the importance of the associated change in water and steam properties. For most analyses this effect is relatively unimportant. As discussed in Subsection 4.11.2.1, core steam production calculations may be sensitive to a two psi error.

4.11.1 Core Vessel Model

The core vessel model is shown in Figure 4.11-5. Eight fluid regions and six core heated regions are modeled. The selected level instrumentation is shown. Fifteen temperature zones associated with the fifteen thermocouple elevations are also shown.

The spans of the selected LDPs differ from the fluid regions and temperature zones and are shown in Table 4.11-1.

LDP levels are relative to their lower pressure taps. To be consistent with other elevations, region levels are defined relative to the inside bottom of the vessel. Region liquid levels are related to LDP readings as follows:

- When the LDP reading is empty or less then empty, the region level is set to either the bottom of the region or the bottom of the LDP span, whichever is greater. In cases where the LDP lower tap is above the bottom of the region, as is the case in the upper plenum, this logic results in a minimum calculated liquid level and a void fraction constrained to a value less than 1.

- When the LDP reading is between empty and full, the density-corrected level is used. The density correction accounts for temperature differences between the fluid in the vessel and the fluid in the reference leg of the instrument line. If this results in a level above the top LDP tap, the next method is used.

- When the LDP reading is full or more than full, the region level is set either to the top of the region or the top of the LDP span, whichever is less. The region is assumed to be full of liquid; the void fraction is set equal to 0. In cases where the LDP upper tap is below the top of the region, step changes in region void fraction and mass will occur when the LDP readings vary between full and less than full.

The effects of this level and mass methodology are shown in Table 4.11-2.

The fifteen temperature zones bound the thermocouple elevations. The midpoints between the thermocouple elevations define the intermediate zone boundaries. The top and bottom zone boundaries are set equal to the model top and bottom. Fluid and steam properties are assumed constant in each zone. Liquid densities are determined on a region basis using the average liquid temperature for the region. All other zone properties are based on the local pressure and temperature. The local pressure is based on the selected pressure tap, the liquid levels, and the density effects of water.

Region liquid masses and volume-based void fractions are determined using lookup tables that relate liquid levels to region volumes. These tables account for axial variations in the region cross-sectional areas. Liquid and vapor masses for the temperature zones are then determined by mapping the region results to the zones.

4.11.2 Core Power and Flow Model

The core is subdivided into six axial heater regions that are 6 in. high. The axial-heater-region power distributions were the same for all tests and were constant during the tests. The core total power is calculated by averaging the redundant power instrumentation. The core total power and axial power distribution are defined below.

Core total power is defined as:

$$PWR_T = \frac{1}{2} \sum_{i=1}^{4} PWR_i \qquad 4.11\text{-}1$$

where:

PWR_T	=	Total heater rod power, kW
PWR_i	=	Heater rod power data, kW

The heater rod instrument list is provided in Table 4.11-3. The power distribution is provided in Table 4.11-4.

Two methods are provided for calculating core steam production: the Tsat method and the DVI line flow method. Both methods view the core as a steady-state control volume. The rate of core mass changes and energy changes are not considered. This limits the validity of both methods during the first several hundred seconds of the transient. During the remainder of the tests, this approximation is expected to have minimal impact. Two important results of this methodology are:

- The liquid mass flow rate from the lower plenum to core is the same as the mixture mass flow rate from the core to upper plenum.

- 100 percent of the power is applied to heating the core flow.

4.11.2.1 Core Steam Production - Tsat Method

Core steam production and saturation line are calculated from core power, core fluid temperature, and local saturation temperature using the following steps:

Step 1: Determine the saturation line by finding the intersection between curves of local saturation temperature and fluid temperature.

Step 2: Determine the power above the saturation line. Power above the saturation line is assumed to generate steam; power below this elevation is assumed to heat water.

Step 3: Determine steam production from power above the saturation line and the enthalpy of vaporization.

Fluid temperatures are defined at the thermocouple elevations. The fluid temperature curve is constructed by linearly interpolating between the elevations. The local pressures are also defined at the thermocouple elevations. The saturation temperature curve is defined by determining the saturation temperature at the local pressure at the thermocouple elevations and linearly interpolating between the elevations. Starting at the bottom and searching in the direction of increasing elevation, the saturation line is found by finding the intersection between the two curves. Thus, the saturation line is the elevation where core heating achieves saturated liquid.

The temperature profiles for the entire vessel are used. As a result, the intersection may occur outside of the bounds of the core. If an intersection is not found, or the intersection is not in the core, then:

- If the core fluid temperatures are above the saturation temperature, the intersection elevation is set equal to the bottom of the core.

- If the core fluid temperatures are below the saturation temperature, the intersection elevation is set equal to the top of the core.

Power above and below the saturation line is defined by:

$$PWR_{ab} = \int_{\text{sat line}}^{\text{top of core}} \frac{PWR_T}{36} \, FTP_z \, dz \qquad 4.11\text{-}2$$

$$PWR_{bl} = PWR_T - PWR_{ab}$$

where:

z	=	Elevation, in.
36	=	Total height of heater region, in.
PWR_{ab}	=	Power above saturation line, kW
PWR_{bl}	=	Power below saturation line, kW
FTP_z	=	Fraction of total power for region bounding elevation z per Table 4.11-4

Several methods for calculating steam and flow were investigated. The modeling of the core for steam and flow calculations is shown in Figure 4.11-6. The calculations are based on properties at the three locations shown. Properties at the saturation line are determined from the saturation temperature calculated by interpolation of the saturation temperature curve. Thermocouple elevations outside of the core and close to the core top and bottom elevations were selected as proxies; the corresponding thermocouple temperatures and local pressures were used to calculate associated properties.

The selected method determines steam production directly from power above the saturation line and the enthalpy of vaporization. Steam production from the core is calculated as:

$$\dot{M}_s = \frac{PWR_{ab}}{h_{fg,sl}} \times C \qquad 4.11\text{-}3$$

where:

C	=	Conversion constant, kW to Btu/sec.
$\dot{M}_s$	=	Steam production, lbm/sec.
$h_{fg,sl}$	=	Enthalpy of vaporization at saturation line, Btu/lbm

The viability of this method for determining steam production is dependent on the accuracy of the saturation line calculation. Since the saturation line is the intersection of the fluid and saturation temperature curves, the accuracy of this elevation is a function of the slope of the two temperature curves. The saturation temperature curve is a function of local pressure and varies only slightly over

the span of the core. The fluid temperature gradient varies widely during the transient as shown for Matrix Test SB01 in Figure 4.11-7. The gradient is very small during steady state operation; and is small during the first several hundred seconds of the transient, and during long term cooling. Since the applicability of this method is a function of the fluid temperature gradient, the range of applicability may vary from test to test.

4.11.2.2 Core Steam Production - DVI Line Flow Method

Core steam production and saturation line are calculated from core power, core inlet enthalpy, and the DVI line flow rate using the following steps:

Step 1: The core inlet enthalpy is based on the fluid temperature and local pressure in the lower plenum. Starting with the bottom core heated region, the enthalpy rise for each of the six heated regions is determined from the DVI line flow rate, less break flow from the cold leg, enthalpy at the bottom of the region, and the core power in the region.

Step 2: The saturation line is identified by locating the first region where the enthalpy exceeds that of saturated liquid and interpolating the enthalpy rise to determine the saturation line elevation in that region. The power above the saturation line is then calculated.

Step 3: Core outlet quality is determined using the steam tables and the enthalpy at the top of the core. Steam production is then determined using the quality and DVI line flow rate.

The saturation line is calculated as:

$$C\,(h_{f,\,sl} - h_{f,\,1})\,\dot{M} = \int_{\text{bottom of core}}^{\text{sat line}} \frac{PWR_T}{36}\,FTP_z\,dz, \text{ for } \dot{M} > 0 \qquad 4.11\text{-}4$$

sat line = bottom of core, for $\dot{M} = 0$

where:

$\dot{M}$ = Liquid flow rate into core = DVI line flow - cold-leg break flow for hot-leg breaks and tests without breaks, the cold-leg break flow is zero

$h_{f,\,sl}$ = Liquid enthalpy at saturation line

$h_{f,1}$ = Liquid enthalpy at core inlet

Core outlet flow quality can be calculated from the liquid flow rate and a core energy balance:

$$h_2 = h_{f,1} + \frac{PWR_T}{\dot{M}} \times C \qquad 4.11\text{-}5$$

$$X_2 = f\,(h_2, P_{TC}) \qquad 4.11\text{-}6$$

The core outlet flow quality shown above applies to the flow exiting the core and not mixture conditions at the top of the core. Thus, core steam production and flow void fraction can be calculated directly without consideration for slip coefficients. The core steam production and flow void fraction are calculated as:

$$\dot{M}_s = X_2 \dot{M} \qquad 4.11\text{-}7$$

$$\alpha_2 = \frac{X_2 \rho_{f,2}}{X_2 \rho_{f,2} + (1 - X_2)\rho_{g,2}} \qquad 4.11\text{-}8$$

where:

h_2	=	Mixture enthalpy at core outlet
$\rho_{g,2}$ $\rho_{f,2}$	=	Vapor and liquid density at core outlet, respectively
X_2	=	Flow quality at core outlet
α_2	=	Flow void fraction at core
P_{TC}	=	Pressure at top of the core
f (h, P)	=	Steam table function for quality

The viability of this method for determining steam production is dependent on the assumption that DVI line flow minus cold-leg break flow is representative of the flow into the core from the lower plenum. This assumption clearly does not apply during steady state operation. During the first several hundred seconds of the transient, this flow is not representative due to draining of various components, which includes the steam generators, hot legs, cold legs, and pressurizer. After approximately [ ]^{a,b,c} seconds, this is a good representation of the core inlet flow. The validity of the flow approximation for the DVI line flow method is further investigated in Subsection 6.2.1.

This method is relatively insensitive to the core temperature gradient. The effects of pressure errors are primarily limited to the change in mixture enthalpy at the top of the core. As a result, this method is well behaved during LTC and is preferred over the Tsat Method for this phase of the transient.

4.11.3 Energy Balance

The total liquid and steam energy is calculated by summing the results for the temperature zones as follows:

$$U_f = \sum_{\text{temperature zones}} M_{f,i}\, c_{P,f,i}\, (T_{f,i} - 32°F) \qquad 4.11\text{-}9$$

$$U_g = \sum_{\text{temperature zones}} M_{g,i}\, c_{P,g,i}\, (T_i - 32°F) \qquad 4.11\text{-}10$$

where the subscripts:

f	=	Liquid phase of water
g	=	Steam
i	=	Temperature zone number

The rate of energy change for the total reactor metal mass (includes downcomer) is based on 33 metal regions associated with metal thermocouples. Approximate metal masses were estimated for each metal region. The rate of energy change of the metal is calculated as:

$$Q_{metal} = \sum_{\text{metal regions}} M_{metal,j}\, c_{P,f,j}\, \frac{\Delta T_{metal,j}}{\Delta t}$$

where the subscript:

j	=	Metal region number

The rate of energy loss from the reactor vessel (including downcomer) to the environment is calculated using the sump methodology of Subsection 4.9.5.5. The reactor vessel and sump are similar in that they are insulated vertical tanks. The reactor vessel and sump modeling differences are limited to the constant multiplier in the equation for the free convection heat transfer coefficient. Subsection 4.9.5.5 defines the applicability of the detailed energy loss calculations for the CMT cold-leg balance line to the sump. The applicability relationship also applies to the RPV.

For reactor vessel-to-ambient energy loss formulas, see Subsection 4.9.5.5 and related sections. The reactor vessel surface was subdivided into four areas, with a different constant multiplier for each area. These multipliers are compared to the sump multiplier in Table 4.11-5. The total heat loss is determined by summing the heat loss for the individual areas.

TABLE 4.11-1 CORE VESSEL MODEL GEOMETRY					
Region	**Level Instrument**	**Bottom of Region**	**Bottom of LDP**	**Top of Region**	**Top of LDP**
Lower plenum	LDP-106 LDP-107	0	2	6.41	10.22
Lower core plate	LDP-108	6.41	2	9.91	10.22
Core	LDP-138	9.91	10.22	50.86	50.17
Core plenum	LDP-139	50.86	50.17	52.75	74.13
Upper core plate	LDP-139	52.75	50.17	53.5	74.13
Upper plenum	LDP-113	53.5	58.71	74.42	77.83
Upper support plate	LDP-115	74.42	77.83	77.42	97.58
Upper head	LDP-115	77.42	77.83	97.58	97.58

TABLE 4.11-2 MASS METHODOLOGY EFFECTS		
Region	**Minimum Level Effects**	**Maximum Level Effects**
Core	Minimum liquid mass > 0 Maximum void fraction < 1	Small step changes in mass and void fraction when level varies to/from top of LDP span
Upper plenum	Minimum liquid mass >> 0 Maximum void fraction << 1	None
Upper head	Minimum liquid mass > 0 Maximum void fraction < 1	None

TABLE 4.11-3 HEATER ROD INSTRUMENTATION	
Pi	**Instrument Name**
P_1	KW-101
P_2	KW-102
P_3	KW-103
P_4	KW-104

TABLE 4.11-4 POWER DISTRIBUTION	
Axial Heater Region	**Fraction of Total Power in Region**
6, top heater region	0.19367
5	0.24293
4	0.22487
3	0.1798
2	0.1172
1, bottom heater region	0.04153

TABLE 4.11-5 CONSTANT MULTIPLIERS FOR THE FREE CONVECTION HEAT TRANSFER COEFFICIENT		
Area	**Coefficient**	**Basis**
Sump	0.09	
Reactor Vessel: Vertical Surface	0.09	Simplified equation for free convection to air from a vertical surface.
Reactor Vessel: Hot & Cold Leg Area	0.15	Simplified equation for free convection to air from horizontal pipe, OD = 5.75"
Reactor Vessel: DVI Nozzle Area	0.21	Simplified equation for free convection to air from horizontal pipe, OD = 1.66"
Reactor Vessel: Bottom Flange Surface Area	0.09	Simplified equation for free convection to air from heated plate facing downward

TABLE 4.11-6 OSU TEST ANALYSIS PLOT PACKAGE FOR SECTION 4.11				
Plot Number	**Component**	**Variables**	**Units**	**Description**
1	Reactor Vessel	N/A	N/A	Reactor Vessel Geometry
2	Reactor Vessel	N/A	N/A	Reactor Vessel Level and Pressure Instrumentation
3	Reactor Vessel	LDP-112 LDP-113	in.	Uncorrected Levels Results of Test SB18
4	Reactor Vessel	Delta-P = PT-108 - PT-107	psi	Pressure Gradients for Tests SB01 and SB18
5	Reactor Vessel	N/A	N/A	Reactor Vessel Model
6	Reactor Vessel	N/A	N/A	Modeling of Core Steam and Flow Calculations
7	Reactor Vessel	Core Temperature Rise	°F	Core Temperature Gradient

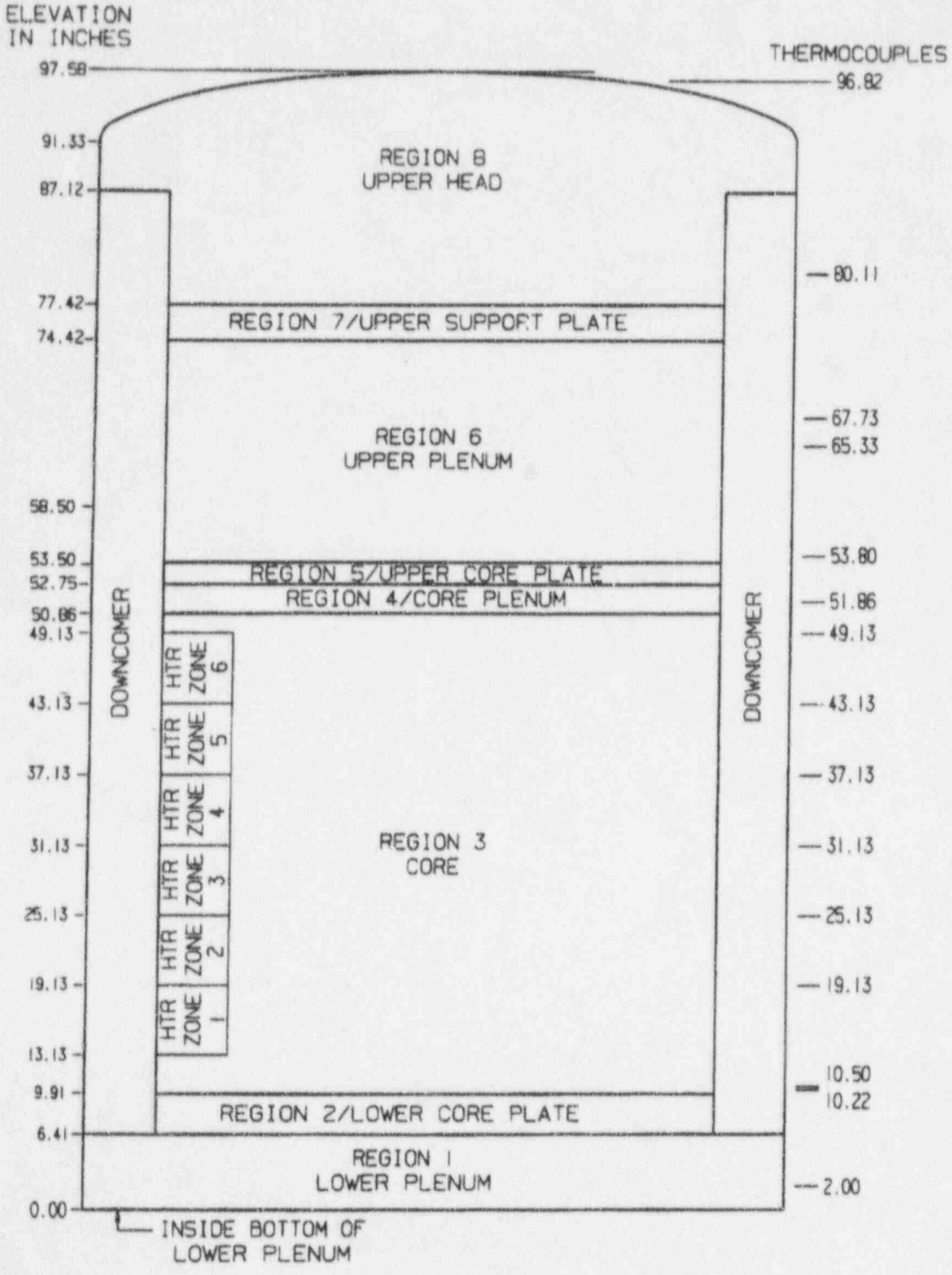

Figure 4.11-1 Reactor Vessel Geometry

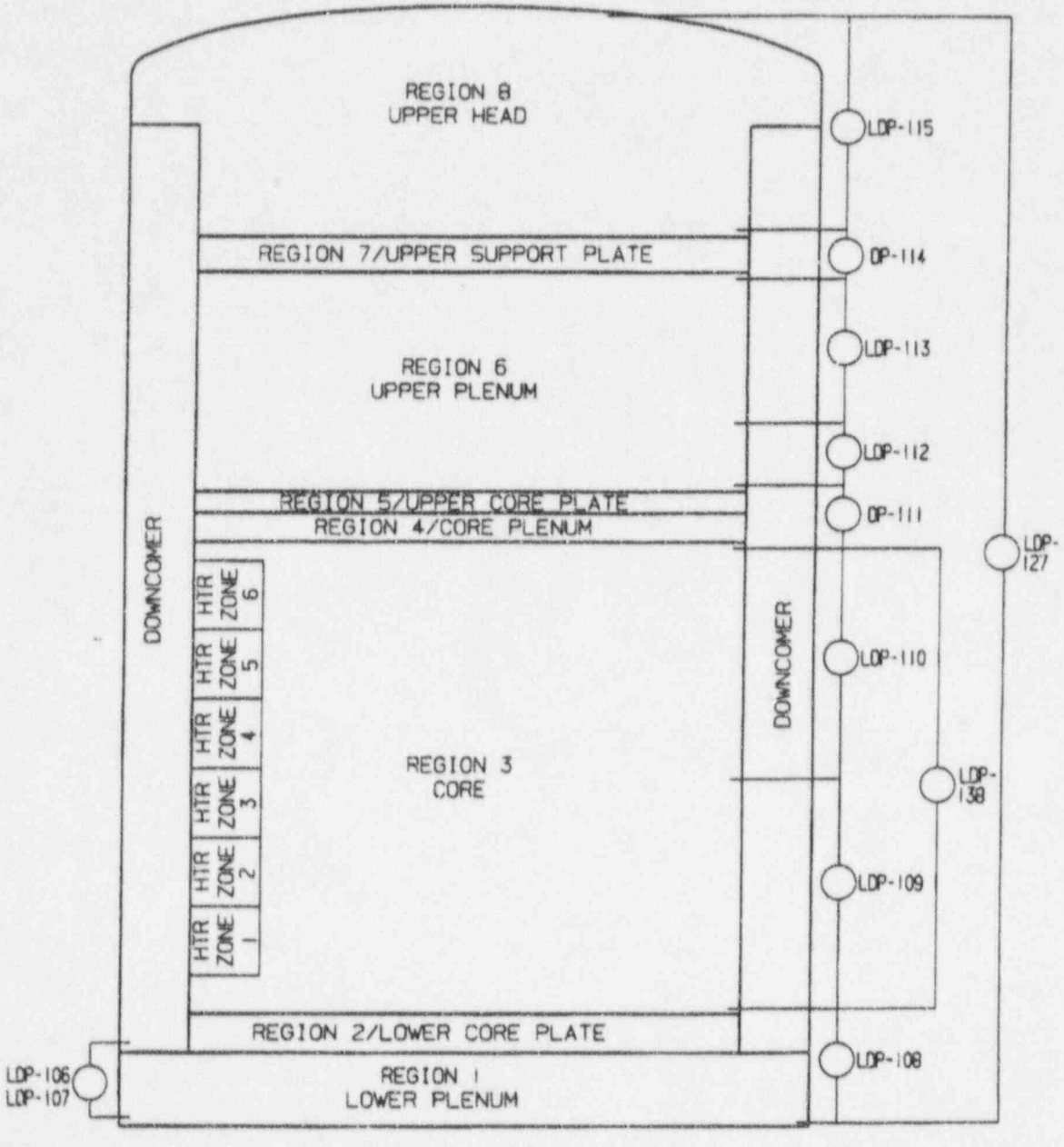

Figure 4.11-2 Reactor Vessel Level Instrumentation

FIGURES 4.11-3 AND 4.11-4
ARE NOT INCLUDED IN THIS NONPROPRIETARY DOCUMENT

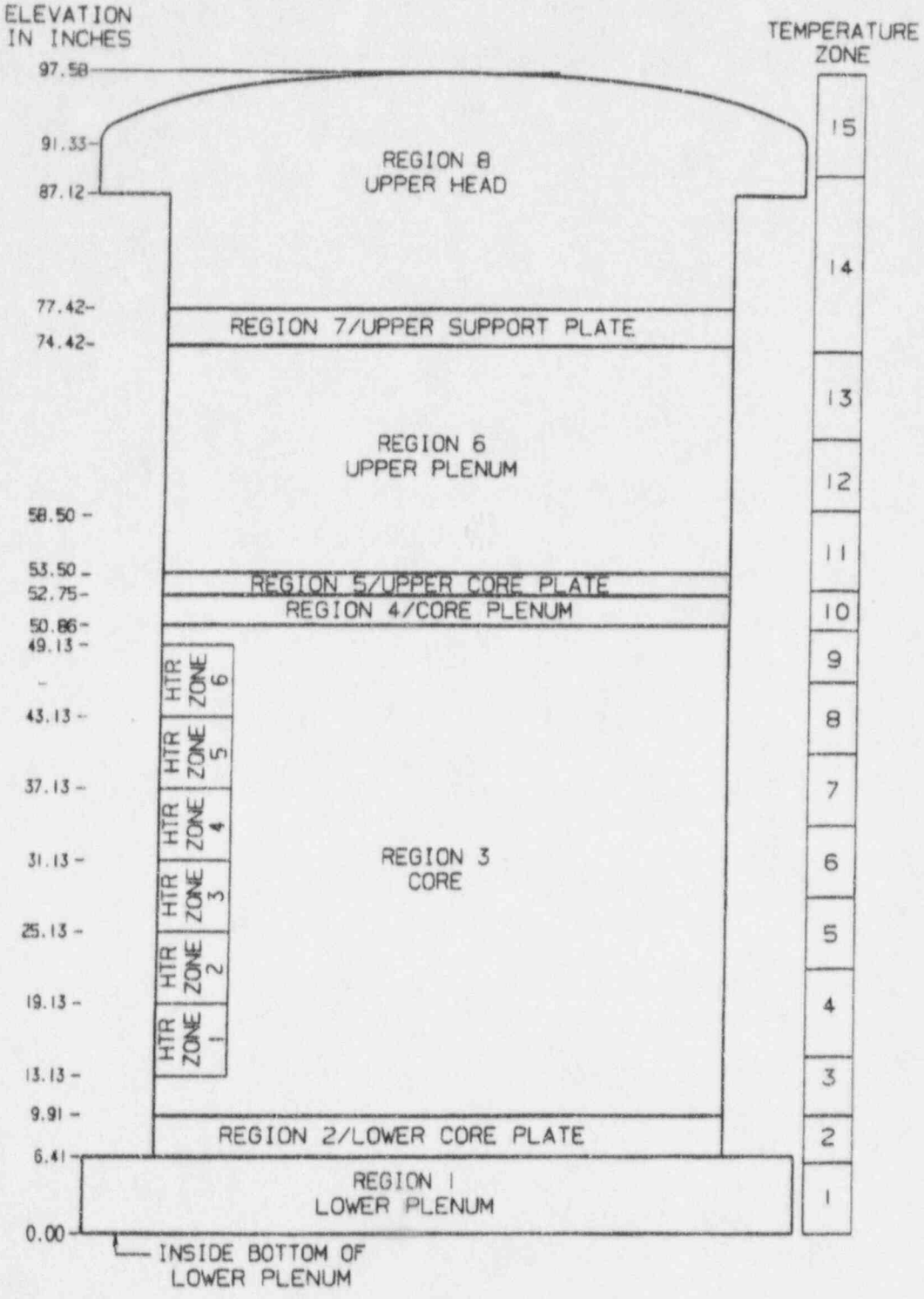

Figure 4.11-5 Reactor Vessel Model

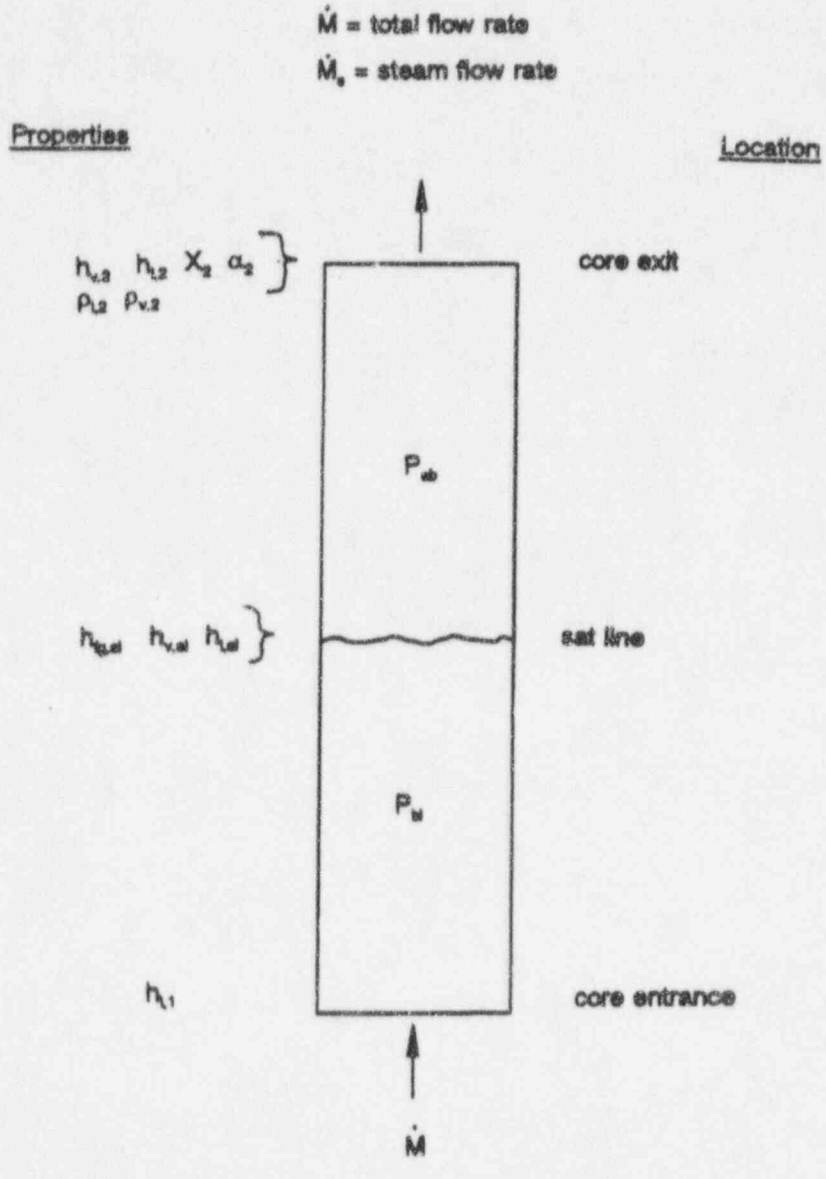

Figure 4.11-6 Modeling of Core Steam and Flow Calculations

FIGURE 4.11-7 IS NOT INCLUDED IN THIS NONPROPRIETARY DOCUMENT

4.12 Downcomer

The downcomer consists of the annular volume in the RPV surrounding the core and upper plenum. Its component interfaces include two DVI lines, four cold legs, reactor vessel lower plenum, and reactor vessel upper head bypass gaps. The downcomer is modeled separately from the other reactor vessel regions. Parameters calculated for the downcomer include liquid level, mass, flow from the DVI lines, and flow in the lower plenum.

Downcomer instrumentation used to analyze the test includes two LDPs that measure liquid level, and thermocouples that provide fluid and metal temperatures. The LDPs are positioned at different circumferential locations and span nearly the full height of the downcomer.

4.12.1 Downcomer Level and Mass

The downcomer fluid temperature distribution is defined by dividing the volume into a vertical array of temperature zones. Where multiple thermocouples are provided at a given elevation, the average temperature is used. Axial midpoints between the thermocouple elevations define the intermediate zone boundaries. The top and bottom zone boundaries are set equal to the top and bottom of the downcomer. Fluid and steam properties are assumed to be constant in each temperature zone. Zone properties are based on local pressure and temperature. Local pressure is based on the pressure at the top of the reactor vessel, the liquid levels, and the density effects of water.

The downcomer liquid level is determined by averaging the two LDP readings and applying density corrections for the density difference between the reference leg and the measured water column. Downcomer liquid and vapor mass are determined using lookup tables that relate liquid levels to volumes. These tables account for axial variations in the cross-sectional areas. Mass calculations are done on a temperature-zone basis and employ the temperature-zone densities.

4.12.2 Fluid Stored Energy

For use in the overall system energy balance calculations, the fluid stored energy in the downcomer is given by the following:

$$U_{H_2O,\,DC} = U_{f,\,DC} + U_{g,\,DC} \qquad 4.12\text{-}1$$

where:

$$U_{f,\,DC} = \sum_{j=1}^{N_{zone,\,DC}} M_{f,DC} \times c_{P_{f,DC}} \times (T_{f,DC} - T_{ref}) \qquad 4.12\text{-}2$$

and:

$$U_{g,DC} = \sum_{j=1}^{N_{zone,DC}} M_{g,DC} \times c_{P_{g,DC}} \times (T_{g,DC} - T_{ref}) \qquad 4.12\text{-}3$$

TABLE 4.12-1
VOLUME VERSUS HEIGHT TABLE FOR DOWNCOMER FLUID VOLUME CALCULATIONS

Height (in.)	Volume ($in.^3$)
0	0
4.41	0
6.0	281.0
22.0	3108.0
38.0	5936.0
78.0	13,004.0
78.11	13,998.0
83.62	13,998.0
98.0	13,998.0

4.13 Steam Generator Primary Side

The AP600 includes two SGs, which under normal operating conditions provide the heat sink for reactor core heat removal and steam source to power the turbine. The OSU test facility incorporates two simulated SGs. For the purposes of developing mass and energy balance equations to represent the thermal hydraulic performance of the RCS primary side, the primary side of the simulated SGs is considered as three interconnected sections:

- Inlet plenum
- Tubes (both uphill and downhill sides)
- Outlet plenum

The mass and energy balance equations are developed by considering the equations for each of these sections.

4.13.1 Inlet Plenum

A general mass balance equation for the inlet plenums may be written as:

$$\frac{d\ M_{IP}}{dt} = \dot{M}_{HL\ X} - \dot{M}_{IP\text{-}TUBE} \qquad 4.13\text{-}1$$

where the subscripts:

HL X	=	Hot leg X = 1 (SG-1) X = 2 (SG-2)
IP	=	SG inlet plenum
IP-TUBE	=	Interface between inlet plenum and tube bundle of SG

Similarly, the energy equation for the SG inlet plenum is written as:

$$Q_{SG} = c_p \frac{d(M\ T)_{SG\ X}}{dt} = \dot{M}_{HL\ X}\ h_{HL\ MIX} - \dot{M}_{IP\text{-}TUBE\ SG\ X}\ h_{IP\text{-}TUBE\ MIX} - Q_{IP\ SG\ X\ METAL} - Q_{IP\ SG\ X\ AMB} \qquad 4.13\text{-}2$$

where the subscripts:

SG X	=	Steam generator X = 1 (SG-1) X = 2 (SG-2)
AMB	=	Ambient conditions associated with inlet plenum
METAL	=	Metal mass of inlet plenum
MIX	=	Fluid mixture conditions

4.13.1.1 Mass Balance

The mass stored in the steam generator inlet plenums is calculated from level measurements in the plenums. The level measurements must be compensated for temperature differences between the fluid in the plenums and that in the sense lines of the instruments. The data channel IDs of the level, pressure, and temperature instruments to be used in calculating fluid mass in the inlet plenums are listed in Table 4.13-1. The following approach was used in performing the temperature compensation of the level instrument output and calculating the fluid mass in the SG inlet plenums.

Step 1: First, compensate the readings of the inlet plenum level transducers to account for temperature differences between fluid in the plenum and fluid in the reference legs of the instrument lines. As noted above, the channel IDs of the two level transducers to be compensated, one for each SG, are identified in Table 4.13-1. The instruments used to measure local pressure and fluid temperatures to be used to accomplish the compensation are also identified in Table 4.13-1.

The LDPs, which provide the SG plenum levels, provide incorrect readings when the pumps are running.

1) The plenum level is to be based on the density-corrected LDP, no pump-flow corrections to be included in the level calculations.

2) The plenum liquid volume and mass is to be based on two alternatives:

   a) Plenums assumed to be liquid solid during pump flow.

   b) Liquid volume and mass to be based on density-corrected LDP after pump flow stops.

3) The time period of pump flow to be defined as:

   a) Starting at the beginning of the test.

b) The time period ends a user-input number of seconds after the flow in both cold legs attached to a SG drops below a user-selected value.

Step 2: The local pressures and temperatures measured by the instruments identified in Table 4.13-1 are used as inputs to calculate the thermodynamic properties of the fluid in the inlet plenums:

$$\rho_f = \rho_f (P, T) \qquad \rho_g = \rho_g (P, T)$$
$$h_f = h_f (P, T) \qquad h_g = h_g (P, T) \qquad 4.13\text{-}3$$

where the subscripts:

f = Liquid phase of water
g = Steam

The data channel IDs of the instruments to be used in the calculation of the thermodynamic properties of the fluid in the SG inlet plenums are given in Table 4.13-1.

Step 3: Using the compensated liquid level and the inlet plenum volume as a function of height, the volume of liquid in the plenum is calculated:

$$V_{f,\ IP\ SG\ X} = V(l)_{IP\ SG\ X} \times LDP\text{-}XXX_{COMP} \qquad 4.13\text{-}4$$

where:

V = Volume, $ft.^3$
V(l) = Volume as a function of elevation, $ft.^3/ft.$ (See Table 4.13-2)
$LDP\text{-}XXX_{COMP}$ = Compensated fluid levels data from level transducer identified as
XXX = 209 (SG-1 inlet plenum) (see Table 4.13-1)
XXX = 214 (SG-2 inlet plenum)

Step 4: The liquid mass inventory in the SG inlet plenum is calculated as:

$$M_{IP\ SG\ X,\ f} = \rho_{f,\ IP\ SG\ X} \times V_{IP\ SG\ X} \qquad 4.13\text{-}5$$

The mass of vapor in the SG inlet plenum is then calculated as:

$$M_{g,\ IP\ SG\ X} = \rho_{g,\ IP\ SG\ X} \times (V_{TOTAL\ SG\ X} - V_{f,\ IPSG\ X}) \qquad 4.13\text{-}6$$

where:

V_{TOTAL} = Total volume of the SG inlet plenum of interest

Step 5: The total fluid mass in the inlet plenum of the SG of interest is then calculated by summing the mass associated with each phase in the plenum:

$$M_{IP\ SG\ X} = (M_{f,\ IP} + M_{g,\ IP})_{SG\ X} \qquad 4.13\text{-}7$$

Step 6: The rate of change in mass inventory of the SG inlet plenum may be approximated by differencing two consecutive calculated values of liquid mass:

$$\frac{dM_{IP\ SG\ X}}{dt} \approx \frac{\Delta M_{IP\ SG\ X}}{\Delta t} = \frac{(M_{IP\ SG\ X,\ i} - M_{IP\ SG\ X,\ i-1})}{t_i - t_{i-1}} \qquad 4.13\text{-}8$$

where the subscript:

i = Index of the data and time arrays

4.13.1.2 Energy Balance

Equation 4.13-2 defines the general form of an energy balance for the SG inlet plenum. The plenum may contain both vapor and liquid at the same time. The energy balance must account for both phases of the working fluid. Thus, the left hand side of Equation 4.13-2 may be expanded as:

$$c_P \cdot \frac{d(M_{IP\ SG\ X}(T - T_{REF}))}{dt} = c_{P,f}\, M_{f,\ IP\ SG\ X} \frac{d(T_f)}{dt} + c_{P,f}\,(T_f - T_{REF}) \frac{d(M_{f,\ IP\ SG\ X})}{dt} + c_{P,g}\, M_{g,\ IP\ SG\ X} \frac{d(T_g)}{dt} + c_{P,g}\,(T_g - T_{REF}) \frac{d(M_{g,\ IP\ SG\ X})}{dt} \qquad 4.13\text{-}9$$

where:

T_{REF} = Reference temperature, 32°F

Writing the preceding equation in its difference form, the rate of change of energy associated with the fluid in the SG inlet plenum is calculated:

$$c_p \frac{d\,(M_{IP\ SG\ X}\ (T-T_{REF}))}{dt} = c_{p,f}\, M_{f,\ IP\ SG\ X} \frac{\Delta T_f}{\Delta t} + c_{p,f}\,(T_f - T_{REF}) \frac{\Delta M_{f,\ IP\ SG\ X}}{\Delta t}$$

4.13-10

$$+ c_{p,g}\, M_{g,\ IP\ SG\ X} \frac{\Delta T_g}{\Delta t} + c_{p,g}\,(T_g - T_{REF}) \frac{\Delta M_{g,\ IP\ SG\ X}}{\Delta t}$$

The data channel IDs of the instruments to be used to evaluate the thermal transport properties for this calculation are listed in Table 4.13-1. Note that the value for T_f will be taken as the minimum of the measured temperature and saturation temperature. The value for T_g will be taken as the maximum of the measured temperature and saturation temperature.

The energy rate of change in stored energy in the SG inlet plenum metal components is expressed as:

$$Q_{IP\ SG\ X\ METAL} = M_{IP\ SG\ X\ METAL} \times c_{p,\ METAL} \times \frac{dT_{METAL}}{dt} \qquad 4.13\text{-}11$$

Representing the preceding equation in its difference form:

$$Q_{IP\ SG\ X\ METAL} = M_{IP\ SG\ x\ METAL} \times c_{P,\ METAL} \times \frac{\Delta T_{METAL}}{\Delta t} \qquad 4.13\text{-}12$$

For these calculations, the outside surface temperature of the SG inlet plenum will be used to represent the average temperature of all the inlet plenum metal. The specific data channel IDs to be used for these calculations are listed in Table 4.13-1.

The heat loss from the inlet plenum of each SG may be represented in the form:

$$Q_{IP\ SG\ X\ AMB} = A_{IP\ SG\ X} \times q \qquad 4.13\text{-}13$$

where:

A	=	Effective area of SG inlet plenum being considered, ft.^{2}
q	=	Flux, Btu/(hr-ft.^{2}) (Flux meters HFM-301 and HFM-302 are used.)

The rate of energy loss to the ambient may be calculated using data collected from the inlet plenum surface temperature instruments identified in Table 4.13-1.

The quality in the inlet plenum is calculated as:

$$X = \frac{M_{g,\ IP\ SG\ X}}{M_{g,\ IP\ SG\ X} + M_{f,\ IP\ SG\ X}} \qquad 4.13\text{-}14$$

For use in the overall system energy balance calculations, the fluid stored energy in SG inlet plenums is given by the following:

$$U_{IP\ SG\ X} = U_{f,\ IP\ SG\ X} + U_{g,\ IP\ SG\ X} \qquad 4.3\text{-}15$$

where:

$$U_{f,\ IP\ SG\ X} = M_{f,\ IP\ SG\ X} \times c_{p_{f,\ IP\ SG\ X}} \times (T_{f,\ IP\ SG\ X} - T_{ref}) \qquad 4.13\text{-}16$$

and:

$$U_{g,\ IP\ SG\ X} = M_{g,\ IP\ SG\ X} \times c_{p_{g,\ IP\ SG\ X}} \times (T_{g,\ IP\ SG\ X} - T_{ref}) \qquad 4.13\text{-}17$$

4.13.2 Steam Generator Tubes

The general mass balance equation for the tubes in each SG may be written as:

$$\frac{dM_{TUBES\ SG\ X}}{dt} = \dot{M}_{IP\text{-}TUBE\ SG\ X} - \dot{M}_{TUBE\text{-}OP\ SG\ X} \qquad 4.13\text{-}18$$

where the subscripts:

TUBE	=	Tube bundle of an SG
TUBE-OP	=	Interface between tube bundle of SG and SG outlet plenum

4.13.2.1 Mass Balance

The mass stored in the tubes of each SG is calculated from level measurements across the hot leg (up-hill side) and cold leg (down-hill side) of the tubes. Like other level measurements taken with the test facility, these measurements must be compensated for temperature differences between the fluid in

the tubes and in the sense lines of the instruments. The data channel IDs of the level, pressure, and temperature instruments to be used in calculating fluid mass in the inlet plenums are listed in Table 4.13-1.

The installation of the common reference leg for the level and pressure transducers on the SG tubes provides for the fluid inventory of the leg to be at the same temperature as the SG secondary side at the initiation of a test. Once the primary-side pressure drops below that of the SG secondary side, the reference leg begins to boil off. This boil-off continues until all fluid in the reference leg that was at or above primary loop saturation temperature has flashed. The boil-off of the reference leg causes the level and pressure transducers to give false indications of water in the tubes and a change in pressure at the top of the tubes. Furthermore, refilling the SG tubes with water is not possible, as the SG secondary side acts as a heat source that is above the saturation temperature of the primary side. Thus, logic has been implemented in the code that, once drained, precludes the tubes from refilling. This approach was taken as data indicated the tubes drain before the primary-side pressure decreases below that of the secondary side.

The following approach is to be used in performing the temperature compensation of the levels instrument output and calculating the fluid mass in the SG inlet plenum.

Step 1: Compensate the levels readings associated with the tube level transducers to account for temperature differences between fluid in the tubes and fluid in the reference legs of the instrument lines. As noted above, the channel IDs of the four level transducers to be compensated, two for each SG, are identified in Table 4.13-1. The instruments used to measure local pressure and fluid temperatures to be used to accomplish the compensation are also identified in Table 4.13-1.

Step 2: The local pressures and temperatures identified in Table 4.13-1 are used as inputs to the ASME steam tables to calculate the thermodynamic properties of the fluid in the inlet plenum:

$$\rho_f = \rho_f(P, T) \qquad \rho_g = \rho_g(P, T)_g$$
$$h_f = h_f(P, T) \qquad h_g = h_g(P, T)_g \qquad \text{4.13-19}$$

Step 3: Using the compensated liquid level and the volume in the SG tubes as a function of height (see Tables 4.13-3 and 4.13-4), the volume of liquid in the tubes of a given SG is calculated as:

$$V_{f,\,\text{TUBES XL}} = V(l)_{\text{TUBES XL}} \times \text{LDP-XXX}_{\text{COMP}} \qquad \text{4.13-20}$$

where the subscript:

XL = Side of the tubes of a given SG being considered:
- XL = HL (hot-leg side)
- XL = CL (cold-leg side)

The total volume of liquid in the tubes of a given SG is then calculated as:

$$V_{f,\ TUBES} = V_{f\ TUBES\ CL} + V_{f,\ TUBES\ HL} \qquad 4.13\text{-}21$$

It follows that the volume of vapor in that SG tubes is calculated as:

$$V_{g,\ TUBES} = V_{TUBES\ TOTAL} - V_{f,\ TUBES} \qquad 4.13\text{-}22$$

where the subscript:

TOTAL = Total volume of the tubes bundle of a given SG, $ft.^3$

Step 4: Accounting for a difference in fluid temperature between the hot leg and cold leg sides of the SG tubes, the liquid mass inventory in each side of the SG tubes of interest is calculated as:

$$M_{f,\ TUBES\ XL} = \rho_f \times V_{f,\ TUBES\ XL} \qquad 4.13\text{-}23$$

The total liquid mass in the SG tubes is then calculated as:

$$M_{f,\ TUBES} = M_{f,\ TUBES\ CL} + M_{f,\ TUBES\ HL} \qquad 4.13\text{-}24$$

The mass of vapor in the tubes of the SG of interest is then calculated as:

$$M_{g,\ TUBES} = \rho_{g,\ TUBES} \times (V_{TOTAL} - V_{f,\ TUBES}) \qquad 4.13\text{-}25$$

Step 5: The total fluid mass in the tubes of the SG of interest is calculated by summing the mass associated with each phase in the tubes:

$$M_{TUBES} = (M_{f,\ TUBES} + M_{g,\ TUBES}) \qquad 4.13\text{-}26$$

Step 6: The rate of change in mass inventory may be approximated by differencing two consecutive calculated values of liquid mass:

$$\frac{dM_{TUBES}}{dt} \approx \frac{\Delta M_{TUBES}}{\Delta t} = \frac{(M_{TUBES,\,i} - M_{TUBES,\,i-1})}{t_i - t_{i-1}} \qquad 4.13\text{-}27$$

where the subscript:

i = Index of the data and time arrays

The total mass flow rate from the inlet plenum into the tubes of a given SG is calculated from Equation 4.13-1. With the change in mass storage of the tubes of a given SG calculated from Equation 4.13-26, the terms of the general mass balance on the SG tube bundle, Equation 4.13-18, may be rearranged to solve for the mass flow from the tubes into the outlet plenum of interest.

4.13.2.2 Energy Balance

Equation 4.13-15 defines the general form of an energy balance for the SG tubes. The tubes may contain both vapor and liquid at the same time. The energy balance must account for both phases of the working fluid. Thus, the left-hand side of Equation 4.13-15 may be expanded as:

$$c_p \frac{d(M\,T)_{TUBES}}{dt} = c_{p,\,f}\left(T_{f,\,TUBES} - T_{REF}\right)\frac{d\,(M_{f,\,TUBES})}{dt} + c_{p,\,f}\,M_{f,\,TUBES}\frac{d(T_{f,\,TUBES})}{dt} + c_{p,\,g}\left(T_{g,\,TUBES} - T_{REF}\right)\frac{d(M_{g,\,TUBES})}{dt} + c_{p,\,g}\,M_{g,\,TUBES}\frac{d(T_{g,\,TUBES})}{dt} \qquad 4.13\text{-}28$$

where:

T_{REF} = Reference temperature; 32°F

Equation 4.13-28 may be further expanded to specifically address the liquid volume on the hot leg ("uphill" side) and cold leg ("downhill" side) of the SG tubes, and written in its difference form to operate on the data:

$$c_p \frac{d(MT)_{TUBES}}{dt} \approx c_{p,f} M_{f,TUBES} \frac{\Delta T_{f,TUBES}}{\Delta t} + c_{p,f} (T_f - T_{REF}) \frac{\Delta M_{f,TUBES}}{\Delta t}$$

$$+ c_{p,g} M_{g,TUBES} \frac{\Delta T_{g,TUBES}}{\Delta t} + c_{p,g} (T_g - T_{REF}) \frac{\Delta M_{g,TUBES}}{\Delta t} \qquad 4.13\text{-}29$$

The data channel IDs of the instruments to be used to evaluate the thermal transport properties are listed in Table 4.13-1. Note that the value for T_f will be taken as the minimum of the average measured temperature and saturation temperature. The value for T_g will be taken as the maximum of the average measured temperature and saturation temperature.

The equation for the rate of change in internal energy of the metal of a tube bundle is written as:

$$Q_{TUBE\ SG\ X\ METAL} = M_{TUBE\ SG\ X\ METAL} \times c_{p,METAL} \times \frac{dT_{TUBE\ SG\ X\ METAL}}{dt} \qquad 4.13\text{-}30$$

Representing the rate of change in energy stored by the metal of the tubes of each SG in difference form:

$$Q_{TUBE,\ SG\ X\ METAL} = M_{TUBE,\ SG\ X\ METAL} \times c_{p,METAL} \times \frac{\Delta T_{TUBE\ SG\ X\ METAL}}{\Delta t} \qquad 4.13\text{-}31$$

The data channel IDs to be used for the metal energy storage calculations are listed in Table 4.13-1.

The quality in the hot-leg side of the tubes is calculated as:

$$X = \frac{M_{g,TUBE\text{-}OP}}{M_{g,TUBE\text{-}OP} + M_{f,TUBE\text{-}OP}} \qquad 4.13\text{-}32$$

For use in the overall system energy balance calculations, the fluid stored energy in the SG tubes is given by the following:

$$U_{TUBE\ SG\ X} = U_{f,TUBE\ SG\ X} + U_{g,TUBE\ SG\ X} \qquad 4.13\text{-}33$$

where:

$$U_{f,\ TUBE\ SG\ X} = M_{f,\ TUBE\ SG\ X} \times c_{p,f} \times (T_{f,\ TUBE\ SG\ X} - T_{ref}) \qquad 4.13\text{-}34$$

and:

$$U_{g,\ TUBE\ SG\ X} = M_{g,\ TUBE\ SG\ X} \times c_{p,g} \times (T_{g,\ TUBE\ SG\ X} - T_{ref}) \qquad 4.13\text{-}35$$

4.13.3 Outlet Plenum

A general mass balance equation for the SG outlet plenums may be written as:

$$\frac{d\ M_{OP\ SG\ X}}{dt} = \dot{M}_{TUBE\text{-}OP\ SG\ X} - \dot{M}_{OP,CL\ X/Y} \qquad 4.13\text{-}36$$

where the subscripts:

CL X/Y	=	Designates cold legs where: X/Y = 1/3 (SG-1) X/Y = 2/4 (SG-2)
OP	=	SG outlet plenum
TUBE-OP	=	Interface between tube bundle and outlet plenum of a SG

Similarly, the energy equation for the SG outlet plenum is written as:

$$c_P \frac{d(MT)_{OP}}{dt} = \dot{M}_{TUBE\text{-}OP}\ h_{TUBE\text{-}OP\ MIX} - \dot{M}_{OP,CL\ X/Y}\ h_{TUBE\text{-}OP\ MIX} - Q_{OP\ SG\ X\ METAL} - Q_{OP\ SG\ X\ AMB} \qquad 4.13\text{-}37$$

4.13.3.1 Mass Balance

The mass stored in the SG outlet plenum is calculated from a level measurement in the plenum. Like other level measurements taken with the test facility, these measurements must be compensated for temperature differences between the fluid in the plenum and that in the sense lines of the instruments. The data channel IDs of the level, pressure, and temperature instruments to be used in calculating fluid mass in the inlet plenums are listed in Table 4.13-1. The approach taken to compensate these level readings is identical to that of the inlet plenum and will not be repeated. The volume versus height values for the SG outlet plenum are provided in Table 4.13-5.

Similarly, calculation of fluid mass in the outlet plenum, and mass flow rates into and out of the outlet plenum are the same as those performed for the inlet plenum and are not repeated here.

4.13.3.2 Energy Balance

The calculation of an energy balance for the SG outlet plenums is similar to that performed for the inlet plenums and is not repeated here. The data channels used in the calculation of the energy balance for the outlet plenums are listed in Table 4.13-1. Since there is no instrumentation on the outlet plenums, heat loss is calculated by scaling the heat loss from the inlet plenum. The metal energy and heat loss to ambient calculations are performed using the inlet plenum surface temperature measurements.

The heat loss from the outlet plenum from each SG is calculated as:

$$Q_{OP\ SG\ X\ AMB} = Q_{IP\ SG\ X\ AMB} \times \frac{T_{OP,f} - T_{amb}}{T_{IP,f} - T_{amb}} \qquad 4.13\text{-}38$$

where:

T_{amb}	=	Ambient temperature
$T_{OP,f}$	=	Fluid temperature in the outlet plenum
$T_{IP,f}$	=	Fluid temperature in the inlet plenum

TABLE 4.13-1
DATA CHANNEL ID FOR SG INLET PLENUM MASS AND ENERGY CALCULATIONS

Location		Data Channel ID for Liquid Levels	Data Channel ID for Pressure Transducers	Data Channel ID for Fluid Thermocouples	Notes
SG-1 inlet plenum		LDP-209	PT-205	TF-205	Metal Surface TEMP = TFM-301
SG-1 tubes	Hot-leg side	LDP-215	PT-201	TF-205 TF-211 TF-217	
	Cold-leg side	LDP-219	PT-201	TF-217 TF-213 TF-201 TF-203	
SG-1 outlet plenum	CL-1	LDP-213	PT-201	TF-201	Subtract elevation head of water in tubes to calculate local pressure
	CL-3	LDP-211	PT-201	TF-203	
SG-2 inlet plenum		LDP-214	PT-202	TF-206	Metal Surface TEMP = TFM-302
SG-2 tubes	Hot-leg side	LDP-218	PT-204	TF-206 TF-212 TF-218	
	Cold-leg side	LDP-222	PT-204	TF-218 TF-214 TF-202 TF-204	
SG-2 outlet plenum	CL-2	LDP-210	PT-204	TF-202	ubtract elevation head of water in tubes to calculate local pressure
	CL-4	LDP-212	PT-204	TF-204	

TABLE 4.13-2 VOLUME VERSUS HEIGHT TABLE FOR STEAM GENERATOR INLET PLENUM	
Height (in.)	**Volume ($in.^3$)**
0.25	105.8
1.25	197.5
2.25	205.8
3.25	427.7
4.25	560.2
5.25	700.3
6.25	830.9
6.75	897.0
7.25	963.1
8.25	1095.4
9.25	1227.7
10.25	1359.9
11.25	1492.2
12.25	1624.5
13.25	1756.7
14.25	1889.0
15.25	2021.2

TABLE 4.13-3 VOLUME VERSUS HEIGHT TABLE FOR STEAM GENERATOR TUBES (DOWN-HILL SIDE)	
Height (in.)	**Volume ($in.^3$)**
0	0
102.0	3918.0

TABLE 4.13-4 VOLUME VERSUS HEIGHT TABLE FOR STEAM GENERATOR TUBES (UP-HILL SIDE)	
Height (in.)	**Volume ($in.^3$)**
0	0
102.0	3918.0

TABLE 4.13-5 VOLUME VERSUS HEIGHT TABLE FOR STEAM GENERATOR OUTLET PLENUM	
Height (in.)	**Volume ($in.^3$)**
3.45	42.73
4.45	78.74
5.45	136.99
6.45	214.72
7.45	309.01
8.45	416.90
9.45	535.39
10.45	661.46
11.45	792.08
11.95	858.15
12.45	924.32
13.45	1056.59
14.45	1188.85
15.45	1321.12
16.45	1453.38
17.45	1585.64
18.45	1717.91
19.45	1850.17
20.45	1982.43

4.14 Steam Generator Secondary Side

The design of the AP600 includes two SGs. Under normal operating conditions, the SGs are a heat sink for reactor core heat removal and a steam source to power the turbine. During a transient, the secondary side becomes a potential heat source to the primary side when the primary side depressurizes and cools below the temperature of the secondary side.

This subsection presents the equations for SG-1 and SG-2. The calculations are the same for both components. The notation is as follows:

SG SS X	=	SG secondary side in general
SG SS 1	=	SG-1 secondary side specifically
SG SS 2	=	SG-2 secondary side specifically

Other notation in this section is as follows:

f	=	Liquid phase of water
g	=	Steam

4.14.1 Inputs and Assumptions

A general mass balance on the SG secondary side may be expressed as:

$$\frac{dM_{SG\ SS\ X}}{dt} = \dot{M}_{f,\ SG\ SS\ X} - \dot{M}_{g,\ SG\ SS\ X} \qquad 4.14\text{-}1$$

For small time-steps, the time rate of change of mass in the SG secondary side may be approximated as:

$$\frac{dM_{SG\ SS\ X}}{dt} \approx \frac{\Delta M_{SG\ SS\ X}}{\Delta t} = \frac{M_{SG\ SS\ X,\ i} - M_{SG\ SS\ X,\ i-1}}{t_i - t_{i-1}} \qquad 4.14\text{-}2$$

where the difference terms represent data from two consecutive calculations or data scans.

In general, the secondary-side liquid inventory mass is calculated in three steps:

1) Determine the temperature-compensated collapsed liquid level in the secondary side

2) Calculate the liquid volume from the collapsed liquid level

3) Calculate the liquid mass using the local thermodynamic properties of water determined from local pressure and fluid temperature measurements

The pertinent data channels associated with the SG-1 secondary side are shown in Table 4.14-1, and the pertinent data channels associated with the SG-2 secondary side are shown in Table 4.14-2. In addition to the flow meters for the individual SGs, another flow meter provides information for the flows out of the secondary-side system. This flow meter is attached to the line that contains combined flow from the two SGs and the data channels associated with this combined flow meter are shown in Table 4.14-3.

Flow from the flow meter data channels (that is, FMM and FVM data channels) use a lower bound of 0.0. Negative values from these flow meters were not used.

The geometry of the SGs is indirectly defined by Table 4.14-4, showing volume as a function of fluid height. In the following equations, this function is expressed as the function $V(level_f)$. Although narrow-range and wide-range data channels were available at the OSU test facility, the calculations assume that the wide-range channels are used. To avoid out-of-range errors, the fluid level readings are bounded to the values shown in Table 4.14-4.

There are no direct interfaces to other components that provide values to equations for this component.

4.14.2 Mass Balance Calculations

4.14.2.1 Steam Generator Secondary Components

The equations listed below hold for SG-1 and SG-2. Only the channel names differ, as shown in Tables 14.4-1 and 14.4-2.

The fluid mass stored in the SG secondary side is calculated from a wide-range level measurement of that volume. Like other level measurements, these readings must be density-compensated. The following approach is used in performing the density compensation of the SG secondary-side level measurements.

The temperature channels are located at equal elevations on opposite sides of the component. For calculations and for LDP compensation, use the average of these two channels:

$$T_f = \frac{T_1 + T_2}{2} \qquad 4.14\text{-}3$$

The density of the fluid in the SG secondary side is obtained from a standard steam table specific volume call:

$$\rho_f = \frac{1.0}{VCL(P_f\ ,\ T_f)} \qquad 4.14\text{-}4$$

The specific heat of the fluid in the SG secondary side is obtained from a standard steam table call:

$$c_{p,f} = CPL(P_f\ ,\ T_f) \qquad 4.14\text{-}5$$

The mass of fluid is calculated:

$$M_f = \rho_f \times V(level_f) \times C \qquad 4.14\text{-}6$$

where:

$V(level_f)$ = Volume as a function of SG secondary side liquid, $in.^3$
C = Conversion constant, $in.^3$ to $ft.^3$

The energy flow rate for this mass is defined:

$$Q_f = M_f \times c_{p,f} \times \frac{\Delta T_f}{\Delta t} \qquad 4.14\text{-}7$$

Since the facility also has flow meters associated with this component, additional calculations can be defined for mass flows in and out of the component.

The enthalpy of the fluid flowing into the SG secondary side is obtained from a standard steam table enthalpy call:

$$h_{IN_f} = HCL(P_{IN_f}\ ,\ T_{IN_f}) \qquad 4.14\text{-}8$$

The density of the fluid flowing into the SG secondary side is obtained from a standard steam table specific volume call:

$$\rho_{IN_i} = \frac{1.0}{VCL(P_{IN_i}, T_{IN_i})} \qquad 4.14\text{-}9$$

The mass flow rate into the SG secondary side is calculated:

$$\dot{M}_{IN_i} = W_{IN_i} \times \rho_{IN_i} \times C \qquad 4.14\text{-}10$$

where:

W = Volumetric flow rate of liquid, gpm
C = Conversion constant, gpm to ft.^{3}/sec.

The energy flow rate of the fluid flowing into the SG secondary side is defined:

$$Q_{IN_i} = h_{IN_i} \dot{M}_{IN_i} \qquad 4.14\text{-}11$$

Likewise, the enthalpy and the specific volume of the vapor flowing out of the SG secondary side are obtained from a standard steam table enthalpy call:

$$h_{OUT_s}, v_{OUT_s} = HSS(P_{OUT_s}, T_{OUT_s}) \qquad 4.14\text{-}12$$

The density of the vapor flowing out of the SG secondary side is defined:

$$\rho_{OUT_s} = \frac{1.0}{v_{OUT_s}} \qquad 4.14\text{-}13$$

The mass flow rate out of the SG secondary side is calculated:

$$\dot{M}_{OUT_s} = W_{OUT_s} \times \rho_{OUT_s} \times C_1 \qquad 4.14\text{-}14$$

where:

W = Volumetric flow rate of steam, $ft.^3/min.$

C_1 = Conversion constant, min. to sec.

Then, the change of the mass for the secondary side is defined:

$$\frac{\Delta M_{SG}}{\Delta t} = \dot{M}_{IN_s} - \dot{M}_{OUT_s} \qquad 4.14\text{-}15$$

The energy flow rate of the vapor flowing out of the SG secondary side is defined:

$$Q_{OUT_s} = h_{OUT_s} \dot{M}_{OUT_s} \qquad 4.14\text{-}16$$

4.14.2.2 Steam Generator System

The flow meter that is associated with the combined flows from both secondary-side components provides values that can be compared to the calculated masses from the other data channels.

A mass-weighted enthalpy at the site of this flow meter is calculated:

$$h_{OUT_{TOTAL}} = \frac{(\dot{M}_{OUT,g,SG1} \times h_{OUT,g,SG1}) + (\dot{M}_{OUT,g,SG2} \times h_{OUT,g,SG2})}{\dot{M}_{OUT,g,SG1} + \dot{M}_{OUT,g,SG2}} \qquad 4.14\text{-}17$$

The specific volume of the vapor flowing out of the SG secondary side is obtained from a standard steam table call:

$$v_{OUT_{TOTAL}} = \text{SSSISSS}\ (\ P_{OUT_{TOTAL}}\ ,\ h_{OUT_{TOTAL}}\ ) \qquad 4.14\text{-}18$$

The density of the vapor flowing out of the SG secondary side is defined:

$$\rho_{OUT_{TOTAL}} = \frac{1.0}{v_{OUT_{TOTAL}}} \qquad 4.14\text{-}19$$

The mass flow rate out of the SG secondary side system is calculated:

$$\dot{M}_{OUT_{TOTAL}} = W_{OUT_{TOTAL}} \times \rho_{OUT_{TOTAL}} \times C_1 \qquad 4.14\text{-}20$$

where:

C_1 = Conversion constant, min. to sec.

TABLE 4.14-1 INSTRUMENT CHANNEL IDs FOR SG-1 SECONDARY-SIDE MASS AND ENERGY CALCULATIONS		
Channel ID	**Notation in this Section**	**Description**
PT-301	P_f	Pressure of the fluid (psig)
TF-305	T_1	Temperature (1) of the fluid (°F)
TF-307	T_2	Temperature (2) of the fluid (°F)
LDP-301	$level_f$	Level of the fluid (wide range) (in.)
FMM-001	W_{IN_i}	Volumetric flow rate of the fluid into the component (gpm)
TF-311	T_{IN_i}	Temperature of the fluid into the component (°F)
PT-001	P_{IN_i}	Pressure of the fluid into the component (psig)
FVM-001	W_{OUT_i}	Volumetric flow rate of the vapor out of the component ($ft.^3$/min.)
PT-301	P_{OUT_i}	Pressure of the vapor out of the component (psig)

TABLE 4.14-2 INSTRUMENT CHANNEL IDs FOR SG-2 SECONDARY-SIDE MASS AND ENERGY CALCULATIONS		
Channel ID	**Notation in this Section**	**Description**
PT-302	P_f	Pressure of the fluid (psig)
TF-306	T_1	Temperature (1) of the fluid (°F)
TF-308	T_2	Temperature (2) of the fluid (°F)
LDP-302	$level_f$	Level of the fluid (wide range) (in.)
FMM-002	W_{IN_s}	Volumetric flow rate of the fluid into the component (gpm)
TF-312	T_{IN_s}	Temperature of the fluid into the component (°F)
PT-001	P_{IN_s}	Pressure of the fluid into the component (psig)
FVM-002	W_{OUT_s}	Volumetric flow rate of the vapor out of the component ($ft.^3$/min.)
PT-302	P_{OUT_s}	Pressure of the vapor out of the component (psig)

TABLE 4.14-3
INSTRUMENT CHANNEL IDs FOR SG SYSTEM
SECONDARY-SIDE MASS AND ENERGY CALCULATIONS

Channel ID	Notation in this Section	Description
FVM-003	$W_{OUT_{TOTAL}}$	Volumetric flow rate of the vapor (ft.^{3}/min.)
PT-002	$P_{OUT_{TOTAL}}$	Pressure of the vapor (psig)

TABLE 4.14-4
FLUID HEIGHT VERSUS VOLUME FOR SG
SECONDARY-SIDE MASS AND ENERGY CALCULATIONS

Secondary Side-1		Secondary Side-2	
Fluid Level (in.)	**Volume (in.^{3})**	**Fluid Level (in.)**	**Volume (in.^{3})**
0.0	963.0	0.0	963.0
46.5	9100.0	46.5	9106.0
94.5	17,984.0	94.5	17,957.0
99.25	19,148.0	99.5	19,317.0
119.0	25,885.0	119.0	26,738.0

4.15 Pressurizer

The pressurizer is a tank-like structure through which mass flows from the primary system to the first three stages of the ADS valves under accident mitigation. At steady-state, the pressurizer has an initial liquid and steam volume. During a transient, the initial pressurizer and primary-side inventory are vented by the ADS through a pipe running from the top of the pressurizer to the IRWST.

Subscript notation in this section is as follows:

f	=	Liquid phase of water
g	=	Steam
PRZR	=	Pressurizer
SL-PRZR	=	Connection between the pressurizer and the surge line
ADS13	=	Connection between the pressurizer and ADS 1-3
AMB	=	Ambient environment
METAL	=	Pressurizer metal

4.15.1 Inputs and Assumptions

A general mass balance for the pressurizer may be expressed as:

$$\frac{dM_{PRZR}}{dt} = \dot{M}_{SL-PRZR} - \dot{M}_{ADS13} \qquad 4.15\text{-}1$$

Similarly, a general energy balance on the pressurizer may be expressed as:

$$c_p \frac{d\,(MT_{PRZR})}{dt} = Q_{SL-PRZR} - Q_{ADS13} - Q_{METAL} - Q_{AMB} \qquad 4.15\text{-}2$$

The pertinent data channels associated with the pressurizer are shown in Table 4.15-1. In addition, the following values are provided by the ADS 1-3 module:

Q_{ADS13}	=	Energy rate from pressurizer by way of ADS 1-3 (Btu/sec.)
$\dot{M}_{ADS13}$	=	Mass flow rate through the ADS 1-3 (lbm/sec.)

The geometry of the pressurizer is indirectly defined by Table 4.15-2, showing volume as a function of fluid height. In the equations below, this function is expressed as $V(level_f)$.

Table 4.15-3 provides the data channels and metal structure information needed for the pressurizer metal segments.

In the calculation of the heat loss to the metal, the heat capacity of a segment is defined as a function of the metal temperature $\left(\text{heat\_cap}(T_{surf}(j))\right)$. Table 4.15-4 provides this function.

4.15.2 Mass Balance Calculation

The fluid level reading from LDP-601 needs to be compensated to account for temperature differences between fluid in the pressurizer and fluid in the reference leg of the instrument line. Since two temperature sensors are defined for the pressurizer, the temperatures are averaged for the fluid temperature:

$$T_f = \frac{T1 + T2}{2.0} \qquad 4.15\text{-}3$$

The density of the fluid in the pressurizer is obtained from an ASME steam table specific volume call:

$$\rho_f = \frac{1.0}{VCL(P_f\ ,\ T_f)} \qquad 4.15\text{-}4$$

The mass of the fluid is then calculated:

$$M_f = \rho_f \times V(level_f) \times C \qquad 4.15\text{-}5$$

where:

C = Conversion constant, $in.^3$ to $ft.^3$

The fluid specific heat, $c_{p,f}$, is defined from a steam table call:

$$c_{p,f} = CPL(P_f\ ,\ T_f) \qquad 4.15\text{-}6$$

The enthalpy of the fluid from the surge line into the pressurizer is defined from a steam table call:

$$h_{SL-PRZR} = HCL(P_f , T_f) \qquad 4.15\text{-}7$$

The void fraction of the pressurizer is defined:

$$vf_f = 1.0 - \frac{V(level_f)}{V_{TOT}} \qquad 4.15\text{-}8$$

where V_{TOT} is the maximum value provided by the fluid height versus volume data in Table 4.15-2. This void fraction is bounded:

$$0.0 \leq vf_f \leq 1.0 \qquad 4.15\text{-}9$$

The vapor specific heat, $c_{p,g}$, and specific volume, v_g, are defined from a steam table call:

$$v_g, c_{p,g} = CPV(P_g , T_g) \qquad 4.15\text{-}10$$

The vapor density is defined:

$$\rho_g = \frac{1.0}{v_g} \qquad 4.15\text{-}11$$

The volume of the vapor in the pressurizer is defined:

$$V_g = V_{TOT} - V_f \qquad 4.15\text{-}12$$

The mass of the vapor is calculated:

$$M_g = \rho_g \times V_g \times C \qquad 4.15\text{-}13$$

The total mass (lbm) in the pressurizer is defined:

$$M_{PRZR} = M_f + M_g \qquad 4.15\text{-}14$$

The rate of change in mass inventory of the pressurizer may be approximated by differencing two consecutive calculated values of the liquid and vapor masses:

$$\frac{dM_{f,\,PRZR}}{dt} \approx \frac{\Delta M_{f,\,PRZR}}{\Delta t} = \frac{M_{f_i} - M_{f_{i-1}}}{t_i - t_{i-1}}$$

$$\frac{dM_{g,\,PRZR}}{dt} \approx \frac{\Delta M_{g,\,PRZR}}{\Delta t} = \frac{M_{g_i} - M_{g_{i-1}}}{t_i - t_{i-1}} \qquad 4.15\text{-}15$$

where the difference terms represent data from two consecutive calculations or data scans.

The total rate of change of the mass inventory of the pressurizer is calculated:

$$\frac{dM_{PRZR}}{dt} \approx \frac{\Delta M_{PRZR}}{\Delta t} = \frac{\Delta M_{f,\,PRZR} + \Delta M_{g,\,PRZR}}{\Delta t} \qquad 4.15\text{-}16$$

The mass rate of flow through ADS 1-3 is calculated in the ADS 1-3 module. The rate of flow from the surge line into the pressurizer may now be solved by rearranging Equation 4.15-1, and solving for the rate of flow from the surge line into the pressurizer:

$$\dot{M}_{SL\text{-}PRZR} = \frac{\Delta M_{PRZR}}{\Delta t} + \dot{M}_{ADS13} \qquad 4.15\text{-}17$$

Thus, the mass flow into the pressurizer from the surge line is calculated using the pressurizer mass storage term and the total ADS mass flow rate.

In addition, the enthalpy of the fluid in the line is provided by a steam table call:

$$h_{SL\text{-}PRZR_i} = HCL\ (\ P_f\ ,\ T_f\ ) \qquad 4.15\text{-}18$$

4.15.3 Energy Balance

The energy flow associated with the pressurizer consists of the following components:

- Rate of change in stored energy of the pressurizer inventory
- Rate of energy transport to the pressurizer from the surge line
- Rate of energy transport from the pressurizer by way of ADS 1-3
- Rate of change in stored energy of the pressurizer metal
- Rate of energy loss to the environment

Expressions for each of these components is developed in the following subsections.

4.15.3.1 Rate of Change of Energy in the Pressurizer Fluid Inventory

The stored energy of the pressurizer inventory must account for both the liquid and vapor phases of the inventory:

$$c_P \frac{d\,(M\,T)_{PRZR}}{dt} = c_{P,f} \frac{d\,(M_f\,T_f)_{PRZR}}{dt} + c_{P,g} \frac{d\,(M_g\,T_g)_{PRZR}}{dt} \qquad 4.15\text{-}19$$

The equation for energy change associated with the liquid phase of the pressurizer inventory may be expressed:

$$c_{P,f} \frac{d(\,M_f\,(T_f - T_{REF})\,)_{PRZR}}{dt} = c_{P,f}\,(T_f - T_{REF}) \frac{d(\,M_{f,PRZR}\,)}{dt} + c_{P,f}\,M_{f,PRZR} \frac{d(\,T_f\,)}{dt} \qquad 4.15\text{-}20$$

where:

T_{REF} = Reference temperature, 32°F

Similarly, the energy change associated with the vapor phase of the pressurizer inventory may be expressed as:

$$c_{P,g}\frac{d(M_g(T_g-T_{REF}))}{dt} = c_{P,g}(T_g-T_{REF})\frac{d(M_g)}{dt} + c_{P,g}M_g\frac{d(T_g)}{dt} \qquad 4.15\text{-}21$$

Expressing the preceding two equations as differences:

$$c_{P,f}\frac{d(M_{f,PRZR}(T_f-T_{REF}))}{dt} \approx c_{P,f}(T_f-T_{REF})\frac{\Delta M_{f,PRZR}}{\Delta t} + c_{P,f}M_{f,PRZR}\frac{\Delta T_f}{\Delta t} \qquad 4.15\text{-}22$$

and:

$$c_{P,g}\frac{d(M_{g,PRZR}(T_g-T_{REF}))}{dt} \approx c_{P,g}(T_g-T_{REF})\frac{\Delta M_{g,PRZR}}{\Delta t} + c_{P,g}M_{g,PRZR}\frac{\Delta T_g}{\Delta t} \qquad 4.15\text{-}23$$

Expanding the two terms on the right-hand side of the preceding two equations, the liquid phase expression becomes:

$$c_{P,f}(T_f-T_{REF})\frac{\Delta M_{f,PRZR}}{\Delta t} = c_{P,f}(T_{f,i}-T_{REF})\frac{M_{f,PRZR,i}-M_{f,PRZR,i-1}}{t_i-t_{i-1}} \qquad 4.15\text{-}24$$

$$c_{P,f}M_{f,PRZR}\frac{\Delta T_f}{\Delta t} = c_{P,f}M_{f,PRZR,i}\frac{T_{f,i}-T_{f,i-1}}{t_i-t_{i-1}}$$

and the vapor phase expression becomes:

$$c_{P,g}\,(T_g - T_{REF})\,\frac{\Delta M_{g,\,PRZR}}{\Delta t} = c_{P,g}\,(T_{g,i} - T_{REF})\,\cdot\frac{M_{g,\,PRZR,\,i} - M_{g,\,PRZR,\,i-1}}{t_i - t_{i-1}}$$

$$c_{P,g}\,M_{g,\,PRZR}\,\frac{\Delta T_g}{\Delta t} = c_{P,g}\,M_{g,\,PRZR,\,i}\,\frac{T_{g,i} - T_{g,i-1}}{t_i - t_{i-1}} \qquad 4.15\text{-}25$$

where the subscript:

i = Index of data and time arrays

Combining the expressions above, the energy rate of the pressurizer is defined:

$$Q_{PRZR} = c_{p,f}M_f\,\frac{T_{f_i} - T_{f_{i-1}}}{t_i - t_{i-1}} + c_{p,g}M_g\,\frac{T_{g_i} - T_{g_{i-1}}}{t_i - t_{i-1}} + c_{p,f}(T_f - T_{REF})\,\frac{M_{f_i} - M_{f_{i-1}}}{t_i - t_{i-1}} + c_{p,g}(T_g - T_{REF})\,\frac{M_{g_i} - M_{g_{i-1}}}{t_i - t_{i-1}} \qquad 4.15\text{-}26$$

4.15.3.2 Energy Transport Rate of ADS Flow

The energy transport associated with the flow through ADS 1-3 is calculated in the module for the ADS 1-3 separator.

4.15.3.3 Heat Loss to Metal

The heat loss to the ambient surrounding from the pressurizer is calculated:

$$Q_{metal} = \sum_{j=1}^{nsurf} (\text{heat\_cap}(T_{surf}(j)) \times M_{metal}(T_{surf}(j)) \times \frac{(T_{surf}(j)_i - T_{surf}(j)_{i-1})}{t_i - t_{i-1}} \qquad 4.15\text{-}27$$

where:

nsurf = Number of metal segments, as defined by Table 4.15-3

The metal segment masses and heat capacities are defined by Table 4.15-4.

4.15.3.4 Heat Loss to Ambient

In the calculation of the heat loss to the ambient surroundings, the pressurizer tank is modeled as having a number of segments, where the number of metal segments is defined as shown by Table 4.15-3. These divisions are chosen to coincide with the available temperature instrumentation. The heat loss for each metal segment is calculated below and then summed for the component. In the following calculations, the following constants are used:

E = Emissivity (0.8)

x = Insulation thickness (2 in.)

k = Mean thermal conductivity of insulation (0.31 Btu-in./hr.-ft.^{2})

C_1 = Conversion of °F to degrees Rankine (459.6)

CSB = Stefan-Boltzmann constant (1.713E-9 Btu/hr.-ft.^{2}-R^4)

C_2 = Conversion of hours to seconds (3600.0)

The heat loss to ambient heat transfer calculation methodology for the pressurizer is analogous to that employed for the other insulated components of the system. Each tank metal segment is treated as an insulated vertical cylinder. The calculations for the pressurizer energy loss to ambient are similar to those for the sumps, as presented in Subsection 4.9.5.5. This similarity is based on the fact that both components are insulated tanks, and both are modelled as vertical cylinders.

The turbulent range form of the free convection heat transfer correlation from Reference 16 applies, based upon the conditions of the OSU test facility air at atmospheric pressure and ambient temperature (averaged over the tests). In the radiation heat transfer correlation, an emissivity of 0.8 is assumed.

The free convection heat transfer coefficient (H_{c_j}) for a metal segment j is defined:

$$H_{c_j} = 0.09 \times \sqrt[3]{T_{surf}(j) - T_{AMB}} \qquad 4.15\text{-}28$$

The coefficient 0.09 in Equation 4.15-28 is obtained from the general form of heat transfer coefficient for air:

$$H_c = 0.19 \left[0.10\ \Delta T \right]^{1/3} = 0.09 \left[\Delta T \right]^{1/3} \qquad 4.15\text{-}29$$

The assumed insulation surface temperature (T_{if_j}) for a metal segment j is defined:

$$T_{if_j} = (0.10 \times (T_{surf_j} - T_{AMB}) + T_{AMB}) + C_1 \qquad 4.15\text{-}30$$

The use of the constant 0.10 in Equation 4.15-30 is based on the assumption that the temperature drop in the insulation is 90 percent of the overall drop in temperature between the metal temperature and the ambient temperature.

The ambient temperature (T_{or}) (°R) is defined:

$$T_{or} = T_{AMB} + C_1 \qquad 4.15\text{-}31$$

The radiant heat transfer coefficient (H_{r_j}) for a metal segment j is defined:

$$H_{r_j} = CSB \times E \times (T_{if_j}^2 + T_{or}^2) \times (T_{if_j} + T_{or}) \qquad 4.15\text{-}32$$

The surface resistance (R_{surf}) for a metal segment j is defined:

$$R_{surf_j} = \frac{1.0}{(H_{c_j} + H_{r_j}) \times A(j)} \qquad 4.15\text{-}33$$

The insulation resistance ($R_{insul}(j)$) for a metal segment j is defined:

$$R_{insul_j} = \frac{x}{k \times mean\_area(j)} \qquad 4.15\text{-}34$$

Given all of the above, the heat loss to the ambient (Btu/sec.) over all metal segments can be defined:

$$Q_{AMB} = \sum_{j=1}^{nsurf} \frac{\frac{T_{surf}(j) - T_{AMB}}{R_{surf_j} + R_{insul_j}}}{C_2} \qquad 4.15\text{-}35$$

4.15.3.5 Energy Transport Rate from the Surge Line

The energy rate of surge line flow (Btu/sec.) is defined as:

$$Q_{SL\text{-}PRZR} = Q_{PRZR} - Q_{ADS13} - Q_{metal} - Q_{AMB} \qquad 4.15\text{-}36$$

TABLE 4.15-1
INSTRUMENT CHANNEL IDS FOR PRESSURIZER MASS AND ENERGY CALCULATIONS

Channel ID	Notation in this Section	Description
PT-604	P_f	Pressure of the fluid (psig)
PT-604	P_g	Pressure of the vapor (psig)
TF-605	T1	Temperature of the fluid (°F)
SC-608	T2	Temperature of the fluid (°F)
LDP-601	$level_f$	Level of the fluid (in.)
TF-602	T_g	Temperature of the vapor (°F)
TF-006	T_{AMB}	Ambient temperature (°F)

TABLE 4.15-2 FLUID HEIGHT VERSUS VOLUME FOR PRESSURIZER MASS CALCULATIONS	
Fluid Level (in.)	**Volume ($in.^3$)**
0.0	0.0
4.625	537.1
12.5	688.7
24.5	2324.9
44.5	4634.9
64.5	7968.0
84.5	9326.8
104.95	11549.1

TABLE 4.15-3 METAL DATA FOR PRESSURIZER METAL ENERGY CALCULATIONS				
Metal Segment Number j	**Temperature Data Channel for $T_{surf}(j)$**	**Metal Mass of segment $M_{metal}(j)$ (lbm)**	**Surface Area A(j) ($ft.^2$)**	**Mean Surface Area mean_area(j) ($ft.^2$)**
1	TFM-604	30.0	3.0	2.28
2	TFM-602	2551.0	17.41	15.25
3	TFM-605	2551.0	17.41	15.25
4	TFM-607	36.0	3.0	2.28

TABLE 4.15-4 TEMPERATURE VERSUS HEAT CAPACITY FOR PRESSURIZER METAL ENERGY CALCULATIONS	
Temperature (°F)	**Heat Capacity (Btu/lbm-°F)**
70.0	0.1085
100.0	0.1109
200.0	0.1175
300.0	0.1223
400.0	0.1256
500.0	0.1279
600.0	0.1297

4.16 Pressurizer Surge Line

The pressurizer surge line is piping that connects the pressurizer to the primary system. During a transient simulation where the ADS is actuated, the surge line becomes part of the relief path from the primary system to the pressurizer, ADS, and containment.

Subscript notation in this section is as follows:

f	=	Liquid phase of water
g	=	Steam
SL	=	Surge line
HL-SL	=	Junction between the hot leg and the surge line
SL-PRZR	=	Connection between the pressurizer and the surge line
ADS13	=	ADS 1-3
AMB	=	Ambient environment
METAL	=	Pressurizer surge line metal

A general mass balance on the pressurizer surge line may be expressed as:

$$\frac{dM_{SL}}{dt} = \dot{M}_{HL-SL} - \dot{M}_{SL-PRZR} \qquad 4.16\text{-}1$$

Similarly, a general energy balance on the pressurizer surge line may be written as:

$$c_P \frac{d\,(MT_{SL})}{dt} = (\dot{M}h_f)_{HL-SL} - (\dot{M}h_f)_{SL-PRZR} - Q_{METAL} - Q_{AMB} \qquad 4.16\text{-}2$$

4.16.1 Inputs and Assumptions

The pertinent data channels associated with the pressurizer surge line are shown in Table 4.16-1. In addition, the following values are provided by the pressurizer calculations:

$\dot{M}_{SL-PRZR}$	=	Mass rate of junction between surge line and pressurizer (lbm/sec.)
$h_{SL-PRZR_f}$	=	Enthalpy of fluid in the junction between surge line and pressurizer (Btu/lbm)

The geometry of the pressurizer surge line is indirectly defined by Table 4.16-2, showing volume as a function of fluid height. In the equations below, this function is expressed as V(level$_f$). The highest volume value in this table is referenced in subsequent equations as V_{max}.

Table 4.16-3 provides the data channels and metal structure information needed for the pressurizer surge line metal segments. Only one metal segment was used to model the pressurizer surge line.

In the calculation of the heat loss to the metal, the heat capacity of a segment is defined as a function of the metal temperature (heat_cap($T_{surf}(j)$)). Table 4.16-4 provides this function.

4.16.2 Mass Balance

The fluid level reading requires compensation because the sensor is outside the actual component. Since only one temperature sensor is defined for the pressurizer surge line, no temperature averaging is required for the LDP compensation.

The density of the fluid in the pressurizer surge line is obtained from a standard steam table specific volume call:

$$\rho_f = \frac{1.0}{VCL(P_f\ ,\ T_f)} \qquad 4.16\text{-}3$$

The mass of the water in the pressurizer surge line is then calculated:

$$M_f = \rho_f \times V(level_f) \times C \qquad 4.16\text{-}4$$

where:

C = Conversion constant, $in.^3$ to $ft.^3$

The specific volume (v_g) and the heat capacity ($c_{p,g}$) of the gas are both obtained from a steam table call:

$$c_{p,g},\ v_g = CPV\ (\ P_g\ ,\ T_g\ ) \qquad 4.16\text{-}5$$

The density of the gas in the pressurizer surge line is:

$$\rho_g = \frac{1.0}{v_g} \qquad 4.16\text{-}6$$

The volume of the gas in the pressurizer surge line is defined:

$$V_g = V_{max} - V_f \qquad 4.16\text{-}7$$

The mass of the gas in the pressurizer surge line is calculated:

$$M_g = \rho_g \times V_g \times C \qquad 4.16\text{-}8$$

The total mass in the pressurizer surge line is defined:

$$M_{SL} = M_g + M_f \qquad 4.16\text{-}9$$

The mass flow rate of the pressurizer surge line from time step i-1 to time step i is defined:

$$\frac{dM_{SL}}{dt} = \frac{M_{SL_i} - M_{SL_{i-1}}}{t_i - t_{i-1}} \qquad 4.16\text{-}10$$

The mass flow rate from the surge line into the pressurizer is calculated from the mass balance on the pressurizer; the ADS 1-3 mass flow rate is measured and the rate of the fluid mass stored in or depleted from the pressurizer is calculated. From Equation 4.16-10, the rate that fluid inventory is either stored in or depleted from the surge line is calculated. Therefore, Equation 4.16-1 may be rearranged to solve for the mass flow rate of the junction between the hot leg and the surge line:

$$\dot{M}_{HL/SL} = \dot{M}_{SL/PRZR} + \frac{dM_{SL}}{dt} \qquad 4.16\text{-}11$$

Note that the flow from the hot leg into the surge line is calculated starting with the ADS 1-3 flow and working in to the primary system to solve for the mass flow rates and fluid mass inventory changes.

4.16.3 Energy Balance

4.16.3.1 Energy in Surge Line

The heat capacity ($c_{p,f}$) of the fluid is obtained from an ASME steam table call:

$$c_{p,f} = CPL\ (\ P_f\ ,\ T_f) \qquad 4.16\text{-}12$$

Assuming that the variation of specific heat of both the liquid and vapor masses of water over the range of pressure conditions experienced in the test is negligible, the left side of Equation 4.16-2 is expanded:

$$Q_{SL} = c_p \frac{d(M_{SL}(T-T_{REF}))}{dt} =$$

$$c_{p,f}M_f \frac{dT_f}{dt} + c_{p,g}M_g \frac{dT_g}{dt} + \qquad 4.16\text{-}13$$

$$c_{p,f}(T_f-T_{REF}) \frac{dM_f}{dt} + c_{p,g}(T_g-T_{REF}) \frac{dM_g}{dt}$$

Given the above equation, the energy rate of the pressurizer surge line is calculated:

$$Q_{SL} = c_p \frac{d(M_{SL}(T-T_{REF}))}{dt} =$$

$$c_{p,f}M_f \frac{T_{f_i} - T_{f_{i-1}}}{t_i - t_{i-1}} + c_{p,g}M_g \frac{T_{g_i} - T_{g_{i-1}}}{t_i - t_{i-1}} + \qquad 4.16\text{-}14$$

$$c_{p,f}(T_f-T_{REF}) \frac{M_{f_i} - M_{f_{i-1}}}{t_i - t_{i-1}} + c_{p,g}(T_g-T_{REF}) \frac{M_{g_i} - M_{g_{i-1}}}{t_i - t_{i-1}}$$

where:

T_{REF} = Reference temperature, 32 °F

4.16.3.2 Heat Loss to Surge Line Piping

The energy rate of the metal is defined as a sum over all the segments of the surge line piping:

$$Q_{METAL} = \sum_{i=0}^{nsurf} M_{metal}(i)\ heat\_cap(T_{surf_i}) \frac{T_{surf_i} - T_{surf_{i-1}}}{t_i - t_{i-1}} \qquad 4.16\text{-}15$$

4.16.3.3 Heat Loss to Ambient Surroundings from Surge Line Piping

In the calculation of the heat loss to the ambient surroundings, the pressurizer surge line is modeled as a horizontal segment, where the number of metal segments is defined as shown by Table 4.16-3. These divisions are chosen to coincide with the available temperature instrumentation. The heat loss is

calculated as shown below for the component. In the following calculations, the following constants are used:

E	=	Emissivity (0.8)
x	=	Insulation thickness (2 in.)
k	=	Mean thermal conductivity of insulation (0.31 Btu-in./hr-ft.^{2})
C_1	=	Conversion of °F to degrees Rankine (459.6)
CSB	=	Stefan-Boltzmann constant (1.713E-9 Btu/hr-ft.^{2}-R^4)
C_2	=	Conversion of hours to seconds (3600.0)

The heat loss to ambient heat transfer calculation methodology for the pressurizer surge line is analogous to that employed for the other insulated components of the system. Each metal segment is treated as an insulated horizontal cylinder. The calculations for the pressurizer surge line energy loss to ambient are similar to the cold-leg balance lines, as presented in Subsection 4.4.6. This similarity is based on the fact that both components are insulated pipes, and both are modelled as horizontal cylinders.

The laminar range form of the free convection heat transfer correlation from Reference 16 applies, based upon the conditions of the OSU test facility air at atmospheric pressure and ambient temperature (averaged over the tests). In the derivation of the coefficient (0.18) in the convection heat transfer correlation, an outside diameter of 6-in. is used. In the radiation heat transfer correlation, an emissivity of 0.8 is assumed.

The free convection heat transfer coefficient (H_{c_j}) for a metal segment j is defined:

$$H_{c_j} = 0.18 \times \sqrt[4]{T_{surf}(j) - T_{AMB}} \qquad 4.16\text{-}16$$

The assumed insulation surface temperature (T_{ir_j}) for a metal segment j is defined:

$$T_{ir_j} = (0.10 \times (T_{surf_j} - T_{AMB}) + T_{AMB}) + C_1 \qquad 4.16\text{-}17$$

The use of the constant 0.10 in Equation 4.16-17 is based on the assumption that the temperature drop in the insulation is 90 percent of the overall drop in temperature between the metal temperature and the ambient temperature.

The ambient temperature (T_{or}) is defined as follows:

$$T_{or} = T_{AMB} + C_1 \qquad 4.16\text{-}18$$

The radiant heat transfer coefficient (H_{r_j}) for a metal segment j is defined:

$$H_{r_j} = CSB \times E \times (T_{sf_j}^2 + T_{or}^2) \times (T_{sf_j} + T_{or}) \qquad 4.16\text{-}19$$

The surface resistance (R_{surf}) for a metal segment j is defined:

$$R_{surf_j} = \frac{1.0}{(H_{c_j} + H_{r_j}) \times A(j)} \qquad 4.16\text{-}20$$

The insulation resistance ($R_{insul}(j)$) for a metal segment j is defined:

$$R_{insul_j} = \frac{x}{k \times mean\_area(j)} \qquad 4.16\text{-}21$$

Given all of the above, the heat loss to the ambient (Btu/sec.) over all metal segments can be defined:

$$Q_{AMB} = \sum_{j=1}^{nsurf} \frac{\frac{T_{surf}(j) - T_{AMB}}{R_{surf_j} + R_{insul_j}}}{C_2} \qquad 4.16\text{-}22$$

4.16.3.4 Hot Leg / Surge Line Junction

Assuming saturated vapor, the enthalpy of the gas in the junction area is provided by a steam table call:

$$h_{HL\text{-}SL,g} = HSV\ (\ P_{HL\text{-}SL}\ ) \qquad 4.16\text{-}23$$

The enthalpy of the fluid in the junction area is provided by a steam table call:

$$h_{HL\text{-}SL,f} = HCL\ (\ P_{HL}\ ,\ T_{HL\text{-}SL}\ ) \qquad 4.16\text{-}24$$

The energy rate of the hot leg surge line area can be calculated:

$$Q_{HL-SL} = Q_{SL} + \dot{M}_{SL-PRZR} h_{SL-PRZR,} + Q_{METAL} + Q_{AMB} \qquad 4.16\text{-}25$$

TABLE 4.16-1 INSTRUMENT CHANNEL IDS FOR PRESSURIZER SURGE LINE MASS AND ENERGY CALCULATIONS		
Channel ID	**Notation in this Section**	**Description**
PT-602	P_f	Pressure of the fluid (psig)
TF-603	T_f	Temperature of the fluid (°F)
PT-604	P_g	Pressure of the gas (psig)
TF-601	T_g	Temperature of the gas (°F)
LDP-602	$level_f$	Level of the fluid (in.)
PT-202	$P_{HL/SL}$	Pressure at the junction of the surge line and hot-leg area (psig)
TF-603	$T_{HL/SL}$	Temperature at the junction of the surge line and hot-leg area (°F)

TABLE 4.16-2 FLUID HEIGHT VERSUS VOLUME FOR PRESSURIZER SURGE LINE MASS CALCULATIONS	
Fluid Level (in.)	**Volume ($in.^3$)**
0.0	0.0
5.0	71.38
23.0	835.14
27.0	1327.01
28.5	1752.14
31.25	2266.26
32.325	2454.11
35.124	2778.14
45.35	2879.24
48.48	2907.06

TABLE 4.16-3 METAL DATA FOR PRESSURIZER SURGE LINE METAL ENERGY CALCULATIONS				
Metal Segment Number j	Temperature Data Channel for $T_{surf}(j)$	Metal Mass of Segment $M_{metal}(j)$ (lbm)	Surface Area A(j) ($ft.^2$)	Mean Surface Area mean_area(j) ($ft.^2$)
1	TFM-603	224.3	38.53	31.71

TABLE 4.16-4 TEMPERATURE VERSUS HEAT CAPACITY FOR PRESSURIZER SURGE LINE METAL ENERGY CALCULATIONS	
Temperature (°F)	Heat capacity (Btu/lbm-°F)
70.0	0.1085
100.0	0.1109
200.0	0.1175
300.0	0.1223
400.0	0.1256
500.0	0.1279
600.0	0.1297

4.17 Cold Legs

The CMT piping design provides for the pressure balance lines for the CMTs to be connected to two of the four cold legs; specifically, the balance line piping is connected to CL-1 and CL-3. CL-2 and CL-4 do not have CMT pressure balance lines associated with them.

4.17.1 Cold Leg with Core Makeup Tank Balance Lines (CL-1 and CL-3)

The break is located at CL-3; the break term applies only to CL-3. The mass balance on the cold legs with CMT balance lines, (CL-1 and CL-3), may be written as:

$$\frac{d\ M_{CL\ w\ BL}}{dt} = \dot{M}_{SG\ 1} - \dot{M}_{BL} - \dot{M}_{DC,\ CL\ w\ BL} - \dot{M}_{BRK} \qquad 4.17\text{-}1$$

where the subscripts:

BL	=	CMT balance lines
CL w BL	=	Cold legs with balance lines (CL-1 and CL-3)
DC	=	Downcomer
SG 1	=	Steam generator-1
BRK	=	Break, applies to CL-3 for selected tests

The change in mass inventory in CL-1 and CL-3 given by the left-hand side of Equation 4.17-1 may be expanded to:

$$\frac{dM_{CL\ w\ BL}}{dt} = \frac{dM_{CL\ 1}}{dt} + \frac{dM_{CL\ 3}}{dt} \qquad 4.17\text{-}2$$

where the subscripts:

CL 1	=	Cold leg-1
CL 3	=	Cold leg-3

4.17.1.1 Mass Terms

Direct measurement of mass flow is provided in the primary system cold legs of the OSU test facility only during operation of the simulated reactor coolant pumps (RCPs). Overall primary system mass balance calculations (Section 4.21) do not evaluate the cold leg as a separate component. Cold-leg flow rate calculations are, therefore, limited to the initial period of pumped flow.

Prior to the start of testing and until the RCPs coast down, cold-leg flow is a single-phase liquid and may, therefore, be measured with the magnetic flow meters located in CL-1 and CL-3.

$$\dot{M}_{CL\ w\ BL} = \dot{M}_{FMM-201} + \dot{M}_{FMM-203} \qquad 4.17\text{-}3$$

where the subscripts:

FMM-201 FMM-203	=	Instrument channel IDs for magnetic flow meters in CL-1 and CL-3, respectively

The single-phase liquid flow rate is calculated as:

$$\dot{M}_{FMM-XXX} = W_{FMM-XXX} \times \rho_f \left(P_{FMM-XXX}, T_{FMM-XXX}\right) \times C \qquad 4.17\text{-}4$$

where:

W	=	Volumetric flow rate of liquid, gpm
C	=	Conversion constant, gpm to $ft.^3/sec.$

and the subscripts:

FMM-XXX	=	data for flow meter XXX where: XXX = 201 (CL-1) XXX = 203 (CL-3)
f	=	Liquid phase of water

The local liquid density is calculated from the ASME steam table routines using pressure, differential pressure, and temperature values from the data channels listed in Table 4.17-1. The local pressure used to evaluate local fluid density is calculated as:

$$P_{FMM-XXX} = P_{PT-XXX} + P_{DP-YYY} \qquad 4.17\text{-}5$$

where the subscripts:

PT-XXX	=	Pressure instrument per Table 4.17-1
DP-YYY	=	Differential pressure instrument per Table 4.17-1

Flow for tests with inoperative flow meters may be inferred from the cold-leg differential pressure cells. Test SB01 has functional flow meters and differential pressure cells and can be used to calibrate this method. The resultant single-phase liquid flow rate is calculated as:

$$\dot{M}_{FMM\text{-}XXX} = \sqrt{\dot{M}^2_{REF\text{-}XXX} \frac{\Delta P_{FMM\text{-}XXX}}{\Delta P_{REF\text{-}XXX}}} \qquad 4.17\text{-}6$$

where:

$\dot{M}_{REF\text{-}XXX}$ = Average flow in lbm/sec through FMM-XXX during the calibration period for Test SB01. The calibration period is the period of full power operation prior to the start of the transient.

$\Delta P_{FMM\text{-}XXX}$ = Differential pressure corresponding to FMM-XXX per Table 4.17-1

$\Delta P_{REF\text{-}XXX}$ = Average value of $\Delta P_{FMM\text{-}XXX}$ during the calibration period for Test SB01

Once flow in the cold legs becomes two-phase, the magnitude of the output from the flow meters is not indicative of the actual flow in those components. The liquid mass in CL-1 and CL-3 is then calculated using local level transducers as follows:

Step 1: Compensate the readings from the downcomer level transducer listed in Table 4.17-2 to account for temperature differences between fluid in the downcomer and fluid in the reference leg of the instrument line. The local pressure and temperature transducers to be used to accomplish the compensation are also identified in Table 4.17-2.

Step 2: Tables of level versus volume were developed for the cold legs. From the collapsed liquid level calculated from Step 1, calculate the liquid volume in the cold leg using linear interpolation:

$$V_{f,\,CL\,X} = f(LDP\text{-}YYY_{COMP}) \qquad 4.17\text{-}7$$

where the subscript:

CL X = CL-1 or CL-3

The elevation of the cold leg relative to the downcomer LDP span extends from [ ]^{a,b,c} in. Thus, the table of volume versus elevation for the cold legs is mapped onto the downcomer levels readings so that:

Downcomer-Compensated Water Level (in.)	Water Level in CL-1 and CL-3 (in.)
[ ]^{a,b,c}	[ ]^{a,b,c}
[ ]^{a,b,c}	[ ]^{a,b,c}

Step 3: The local pressures and temperatures measured using the instruments identified in Table 4.17-2 are used as inputs to the ASME steam tables to calculate the density of the liquid and vapor in the pressurizer in the cold legs:

$$\rho_{f,\,CL\,X} = \rho(P_{PT\text{-}XXX},\ T_{TF\text{-}XXX})$$
$$\rho_{g,\,CL\,X} = \rho(P_{PT\text{-}XXX},\ T_{TF\text{-}ZZZ}) \qquad 4.17\text{-}8$$

where the subscripts:

PT-XXX = Channel ID for local pressure measurement in downcomer
TF-XXX = Channel ID for local temperature measurement of liquid temperatures
TF-ZZZ = Channel ID for local temperature measurement of vapor temperatures

Step 4: Using the local thermodynamic properties of water as determined from local pressure and fluid temperature measurements, the liquid and vapor mass in the pressurizer is calculated as:

$$M_{f,\,CL\,X} = \rho_{f,\,CL\,X} \times V_{f,\,CL\,X}$$
$$M_{g,\,CL\,X} = \rho_{g,\,CL\,X} \times (V_{TOT,\,CL\,X} - V_{f,\,CL\,X}) \qquad 4.17\text{-}9$$

where the subscript:

TOT = Total volume of component

Step 5: The rate of change in mass inventory of the cold leg may be approximated by differencing two consecutive calculated values of the liquid and vapor masses:

$$\frac{dM_{f,\,CL\,X}}{dt} \approx \frac{\Delta M_{f,\,CL\,X}}{\Delta t} = \frac{M_{f,\,CL\,X,\,i} - M_{f,\,CL\,X,\,i-1}}{t_i - t_{i-1}}$$

$$\frac{dM_{g,\,CL\,X}}{dt} \approx \frac{\Delta M_{g,\,CL\,X}}{\Delta t} = \frac{M_{g,\,CL\,X,\,i} - M_{g,\,CL\,X,\,i-1}}{t_i - t_{i-1}} \qquad 4.17\text{-}10$$

where the subscript:

i = A specific value in the time and corresponding data array

The total rate of change of the mass inventory of CL-1 or CL-3 is then calculated as:

$$\frac{dM_{CL\ w\ BL}}{dt} \approx \frac{\Delta M_{CL\ w\ BL}}{\Delta t}$$

$$\approx \frac{\Delta M_{f,\,CL\,1} + \Delta M_{g,\,CL\,1} + \Delta M_{f,\,CL\,3} + \Delta M_{g,\,CL\,3}}{\Delta t} \qquad 4.17\text{-}11$$

4.17.1.2 Energy Terms

The fluid in these two cold legs may, depending on the time and nature of the test, be in either a liquid or a vapor phase. Therefore, the change of energy for either CL-1 or CL-3 may be written as:

$$c_P \frac{d(M_{CL\,X}\,T)}{dt} = c_{P,\,f}\,M_{CL\,X,\,f}\frac{d(T_f)}{dt} + c_{P,\,f}\,T_f\frac{d(M_{CL\,X,\,f})}{dt}$$

$$+ c_{P,\,g}\,M_{CL\,X,\,g}\frac{d(T_g)}{dt} + c_{P,\,g}\,T_g\frac{d(M_{CL\,X,\,g})}{dt} \qquad 4.17\text{-}12$$

Writing the previous equation in its difference form:

$$c_P \frac{d(M_{CL\,X}\,T)}{dt} = c_{P,f}\,M_{CL\,X,f}\frac{\Delta T_f}{\Delta t} + c_{P,f}\,T_f\frac{\Delta M_{CL\,X,f}}{\Delta t} + c_{P,g}\,M_{CL\,X,g}\frac{\Delta T_g}{\Delta t} + c_{P,g}\,T_g\frac{\Delta M_{CL\,X,g}}{\Delta t} \qquad 4.17\text{-}13$$

The data channel IDs for the instruments to be used to define the thermal transport properties are identified in Table 4.17-2.

The rate of energy change of the metal mass for CL-1 and CL-3 is calculated as:

$$Q_{CL\ w\ BL\ METAL} = Q_{CL\ 1\ METAL} + Q_{CL\ 3\ METAL} \qquad 4.17\text{-}14$$

expanding,

$$Q_{CL\ X\ METAL} = M \times c_P \times \frac{\Delta T_{TFM\text{-}20X}}{\Delta t} \qquad 4.17\text{-}15$$

where the subscript:

TFM-20X = Temperature-sensing element to be used for this calculation:
X = 1 CL-1
X = 3 CL-3

Similarly, the heat flux from the surface of the cold leg is calculated as:

$$Q_{CL\ w\ BL\ AMB} = Q_{CL\ 1\ AMB} + Q_{CL\ 3\ AMB} \qquad 4.17\text{-}16$$

The cold legs and CMT balance lines are similar in that they are predominantly horizontal pipes. The cold-leg surface heat flux calculations and equations are, therefore, identical to those of the CMT balance line. The balance line equations are provided in Subsection 4.4.6 and the associated cold-leg instrumentation is listed in Table 4.17-2.

4.17.2 Cold Leg without Core Makeup Tank Balance Lines (Cold Leg-2 and Cold Leg-4)

The mass balance on the cold legs without CMT balance lines (CL-2 and CL-4) may be written as:

$$\frac{d\ M_{CL\ w/o\ BL}}{dt} = \dot{M}_{SG\ 2} - \dot{M}_{DC,\ CL\ w/o\ BL} \qquad 4.17\text{-}17$$

where the subscripts:

CL w/o BL	=	Cold legs without balance lines (CL-2 and CL-4)
DC	=	Downcomer
SG 2	=	Steam generator-2

The change in mass inventory in CL-2 and CL-4 given by the left hand side of Equation 4.17-17 above may be expanded to:

$$\frac{dM_{CL\ w/o\ BL}}{dt} = \frac{dM_{CL\ 2}}{dt} + \frac{dM_{CL\ 4}}{dt} \qquad 4.17\text{-}18$$

where the subscripts:

CL 2	=	Cold leg-2
CL 4	=	Cold leg-4

4.17.2.1 Mass Terms

Direct measurement of mass flow is provided in the primary system cold legs of the OSU test facility only during operation of the simulated reactor coolant pumps (RCPs). Overall primary system mass balance calculations (Section 4.21) do not evaluate the cold leg as a separate component. Cold leg flow rate calculations are, therefore, limited to the initial period of pumped flow.

Prior to the start of testing and until the RCPs coast down, cold-leg flow is a single-phase liquid and may, therefore, be measured with the magnetic flow meters located in CL-2 and CL-4. Therefore:

$$\dot{M}_{CL\ w/o\ BL} = \dot{M}_{FMM-202} + \dot{M}_{FMM-204} \qquad 4.17\text{-}19$$

where the subscripts:

FMM-202 FMM-204	=	Instrument channel IDs for magnetic flow meters in CL-2 and CL-4, respectively

All other parameters and subscripts are as previously defined. The single-phase liquid flow rate is calculated as:

$$\dot{M}_{FMM\text{-}XXX} = W_{FMM\text{-}XXX} \times \rho_f \left(P_{FMM\text{-}XXX}, T_{FMM\text{-}XXX}\right) \times C \qquad 4.17\text{-}20$$

where:

W	=	Volumetric flow rate of liquid, gpm
C	=	Conversion constant, gpm to $ft.^3/sec.$

and the subscripts:

FMM-XXX	=	Data for flow meter XXX where XXX = 202 CL-2 204 CL-4
f	=	Liquid phase of water

The local liquid density is calculated from the ASME steam table routines using pressure, differential pressure, and temperature values from the data channels listed in Table 4.17-3. The local pressure used to evaluate local fluid density is calculated as:

$$P_{FMM\text{-}XXX} = PT\text{-}XXX + DP\text{-}YYY \qquad 4.17\text{-}21$$

where the subscripts:

PT-XXX	=	Pressure instrument per Table 4.17-3
DP-YYY	=	Differential pressure instrument per Table 4.17-3

Flow for tests with inoperative flow meters may be inferred from the cold leg differential pressure cells. Test SB01 has functional flow meters and differential pressure cells and can be used to calibrate this method. The resultant single-phase liquid flow rate is calculated as:

$$\dot{M}_{FMM\text{-}XXX} = \sqrt{\dot{M}^{2}_{REF\text{-}XXX} \frac{\Delta P_{FMM\text{-}XXX}}{\Delta P_{REF\text{-}XXX}}} \qquad 4.17\text{-}22$$

where:

$\dot{M}_{REF\text{-}XXX}$ = Average flow in lbm/sec through FMM-XXX during the calibration period for Test SB01. The calibration period is the period of full power operation prior to the start of the transient.

$\Delta P_{FMM\text{-}XXX}$ = Differential pressure corresponding to FMM-XXX per Table 4.17-3

$\Delta P_{REF\text{-}XXX}$ = Average value of $\Delta P_{FMM\text{-}XXX}$ during the calibration period for Test SB01

Once flow in the cold legs becomes two-phase, the magnitude of the output from the flow meters is not indicative of the actual flow in those components. The liquid mass in CL-2 and CL-4 is then calculated using local level transducers as follows:

Step 1: Compensate the readings from the downcomer level transducer listed in Table 4.17-4 to account for temperature differences between fluid in the downcomer and the fluid in the reference leg of the instrument line. The local pressure and temperature transducers to be used to accomplish the compensation are also identified in Table 4.17-4.

Step 2: Tables of level versus volume were developed for the cold legs. From the collapsed liquid level calculated from Step 1, calculate the liquid volume in the pressurizer, $V_{f,\,CL\,X}$, as follows:

$$V_{f,\,CL\,X} = f\,(LDP\text{-}YYY_{COMP}) \qquad 4.17\text{-}23$$

where the subscript:

CL X = CL-2 or CL-4

The elevation of the cold leg extends from [ ]^{a,b,c} in. The table of volume versus elevation for CL-2 and CL-4 is mapped onto the downcomer levels readings, such that:

Downcomer-Compensated Water Level (in.)	Water Level in CL-2 and CL-4 (in.)
[ ]^{a,b,c}	[ ]^{a,b,c}
[ ]^{a,b,c}	[ ]^{a,b,c}

Step 3: The local pressures and temperatures measured using the instruments identified in Table 4.17-4 are used as inputs to the ASME steam tables to calculate the density of the liquid and vapor in the pressurizer in the cold legs:

$$\rho_{f,\,CL\,X} = \rho(P_{PT\text{-}XXX},\ T_{TF\text{-}XXX})$$
$$\rho_{g,\,CL\,X} = \rho(P_{PT\text{-}XXX},\ T_{TF\text{-}ZZZ}) \qquad 4.17\text{-}24$$

where the subscripts:

PT-XXX	=	Channel ID for local pressure measurement in downcomer
TF-XXX	=	Channel ID for local temperature measurement of liquid and vapor temperatures
TF-ZZZ	=	Channel ID for local temperature measurement of vapor temperatures

Step 4: Using the local thermodynamic properties of water as determined from local pressure and fluid temperature measurements, the liquid and vapor mass in the pressurizer is calculated as:

$$M_{f,\,CL\,X} = \rho_{f,\,CL\,X} \times V_{f,\,CL\,X}$$
$$M_{g,\,CL\,X} = \rho_{g,\,CL\,X} \times (V_{TOT,\,CL\,X} - V_{f,\,CL\,X}) \qquad 4.17\text{-}25$$

where the subscript:

TOT	=	Total volume of component

Step 5: The rate of change in mass inventory of the cold leg may be approximated by differencing two consecutive calculated values of the liquid and vapor masses:

$$\frac{dM_{f,\,CL\,X}}{dt} = \frac{\Delta M_{f,\,CL\,X}}{\Delta t} = \frac{M_{f,\,CL\,X,\,i} - M_{f,\,CL\,X,\,i-1}}{t_i - t_{i-1}}$$

$$\frac{dM_{g,\,CL\,X}}{dt} = \frac{\Delta M_{g,\,CL\,X}}{\Delta t} = \frac{M_{g,\,CL\,X,\,i} - M_{g,\,CL\,X,\,i-1}}{t_i - t_{i-1}} \qquad 4.17\text{-}26$$

where the subscript:

i = A specific value in the time and corresponding data array

The total rate of change of the mass inventory of CL-2 or CL-4 is then calculated as:

$$\frac{dM_{CL\ w/o\ BL}}{dt} = \frac{\Delta M_{CL\ w/o\ BL}}{\Delta t}$$

$$= \frac{\Delta M_{f,\,CL\,2} + \Delta M_{g,\,CL\,2} + \Delta M_{f,\,CL\,4} + \Delta M_{g,\,CL\,4}}{\Delta t} \qquad 4.17\text{-}27$$

4.17.2.2 Energy Terms

The fluid in these two cold legs may, depending on the time and nature of the test, be in either a liquid or a vapor phase. The change of energy for either CL-2 or CL-4 may be written as:

$$c_p \frac{d(\,M_{CL\,X}\,T\,)}{dt} = c_{p,\,f}\,M_{CL\,X,\,f}\,\frac{d(\,T_f\,)}{dt} + c_{p,\,f}\,T_f\,\frac{d(\,M_{CL\,X,\,f}\,)}{dt}$$

$$+ c_{p,\,g}\,M_{CL\,X,\,g}\,\frac{d(\,T_g\,)}{dt} + c_{p,\,g}\,T_g\,\frac{d(\,M_{CL\,X,\,g}\,)}{dt} \qquad 4.17\text{-}28$$

Writing the previous equation in its difference form:

$$c_P \frac{d(M_{CL\,X}\,T)}{dt} = c_{P,f}\,M_{CL\,X,f}\frac{\Delta T_f}{\Delta t} + c_{P,f}\,T_f\frac{\Delta M_{CL\,X,f}}{\Delta t} + c_{P,g}\,M_{CL\,X,g}\frac{\Delta T_g}{\Delta t} + c_{P,g}\,T_g\frac{\Delta M_{CL\,X,g}}{\Delta t} \quad 4.17\text{-}29$$

The data channel IDs for the instruments to be used to define the thermal transport properties are identified in Table 4.17-4.

The rate of energy change of the metal mass for CL-2 and CL-4 is calculated as:

$$Q_{CL\ w/o\ BL\ METAL} = Q_{CL\ 2\ METAL} + Q_{CL\ 4\ METAL} \quad 4.17\text{-}30$$

expanding,

$$Q_{CL\ X\ METAL} = M \times c_P \times \frac{\Delta T_{TFM\text{-}20X}}{\Delta t} \quad 4.17\text{-}31$$

where the subscript:

TFM-20X = Temperature-sensing element to be used for this calculation:
X = 2 CL - 2
X = 4 CL - 4

Similarly, the heat flux from the surface of the cold leg is calculated as:

$$Q_{CL\ w/o\ BL\ AMB} = Q_{CL\ 2\ AMB} + Q_{CL\ 4\ AMB} \quad 4.17\text{-}32$$

The cold legs and CMT balance lines are similar in that they are predominantly horizontal pipes. The cold-leg surface heat flux calculations and equations are, therefore, identical to those of the CMT balance lines. The balance line equations are provided in Subsection 4.4.6 and the associated cold-leg instrumentation is listed in Table 4.17-4.

TABLE 4.17-1 DATA CHANNEL IDs USED TO CALCULATE LOCAL FLUID PROPERTIES FOR FLOW METERS				
Applicable Conditions	**Channel IDs for Liquid Flow Meter and DP**	**Data Channel ID for Pressure Transducers**	**Data Channel ID for Differential Pressure Transducers**	**Data Channel ID for Fluid Thermocouples**
Cold-leg inventory is all liquid	FMM-201 DP-203	PT-101	DP-121	TF-107
	FMM-203 DP-205	PT-103	DP-123	TF-103

TABLE 4.17-2 DATA CHANNEL IDs USED TO CALCULATE FLUID PROPERTIES FOR LEVELS TRANSDUCERS					
Applicable Conditions	**Location**	**Data Channel ID for Liquid Levels**	**Data Channel ID for Local Pressure**	**Data Channel ID for Fluid Temperature**	**Data Channel ID for Energy Balance Calculations**
Compensated water level when water level in downcomer is above bottom of cold leg	Downcomer annulus at ≈ 180°az (≈ 270°az for backup)	LDP-140 LDP-116	PT-111	TF-152 TF-155 TF-158	
Density and enthalpy of liquid in cold legs	CL-1		PT-101	TF-107 (liquid) SC-105 (vapor)	
	CL-3		PT-103	TF-103 (liquid) SC-101 (vapor)	
Change in stored energy of cold legs	CL-1				TFM-201
	CL-3				TFM-203
Heat loss to ambient	CL-1				HFM-201
	CL-3				HFM-203
Ambient temperature	All CL				TF-006

TABLE 4.17-3 DATA CHANNEL IDs USED TO CALCULATE LOCAL FLUID PROPERTIES FOR FLOW METERS				
Applicable Conditions	**Channel ID for Liquid Flow Meter and DP**	**Data Channel ID for Pressure Transducers**	**Data Channel ID for Differential Pressure Transducers**	**Data Channel ID for Fluid Thermocouples**
Cold-leg inventory is all liquid	FMM-202 DP-202	PT102	DP-122	TF-108
	FMM-204 DP-204	PT-104	DP-124	TF-104

TABLE 4.17-4 DATA CHANNEL IDs USED TO CALCULATE FLUID PROPERTIES FOR LEVELS TRANSDUCERS					
Applicable Conditions	**Location**	**Data Channel ID for Liquid Levels**	**Data Channel ID for Local Pressure**	**Data Channel ID for Fluid Temperature**	**Data Channel ID for Energy Balance Calculations**
Compensated water level when water level in downcomer is above bottom of cold leg	Downcomer annulus at ≈ 180°az (≈ 270°az for backup)	LDP-140 LDP-116	PT-111	TF-152 TF-155 TF-158	
Density and enthalpy of liquid in cold legs	CL-2		PT-102	TF-108 (liquid) SC-106 (vapor)	
	CL-4		PT-104	TF-104 (liquid) SC-102 (vapor)	
Change in stored energy of cold legs	CL-2				TFM-202
	CL-4				TFM-204
Heat loss to ambient	CL-2				HFM-202
	CL-4				HFM-204
Ambient temperature	All CL				TF-006

4.18 Hot Legs

The OSU test facility incorporates the two hot legs of the AP600. Each hot leg has an ADS-4 line associated with it. In addition, one hot leg, designated as HL-2, also has the pressurizer surge line and the PRHR feed line associate with it. The pressurizer surge line connection to HL-2 provides a flow path from the primary system to ADS 1-3. Considering the various flow paths, the mass balance for HL-1 and HL-2, respectively, may be written as:

$$\frac{d\ M_{HL\ 1}}{dt} = \dot{M}_{UP\text{-}HL\ 1} - \dot{M}_{ADS\ 4\text{-}1} - \dot{M}_{SG\ 1} \qquad 4.18\text{-}1$$

and

$$\frac{d\ M_{HL\ 2}}{dt} = \dot{M}_{UP\text{-}HL\ 2} - \dot{M}_{SL} - \dot{M}_{ADS\ 4\text{-}2} - \dot{M}_{PRHR} - \dot{M}_{SG\ 2} \qquad 4.18\text{-}2$$

where the subscripts:

ADS 4-X = ADS-4
X = 1, HL-1
= 2, HL-2

HL 1, HL 2 = HL-1 or HL-2, respectively

SG 1, SG 2 = Steam generator-1 or steam generator-2, respectively

SL = Junction between HL-2 and the pressurizer surge line

UP - HL 1, = Junction between the RPV upper plenum and HL-1

UP - HL 2 = Junction bewteen the RPV upper plenum and HL-2

There is no direct measurement of mass flow in the primary system hot legs of the OSU test facility; hot-leg flows may be inferred by continuity and/or energy balances performed on the system. Overall primary system mass balance calculations (Section 4.21) do not evaluate the hot leg as a separate component. Hot-leg flow rates are, therefore, not calculated. Hot-leg calculations include fluid inventory, the rate of change in fluid and metal energy, and heat loss to ambient.

4.18.1 Mass Storage in the Hot Legs

The hot leg may be in one of three states; all liquid, all vapor, or a mixture of liquid and vapor. The output from the appropriate level transducers listed in Table 4.18-1 is used to first calculate the liquid inventory and mass in the hot leg, and then corresponding vapor inventory and mass. This calculation is accomplished as follows:

Step 1: Compensate the readings from HL-1 level transducers listed in Table 4.18-1 to account for temperature differences between fluid in the hot leg and fluid in the reference leg of the instrument line. The instruments used to measure local pressure and fluid temperatures to be used to accomplish the compensation are also identified in Table 4.18-1.

Step 2: The local pressures and temperatures measured by the instruments identified in Table 4.18-1 are used as inputs to the ASME steam tables to calculate the density of the fluid in the hot legs:

$$\rho_{f,\,HL\,X} = \rho_f\,(P,T)$$
$$\rho_{g,\,HL\,X} = \rho\,(P,T) \qquad 4.18\text{-}3$$

where the subscripts:

f = Liquid phase
g = Steam

Step 3: Tables of level versus volume were developed for the two hot legs. Using the compensated liquid level and the table of hot-leg volume as a function of height, the volume, in $ft.^3$, of liquid in the hot leg is determined using linear interpolation:

$$V_{f,\,HL\,1} = f(LDP\text{-}XXX_{COMP}) \qquad 4.18\text{-}4$$

Step 4: The liquid mass inventory in the hot leg is calculated as:

$$M_{f,\,HL\,X} = \rho_{f,\,HL\,X} \times V_{f,\,HL\,X} \qquad 4.18\text{-}5$$

and the vapor mass is calculated as:

$$M_{g,\,HL\,X} = \rho_{g,\,HL\,X} \times (V_{TOT,\,HL\,X} - V_{f,\,HL\,X}) \qquad 4.18\text{-}6$$

where the subscript:

g	=	Vapor conditions at the local hot-leg pressures and temperatures
TOT	=	Total, or liquid + vapor

The total fluid mass in the hot leg is calculated as:

$$M_{HL\ X} = M_{f,\ HL\ X} + M_{g,\ HL\ X} \qquad 4.18\text{-}7$$

Step 5: The rate of change in mass inventory of the hot leg may be approximated by differencing two consecutive calculated values of liquid mass:

$$\frac{dM_{HL\ X}}{dt} \approx \frac{\Delta M_{HL\ X}}{\Delta t} = \frac{M_{HL\ X,\ i} - M_{HL\ X,\ i-1}}{t_i - t_{i-1}} \qquad 4.18\text{-}8$$

where the subscript:

i	=	Index of the data and time arrays

4.18.2 Energy Terms

The fluid in the two hot legs may, depending upon the time and nature of the test, be either in a liquid or a vapor phase. Thus, the change of energy for the fluid in either HL-1 or HL-2 may be written as:

$$c_P \frac{d(M_{HL\ X}\ T)}{dt} = c_{P,\ f}\ M_{HL\ X,\ f} \frac{d(T_f)}{dt} + c_{P,\ f}\ T_f \frac{d(M_{HL\ X,\ f})}{dt} + c_{P,\ g}\ M_{HL\ X,\ g} \frac{d(T_g)}{dt} + c_{P,\ g}\ T_g \frac{d(M_{HL\ X,\ g})}{dt} \qquad 4.18\text{-}9$$

where the subscript:

g	=	Steam
f	=	Liquid phase of water
HL X	=	X = 1 for HL 1
		X = 2 for HL 2

Writing the above equation in its difference form:

$$c_P \frac{d(M_{HL\ X}\ T)}{dt} \approx c_{P,f} M_{HL\ X,f} \frac{\Delta T_f}{\Delta t} + c_{P,f} T_f \frac{\Delta M_{HL\ X,f}}{\Delta t} + c_{P,g} M_{HL\ X,g} \frac{\Delta T_g}{\Delta t} + c_{P,g} T_g \frac{\Delta M_{HL\ X,g}}{\Delta t} \quad 4.18\text{-}10$$

The data channel IDs for the instruments to be used to define the thermal transport properties are identified in Table 4.18-1.

The rate of energy change of the metal mass for HL-1 and HL-2 is calculated as:

$$Q_{HL\ X\ METAL} = M_{METAL} \times c_P \times \frac{\Delta T_{TFM\text{-}20Y}}{\Delta t} \quad 4.18\text{-}11$$

where the subscript:

TFM-20Y Designates the temperature sensing element to be used for this calculation:
where Y = 5 $\Rightarrow$ HL-1
6 $\Rightarrow$ HL-2

The hot legs and CMT balance lines are similar in that they are predominantly horizontal pipes. The hot-leg surface heat flux calculations and equations are, therefore, identical to those of the CMT balance line. The balance line equations are provided in Subsection 4.4.6 and the associated hot-leg instrumentation is provided in Table 4.18-1.

TABLE 4.18-1
DATA CHANNEL IDs USED IN HOT-LEG MASS AND ENERGY CALCULATIONS

Applicable Conditions	Location	Data Channel ID for Liquid Levels	Data Channel ID for Local Pressure	Data Channel ID for Fluid Temperature	Data Channel ID for Energy Balance Calculations
Fluid conditions in hot leg	HL-1	HPS-205(1)			
	HL-2	HPS-206(1)			
Compensated levels readings in hot legs	HL-1	LDP-207	PT-202	TF-205	
	HL-2	LDP-208	PT-202	TF-206	
Density and enthalpy of liquid in hot legs	HL-1		PT-202	TF-143 (liquid) SC-141 (vapor)	
	HL-2		PT-202	TF-142 (liquid) SC-140 (vapor)	
Change in stored energy of hot legs	HL-1				TFM-205
	HL-2				TFM-206
Heat loss to ambient	HL-1				HFM-205
	HL-2				HFM-206
Ambient temperature	HL-1 HL-2				TF-006

Note:
(1) Heated phase switch is used to determine state of fluid in hot legs: liquid solid = 100, full scale reading
two-phase = $0 < x < 100$
vapor solid = 0

4.19 Pressure Conversions

A number of input pressures need to be converted from psig to psia and placed onto the results plot file. As with other calculations involving input pressures in the various modules, the ambient pressure data channel (PT-003) is used for the conversion, as opposed to a constant of 14.7 psi. The units of the resulting pressure values is psia. A list of pressures converted from psig to psia is given in Table 4.19-1.

TABLE 4.19-1 PRESSURE CONVERSIONS	
Data Channel	**Channel Description**
DP-905	Break Separ Ent DP
PT-001	MFP Dischrg Pressure
PT-002	MS Header Pressure
PT-101	CL1 Press @RV Flange
PT-102	CL2 Press @RV Flange
PT-103	CL3 Press @RV Flange
PT-104	CL4 Press @RV Flange
PT-107	RV Upper Head Press
PT-108	RV Bottom Pressure
PT-109	DVI1 Pres @RV Flange
PT-110	DVI2 Pres @RV Flange
PT-111	RV Dwncmer Press-Top
PT-112	RV Dwncmer Press-Bot
PT 113	Rctr Blw Mid Spc Grd
PT-201	SG1 Long Tube Press
PT-202	HL-2 Pressure
PT-203	PR Upstrm of Break-1
PT-204	SG2 Long Tube Press
PT-205	HL-1 Pressure
PT-206	PR Upstrm of Break-2
PT-301	SG1 Sec Steam Press
PT-302	SG2 Sec Steam Press
PT-401	ACC-1 Pressure
PT-402	ACC-2 Pressure
PT-501	CMT-1 Pressure
PT-502	CMT-2 Pressure

TABLE 4.19-1 (Continued) PRESSURE CONVERSIONS	
Data Channel	**Channel Description**
PT-602	PZR NR Pressure
PT-603	PZR NR Pressure
PT-604	PZR WR Pressure
PT-605	ADS1-3 Separtr Press
PT-606	IRWST Sparger Press
PT-610	ADS4-2 Separtr Press
PT-611	ADS4-1 Separtr Press
PT-701	IRWST Pressure
PT-801	CVSP Discharge Press
PT-802	RNSP Discharge Press
PT-901	Primary Sump Press
PT-902	BAMS Header Pressure
PT-905	Break Separatr Press

4.20 Adjusted Data

During the analysis of various tests, oscillations in a number of reactor vessel core thermocouples were identified. The oscillations consisted of temperature excursions of up to 40°F, which lasted for as little as one recorded data point when data was recorded every two seconds. An example from near the top of the core is shown in Figure 4.20-1. Similar problems were also identified for two accumulator thermocouples.

These oscillations were investigated and concluded to be inconsistent with the thermal and hydraulic phenomena present in the core; the oscillations could not be explained given the potential local boiling effects, the low local power densities, and the heater rod heat capacities. Therefore, the oscillations are attributed to instrumentation noise.

The oscillations were eliminated by smoothing the data. Several options were investigated and locally weighted regression,[17] as implemented in the Westinghouse NSAPLOT plot package, was selected. In this method, fitted values are computed by using a nearest neighbor routine and robust locally weighted regression with a weighing function. The effect of this method is to create a smoothed curve by combining a series of adjacent curves, where each curve was generated by regressing a different set of data points. Regression parameters were investigated by trial and error. The parameters were selected to eliminate a sufficient portion of the oscillations to support detailed analysis of the core, while maintaining the underlying data. An example of the results is shown in Figures 4.20-1 through 4.20-5. The raw data is shown for two different time scales in Figures 4.20-1 and 4.20-3. The corresponding smoothed data is shown in Figures 4.20-2 and 4.20-4. The raw and smoothed data are shown together in Figure 4.20-5. To ensure consistent results, all core thermocouple data were smoothed. The list of thermocouple channel names and the associated smoothing parameter values are shown in Table 4.20-1.

Based on this initial evaluation, it was determined that the OSU test analysis software must use an optional input file which would contain data which superseded the data on the input file from the timesync software. This adjusted data file would contain a subset of input data with the same channel names, but which have been smoothed by NSAPLOT. When the OSU test analysis software requires a data element from the input data file, this adjusted data file is searched first. This ensures that the smoothed data is used instead of the input data.

TABLE 4.20-1 CHANNELS FOR DATA SMOOTHING	
Channel Name	**NSAPLOT Smoothing Function lowess (Fit, Iterations, Delta)**
TR-001-1	lowess (-120, 2, 0)
TR-001-2	lowess (-120, 2, 0)
TR-001-3	lowess (-120, 2, 0)
TR-001-4	lowess (-120, 2, 0)
TR-001-5	lowess (-120, 2, 0)
TR-001-6	lowess (-120, 2, 0)
TR-001-7	lowess (-120, 2, 0)
TR-001-8	lowess (-120, 2, 0)
TR-303-1	lowess (-120, 2, 0)
TR-303-2	lowess (-120, 2, 0)
TR-303-3	lowess (-120, 2, 0)
TR-303-4	lowess (-120, 2, 0)
TR-303-5	lowess (-120, 2, 0)
TR-303-6	lowess (-120, 2, 0)
TR-303-7	lowess (-120, 2, 0)
TR-303-8	lowess (-120, 2, 0)
TR-308-1	lowess (-120, 2, 0)
TR-308-2	lowess (-120, 2, 0)
TR-308-3	lowess (-120, 2, 0)
TR-313-1	lowess (-120, 2, 0)
TR-313-2	lowess (-120, 2, 0)
TR-313-3	lowess (-120, 2, 0)
TR-313-4	lowess (-120, 2, 0)
TR-313-5	lowess (-120, 2, 0)

TABLE 4.20-1 (Continued) CHANNELS FOR DATA SMOOTHING	
Channel Name	**NSAPLOT Smoothing Function lowess (Fit, Iterations, Delta)**
TR-313-7	lowess (-120, 2, 0)
TR-313-8	lowess (-120, 2, 0)
TR-318-1	lowess (-120, 2, 0)
TR-318-2	lowess (-120, 2, 0)
TR-318-3	lowess (-120, 2, 0)
SCTH1014	lowess (-120, 2, 0)
SCTH1033	lowess (-120, 2, 0)
SCTH5014	lowess (-120, 2, 0)
SCTH3194	lowess (-120, 2, 0)
SCTH1044	lowess (-120, 2, 0)
SCTH5074	lowess (-120, 2, 0)
TH-601	lowess (-120, 2, 0)
TH-602	lowess (-120, 2, 0)
TH-60.	lowess (-120, 2, 0)
TH-101-1	lowess (-120, 2, 0)
TH-101-2	lowess (-120, 2, 0)
TH-101-3	lowess (-120, 2, 0)
TH-103-1	lowess (-120, 2, 0)
TH-103-2	lowess (-120, 2, 0)
TH-103-4	lowess (-120, 2, 0)
TH-104-1	lowess (-120, 2, 0)
TH-104-2	lowess (-120, 2, 0)
TH-104-3	lowess (-120, 2, 0)
TH-302-1	lowess (-120, 2, 0)
TH-302-2	lowess (-120, 2, 0)

TABLE 4.20-1 (Continued) CHANNELS FOR DATA SMOOTHING	
Channel Name	**NSAPLOT Smoothing Function lowess (Fit, Iterations, Delta)**
TH-302-3	lowess (-120, 2, 0)
TH-302-4	lowess (-120, 2, 0)
TH-304-1	lowess (-120, 2, 0)
TH-304-2	lowess (-120, 2, 0)
TH-304-4	lowess (-120, 2, 0)
TH-307-1	lowess (-120, 2, 0)
TH-307-2	lowess (-120, 2, 0)
TH-307-3	lowess (-120, 2, 0)
TH-307-4	lowess (-120, 2, 0)
TH-309-1	lowess (-120, 2, 0)
TH-309-2	lowess (-120, 2, 0)
TH-309-3	lowess (-120, 2, 0)
TH-309-4	lowess (-120, 2, 0)
TH-312-1	lowess (-120, 2, 0)
TH-312-2	lowess (-120, 2, 0)
TH-312-3	lowess (-120, 2, 0)
TH-312-4	lowess (-120, 2, 0)
TH-314-1	lowess (-120, 2, 0)
TH-314-2	lowess (-120, 2, 0)
TH-319-1	lowess (-120, 2, 0)
TH-319-2	lowess (-120, 2, 0)
TH-319-3	lowess (-120, 2, 0)
TH-501-1	lowess (-120, 2, 0)
TH-501-2	lowess (-120, 2, 0)
TH-501-3	lowess (-120, 2, 0)

TABLE 4.20-1 (Continued) CHANNELS FOR DATA SMOOTHING	
Channel Name	**NSAPLOT Smoothing Function lowess (Fit, Iterations, Delta)**
TH-304-3	lowess (-120, 2, 0)
TH-503-1	lowess (-120, 2, 0)
TH-503-2	lowess (-120, 2, 0)
TH-503-3	lowess (-120, 2, 0)
TH-503-4	lowess (-120, 2, 0)
TH-505-1	lowess (-120, 2, 0)
TH-505-2	lowess (-120, 2, 0)
TH-505-3	lowess (-120, 2, 0)
TH-505-4	lowess (-120, 2, 0)
TH-507-1	lowess (-120, 2, 0)
TH-507-2	lowess (-120, 2, 0)
TH-507-3	lowess (-120, 2, 0)
TH-314-3	lowess (-120, 2, 0)
TF-401	lowess (-60, 2, 0)
TF-402	lowess (-60, 2, 0)

TABLE 4.20-2 OSU TEST ANALYSIS PLOT PACKAGE FOR SECTION 4.20				
Plot Number	**Component**	**Variables**	**Units**	**Description**
1	Reactor Vessel	TR-001-7	°F	Raw Core Thermocouple Data
2	Reactor Vessel	TR-001-7	°F	Smoothed Core Thermocouple Data
3	Reactor Vessel	TR-001-7	°F	Raw Core Thermocouple Data
4	Reactor Vessel	TR-001-7	°F	Smoothed Core Thermocouple Data
5	Reactor Vessel	TR-001-7 TR-001-7	°F °F	Raw Core Thermocouple Data Smoothed Core Thermocouple Data

THE FIGURES LISTED IN TABLE 4.20-2
ARE NOT INCLUDED IN THIS NONPROPRIETARY DOCUMENT

4.21 System Mass Analysis

To evaluate the OSU results, an overall mass inventory calculation and a mass balance of the primary system were performed. To investigate the effects of instrumentation accuracy, IRWST and sump mass balances were also performed. The IRWST and sump were selected because all flow paths to and from these components were metered.

Sections 4.1 through 4.20 and Subsections 4.21.1 through 4.21.4 provide methodologies for the tests with cold-leg breaks, which included Matrix Tests SB01 and SB18. Subsection 4.21.5 provides changes to these methodologies required to address other break configurations.

4.21.1 Total System Mass Inventory

The total system mass inventory is calculated at each transient time point by summing the fluid contributions from all the components modeled in the OSU analysis code, with the exception of the SG secondary-side. These fluid masses include:

Masses	Component
M_{ACCi}	Two accumulators
M_{ADS13}	ADS 1-3 separator tank
M_{ADS4i}	ADS 4-1 and ADS 4-2 separator tanks
M_{BRK}	Break separator tank
M_{CLi}	Four cold legs
$M_{TOT\text{-}CMTi}$	CMT plus CMT to cold leg balance lines for two CMTs
M_{RPV}	RPV excluding downcomer
M_{DC}	Downcomer
M_{HLi}	Two hot legs
M_{IRWST}	IRWST
$M_{TOT\text{-}PZR}$	Pressurizer plus surge line
M_{PRHR}	PRHR HX
$M_{TOT\text{-}SGi}$	Primary side, SG inlet plenum plus outlet plenum plus U-tubes for two SGs
$M_{TOT\text{-}SUMP}$	Primary plus secondary sump

The total system mass inventory is calculated as:

$$M_{TOT} = \sum_{i=1}^{2} M_{ACCi} + M_{ADS13} + \sum_{i=1}^{2} M_{ADS4i} + M_{BRK} + \sum_{i=1}^{4} M_{CLi} + \sum_{i=1}^{2} M_{TOT\text{-}CMTi} \quad 4.21\text{-}1$$

$$+ M_{RPV} + M_{DC} + \sum_{i=1}^{2} M_{HLi} + M_{IRWST} + M_{TOT\text{-}PZR} + M_{PRHR} + \sum_{i=1}^{2} M_{TOT\text{-}SGi} + M_{TOT\text{-}SUMP}$$

As well as the total system mass inventory, the following additional mass inventories are calculated:

1. Pressure vessel inventory:

$$M_{PV} = M_{RPV} + M_{DC} \quad 4.21\text{-}2$$

2. Primary system mass:

$$M_{PRIM} = \sum_{i=1}^{4} M_{CLi} + M_{RPV} + M_{DC} + \sum_{i=1}^{2} M_{HLi} + M_{TOT\text{-}PZR} + \sum_{i=1}^{2} M_{TOT\text{-}SGi} + M_{PRHR} \quad 4.21\text{-}3$$

3. Total mass in all water sources:

$$M_{SOURCE} = \sum_{i=1}^{2} M_{ACCi} + \sum_{i=1}^{2} M_{TOT\text{-}CMTi} + M_{IRWST} + M_{TOT\text{-}SUMP} \quad 4.21\text{-}4$$

4.21.2 Primary System Mass Balance

In additional to the measured primary system mass inventory given above, the primary system mass can be inferred using the initial measured mass and integrated flow. The inferred mass is calculated as:

$$M^{*}_{PRIM} = M_{PRIM}\big|_{initial} + M_{IN} - M_{OUT} \quad 4.21\text{-}5$$

where:

M_{IN} = Total mass gained by the primary system from all sources, where the sources combine to form flow to the two DVI lines

$$M_{IN} = \int_0^t \left\{ \dot{M}_{DVI1} + \dot{M}_{DVI2} \right\} dt \qquad 4.21\text{-}6$$

$$\dot{M}_{DVi} = \dot{M}_{ACCi,f} + \dot{M}_{TOT\text{-}CMTi,f} + \dot{M}_{IRWST,f\text{-}i} + \dot{M}_{TOT\text{-}SUMP,f\text{-}i} \qquad 4.21\text{-}7$$

M_{OUT} = Total mass (liquid + steam) lost by the primary system to the sinks

$$\dot{M}_{OUT} = \dot{M}_{ADS13,mix} + \dot{M}_{ADS41,mix} + \dot{M}_{ADS42,mix} + \dot{M}_{BRK,mix} + \dot{M}_{CMT1,mix} + \dot{M}_{CMT2,mix} \qquad 4.21\text{-}8$$

where the superscript:

* = An inferred mass

where the subscripts:

f = Liquid flow path from components
f-i = One of two liquid flow paths from components with two flow paths (SUMP & IRWST)
mix = Mixture (liquid + vapor) flow path to components

The primary system mass balance error is calculated as:

$$M_{PRIM,ERROR} = M_{PRIM} - M^{*}_{PRIM} \qquad 4.21\text{-}9$$

4.21.3 Sump Mass Balance

All flow paths to and from the combination of the primary plus secondary sumps are metered. Thus, a sump mass balance gives insight into instrumentation accuracy. The sump mass can be inferred using the initial measured mass and integrated flows. The inferred mass is calculated as:

$$M^{*}_{TOT\text{-}SUMP} = M_{TOT\text{-}SUMP}\Big|_{initial}$$

$$+ \int_{t_o}^{t} \left\{ \dot{M}_{ADS41,f} + \dot{M}_{ADS42,f} + \dot{M}_{BRK,f} + \dot{M}_{IRWST,f\text{-}over} \right\} dt \qquad 4.21\text{-}10$$

$$- \int_{t_o}^{t} \left\{ \dot{M}_{TOT\text{-}SUMP,f\text{-}1} + \dot{M}_{TOT\text{-}SUMP,f\text{-}2} + \dot{M}_{TOT\text{-}SUMP,g} \right\} dt$$

where the subscripts:

f-over	=	Liquid overflow
g	=	Steam flow path

The sump mass balance error is calculated as:

$$M_{TOT\text{-}SUMP,ERROR} = M_{TOT\text{-}SUMP} - M^{*}_{TOT\text{-}SUMP} \qquad 4.21\text{-}11$$

4.21.4 In-Containment Refueling Water Storage Tank Mass Balance

All flow paths to and from the IRWST are metered. Thus, an IRWST mass balance gives insight into instrumentation accuracy. The IRWST mass can be inferred using the initial measured mass and integrated flow. The inferred mass is calculated as:

$$M^{*}_{IRWST} = M_{IRWST}\Big|_{initial} + \int_{t_o}^{t} \left\{ \dot{M}_{ADS13,f} + \dot{M}_{ADS13,g} \right\} dt$$

$$4.21\text{-}12$$

$$- \int_{t_o}^{t} \left\{ \dot{M}_{IRWST,f\text{-}1} + \dot{M}_{IRWST,f\text{-}2} + \dot{M}_{IRWST,f\text{-}over} + \dot{M}_{IRWST,g} \right\} dt$$

The IRWST mass balance error is calculated as:

$$M_{IRWST,ERROR} = M_{IRWST} - M^{*}_{IRWST} \qquad 4.21\text{-}13$$

4.21.5 Variations in Mass Balance Models with Break Location

Various tests included changes to the piping to facilitate different break configurations. The following outlines these changes on a test-by-test basis. Input flags have been used to determine what logic should be used for each test. Modeling of the various break configurations in the OSU test analysis program is limited to the system mass analyses of Section 4.21 and the DVI flow related, core calculations of Section 4.11.

4.21.5.1 Core Makeup Tank/Cold Leg Balance-Line Break – Double-Ended Guillotine of Balance Line-1

This break configuration applies to Matrix Test SB10.

Flow from the cold-leg side of the break was directed into the break separator, and flow from the CMT side was directed to the 5-in. ADS 4-2 separator. Both sides of ADS-4 were piped to the 8-in. ADS 4-1 separator. The break flow path included flow to the break separator and to the ADS 4-2 separator. Changes to equations in Subsections 4.21.1 through 4.21.4 are shown below.

Equation 4.21-8 becomes:

$$\dot{M}_{OUT} = \dot{M}_{ADS13,mix} + \dot{M}_{ADS41,mix} + \dot{M}_{BRK,mix} + \dot{M}_{CMT2,mix} \qquad 4.21\text{-}14$$

4.21.5.2 Direct Vessel Injection Line Break – Double-Ended Guillotine of Direct Vessel Injection-1

This break configuration applies to Matrix Test SB12.

The reactor break flow was piped to the break separator while the CMT/accumulator/IRWST side of DVI-1 was aligned directly to the sump, and the sump side of DVI-1 was dead-ended. The reactor side break flow was therefore measured by FMM-905 and FVM-905. CMT/accumulator/IRWST side of the break had liquid flow measured by {FMM-401 + FMM-501 + FMM-701} and the steam flow by FVM-906. The latter was the steam flow through the primary sump exhaust.

From a mass balance point of view, there was no impact on the integrated mass lost from the primary system. Mass flow into the primary system excluded all contributions that would have normally flowed through DVI line-1.

Both CMT discharge flow meters were over-ranged during this test. The CMT-1 meter, FMM-501, was over-ranged for most of the first 200 seconds of the transient and had multiple shifts in its zero-flow offset. The CMT-2 meter, FMM-504, was over-ranged for two relatively short time periods and

did not exhibit significant zero-flow offset shifts. To minimize errors introduced by these problems, CMT balance line flow was not included in the primary system mass balance.

Changes to equations in Subsections 4.21.1 through 4.21.4 are shown below. Reverse flow for DVI-1 is flow lost by the primary system and is included in M_{OUT}. Equation 4.21-7 for DVI-1 becomes:

$$\dot{M}_{DVI1} = 0 \qquad 4.21\text{-}15$$

Equation 4.21-8 becomes:

$$\dot{M}_{OUT} = \dot{M}_{ADS13,mix} + \dot{M}_{ADS41,mix} + \dot{M}_{ADS42,mix} + \dot{M}_{BRK,mix} \qquad 4.21\text{-}16$$

Equation 4.21-10 becomes:

$$M^{*}_{TOT\text{-}SUMP} = M_{TOT\text{-}SUMP}\Big|_{initial} + \int_{t_0}^{t} \left\{ \dot{M}_{ADS41,f} + \dot{M}_{ADS42,f} + \dot{M}_{BRK,f} + \dot{M}_{IRWST,f\text{-}over} \right\} dt + \int_{t_0}^{t} \left\{ \dot{M}_{ACC1,f} + \dot{M}_{TOT\text{-}CMT1,f} + \dot{M}_{IRWST,f\text{-}1} \right\} dt - \int_{t_0}^{t} \left\{ \dot{M}_{TOT\text{-}SUMP,f\text{-}2} + \dot{M}_{TOT\text{-}SUMP,g} \right\} dt \qquad 4.21\text{-}17$$

4.21.5.3 Direct Vessel Injection Line Break – 2-in. Direct Vessel Injection Line-1 Break

This break configuration applies to Matrix Test SB13.

The break separator was connected to the DVI line by two valves to allow both reactor and CMT/accumulator sides of the break to be piped directly to the break separator. Thus, the break separator measured all the break flow directly. Flow measurements for the affected accumulator, CMT, and IRWST line-1 are applicable.

Changes to equations in Subsections 4.21.1 through 4.21.4 are shown below. Reverse flow for DVI-1 is flow lost by the primary system and is included in M_{OUT}. Equation 4.21-7 for DVI-1 becomes:

$$\dot{M}_{DVI1} = 0 \qquad 4.21\text{-}18$$

Equation 4.21-8 becomes:

$$\dot{M}_{OUT} = \dot{M}_{ADS13,mix} + \dot{M}_{ADS41,mix} + \dot{M}_{ADS42,mix} + \dot{M}_{BRK,mix} - \dot{M}_{IRWST,f-1} - \dot{M}_{CMT1,f} - \dot{M}_{ACC1,f} - \dot{M}_{SUMP,f-1} \quad 4.21\text{-}19$$

4.21.5.4 Direct Vessel Injection Line Break – Double-Ended Guillotine of Direct Vessel Injection Line-1 with Additional Failures

This break configuration applies to Matrix Test SB28.

The break configuration is the same as in SB12 and the same break flow measurement requirements are applicable. It should be noted that accumulator-1 was isolated and did not discharge; thus, FMM-401 should read zero throughout.

Changes to equations in Subsections 4.21.1 through 4.21.4 are shown below. Reverse flow for DVI-1 is applied to M_{OUT}. Equation 4.21-7 for DVI-1 becomes:

$$\dot{M}_{DVI1} = 0 \quad 4.21\text{-}20$$

Equation 4.21-8 becomes:

$$\dot{M}_{OUT} = \dot{M}_{ADS13,mix} + \dot{M}_{ADS41,mix} + \dot{M}_{ADS42,mix} + \dot{M}_{BRK,mix} - \dot{M}_{IRWST,f-1} - \dot{M}_{CMT1,f} - \dot{M}_{SUMP,f-1} \quad 4.21\text{-}21$$

4.21.5.5 Hot-Leg Break – 2-in. Hot Leg-2 Break

This break configuration applies to Matrix Test SB15.

The break was routed to the break separator in a configuration similar to the cold-leg breaks. Thus, there are no changes to the equations in Subsections 4.21.1 through 4.21.4.

4.21.5.6 Inadvertent Automatic Depressurization System

This break configuration applies to Matrix Tests SB14 and SB26.

This test models an inadvertent ADS valve opening and does not include any breaks. Changes to equations in Subsections 4.21.1 through 4.21.4 are shown below. The break flow should be zero throughout and is not applied to M_{OUT}. Equation 4.21-8 becomes:

$$\dot{M}_{OUT} = \dot{M}_{ADS13,mix} + \dot{M}_{ADS41,mix} + \dot{M}_{ADS42,mix} + \dot{M}_{CMT1,mix} + \dot{M}_{CMT2,mix} \qquad 4.22\text{-}22$$

4.21.5.7 Inadvertent S-Signal

This break configuration applies to Matrix Test SB31.

This test models an inadvertent S-signal and does not include any breaks. Changes to equations of Subsections 4.21.1 through 4.21.4 are shown below. The break flow should be zero throughout and is not applied to M_{OUT}. Equation 4.21-8 becomes:

$$\dot{M}_{OUT} = \dot{M}_{ADS13,mix} + \dot{M}_{ADS41,mix} + \dot{M}_{ADS42,mix} + \dot{M}_{CMT1,mix} + \dot{M}_{CMT2,mix} \qquad 4.22\text{-}23$$

4.21.5.8 Additional Inflow for Tests with Nonsafety-Related Systems

This break configuration applies to Matrix Tests SB04 and SB24.

Mass flow from the nonsafety systems, the CVS and the RNS to the primary system must be included. Single-phase liquid flow is calculated as:

$$\dot{M}_{CVS} = W_{FMM-801} \times \rho_f(P_{FMM-801}, T_{FMM-801}) \times C \qquad 4.21\text{-}24$$

$$\dot{M}_{RNS} = W_{FMM-802} \times \rho_f(P_{FMM-802}, T_{FMM-802}) \times C \qquad 4.21\text{-}25$$

where:

W	=	Volumetric flow rate of liquid, gpm
C	=	Conversion constant, gpm to ft^3/sec.

and the subscript:

FMM-XXX	=	Data for flow meter XXX

Local density is calculated from the ASME steam tables. Flow meter data channels are listed in Table 4.21-1.

Changes to equations in Subsections 4.21.1 through 4.21.4 are shown below. Two additional flow measurements are applied to M_{IN}. Equation 4.21-6 becomes:

$$M_{IN} = \int_{t_0}^{t} \left\{ \dot{M}_{DVI1} + \dot{M}_{DVI2} + \dot{M}_{CVS} + \dot{M}_{RNS} \right\} dt \qquad 4.21\text{-}26$$

The CVS and RNS flow is also included with the DVI line flow in the DVI flow related, core calculations of Section 4.11.

TABLE 4.21-1 DATA CHANNEL IDs USED FOR FLOW METER CALCULATIONS			
Applicable Conditions	**Channel ID for Liquid Flow Meter**	**Channel ID for Pressure Transducer**	**Channel ID for Fluid Thermocouple**
CVS	FMM-801	PT-801	TF-801
RNS	FMM-802	PT-802	TF-802

4.22 Overall System Energy Balance

An overall energy balance on the test facility is achieved by considering the primary system, the IRWST, sumps, ADS and break separators as a control volume. Energy is added to the volume through the heated rods in the core. Energy is extracted via losses to the environment, steam exhaust from the break, IRWST, sumps and ADS-4, and energy loss from the primary to secondary side of the SGs. Finally, the change in the internal energy of the fluid and metal heat capacities within the control volume is included to complete the energy balance. The overall system energy balance for the OSU test facility is written as follows:

$$U_{DEF} = U_{RODS} - U_{STM\ XHST} - U_{AMB} - U_{SG} + (U - U_o)_{FL} + (U - U_o)_{METAL} \qquad 4.22\text{-}1$$

where:

U_{DEF}	=	Deficit in the overall energy balance (Btu)
U_{RODS}	=	Integrated power in the heated rods (Btu)
$U_{STM\ XHST}$	=	Integrated rate of energy loss from steam exhaust (Btu)
U_{AMB}	=	Integrated rate of energy loss to the ambient (Btu)
U_{SG}	=	Integrated rate of energy loss from the SGs (Btu)
ΔU_{FL}	=	Change in the energy of the fluid in the control volume (Btu)
ΔU_{METAL}	=	Change in the energy of the metal in the control volume (Btu)

Heat transfer that occurs internal to the control volume, as in the PRHR/IRWST, is accounted for implicitly in the overall heat balance.

Integrated rod power is defined by the following equation:

$$U_{RODS} = \int Q_{RODS} dt = \sum Q_{RODS_j} \Delta t_j \qquad 4.22\text{-}2$$

where:

Q_{RODS_j}	=	Measured power over time step, Δt_j

The total heat loss from steam exhaust is given by:

$$Q_{STM\ XHST} = Q_{BRK} + Q_{ADS4} + Q_{IRWST} + Q_{SUMP} \qquad 4.22\text{-}3$$

where:

$Q_{STM\ XHST}$	=	Total exhaust heat loss rate (Btu/sec.)
Q_{BRK}	=	Steam exhaust heat loss rate from the break (Btu/sec.)
Q_{ADS4}	=	Steam exhaust heat loss rate from ADS-4 (Btu/sec.)

Q_{IRWST} = Steam exhaust heat loss rate from the IRWST (Btu/sec.)
Q_{SUMP} = Steam exhaust heat loss rate from the sumps (Btu/sec.)

The integrated rate of energy loss from the steam exhaust is given by:

$$U_{STM\ XHST} = \int Q_{STM\ XHST} dt = \sum Q_{STM\ XHST,j} \Delta t_j \qquad 4.22\text{-}4$$

where:

$Q_{STM\ XHST,j}$ = Total heat loss rate from the steam exhaust for a time step, Δt_j

Heat loss to the surroundings is determined by summing heat loss calculated for the various components.

$$Q_{AMB} = \sum Q_{AMB,i} \qquad 4.22\text{-}5$$

where:

Q_{AMB} = Total heat loss to the ambient (Btu/sec.)
$Q_{AMB,i}$ = Heat loss to the ambient for each component, including the RPV, pressurizer, CMTs, Steam generators, IRWST, sumps, separators, and piping (Btu/sec.)

The integrated heat loss to the ambient is given by the following equation:

$$U_{AMB} = \int Q_{AMB} dt = \sum Q_{AMB,j} \Delta t_j \qquad 4.22\text{-}6$$

where:

$Q_{AMB,j}$ = Total heat loss to the ambient over a given time step, Δt_j (Btu/sec.)

The heat loss from the primary side to the secondary side of the SGs is given by:

$$Q_{SG} = Q_{SG1} + Q_{SG2} \qquad 4.22\text{-}7$$

where:

Q_{SG} = Total heat loss from the two SGs (Btu/sec.)
Q_{SG1} = Heat loss from SG-1 (Btu/sec.)
Q_{SG2} = Heat loss from SG-2 (Btu/sec.)

The integrated heat loss from the primary system through the SGs is given by:

$$U_{SG} = \int Q_{SG} dt = \sum Q_{SG,j} \Delta t_j \qquad 4.22\text{-}8$$

where:

$Q_{SG,j}$ = Total heat loss through the SGs over time step, Δt_j (Btu/sec.)

The change in the fluid energy relative to time zero is calculated by summing the fluid energy for each component in the control volume at each time step, then subtracting the value at time zero.

$$\Delta U_{FL} = \sum U_{FL,i,j} - \sum U_{FL,i,o} \qquad 4.22\text{-}9$$

where:

$\sum U_{FL,i,j}$ = Energy content of the fluid in component i at time t_j (Btu)

$\sum U_{FL,i,o}$ = Energy content of the fluid in component i at time t_o (Btu)

The components include the RPV, downcomer, pressurizer, SGs (primary side), CMTs, accumulators PRHR, IRWST, sumps, separators, and piping.

The change in the metal energy relative to time zero is calculated by summing the metal energy for each component in the control volume at each time step, then subtracting the value at time zero.

$$\Delta U_{METAL} = \sum U_{METAL,i,j} - \sum U_{METAL,i,o} \qquad 4.22\text{-}10$$

where:

$\sum U_{METAL,i,j}$ = Energy content of the metal in component i at time t_j (Btu)

$\sum U_{METAL,i,o}$ = Energy content of the metal in component i at time t_o (Btu)

The components include the RPV, downcomer, pressurizer, SGs (primary side), CMTs, accumulators, PRHR, IRWST, sumps, separators, and piping.

5.0 ANALYSIS OF OSU TEST DATA

The phenomena identification ranking table (PIRT) for AP600 small-break loss-of-coolant accident (SBLOCA) with long-term cooling (Table 1.3-1) provided a guide for development of the OSU testing program. The PIRT was used to identify the instrumentation needed to record specific phenomena and also the manner in which the tests were performed. An initial acceptance evaluation of the tests against the requirements documented in the PIRT was performed in the OSU Final Data Report[1], which also included an evaluation of critical instruments and the acceptability of the initial conditions.

SBLOCA transients which transitioned into the long-term cooling (LTC) phase were performed in the OSU test. These tests were divided into phases characterized by the primary system pressure and thermal-hydraulic phenomena which occurred. The following phases were selected for the purpose of detailed evaluation of the SBLOCA and LTC:

- Blowdown phase
- Natural circulation phase
- ADS phase
- IRWST injection phase
- Sump injection phase

The analysis of the OSU test data was performed using the test data reduction computer code specifically developed to perform a continuous mass and energy balance for each component of the system (Section 4.0). The collapsed liquid levels were also computed for the various components, including the power channel. The two-phase level in the power channel was calculated to determine the extent of coolant coverage of the heater bundle during the entire test.

This section presents an analysis of the test data from the Matrix Tests listed in Table 3.2-1. A discussion of each test is provided along with a set of standard plots that quantify the performance of the test. Additional plots are included to aid in characterizing the phenomena observed during each test.

5.1 Analysis of Matrix Test SB01

Matrix Test SB01 (OSU Test U0001) modeled a 2-in. cold-leg break SBLOCA with LTC and without operation of the nonsafety-related systems. The break was located at the bottom of CL-3 on the core makeup tank side of the facility. The test included a simulated failure of one of the ADS-4 lines. Since SB01 is the base case LOCA test, more detail is included in Section 5.1 than in subsequent sections.

The analysis of Matrix Test SB01 is divided into three sections:

- General facility performance (Subsection 5.1.1) describes the overall response of the system throughout the test. The performance of the facility is characterized by the figures listed in Table 5.1.1-1.

- SBLOCA (Subsection 5.1.2) provides a discussion of the system behavior from the start of the test, through system depressurization, to approximately [ ]^{a,b,c} seconds into the transient, and includes the initial system blowdown, the establishment of natural circulation, and the initial portion of the IRWST injection cooling (Figure 5.2-2).

- LTC (Subsection 5.1.3) discusses the behavior of the remainder of the test after [ ]^{a,b,c} seconds and includes the completion of IRWST injection and the establishment of sump injection.

The refill and subsequent recirculation of the CMT is considered as a separate discussion within Subsection 6.1.1. The period between SBLOCA and LTC is not discussed specifically since the system was behaving in a stable manner.

5.1.1 Facility Performance

The simulated break was located on the bottom of cold leg 3. A flow nozzle simulating one ADS-4 valve was installed in the ADS 4-1 line (HL-1 to the ADS 4-1 separator) to provide the single-failure simulation. A flow nozzle simulating two valves was installed in the ADS 4-2 line (HL-2 to the ADS 4-2 separator). Additionally, flow nozzles simulating two ADS 1-3 pairs of valves were installed in the ADS 1-3 inlet lines.

The reactor heater control decay algorithm maintained maximum reactor heater power output for [ ]^{a,b,c} seconds, and then the power was programmed to begin to decay, simulating the total post-trip energy input of the AP600 nuclear fuel. This test was performed with reactor heater rod HTR-C2-317 removed and replaced with a dummy rod.

Facility performance is divided into separate discussions of the five phases of the test:

- Blowdown
- Natural circulation
- ADS
- IRWST injection
- Sump injection

The overall performance of the 30,000-second (8-hour) test is shown in Figures 5.1.1-1 to 5.1.1-4. Figure 5.1.1-1 shows the pressurizer pressure throughout the test with the various phases and operating components indicated for each phase. For clarity, the time scale is cut between 2000 and 12,000 seconds since there was no change in the operating mode during this period. Figure 5.1.1-2 shows the total injection flow rates into the DVI line from the various systems as a function of time. Figure 5.1.1-3 shows the calculated quantity of steam generated in the core throughout the test. Figure 5.1.1-4 shows the variation in average measured core outlet temperature and peak clad temperature relative to the core outlet saturation temperature.

Figures 5.1.1-1 and 5.1.1-2 shows that a continuous flow of water into the reactor vessel was provided by the passive safety-related systems as the primary system was depressurizing. The operation of the passive safety injection systems overlapped so that, as one system drained or emptied, another provided flow into the simulated reactor vessel for continuous core cooling.

Sufficient flow to the core was maintained so that the measured average core outlet temperature was saturated or subcooled for significant portions of the transient, and the core steam flow was less than the passive safety system injection flow (Figures 5.1.1-2 and 5.1.1-3). As the system transitioned into

LTC, the water injected from the sump was hot since it originated in the primary system. The hotter sump water combined with the lower driving head during the sump injection resulted in continuous steam generation in the heater rod bundle (Figure 5.1.1-3) after [ ]^{a,b,c} seconds. This steam was then vented, primarily through the ADS-4 valves.

5.1.1.1 Blowdown Phase

The blowdown phase corresponds to the first [ ]^{a,b,c} seconds of Matrix Test SB01 (Figure 5.1.1-1). The test was initiated (0 time) by opening the break valve located at the bottom of CL-3 and the blowdown phase was completed when steam pressure reached the steam generator (SG) safety valve setpoint. The hot leg of the reactor coolant system (RCS) was at 420°F and 370 psig prior to test initiation. The simulated S signal was generated at 0.5 seconds after the break signal and initiated the following actions.

In the first [ ]^{a,b,c} seconds, the SG safety relief setpoint pressure was raised to [ ]^{a,b,c} psig, and the reactor shifted to power (kW) control mode with a programmed power demand for 600-kW total power. The main feedwater pump tripped and the feedwater was isolated at [ ]^{a,b,c} seconds. The passive residual heat removal heat exchanger (PRHR HX) outlet valve and CMT discharge valves opened at [ ]^{a,b,c} seconds, and the reactor coolant pumps (RCPs) tripped at [ ]^{a,b,c} seconds after the break signal.

Forced flow continued through the PRHR HX and the CMTs until the RCPs stopped at about [ ]^{a,b,c} seconds, at which time PRHR HX flow changed to natural circulation. As the RCS depressurized and coolant escaped through the break, the pressurizer level decreased rapidly and steam formation began in the reactor vessel upper head. At about [ ]^{a,b,c} seconds, the level in the reactor vessel indicated the vessel was beginning to lose inventory as the vessel drained and some liquid flashed to steam. The upper plenum volume began to show a collapsed level decrease indicating that there was steam collecting in this volume at about [ ]^{a,b,c} seconds.

As primary system pressure fell to near a steady-state condition, the system transitioned into the natural circulation phase once the pumps coasted down and the system reached the SG pressure relief setpoint at 335 psig at about [ ]^{a,b,c} seconds. During this period, there was initially liquid solid natural circulation in the PRHR and CMT systems. The CMTs provided recirculating flow to the reactor vessel, while the PRHR removed energy from the primary system.

5.1.1.2 Natural Circulation Phase

The upper head drained to two-thirds empty after [ ]^{a,b,c} seconds. The mass loss through the break caused a rapid decrease in pressurizer level and emptied the pressurizer at about [ ]^{a,b,c} seconds. The pressurizer surge line was completely emptied at about [ ]^{a,b,c} seconds. The primary system was initially at a pressure above the SG secondary-side pressure, therefore the SGs continued to remove energy from the primary system. As the system continued to drain, the SG tubes started to

drain at [ ]^{a,b,c} seconds, and the SGs transitioned into a two-phase recirculation behavior. The cold legs developed a void fraction at about [ ]^{a,b,c} seconds, at which time the CMT balance lines began to drain. CMT-1 and CMT-2 levels began to decrease, making the transition from recirculation to draindown at about [ ]^{a,b,c} seconds, respectively, at which time the injection flow from the CMTs increased (Figure 5.1.1-2). At about [ ]^{a,b,c} seconds, a condensation/depressurization event took place in CMT-1, as indicated by a rapid refill of the CMT-1 balance line as steam from the balance line was condensed in the CMT. Water from the cold leg was drawn up the balance line into the CMT as the balance line filled.

As the system continued to drain, the hot-leg level began to decrease at about [ ]^{a,b,c} seconds, and the steam generation reached its maximum of [ ]^{a,b,c} lbm/sec. at [ ]^{a,b,c} seconds (Figure 5.1.1-3). The U-tubes of both SGs were completely empty by about [ ]^{a,b,c} seconds and became superheated at about [ ]^{a,b,c} seconds. The horizontal sections of the hot legs started to drain at about [ ]^{a,b,c} seconds. The hot legs remained at saturation temperature and never superheated, even though they were partially or completely empty, due to a small flow of saturated steam from the reactor heater bundle to the SGs.

The collapsed liquid level inside the reactor pressure vessel reached a near-term minimum value at [ ]^{a,b,c} seconds but the core remained covered with a two-phase mixture during this period. The maximum steam generation rate shown in Figure 5.1.1-3, also occurred at this time as the flow from the CMT was decreasing.

When the RCS depressurized to about [ ]^{a,b,c} psig at about [ ]^{a,b,c} seconds, accumulator injection into the DVI line began (Figures 5.1.1-1 and 5.1.1-2). At [ ]^{a,b,c} seconds, CMT-1 reached the ADS-1 setpoint, and the ADS-1 valve opened, to initiate ADS blowdown.

5.1.1.3 Automatic Depressurization System Phase

The ADS flow path, in conjunction with the break, caused RCS pressure to decrease at a more rapid rate, redistributing the mass inventory of the system. The opening of the ADS-1 valve resulted in two-phase flow going through the pressurizer to the ADS 1-3 separator and into the IRWST through the sparger. The opening of the ADS-1 valve, followed by the ADS-2 valve about 1 minute later, caused an increase in the rate of RCS depressurization. As the different ADS stages opened, the primary vent path shifted from the cold-leg break to the ADS valves through the pressurizer.

The accumulators started discharging into the DVI line, which reduced CMT-1 injection flow to [ ]^{a,b,c} over the following [ ]^{a,b,c} seconds and CMT-2 injection flow to less than [ ]^{a,b,c} gpm over the following [ ]^{a,b,c} seconds by closing the CMT discharge line check valves until the accumulators were almost empty and depressurized. With the accumulators at their maximum injection rate, the RCS refilled and the surge line and pressurizer began to reflood at about [ ]^{a,b,c} seconds, and the pressurizer attained its maximum level at [ ]^{a,b,c} seconds. Once the accumulators were empty, the pressurizer and surge line drained again and were completely empty at [ ]^{a,b,c} seconds.

The pressurizer was slightly subcooled at about [ ]^{a,b,c} seconds, remained subcooled until primary sump injection began, and then heated to saturation temperature. The pressurizer remained at saturation temperature until about [ ]^{a,b,c} seconds when the temperature began to rise into the superheated range.

The RCS pressure had decreased to [ ]^{a,b,c} psig at about [ ]^{a,b,c} seconds, when the two IRWST injection valves automatically opened, but IRWST injection could not occur until the RCS pressure decreased to near containment pressure. As ACC-1 and ACC-2 completed injection at [ ]^{a,b,c} and [ ]^{a,b,c} seconds, CMT-2 injection flow started to increase at [ ]^{a,b,c} seconds, and CMT-1 injection flow started to increase at [ ]^{a,b,c} seconds. About 50 percent of the nitrogen gas inventory used to pressurize the accumulator was injected into the DVI lines (Subsection 6.1.4), momentarily cooling the injection lines. The nitrogen caused a momentary decrease in DVI-1 flow of about [ ]^{a,b,c} gpm and a decrease in ACC-1 outlet temperature of about [ ]^{a,b,c} °F at [ ]^{a,b,c} seconds. On the ACC-2 side, there was no indicated change in DVI-2 flow, although the ACC-2 outlet temperature decreased [ ]^{a,b,c} °F at [ ]^{a,b,c} seconds.

During the accumulator injection period, at about [ ]^{a,b,c} seconds, there was sufficient injection of subcooled liquid to suppress boiling in the core region. The downcomer was filled with subcooled liquid which resulted in the collapse of the superheated steam bubble in the upper portion of the reactor vessel downcomer annulus. As pressure decreased in the upper annulus the downcomer fluid accelerated upward and impacted on the bottom of the core barrel flange where the core bypass holes are located. The impact of the downcomer liquid on the solid surface of the core barrel flange was heard during the test.

During accumulator injection, PRHR flow decreased to near [ ]^{a,b,c} and the PRHR level decreased. The majority of the nitrogen was discharged into the DVI lines at about [ ]^{a,b,c} seconds, respectively with small subsequent periodic outflows marked by spikes in the DVI line flow. The PRHR HX inlet fluid temperature became subcooled while the ADS-4 valves opened at [ ]^{a,b,c} seconds and over the next [ ]^{a,b,c} seconds dropped to and paralleled the PRHR HX outlet fluid temperature. Again, this is an indication that there was no flow through the PRHR HX during this time frame. From [ ]^{a,b,c} seconds, both DVI nozzle temperatures increased from essentially ambient conditions to as high as [ ]^{a,b,c} °F and then returned to ambient condition. The DVI fluid temperature increase was caused by two factors. First, there was rapid heating of the remaining water injected from the CMTs. Second, the reactor vessel downcomer level was at the DVI nozzle level during this period, possibly partially uncovering the nozzles. The DVI fluid temperature transient was terminated when IRWST injection began refilling the reactor vessel at about [ ]^{a,b,c} seconds, and temperatures returned to ambient conditions when the CMTs were empty of hot liquid.

Steam generation in the reactor vessel was reestablished at about [ ]^{a,b,c} seconds and the reactor vessel inventory began to decrease. At [ ]^{a,b,c} seconds, the ADS 4-1 and ADS 4-2 valves opened automatically when the CMT-1 level reached its low-low level setpoint. ADS-4 actuation started a decline in RCS inventory that could not be overcome until IRWST injection began. There was initially

an excess of mass in the system to be vented through ADS-4 before IRWST injection could occur. CMT-1 and CMT-2 were completely empty at [ ]^{a,b,c} seconds, respectively.

The collapsed reactor vessel level reached a minimum value of about [ ]^{a,b,c} in. at [ ]^{a,b,c} seconds. Although this level is below the top of the heater rod heated length, the actual level of the top of the two-phase mixture is much higher, as shown in the behavior of the core outlet thermocouples (Figure 5.1.1-4), which do not exceed saturation temperatures.

At about [ ]^{a,b,c} seconds, the RCS system pressure decreased to about [ ]^{a,b,c} psig, which was sufficiently low that the IRWST static head was greater than RCS pressure, and IRWST injection began.

5.1.1.4 In-Containment Refueling Water Storage Tank Injection Phase

IRWST injection was split between the two DVI lines beginning at [ ]^{a,b,c} seconds and continually diminished (Figure 5.1.1-2) as the differential head between the IRWST and the RCS decreased with draining of the IRWST. IRWST injection was sufficient for the primary system to refill. The pressurizer and pressurizer surge line emptied a second time at about [ ]^{a,b,c} seconds, respectively.

When the pressurizer had a liquid level, ADS 1-3 separator and sparger pressure became negative by as much as [ ]^{a,b,c} psig. These values remained negative from [ ]^{a,b,c} seconds as steam in the ADS lines was condensed in the IRWST. The negative pressure was broken as the level in the IRWST decreased below the sparger nozzles. No vacuum breaker was installed on the sparger line inside the IRWST for this test. A vacuum breaker is included in the AP600 plant design, thus this OSU test response may not be typical of the AP600. The surge line then began to reflood almost immediately at [ ]^{a,b,c} seconds and the pressurizer at about [ ]^{a,b,c} seconds. The reflood was caused by RCS levels increasing above the reactor vessel nozzles because IRWST injection exceeded the inventory losses, and by the condensation in the ADS 1-3 lines. The maximum pressurizer level attained was about [ ]^{a,b,c} in. at [ ]^{a,b,c} seconds, but it immediately began to decrease. The pressurizer was empty at [ ]^{a,b,c} seconds and remained empty for the remainder of the test. The surge line stayed full until [ ]^{a,b,c} seconds when the level decreased to about [ ]^{a,b,c} in. and remained there until [ ]^{a,b,c} seconds. The level again decreased to about [ ]^{a,b,c} in. at [ ]^{a,b,c} seconds and oscillated between about [ ]^{a,b,c} in. for the remainder of the test.

Both CMT balance lines began to refill at about [ ]^{a,b,c} seconds when the IRWST injection increased the reactor vessel level sufficiently to begin covering and refilling the cold legs. At about [ ]^{a,b,c} seconds, when the CMT-2 balance line had completely refilled, CMT-2 began to rapidly refill and reached the [ ]^{a,b,c} in. level (about two-thirds full) at about [ ]^{a,b,c} seconds. The CMT refill is discussed in more detail in Subsection 6.1.1. After the CMTs were partially refilled, there was no injection flow from the CMTs because the higher static head of the IRWST held the CMT discharge line check valves closed.

Steam generation started again at about [ ]^{a,b,c} seconds and continued for the remainder of the test (Figure 5.1.1-3). CMT-1 and CMT-2 remained at essentially constant levels for several thousand seconds and then began slow draindowns at about [ ]^{a,b,c} seconds, respectively. The draindown for both CMTs was slow and did not occur until the IRWST relative level was [ ]^{a,b,c} in. below that of the CMTs. Data indicate that the CMTs drained for a while, and then the differential head between the IRWST and the CMTs again closed the CMT discharge check valves, terminating draining until the differential shifted the other way and draining recommenced. Both CMTs were completely empty at about [ ]^{a,b,c} seconds, which coincides closely with the primary sump injection valve opening at [ ]^{a,b,c} seconds. A possible correlation is that when the primary sump valve opened, the IRWST had just reached its minimum level of about [ ]^{a,b,c} in., which is about [ ]^{a,b,c} in. below the instrumented level for the CMTs, and that there was still a slight negative pressure remaining in the CMTs. Also, when the primary sump injection valves opened, there was a short period in which the IRWST and primary sump levels equalized, causing a decrease in RCS fluid levels and resulting in a rapid drop in CMT levels from about [ ]^{a,b,c} in.

Starting at about [ ]^{a,b,c} seconds, there was a series of pressure, level, and flow oscillations that occurred throughout the components of the facility lasting until about [ ]^{a,b,c} seconds. These oscillations will be discussed in detail in Subsection 6.1.3.

At [ ]^{a,b,c} seconds, the PRHR HX inlet fluid temperature instantly increased from [ ]^{a,b,c} °F to saturation temperature. The temperature increased at about [ ]^{a,b,c} seconds after pressure, level, and flow oscillations began in the facility and was possibly caused by the inlet line burping, which once again allowed the line to fill with saturated steam. Following the burp, all of the PRHR HX temperatures began to slowly approach saturation.

The break separator level began to increase at the same rate as the primary sump at about [ ]^{a,b,c} seconds. This increase occurred when the sump level reached the height of the break separator loop seal. As a result of this increase, the break separator level reached the height of the break in CL-3, causing break flow to reverse and flow from the break separator into the RCS through the break at about [ ]^{a,b,c} seconds. Break flow then remained essentially zero or slightly negative throughout the rest of the test.

5.1.1.5 Sump Injection Phase

Primary sump injection (Figure 5.1.1-2) began through the check valves around the sump injection valves at about [ ]^{a,b,c} seconds, when primary sump and IRWST levels were essentially equal. At [ ]^{a,b,c} seconds, the primary sump injection valves automatically opened when the IRWST reached its low-low level setpoint of [ ]^{a,b,c} in.

In the LTC mode of operation, primary system inventory was lost through the ADS 4-1 and ADS 4-2 valves to the primary sump. System inventory was made up through primary sump and IRWST injection through the DVI lines and some small flow from the primary sump through the break

separator and into the break. The driving force for this flow was the difference between the liquid head in the downcomer and the corresponding head in the simulated core. The two-phase mixture produced in the core flowed out through the hot legs and ADS-4 to the primary sump, and the somewhat cooler fluid in the sump returned from the bottom of the sump to the reactor vessel downcomer via the DVI lines.

When sump injection began, the reactor vessel downcomer fluid temperatures rapidly increased to the sump flow injection temperature. The core steam generation increased (Figure 5.1.1-3) due to injection of hotter sump fluid. When the primary sump injection valves opened, the DVI flow decreased, and the sump and IRWST levels equalized. During the reduced DVI flow period, there was an upward spike in reactor downcomer temperatures. The upper downcomer fluid temperature, indicated by thermocouples located above the DVI nozzle elevation, increased to saturation at this time and remained at saturation for the rest of the test. Figure 5.1.1-3 shows a corresponding increase in steam generation rate.

Overflow from the primary sump to the secondary sump started at about [ ]^{a,b,c} seconds. When primary sump injection started through the check valves, flowing around the sump injection valve lines, IRWST injection from each line was about [ ]^{a,b,c} lbm/sec. and another [ ]^{a,b,c} lbm/sec. from each sump line to each DVI line. With the opening of the primary sump valves [ ]^{a,b,c} seconds, injection flow increased to approximately [ ]^{a,b,c} lbm/sec. through each DVI line. About one-third of the flow from sump-1 was diverted back into the IRWST with the remainder flowing to the DVI nozzle due to the smaller pressure drop in the IRWST to sump line (2.5-in. diameter versus 1.5-in. diameter for sump-2). One-fourth of DVI-2 flow was provided by flow from the IRWST and the remainder from the sump-2 line.

The PRHR HX outlet temperature remained subcooled in the range of [ ]^{a,b,c} °F during most of the test, but after sump injection, it began to rise and was just reaching saturation temperature at the end of the test. The PRHR HX was inactive during this phase, since the IRWST had drained.

TABLE 5.1.1-1
OSU TEST ANALYSIS PLOT PACKAGE FOR SUBSECTION 5.1.1

Plot No.	Component	Variables	Units	Description
1	Pressurizer	CPT-604	psia	System pressure and event history
2	Water injection	WWTDVI1+WWTDVI2, WOUTACC1+WOUTACC2, WWTIRWI1+WWTIRWI2, WWTSMPIT	lbm/sec.	Total of CMT, accumulator, IRWST, and sump injection flows
3	Reactor vessel	RPVASOU2	lbm/sec.	Steam generation in reactor vessel
4	Reactor vessel	T08RPV, HTMXRPV, TSAT	°F	Reactor vessel outlet temperature, maximum clad temperature and fuel exit saturation temperature

THE FIGURES LISTED IN TABLE 5.1.1-1
ARE NOT INCLUDED IN THIS NONPROPRIETARY DOCUMENT

5.1.2 Short-Term Transient

For the 2-in., cold-leg break, Matrix Test SB01, the short-term transient covered the first [ ]^{a,b,c} seconds. As can be seen from Figures 5.1.2-1 and 5.1.2-2, this period included full depressurization of the facility through all four stages of the ADS together with CMT and accumulator injection plus the initial stages of IRWST injection. The mass and energy distribution for this phase of the transient is discussed here based on the plot package detailed in Table 5.1.2-1. These plots concentrate on the primary system including the accumulators, CMTs, IRWST, sumps, and flow from the primary system via the ADS, break, and IRWST overflow.

5.1.2.1 Maintenance of Core Cooling

Reactor Pressure Vessel and Downcomer Mass Distribution

For the short-term transient, the most important criteria was the maintenance of sufficient core inventory to supply adequate cooling of the heater rods. Figure 5.1.2-57 shows that there were no significant excursions in heater rod temperatures and, therefore, sufficient core inventory was maintained through this phase of the transient to remove the decay heat from the rods. However, for significant portions of the transient a two-phase mixture is present in the core and upper plenum regions. The following discussion tracks the variation in water level and mass throughout the reactor vessel and downcomer.

The total fluid mass in the reactor pressure vessel (RPV) is shown in Figure 5.1.2-40. Here, and throughout the report the overall RPV inventory is described in terms of the eight regions shown in Figure 4.11-1 plus a separate downcomer region. The initial RPV inventory is [ ]^{a,b,c} lbm. During the course of the short-term transient, the vessel inventory experiences two mass minimums: [ ]^{a,b,c} lbm before accumulator injection and [ ]^{a,b,c} lbm before IRWST injection. Steam generation was near maximum at these times (Figure 5.1.2-55). By the end of the short-term transient, vessel inventory recovered to a steady [ ]^{a,b,c} lbm. Similar variations were seen in the core fluid mass and water level shown in Figures 5.1.2-44 and 5.1.2-45. The minimum core level occurred before IRWST injection. It can be seen from Figure 5.1.2-45 that during this phase of the transient, the collapsed liquid level dropped to [ ]^{a,b,c} in. below the top of the heated rod length. By the end of the short-term transient, the effect of IRWST injection ended all core boiling (Figure 5.1.2-55), and the core was again water-solid.

It was noticed in the analysis of the SBLOCA simulations on the SPES-2 facility[3] that following the pump trip there were short-period oscillations in primary system flow, temperature, and pressure. A small number of oscillations were also observed in the OSU test response after the end of the initial blowdown (see, for example, the pressure response in Figure 5.1.2-1 and the reactor vessel mass in Figure 5.1.2-40). In the SPES-2 tests, the oscillations were clearly driven by power-to-flow mismatches in the core due to high core power levels, which were needed in SPES-2 to compensate for high ambient losses. The short-term oscillations observed in the OSU results are believed to be a result of pressure oscillations following the initial blowdown.

The fluid mass in the core region is shown in Figure 5.1.2-44. Once again, the two minimums occur prior to accumulator injection and prior to IRWST injection. The minimum core inventory is [ ]^{a,b,c} lbm.

The collapsed liquid level in the upper plenum region spanned by LDP-138 and the associated fluid mass are shown in Figures 5.1.2-49 and 5.1.2-48. It can be seen that, during the period before accumulator injection, the collapsed liquid level in the upper plenum dropped below the hot-leg elevation. During accumulator injection, the steam bubble in the upper plenum partially condensed and the water level briefly rose above the hot legs. Following the end of accumulator injection, flow from the CMTs was not sufficient to maintain the upper plenum level, and the region of LDP-113 completely drained of water. IRWST injection caused the upper plenum to refill, and this region became water-solid again at approximately [ ]^{a,b,c} seconds.

The fluid mass and collapsed liquid level for the head region are given in Figures 5.1.2-50 and 5.1.2-51. During the first [ ]^{a,b,c} seconds, the head inventory reaches a minimum of [ ]^{a,b,c} lbm of water. Accumulator injection was sufficient to maintain a level in the head region. At the end of accumulator injection and before IRWST injection began, the upper head drained. Once IRWST injection began, liquid level in the upper head was reestablished.

The mass of fluid and collapsed liquid level in the reactor vessel downcomer are shown in Figures 5.1.2-41 and 5.1.2-42. During the blowdown phase of the transient, the level dropped to the elevation of the cold legs. This elevation was maintained until the cold legs were fully drained. Following this time, the collapsed level remained between the DVI and hot-leg elevations until IRWST injection once again raised the level above the cold legs and cold leg refill commenced.

Loop Mass Distribution

For this discussion the loop was considered to consist of the hot- and cold-leg pipe work, the SG primary side, and the pressurizer plus surge line.

The total fluid mass and water level for the pressurizer are shown in Figures 5.1.2-34 and 5.1.2-35. During the blowdown phase of the transient ([ ]^{a,b,c} seconds), the pressurizer drained rapidly, becoming completely empty of water at about [ ]^{a,b,c} seconds. The pressurizer remained empty until ADS-1 actuation at [ ]^{a,b,c} seconds. At this time, water was drawn back into the pressurizer as steam and water flowed out of the ADS. A fluid inventory of over [ ]^{a,b,c} lbm was maintained until ADS-4 actuation at [ ]^{a,b,c} seconds. This caused an initial outsurge through the surge line, followed by a more gradual draining of the pressurizer as mass flowed out of the hot legs via the ADS-4 valves. The pressurizer fully drained at [ ]^{a,b,c} seconds and remained empty for the remainder of the transient.

Mass data for the SG U-tubes and their associated inlet and outlet plena are shown in Figures 5.1.2-32 and 5.1.2-31. The SG tubes gradually drained until ADS actuation when all the tubes and plena were empty of water. SG-1 on the broken loop drained before SG-2. Any flow through the SGs ceased

once the tubes drained and steam trapped the U-tubes became superheated. Once the SG tubes drained, natural circulation around the primary loop circuit ceased. The SG U-tubes remained empty for the remainder of the short-term transient.

The mass of water and vapor in the hot legs are shown in Figures 5.1.2-58 and 5.1.2-59. The water mass calculated for HL-1 is not considered valid for this test as it did not indicate the appropriate level of draining. The hot legs maintained their water inventory until [ ]^{a,b,c} seconds into the transient when they started to drain (Figure 5.1.2-58). The hot legs completely drained within [ ]^{a,b,c} seconds. Actuation of ADS-1 caused a rapid increase in void fraction in both hot legs. A larger void fraction was maintained in HL-1 as steam was preferentially removed from HL-2 by PRHR. Figure 5.1.2-59 reveals that, at around [ ]^{a,b,c} seconds, the small amount of steam remaining in HL-2 was removed, and the water level in that hot leg increased as a result of condensation in the PRHR HX drawing a vacuum and raising the level on loop 2.

The liquid and vapor mass for the four cold legs are shown in Figures 5.1.2-60 and 5.1.2-61. Following initial blowdown, all four cold legs became two-phase, although there was a greater void fraction in CL-1 and CL-4 compared with CL-2 and CL-3 (Figure 5.1.2-61). The mass variation in all four cold legs appears very similar. The mass variations were derived from levels in the reactor vessel downcomer because the level instruments on the cold legs are unreliable. All the cold legs were completely drained after ADS actuation and refilled at [ ]^{a,b,c} seconds when flow from the IRWST refilled the reactor vessel downcomer to the level of the cold legs (Figure 5.1.2-42). The cold legs did not drain uniformly, but rather, CL-3 (with the break) drained first, followed by CL-1 with CL-2 and CL-4 delayed. Figure 5.1.2-31 shows that the SG outlet plenum on loop 1 drained at about [ ]^{a,b,c} seconds before that on loop 2, confirming the expected asymmetry in cold-leg behavior.

Mass Injected to the Primary System

The CMTs transitioned from a recirculation to a mass injection mode at approximately [ ]^{a,b,c} seconds when the cold leg started to drain. Draindown of the CMTs continued until the CMT check valves were closed by flow from the accumulators. CMT draindown restarted at the end of accumulator injection, continuing until IRWST injection began (Figures 5.1.2-5 and 5.1.2-6).

The accumulators drained about [ ]^{a,b,c} seconds before activation of the ADS. The accumulators started discharging into the DVI line when the system pressure dropped below the pressure in each accumulator. Accumulator injection began at approximately [ ]^{a,b,c} seconds and continued until the accumulator emptied at approximately [ ]^{a,b,c} seconds (Figure 5.1.2-23). Complete discharge from the accumulators was indicated by a sharp decrease in the temperature of the fluid exiting each accumulator due to the discharge of expansion-cooled nitrogen cover gas, which was released into the primary system (Subsection 6.1.4). Flow from the CMTs was significantly reduced during the discharge of the accumulators and increased again once accumulator discharge was completed.

It should be noted that, for Matrix Test SB01, the indicated flow measurement from ACC-2 was not valid due to an error in the data acquisition for that instrument. The integrated mass flow has, however, been included in the mass balance since the total indicated outflow was only in error by a small amount (Figure 5.1.2-26).

The IRWST injection valves opened when the reactor vessel pressure low-low level setpoint was reached. Injection flow only started when the reactor vessel pressure became less than the static head from the IRWST. Figure 5.1.2-16 shows that the IRWST injection began at approximately [ ]^{a,b,c} seconds after CMT flow ceased. IRWST flow gradually increased to a peak value of [ ]^{a,b,c} lbm/sec. ([ ]^{a,b,c} lbm/sec. per injection line) at [ ]^{a,b,c} seconds before gradually decreasing.

Mass Ejected from the Primary System

At time zero in the transient, a 2-in. break was initiated at the bottom of CL-3. The mass flow rate from the primary system through the break is shown in Figures 5.1.2-67 and 5.1.2-68. For the first [ ]^{a,b,c} seconds following the break, [ ]^{a,b,c} lbm of steam and water left the primary system via the break (Figure 5.1.2-62). During this period, the primary system depressurized to around 300 psi (Figure 5.1.2-1). By the onset of ADS actuation, the cold legs drained, and there was almost no water flow out of the break. Between [ ]^{a,b,c} seconds, ADS 1-3 activated and the system depressurized rapidly. Break flow significantly decreased once the ADS activated, since the ADS valve area was significantly larger than the break. At around [ ]^{a,b,c} seconds, ADS-4 was initiated, and the primary system depressurized until IRWST injection commenced at [ ]^{a,b,c} seconds.

Actuation of ADS 1-3 rapidly terminated the flow of steam from the break, although this was replaced by steam flow through the ADS 1-3 valves for the next [ ]^{a,b,c} seconds (Figure 5.1.2-63). This steam flow was accompanied by an outflow of water from ADS 1-3 at a peak rate of over 4 lbm/sec. (Figure 5.1.2-66). After [ ]^{a,b,c} seconds into the accident simulation, the mass flowing through ADS 1-3 was composed almost entirely of water. The rate of flow through the ADS continued at a gradually reducing rate until [ ]^{a,b,c} seconds when the ADS-4 valves opened, causing flow through ADS 1-3 to terminate and be replaced by flow through the lower resistance ADS-4 paths. For ADS 4-1, there was a near-steady water flow rate of [ ]^{a,b,c} lbm/sec. from the time of initiation. However, for ADS 4-2, there was an initial outsurge at [ ]^{a,b,c} lbm/sec. followed by a drop to near zero and an increase to over [ ]^{a,b,c} lbm/sec. (Figure 5.1.2-66).

The integrated mass flow out of the primary system via the ADS and the break are shown in Figures 5.1.2-62 to 5.1.2-64. During the first [ ]^{a,b,c} seconds of the transient, over [ ]^{a,b,c} lbm of water left the primary system. Of this, the [ ]^{a,b,c} lbm flowing through ADS 1-3 was deposited in the IRWST. The [ ]^{a,b,c} lbm leaving the ADS-4 system and the liquid part of the [ ]^{a,b,c} lbm flowing through the break were added to the liquid overflow from the IRWST and deposited nearly [ ]^{a,b,c} lbm of water into the primary sump (Figure 5.1.2-28). By the end of the short-term transient, the water level in the primary sump reached nearly [ ]^{a,b,c} in. (Figure 5.1.2-29).

At [ ]^{a,b,c} seconds into the transient, the cold legs refilled enough to allow a restart of approximately [ ]^{a,b,c} lbm/sec. of water flow through the break, so that the total rate of water flow from the primary system to the sump was approximately [ ]^{a,b,c} lbm/sec. At this time, the flow rate into the reactor vessel through the DVI lines was approximately [ ]^{a,b,c} lbm/sec.

Mass Balance

Figure 5.1.2-70 presents the variation in the total system inventory during the short-term transient. Following the initiation of the break, there was an increase in system mass of approximately [ ]^{a,b,c} lbm. By the end of the short-term transient, the system inventory decreased by approximately [ ]^{a,b,c} lbm compared with the post-break value. During this period of the transient, about [ ]^{a,b,c} lbm of water was lost from the primary system as steam (Figure 5.1.2-63).

In addition to the overall reduction in system inventory, some reductions and recoveries (dips) were observed. There was a general decrease in system inventory following the initiation of ADS 1-3 until the start of ADS-4 venting (around [ ]^{a,b,c} seconds). Two other marked dips were also observed at around [ ]^{a,b,c} seconds. These two dips resulted from corresponding changes in the primary sump inventory, which have been observed in the level data from which the masses were calculated. The readings on the load cells for the sump did not show corresponding dips, and there were no indications of flow out of the sump at this time. It is, therefore, believed that these resulted from corresponding increases in pressure above the sump water level and lead to an artificially low differential pressure of the sump and a reduced level indication. The necessary pressure increase could have resulted from condensation in the exhaust line causing a build up in steam until the pressure was great enough to drive the venting through the check valve.

A mass balance analysis has been performed on the primary system. Figure 5.1.2-71 plots the measured primary system mass determined by summing the contributions from the reactor vessel, downcomer, hot and cold legs, SG primary side, pressurizer, and surge line plus the PRHR HX. The second curve on Figure 5.1.2-71 provides an alternative primary system mass determined from the mass balance, that is given by:

$$M'_{prim}(t) = M_{prim}(0) + M_{in}(t) - M_{out}(t) \qquad 5.1.2\text{-}1$$

where:

$M'_{prim}(t)$	=	Mass calculated primary system mass
$M_{prim}(0)$	=	Measured primary system mass at the start of transient
$M_{in}(t)$	=	Total integrated mass injected from all sources (i.e., accumulators, CMT, IRWST, and sumps) to time t
$M_{out}(t)$	=	Mass lost from primary system to time t via CMT balance lines, ADS 1-3, ADS-4, and break

The difference in the two primary system mass curves is shown in Figure 5.1.2-72 as the mass balance error.

During the short-term transient, there was, in general, an overestimate of the mass in the primary system from the measured data of up to [ ]^{a,b,c} lbm relative to that calculated from the mass balance, although there was an underestimate following ADS 1-3 initiation. There are two main contributions to this excess mass. First, the measured primary system inventory did not include all of the pipework in the system, and there was approximately [ ]^{a,b,c} lbm of mass missing from the initial inventory. This mass was deposited in and lost from the measured system as pipes drained and refilled. Some of the additional mass was subsequently lost via one of the leakage paths. Second, the instrumentation on the hot legs is believed to have given erroneous level measurements during certain portions of the transient. Figure 5.1.2-58 shows that, for this test, only one hot leg appears to drain, and this contributes an overestimate of [ ]^{a,b,c} lbm. By the end of the short-term transient, the apparent mass-balance error was approximately [ ]^{a,b,c} lbm.

Figure 5.1.2-73 shows the total integrated mass flow from and to the primary system, together with the water inventory remaining in the sources of cooling water. During the short-term transient, there was a net loss of water from the primary system of approximately [ ]^{a,b,c} lbm of which only a small quantity was deposited in the sources. Of the lost primary system inventory, [ ]^{a,b,c} lbm was lost as steam. The rest has been added to the water stored in the ADS and break separators.

Pressure Decay

Figure 5.1.2-1 shows the primary system pressure during the test. Throughout the LOCA portion of this test, the pressure was controlled by the saturation pressure of the hottest fluid in the primary system. At initiation of the break, the controlling fluid volume was the pressurizer and surge line; however, within the first [ ]^{a,b,c} seconds (after the initial blowdown phase), this shifted to the reactor vessel. Figure 5.1.2-3 shows that the temperature of the upper plenum was equal to the saturation temperature corresponding to the primary system pressure measured in the upper head during the natural circulation phase and into the ADS phase. The pressure stabilized at the saturation pressure for the upper plenum and then continued a slow pressure decrease responding to the cooling caused by CMT injection. Figure 5.1.2-1 shows an increase in the pressure decay rate that occurred at approximately [ ]^{a,b,c} seconds when the CMTs transitioned from natural circulation injection to draindown injection, which essentially doubled the injection rate of cold water into the DVI line. The higher injection rate resulted in a more rapid temperature drop in the upper plenum (core outlet in Figure 5.1.2-3), which was reflected in a more rapid pressure decay. With the actuation of ADS-1 at approximately [ ]^{a,b,c} seconds, the pressure dropped rapidly due to the increased rate of mass ejected from the system, and the increased flow of cold water into the downcomer and the core (Figure 5.1.2-63). This continued to reduce the power channel inlet plenum temperature and subcool the heater rods in the core due to the higher flow. Since the reactor vessel outlet plenum became subcooled at about [ ]^{a,b,c} seconds, the hottest fluid in the system was in the pressurizer, the cold legs, and the CMTs, and the pressure was partially supported by the flashing of fluid in one or several of

these locations. When accumulator discharge ended at between [ ]^{a,b,c} seconds, the reactor vessel temperature again increased to the saturation temperature and took control of the system pressure for the remainder of the LOCA phase.

5.1.2.2 Energy Inventory

Heat removal from the reactor core follows a sequence similar to pressure decay for SBLOCA tests. Before the reactor trips, nearly all the energy generated in the core is removed by the SGs and out of the break with a small fraction lost to surrounding heat sinks. When the reactor trips, the primary system pumps trip, and flow through the SG tubes is sharply reduced. Coupled with the isolation of the SG secondary side, the effect is to significantly reduce heat removal by the SGs. At that time, the PRHR HX isolation valves open, and energy is removed to the IRWST as well as out of the break.

As the system drains, primary system pressure is reduced, and the sensible heat of the coolant and metal add to the core heat load. The CMTs start to drain, and the ADS is activated. At that time, heat removal is accomplished through ADS flow, and the PRHR HX becomes less effective. Finally, ADS-4 is actuated, the primary system is completely depressurized, and the IRWST is actuated. The LOCA phase of the test is then completed.

The behavior of the components involved in the energy removal is discussed below.

Core

The power output of the core is shown in Figure 5.1.2-2. After reactor trip, the core power is representative of decay heat levels expected in the AP600 core. Flow through the core is shown in Figure 5.1.2-56 and the steam generation rate is given in Figure 5.1.2-55. As discussed in Section 4.11, the steam production rate has been calculated by two methods, the Tsat method and the DVI line flow method.

Figures 5.1.2-53, 5.1.2-54, and 5.1.2-55 reproduce the saturation line elevation power split above the saturation elevation and steam generation rates from the two methods. Both methods give similar predictions, but neither method gives valid predictions before [ ]^{a,b,c} seconds because of flow oscillations during natural circulation in the primary system.

Both methods for calculating the steam generation predict that the maximum steam generation rate during the LOCA phase will occur at approximately [ ]^{a,b,c} seconds, just prior to IRWST injection. The peak cladding temperature is shown in Figure 5.1.2-57 and indicates that the core is adequately cooled at all times during the test.

Steam Generator Heat Transfer

SGs remove most of the heat from the primary system during normal operation; however, heat transfer from the primary-to-secondary side is significantly reduced after the pumps trip. This is due to reduced flow in the tubes, which causes a sharp reduction in the tube-side heat transfer coefficient. In addition, the secondary side is isolated, which causes the temperature and pressure to remain high as primary-side pressure rapidly decreases.

Passive Residual Heat Removal Heat Transfer

The PRHR is designed to remove heat from the primary system from the time when the SGs become thermally isolated prior to the initiation of the ADS. One measure of the effectiveness of the PRHR is the increase in the fluid internal energy in the IRWST, which serves as the heat sink for the PRHR. Figure 5.1.2-33 shows the SG primary and secondary pressure together with the PRHR integrated heat transfer as represented by the IRWST fluid energy after allowing for the contribution from ADS 1-3 inflow. PRHR flow began at about [ ]^{a,b,c} seconds when the SG heat removal ended. The heat removal rate was approximately [ ]^{a,b,c} Btu/sec. until [ ]^{a,b,c} seconds when ADS-1 activated. At that time, the heating rate in the IRWST increased to [ ]^{a,b,c} Btu/sec. due to condensation of steam vented through ADS 1-3 and heating from the PRHR continues. PRHR heat transfer rate decreased when the accumulators discharged at about [ ]^{a,b,c} seconds as the core became subcooled.

Automatic Depressurization System and Break

Energy removal from the ADS and break are shown in Figure 5.1.2-69. Fluid energy exiting the break increased at a constant rate until ADS-1 actuated. For ADS-1, ADS-2, and ADS-3, compared to the break, the energy removal occurred at a somewhat lower rate due to the reduced system pressure. When ADS-4 actuated, energy removal switched from ADS 1-3 to the larger flow path of ADS-4. The ADS effectively reduced the primary system pressure to allow gravity-injection flow from the IRWST. This flow sufficiently subcooled the primary system, ending core boiling, partially collapsing the steam bubble in the upper plenum and bringing the system to near atmospheric pressure.

Overall Energy Balance

Figure 5.1.2-74 shows all the energy components in the heat balance for the system during the LOCA phase ([ ]^{a,b,c} seconds). Throughout the event, the heater rod bundle power was the dominant heat input to the system, and before the start of the event, the SGs provided the dominant heat removal. At the start of the event, the SG secondary side was isolated, and the RCPs tripped. During this period, heat removal by the SG was reduced as natural circulation flow occurred in the primary system. As the primary system depressurized, the pressure reached the secondary-side pressure, and heat transfer through the SGs effectively ended.

The steam component of the break flow was leaving the control volume at the start of the event until ADS actuation. Heat loss via this path was nearly [ ]^{a,b,c} Btu/sec., which is far greater than the reactor decay power ([ ]^{a,b,c} Btu/sec.). The remaining energy lost through the break exhaust resulted from a decrease in the fluid internal energy as the primary system depressurized.

After ADS 1-3 actuated, the break flow effectively ended, and ADS heat was deposited into the IRWST. Thus, the fluid internal energy in the control volume increased from this time until the end of the SBLOCA phase as the IRWST water temperature increased. Also at that time, the metal masses in the control volume lost energy as primary system temperature decreased. This resulted in energy being lost at a rate of nearly [ ]^{a,b,c} Btu/sec. between [ ]^{a,b,c} seconds. After [ ]^{a,b,c} seconds, the metal masses lost energy at a much lower rate, which is consistent with the primary system fluid temperature decay. Ambient losses were reduced from a maximum of [ ]^{a,b,c} Btu/sec. at full power conditions to [ ]^{a,b,c} Btu/sec. at the end of the LOCA phase.

A large increase was observed in the deficit between the rod bundle power and the various sources of energy dissipation from the control volume after the initiation of ADS 1-3, and again after the initiation of ADS-4 at approximately [ ]^{a,b,c} seconds. Steam exhaust included steam from the IRWST and the steam portion of the flow from ADS-4. However, relatively little steam was measured by the vapor flow meters. Further discussion of this steam flow is provided in the mass and energy balance in Sections 6.2.2 and 6.2.3.

TABLE 5.1.2-1
OSU TEST ANALYSIS STANDARD PLOT PACKAGE FOR SUBSECTION 5.1.2

Plot No.	Component	Variables	Units	Description
1	Pressurizer	CPT-604	psia	System pressure
2	RPV	RPVPWR	kW	Core power
3	RPV	T01RPV, T08RPV, ST08RPV	°F	Core inlet/outlet temperature, saturation temperature
4	SG	CPT-201, CPT-204, CPT-301, CPT-302	psia	Primary and secondary pressures in SG
5	DVI-1	WWTDVIL1, WWTIRWI1, WOUTACC1, WWTIRWI3	lbm/sec.	Individual components and total flow in DVI-1
6	DVI-2	WWTDVIL2, WWTIRWI2, WOUTACC2, WWTIRWI4	lbm/sec.	Individual components and total flow in DVI-2
7	CMT	AMCMT1B, AMCMT2B	lbm	Fluid mass in CMTs (excludes balance lines)
8	CMT	CLDP-502, CLDP-507	in.	Collapsed liquid level in CMTs
9	CMT	MIWDVIL1, MIWDVIL2	lbm	Integrated mass out of CMTs
10	CMT	WWTDVIL1, WWTDVIL2	lbm/sec.	Flow out of CMTs
11	CMT	WWTCLBL1, WWTCLBL2	lbm/sec.	Flow into CMTs
12	CMT	CLDP-509, CLDP510	in.	Level CL-CMT balance lines
13	CMT	UCMT1, UCMT2	Btu	Fluid energy in CMTs
14	IRWST	IRWST	lbm	Mass of fluid in IRWST
15	IRWST	CLDP-701	in.	Collapsed liquid level in IRWST
16	IRWST	WWTIRWI1, WWTIRWI2	lbm/sec.	Flow from IRWST to DVI lines
17	IRWST	IRWSTOR	lbm/sec.	Overflow from IRWST to sump
18	IRWST	ADS13TMR	lbm/sec.	Total ADS flow into IRWST
19	IRWST	ADS13TIR, MIIRWI1, MIIRWI2, MIIRWIO	lbm	Integrated mass out of IRWST
20	IRWST	UIRWST	Btu	Fluid energy in IRWST
21	PRHR	CLDP-802	in.	Collapsed liquid level in PRHR HX

TABLE 5.1.2-1 (Continued)
OSU TEST ANALYSIS STANDARD PLOT PACKAGE FOR SUBSECTION 5.1.2

Plot No.	Component	Variables	Units	Description
22	PRHR	WWOTPRHR	lbm/sec.	Measured outlet flow from PRHR tube
23	Accumulator	AMACC1, AMACC2	lbm	Mass of fluid in accumulators
24	Accumulator	CLDP-401, CLDP-402	in.	Collapsed liquid level in accumulators
25	Accumulator	WOUTACC1, WOUTACC2	lbm/sec.	Flow from accumulators
26	Accumulator	MOUTACC1, MOUTACC2	lbm	Integrated mass out of accumulators
27	Accumulator	UACC1, UACC2	Btu	Fluid energy in accumulators
28	Primary sump	AMPSMP	lbm	Primary sump fluid mass
29	Primary sump	CLDP-901	in.	Primary sump level
30	Primary sump	UPSMP	Btu	Primary sump fluid energy
31	SG	MSSGIP1, MSSGIP2, MSSGOP1, MSSGOP2	lbm	Mass of fluid in SG primary side inlet/outlet plena
32	SG	MSSGHT1, MSSGHT2, MSSGCT1, MSSGCT2	lbm	Mass of fluid in SG primary side hot and cold tubes
33	SG/PRHR	CPT-201, CPT-301, QPRHRI	psia & Btu	SG1 pressure and PRHR integrated heat output
34	Pressurizer	PZM	lbm	Fluid mass in pressurizer
35	Pressurizer	CLDP-601	in.	Collapsed liquid level in pressurizer
36	Pressurizer	UPZ	Btu	Fluid energy in pressurizer
37	Surge line	PLM	lbm	Fluid mass in surge line
38	Surge line	CLDP-602	in.	Collapsed liquid level in surge line
39	Surge line	UPSL	Btu	Fluid energy in surge line
40	RPV	MWRPV	lbm	Total fluid mass in reactor vessel
41	RPV	DCM	lbm	Fluid mass in downcomer
42	RPV	LDP01DC	in.	Collapsed liquid level in downcomer compared to various reference elevations
43	RPV	MW01RPV	lbm	Fluid mass in lower plenum
44	RPV	MW03RPV	lbm	Fluid mass in core region
45	RPV	LDP03RPV	in.	Collapsed liquid level in core
46	RPV	RPVAVDF2		Core exit void fraction
47	RPV	RPVAQOU2		Core exit quality
48	RPV	MW06RPV	lbm	Fluid mass in the upper plenum
49	RPV	LDP06RPV	in.	Collapsed liquid level in the upper plenum
50	RPV	MW08RPV	lbm	Fluid mass in the upper head
51	RPV	LDP08RPV	in.	Collapsed liquid level in the upper head

TABLE 5.1.2-1 (Continued)
OSU TEST ANALYSIS STANDARD PLOT PACKAGE FOR SUBSECTION 5.1.2

Plot No.	Component	Variables	Units	Description
52	RPV	URPV	Btu	Total fluid energy in reactor vessel
53	RPV	RPVXE, RPVASL2	ft	Level of Tsat line
54	RPV	RPVPab, RPVAPab2, RPVPWR	kW	Heated rod power above and below Tsat level and total
55	RPV	RPVRXV, RPVASOU2	lbm/sec.	Core steam generation rate
56	RPV	RPVALIN2	lbm/sec.	Calculated core flow
57	RPV	HTMXRPV, ST08RPV	°F	Maximum clad temperature and saturation temperature
58	Hot leg	MWHL1, MWHL2	lbm	Water mass in hot legs
59	Hot leg	MVHL1, MVHL2	lbm	Vapor mass in hot legs
60	Cold leg	CL1WMS, CL2WMS, CL3WMS, CL4WMS	lbm	Water mass in cold legs
61	Cold leg	CL1VMS, CL2VMS, CL3VMS, CL4VMS	lbm	Vapor mass in cold legs
62	ADS and break	BRKSTIR, ADS13TIR, ADS41TIR, ADS42TIR	lbm	Total discharged mass for ADS 1-3, ADS-4s, and break
63	ADS and break	BRKTIVF, AD13TIVF, AD41TIVF, AD42TIVF	lbm	Total integrated vapor flow for ADS and break
64	ADS and break	BRKTILF, AD13TILF, AD41TILF, AD42TILF	lbm	Total integrated liquid flow for ADS and break
65	ADS and break	ADS13SVR, ADS41SVR, ADS42SVR	lbm/sec.	Vapor flow out ADS 1-3 and ADS-4
66	ADS and break	ADS13SLR, ADS41SLR, ADS42SLR	lbm/sec.	Liquid flow out ADS 1-3 and ADS-4
67	ADS and break	BRKSSVR	lbm/sec.	Vapor flow out of break
68	ADS and break	BRKSSLR	lbm/sec.	Liquid flow out of break
69	ADS and break	BRKSPEI, ADS13EI, ADS41EI, ADS42EI	Btu	Integrated fluid energy for ADS 1-3, ADS-4, and break
70	Mass balance	TOTMASS	lbm	Total system mass inventory
71	Mass balance	PRIMMASS, PRIMASS2	lbm	Measured primary system inventory and value from mass balance
72	Mass balance	MERROR	lbm	Mass balance error
73	Mass balance	MIN, MOUT SRCMASS	lbm	Integrated mass flow in and out of primary system and source mass
74	Energy balance	Various	Btu	Components of energy balance

THE FIGURES LISTED IN TABLE 5.1.2-1
ARE NOT INCLUDED IN THIS NONPROPRIETARY DOCUMENT

5.1.3 Long-Term Transient

The long-term transient covers the transition from IRWST to sump injection and provides information on the LTC response of the AP600. For the 2-in. cold-leg break, Matrix Test SB01, the long-term transient encompasses the time frame of [ ]^{a,b,c} seconds to the end of the test near [ ]^{a,b,c} seconds. The behavior of the test facility during this period of the transient is discussed in this subsection using the plot package detailed in Table 5.1.3-1. These results concentrate on the components of the primary system that remain active during the LTC phase, that is, the RPV, the hot legs, ADS-4, the sumps, and the IRWST.

5.1.3.1 Maintenance of Core Cooling

Reactor Pressure Vessel and Downcomer Mass Distribution

For the long-term transient, the passive core cooling systems must supply sufficient flow to prevent any overheating of the heater rods. During the time frame of [ ]^{a,b,c} seconds, the decay heat simulation of the heated rods reduced power from 175 to 120 kW (Figure 5.1.3-1). As seen in Figure 5.1.3-38, there were no significant excursions in heater rod temperatures and, therefore, sufficient core flow was maintained throughout the long-term transient.

The mass of water in the reactor pressure vessel is shown in Figure 5.1.3-25. After an initial decline, the reactor vessel water mass settled at an average value of [ ]^{a,b,c} lbm until the sump injection valves opened at around [ ]^{a,b,c} seconds. From [ ]^{a,b,c} seconds, oscillations in vessel inventory were observed. These oscillations can be seen in measurements throughout the primary system, and they are discussed further in Subsection 6.1.3. The onset of sump injection caused a drop in vessel inventory to a constant value of [ ]^{a,b,c} lbm, which is 67 percent of the initial vessel water inventory. At approximately [ ]^{a,b,c} seconds, the water mass increased to [ ]^{a,b,c} lbm in response to a partial collapse of the steam bubble in the head region (Figure 5.1.3-33) and remained at this level during the last [ ]^{a,b,c} seconds of the transient.

Core water mass and the collapsed liquid level are shown in Figures 5.1.3-28 and 5.1.3-29. From [ ]^{a,b,c} seconds, the core remained near water-solid with only a very low level of boiling (Figure 5.1.3-36); however, after the sump injection valves opened, the increase in core temperature resulting from the influx of hot sump water (Figures 5.1.3-2 to 5.1.3-5) reduced the core collapsed liquid level to just below the top of the heater rods. At this time, the level at which the core fluid temperatures reached saturation dropped (Figure 5.1.3-34), and the amount of boiling increased along the upper regions of the heater rods. The level of boiling continued at a constant rate until the end of the accident simulation (Figure 5.1.3-36). Note that the long-term transient core steam generation calculation is based only on the DVI line flow method, since the Tsat method is very sensitive to small changes in local pressure.

The collapsed liquid level in the upper plenum region is shown in Figure 5.1.3-32. Right before sump injection began, the collapsed liquid level in the upper plenum remained at the top of the hot legs. Following the influx of hot water from the sumps, the level dropped to the top of the DVI lines and remained there for the remainder of the transient.

The mass of fluid and collapsed liquid level in the reactor vessel downcomer are shown in Figures 5.1.3-26 and 5.1.3-27. Before the start of sump injection, the collapsed liquid level in the downcomer was at the level of the center of the cold legs. The start of sump injection through the injection valves at [ ]^{a,b,c} seconds caused a readjustment of the levels around the primary system, and, subsequently, the downcomer level remained at the bottom of the hot legs for the remainder of the transient.

Figure 5.1.3-4 shows the response of the downcomer water temperatures during the LTC phase of the transient. Initial sump injection via the check valves caused a sudden rise in downcomer water temperature as the hotter sump water entered the downcomer. The opening of the main sump injection valve momentarily increased downcomer temperature as DVI flow temporarily decreased (Figures 5.1.3-6 and 5.1.3-7). During the long-term phase of the transient, the downcomer water temperatures increased gradually, but it can be seen that the temperature remained well subcooled. The downcomer, therefore, provides a potential site for steam condensation. Such a process is believed to be involved in driving the oscillations observed between [ ]^{a,b,c} seconds into the transient (Subsection 6.1.3).

Loop Mass Distribution

During the LTC phase of the transient, there was a low level of boiling in the upper regions of the core. The following are five potential paths for the steam:

- To the hot legs and out of the ADS-4 valves
- To HL-2, through the pressurizer and ADS 1-3 valves to be deposited in the IRWST
- To HL-2, through the PRHR HX to the SG outlet
- To the hot legs, through the SGs to the cold legs to return to the reactor vessel or flow out of the break
- To the head region and into the downcomer, potentially condensing in the downcomer, or, if the downcomer water level is below the cold legs, venting through the cold legs to the CMTs and break

Figures 5.1.3-39 and 5.1.3-40 show that during sump injection, two-phase flow occurred in the hot legs. Figure 5.1.3-23 shows that throughout this phase of the transient, the pressurizer surge line

remained filled with water. Figure 5.1.3-21 shows that the inlet plenum on SG-2 also remained plugged with water. It was expected that the inlet plenum on SG-1 also contained a small amount of water, although for this test, the level measurement was over-ranged and SG-2 results have been used for SG-1. There is no evidence of flow through the PRHR HX during the long term-transient. Therefore, for steam entering the hot legs, the only available flow path was out of the primary loop to the sumps via the ADS-4 valves. However, there was no evidence on the steam vortex meters for vapor flow out of the ADS. Note that the vortex meters have a deadband, and low flow was not detected. The expected rate of loss of steam through each ADS-4 valve during the long-term transient is of that order. As discussed in Subsection 6.2.2, examination of the fluid thermocouples in the steam lines from the ADS-4 separator shows the temperature at or above saturation for all of the transient beyond 15,000 seconds, which indicates that steam was leaving the system by this path at a low flow rate.

Mass Ejected from the Primary System

Integrated mass flow out of the primary system via the ADS and the break is shown in Figure 5.1.3-43. By the end of the accident simulation, approximately [ ]^{a,b,c} lbm of water had flowed out of the primary system. During the LTC phase of the transient, the only significant outflow was through the ADS-4 valves, with a small apparent flow through the break. The apparent break flow does not represent flow out of the primary system, but indicates continued interaction between the break separator and the sump. The most marked manifestation of this interaction is at [ ]^{a,b,c} seconds when the primary sump began to flow into the secondary sump causing oscillating flow indications in the liquid flow out of the break separator. This is confirmed by Figures 5.1.3-44 and 5.1.3-45, which show flow through the ADS and the break. During the sump injection phase of the transient, outflow in the form of liquid exited out of the ADS-4 valves. Water flowed through each of these at an average rate of [ ]^{a,b,c} lbm/sec.

During the long-term transient, there was no evidence from the vortex meters for steam flowing out of the primary system via the ADS-4 valves. It is, therefore, not obvious where the steam generated in the core was ducted. As discussed in Subsection 6.1.3, there is evidence for steam flowing from the upper head to the downcomer via the bypass holes, but this estimated flow is not enough to account for all the steam generated in the core. The system mass inventory (Subsection 5.1.3.5) indicates a flow of [ ]^{a,b,c} lbm/sec. and is required to explain the fall in measured system mass inventory. As noted above and in Subsection 6.2.2, fluid temperatures in the vapor lines out of the ADS-4 stage separators indicate that steam left the primary system via the ADS.

At approximately [ ]^{a,b,c} seconds into the transient, the level in the primary sump (Figure 5.1.3-14) reached the point at which overflow to the secondary sump occurred. At this time, there was approximately [ ]^{a,b,c} lbm of water collected in the primary sump. From the start of primary sump overflow to the end of the transient, [ ]^{a,b,c} lbm of water was transferred to the secondary sump (Figure 5.1.3-16).

Mass Injected to the Primary System

The total DVI line flow, CMT flow, and IRWST flow are shown in Figures 5.1.3-6 and 5.1.3-7; flow from the primary sump is shown in Figure 5.1.3-19. From around [ ]^{a,b,c} seconds, there was a contribution to the DVI flow from the CMTs as they finished post-refill draindown.

During the presump injection phase of the transient, IRWST flow proceeded at a gradually reducing rate with the effect of the primary system oscillations superimposed. At [ ]^{a,b,c} seconds, flow from the primary sump began through the check valves around the main injection valves. After the initial outsurge, a flow rate of [ ]^{a,b,c} lbm/sec. was achieved. At around [ ]^{a,b,c} seconds, the level in the IRWST fell to [ ]^{a,b,c} in. and the primary sump injection valves opened, allowing additional flow to the primary system from the sump with an initial surge of water at a peak rate of [ ]^{a,b,c} lbm/sec. (Figure 5.1.3-19). As the levels in the primary system adjusted, flow through the DVI lines ceased temporarily before restarting again. Following the start of sump injection through the main valve, flow through DVI-1 resulted entirely from sump injection (Figure 5.1.3-6) while for DVI-2, flow was mainly from the IRWST (around [ ]^{a,b,c} lbm/sec.) with a small contribution from the primary sump flow (Figure 5.1.3-7). Both DVI lines delivered water to the reactor vessel at a near-constant rate of just under [ ]^{a,b,c} lbm/sec. for the entire period of the transient following the opening of the sump injection valves. Note that IRWST flow rates were based on measured positive flows. During sump injection, there was reverse flow from the primary sump to the IRWST via the DVI-1 line.

During sump injection, [ ]^{a,b,c} lbm of water was delivered from the primary sump to the primary system in addition to [ ]^{a,b,c} lbm from the IRWST (Figure 5.1.3-20). During this time, a total of around [ ]^{a,b,c} lbm of water left the primary system via the ADS-4 valves. The inventory of water available for injection to the primary system was not reduced significantly by the end of the transient (Figure 5.1.3-13).

During the long-term transient, the water level in the break separator was sufficient to allow flow back into the primary system through the break. This is representative of the behavior expected in the AP600 where the level of water in the sump would reach the break elevation.

Mass Balance

Figure 5.1.3-46 shows the variation in the total system mass inventory during the entirety of Matrix Test SB01. Following the short-term transient, the total inventory remained between [ ]^{a,b,c} lbm below the initial value. Initially, there was an increase in inventory until [ ]^{a,b,c} seconds when the inventory fell. From [ ]^{a,b,c} seconds to the start of sump injection, the inventory remained essentially constant. After sump injection began, there was an increase in inventory followed by a gradual reduction, so that by the end of the LTC phase of the transient, [ ]^{a,b,c} lbm of water was also lost. This reduction was consistent with a flow rate of steam out of the system of [ ]^{a,b,c} lbm/sec. Note that the vortex flow meters have a deadband, and thus,

the vortex meters would not register the low flow of steam passing through each ADS-4 valve; therefore, this inventory loss was not measured directly.

Figure 5.1.3-46 shows dips of about [200] lbm superimposed on the general trends in mass inventory. As in the short-term transient, these dips resulted from corresponding changes in the sump inventory, observed in the level data from which the masses were calculated (Figures 5.1.3-13, 5.1.3-14, 5.1.3-16, and 5.1.3-17). The readings on the load cells for the two sumps did not show corresponding dips, and there were no indications of increased flow at this time; thus, the dips are believed to be the result of corresponding pressure variations in the differential pressure taps and not mass changes.

The mass balance calculation has been performed for the entire transient, and the results are presented in Figures 5.1.3-47 to 5.1.3-49. During the long-term phase of the transient, the measured water inventory in the primary system remained approximately constant at [950] lbm. The mass balance calculations do not fully allow for reverse flow from the break separator to the primary circuit.

5.1.3.2 Energy Balance

Figure 5.1.3-50 shows all the energy components in the heat balance for the system during the LTC phase. During this phase, the heater rod bundle power was the dominant heat input to the system. The SG heat transfer ended during the LOCA phase and did not contribute to the overall energy balance during the LTC phase. Thus, for the LTC phase, the active components in the overall energy balance were rod bundle power, change in the fluid internal energy, change in the metal internal energy, ambient losses, and steam exhaust from the control volume.

The fluid energy in the control volume increased steadily until sump injection began at (approximately [ ]^{a,b,c} seconds). At that time, fluid throughout the system approached saturated conditions, and the rate of increase was reduced. At the same time, metal mass temperatures increased and the primary system temperature increased in response to the hotter water from the sump. Also, ambient losses increased slightly as the control volume temperatures increased. The sum of these increases is much less than the rod bundle power and must be a result of steam exhausting from the control volume. This assumption is consistent with the mass balance deficit discussed previously.

The steam component of the ADS-4 flow left the control volume from actuation of ADS-4. For the LTC phase, this quantity is essentially zero, as measured by the vapor flow meters. It is concluded that the vapor flow meters in the ADS-4 separators did not measure the relatively small steam flow rates accurately. Further discussion of this steam flow is provided in the mass and energy balance in Sections 6.2.2 and 6.2.3.

TABLE 5.1.3-1
OSU TEST ANALYSIS STANDARD PLOT PACKAGE FOR SUBSECTION 5.1.3
LONG-TERM TRANSIENT

Plot No.	Component	Variables	Units	Description
1	RPV	RPVPWR	kW	Core power
2	Primary sump	TSMPI1, TSMPI2	°F	Sump injection line temperatures
3	DVI	TDVIL1, TDVIL2	°F	DVI line temperatures
4	RPV	T01DC, T02DC, T03DC, ST01DC	°F	Water and saturation temperatures in downcomer
5	RPV	T01RPV, T08RPV, ST08RPV	°F	Core inlet/outlet temperature, saturation temperature
6	DVI-1	WWTDVIL1, WWTIRWI1, WWTIRWI3	lbm/sec.	Individual components and total flow in DVI-1
7	DVI-2	WWTDVIL2, WWTIRWI2, WWTIRWI4	lbm/sec.	Individual components and total flow in DVI-2
8	CMT	CLDP-502, CLDP-507	in.	Collapsed liquid level in CMTs
9	CMT	CLDP-509, CLDP510	in.	Level CL-CMT balance lines
10	IRWST	IRWST	lbm	Mass of fluid in IRWST
11	IRWST	CLDP-701	in.	Collapsed liquid level in IRWST
12	IRWST	UIRWST	Btu	Fluid energy in IRWST
13	Primary sump	AMPSMP	lbm	Primary sump fluid mass
14	Primary sump	CLDP-901	in.	Primary sump level
15	Primary sump	UPSMP	Btu	Primary sump fluid energy
16	Secondary sump	AMSSMP	lbm	Secondary sump fluid mass
17	Secondary sump	CLDP-902	in.	Secondary sump level
18	Secondary sump	USSMP	Btu	Secondary sump fluid energy
19	Primary sump	WSTSMPET, WWTSMPIT	lbm/sec.	Primary sump steam and liquid injection rate
20	Primary sump	MISMPI1, MISMPI2, MISMPIT, MIIRWT	lbm	Integrated primary sump and IRWST flows
21	SG	MSSGIP1, MSSGIP2, MSSGOP1, MSSGOP2	lbm	Mass of fluid in SG side inlet/outlet plena
22	Surge line	PLM	lbm	Fluid mass in surge line
23	Surge line	CLDP-602	in.	Collapsed liquid level in surge line
24	Surge line	UPSL	Btu	Fluid energy in surge line
25	RPV	MWRPV	lbm	Total fluid mass in reactor vessel

TABLE 5.1.3-1 (Continued)
OSU TEST ANALYSIS STANDARD PLOT PACKAGE FOR SUBSECTION 5.1.3
LONG-TERM TRANSIENT

Plot No.	Component	Variables	Units	Description
26	RPV	DCM	lbm	Fluid mass in downcomer
27	RPV	LDP01DC	in.	Collapsed liquid level in downcomer compared to various reference elevations
28	RPV	MW03RPV	lbm	Fluid mass in core region
29	RPV	LDP03RPV	in.	Collapsed liquid level in core
30	RPV	RPVAVDF2		Core exit void fraction
31	RPV	RPVAQOU2		Core exit quality
32	RPV	LDP06RPV	in.	Collapsed liquid level in the upper plenum
33	RPV	MW08RPV	lbm	Fluid mass in the upper head
34	RPV	RPVASL2	ft.	Level of Tsat line
35	RPV	RPVAPab2, RPVPWR	kW	Heated rod power above and below Tsat level and total
36	RPV	RPVASOU2	lbm/sec.	Core steam generation rate
37	RPV	RPVALIN2	lbm/sec.	Calculated core flow
38	RPV	HTMXRPV, ST08RPV	°F	Maximum clad temperature, saturation temperature and delta
39	Hot leg	MWHL1, MWHL2	lbm	Water mass in hot legs
40	Hot leg	MVHL1, MVHL2	lbm	Vapor mass in hot legs
41	Cold leg	CL1WMS, CL2WMS, CL3WMS, CL4WMS	lbm	Water mass in cold legs
42	Cold leg	CL1VMS, CL2VMS, CL3VMS, CL4VMS	lbm	Vapor mass in cold legs
43	ADS and break	BRKSTIR, ADS13TIR, ADS41TIR, ADS42TIR	lbm	Total discharged mass for ADS 1-3, ADS-4, and break
44	ADS and break	ADS13TLR, ADS41TLR, ADS42TLR	lbm/sec.	Liquid flow out ADS 1-3 and ADS-4
45	ADS and break	BRKSTLR	lbm/sec.	Liquid flow and total flow out of break
46	Mass balance	TOTMASS	lbm	Total system mass inventory
47	Mass balance	PRIMMASS, PRIMASS2	lbm	Measured primary system inventory and valve from mass balances
48	Mass balance	MERROR	lbm	Mass balance error
49	Mass balance	MIN, MOUT SRCMASS	lbm	Integrated mass flow in and out of primary system and source mass
50	Energy balance	Various	Btu	Component of energy balance
51	ADS-4	ADS41TLR, ADS42TLR	lbm/sec.	Oscillations in ADS-4 liquid flow
52	Surge line	CLDP-602	in.	Oscillations in surgeline level

TABLE 5.1.3-1 (Continued)
OSU TEST ANALYSIS STANDARD PLOT PACKAGE FOR SUBSECTION 5.1.3
LONG-TERM TRANSIENT

Plot No.	Component	Variables	Units	Description
53	RPV	CPT-107	psia	Oscillations in upper head pressure
54	RPV	CLDP-113	in.	Oscillations in upper plenum level
55	RPV	LDP03RPV	in.	Oscillations in core level
56	RPV	LDP01DC	in.	Oscillations in downcomer level

THE FIGURES LISTED IN TABLE 5.1.3-1
ARE NOT INCLUDED IN THIS NONPROPRIETARY DOCUMENT

5.2 Analysis of Matrix Test SB18

Matrix Test SB18 (OSU Test U0018) simulated a 2-in. cold-leg (CL) break SBLOCA with LTC and without operation of nonsafety-related systems. The break was located at the bottom of CL-3 with a simulated failure of one of the ADS-4 lines. CL-3 is on the CMT side of the facility.

The analysis of Matrix Test SB18 is divided into three sections:

- General facility performance (Subsection 5.2.1) describes the overall response of the system throughout the test. The performance of the facility is characterized by the figures listed in Table 5.1.1-1.

- SBLOCA (Subsection 5.2.2) provides a discussion of the system behavior from the start of the test, through system depressurization, to approximately [ ]^{a,b,c} seconds into the transient, and includes the initial system blowdown, the establishment of natural circulation, and the initial portion of the IRWST injection cooling (Figure 5.2-2).

- LTC (Subsection 5.2.3) discusses the behavior of the remainder of the test and includes the completion of IRWST injection and the establishment of sump injection.

The refill and subsequent recirculation of the CMT is considered as a separate discussion within Subsection 6.1.1. The period between SBLOCA and LTC is not discussed specifically since the system was behaving in a stable manner.

Matrix Test SB18 was a duplication of Matrix Test SB01. The purpose of performing Matrix Test SB18 was to confirm the ability of the facility to replicate its response to a SBLOCA, with the same configuration from the beginning to the end of the test program.

The differences between SB01 and SB18 are as follows:

- In SB18, a vacuum breaker was installed on the ADS 1-3 sparger line inside the IRWST to eliminate negative pressures in the pressurizer and ADS 1-3 separator.

- In SB18, pressurizer heater logic was changed so that the PLC initiated a signal to open the pressurizer heater SCR contactor at [ ]^{a,b,c} seconds after S signal actuation, thereby ensuring de-energization of the heaters.

- In SB18, to prevent heating at the top of the CMTs prior to break valve opening, CMT balance line isolation valves were closed and opened by the operator 1 minute after the TEST pushbutton was pressed.

5.2.1 Facility Performance

A flow nozzle simulating one ADS-4 valve was installed in the ADS 4-1 line, hot leg-1 (HL-1) to the ADS 4-1 separator, to provide the single failure simulation. A flow nozzle simulating two valves was installed in the ADS 4-2 line (HL-2 to the ADS 4-2 separator). Additionally, flow nozzles simulating two lines of flow each were installed in the ADS 1-3 inlet lines.

The reactor heater control decay algorithm maintained the maximum reactor heater power output for [ ]^{a,b,c} seconds, and then the power was programmed to begin to decay, simulating the total decay energy input of the AP600 nuclear fuel. This test was performed with reactor heater rod HTR-C2-317 electrically disconnected to simulate the heater conditions during the performance of Matrix Test SB01.

The facility performance is divided into separate discussions of the five phases of the test:

- Blowdown
- Natural circulation
- ADS
- IRWST injection
- Sump injection

The overall performance over the [ ]^{a,b,c} second test is shown in Figures 5.2.1-1 to 5.2.1-4. Figure 5.2.1-1 shows the pressurizer pressure throughout the test, indicating the various phases and operating components. For clarity, the time scale is split out between 1600 and 13,000 seconds since there was no change in the operating mode during this period. Figure 5.2.1-2 shows the total injection flow rates into the DVI line from the various systems as a function of time. Figure 5.2.1-3 shows the quantity of steam generated in the core throughout the test. Figure 5.2.1-4 shows the variation in average measured core outlet temperature and peak clad temperature relative to the core outlet saturation temperature.

Figures 5.2.1-1 and 5.2.1-2 show that a continuous flow of water into the reactor vessel is provided by passive safety-related systems as the primary system was depressurizing. The operation passive safety-related systems overlapped so that as one system drained or emptied, another provided flow into the simulated reactor vessel for continuous core cooling.

Sufficient flow to the core was maintained so that the average measured core outlet temperature is just saturated or subcooled for significant portions of the transient, and the core steam flow is less than the passive safety-related system injection flow, as seen by comparing Figures 5.2.1-2, 5.2.1-3, and 5.2.1-4. As the system transitions into LTC, the water injected from the sump was hot since it originated in the primary system. The hot injection water temperature after [ ]^{a,b,c} seconds resulted in continuous steam generation in the heater rod bundle as seen in Figure 5.2.1-3. The resulting steam generation is vented primarily through the ADS-4 valves.

5.2.1.1 Blowdown Phase

The blowdown phase corresponds to the first [ ]^{a,b,c} seconds of Test SB18, as shown in Figure 5.2.1-1, and is completed when the steam pressure reaches the SG safety valve setpoint. As with Matrix Test SB01, the test was initiated at time zero by opening the break valve. The hot leg of the RCS was at the same temperature and pressure (420°F at 372 psig) prior to the initiation of the test as for Test SB01. The simulated S signal was generated 0.5 seconds after the break signal and initiated the following actions.

In the first [ ]^{a,b,c} seconds, the SG pressure setpoint was raised to 335 psig, the reactor shifted to power (kW) control mode with a programmed power demand for 600 kW total power, the main feedwater pump tripped and feedwater was isolated (at [ ]^{a,b,c} seconds), the PRHR HX outlet valve and CMT discharge valves opened (at [ ]^{a,b,c} seconds), and the RCPs tripped [ ]^{a,b,c} seconds into the event.

Forced flow was continued through the PRHR HX and the CMTs until the RCPs stopped at approximately [ ]^{a,b,c} seconds, at which time the PRHR HX flow changed to natural circulation. As the RCS depressurized and coolant escaped through the break, pressurizer level decreased rapidly and steam formation began in the reactor vessel upper head. At about [ ]^{a,b,c} seconds, the level in the upper head of the reactor vessel indicated the vessel was beginning to lose inventory as the vessel drained and some liquid flashed to steam.

As the primary system pressure fell to near a steady-state condition, the system transitioned into the natural circulation phase once the pumps coasted down; the system reached the SG pressure setpoint at 335 psig at approximately [ ]^{a,b,c} seconds. During this time period, there was initially forced flow and then liquid single-phase natural circulation in the PRHR and CMT. The CMTs provided recirculating flow to the reactor vessel, while the PRHR removed energy from the primary system.

5.2.1.2 Natural Circulation Phase

The cold legs developed a void fraction at approximately [ ]^{a,b,c} seconds at which time the CMT balance lines began to drain. CMT-1 and CMT-2 levels began to decrease, making the transition from recirculation to draindown at about [ ]^{a,b,c} seconds, respectively, and the injection flow from the CMTs increased (Figure 5.2.1-2). As the system continued to drain, the SG tubes started to drain at [ ]^{a,b,c} seconds, and the SGs transitioned into a two-phase recirculation behavior. The mass loss through the break decreased the pressurizer level and emptied the pressurizer at approximately [ ]^{a,b,c} seconds. At both [ ]^{a,b,c} seconds, a condensation/depressurization event took place in CMT-1, as indicated by a rapid refill of the CMT-1 balance line as steam from the balance line was condensed in the CMT. Water from the cold leg was drawn up the balance line into the CMT as the balance line filled.

The upper head continued to drain and was empty at [ ]^{a,b,c} seconds. Steam generation in the reactor vessel reached its maximum ([ ]^{a,b,c} lbm/sec., Figure 5.2.1-3) at [ ]^{a,b,c} seconds. The

pressurizer surge line was completely emptied at approximately [ ]^{a,b,c} seconds. The primary system was at a pressure above the SG secondary side pressure, which continued to remove energy until approximately [ ]^{a,b,c} seconds when the tubes become superheated.

As the system continued to drain, the U-tubes of both SGs were completely empty by approximately [ ]^{a,b,c} seconds, and the HL-1 and HL-2 levels began to decrease at about [ ]^{a,b,c} seconds. The horizontal sections of the hot legs started to drain at about [ ]^{a,b,c} seconds. The hot legs remained at saturation temperature and never superheated, even though they were partially or completely empty due to a small flow of saturated steam from the reactor heater bundle to the SGs.

At [ ]^{a,b,c} seconds, CMT-1 reached the ADS-1 setpoint, and the ADS-1 valve opened to initiate ADS blowdown.

5.2.1.3 Automatic Depressurization System Phase

The ADS flow path, in conjunction with the break, decreased RCS pressure at a rapid rate, redistributing the mass inventory of the system. The opening of the ADS-1 valve released two-phase flow through the pressurizer to the ADS 1-3 separator and into the IRWST through the sparger. The opening of the ADS-1 valve, followed by the ADS-2 valve approximately 1 minute later, increased the rate of RCS depressurization. As the different ADS stages opened, the primary vent path shifted from the cold leg break to the ADS valves through the pressurizer.

The collapsed liquid level inside the reactor core barrel reached a near-term minimum value at [ ]^{a,b,c} seconds, but the core remained covered during this time period with a two-phase mixture. When the RCS depressurized to approximately [ ]^{a,b,c} psia at about [ ]^{a,b,c} seconds, accumulator injection into the DVI line began (Figures 5.2.1-1 and 5.2.1-2).

The accumulators discharged into the DVI line, which reduced CMT-1 injection flow during accumulator injection by closing off the CMT discharge line check valves until the accumulators were almost empty and depressurized. With the accumulators at their maximum injection rate, the RCS refilled and the surge line and pressurizer began to reflood at about [ ]^{a,b,c} seconds; the pressurizer attained its maximum level at [ ]^{a,b,c} seconds. Once the accumulators were empty, the pressurizer and surge line then drained down and were completely empty at [ ]^{a,b,c} seconds.

When RCS pressure decreased to [ ]^{a,b,c} psig at approximately [ ]^{a,b,c} seconds, the two IRWST injection valves automatically opened, but IRWST injection could not occur until the RCS pressure decreased to near atmospheric pressure. As the accumulators completed injection at [ ]^{a,b,c} seconds for ACC-1 and [ ]^{a,b,c} seconds for ACC-2, CMT-1 and CMT-2 injection flow started to increase at [ ]^{a,b,c} seconds. Approximately 50 percent of the nitrogen gas in the accumulator was injected into the DVI lines (see Subsection 6.1.4), momentarily cooling the injection lines at the end of accumulator injection. The nitrogen caused a decrease in ACC-1 and ACC-2 outlet temperature of about [ ]^{a,b,c} °F at approximately [ ]^{a,b,c} seconds. There was no indicated change in total DVI flow in either DVI line.

During the accumulator injection period, there was sufficient injection of subcooled liquid to suppress boiling in the core region. The downcomer was filled with subcooled liquid, which resulted in the collapse of the superheated steam bubble in the upper portion of the reactor vessel downcomer annulus. As the pressure decreased in this region, the downcomer fluid accelerated upward and impacted on the bottom of the core barrel flange where the core bypass holes are located. The impact of the downcomer liquid on the solid surface of the core barrel flange was heard during the test.

During accumulator injection, the PRHR level decreased. The PRHR HX inlet temperature became subcooled coincident with the ADS-4 valves opening at [ ]^{a,b,c} seconds, and over the next [ ]^{a,b,c} seconds, dropped to and paralleled the outlet temperature.

From [ ]^{a,b,c} seconds, both DVI nozzle fluid temperatures increased from essentially ambient conditions to as high as [ ]^{a,b,c}°F as the CMT fluid heated The DVI fluid temperature transient was terminated when the CMT inventory was exhausted, and the IRWST injection began refilling the reactor vessel at about [ ]^{a,b,c} seconds; temperatures returned to ambient when the CMTs were empty, terminating the hot liquid injection. This temperature transient does not appear to have affected any other facility parameters.

Steam generation in the reactor vessel (RPV) was re-established in the period between about [ ]^{a,b,c} seconds after accumulator injection ended and the system began to drain again. At [ ]^{a,b,c} seconds, the ADS 4-1 and ADS 4-2 valves opened automatically when CMT-1 level reached its low-low level setpoint. ADS-4 actuation started a decline in RCS inventory up until IRWST injection began. There was initially too much mass in the system to be vented through ADS-4 before IRWST injection could occur. CMT-1 and CMT-2 were completely empty at [ ]^{a,b,c} seconds, respectively.

The pressurizer was slightly subcooled at about [ ]^{a,b,c} seconds and remained subcooled until the data acquisition ceased at approximately [ ]^{a,b,c} seconds.

At about [ ]^{a,b,c} seconds, the RCS drained sufficiently to decrease system pressure to about [ ]^{a,b,c} psig, which was sufficiently low that the IRWST static head was greater than RCS pressure, and IRWST injection began.

5.2.1.4 In-Containment Refueling Water Storage Tank Injection Phase

IRWST injection started at about [ ]^{a,b,c} seconds and proceeded at a continually diminishing rate (Figure 5.2.1-2) as the differential head between the IRWST and the RCS decreased with the drainage of the IRWST. The IRWST injection was sufficient to begin refilling the primary system. The pressurizer and pressurizer surge line emptied for the second time at approximately [ ]^{a,b,c} seconds, respectively. No reflood of the pressurizer occurred because of the vacuum breaker installed on the ADS 1-3 sparger line inside the IRWST.

Both CMT balance lines began to refill about [ ]^{a,b,c} seconds when the IRWST injection increased the reactor vessel level, sufficiently covering and refilling the cold legs. At about [ ]^{a,b,c} seconds, when the CMT-2 balance line had completely refilled, CMT-2 began to rapidly refill and reached the [ ]^{a,b,c} in. level (about [ ]^{a,b,c} percent full) at about [ ]^{a,b,c} seconds. The CMT refill will be discussed in more detail in Subsection 6.1.1. After the CMTs were partially refilled, there was no injection flow from the CMTs because the higher static head of the IRWST held the CMT discharge line check valves closed.

Steam generation started again at about [ ]^{a,b,c} seconds and continued for the remainder of the test (Figure 5.2.1-3). CMT-1 and CMT-2 remained at essentially constant levels for several thousand seconds and then began slow draindowns at about [ ]^{a,b,c} seconds, respectively. The draindown for both CMTs was slow and did not occur until IRWST relative level was [ ]^{a,b,c} in. below that of the CMTs. Data indicate that the CMTs drained for a while, and then the differential head between the IRWST and the CMTs again closed the CMT discharge check valves, terminating draining until the differential shifted the other way and draining recommenced. Both CMTs were completely empty at about [ ]^{a,b,c} seconds, which coincides closely with the primary sump injection valve opening at [ ]^{a,b,c} seconds. Failure of the DAS from [ ]^{a,b,c} seconds until the completion of the test stopped any further description of the test events.

The break separator level began to increase at the same rate as the primary sump at about [ ]^{a,b,c} seconds. This occurred when sump level reached the height of the break separator loop seal. As a result of this level increase, break separator level reached the height of the break in CL-3, causing break flow to reverse and flow from the break separator into the RCS through the break at about [ ]^{a,b,c} seconds. The break flow then remained essentially zero or slightly negative throughout the rest of the test.

At approximately [ ]^{a,b,c} seconds, the PRHR inlet temperature started rising to the saturation temperature while the discharge temperature remained steady at approximately [ ]^{a,b,c}°F for the remainder of the data collection period.

5.2.1.5 Sump Injection Phase

Primary sump injection (Figure 5.2.1-2) began through the check valves around the sump injection valves at about [ ]^{a,b,c} seconds, or some [ ]^{a,b,c} seconds earlier in Matrix Test SB18 than in Matrix Test SB01. When sump injection began, the reactor vessel downcomer fluid temperatures rapidly increased to the sump flow injection temperature. Primary sump injection valves opened at [ ]^{a,b,c} seconds when the IRWST reached its low-low level setpoint of [ ]^{a,b,c} in., and the test was stopped 30 minutes later. Detailed data between [ ]^{a,b,c} seconds and the end of the test is missing for one instrument rack and thus, this phase of the transient cannot be analyzed.

TABLE 5.2.1-1
OSU TEST ANALYSIS PLOT PACKAGE FOR SUBSECTION 5.2.1

Plot No.	Component	Variables	Units	Description
1	Pressurizer	CPT-604	psia	System pressure and event history
2	Water injection	WWTDVI1+WWTDVI2, WOUTACC1+WOUTACC2, WWTIRWI1+WWTIRWI2, WWTSMPIT	lbm/sec.	Total of CMT, accumulator, IRWST, and sump injection flows
3	Reactor vessel	RPVASOU2	lbm/sec.	Steam generation in reactor vessel
4	Reactor vessel	T08RPV, HTMXRPV, TSAT	°F	Reactor vessel outlet temperature, maximum clad temperature and fuel exit saturation temperature

THE FIGURES LISTED IN TABLE 5.2.1-1
ARE NOT INCLUDED IN THIS NONPROPRIETARY DOCUMENT

5.2.2 Short-Term Transient

For the 2-in. cold leg break, Test SB18 (a repeat of SB01), the short-term transient encompassed the first [ ]^{a,b,c} seconds. As shown in Figures 5.2.2-1 and 5.2.2-2, this period included the full depressurization of the facility through all four stages of the ADS, together with CMT and accumulator injection plus the initial stages of IRWST injection. The mass and energy distribution results for this phase of the transient were based on the plot package detailed in Table 5.2.2-1. These plots concentrate on the primary system, including the accumulators, CMTs, IRWST, and the sumps and the flows from the primary system via the ADS, break, and IRWST overflow.

5.2.2.1 Maintenance of Core Cooling

Reactor Pressure Vessel and Downcomer Mass Distribution

For the short-term transient, the most important criteria is the maintenance of sufficient core inventory to supply adequate cooling of the heater rods. Figure 5.2.2-57 shows that there are no significant excursions in heater rod temperatures and, therefore, sufficient core inventory was maintained through this phase of the transient to remove the decay heat from the rods. However, a two-phase mixture will be present in the core and upper plenum regions for significant portions of the transient. The following discussion tracks the variation in water level and mass throughout the RPV and downcomer.

The total fluid mass in the RPV is shown in Figure 5.2.2-40. The initial vessel inventory was [ ]^{a,b,c} lbm. During the course of the short-term transient, the vessel inventory experienced two minimum values, one of [ ]^{a,b,c} lbm before accumulator injection and one of [ ]^{a,b,c} lbm before IRWST injection. Steam generation was near maximum at these times, as shown in Figures 5.2.2-55. By the end of the short-term transient, the vessel inventory recovered to a steady [ ]^{a,b,c} lbm. Similar variations are shown in the core fluid mass and water level reproduced in Figures 5.2.2-44 and 5.2.2-45. Minimum core level occurred before IRWST injection. During this phase of the transient, the collapsed liquid level dropped to [ ]^{a,b,c} in. below the top of the heated rod length (Figure 5.2.2-45). By the end of the short-term transient, the effect of IRWST injection ended all core boiling (Figure 5.2.2-55), and the core was again water-solid.

In the analysis of the SBLOCA simulations on the SPES-2 facility[3] following the pump trip, there were short-term oscillations in primary system flow, temperature, and pressure. A small number of oscillations were also observed in the OSU test response at the end of the initial blowdown (see for example the pressure response (Figure 5.2.2-1) and the RPV mass (Figure 5.2.2-40)). In the SPES-2 tests, the oscillations were driven by power-to-flow mismatches in the core due to the high core power levels that were needed in SPES-2 to compensate for the high ambient losses. The short-term oscillations observed in OSU results are believed to be a result of pressure oscillations following the initial blowdown.

The fluid mass in the core region is shown in Figure 5.2.2-44. Once again, the two minimum values occurred prior to accumulator injection and prior to IRWST injection. The minimum core inventory is [ ]^{a,b,c} lbm.

The collapsed liquid level in the upper plenum region spanned by LDP-138 and the associated fluid mass are shown in Figures 5.2.2-49 and 5.2.2-48. During the period before accumulator injection, the collapsed liquid level in the upper plenum dropped below the hot-leg elevation. During the accumulator injection, the steam bubble in the upper plenum partially condensed, and the water level briefly rose above the hot legs. Following the end of accumulator injection, the flow from the CMTs was not sufficient to maintain the upper plenum level, and this region completely drained of water. The start of IRWST injection refilled the upper plenum, and this region became near water-solid again at approximately [ ]^{a,b,c} seconds.

The fluid mass and collapsed liquid level for the head region are given in Figure 5.2.2-50 and 5.2.2-51. During the first [ ]^{a,b,c} seconds, the head inventory drained. Following the end of accumulator injection, the head region again drained. Both accumulator injection and IRWST injection were sufficient to supply a level of water in the head.

The mass of fluid and collapsed liquid level in the RPV downcomer are shown in Figures 5.2.2-41 and 5.2.2-42. During the blowdown phase of the transient, the level dropped to the elevation of the cold legs. This elevation was maintained until the cold legs were fully drained. Following this time, the collapsed level remained between the DVI and hot-leg elevations, until IRWST injection once again raised the level above the cold legs and cold-leg refill commenced.

Loop Mass Distribution

For this discussion, the loop was considered to consist of the hot- and cold-leg pipe work, the SG primary side, and the pressurizer plus surge line.

The total fluid mass and water level for the pressurizer are shown in Figures 5.2.2-34 and 5.2.2-35. During the blowdown phase of the transient ([ ]^{a,b,c}) seconds, the pressurizer drained rapidly, becoming completely empty of water at about [ ]^{a,b,c} seconds. The pressurizer remained empty until ADS-1 actuation at [ ]^{a,b,c} seconds. At that time, water was drawn back into the pressurizer as steam and water flow out of the ADS. A fluid inventory of over [ ]^{a,b,c} lbm was maintained until ADS-4 actuation at [ ]^{a,b,c} seconds. This caused an initial outsurge through the surge line, followed by a more gradual draining of the pressurizer as mass flowed out of the hot legs via the ADS-4 valves. The pressurizer fully drained at [ ]^{a,b,c} seconds and remained empty for the remainder of the transient.

Mass data for the SG U-tubes and their associated inlet and outlet plena are shown in Figures 5.2.2-32 and 5.2.2-31. The SG tubes gradually drained until ADS actuation, when all the tubes and plena were empty of water. The SG on the broken loop (loop 1) drained before that on loop 2. Any flow

through the SGs ceased on the tubes were drained and the steam trapped within the U-tubes became superheated. Once the SG tubes drained, natural circulation around the primary loop circuit ceased.

The SG U-tubes remained empty for the remainder of the short-term transient. However, both inlet and outlet plena on SG-2 show an influx of water [ ]^{a,b,c} seconds into the transient. This corresponds to the time at which the primary system reached atmospheric pressure. Figure 5.2.2-59 shows that in approximately [ ]^{a,b,c} seconds, the small amount of steam remaining in HL-2 was removed, and the water level in that hot leg increased. This is believed to result from condensation in the PRHR drawing a vacuum and raising the level on loop 2.

The mass of water and vapor in the hot legs is shown in Figures 5.2.2-58 and 5.2.2-59. The hot legs maintained their water inventory until [ ]^{a,b,c} seconds into the transient, when they started to drain (Figure 5.2.2-58), and were completely drained by [ ]^{a,b,c} seconds. Actuation of ADS-1 caused a rapid increase in void fraction in both hot legs. A larger void fraction was maintained in HL-1 as steam was preferentially removed from HL-2 by the PRHR.

The liquid and vapor mass for the four cold legs are shown in Figures 5.2.2-60 and 5.2.2-61. Following the initial blowdown, all four cold legs became two-phase although there was a greater void fraction in CL-1 and CL-4 as compared to CL-2 and CL-3 (Figure 5.2.2-61). The mass variation in all four cold legs appears very similar, as these have been derived from levels in the RPV downcomer. Derived values were used because the level instruments on the cold legs have been found to be unreliable. All the cold legs completely drained after ADS initiation and refilled at [ ]^{a,b,c} seconds when flow from the IRWST refilled the RPV downcomer to the level of the cold legs (Figure 5.2.2-42). The cold legs did not drain uniformly. Instead, CL-3 (with the break) drained first, followed by CL-1, with CL-2 and CL-4 delayed. Figure 5.2.2-31 shows that the SG outlet plenum on loop 1 drains at [ ]^{a,b,c} seconds slightly more than and before loop 2; therefore, the expected asymmetry in cold-leg behavior did occur.

Mass Injected to the Primary System

The CMTs transitioned from a recirculation to a mass injection mode at approximately [ ]^{a,b,c} seconds when the cold leg started to drain. Draindown of the CMTs continued until the CMT check valves were closed by the flow from the accumulators. CMT draindown restarted at the end of accumulator injection, continuing until IRWST injection began (Figures 5.2.2-6 and 5.2.2.-7).

The accumulators started draining approximately 20 seconds after activation of the ADS. Accumulators started discharging into the DVI line when the system pressure dropped below the pressure preset in each accumulator. Accumulator injection began at approximately [ ]^{a,b,c} seconds and continued until the accumulator was empty at approximately [ ]^{a,b,c} seconds (Figure 5.2.2-23). Complete discharge from the accumulators was indicated by a sharp decrease in the temperature of the fluid exiting each accumulator due to the discharge of expansion-cooled, nitrogen-cover gas, which

was released into the primary system (see Subsection 6.1.4). Flow from the CMTs was significantly reduced during the discharge of the accumulators and increased once accumulator discharge ended.

The IRWST injection valves were opened when the reactor vessel pressure low-low setpoint was reached. Injection flow started when the reactor vessel pressure became less than the static head from the IRWST. Figure 5.2.2-16 shows that the IRWST injection began at approximately [ ]^{a,b,c} seconds after the CMT flow ceased. The IRWST flow gradually increased to a peak value of [ ]^{a,b,c} lbm/sec. ([ ]^{a,b,c} lbm/sec. per injection line) at [ ]^{a,b,c} seconds before gradually decreasing.

Mass Ejected from the Primary System

At time zero in the transient, a 2-in. break was initiated at the bottom of CL-2. The rate of flow of mass out of the primary system, via the break, is shown in Figures 5.2.2-66 to 5.2.2-68. For the first [ ]^{a,b,c} seconds following the break, [ ]^{a,b,c} lbm of steam and water escaped from the primary system via the break (Figure 5.2.2-62). During that period, the primary system depressurized to around [ ]^{a,b,c} psi (Figure 5.2.2-1). By the onset of ADS actuation, the cold legs drained, and there was almost no water flow out of the break. Between [ ]^{a,b,c} and [ ]^{a,b,c} seconds, ADS 1-3 activated, and the system depressurized rapidly. The break flow significantly decreased once ADS activated, since the ADS valve area is significantly larger than the break. At around [ ]^{a,b,c} seconds, the ADS-4 was initiated, and the primary system continued to depressurize until IRWST injection commenced at [ ]^{a,b,c} seconds.

The actuation of ADS 1-3 terminated the flow of steam from the break, although this was replaced by steam flow through the ADS 1-3 valves for the next [ ]^{a,b,c} seconds (Figure 5.2.2-63). This steam flow was accompanied by an outflow of water from the ADS 1-3 at a peak rate of over [ ]^{a,b,c} lbm/sec. (Figure 5.2.2-66). After [ ]^{a,b,c} seconds the mass flowing through ADS 1-3 was composed almost entirely of water. The rate of flow through the ADS continued at a gradually reducing rate until [ ]^{a,b,c} seconds when the ADS-4 valves opened, terminating flow through the ADS 1-3 and replacing this flow with flow through the lower-resistance ADS-4 paths. For ADS 4-1, there was a near-steady water flow at a rate of [ ]^{a,b,c} lbm/sec. from the time of initiation. However, there was an initial outsurge at [ ]^{a,b,c} lbm/sec. for ADS 4-2, which was followed by a drop to near zero and then an increase to over [ ]^{a,b,c} lbm/sec. (Figure 5.2.2-66).

The integrated mass flow out of the primary system via the ADS and the break are shown in Figures 5.2.2-62 to 5.2.2-66. During the first [ ]^{a,b,c} seconds of the transient, over [ ]^{a,b,c} lbm of water escaped from the primary system. Of this, the [ ]^{a,b,c} lbm flowing through ADS 1-3 was deposited in the IRWST. The [ ]^{a,b,c} lbm leaving ADS-4 and the liquid part of the [ ]^{a,b,c} lbm flowing through the break were added to the overflow from the IRWST to deposit [ ]^{a,b,c} lbm of water in the primary sump (Figure 5.2.2-28). By the end of the short-term transient, the water level in the primary sump reached nearly [ ]^{a,b,c} in. (Figure 5.2.2-29).

At [ ]^{a,b,c} seconds into the transient, the cold legs refilled enough to restart water flow through the break. This proceeded at a rate of approximately [ ]^{a,b,c} lbm/sec. at the end of the short-term transient, so that the total rate of water flow from the primary system to the sump was approximately [ ]^{a,b,c} lbm/sec. At that time, the flow rate into the RPV through the DVI lines was about [ ]^{a,b,c} lbm/sec.

Mass Balance

Figure 5.2.2-70 presents the variation in the total system inventory during the short-term phase of the transient. In addition to the random variations associated with the measurement uncertainties and some inventory dips, there is a general reduction in inventory of around [ ]^{a,b,c} lbm from the initial value. During this phase of the transient, around [ ]^{a,b,c} lbm of steam was lost from the system (Figure 5.2.3-63).

A mass balance analysis was performed on the primary system. Figure 5.2.2-71 plots the measured primary system mass determined by summing the contributions from the RPV, downcomer, hot and cold legs, SG primary, pressurizer, and surge line plus the PRHR. The second curve on Figure 5.2.2-71 provides an alternative primary system mass determined from the mass balance, that is given by:

$$M'_{prim}(t) = M_{prim}(0) + M_{in}(t) - M_{out}(t) \qquad 5.2.2\text{-}1$$

where:

$M'_{prim}(t)$	=	Mass balance calculated primary system mass
$M_{prim}(0)$	=	Measured primary system mass at the start of the transient
$M_{in}(t)$	=	Total integrated mass injected from all sources (i.e., accumulators, CMT, IRWST, and sumps) to time t
$M_{out}(t)$	=	Mass lost from the primary system to time t via the CMT balance lines, ADS 1-3, ADS-4, and break

The difference in the two primary system mass curves is shown in Figure 5.2.2-72 as the mass-balance error.

During the short-term transient, there is an apparent systematic overestimate of the mass in the primary system from the measured data of up to [ ]^{a,b,c} lbm, relative to that calculated from the mass balance. There are two main contributions to this excess mass. First, the measured primary system inventory does not include all of the pipework in the system and there is about [ ]^{a,b,c} lbm of mass missing from the initial inventory. This mass will be deposited in, and lost from, the measured system as pipes drain and refill. Some of the additional mass is subsequently lost via one of the leakage paths. Second, the instrumentation on the hot legs may be giving erroneous level measurements during certain portions of the transient. Figure 5.2.2-58 shows that neither hot leg appears to drain in

this test, which contributes to an overestimate of some [ ]^{a,b,c} lbm. By the end of the short-term transient, the apparent mass-balance error is about [ ]^{a,b,c} lbm.

Figure 5.2.2-73 shows the total integrated-mass flow from and to the primary system, together with the water inventory remaining in the sources of cooling water. During the short-term transient, there was a net loss of water from the primary system of approximately [ ]^{a,b,c} lbm, of which only a small quantity was deposited in the sources. As noted above, the overall system mass inventory shows that of the lost primary system mass, [ ]^{a,b,c} lbm has been lost as steam. The rest was added to the water stored in the ADS and break separators.

Pressure Decay

Figure 5.2.2-1 shows the primary system pressure during the test. Throughout the LOCA portion of this test, the pressure was controlled by the saturation pressure of the hottest fluid in the primary system. At initiation of the break, the controlling fluid volume was the pressurizer and surge line; however, within the first [ ]^{a,b,c} seconds, (after the initial blowdown phase) this shifted to the RPV. Figure 5.2.2-3 shows that the average temperature of the upper plenum was equal to the saturation temperature corresponding to the primary system pressure measured in the upper head during the natural circulation phase and into the ADS phase.

The pressure stabilized at the saturation pressure for the upper plenum, and then continued a slow pressure decay responding to the cooling caused by the CMT injection. Figure 5.2.2-1 shows an increase in the pressure decay rate occurred at about [ ]^{a,b,c} seconds, when the CMTs transitioned from natural circulation injection to draindown injection, which essentially doubled the injection rate of cold water into the DVI line. The higher injection rate resulted in a rapid temperature drop in the upper plenum (core outlet in Figure 5.2.2-3), which was reflected in a more rapid pressure decay. With the actuation of ADS-1 at about [ ]^{a,b,c} seconds, the pressure dropped rapidly due to the increased rate of mass ejected from the system (Figure 5.2.2-56), and the increased flow of cold water injected into the downcomer and flowing through the core. This continued to reduce power channel inlet plenum temperature, and subcooled the heater rods in the core due to the higher flow.

Since the RPV outlet plenum became subcooled at about [ ]^{a,b,c} seconds, the hottest fluid in the system was in the pressurizer, the cold legs, and the CMTs, and the pressure was partially supported by the flashing of the fluid in one or several of these locations. When the accumulator discharge ended (about [ ]^{a,b,c} seconds), the RPV temperature again increased to the saturation temperature and took control of the system pressure for the rest of the LOCA phase. Also at the end of accumulator injection, a large amount of noncondensible gas was injected into the primary system and could have affected the heat transfer performance of the PRHR and the CMTs.

5.2.2.2 Energy Inventory

Heat removal from the reactor core follows a sequence similar to the pressure decay for the SBLOCA tests. Before reactor trip, nearly all the energy generated in the core is removed by the SGs and out of the break with a small fraction lost to the surroundings. When the reactor tripped, the primary system pumps tripped, and flow through the SG tubes was sharply reduced. Coupled with the isolation of the SG secondary side, the result was to significantly reduce heat removal by the SGs. At that time, the PRHR isolation valves opened, and energy was removed to the IRWST as well as out of the break.

As the system drained, the primary system pressure was reduced, and the sensible heat of the coolant and metal added to the core heat load. The CMTs started to drain, and the ADS activated. At that time, heat removal was accomplished through the ADS flow, and the PRHR became less effective. Finally, ADS-4 actuated, the primary system completely depressurized, and the IRWST actuated. The LOCA phase of the test was then completed.

The behavior of the components involved in the energy removal is discussed below.

Core

The power output of the core is shown in Figure 5.2.2-2. After reactor trip, the core power is representative of decay heat levels expected in the AP600 core. Flow through the core is shown in Figure 5.2.2-56, and the steam generation rate is given in Figure 5.2.2-55. As discussed in Section 4.0, the steam generation rate can be calculated by two methods, the Tsat method and the DVI line flow method.

Figures 5.2.2-53, 5.2.2-54, and 5.2.2-55 reproduce the saturation line elevation, power split above the saturation elevation and steam generation rates from the two methods. Both methods give similar predictions. Note that neither method gives valid predictions before [ ]^{a,b,c} seconds because of flow oscillations during natural circulation in the primary system.

The maximum steam generation rate during the LOCA phase occurred at approximately [ ]^{a,b,c} seconds, which was just prior to IRWST injection. The peak cladding temperature is shown in Figure 5.2.2-57, and indicates that the core was adequately cooled at all times during the test.

Steam Generator Heat Transfer

The SGs remove most of the heat from the primary system during normal operation. However, heat transfer from the primary to secondary side was significantly reduced after the pumps trip. This was due to reduced flow in the tubes, which caused a sharp reduction in the tube-side heat transfer coefficient. In addition, the secondary side was isolated, which caused the temperature and pressure to remain high as the primary-side pressure rapidly decreased.

Passive Residual Heat Removal Heat Transfer

The PRHR is designed to remove heat from the primary system from the time when the SGs become thermally isolated due to the initiation of the ADS. One measure of the effectiveness of the PRHR is the increase in the fluid internal energy in the IRWST, which serves as the heat sink for the PRHR. Figure 5.2.2-33 shows the fluid internal energy in the IRWST during the first [ ]^{a,b,c} seconds of the test. The PRHR began operating at about [ ]^{a,b,c} seconds as the SG heat removal ended. The heat removal rate was approximately [ ]^{a,b,c} Btu/sec. until [ ]^{a,b,c} seconds when ADS-1 activated. At that time, the heating rate in the IRWST increased to [ ]^{a,b,c} Btu/sec. due to steam condensing from the ADS 1-3, and heating from the PRHR. The PRHR heat removal decreased when the accumulators discharged at about [ ]^{a,b,c} seconds as the core became subcooled.

Automatic Depressurization System and Break

The energy removal from the ADS and break are shown in Figure 5.2.2-69. The fluid energy exiting the break increased at a constant rate until ADS-1 was actuated. For ADS-1, ADS-2, and ADS-3, compared to the break, the energy removal occurred at a somewhat lower rate due to reduced system pressure. When ADS-4 was actuated, energy removal switched from ADS 1-3 to the larger flow path ADS-4. The ADS effectively reduced the primary system pressure to start gravity injection flow from the IRWST. This flow was sufficient to subcool the primary system, ending core boiling and partially collapsing the steam bubble in the upper plenum to bring the system to near atmospheric pressure.

Overall Energy Balance

Figure 5.2.2-74 shows all the energy components in the heat balance for the system during the LOCA phase ([ ]^{a,b,c} seconds). Throughout the event, the heater rod bundle power was the dominant heat input to the system, and before the start of the event, the SGs provided the dominant heat removal. At the start of the event, the SG secondary side was isolated, and the RCPs tripped. During this period, heat removal by the SG was reduced as natural circulation flow occurred in the primary system. As the primary system depressurized, the pressure reached the secondary-side pressure, and heat transfer effectively ended.

From the start of the event, the steam component of the break flow left the control volume until the actuation of ADS. Heat loss via this path was nearly [ ]^{a,b,c} Btu/sec., which was far greater than the reactor decay power [ ]^{a,b,c} Btu/sec. The remaining energy lost through the break exhaust consisted of a decrease in the fluid internal energy as the primary system depressurized.

After ADS 1-3 was actuated, the break flow effectively ended, and the ADS heat was deposited into the IRWST. Thus, the fluid internal energy in the control volume increased until the end of the LOCA phase, as the IRWST water temperature increased. Also, at this time, the metal masses in the control volume lost energy as primary system temperature decreased. As a result, energy was deposited at a rate of nearly [ ]^{a,b,c} Btu/sec. between [ ]^{a,b,c} seconds. After [ ]^{a,b,c}

seconds, the metal masses lost energy at a much lower rate, which was consistent with the primary system fluid temperature decay. Ambient losses were reduced from a maximum of [ ]^{a,b,c} Btu/sec. at full-power conditions tc [ ]^{a,b,c} Btu/sec. at the end of the LOCA phase.

A large increase was observed in the deficit between the rod bundle power and the various sources of energy dissipation from the control volume after the initiation of ADS 1-3, and again after the initiation of ADS-4 at approximately [ ]^{a,b,c} seconds. The steam exhaust included steam from the IRWST and the steam portion of the flow from ADS-4. However, relatively little steam flow was measured by the vapor flow meters. Further discussion of this steam flow is provided in the mass and energy balance in Sections 6.2.2 and 6.2.3.

TABLE 5.2.2-1 OSU TEST ANALYSIS STANDARD PLOT PACKAGE FOR SUBSECTION 5.2.2				
Plot No.	**Component**	**Variables**	**Units**	**Description**
1	Pressurizer	CPT-604	psia	System pressure
2	RPV	RPVPWR	kW	Core power
3	RPV	T01RPV, T08RPV, ST08RPV	°F	Core inlet/outlet temperature, saturation temperature
4	SG	CPT-201, CPT-204, CPT-301, CPT-302	psia	Primary and secondary pressures in SG
5	DVI-1	WWTDVIL1, WWTIRWI1, WOUTACC1, WWTIRWI3	lbm/sec.	Individual components and total flow in DVI-1
6	DVI-2	WWTDVIL2, WWTIRWI2, WOUTACC2, WWTIRWI4	lbm/sec.	Individual components and total flow in DVI-2
7	CMT	AMCMT1B, AMCMT2B	lbm	Fluid mass in CMTs (excludes balance lines)
8	CMT	CLDP-502, CLDP-507	in.	Collapsed liquid level in CMTs
9	CMT	MIWDVIL1, MIWDVIL2	lbm	Integrated mass out of CMTs
10	CMT	WWTDVIL1, WWTDVIL2	lbm/sec.	Flow out of CMTs
11	CMT	WWTCLBL1, WWTCLBL2	lbm/sec.	Flow into CMTs
12	CMT	CLDP-509, CLDP510	in.	Level CL-CMT balance lines
13	CMT	UCMT1, UCMT2	Btu	Fluid energy in CMTs
14	IRWST	IRWST	lbm	Mass of fluid in IRWST
15	IRWST	CLDP-701	in.	Collapsed liquid level in IRWST
16	IRWST	WWTIRWI1, WWTIRWI2	lbm/sec.	Flow from IRWST to DVI lines
17	IRWST	IRWSTOR	lbm/sec.	Overflow from IRWST to sump
18	IRWST	ADS13TMR	lbm/sec.	Total ADS flow into IRWST
19	IRWST	ADS13TIR, MIIRWI1, MIIRWI2, MIIRWIO	lbm	Integrated mass out of IRWST
20	IRWST	UIRWST	Btu	Fluid energy in IRWST
21	PRHR	CLDP-802	in.	Collapsed liquid level in PRHR HX

TABLE 5.2.2-1 (Continued) OSU TEST ANALYSIS STANDARD PLOT PACKAGE FOR SUBSECTION 5.2.2				
Plot No.	**Component**	**Variables**	**Units**	**Description**
22	PRHR	WWOTPRHR	lbm/sec.	Measured outlet flow from PRHR tube
23	Accumulator	AMACC1, AMACC2	lbm	Mass of fluid in accumulators
24	Accumulator	CLDP-401, CLDP-402	in.	Collapsed liquid level in accumulators
25	Accumulator	WOUTACC1, WOUTACC2	lbm/sec.	Flow from accumulators
26	Accumulator	MOUTACC1, MOUTACC2	lbm	Integrated mass out of accumulators
27	Accumulator	UACC1, UACC2	Btu	Fluid energy in accumulators
28	Primary sump	AMPSMP	lbm	Primary sump fluid mass
29	Primary sump	CLDP-901	in.	Primary sump level
30	Primary sump	UPSMP	Btu	Primary sump fluid energy
31	SG	MSSGIP1, MSSGIP2, MSSGOP1, MSSGOP2	lbm	Mass of fluid in SG primary side inlet/outlet plena
32	SG	MSSGHT1, MSSGHT2, MSSGCT1, MSSGCT2	lbm	Mass of fluid in SG primary side hot and cold tubes
33	SG/PRHR	CPT-201, CPT-301, QPRHRI	psia & Btu	SG1 pressure and PRHR integrated heat output
34	Pressurizer	PZM	lbm	Fluid mass in pressurizer
35	Pressurizer	CLDP-601	in.	Collapsed liquid level in pressurizer
36	Pressurizer	UPZ	Btu	Fluid energy in pressurizer
37	Surge line	PLM	lbm	Fluid mass in surge line
38	Surge line	CLDP-602	in.	Collapsed liquid level in surge line
39	Surge line	UPSL	Btu	Fluid energy in surge line
40	RPV	MWRPV	lbm	Total fluid mass in reactor vessel
41	RPV	DCM	lbm	Fluid mass in downcomer
42	RPV	LDP01DC	in.	Collapsed liquid level in downcomer compared to various reference elevations
43	RPV	MW01RPV	lbm	Fluid mass in lower plenum
44	RPV	MW03RPV	lbm	Fluid mass in core region
45	RPV	LDP03RPV	in.	Collapsed liquid level in core
46	RPV	RPVAVDF2		Core exit void fraction
47	RPV	RPVAQOU2		Core exit quality
48	RPV	MW06RPV	lbm	Fluid mass in the upper plenum
49	RPV	LDP06RPV	in.	Collapsed liquid level in the upper plenum
50	RPV	MW08RPV	lbm	Fluid mass in the upper head
51	RPV	LDP08RPV	in.	Collapsed liquid level in the upper head

TABLE 5.2.2-1 (Continued)
OSU TEST ANALYSIS STANDARD PLOT PACKAGE FOR SUBSECTION 5.2.2

Plot No.	Component	Variables	Units	Description
52	RPV	URPV	Btu	Total fluid energy in reactor vessel
53	RPV	RPVXE, RPVASL2	ft	Level of Tsat line
54	RPV	RPVPab, RPVAPab2, RPVPWR	kW	Heated rod power above and below Tsat level and total
55	RPV	RPVRXV, RPVASOU2	lbm/sec.	Core steam generation rate
56	RPV	RPVALIN2	lbm/sec.	Calculated core flow
57	RPV	HTMXRPV, ST08RPV	°F	Maximum clad temperature and saturation temperature
58	Hot leg	MWHL1, MWHL2	lbm	Water mass in hot legs
59	Hot leg	MVHL1, MVHL2	lbm	Vapor mass in hot legs
60	Cold leg	CL1WMS, CL2WMS, CL3WMS, CL4WMS	lbm	Water mass in cold legs
61	Cold leg	CL1VMS, CL2VMS, CL3VMS, CL4VMS	lbm	Vapor mass in cold legs
62	ADS and break	BRKSTIR, ADS13TIR, ADS41TIR, ADS42TIR	lbm	Total discharged mass for ADS 1-3, ADS-4s, and break
63	ADS and break	BRKTIVF, AD13TIVF, AD41TIVF, AD42TIVF	lbm	Total integrated vapor flow for ADS and break
64	ADS and break	BRKTILF, AD13TILF, AD41TILF, AD42TILF	lbm	Total integrated liquid flow for ADS and break
65	ADS and break	ADS13SVR, ADS41SVR, ADS42SVR	lbm/sec.	Vapor flow out ADS 1-3 and ADS-4
66	ADS and break	ADS13SLR, ADS41SLR, ADS42SLR	lbm/sec.	Liquid flow out ADS 1-3 and ADS-4
67	ADS and break	BRKSSVR	lbm/sec.	Vapor flow out of break
68	ADS and break	BRKSSLR	lbm/sec.	Liquid flow out of break
69	ADS and break	BRKSPEI, ADS13EI, ADS41EI, ADS42EI	Btu	Integrated fluid energy for ADS 1-3, ADS-4, and break
70	Mass balance	TOTMASS	lbm	Total system mass inventory
71	Mass balance	PRIMMASS, PRIMASS2	lbm	Measured primary system inventory and value from mass balance
72	Mass balance	MERROR	lbm	Mass balance error
73	Mass balance	MIN, MOUT SRCMASS	lbm	Integrated mass flow in and out of primary system and source mass
74	Energy balance	Various	Btu	Components of energy balance

THE FIGURES LISTED IN TABLE 5.2.2-1
ARE NOT INCLUDED IN THIS NONPROPRIETARY DOCUMENT

5.2.3 Long-Term Transient

The long-term transient covered the transition from IRWST to sump injection and provided information on the LTC response of AP600. For the 2-in. cold-leg break, Test SB18, the DAS did not record all the instrumentation signals beyond [ ]^{a,b,c} seconds; therefore, the sump injection phase cannot be analyzed beyond this point. In this case, the long-term transient covered the time frame from [ ]^{a,b,c} seconds. By this time, the initial stages of flow from the primary sump had begun via the check valves around the main injection valves, but the main sump injection valves had not opened. The behavior of the test facility during this period of the transient is discussed in this subsection using the plot package detailed in Table 5.2.3-1. These results concentrate on the components of the primary system that remain active during the LTC phase, that is the RPV, the hot legs, ADS-4, the sumps, and the IRWST.

5.2.3.1 Maintenance of Core Cooling

Reactor Pressure Vessel and Downcomer Mass Distribution

For the long-term transient, the passive core cooling systems must supply sufficient flow to prevent any overheating of the heater rods. At [ ]^{a,b,c} seconds, the decay heat simulation of the heated rods reduced the power from [ ]^{a,b,c} kW (Figure 5.2.3-1). As shown in Figure 5.2.3-38, there are no significant excursions in heated rod temperatures and therefore, sufficient core flow was maintained throughout the long-term transient.

The mass of water in the RPV is shown in Figure 5.2.3-25. After an initial decline, the reactor vessel water mass settled at an average value of around [ ]^{a,b,c} lbm where it remained until the end of the test. From [ ]^{a,b,c} seconds, oscillations in vessel inventory can be observed. These oscillations are evident in measurements throughout the primary system and are discussed further in Subsection 6.1.3.

The core water mass and collapsed liquid level are shown in Figures 5.2.3-28 and 5.2.3-29. During the transient, the core remained nearly water-solid with only a low level of boiling (Figure 5.2.3-36). The level at which the core fluid reached saturation temperature was around [ ]^{a,b,c} in. for the period of the transient (Figure 5.2.3-34). Figure 5.2.3-29 shows that at the end of the transient, the effect of the hot water arriving from the sump was detected as a decreased core collapsed liquid level.

The collapsed liquid level in the upper plenum region is shown in Figure 5.2.3-32. During the period before sump injection began, the collapsed liquid level in the upper plenum remained at the top of the hot legs. Following the start of the hot water influx from the sumps, the level dropped to the middle of the hot legs.

The mass of fluid and collapsed liquid level in the RPV downcomer are shown in Figures 5.2.3-26 and 5.2.3-27. Before sump injection began, the collapsed liquid level in the downcomer was at the level of the center of the cold legs. By the end of the transient, the effect of the initial stages of sump injection reduced the downcomer collapsed liquid level to the hot-leg elevation.

Loop Mass Distribution

As discussed, the LTC phase of the transient shows that there is a low level of boiling in the upper regions of the core. However, due to a failure of the DAS, analysis of the long-term transient is not detailed enough to track the behavior of this steam.

Mass Ejected from the Primary System

The integrated mass flow out of the primary system via the ADS and the break is shown in Figure 5.2.3-43. By the end of the transient, [ ]^{a,b,c} lbm of water flowed out of the primary system. During the LTC phase of the transient, the only significant outflow was through the ADS-4 valves with a small apparent flow through the break. The apparent break flow did not represent a flow out of the primary system, but indicated continued interaction between the break separator and the sump. The most marked manifestation of this interaction is at [ ]^{a,b,c} seconds when the primary sump began to overflow into the secondary sump. This caused oscillating flow indications in the liquid flow out of the break separator. This is confirmed by Figures 5.2.3-44 to 5.2.3-45, which show the flows through the ADS and the break. During the sump injection phase of the transient, outflow was in the form of liquid out of the ADS-4 valves. Water flowed through each of these at an average rate of [ ]^{a,b,c} lbm/sec. Although no steam flow was recorded by the vortex meters to show steam escaping from the system via ADS-4, as discussed in Subsection 6.2.2, steam most likely left the system by this route at a very low flow rate.

At approximately [ ]^{a,b,c} seconds into the transient, the level in the primary sump (Figure 5.2.3-14) reached the point at which overflow to the secondary sump occurred. At that time, there was [ ]^{a,b,c} lbm of water collected in the primary sump. From the beginning of primary sump overflow to the end of the analysis, [ ]^{a,b,c} lbm of water was transferred to the secondary sump.

Mass Injected to the Primary System

The total DVI line flow, CMT flow, and IRWST flows are shown in Figures 5.2.3-6 and 5.2.3-7, and the flow from the primary sump is shown in Figure 5.2.3-19. From around [ ]^{a,b,c} seconds, there was a contribution to the DVI flow from the CMTs as they finished their post-refill draindown.

During the presump injection phase of the transient, the IRWST flow proceeded at a gradually reduced rate, with the effect of the primary system oscillations superimposed. At [ ]^{a,b,c} seconds, flow from the primary sump began through the check valves around the main injection valves. At the end of the analysis, the level in the IRWST fell to [ ]^{a,b,c} in., which was above the level at which the primary sump injection valves opened.

Mass Balance

Figure 5.2.3-46 shows the variation in the total system mass inventory during the entirety of Test SB18. Following the short-term transient, total inventory increased by [ ]^{a,b,c} lbm to approximately [ ]^{a,b,c} lbm above the initial value at the time sump injection around the main valve started. The initiation of sump injection led to [ ]^{a,b,c} lbm increase in inventory.

The mass balance calculation described in Subsection 5.2.2.1 was performed for the entirety of the transient, and the results are presented in Figures 5.2.3-47 to 5.2.3-49. From [ ]^{a,b,c} seconds, the error remained between ± [ ]^{a,b,c} lbm. Following the overflow from the primary to secondary sump, the error increased due to the interaction between the break separator and sumps.

5.2.3.2 Energy Balance

Figure 5.2.3-50 shows all the energy components in the heat balance for the system during the LTC phase. The LTC phase for this test was abbreviated because the data acquisition system stopped recording data prematurely. During this phase, the heater rod bundle power was the dominant heat input to the system. The SG heat transfer ended during the LOCA phase and did not contribute to the overall energy balance during the LTC phase. Thus, for the LTC phase, the active components in the overall energy balance were the rod bundle power, the change in the fluid internal energy, the change in the metal internal energy, and ambient losses, and the steam exhausted from the control volume.

The fluid energy in the control volume increased steadily until sump injection began (approximately [ ]^{a,b,c} seconds). At that time, the fluid throughout the system approached saturated conditions, and the rate of increase was lower. At the same time, the metal mass temperatures increased as the primary system temperature increased. Also, the ambient losses increased slightly as the control volume temperatures increased.

The steam component of the ADS-4 flow left the control volume after the actuation of ADS-4. For times subsequent to the LOCA phase, this quantity was essentially zero, as measured by the vapor flow meters. It is concluded that the vapor flow meters in the ADS-4 separators did not measure the relatively small steam flow rates accurately. Further discussion of this steam flow is provided in the mass and energy balance in Sections 6.2.2 and 6.2.3.

TABLE 5.2.3-1
OSU TEST ANALYSIS STANDARD PLOT PACKAGE FOR SUBSECTION 5.2.3
LONG-TERM TRANSIENT

Plot No.	Component	Variables	Units	Description
1	RPV	RPVPWR	kW	Core power
2	Primary sump	TSMPI1, TSMPI2	°F	Sump injection line temperatures
3	DVI	TDVIL1, TDVIL2	°F	DVI line temperatures
4	RPV	T01DC, T02DC, T03DC, ST01DC	°F	Water and saturation temperatures in downcomer
5	RPV	T01RPV, T08RPV, ST08RPV	°F	Core inlet/outlet temperature, saturation temperature
6	DVI-1	WWTDVIL1, WWTIRWI1, WWTIRWI3	lbm/sec.	Individual components and total flow in DVI-1
7	DVI-2	WWTDVIL2, WWTIRWI2, WWTIRWI4	lbm/sec.	Individual components and total flow in DVI-2
8	CMT	CLDP-502, CLDP-507	in.	Collapsed liquid level in CMTs
9	CMT	CLDP-509, CLDP510	in.	Level CL-CMT balance lines
10	IRWST	IRWST	lbm	Mass of fluid in IRWST
11	IRWST	CLDP-701	in.	Collapsed liquid level in IRWST
12	IRWST	UIRWST	Btu	Fluid energy in IRWST
13	Primary sump	AMPSMP	lbm	Primary sump fluid mass
14	Primary sump	CLDP-901	in.	Primary sump level
15	Primary sump	UPSMP	Btu	Primary sump fluid energy
16	Secondary sump	AMSSMP	lbm	Secondary sump fluid mass
17	Secondary sump	CLDP-902	in.	Secondary sump level
18	Secondary sump	USSMP	Btu	Secondary sump fluid energy
19	Primary sump	WSTSMPET, WWTSMPIT	lbm/sec.	Primary sump steam and liquid injection rate
20	Primary sump	MISMPI1, MISMPI2, MISMPIT, MIIRWT	lbm	Integrated primary sump and IRWST flows
21	SG	MSSGIP1, MSSGIP2, MSSGOP1, MSSGOP2	lbm	Mass of fluid in SG side inlet/outlet plena
22	Surge line	PLM	lbm	Fluid mass in surge line
23	Surge line	CLDP-602	in.	Collapsed liquid level in surge line
24	Surge line	UPSL	Btu	Fluid energy in surge line
25	RPV	MWRPV	lbm	Total fluid mass in reactor vessel

TABLE 5.2.3-1 (Continued)
OSU TEST ANALYSIS STANDARD PLOT PACKAGE FOR SUBSECTION 5.2.3
LONG-TERM TRANSIENT

Plot No.	Component	Variables	Units	Description
26	RPV	DCM	lbm	Fluid mass in downcomer
27	RPV	LDP01DC	in.	Collapsed liquid level in downcomer compared to various reference elevations
28	RPV	MW03RPV	lbm	Fluid mass in core region
29	RPV	LDP03RPV	in.	Collapsed liquid level in core
30	RPV	RPVAVDF2		Core exit void fraction
31	RPV	RPVAQOU2		Core exit quality
32	RPV	LDP06RPV	in.	Collapsed liquid level in the upper plenum
33	RPV	MW08RPV	lbm	Fluid mass in the upper head
34	RPV	RPVASL2	ft.	Level of Tsat line
35	RPV	RPVAPab2, RPVPWR	kW	Heated rod power above and below Tsat level and total
36	RPV	RPVASOU2	lbm/sec.	Core steam generation rate
37	RPV	RPVALIN2	lbm/sec.	Calculated core flow
38	RPV	HTMXRPV, ST08RPV	°F	Maximum clad temperature, saturation temperature and delta
39	Hot leg	MWHL1, MWHL2	lbm	Water mass in hot legs
40	Hot leg	MVHL1, MVHL2	lbm	Vapor mass in hot legs
41	Cold leg	CL1WMS, CL2WMS, CL3WMS, CL4WMS	lbm	Water mass in cold legs
42	Cold leg	CL1VMS, CL2VMS, CL3VMS, CL4VMS	lbm	Vapor mass in cold legs
43	ADS and break	BRKSTIR, ADS13TIR, ADS41TIR, ADS42TIR	lbm	Total discharged mass for ADS 1-3, ADS-4, and break
44	ADS and break	ADS13TLR, ADS41TLR, ADS42TLR	lbm/sec.	Liquid flow out ADS 1-3 and ADS-4
45	ADS and break	BRKSTLR	lbm/sec.	Liquid flow and total flow out of break
46	Mass balance	TOTMASS	lbm	Total system mass inventory
47	Mass balance	PRIMMASS, PRIMASS2	lbm	Measured primary system inventory and valve from mass balances
48	Mass balance	MERROR	lbm	Mass balance error
49	Mass balance	MIN, MOUT SRCMASS	lbm	Integrated mass flow in and out of primary system and source mass
50	Energy balance	Various	Btu	Component of energy balance
51	ADS-4	ADS41TLR, ADS42TLR	lbm/sec.	Oscillations in ADS-4 liquid flow
52	Surge line	CLDP-602	in.	Oscillations in surgeline level
53	RPV	CPT-107	psia	Oscillations in upper head pressure

TABLE 5.2.3-7 (Continued)
OSU TEST ANALYSIS STANDARD PLOT PACKAGE FOR SUBSECTION 5.2.3
LONG-TERM TRANSIENT

Plot No.	Component	Variables	Units	Description
54	RPV	CLDP-113	in.	Oscillations in upper plenum level
55	RPV	LDP03RPV	in.	Oscillations in core level
56	RPV	LDP01DC	in.	Oscillations in downcomer level

THE FIGURES LISTED IN TABLE 5.2.3-1
ARE NOT INCLUDED IN THIS NONPROPRIETARY DOCUMENT

5.3 Analysis of Matrix Test SB06

Matrix Test SB06 (OSU Test U0006) simulated a 4-in. cold-leg break SBLOCA with LTC and without the operation of the nonsafety-related systems. The break was located on the bottom of CL-3 and except for the break size, this test was similar to SB01, including the simulated failure of one of the ADS-4 lines.

The analysis of Matrix Test SB06 is divided into three subsections as follows:

- Facility performance is discussed in Subsection 5.3.1, which provides a brief outline of the response of the test facility.

- The short-term transient for SB06 encompassed the start of the simulation up to [ ]^{a,b,c} seconds. This period includes blowdown, natural circulation, ADS, and initial IRWST stages of the transient.

- The analysis of the long-term transient for SB06 encompassed the time frame from 1500 seconds to the end of the test. This phase of the transient includes the IRWST injection and covers the transition to sump injection. The long-term transient actually started at IRWST injection, which is discussed as part of the short-term transient and so, the discussion of the long-term transient provided here begins at [ ]^{a,b,c} seconds. At [ ]^{a,b,c} seconds, CMT-1 began to refill and CMT-2 followed [ ]^{a,b,c} seconds later. CMT refill phenomena are discussed further in Subsection 6.1.1.

The discussion of the short and long-term phase of the transient focuses on important thermal-hydraulic phenomena identified in the PIRT (Table 1.3-1). Key indicators of the quality of the analysis on which this discussion is based are the mass and energy balance results. These are discussed in detail in Subsections 6.2.2 and 6.2.3.

5.3.1 Facility Performance

The performance of the OSU test facility during Matrix Test SB06 in reference to the five transient phases is outlined in the following:

- Blowdown
- Natural circulation
- ADS
- IRWST injection
- Sump injection

The overall performance of the facility during the transient is shown in Figures 5.3.1-1 to 5.3.1-4. Figure 5.3.1-1 shows the pressurizer pressure throughout the test with various phases and operating components. The time scale was reduced for clarity since there were only small changes in system pressure during the long-term phase of the transient. Figure 5.3.1-2 shows the total DVI line flow and its composition from the various sources at each time in the transient. Figure 5.3.1-3 shows the calculated core steam generation rate throughout the test and Figure 5.3.1-4 the variation in average measured core outlet temperature and peak clad temperature relative to the core outlet saturation temperature.

Figures 5.3.1-1 and 5.3.1-2 show that throughout the transient there was a continuous flow of cooling water to the core from the passive safety-related systems. Once initiated, the ADS rapidly depressurized the primary system and thus enhanced CMT and accumulator injection flow rates. Ultimately, the ADS-4 valves reduced the system pressure sufficiently to allow gravity-driven IRWST injection to begin. Operation of the passive injection systems overlapped so that as one source of water drained the next was available to continue the cooling process. The level of steam generation in the core and the response of the average measured core outlet fluid temperatures and maximum clad temperatures is shown in Figures 5.3.1-3 and 5.3.1-4. These figures show that the cooling flow prevented excessive core heating, and the core remained covered. The core remained subcooled for large periods of the transient and when steam production occurred, the rate of generation remained well below the rate at which water is delivered to the core.

5.3.1.1 Blowdown Phase

The blowdown phase began at time zero when the break was initiated and continued until the primary system pressure was in equilibrium with the secondary-side pressure at about [ ]^{a,b,c} seconds. During this phase of the transient, cooling flow was provided from the two CMTs, which remained in the recirculation mode and heat was removed from the primary system via the SG. The pressurizer and surge line completely drained at [ ]^{a,b,c} and [ ]^{a,b,c} seconds, respectively.

5.3.1.2 Natural Circulation Phase

In this LOCA simulation, after a brief period of stability, the single and two-phase natural circulation phase was marked by a gradual reduction in system pressure rather than by the more stable pressure observed in SB01. During this phase of the transient, the SG tubes drained by about [ ]^{a,b,c} seconds and at this time, heat removal from the primary system continued via the PRHR. In response to voiding in CL-3, CMT-1 transitioned to draindown mode at [ ]^{a,b,c} seconds, after the end of the blowdown phase, and the falling CMT level reached the ADS low-level setpoint at [ ]^{a,b,c} seconds. At [ ]^{a,b,c} seconds, both accumulators began to inject at [ ]^{a,b,c} lbm/sec. without affecting the CMT outflow. The rate of accumulator injection gradually rose to [ ]^{a,b,c} lbm/sec. over the next [ ]^{a,b,c} seconds. The natural circulation phase of the transient continued to [ ]^{a,b,c} seconds when the ADS-1 valve opened. The minimum RPV inventory of [ ]^{a,b,c} lbm was observed at about [ ]^{a,b,c} seconds.

5.3.1.3 Automatic Depressurization System Phase

ADS-1 actuation was followed by ADS-2 and ADS-3 [ ]^{a,b,c} and [ ]^{a,b,c} seconds later. Coinciding with the initiation of the ADS, a more rapid phase of accumulator injection began. The influx of cold water combined with increased venting via the ADS led to a rapid depressurization of the primary system. Actuation of ADS-4 at [ ]^{a,b,c} seconds completed depressurization to a level which allowed IRWST injection at [ ]^{a,b,c} seconds via DVI-1 and [ ]^{a,b,c} seconds via DVI-2. During the more rapid phase of accumulator injection, increased flow path resistance reduced flow out of the CMTs. As the accumulators drained, CMT flow resumed. The accumulators were fully drained [ ]^{a,b,c} seconds before IRWST injection began. CMT flow became more sporadic [ ]^{a,b,c} seconds after the start of IRWST injection, but the CMTs never fully drained during the short-term transient.

Actuation of ADS-2 rapidly refilled the pressurizer as water and steam flowed out of the ADS. The pressurizer gradually drained by [ ]^{a,b,c} seconds.

5.3.1.4 In-Containment Refueling Water Storage Tank Injection

IRWST injection signaled the transition from the short- to long-term phase of the transient. The initial phase of IRWST injection involved an increase in flow through the two DVI lines, which was followed by a gradual reduction as the driving head between the IRWST tank and the RCS fell due to the reduced IRWST water level. Once maximum flow was established, the influx of water from the IRWST was enough to keep the core subcooled until [ ]^{a,b,c} seconds. Steam was subsequently generated in the core for the remainder of the transient. The IRWST injection phase between [ ]^{a,b,c} seconds, was marked by oscillations in pressure and level throughout the primary system. These oscillations were also observed in the ADS-4 liquid flow rates.

5.3.1.5 Sump Injection

Flow from the primary sump began at [ ]^{a,b,c} seconds, via the check valves around the main sump injection valves, when the relative sump and IRWST driving heads allowed this. The test was terminated before the IRWST level fell to [ ]^{a,b,c} in. and thus, the main sump injection valves were not actuated.

TABLE 5.3.1-1 OSU TEST ANALYSIS PLOT PACKAGE FOR SUBSECTION 5.3.1				
Plot No.	**Component**	**Variables**	**Units**	**Description**
1	Pressurizer	CPT-604	psia	System pressure and event history
2	Water injection	WWTDVI1+WWTDVI2, WOUTACC1+WOUTACC2, WWTIRWI1+WWTIRWI2, WWTSMPIT	lbm/sec.	Total of CMT, accumulator, IRWST, and sump injection flows
3	Reactor vessel	RPVASOU2	lbm/sec.	Steam generation in reactor vessel
4	Reactor vessel	T08RPV, HTMXRPV, TSAT	°F	Reactor vessel outlet temperature, maximum clad temperature and fuel exit saturation temperature

THE FIGURES LISTED IN TABLE 5.3.1-1
ARE NOT INCLUDED IN THIS NONPROPRIETARY DOCUMENT

5.3.2 Short-Term Transient

For the 4-in. cold-leg break LOCA simulation, Matrix Test SB06, the short-term transient encompassed the time frame up to [ ]^{a,b,c} seconds. As can be seen from Figures 5.3.1-1, this period included the full depressurization of the facility through all four stages of the ADS together with CMT and accumulator injection plus the initial stages of IRWST injection. The variation in mass, energy, pressure, and temperature throughout this stage of the transient are illustrated in the plot package outlined in Table 5.3.2-1. The plots concentrate on the primary system including the accumulators, CMTs, IRWST, primary sump and flows from the primary system via the ADS, break and IRWST overflow.

There were two principal parameters of interest for the short-term transient:

- Adequate flow from the passive systems to the reactor vessel must be maintained.
- Adequate flow into the core must be maintained to ensure that decay heat was removed from the simulated fuel rods, without a temperature excursion.

These parameters are addressed in the following discussion.

5.3.2.1 Maintenance of Core Cooling

Mass Injected to the Primary System

Figures 5.3.2-6 and 5.3.2-7 show the combined effect of the injection flows for the short-term phase of the transient. Separate plots of the individual contributions to the total flow can be located by consulting the plot package index given in Table 5.3.2-1.

Figures 5.3.2-5 and 5.3.2-6 show how the CMTs, accumulators and IRWST combined to supply a continuous flow of cooling water to the core. During the first [ ]^{a,b,c} seconds, cooling flow was provided by the CMTs and then was supplemented by gradually increasing flow from both accumulators. The flow from the CMTs began at an initial value of [ ]^{a,b,c} lbm/sec., and increased to over [ ]^{a,b,c} lbm/sec. when the CMTs transitioned to draindown at [ ]^{a,b,c} seconds. Following the start of accumulator injection, the CMT flow gradually reduced as the driving head fell in response to the CMT water heat-up and draindown until [ ]^{a,b,c} seconds, when depressurization following ADS-1 initiation generated more rapid accumulator injection. The rapid accumulator flow temporarily stopped CMT flow, but led to an overall increase in flow to the core to a peak value of [ ]^{a,b,c} lbm/sec. Following the end of accumulator injection, the CMTs again provided cooling flow until the flow from the IRWST caused CMT draindown to end. Since IRWST injection began before the CMTs had fully drained, there was no period of the short-term transient when the passive safety-related systems failed to provide flow to the RPV.

Reactor Pressure Vessel and Downcomer Behavior

The effect of water flow on the average measured core inlet/outlet temperatures and peak heater rod temperatures during the short-term phase of the transient can be seen in Figures 5.3.2-3 and 5.3.2-57. The core outlet temperature reached the saturation point at approximately [ ]^{a,b,c} seconds. Except for the period of rapid accumulator injection, the core exit temperature then remained at the saturation level for about [ ]^{a,b,c} seconds, when the influx of water from the IRWST became sufficient to again subcool the core. The core then remained subcooled until approximately [ ]^{a,b,c} seconds.

Figure 5.3.2-57 shows that there were no significant excursions in heated rod temperatures throughout the short-term transient; therefore, sufficient core inventory and flow was maintained through this phase of the transient to remove the simulated decay heat generation. For significant portions of the transient, a two-phase mixture was present in the core and upper plenum regions, with core boiling kept at a low level. The following discussion tracks the variation in water level and mass throughout the RPV and downcomer.

The mass and level for the core region are shown in Figures 5.3.2-44 and 5.3.2-45. The collapsed liquid level in the core indicates that the heater rods remained covered with a single or two-phase mixture throughout the short-term transient. The minimum core inventory of [ ]^{a,b,c} lbm occurred at [ ]^{a,b,c} seconds into the transient, before the initial accumulator injection was established. As shown in Figure 5.3.2-45, during this phase of the transient, the collapsed liquid level dropped to [ ]^{a,b,c} in. below the top of the heated rod length. The average void fraction of the core two-phase mixture may be estimated by dividing the measured core collapsed liquid level by the [ ]^{a,b,c} in. heated rod length. In this test, the minimum collapsed liquid level corresponded to a core void fraction of [ ].^{a,b,c}

The collapsed liquid level in the upper plenum region covered by LDP-113, and the associated fluid mass are shown in Figures 5.3.2-49 and 5.3.2-48. It can be seen that during the period before accumulator injection, the upper plenum within the span of LDP-113 fully drained. The start of rapid accumulator injection caused a refill to the elevation of the cold legs. Following the end of accumulator injection, the region of the upper plenum spanned by the LDP cell fully drained by [ ]^{a,b,c} seconds and remained so until IRWST injection supplied sufficient inventory to initiate a refill.

Figures 5.3.2-50 and 5.3.2-51 show that the upper head drained very rapidly during SB06, but maintained a collapsed liquid level until after the upper plenum drained. The upper head refilled slightly during accumulator injection, and again when IRWST injection was fully established, but otherwise remained drained during the short-term transient.

The mass of fluid and collapsed liquid level in the RPV downcomer are shown in Figures 5.3.2-41 and 5.3.2-42. The downcomer collapsed liquid level fell to the bottom of the cold-leg piping during the first [ ]^{a,b,c} seconds, where it remained until IRWST injection was fully established. At the time of rapid accumulator injection, there was evidence of splashing between the core and downcomer.

IRWST injection maintained the collapsed liquid level at the center of the cold legs. As in SB21, the downcomer level showed irregular oscillations. For SB06, these began at [ ]^{a,b,c} seconds, and continued until [ ]^{a,b,c} seconds. As in SB21, these may be indications of continued flow through the SG tubes. There is also evidence of splashing between the core and downcomer at this time, as well as between [ ]^{a,b,c} seconds.

5.3.2.2 Energy Transport from the Primary System

Following the break, energy was deposited in the primary system fluid by the heater rods to simulate decay heat and the primary system metal as it cools down. Some fluid energy was lost to ambient and out of the break. Energy must be removed from the primary system to prevent excessive fluid and heater rod temperature excursions. In the AP600 plant, heat removal is designed to be achieved by a combination of the SGs and the PRHR plus the ADS.

Steam Generator and Passive Residual Heat Removal Heat Transfer

During normal operation, most of the primary system heat was removed via the SGs; however, once the RCPs tripped, the reduced system flow caused a reduction in primary- to secondary-side heat transfer. The SGs were only available as heat sinks until the primary system pressure dropped to that of the secondary side, then the two sides were in thermal equilibrium. The PRHR is designed to remove heat from the primary system once the safety signal opens the isolation valve. The PRHR will continue to remove energy after the SGs are thermally isolated until ADS actuates. Once the ADS is actuated, it becomes the predominant path for the removal of energy from the primary system.

Figure 5.3.2-33 shows the SG primary- and secondary-side pressure together with the PRHR integrated heat transfer as represented by the IRWST fluid energy after allowing for the contribution from ADS 1-3 inflow. The SGs were potential sinks for primary system heat while the primary-side pressure was above that of the secondary side, that is before [ ]^{a,b,c} seconds. PRHR heat removal began [ ]^{a,b,c} seconds into the test and the PRHR was responsible for all the IRWST heat-up until ADS-1 activation. Following the actuation of the ADS, PRHR heat transfer continued for a further [ ]^{a,b,c} seconds. This was a distinct departure from the behavior observed in the smaller break cases. During the active phase, the PRHR transferred heat to the IRWST at an average rate of [ ]^{a,b,c} Btu/sec.

Energy Transport via the Break and Automatic Depressurization System

The mass flow rate from the primary system via the break is shown in Figures 5.3.2-67 and 5.3.2-68. During the first [ ]^{a,b,c} seconds following the break, nearly [ ]^{a,b,c} lbm of water appeared to flow out of the primary system via the break (Figure 5.3.2-62). As shown in Figure 5.3.2-71, there was no evidence for such a loss of primary system inventory from the mass balance. The apparent mass flow resulted from the indicated increase in break separator inventory caused by a rise in pressure above the

fluid in response to the opening of the break. The first [ ]^{a,b,c} seconds of Figures 5.3.2-67 and 5.3.2-68 should therefore be ignored as far as mass loss from the break is concerned.

Following initiation of ADS 1-3, flow through the break continued and was augmented by steam and liquid flow through the ADS 1-3 valves. Between [ ]^{a,b,c} and [ ]^{a,b,c} seconds, ADS 1-3 caused the system to depressurize rapidly and at [ ]^{a,b,c} seconds, ADS-4 was initiated and the primary system continued to depressurize to containment pressure.

Beyond [ ]^{a,b,c} seconds, there was continued flow through the break as cold-leg refill was occurring. Flow through the ADS continued at a declining rate until [ ]^{a,b,c} seconds when the flow through the ADS stages 1-3 terminated and was replaced by flow through the lower resistance ADS-4 paths for the rest of the short-term transient.

Integrated mass flow from the primary system via the ADS and the break is shown in Figure 5.3.2-62 and the corresponding integrated energy flow is shown in Figure 5.3.2-69. The total system inventory plot given in Figure 5.3.2-70 indicates that during the short-term transient up to [ ]^{a,b,c} lbm of inventory was lost as steam through the break. This is consistent with the quantity of steam measured flowing through the break (Figure 5.3.2-63).

TABLE 5.3.2-1
OSU TEST ANALYSIS STANDARD PLOT PACKAGE FOR SUBSECTION 5.3.2

Plot No.	Component	Variables	Units	Description
1	Pressurizer	CPT-604	psia	System pressure
2	RPV	RPVPWR	kW	Core power
3	RV	T01RPV, T08RPV, ST08RPV	°F	Core inlet/outlet temperature, saturation temperature
4	SG	CPT-201, CPT-204, CPT-301, CPT-302	psia	Primary and secondary pressures in SG
5	DVI-1	WWTDVIL1, WWTIRWI1, WOUTACC1, WWTIRWI3	lbm/sec.	Individual components and total flow in DVI-1
6	DVI-2	WWTDVIL2, WWTIRWI2, WOUTACC2, WWTIRWI4	lbm/sec.	Individual components and total flow in DVI-2
7	CMT	AMCMT1B, AMCMT2B	lbm	Fluid mass in CMTs (excludes balance lines)
8	CMT	CLDP-502, CLDP-507	in.	Collapsed liquid level in CMTs
9	CMT	MIWDVIL1, MIWDVIL2	lbm	Integrated mass out of CMTs
10	CMT	WWTDVIL1, WWTDVIL2	lbm/sec.	Flow out of CMTs
11	CMT	WOUTCLB1, WOUTCLB2	lbm/sec.	Flow into CMTs
12	CMT	CLDP-509, CLDP510	in.	Level CL-CMT balance lines
13	CMT	UCMT1, UCMT2	Btu	Fluid energy in CMTs
14	IRWST	IRWST	lbm	Mass of fluid in IRWST
15	IRWST	CLDP-701	in.	Collapsed liquid level in IRWST
16	IRWST	WWTIRWI1, WWTIRWI2	lbm/sec.	Flow from IRWST to DVI lines
17	IRWST	IRWSTOR	lbm/sec.	Overflow from IRWST to sump
18	IRWST	ADS13TMR	lbm/sec.	Total ADS flow into IRWST
19	IRWST	ADS13TIR, MIIRWI1, MIIRWI2, MIIRWIO	lbm	Integrated mass out of IRWST
20	IRWST	UIRWST	Btu	Fluid energy in IRWST
21	PRHR	CLDP-802	in.	Collapsed liquid level in PRHR HX

TABLE 5.3.2-1 (Continued) OSU TEST ANALYSIS STANDARD PLOT PACKAGE FOR SUBSECTION 5.3.2				
Plot No.	**Component**	**Variables**	**Units**	**Description**
22	PRHR	WWOTPRHR	lbm/sec.	Measured outlet flow from PRHR tube
23	Accumulator	AMACC1, AMACC2	lbm	Mass of fluid in accumulators
24	Accumulator	CLDP-401, CLDP-402	in.	Collapsed liquid level in accumulators
25	Accumulator	WOUTACC1, WOUTACC2	lbm/sec.	Flow from accumulators
26	Accumulator	MOUTACC1, MOUTACC2	lbm	Integrated mass out of accumulators
27	Accumulator	UACC1, UACC2	Btu	Fluid energy in accumulators
28	Primary sump	AMPSMP	lbm	Primary sump fluid mass
29	Primary sump	CLDP-901	in.	Primary sump level
30	Primary sump	UPSMP	Btu	Primary sump fluid energy
31	SG	MSSGIP1, MSSGIP2, MSSGOP1, MSSGOP2	lbm	Mass of fluid in SG primary side inlet/outlet plena
32	SG	MSSGHT1, MSSGHT2, MSSGCT1, MSSGCT2	lbm	Mass of fluid in SG primary side hot and cold tubes
33	SG/PRHR	CPT-201, CPT-301, QPRHR1	psia & Btu	SG1 pressure and PRHR integrated heat output
34	Pressurizer	PZM	lbm	Fluid mass in pressurizer
35	Pressurizer	CLDP-601	in.	Collapsed liquid level in pressurizer
36	Pressurizer	UPZ	Btu	Fluid energy in pressurizer
37	Surge line	PLM	lbm	Fluid mass in surge line
38	Surge line	CLDP-602	in.	Collapsed liquid level in surge line
39	Surge line	UPSL	Btu	Fluid energy in surge line
40	RPV	MWRPV	lbm	Total fluid mass in reactor vessel
41	RPV	DCM	lbm	Fluid mass in downcomer
42	RPV	LDP01DC	in.	Collapsed liquid level in downcomer compared to various reference elevations
43	RPV	MW01RPV	lbm	Fluid mass in lower plenum
44	RPV	MW03RPV	lbm	Fluid mass in core region
45	RPV	LDP03RPV	in.	Collapsed liquid level in core
46	RPV	RPVAVDF2		Core exit void fraction
47	RPV	RPVAQOU2		Core exit quality
48	RPV	MW06RPV	lbm	Fluid mass in the upper plenum
49	RPV	LDP06RPV	in.	Collapsed liquid level in the upper plenum
50	RPV	MW08RPV	lbm	Fluid mass in the upper head
51	RPV	LDP08RPV	in.	Collapsed liquid level in the upper head

TABLE 5.3.2-1 (Continued) OSU TEST ANALYSIS STANDARD PLOT PACKAGE FOR SUBSECTION 5.3.2				
Plot No.	**Component**	**Variables**	**Units**	**Description**
52	RPV	URPV	Btu	Total fluid energy in reactor vessel
53	RPV	RPVXE, RPVASL2	in.	Level of Tsat line
54	RPV	RPVPab, RPVAPab2, RPVPWR	kW	Heated rod power above and below Tsat level and total
55	RPV	RPVRXV, RPVASOU2	lbm/sec.	Core steam generation rate
56	RPV	RPVALIN2	lbm/sec.	Calculated core flow
57	RPV	HTMXRPV, ST08RPV	°F	Maximum clad temperature and saturation temperature
58	Hot leg	MWHL1, MWHL2	lbm	Water mass in hot legs
59	Hot leg	MVHL1, MVHL2	lbm	Vapor mass in hot legs
60	Cold leg	CL1WMS, CL2WMS, CL3WMS, CL4WMS	lbm	Water mass in cold legs
61	Cold leg	CL1VMS, CL2VMS, CL3VMS, CL4VMS	lbm	Vapor mass in cold legs
62	ADS and break	BRKSTIR, ADS13TIR, ADS41TIR, ADS42TIR	lbm	Total discharged mass for ADS 1-3, ADS-4s, and break
63	ADS and break	BRKTIVF, AD13TIVF, AD41TIVF, AD42TIVF	lbm	Total integrated vapor flow for ADS and break
64	ADS and break	BRKTILF, AD13TILF, AD41TILF, AD42TILF	lbm	Total integrated liquid flow for ADS and break
65	ADS and break	ADS13SVR, ADS41SVR, ADS42SVR	lbm/sec.	Vapor flow out ADS 1-3 and ADS-4
66	ADS and break	ADS13SLR, ADS41SLR, ADS42SLR	lbm/sec.	Liquid flow out ADS 1-3 and ADS-4
67	ADS and break	BRKSSVR	lbm/sec.	Vapor flow out of break
68	ADS and break	BRKSSLR	lbm/sec.	Liquid flow out of break
69	ADS and break	BRKSPEI, ADS13EI, ADS41EI, ADS42EI	Btu	Integrated fluid energy for ADS 1-3, ADS-4, and break
70	Mass balance	TOTMASS	lbm	Total system mass inventory
71	Mass balance	PRIMMASS, PRIMASS2	lbm	Measured primary system inventory and value from mass balance
72	Mass balance	MERROR	lbm	Mass balance error
73	Mass balance	MIN, MOUT SRCMASS	lbm	Integrated mass flow in and out of primary system and source mass
74	Energy balance	Various	Btu	Components of energy balance

THE FIGURES LISTED IN TABLE 5.3.2-1
ARE NOT INCLUDED IN THIS NONPROPRIETARY DOCUMENT

5.3.3 Long-Term Transient

The long-term transient started with initiation of IRWST injection, covers the transition from IRWST to sump injection, and provides information on the long-term cooling response of the AP600 plant. For the large cold-leg break, Matrix Test SB06, the long-term transient analyzed runs from [ ]^{a,b,c} seconds to the end of the test at near [ ]^{a,b,c} seconds. The behavior of the test facility during this period of the transient is discussed in this subsection using the plot package detailed in Table 5.3.3-1. This analysis concentrates on the components of the primary system that remained active during the long-term cooling phase, that is, the RPV, the hot legs, ADS-4, the sumps, and the IRWST.

During the long-term transient, the main thermal-hydraulic phenomena of interest were:

- Maintenance of core cooling and removal of energy from the primary system.
- Level oscillations (from [ ]^{a,b,c} seconds, there were system-wide level and pressure oscillations, which are discussed further in Subsection 6.1.3).

5.3.3.1 Maintenance of Core Cooling

Mass Injected into Primary System

Total DVI line flow, CMT flow and IRWST flows are shown in Figures 5.3.3-6 and 5.3.3-7 and the flow from the primary sump is shown in Figure 5.3.3-19. From around [ ]^{a,b,c} seconds, there was a contribution to the DVI flow from the CMTs as the CMTs reached post-refill draindown.

During the IRWST injection phase of the transient, IRWST flow proceeded at a gradually declining rate with the effect of the primary system oscillations superimposed. At [ ]^{a,b,c} seconds, flow from the primary sump began through check valves around the main injection valves. This caused the IRWST flow to cease. The test was not continued to the point where the IRWST level fell to the low-low setpoint and thus, the main sump injection valves were not actuated.

Reactor Pressure Vessel and Downcomer Response

The effect of the water inflow on the average measured downcomer fluid temperatures, core inlet and core outlet temperatures, and peak clad temperatures during the long-term phase of the transient is shown in Figures 5.3.3-4, 5.3.3-5, and 5.3.3-38. Figure 5.3.3-4 shows that there is a general increase in average downcomer fluid temperatures during the long-term transient. By the end of the test, this average temperature reached an equilibrium [ ]^{a,b,c} °F below saturation. Figure 5.3.3-5 shows that the core average outlet fluid temperature remained at saturation during the long-term transient. Figures 5.3.3-34 to 5.3.3-36 show that the DVI line flow method discussed in Section 4.11 indicates that a small level of boiling was maintained throughout the long-term transient. Nevertheless, the level

of boiling was small and the test results showed that the inflow from the IRWST was sufficient to maintain cooling.

Figure 5.3.3-38 shows that throughout the long-term transient there were no significant excursions in heater rod temperatures; therefore, sufficient core inventory and flow was maintained through this phase of the transient to remove the decay heat generated. For significant portions of the transient, a two-phase mixture was present in the core and upper plenum regions. The following discussion tracks the variation in water level and mass throughout the RPV and downcomer.

Mass and level for the core region are shown in Figures 5.3.3-28 and 5.3.3-29. The collapsed liquid level in the core indicated that the heater rods were always covered with a single- or two-phase mixture. During the initial core oscillations, the maximum core void fraction was [ ],[a,b,c] and for much of the transient the average core void fraction was [ ].[a,b,c] During the long-term transient represented, the calculated steam generation rate maintained an average value of around [ ][a,b,c] lbm/sec. (Figure 5.3.3-36).

The collapsed liquid level in the upper plenum region covered by LDP-113, is shown in Figure 5.3.3-32. For the entire long-term transient, the average collapsed liquid level was at, or above, the hot-leg elevation. The effect of the oscillations during the long term transient were observed.

The mass of water in the RPV is shown in Figure 5.3.3-25. For the entire long-term transient, the RPV water mass remained at an average value of [ ][a,b,c] lbm, which is [ ][a,b,c] percent of the initial vessel water inventory. From [ ][a,b,c] seconds, oscillations in vessel inventory were observed. Figures 5.3.3-51 to 5.3.3-56 illustrate these oscillations using plots on a restricted time frame from [ ][a,b,c] seconds. These oscillations are observed in primary system measurements from the upper plenum to the ADS-4 flows. The oscillations occurred with a period of about [ ][a,b,c] seconds. The oscillations in the ADS flow lagged behind those in the upper head pressure. These oscillations and possible mechanisms for their production are discussed further in Subsection 6.1.3.

The mass of fluid and collapsed liquid level in the RPV downcomer are shown in Figures 5.3.3-26 and 5.3.3-27. The collapsed liquid level remained above the cold legs until the end of the test. Until [ ][a,b,c] seconds, there were irregular oscillations which may be related to continued steam flow and core to downcomer splashing.

5.3.3.2 Energy Transport from the Primary System

During the long-term transient, energy continued to be deposited in the primary system from the heater rods, metal and fluid flowing from the primary sump. The SGs and PRHR remained inactive throughout this phase of the transient, and the primary path for energy out of the primary system was via the ADS-4 valves.

Integrated mass flow from the primary system via the ADS and the break is shown in Figure 5.3.3-43. This figure shows that during the LTC phase of the transient, the only significant energy outflows are through the ADS-4 valves and, until [ ]^{a,b,c} seconds, the break. This is confirmed by Figures 5.3.3-44 to 5.3.3-45, which show flow through the ADS and break. After [ ]^{a,b,c} seconds, there was reverse flow through the break as is indicated by the reducing integrated flow shown in Figure 5.3.3-43.

Figure 5.3.3-36 shows the calculated steam generation rate as determined by the DVI line flow method. During the long-term transient, steam was being generated at an average rate of [ ]^{a,b,c} lbm/sec., although the steam vortex meters indicate little or no flow out of the ADS-4 valves. However, examination of the fluid thermocouples on the outlet of both the ADS-4 valves indicated that they reached saturation temperature during much of the transient after [ ]^{a,b,c} seconds. Furthermore, it can be concluded from the discussion in Subsection 6.1.3 that it was not possible for all the steam generated in the core to flow from the upper head to the downcomer via the bypass holes. It can therefore be concluded that steam was leaving the primary system via the ADS-4 valves although the steam vortex meters did not measure any steam flow.

Figure 5.3.3-50 shows all the components contributing to the system energy balance. Further discussion of steam loss from the primary system is provided in the mass and energy balance discussions of Section 6.2.

TABLE 5.3.3-1
OSU TEST ANALYSIS STANDARD PLOT PACKAGE FOR SUBSECTION 5.3.3
LONG-TERM TRANSIENT

Plot No.	Component	Variables	Units	Description
1	RPV	RPVPWR	kW	Core power
2	Primary sump	TSMPI1, TSMPI2	°F	Sump injection line temperatures
3	DVI	TDVIL1, TDVIL2	°F	DVI line temperatures
4	RPV	T01DC, T02DC, T03DC, ST01DC	°F	Water and saturation temperatures in downcomer
5	RPV	T01RPV, T08RPV, ST08RPV	°F	Core inlet/outlet temperature, saturation temperature
6	DVI-1	WWTDVIL1, WWTIRWI1, WWTIRWI3	lbm/sec.	Individual components and total flow in DVI-1
7	DVI-2	WWTDVIL2, WWTIRWI2, WWTIRWI4	lbm/sec.	Individual components and total flow in DVI-2
8	CMT	CLDP-502, CLDP-507	in.	Collapsed liquid level in CMTs
9	CMT	CLDP-509, CLDP510	in.	Level CL-CMT balance lines
10	IRWST	IRWST	lbm	Mass of fluid in IRWST
11	IRWST	CLDP-701	in.	Collapsed liquid level in IRWST
12	IRWST	UIRWST	Btu	Fluid energy in IRWST
13	Primary sump	AMPSMP	lbm	Primary sump fluid mass
14	Primary sump	CLDP-901	in.	Primary sump level
15	Primary sump	UPSMP	Btu	Primary sump fluid energy
16	Secondary sump	AMSSMP	lbm	Secondary sump fluid mass
17	Secondary sump	CLDP-902	in.	Secondary sump level
18	Secondary sump	USSMP	Btu	Secondary sump fluid energy
19	Primary sump	WSTSMPET, WWTSMPIT	lbm/sec.	Primary sump steam and liquid injection rate
20	Primary sump	MISMPI1, MISMPI2, MISMPIT, MIIRWT	lbm	Integrated primary sump and IRWST flows
21	SG	MSSGIP1, MSSGIP2, MSSGOP1, MSSGOP2	lbm	Mass of fluid in SG side inlet/outlet plena
22	Surge line	PLM	lbm	Fluid mass in surge line
23	Surge line	CLDP-602	in.	Collapsed liquid level in surge line
24	Surge line	UPSL	Btu	Fluid energy in surge line
25	RPV	MWRPV	lbm	Total fluid mass in reactor vessel

TABLE 5.3.3-1 (Continued)
OSU TEST ANALYSIS STANDARD PLOT PACKAGE FOR SUBSECTION 5.3.3
LONG-TERM TRANSIENT

Plot No.	Component	Variables	Units	Description
26	RPV	DCM	lbm	Fluid mass in downcomer
27	RPV	LDP01DC	in.	Collapsed liquid level in downcomer compared to various reference elevations
28	RPV	MW03RPV	lbm	Fluid mass in core region
29	RPV	LDP03RPV	in.	Collapsed liquid level in core
30	RPV	RPVAVDF2		Core exit void fraction
31	RPV	RPVAQOU2		Core exit quality
32	RPV	LDP06RPV	in.	Collapsed liquid level in the upper plenum
33	RPV	MW08RPV	lbm	Fluid mass in the upper head
34	RPV	RPVASL2	in.	Level of Tsat line
35	RPV	RPVAPab2, RPVPWR	kW	Heated rod power above and below Tsat level and total
36	RPV	RPVASOU2	lbm/sec.	Core steam generation rate
37	RPV	RPVALIN2	lbm/sec.	Calculated core flow
38	RPV	HTMXRPV, ST08RPV	°F	Maximum clad temperature, saturation temperature and delta
39	Hot leg	MWHL1, MWHL2	lbm	Water mass in hot legs
40	Hot leg	MVHL1, MVHL2	lbm	Vapor mass in hot legs
41	Cold leg	CL1WMS, CL2WMS, CL3WMS, CL4WMS	lbm	Water mass in cold legs
42	Cold leg	CL1VMS, CL2VMS, CL3VMS, CL4VMS	lbm	Vapor mass in cold legs
43	ADS and break	BRKSTIR, ADS13TIR, ADS41TIR, ADS42TIR	lbm	Total discharged mass for ADS 1-3, ADS-4, and break
44	ADS and break	ADS13TLR, ADS41TLR, ADS42TLR	lbm/sec.	Liquid flow out ADS 1-3 and ADS-4
45	ADS and break	BRKSTLR	lbm/sec.	Liquid flow and total flow out of break
46	Mass balance	TOTMASS	lbm	Total system mass inventory
47	Mass balance	PRIMMASS, PRIMASS2	lbm	Measured primary system inventory and valve from mass balances
48	Mass balance	MERROR	lbm	Mass balance error
49	Mass balance	MIN, MOUT SRCMASS	lbm	Integrated mass flow in and out of primary system and source mass
50	Energy balance	Various	Btu	Component of energy balance
51	ADS-4	ADS41TLR, ADS42TLR	lbm/sec.	Oscillations in ADS-4 liquid flow
52	Surge line	CLDP-602	in.	Oscillations in surge line level

TABLE 5.3.3-1 (Continued)
OSU TEST ANALYSIS STANDARD PLOT PACKAGE FOR SUBSECTION 5.3.3
LONG-TERM TRANSIENT

Plot No.	Component	Variables	Units	Description
53	RPV	CPT-107	psia	Oscillations in upper head pressure
54	RPV	CLDP-113	in.	Oscillations in upper plenum level
55	RPV	LDP03RPV	in.	Oscillations in core level
56	RPV	LDP01DC	in.	Oscillations in downcomer level

THE FIGURES LISTED IN TABLE 5.3.3-1
ARE NOT INCLUDED IN THIS NONPROPRIETARY DOCUMENT

5.4 Analysis of Matrix Test SB09

Matrix Test SB09 (OSU Test U0009) simulated a 2-in. LOCA in the CL-3 to CMT-1 balance line with LTC and without the operation of the nonsafety-related systems. The break was located on the horizontal section of the balance line before the vertical rise to CMT-1. Except for the break location, this test was similar to SB01, including the simulated failure of one of the ADS-4 lines. Changes to the OSU facility since the performance of SB01 are noted in the Final Data Report.[1]

The analysis of Matrix Test SB09 is divided into three subsections as follows:

- Facility performance is discussed in Subsection 5.4.1. It provides a brief outline of the response of the test facility; further details are available in the Final Data Report.[1]

- The short-term transient for SB09 encompassed the start of the simulation up to [ ]^{a,b,c} seconds. This period included the blowdown, natural circulation, ADS, and initial IRWST stages of the transient.

- The analysis of the long-term transient for SB09 encompassed the time frame from [ ]^{a,b,c} seconds to the end of the test. This phase of the transient includes the IRWST injection and covers the transition to sump injection. The long-term transient actually started at IRWST injection, which is discussed as part of the short-term transient. Between the end of the short-term transient and [ ]^{a,b,c} seconds, the system remained relatively inactive with the exception of the CMT-2 refill. At [ ]^{a,b,c} seconds, CMT-2 began to refill; CMT-1 [ ]^{a,b,c} during the SB09 transient. CMT refill phenomena are discussed further in Subsection 6.1.1, and the discussion of the long-term transient provided here begins at [ ]^{a,b,c} seconds.

The discussion of the short- and long-term phase of the transient focuses on important thermal-hydraulic phenomena identified in the PIRT (Table 1.3-1). Key indicators of the quality of the analysis on which this discussion is based are the mass and energy balance results. These are discussed in detail in Subsections 6.2.2 and 6.2.3.

5.4.1 Facility Performance

The performance of the OSU test facility during Matrix Test SB09 in reference to the five transient phases is outlined in the following:

- Blowdown
- Natural circulation
- ADS
- IRWST injection
- Sump injection

The overall performance of the facility during the transient is shown in Figures 5.4.1-1 to 5.4.1-4. Figure 5.4.1-1 shows the pressurizer pressure throughout the test with various phases and operating components delineated on the figure. The time scale was reduced for clarity since there were only small changes in system pressure during the long-term phase of the transient. Figure 5.4.1-2 shows the total DVI line flow and its composition from the various sources at each time in the transient. Figure 5.4.1-3 shows the calculated core steam generation rate throughout the test. Figure 5.4.1-4 shows the variation in average measured core outlet temperature and peak clad temperature relative to the core outlet saturation temperature.

Figures 5.4.1-1 and 5.4.1-2 show that there was a continuous flow of water to the core from the passive safety-related systems throughout the transient. Once initiated, the ADS lines rapidly depressurized the primary system, enhancing the CMT and accumulator injection flow rates. Ultimately, the ADS-4 valves reduced the system pressure sufficiently to start gravity-driven IRWST injection. The passive injection systems operation overlapped so that as one source of water drained the next was available to continue the cooling process. The level of steam generation in the core and the response of the average measured core outlet fluid temperatures and maximum clad temperatures are shown in Figures 5.4.1-3 and 5.4.1-4. These figures show that the cooling flow prevented core heatup, and the core remained covered. The core remained subcooled for large periods of the transient. When steam was produced, the rate of generation remained well below the rate at which water was delivered to the core.

5.4.1.1 Blowdown Phase

The blowdown phase began at time zero when the break was initiated and continued until the primary circuit pressure is in equilibrium with the secondary-side pressure at around [ ]^{a,b,c} seconds. During this phase of the transient, cooling flow was provided from the intact CMT, while the CMT with a broken balance line injected very little mass. CMT-2 remained in the recirculation mode until almost the end of this phase, and heat was removed from the primary circuit via the SGs. The pressurizer and surge line completely drained at [ ]^{a,b,c} and [ ]^{a,b,c} seconds, respectively.

5.4.1.2 Natural Circulation Phase

In this LOCA simulation, the single- and two-phase natural circulation phase initially continued the gradual reduction in system pressure characteristic of blowdown; later on in this phase of the transient, the rate of depressurization increased significantly once all the SG tubes had drained at about [ ]^{a,b,c} seconds. The tubes in SG-2 in the nonbalance line loop completed draining almost [ ]^{a,b,c} seconds later than those in SG-1. After [ ]^{a,b,c} seconds, heat removal from the primary circuit continued via the PRHR and the break. In response to the enhanced depressurization rate, CMT-2 transitioned into a rapid draindown at [ ]^{a,b,c} seconds, and the falling CMT level reached the ADS low-level setpoint so that the ADS-1 valve began to open at [ ]^{a,b,c} seconds. By [ ]^{a,b,c} seconds, both accumulators began to inject.

5.4.1.3 Automatic Depressurization System Phase

ADS-1 actuation was followed by ADS-2 and ADS-3 [ ]^{a,b,c} and [ ]^{a,b,c} seconds later. An increased accumulator injection rate was observed with initiation of ADS-2. The influx of cold water combined with increased venting via the ADS led to an even more rapid depressurization of the primary system. Actuation of ADS-4 at [ ]^{a,b,c} seconds completed the depressurization to the extent that the IRWST began injecting at [ ]^{a,b,c} seconds via DVI-2 and [ ]^{a,b,c} seconds via DVI-1. During the rapid accumulator injection, increased flow path resistance reduced flow out of CMT-2 and stopped flow out of CMT-1. CMT flow resumed at rates approaching [ ]^{a,b,c} lbm/sec. as the accumulators drained. Because the CMT-1 balance line contained the break, CMT-1 injection was delayed and overlapped with IRWST-2 injection for more than [ ]^{a,b,c} seconds. CMT-1 flow continued concurrently with in [ ]^{a,b,c} seconds of IRWST-1 injection. The minimum RPV mass inventory of [ ]^{a,b,c} lbm occurred just before IRWST injection began.

Actuation of ADS-1 and ADS-2 rapidly refilled the pressurizer as water and steam flowed out of the ADS. The pressurizer gradually drained by [ ]^{a,b,c} seconds.

5.4.1.4 In-Containment Refueling Water Storage Tank Injection

IRWST injection signals the transition from the short- to long-term phase of the transient. Initially, IRWST injection was delivered solely through the IRWST-2 DVI line with flow gradually increasing as the driving head between the IRWST and the RCS increased. The pressure differential increased because RCS pressure decreased as the core steam generation decreased from [ ]^{a,b,c} lbm/sec. at IRWST-2 initiation to zero at [ ]^{a,b,c} seconds. The maximum IRWST flow was established shortly thereafter, then it gradually decreased with the decrease in pressure differential as the IRWST continued to drain. The influx of water from the IRWST was enough to keep the core subcooled until [ ]^{a,b,c} seconds. Steam was subsequently generated in the core for the remainder of the transient. Following the restart of core steam generation, IRWST injection between [ ]^{a,b,c} seconds was marked by oscillations in pressure and level throughout the primary system. These oscillations were also observed in the ADS-4 liquid flow rates.

5.4.1.5 Sump Injection

Sump flow began at [ ]^{a,b,c} seconds through the check valves around the main sump injection valve when the driving head from the sump was sufficient for flow to initiate in DVI-2. Sump injection through DVI-1 began to enter the IRWST once the main sump injection valves opened; at that time DVI-2 exhibited a corresponding increase in flow out of the IRWST, which meant that there was no increase in IRWST inventory. Flow through the main sump injection valves began when those valves opened at about [ ]^{a,b,c} seconds.

TABLE 5.4.1-1 OSU TEST ANALYSIS PLOT PACKAGE FOR SUBSECTION 5.4.1				
Plot No.	**Component**	**Variables**	**Units**	**Description**
1	Pressurizer	CPT-604	psia	System pressure and event history
2	Water injection	WWTDVI1+WWTDVI2, WOUTACC1+WOUTACC2, WWTIRWI1+WWTIRWI2, WWTSMPIT	lbm/sec.	Total of CMT, accumulator, IRWST, and sump injection flows
3	Reactor vessel	RPVASOU2	lbm/sec.	Steam generation in reactor vessel
4	Reactor vessel	T08RPV, HTMXRPV, TSAT	°F	Reactor vessel outlet temperature, maximum clad temperature and fuel exit saturation temperature

THE FIGURES LISTED IN TABLE 5.4.1-1
ARE NOT INCLUDED IN THIS NONPROPRIETARY DOCUMENT

5.4.2 Short-Term Transient

For the 2-in. balance line break LOCA simulation, Matrix Test SB09, the short-term transient encompassed the time frame up to 3000 seconds. As shown in Figure 5.4.1-1, this period included full depressurization of the facility through all four stages of the ADS, together with CMT and accumulator injection plus the initial stages of IRWST injection. The variation in mass, energy, pressure, and temperature throughout this stage of the transient are illustrated in the plot package outlined in Table 5.4.2-1. The plots concentrate on the primary system, including the accumulators, CMTs, IRWST, primary sump and flows from the primary system via the ADS, break, and IRWST overflow.

There were two principal parameters to be examined for the short-term transient:

- Adequate flow from the passive systems to the reactor vessel must be maintained.
- Adequate flow into the core must be maintained to ensure that decay heat was removed from the simulated fuel rods, without a temperature excursion.

These parameters are addressed in the following discussion.

5.4.2.1 Maintenance of Core Cooling

Mass Injected to the Primary System

Figures 5.4.2-6 and 5.4.2-7 show the combined effect of the injection flows for the short-term phase of the transient. Separate plots of the individual contributions to the total flow can be located by consulting the plot package index given in Table 5.4.2-1.

Figures 5.4.2-5 and 5.4.2-6 show how the CMTs, accumulators, and IRWST supplied a continuous flow of water to the core. During the first [ ]^{a,b,c} seconds, cooling flow was provided primarily by CMT-2, since CMT-1 flow was severely limited by the break in its balance line. By [ ]^{a,b,c} seconds, CMT flow was supplemented by flow from both accumulators. The rate of flow from the CMTs was reduced or stopped by accumulator injection. Accumulator flow produced maximum DVI injection rates during the entire transient with values of [ ]^{a,b,c} lbm/sec. and above in each DVI line. Following the end of accumulator injection, the CMTs again provided cooling flow. Because CMT-1 was still almost full at the end of accumulator injection, it provided greater flow than CMT-2 through the remainder of the CMT drain period. While CMT-2 emptied [ ]^{a,b,c} seconds before the flow from IRWST-2 began, CMT-1 was still injecting at a rate of [ ]^{a,b,c} lbm/sec. so continuous injection was maintained. IRWST-1 injection began [ ]^{a,b,c} seconds before the CMT-1 draindown completed. Since continuous IRWST injection through both DVI lines began before CMT-2 had fully drained, there was no period of the short-term transient when the passive safety systems failed to provide flow to the RPV.

Reactor Pressure Vessel and Downcomer Behavior

The effect of water flow on the average measured core inlet/outlet temperatures and peak clad temperatures during the short-term phase of the transient is shown in Figures 5.4.2-3 and 5.4.2-57. The core outlet temperature first reached the saturation point at [ ]^{a,b,c} seconds. The core outlet fluid temperature became subcooled again returning to the saturation level for the period between [ ]^{a,b,c} seconds, after which, the influx of water from the accumulators kept the core subcooled until [ ]^{a,b,c} secs. At [ ]^{a,b,c} seconds, the influx of water from the IRWST was sufficient to subcool the core again. The core then remained subcooled until the end of the short-term transient.

Figure 5.4.2-57 shows that there were no significant excursions in heated rod temperatures throughout the short-term transient, therefore, sufficient core inventory and flow were maintained through this phase of the transient to remove the decay heat generated. For significant portions of the transient, a two-phase mixture was present in the core and upper plenum regions, with core boiling kept at a low level.

The following discussion tracks the variation in water level and mass throughout the reactor vessel and downcomer. The mass and level for the core region are shown in Figures 5.4.2-44 and 5.4.2-45. The collapsed liquid level in the core indicates that the heated rods remained covered with a single- or two-phase mixture throughout the short-term transient. The minimum core inventory of [ ]^{a,b,c} lbm occurred at about [ ]^{a,b,c} seconds into the transient before the initial accumulator injection was fully established. As shown in Figure 5.4.2-45, the collapsed liquid level dropped to [ ]^{a,b,c} in. below the top of the heated rod length during this phase of the transient. The average void fraction of the core two-phase mixture may be estimated by dividing the measured core collapsed liquid level by the [ ]^{a,b,c} in. heated rod length. In this test, the minimum collapsed liquid level corresponded to a core void fraction of [ ].^{a,b,c} By the end of the short-term transient, the effect of IRWST injection ended core boiling (Figure 5.4.2-55), and the core was again water-solid.

The collapsed liquid level in the upper plenum region and the associated fluid mass are shown in Figures 5.4.2-49 and 5.4.2-48. Figures 5.4.2-50 and 5.4.2-51 show that the upper head had only partially drained while accumulator injection and ADS-1 actuation occurred; then it rapidly refilled by about [ ]^{a,b,c} in. during Matrix Test SB09. The upper head resumed draining and refilled later in the short-term transient during maximum IRWST injection.

The mass of fluid and collapsed liquid level in the RPV downcomer are shown in Figures 5.4.2-41 and 5.4.2-42. The downcomer collapsed liquid level fell to the bottom of the cold-leg piping during the first [ ]^{a,b,c} seconds. IRWST injection maintained the collapsed liquid level within the cold-leg pipe perimeter after [ ]^{a,b,c} seconds in the transient.

5.4.2.2 Energy Transport from the Primary System

Following the break, energy was deposited in the primary circuit fluid by the heater rods to simulate decay heat and by the primary circuit metal as it cooled down. Some fluid energy was lost to the atmosphere and out of the break. Excess energy must be removed from the primary system to prevent excessive fluid and heater rod temperature excursions. The AP600 is designed to remove heat by a combination of the SGs and the PRHR plus the ADS.

Steam Generator and Passive Residual Heat Removal Heat Transfer

During normal operation, most of the primary system heat was removed via the SGs; however, once the RCPs tripped, the reduced system flow decreased primary-to-secondary side heat transfer. The SGs were only available as heat sinks until the primary system pressure dropped to that of the secondary side; afterward, the two sides were then in thermal equilibrium. The PRHR is designed to remove heat from the primary system, once the safety signal opens the isolation valve. The PRHR continued to remove energy after the SGs were thermally isolated until ADS actuated. Once ADS actuated, ADS 1-3 became the predominant path for the removal of energy from the primary circuit.

Figure 5.4.2-33 shows the SG pressure equalization together with the PRHR integrated heat transfer as represented by the IRWST fluid energy after allowing for the contribution from ADS 1-3 inflow. As shown, heat was transferred to the secondary side of the SGs for only the first [ ]^{a,b,c} seconds. PRHR heat removal began [ ]^{a,b,c} seconds into the test, and the PRHR was responsible for all the IRWST heat-up until ADS-1 activation, after which the PRHR heat transfer was significantly reduced. During the natural circulation phase, the PRHR transferred heat to the IRWST at an average rate of [ ]^{a,b,c} Btu/sec.

Energy Transport via the Break and Automatic Depressurization System

The mass flow rate from the primary system via the break is shown in Figures 5.4.2-67 and 5.4.2-68. During the first [ ]^{a,b,c} seconds, break flow rose to a maximum value of over [ ]^{a,b,c} lbm/sec. of water, then diminished as system pressure fell. At [ ]^{a,b,c} seconds, mass appeared to flow out of the primary circuit via the break (Figure 5.4.2-62) at an increased rate. Figure 5.4.2-71 shows the same trend. Apparently, this mass flow increase resulted from a decrease in the enthalpy of the fluid exiting the break.

Following initiation of ADS 1-3, flow through the break dropped greatly as steam and liquid flow through the ADS 1-3 valves became the primary mass release path. Between [ ]^{a,b,c} and [ ]^{a,b,c} seconds, ADS 1-3 caused the system to depressurize rapidly at [ ]^{a,b,c} seconds, ADS-4 was initiated and the primary system continued its depressurization to the BAMS header pressure.

Beyond [ ]^{a,b,c} seconds, there was continued flow through the break as cold leg refill was occurring due to accumulator injection. Liquid flow through the break in the balance line continued at a

declining rate until [ ]^{a,b,c} seconds, the flow through the break was then minimal for the rest of the short-term transient.

Integrated mass flow from the primary system via the ADS and the break is shown in Figure 5.4.2-62. The corresponding integrated energy flow is shown in Figure 5.4.2-69. The total system inventory plot given in Figure 5.4.2-70 indicates that only [ ]^{a,b,c} lbm of inventory left the system during the short-term transient. Components of the energy balance are shown in Figure 5.4.2-74.

TABLE 5.4.2-1
OSU TEST ANALYSIS STANDARD PLOT PACKAGE FOR SUBSECTION 5.4.2

Plot No.	Component	Variables	Units	Description
1	Pressurizer	CPT-604	psia	System pressure
2	RPV	RPVPWR	kW	Core power
3	RPV	T01RPV, T08RPV, ST08RPV	°F	Core inlet/outlet temperature, saturation temperature
4	SG	CPT-201, CPT-204, CPT-301, CPT-302	psia	Primary and secondary pressures in SG
5	DVI-1	WWTDVIL1, WWTIRWI1, WOUTACC1, WWTIRWI3	lbm/sec.	Individual components and total flow in DVI-1
6	DVI-2	WWTDVIL2, WWTIRWI2, WOUTACC2, WWTIRWI4	lbm/sec.	Individual components and total flow in DVI-2
7	CMT	AMCMT1B, AMCMT2B	lbm	Fluid mass in CMTs (excludes balance lines)
8	CMT	CLDP-502, CLDP-507	in.	Collapsed liquid level in CMTs
9	CMT	MIWDVIL1, MIWDVIL2	lbm	Integrated mass out of CMTs
10	CMT	WWTDVIL1, WWTDVIL2	lbm/sec.	Flow out of CMTs
11	CMT	WOUTCLB1, WOUTCLB2	lbm/sec.	Flow into CMTs
12	CMT	CLDP-509, CLDP510	in.	Level CL-CMT balance lines
13	CMT	UCMT1, UCMT2	Btu	Fluid energy in CMTs
14	IRWST	IRWST	lbm	Mass of fluid in IRWST
15	IRWST	CLDP-701	in.	Collapsed liquid level in IRWST
16	IRWST	WWTIRWI1, WWTIRWI2	lbm/sec.	Flow from IRWST to DVI lines
17	IRWST	IRWSTOR	lbm/sec.	Overflow from IRWST to sump
18	IRWST	ADS13TMR	lbm/sec.	Total ADS flow into IRWST
19	IRWST	ADS13TIR, MIIRWI1, MIIRWI2, MIIRWIO	lbm	Integrated mass out of IRWST
20	IRWST	UIRWST	Btu	Fluid energy in IRWST
21	PRHR	CLDP-802	in.	Collapsed liquid level in PRHR HX

TABLE 5.4.2-1 (Continued) OSU TEST ANALYSIS STANDARD PLOT PACKAGE FOR SUBSECTION 5.4.2				
Plot No.	**Component**	**Variables**	**Units**	**Description**
22	PRHR	WWOTPRHR	lbm/sec.	Measured outlet flow from PRHR tube
23	Accumulator	AMACC1, AMACC2	lbm	Mass of fluid in accumulators
24	Accumulator	CLDP-401, CLDP-402	in.	Collapsed liquid level in accumulators
25	Accumulator	WOUTACC1, WOUTACC2	lbm/sec.	Flow from accumulators
26	Accumulator	MOUTACC1, MOUTACC2	lbm	Integrated mass out of accumulators
27	Accumulator	UACC1, UACC2	Btu	Fluid energy in accumulators
28	Primary sump	AMPSMP	lbm	Primary sump fluid mass
29	Primary sump	CLDP-901	in.	Primary sump level
30	Primary sump	UPSMP	Btu	Primary sump fluid energy
31	SG	MSSGIP1, MSSGIP2, MSSGOP1, MSSGOP2	lbm	Mass of fluid in SG primary side inlet/outlet plena
32	SG	MSSGHT1, MSSGHT2, MSSGCT1, MSSGCT2	lbm	Mass of fluid in SG primary side hot and cold tubes
33	SG/PRHR	CPT-201, CPT-301, QPRHR1	psia & Btu	SG1 pressure and PRHR integrated heat output
34	Pressurizer	PZM	lbm	Fluid mass in pressurizer
35	Pressurizer	CLDP-601	in.	Collapsed liquid level in pressurizer
36	Pressurizer	UPZ	Btu	Fluid energy in pressurizer
37	Surge line	PLM	lbm	Fluid mass in surge line
38	Surge line	CLDP-602	in.	Collapsed liquid level in surge line
39	Surge line	UPSL	Btu	Fluid energy in surge line
40	RPV	MWRPV	lbm	Total fluid mass in reactor vessel
41	RPV	DCM	lbm	Fluid mass in downcomer
42	RPV	LDP01DC	in.	Collapsed liquid level in downcomer compared to various reference elevations
43	RPV	MW01RPV	lbm	Fluid mass in lower plenum
44	RPV	MW03RPV	lbm	Fluid mass in core region
45	RPV	LDP03RPV	in.	Collapsed liquid level in core
46	RPV	RPVAVDF2		Core exit void fraction
47	RPV	RPVAQOU2		Core exit quality
48	RPV	MW06RPV	lbm	Fluid mass in the upper plenum
49	RPV	LDP06RPV	in.	Collapsed liquid level in the upper plenum
50	RPV	MW08RPV	lbm	Fluid mass in the upper head
51	RPV	LDP08RPV	in.	Collapsed liquid level in the upper head

TABLE 5.4.2-1 (Continued) OSU TEST ANALYSIS STANDARD PLOT PACKAGE FOR SUBSECTION 5.4.2				
Plot No.	**Component**	**Variables**	**Units**	**Description**
52	RPV	URPV	Btu	Total fluid energy in reactor vessel
53	RPV	RPVXE, RPVASL2	in.	Level of Tsat line
54	RPV	RPVPab, RPVAPab2, RPVPWR	kW	Heated rod power above and below Tsat level and total
55	RPV	RPVRXV, RPVASOU2	lbm/sec.	Core steam generation rate
56	RPV	RPVALIN2	lbm/sec.	Calculated core flow
57	RPV	HTMXRPV, ST08RPV	°F	Maximum clad temperature and saturation temperature
58	Hot leg	MWHL1, MWHL2	lbm	Water mass in hot legs
59	Hot leg	MVHL1, MVHL2	lbm	Vapor mass in hot legs
60	Cold leg	CL1WMS, CL2WMS, CL3WMS, CL4WMS	lbm	Water mass in cold legs
61	Cold leg	CL1VMS, CL2VMS, CL3VMS, CL4VMS	lbm	Vapor mass in cold legs
62	ADS and break	BRKSTIR, ADS13TIR, ADS41TIR, ADS42TIR	lbm	Total discharged mass for ADS 1-3, ADS-4s, and break
63	ADS and break	BRKTIVF, AD13TIVF, AD41TIVF, AD42TIVF	lbm	Total integrated vapor flow for ADS and break
64	ADS and break	BRKTILF, AD13TILF, AD41TILF, AD42TILF	lbm	Total integrated liquid flow for ADS and break
65	ADS and break	ADS13SVR, ADS41SVR, ADS42SVR	lbm/sec.	Vapor flow out ADS 1-3 and ADS-4
66	ADS and break	ADS13SLR, ADS41SLR, ADS42SLR	lbm/sec.	Liquid flow out ADS 1-3 and ADS-4
67	ADS and break	BRKSSVR	lbm/sec.	Vapor flow out of break
68	ADS and break	BRKSSLR	lbm/sec.	Liquid flow out of break
69	ADS and break	BRKSPEI, ADS13EI, ADS41EI, ADS42EI	Btu	Integrated fluid energy for ADS 1-3, ADS-4, and break
70	Mass balance	TOTMASS	lbm	Total system mass inventory
71	Mass balance	PRIMMASS, PRIMASS2	lbm	Measured primary system inventory and value from mass balance
72	Mass balance	MERROR	lbm	Mass balance error
73	Mass balance	MIN, MOUT SRCMASS	lbm	Integrated mass flow in and out of primary system and source mass
74	Energy balance	Various	Btu	Components of energy balance

THE FIGURES LISTED IN TABLE 5.4.2-1
ARE NOT INCLUDED IN THIS NONPROPRIETARY DOCUMENT

5.4.3 Long-Term Transient

The long-term transient started with initiation of IRWST injection, covered the transition from IRWST to sump injection, and provided information on the LTC response of the AP600. For the 2-in. cold-leg balance line break, Matrix Test SB09, the long-term transient analyzed begins at [ ]^{a,b,c} seconds and extends to the end of the test at [ ]^{a,b,c} seconds. The behavior of the test facility during this period of the transient is discussed in this subsection using the plot package detailed in Table 5.4.3-1. This analysis concentrates on the components of the primary system that remained active during the LTC phase, that is, the RPV, the hot legs, ADS-4, the sumps, and the IRWST.

Thermal-hydraulic phenomena of interest for the long-term transient are:

- Maintenance of core cooling and removal of energy from the primary system.
- Level oscillations (from [ ]^{a,b,c} seconds. There were system wide level and pressure oscillations, which are discussed further in Subsection 6.1.3).

5.4.3.1 Maintenance of Core Cooling

Mass Injected into Primary System

Total DVI line flow, CMT flow, and IRWST flows are shown in Figures 5.4.3-6 and 5.4.3-7. Flow from the primary sump is shown in Figure 5.4.3-19. From around [ ]^{a,b,c} seconds, there was a contribution to the DVI flow from the CMT-2 as the previously refilled CMT-2 drained. CMT-1 did not refill during test SB09.

During the pre-sump injection phase of the transient, IRWST flow proceeded at a gradually decreasing rate with the effect of the primary system oscillations superimposed. At [ ]^{a,b,c} seconds, flow from the primary sump began through the main injection valves, which opened as the IRWST has reached the low-low level set-point. This resulted in a reversal of flow through the IRWST injection line-1 almost equal to the IRWST flow into DVI-2. The net result was that the IRWST level decreased less than [ ]^{a,b,c} in. between the inception of sump injection flow through the primary injection valves and the end of the transient. The initial sump injection through the check valves around the main injection valves at [ ]^{a,b,c} seconds decreased the IRWST rate by about [ ]^{a,b,c} percent in each of the DVI lines.

Reactor Pressure Vessel and Downcomer Response

The effect of water inflow on the average measured downcomer fluid temperatures, core inlet and core outlet temperatures, and heater rod temperatures during the long-term phase of the transient is shown in Figures 5.4.3-4, 5.4.3-5, and 5.4.3-38. Figure 5.4.3-4 shows that there was a general increase in average downcomer fluid temperatures during the long-term transient. By the end of the test, this

average temperature reached a value about [ ]^{a,b,c} °F below saturation. Figure 5.4.3-5 shows that the core exit temperature remained at or near saturation for the majority of the long-term transient after [ ]^{a,b,c} secs. Figures 5.4.3-34 to 5.4.3-36 show that the DVI line flow method described in Section 4.11 indicates that a small level of boiling was maintained after [ ]^{a,b,c} seconds into the transient. Nevertheless, the level of boiling was small, and the test results showed that the inflow from the IRWST and sumps was sufficient to maintain cooling.

Figure 5.4.3-38 shows that there were no significant excursions in heated rod temperatures throughout the long-term transient therefore, sufficient core inventory and flow was maintained through this phase of the transient to remove the decay heat generated. For significant portions of the transient, a two-phase mixture was present in the core and upper plenum regions.

The following discussion tracks the variation in water level and mass throughout the reactor vessel and downcomer. The mass and level for the core region are shown in Figures 5.4.3-28 and 5.4.3-29. The collapsed liquid level in the core indicated that the heated rods, were always covered with a single- or two-phase mixture. During the sump injection stage of the transient (beyond [ ]^{a,b,c} seconds), the collapsed liquid level remained just below the top of the heated rods, and the core void fraction was [ ].^{a,b,c} The reduction in the core collapsed liquid level following the start of sump injection produced no marked impact on core cooling; in this test the sump water was relatively cold (Figures 5.4.3-4 and 5.4.3-5). During sump injection the calculated steam generation rate was at a maximum of about [ ]^{a,b,c} lbm/sec. (Figure 5.4.3-36).

The collapsed liquid level in the upper plenum region is shown in Figure 5.4.3-32; the level remained between the hot leg and DVI line elevations throughout the transient. Figure 5.4.3-33 shows the mass of water in the upper head, which remained below [ ]^{a,b,c} lbm from the inception of sump injection until the end of the test.

The mass of water in the RPV is shown in Figure 5.4.3-25. For the sump injection portion of the long-term transient, the reactor vessel water mass reached an equilibrium value of about [ ]^{a,b,c} lbm, which is [ ]^{a,b,c} percent of the initial vessel water inventory. From [ ]^{a,b,c} seconds, oscillations in vessel inventory were observed. Figures 5.4.3-51 to 5.4.3-56 illustrate these oscillations using plots on a restricted time frame from [ ]^{a,b,c} seconds. These oscillations are observed in primary system measurements from the upper plenum to the ADS-4 flows. The SB09 oscillations have a less uniform period during this time interval than do the oscillations observed in other tests. The oscillations in ADS flow lagged behind those in the upper head pressure by around [ ]^{a,b,c} seconds. These oscillations and possible mechanisms for their production are discussed further in Subsection 6.1.3.

The mass of fluid and collapsed liquid level in the RPV downcomer are shown in Figures 5.4.3-26 and 5.4.3-27. The collapsed liquid level remained above the cold leg midplane until [ ]^{a,b,c} seconds when it started to fall to an elevation below the center of the hot legs. This was close to the time that CMT-2 completed draindown and corresponds to the time the cold legs began to drain

(Figure 5.4.3-41) and the ADS-4 valve liquid flow increased (Figure 5.4.3-44). There was no effect on downcomer level resulting from the start of injection through the primary sump valves.

5.4.3.2 Energy Transport from the Primary System

During the long-term transient, energy continued to be deposited in the primary system from the heated rods, metal, and fluid flowing from the primary sump. The SGs and PRHR remained inactive throughout this phase of the transient, and the principal path for energy out of the primary system was via the ADS-4 valves.

Integrated mass flow from the primary system via the ADS and the break is shown in Figure 5.4.3-43. During the LTC phase of the transient, the only significant outflow was through the ADS-4 valves. After [ ]^{a,b,c} seconds, there was some reverse flow through the break as is indicated by the reduction in the integrated flow shown in Figure 5.4.3-43; the break flow integral returned to its pre-[ ]^{a,b,c} second value prior to sump injection. During the sump injection phase of the transient, outflow from the ADS-4 valves was liquid. By the end of the test, liquid flowed out through these valves at a combined average rate of [ ]^{a,b,c} lbm/sec.

Figure 5.4.3-36 shows the calculated steam generation rate as determined by the DVI line flow method. During the sump injection phase of the transient, steam was generated at up to [ ]^{a,b,c} lbm/sec., although the steam vortex meters indicate little or no flow out of the ADS-4 valves. However, there are two indications that steam is leaving the primary system by this route.

- Figure 5.4.3-46 shows total measured system fluid inventory. During this phase of the transient after the start of primary sump injection (from [ ]^{a,b,c} seconds, that is, when core steam generation was most significant), the total system inventory fell by about [ ]^{a,b,c} lbm. This amount corresponds to a steam flow rate of [ ]^{a,b,c} lbm/sec., which would not have been detected by the vortex meters.

- Examination of the fluid thermocouples on the outlet of the ADS-4 valves indicates that temperatures remained at or above saturation temperature following the start of sump injection.

It was not possible for all the steam generated in the core to flow from the upper head to the downcomer via the bypass holes (Subsection 6.1.3). Therefore, steam was leaving the primary system via ADS-4. Figure 5.4.3-50 shows all the components to the system energy balance. Further discussion of steam loss from the primary circuit is provided in the mass and energy balance discussions of Section 6.2.

TABLE 5.4.3-1
OSU TEST ANALYSIS STANDARD PLOT PACKAGE FOR SUBSECTION 5.4.3
LONG-TERM TRANSIENT

Plot No.	Component	Variables	Units	Description
1	RPV	RPVPWR	W	Core power
2	Primary sump	TSMPI1, TSMPI2	°F	Sump injection line temperatures
3	DVI	TDVIL1, TDVIL2	°F	DVI line temperatures
4	RPV	T01DC, T02DC, T03DC, ST01DC	°F	Water and saturation temperatures in downcomer
5	RPV	T01RPV, T08RPV, ST08RPV	°F	Core inlet/outlet temperature, saturation temperature
6	DVI-1	WWTDVIL1, WWTIRWI1, WWTIRWI3	lbm/sec.	Individual components and total flow in DVI-1
7	DVI-2	WWTDVIL2, WWTIRWI2, WWTIRWI4	lbm/sec.	Individual components and total flow in DVI-2
8	CMT	CLDP-502, CLDP-507	in.	Collapsed liquid level in CMTs
9	CMT	CLDP-509, CLDP510	in.	Level CL-CMT balance lines
10	IRWST	IRWST	lbm	Mass of fluid in IRWST
11	IRWST	CLDP-701	in.	Collapsed liquid level in IRWST
12	IRWST	UIRWST	Btu	Fluid energy in IRWST
13	Primary sump	AMPSMP	lbm	Primary sump fluid mass
14	Primary sump	CLDP-901	in.	Primary sump level
15	Primary sump	UPSMP	Btu	Primary sump fluid energy
16	Secondary sump	AMSSMP	lbm	Secondary sump fluid mass
17	Secondary sump	CLDP-902	in.	Secondary sump level
18	Secondary sump	USSMP	Btu	Secondary sump fluid energy
19	Primary sump	WSTSMPET, WWTSMPIT	lbm/sec.	Primary sump steam and liquid injection rate
20	Primary sump	MISMPI1, MISMPI2, MISMPIT, MIIRWT	lbm	Integrated primary sump and IRWST flows
21	SG	MSSGIP1, MSSGIP2, MSSGOP1, MSSGOP2	lbm	Mass of fluid in SG side inlet/outlet plena
22	Surge line	PLM	lbm	Fluid mass in surge line
23	Surge line	CLDP-602	in.	Collapsed liquid level in surge line
24	Surge line	UPSL	Btu	Fluid energy in surge line
25	RPV	MWRPV	lbm	Total fluid mass in reactor vessel

TABLE 5.4.3-1 (Continued)
OSU TEST ANALYSIS STANDARD PLOT PACKAGE FOR SUBSECTION 5.4.3
LONG-TERM TRANSIENT

Plot No.	Component	Variables	Units	Description
26	RPV	DCM	lbm	Fluid mass in downcomer
27	RPV	LDP01DC	in.	Collapsed liquid level in downcomer compared to various reference elevations
28	RPV	MW03RPV	lbm	Fluid mass in core region
29	RPV	LDP03RPV	in.	Collapsed liquid level in core
30	RPV	RPVAVDF2		Core exit void fraction
31	RPV	RPVAQOU2		Core exit quality
32	RPV	LDP06RPV	in.	Collapsed liquid level in the upper plenum
33	RPV	MW08RPV	lbm	Fluid mass in the upper head
34	RPV	RPVASL2	in.	Level of Tsat line
35	RPV	RPVAPab2, RPVPWR	kW	Heated rod power above and below Tsat level and total
36	RPV	RPVASOU2	lbm/sec.	Core steam generation rate
37	RPV	RPVALIN2	lbm/sec.	Calculated core flow
38	RPV	HTMXRPV, ST08RPV	°F	Maximum clad temperature, saturation temperature and delta
39	Hot leg	MWHL1, MWHL2	lbm	Water mass in hot legs
40	Hot leg	MVHL1, MVHL2	lbm	Vapor mass in hot legs
41	Cold leg	CL1WMS, CL2WMS, CL3WMS, CL4WMS	lbm	Water mass in cold legs
42	Cold leg	CL1VMS, CL2VMS, CL3VMS, CL4VMS	lbm	Vapor mass in cold legs
43	ADS and break	BRKSTIR, ADS13TIR, ADS41TIR, ADS42TIR	lbm	Total discharged mass for ADS 1-3, ADS-4, and break
44	ADS and break	ADS13TLR, ADS41TLR, ADS42TLR	lbm/sec.	Liquid flow out ADS 1-3 and ADS-4
45	ADS and break	BRKSTLR	lbm/sec.	Liquid flow and total flow out of break
46	Mass balance	TOTMASS	lbm	Total system mass inventory
47	Mass balance	PRIMMASS, PRIMASS2	lbm	Measured primary system inventory and valve from mass balances
48	Mass balance	MERROR	lbm	Mass balance error
49	Mass balance	MIN, MOUT SRCMASS	lbm	Integrated mass flow in and out of primary system and source mass
50	Energy balance	Various	Btu	Component of energy balance
51	ADS-4	ADS41TLR, ADS42TLR	lbm/sec.	Oscillations in ADS-4 liquid flow
52	Surge line	CLDP-602	in.	Oscillations in surgeline level

TABLE 5.4.3-1 (Continued)
OSU TEST ANALYSIS STANDARD PLOT PACKAGE FOR SUBSECTION 5.4.3
LONG-TERM TRANSIENT

Plot No.	Component	Variables	Units	Description
53	RPV	CPT-107	psia	Oscillations in upper head pressure
54	RPV	CLDP-113	in.	Oscillations in upper plenum level
55	RPV	LDP03RPV	in.	Oscillations in core level
56	RPV	LDP01DC	in.	Oscillations in downcomer level

THE FIGURES LISTED IN TABLE 5.4.3-1
ARE NOT INCLUDED IN THIS NONPROPRIETARY DOCUMENT

5.5 Analysis of Matrix Test SB10

Matrix Test SB10 (OSU Test U0110) simulated the double-ended rupture of the CL-3 to CMT-1 balance line with long-term cooling (LTC) and without the operation of the nonsafety-related systems. The break was located on the horizontal section of the balance line before the vertical rise to CMT-1. Except for the break size, this test was similar to SB09, including the simulated failure of one of the ADS-4 lines. Changes to the OSU facility since the performance of SB01 are noted in the Final Data Report.[1]

The analysis of Matrix Test SB10 is divided into three subsections as follows:

- Facility performance is discussed in Subsection 5.5.1. It provides a brief outline of the response of the test facility; further details are available in the Final Data Report.[1]

- The short-term transient for SB10 encompassed the start of the simulation up to [ ]^{a,b,c} seconds. This period includes blowdown, natural circulation, ADS and initial IRWST stages of the transient.

- The analysis of the long-term transient SB10, encompassed the time frame from [ ]^{a,b,c} seconds to the end of the test. This phase of the transient includes IRWST injection and covered the transition to sump injection. The long-term transient actually starts at IRWST injection, which is discussed as part of the short-term transient. Between the end of the short-term transient and [ ]^{a,b,c} seconds, the system remained relatively inactive with the exception of the CMT-2 refill. At [ ]^{a,b,c} seconds, CMT-2 began to refill; CMT-1 did not empty until [ ] seconds and [ ]^{a,b,c} during the SB10 transient. CMT refill phenomena are discussed further in Subsection 6.1.1, and the discussion of the long-term transient provided in this section begins at [ ]^{a,b,c} seconds.

The discussion of the short and long-term phase of the transient focuses on important thermal-hydraulic phenomena identified in the PIRT (Table 1.3-1). Key indicators of the quality of the analysis on which this discussion is based are the mass and energy balance results. These are discussed in detail in Subsections 6.2.2 and 6.2.3.

5.5.1 Facility Performance

The performance of the OSU test facility during Matrix Test SB10 in reference to the five transient phases is outlined in the following:

- Blowdown
- Natural circulation
- ADS
- IRWST injection
- Sump injection

The overall performance of the facility during the transient is shown in Figures 5.5.1-1 to 5.5.1-4. Figure 5.5.1-1 shows the pressurizer pressure throughout the test with various phases and operating components delineated on the figures. The time scale was reduced for clarity since there were only small changes in system pressure during the long-term phase of the transient. Figure 5.5.1-2 shows the total DVI line flow and its composition from the various sources at each time in the transient. Figure 5.5.1-3 shows the calculated core steam generation rate throughout the test. Figure 5.5.1-4 shows the variation in average measured core outlet temperature and peak clad temperature relative to the core outlet saturation temperature.

Figures 5.5.1-1 and 5.5.1-2 show that there was a continuous flow of water to the core from the passive safety-related systems throughout the transient. Once initiated, the ADS rapidly depressurized the primary system and thus enhanced the CMT and accumulator injection flow rates. Ultimately, the ADS-4 valves reduced the system pressure sufficiently to allow gravity-driven IRWST injection to commence. The passive injection systems operation overlapped so that as one source of water drained the next was available to continue the cooling process. The level of steam generation in the core and the response of the average measured core outlet fluid temperatures and maximum clad temperatures is shown in Figures 5.5.1-3 and 5.5.1-4. These figures show that the cooling flow prevented core heatup, and the core remained covered. The core remained subcooled for large periods of the transient, and when steam was produced the rate of generation remained below the rate at which water was delivered to the core.

5.5.1.1 Blowdown Phase

The blowdown phase began at time zero when the break was initiated and continued until the primary circuit pressure was in equilibrium with the secondary-side pressure at about [ ]^{a,b,c} seconds. During this phase of the transient, cooling flow was provided from the intact CMT, while the CMT with a broken balance line injected no mass. CMT-2 remained in the recirculation mode until the end of the blowdown phase, and heat was removed from the primary circuit via the steam generators (SGs). The pressurizer and surge line completely drained at [ ]^{a,b,c} and [ ]^{a,b,c} seconds respectively.

5.5.1.2 Natural Circulation Phase

In this LOCA simulation, single and two-phase natural circulation initially continued the gradual reduction in system pressure that is characteristic of blowdown; later in this phase of the transient, the rate of depressurization increased significantly once all the SG tubes had almost completely drained at about [ ]^{a,b,c} seconds. The tubes in SG-2 completed draining almost [ ]^{a,b,c} seconds earlier than those in SG-1 because primary circuit mass was drawn to loop-1, where the relatively large balance line break was located. After [ ]^{a,b,c} seconds, heat removal from the primary system continued via the PRHR and the break. In response to the double-ended balance line break, CMT-2 transitioned into a rapid draindown at [ ]^{a,b,c} seconds, and the falling CMT level reached the ADS low-level setpoint so that the ADS-1 valve began to open at [ ]^{a,b,c} seconds. Both accumulators had begun to inject at [ ]^{a,b,c} seconds and delivered at a rate of about [ ]^{a,b,c} lbm/sec. before ADS actuation due to the depressurization caused by the break.

5.5.1.3 Automatic Depressurization System Phase

ADS-1 actuation was followed by ADS-2 and ADS-3 [ ]^{a,b,c} and [ ]^{a,b,c} seconds later. Coinciding with initiation of ADS-2 an increased accumulator injection rate was observed. The influx of cold water combined with increased venting via the ADS led to an even more rapid depressurization of the primary circuit. Actuation of ADS-4 at [ ]^{a,b,c} seconds completed the depressurization and allowed the IRWST to begin injecting at [ ]^{a,b,c} seconds via DVI-2 and [ ]^{a,b,c} seconds via DVI-1. During the rapid accumulator injection, increased flow path resistance reduced flow out of CMT-2, and actually stopped it after ADS actuation. No flow was observed out of CMT-1 until about [ ]^{a,b,c} seconds after IRWST-1 injection had begun. Since both the CMT and IRWST lines attached to DVI-1 were open to containment, and the IRWST had greater gravity head, earlier injection through IRWST 1 was expected for this double-ended balance line break. As the accumulators drained, CMT-2 flow resumed at rates approaching [ ]^{a,b,c} lbm/sec. Because the CMT-1 balance line contained the break, CMT-1 injection was delayed until after IRWST-1 and IRWST-2 injection had been achieved for almost [ ]^{a,b,c} seconds. CMT-1 flow continued concurrently with IRWST-1 injection thereafter. The minimum RPV mass inventory of [ ]^{a,b,c} lbm occurred shortly after accumulator injection began.

Actuation of ADS-1 and ADS-2 rapidly refilled the pressurizer as water and steam flowed out of the ADS. The pressurizer gradually drained by [ ]^{a,b,c} seconds.

5.5.1.4 In-Containment Refueling Water Storage Tank Injection

IRWST injection was the transition from the short- to long-term phase of the transient. Initially, IRWST injection began through the IRWST-1 DVI line, and flow through IRWST-2 started a few seconds thereafter. Both of these flows exhibited a gradual increase as the driving head between the IRWST tank and the RCS increased. This pressure differential increased because RCS pressure decreased as the core steam generation decreased from [ ]^{a,b,c} lbm/sec. at IRWST-2 initiation to zero

by [ ]^{a,b,c} seconds. Maximum IRWST flow was established a short time later, and afterward, it gradually decreased with the decrease in pressure differential as the IRWST continued to drain. The influx of water from the IRWST was enough to keep the core subcooled until [ ]^{a,b,c} seconds. Steam was subsequently generated in the core for the remainder of the transient. Oscillations in pressure and level were observed in the primary circuit between [ ]^{a,b,c} and [ ]^{a,b,c} seconds.

5.5.1.5 Sump Injection

Sump flow began at [ ]^{a,b,c} seconds through the check valves around the DVI-2 main sump injection valve since the driving head from the sump was sufficient for flow to initiate. Sump injection flow in DVI-1 began a short time later. Sump injection through DVI-1 began to enter the IRWST once the main sump injection valves opened; at that time DVI-2 exhibited a corresponding increase in the flow out of the IRWST, which meant that there was no increase in IRWST inventory. Flow through the main sump injection valves began when those valves opened at about [ ]^{a,b,c} seconds.

TABLE 5.5.1-1
OSU TEST ANALYSIS PLOT PACKAGE FOR SUBSECTION 5.5.1

Plot No.	Component	Variables	Units	Description
1	Pressurizer	CPT-604	psia	System pressure and event history
2	Water injection	WWTDVI1+WWTDVI2, WOUTACC1+WOUTACC2, WWTIRWI1+WWTIRWI2, WWTSMPIT	lbm/sec.	Total of CMT, accumulator, IRWST, and sump injection flows
3	Reactor vessel	RPVASOU2	lbm/sec.	Steam generation in reactor vessel
4	Reactor vessel	T08RPV, HTMXRPV, TSAT	°F	Reactor vessel outlet temperature, maximum clad temperature and fuel exit saturation temperature

THE FIGURES LISTED IN TABLE 5.5.1-1
ARE NOT INCLUDED IN THIS NONPROPRIETARY DOCUMENT

5.5.2 Short-Term Transient

For the double-ended balance line break LOCA simulation, Matrix Test SB10, the short-term transient encompassed the time frame up to 2000 seconds. As shown in Figure 5.5.1-1, this period included the full depressurization of the facility through all four stages of the ADS, together with CMT and accumulator injection plus the initial stages of IRWST injection. The variation in mass, energy, pressure, and temperature throughout this stage of the transient are illustrated in the plot package outlined in Table 5.5.2-1. The plots concentrate on the primary system, including the accumulators, CMTs, IRWST, primary sump and flow from the primary system via the ADS, break, and IRWST overflow.

There were two principal parameters to be examined for the short-term transient:

- Adequate flow from the passive systems to the reactor vessel must be maintained.
- Adequate flow into the core must be maintained to ensure that decay heat was removed from the simulated fuel rods without a temperature excursion.

These parameters are addressed in the following discussion.

5.5.2.1 Maintenance of Core Cooling

Mass Injected to the Primary System

Figures 5.5.2-6 and 5.5.2-7 show the combined effect of the injection flow for the transient. Separate plots of the individual contributions to the total flow can be located by consulting the plot package index given in Table 5.5.2-1.

Figures 5.5.2-5 and 5.5.2-6 show how the CMTs, accumulators, and IRWST supplied a continuous flow of water to the core. During the first [ ]^{a,b,c} seconds, cooling flow was provided primarily by CMT-2, since CMT-1 flow was negligible due to the break in its balance line. By [ ]^{a,b,c} seconds, CMT flow was supplemented by flow from both accumulators. The rate of flow from CMT-2 was stopped for awhile by the accumulator injection. Accumulator flow produced the maximum DVI injection rates during the entire transient, with values of [ ]^{a,b,c} lbm/sec. and above in each DVI line. Following the end of accumulator injection, CMT-2 once again provided the cooling flow into the RPV. IRWST-1 injection began [ ]^{a,b,c} seconds before the CMT-2 draindown was completed. Since continuous IRWST injection through both DVI lines began before CMT-2 had fully drained, there was no period of the short-term transient when the passive safety-related systems failed to provide flow to the RPV.

Reactor Pressure Vessel and Downcomer Behavior

The effect of water flow on the average measured core inlet/outlet temperatures and peak clad temperatures during the short-term phase of the transient is shown in Figures 5.5.2-3 and 5.5.2-57. The core outlet temperature first reached the saturation point at [ ]^{a,b,c} seconds. The core outlet temperature then remained at saturation for almost the entire interval until about [ ]^{a,b,c} seconds when the influx of water from the CMT and IRWST became sufficient to again subcool the core. The core then remained subcooled beyond the end of the short-term transient.

Figure 5.5.3-57 shows that there were no significant excursions in heated rod temperatures throughout the short-term transient; therefore, sufficient core inventory and flow were maintained throughout this phase of the transient to remove the simulated decay heat generation. For significant portions of the transient, a two-phase mixture was present in the core and upper plenum regions, with core boiling kept at a low level.

The following discussion tracks the variation in water level and mass throughout the reactor vessel and downcomer. The mass and level for the core region are shown in Figures 5.5.3-44 and 5.5.3-45. The collapsed liquid level in the core indicated that the heated rods remained covered with a single- or two-phase mixture throughout the short-term transient. The minimum core inventory of [ ]^{a,b,c} lbm occurred at about [ ]^{a,b,c} seconds into the transient, before the initial accumulator injection was fully established. As seen in Figure 5.5.2-45, the collapsed liquid level dropped to [ ]^{a,b,c} in. below the top of the heated rod length during this phase of the transient. The average void fraction of the core two-phase mixture may be estimated by dividing the measured core collapsed liquid level by the [ ]^{a,b,c} in. heated rod length. In this test, the minimum collapsed liquid level corresponds to a core void fraction of [ ].^{a,b,c} By the end of the short-term transient, the effect of IRWST injection ended core boiling (Figure 5.5.2-55) and the core was again water-solid.

The collapsed liquid level in the upper plenum region and the associated fluid mass are shown in Figures 5.5.2-49 and 5.5.2-48; the level decreases, is replenished by accumulator injection, decreases again, and is replenished again by IRWST injection. In the [ ]^{a,b,c} second time interval, liquid splashed from the upper plenum to the downcomer and back again twice; the downcomer level twice reached the upper head bypass plate during this rapid condensation event, as discussed in the Final Data Report.[1] Figures 5.5.2-50 and 5.5.2-51 show that the upper head, which had drained by the time of significant accumulator injection, refilled along with the upper plenum during the initial rapid condensation event of SB10. The upper head eventually drained, only to refill later during the short-term transient due to another rapid condensation event at [ ]^{a,b,c} seconds in the downcomer. This refill occurred at the time of maximum combined CMT/IRWST injection in the downcomer.

The mass of fluid and collapsed liquid level in the RPV downcomer is shown in Figures 5.5.2-41 and 5.5.2-42. The downcomer collapsed liquid level fell to the cold-leg elevation during the first [ ]^{a,b,c} seconds, and rapidly refilled to the bypass plate during the interaction with the upper plenum. The level decreased and then recovered in the [ ]^{a,b,c} second time interval as the upper head

partially filled and then drained. IRWST injection maintained the collapsed liquid level within the cold-leg pipe perimeter after [ ]^{a,b,c} seconds in the short-term transient.

5.5.2.2 Energy Transport from the Primary System

Following the break, energy was deposited in the primary circuit fluid by the heater rods to simulate decay heat and the primary circuit metal as it cools down. Some fluid energy was lost to the atmosphere and out of the break. Excess energy must be removed from the primary system to prevent excessive fluid and heater rod temperature excursions. In the AP600, heat removal is designed to be achieved by a combination of the SGs and the PRHR plus the ADS.

Steam Generator and Passive Residual Heat Removal Heat Transfer

During normal operation, most of the primary system heat was removed via the SGs; however, once the RCPs tripped, the reduced system flow caused a reduction in primary- to secondary-side heat transfer. The SGs were only available as heat sinks until primary-side system pressure dropped to that of the secondary side. The two sides of the SG were in thermal equilibrium for a time, then the secondary side became a heat source to the primary system, and the SG tubes drained rapidly. The PRHR is designed to remove heat from the primary system once the safety signal opens the PRHR isolation valve. The PRHR will continue to remove energy via natural circulation after the SGs are thermally isolated until ADS actuates. Once the ADS is actuated, ADS 1-3 becomes the predominant path for the removal of energy from the primary system.

Figure 5.5.2-33 shows the SG pressure equalization together with the PRHR integrated heat transfer as represented by the IRWST fluid energy after allowing for the contribution from ADS 1-3 inflow. As shown, heat was transferred to the secondary side of the SGs for only the first [ ]^{a,b,c} seconds of the test. PRHR heat removal began about [ ]^{a,b,c} seconds into the test, and the PRHR was responsible for all the IRWST heat-up until ADS-1 activation, after which PRHR heat transfer was significantly reduced. During the natural circulation phase, the PRHR transferred heat to the IRWST at an average rate of about [ ]^{a,b,c} Btu/sec.

Energy Transport via the Break and Automatic Depressurization System

The mass flow rate from the primary system via the break is shown in Figures 5.5.2-67 and 5.5.2-68. Immediately, the break flow rose to a maximum value near [ ]^{a,b,c} lbm/sec. of water, then diminished as system pressure fell. At [ ]^{a,b,c} seconds, mass flow out of the break (Figure 5.5.2-62) decreased as the SG draining ended. Figure 5.5.2-71 shows the equivalent trend. Then, following the initiation of ADS 1-3, flow through the break dropped somewhat as steam and liquid flow through the ADS 1-3 valves began; ADS 1-3 then became the primary mass release path.

Beyond [ ]^{a,b,c} seconds, flow through the break continued as the downcomer level refilled to the cold-leg elevation; refill was occurring due to IRWST and CMT-2 injection. Liquid flow through the

break in the balance line continued at a declining rate until almost [ ]^{a,b,c} seconds, afterward flow through the break was minimal for the rest of the short-term transient.

Integrated mass flow from the primary system via the ADS and the break is shown in Figure 5.5.2-62. The corresponding integrated energy flow is shown in Figure 5.5.2-69. The total system inventory plot given in Figure 5.5.2-70 indicates that only [ ]^{a,b,c} lbm of inventory left the system during the short-term transient. Components of the energy balance are shown in Figure 5.5.2-74.

TABLE 5.5.2-1 OSU TEST ANALYSIS STANDARD PLOT PACKAGE FOR SUBSECTION 5.5.2				
Plot No.	**Component**	**Variables**	**Units**	**Description**
1	Pressurizer	CPT-604	psia	System pressure
2	RPV	RPVPWR	kW	Core power
3	RPV	T01RPV, T08RPV, ST08RPV	°F	Core inlet/outlet temperature, saturation temperature
4	SG	CPT-201, CPT-204, CPT-301, CPT-302	psia	Primary and secondary pressures in SG
5	DVI-1	WWTDVIL1, WWTIRWI1, WOUTACC1, WWTIRWI3	lbm/sec.	Individual components and total flow in DVI-1
6	DVI-2	WWTDVIL2, WWTIRWI2, WOUTACC2, WWTIRWI4	lbm/sec.	Individual components and total flow in DVI-2
7	CMT	AMCMT1B, AMCMT2B	lbm	Fluid mass in CMTs (excludes balance lines)
8	CMT	CLDP-502, CLDP-507	in.	Collapsed liquid level in CMTs
9	CMT	MIWDVIL1, MIWDVIL2	lbm	Integrated mass out of CMTs
10	CMT	WWTDVIL1, WWTDVIL2	lbm/sec.	Flow out of CMTs
11	CMT	WOUTCLB1, WOUTCLB2	lbm/sec.	Flow into CMTs
12	CMT	CLDP-509, CLDP510	in.	Level CL-CMT balance lines
13	CMT	UCMT1, UCMT2	Btu	Fluid energy in CMTs
14	IRWST	IRWST	lbm	Mass of fluid in IRWST
15	IRWST	CLDP-701	in.	Collapsed liquid level in IRWST
16	IRWST	WWTIRWI1, WWTIRWI2	lbm/sec.	Flow from IRWST to DVI lines
17	IRWST	IRWSTOR	lbm/sec.	Overflow from IRWST to sump
18	IRWST	ADS13TMR	lbm/sec.	Total ADS flow into IRWST
19	IRWST	ADS13TIR, MIIRWI1, MIIRWI2, MIIRWIO	lbm	Integrated mass out of IRWST
20	IRWST	UIRWST	Btu	Fluid energy in IRWST
21	PRHR	CLDP-802	in.	Collapsed liquid level in PRHR HX

TABLE 5.5.2-1 (Continued) OSU TEST ANALYSIS STANDARD PLOT PACKAGE FOR SUBSECTION 5.5.2				
Plot No.	**Component**	**Variables**	**Units**	**Description**
22	PRHR	WWOTPRHR	lbm/sec.	Measured outlet flow from PRHR tube
23	Accumulator	AMACC1, AMACC2	lbm	Mass of fluid in accumulators
24	Accumulator	CLDP-401, CLDP-402	in.	Collapsed liquid level in accumulators
25	Accumulator	WOUTACC1, WOUTACC2	lbm/sec.	Flow from accumulators
26	Accumulator	MOUTACC1, MOUTACC2	lbm	Integrated mass out of accumulators
27	Accumulator	UACC1, UACC2	Btu	Fluid energy in accumulators
28	Primary sump	AMPSMP	lbm	Primary sump fluid mass
29	Primary sump	CLDP-901	in.	Primary sump level
30	Primary sump	UPSMP	Btu	Primary sump fluid energy
31	SG	MSSGIP1, MSSGIP2, MSSGOP1, MSSGOP2	lbm	Mass of fluid in SG primary side inlet/outlet plena
32	SG	MSSGHT1, MSSGHT2, MSSGCT1, MSSGCT2	lbm	Mass of fluid in SG primary side hot and cold tubes
33	SG/PRHR	CPT-201, CPT-301, QPRHRI	psia & Btu	SG1 pressure and PRHR integrated heat output
34	Pressurizer	PZM	lbm	Fluid mass in pressurizer
35	Pressurizer	CLDP-601	in.	Collapsed liquid level in pressurizer
36	Pressurizer	UPZ	Btu	Fluid energy in pressurizer
37	Surge line	PLM	lbm	Fluid mass in surge line
38	Surge line	CLDP-602	in.	Collapsed liquid level in surge line
39	Surge line	UPSL	Btu	Fluid energy in surge line
40	RPV	MWRPV	lbm	Total fluid mass in reactor vessel
41	RPV	DCM	lbm	Fluid mass in downcomer
42	RPV	LDP01DC	in.	Collapsed liquid level in downcomer compared to various reference elevations
43	RPV	MW01RPV	lbm	Fluid mass in lower plenum
44	RPV	MW03RPV	lbm	Fluid mass in core region
45	RPV	LDP03RPV	in.	Collapsed liquid level in core
46	RPV	RPVAVDF2		Core exit void fraction
47	RPV	RPVAQOU2		Core exit quality
48	RPV	MW06RPV	lbm	Fluid mass in the upper plenum
49	RPV	LDP06RPV	in.	Collapsed liquid level in the upper plenum
50	RPV	MW08RPV	lbm	Fluid mass in the upper head
51	RPV	LDP08RPV	in.	Collapsed liquid level in the upper head

TABLE 5.5.2-1 (Continued)
OSU TEST ANALYSIS STANDARD PLOT PACKAGE FOR SUBSECTION 5.5.2

Plot No.	Component	Variables	Units	Description
52	RPV	URPV	Btu	Total fluid energy in reactor vessel
53	RPV	RPVXE, RPVASL2	in.	Level of Tsat line
54	RPV	RPVPab, RPVAPab2, RPVPWR	kW	Heated rod power above and below Tsat level and total
55	RPV	RPVRXV, RPVASOU2	lbm/sec.	Core steam generation rate
56	RPV	RPVALIN2	lbm/sec.	Calculated core flow
57	RPV	HTMXRPV, ST08RPV	°F	Maximum clad temperature and saturation temperature
58	Hot leg	MWHL1, MWHL2	lbm	Water mass in hot legs
59	Hot leg	MVHL1, MVHL2	lbm	Vapor mass in hot legs
60	Cold leg	CL1WMS, CL2WMS, CL3WMS, CL4WMS	lbm	Water mass in cold legs
61	Cold leg	CL1VMS, CL2VMS, CL3VMS, CL4VMS	lbm	Vapor mass in cold legs
62	ADS and break	BRKSTIR, ADS13TIR, ADS41TIR, ADS42TIR	lbm	Total discharged mass for ADS 1-3, ADS-4s, and break
63	ADS and break	BRKTIVF, AD13TIVF, AD41TIVF, AD42TIVF	lbm	Total integrated vapor flow for ADS and break
64	ADS and break	BRKTILF, AD13TILF, AD41TILF, AD42TILF	lbm	Total integrated liquid flow for ADS and break
65	ADS and break	ADS13SVR, ADS41SVR, ADS42SVR	lbm/sec.	Vapor flow out ADS 1-3 and ADS-4
66	ADS and break	ADS13SLR, ADS41SLR, ADS42SLR	lbm/sec.	Liquid flow out ADS 1-3 and ADS-4
67	ADS and break	BRKSSVR	lbm/sec.	Vapor flow out of break
68	ADS and break	BRKSSLR	lbm/sec.	Liquid flow out of break
69	ADS and break	BRKSPEI, ADS13EI, ADS41EI, ADS42EI	Btu	Integrated fluid energy for ADS 1-3, ADS-4, and break
70	Mass balance	TOTMASS	lbm	Total system mass inventory
71	Mass balance	PRIMMASS, PRIMASS2	lbm	Measured primary system inventory and value from mass balance
72	Mass balance	MERROR	lbm	Mass balance error
73	Mass balance	MIN, MOUT SRCMASS	lbm	Integrated mass flow in and out of primary system and source mass
74	Energy balance	Various	Btu	Components of energy balance

THE FIGURES LISTED IN TABLE 5.5.2-1
ARE NOT INCLUDED IN THIS NONPROPRIETARY DOCUMENT

5.5.3 Long-Term Transient

The long-term transient started with initiation of IRWST injection, covered the transition from IRWST to sump injection, and provided information on the LTC response of the AP600. For the double-ended cold-leg balance line (CLBL) break, Matrix Test SB10, the long-term transient analyzed runs from [ ]^{a,b,c} seconds to the end of the test to about [ ]^{a,b,c} seconds. The behavior of the test facility during this period of the transient is discussed in this subsection using the plot package detailed in Table 5.5.3-1. This analysis concentrates on the components of the primary system that remained active during the LTC phase, that is, the RPV, the hot legs, ADS-4, the sumps, and the IRWST.

The main thermal-hydraulic phenomena of interest for the long-term transient are:

- Maintenance of core cooling and removal of energy from the primary system.
- Level oscillations (from [ ]^{a,b,c} seconds. There were system wide level and pressure oscillations, which are discussed further in Subsection 6.1.3)

5.5.3.1 Maintenance of Core Cooling

Mass Injected into Primary System

Total DVI line flow, CMT flow and IRWST flow are shown in Figures 5.5.3-6 and 5.5.3-7, and flow from the primary sump is shown in Figure 5.5.3-19. As shown in this figure, from about [ ]^{a,b,c} seconds, there was a large contribution to the DVI flow from the CMT-2 as the previously refilled CMT-2 drained. CMT-1 did not empty completely during test SB10 until [ ]^{a,b,c} seconds as a result of the break location. It provided a relatively small amount of flow between [ ]^{a,b,c} seconds until it emptied.

Prior to sump injection, during the IRWST injection phase of the transient, IRWST flow proceeded at a gradually decreasing rate with the effect of the primary system oscillations and CMT-1 delivery superimposed. At [ ]^{a,b,c} seconds, flow from the primary sump began through the main injection valves which had opened once the IRWST reached the low-low level set-point. This resulted in a reversal of flow through the IRWST injection line-1 almost equal to the IRWST flow into DVI-2. The net result was that the IRWST level decreased less than [ ]^{a,b,c} in. between the inception of sump injection flow through the primary injection valves and the end of the transient. The initial sump injection through the check valves around the main injection valves at [ ]^{a,b,c} seconds decreased the IRWST injection rate by about [ ]^{a,b,c} percent in each of the DVI lines.

Reactor Pressure Vessel and Downcomer Response

The effect of the water inflow on the average measured downcomer fluid temperatures, core inlet and core outlet temperatures, and heater rod temperatures during the long-term phase of the transient is

shown in Figures 5.5.3-4, 5.5.3-5 and 5.5.3-38. Figure 5.5.3-4 shows that there was a general increase in average downcomer fluid temperatures during the long-term transient. By the end of the test, this average temperature reached a value about [ ]^{a,b,c}F below saturation. Figure 5.5.3-5 shows that the core exit temperature remained near saturation for the majority of the long-term transient. Figures 5.5.3-34 to 5.5.3-36 show the DVI line flow method described in Section 4.11 indicating that a small level of boiling was maintained after [ ]^{a,b,c} seconds into the transient. Nevertheless, the level of boiling was small, and the test results showed that the inflow from the IRWST and sumps was sufficient to maintain cooling.

Figure 5.5.3-38 shows that there were no significant excursions in heated rod temperatures throughout the long-term transient; therefore, sufficient core inventory and flow was maintained throughout this phase of the transient to remove the decay heat generated. For significant portions of the transient, a two-phase mixture was present in the core and upper plenum regions.

The following discussion tracks the variation in water level and mass throughout the reactor vessel and downcomer. The mass and level for the core region are shown in Figures 5.5.3-28 and 5.5.3-29. The collapsed liquid level in the core indicated that the heated rods were always covered with a single- or two-phase mixture. During the sump injection stage of the transient (beyond [ ]^{a,b,c} seconds), the collapsed liquid level remained just below the top of the heated rods, and the core void fraction was [ ].^{a,b,c} The reduction in the core collapsed liquid level following the start of sump injection produced no marked impact on core cooling; in this test the sump water was relatively warm (Figures 5.5.3-4 and 5.5.3-5). During sump injection, the calculated steam generation rate was at a maximum of about [ ]^{a,b,c} lbm/sec. (Figure 5.5.3-36).

The collapsed liquid level in the upper plenum region is shown in Figure 5.5.3-32; the level remained between the hot leg and DVI line elevations during the sump injection transient. Figure 5.5.3-33 shows the mass of water in the upper head, which drained shortly after the inception of sump injection and thereafter remained nearly empty until the end of the test.

The mass of water in the RPV is shown in Figure 5.5.3-25. For the sump injection portion of the long-term transient, the reactor vessel water mass reached an equilibrium value of about [ ]^{a,b,c} lbm, which was [ ]^{a,b,c} percent of the initial vessel water inventory. Between [ ]^{a,b,c} seconds, oscillations in vessel inventory were observed. Figures 5.5.3-51 to 5.5.3-56 illustrate these oscillations using plots on a restricted time frame from [ ]^{a,b,c} seconds. These oscillations are observed in primary system measurements from the upper plenum to the ADS-4 flows. The oscillations in the ADS flow lagged behind those in the upper head pressure by around [ ]^{a,b,c} seconds. These oscillations and possible mechanisms for their production are discussed further in Subsection 6.1.3.

The history of fluid mass and collapsed liquid level in the RPV downcomer during the test are shown in Figures 5.5.3-26 and 5.5.3-27. The collapsed liquid level remained above the cold-leg midplane until [ ]^{a,b,c} seconds, and afterward the level was at or just below the mid-level cold-leg elevation

for the remainder of the transient. The cold legs did not drain (Figure 5.5.3-41) in this transient. The double-ended balance line break at an elevation above the cold legs kept the liquid level high in the downcomer and into the cold legs throughout sump injection. Liquid continued to flow through the break for the remainder of the transient (Figure 5.5.3-45). There was no effect on downcomer level resulting from the start of injection through the primary sump valves.

5.5.3.2 Energy Transport from the Primary System

During the long-term transient, energy continued to be deposited in the primary system from the heated rods, metal, and fluid flowing from the primary sump. The SGs and PRHR remained inactive throughout this phase of the transient, and the principal path for energy out of the primary system was via the ADS-4 valves.

Integrated mass flow from the primary system via the ADS and the break is shown in Figure 5.5.3-43. During the LTC phase of the transient, the most significant energy outflows are through ADS-4 valves. Because the ADS-4 lines were both connected to the ADS separator for test SB10, ADS4A flow shown in Figure 5.5.3-43 represents the total flow for the ADS-4 paths. After [ ]^{a,b,c} seconds, flow through the break previously identified is reflected in the integrated flow shown in Figure 5.5.3-43. By the end of the test, water flowed out through the ADS-4 valves at a combined average rate of [ ]^{a,b,c} lbm/sec.

Figure 5.5.3-36 shows the calculated steam generation rate as determined by the DVI line flow method. During the sump injection phase of the transient, steam was generated at about [ ]^{a,b,c} lbm/sec., indicate little or no flow from the steam vortex meters out of the ADS-4 valves. Steam left the primary circuit by this route as shown by the following.

- Figure 5.5.3-46 shows total measured system fluid inventory. During this phase of the transient after the start of primary sump injection (from [ ]^{a,b,c} seconds, that is, when core steam generation was most significant, the total system inventory fell by over [ ]^{a,b,c} lbm. This amount corresponds to a steam flow rate of [ ]^{a,b,c} lbm/sec., which would not have been detected by the vortex meters.

- Examination of the fluid thermocouples on the outlet of the ADS-4 valves indicates that temperatures remained at or above saturation temperature following the start of sump injection.

Furthermore, as discussed in Subsection 6.1.3, it was not possible for all the steam generated in the core to flow from the upper head to the downcomer via the bypass holes. It can therefore be concluded that steam was leaving the primary system via ADS-4. Figure 5.5.3-50 shows all the components to the system energy balance. Further discussion of steam loss from the primary circuit is provided in the mass and energy balance discussions of Section 6.2.

TABLE 5.5.3-1
OSU TEST ANALYSIS STANDARD PLOT PACKAGE FOR SUBSECTION 5.5.3
LONG-TERM TRANSIENT

Plot No.	Component	Variables	Units	Description
1	RPV	RPVPWR	kW	Core power
2	Primary sump	TSMPI1, TSMPI2	°F	Sump injection line temperatures
3	DVI	TDVIL1, TDVIL2	°F	DVI line temperatures
4	RPV	T01DC, T02DC, T03DC, ST01DC	°F	Water and saturation temperatures in downcomer
5	RPV	T01RPV, T08RPV, ST08RPV	°F	Core inlet/outlet temperature, saturation temperature
6	DVI-1	WWTDVIL1, WWTIRWI1, WWTIRWI3	lbm/sec.	Individual components and total flow in DVI-1
7	DVI-2	WWTDVIL2, WWTIRWI2, WWTIRWI4	lbm/sec.	Individual components and total flow in DVI-2
8	CMT	CLDP-502, CLDP-507	in.	Collapsed liquid level in CMTs
9	CMT	CLDP-509, CLDP510	in.	Level CL-CMT balance lines
10	IRWST	IRWST	lbm	Mass of fluid in IRWST
11	IRWST	CLDP-701	in.	Collapsed liquid level in IRWST
12	IRWST	UIRWST	Btu	Fluid energy in IRWST
13	Primary sump	AMPSMP	lbm	Primary sump fluid mass
14	Primary sump	CLDP-901	in.	Primary sump level
15	Primary sump	UPSMP	Btu	Primary sump fluid energy
16	Secondary sump	AMSSMP	lbm	Secondary sump fluid mass
17	Secondary sump	CLDP-902	in.	Secondary sump level
18	Secondary sump	USSMP	Btu	Secondary sump fluid energy
19	Primary sump	WSTSMPET, WWTSMPIT	lbm/sec.	Primary sump steam and liquid injection rate
20	Primary sump	MISMPI1, MISMPI2, MISMPIT, MIIRWT	lbm	Integrated primary sump and IRWST flows
21	SG	MSSGIP1, MSSGIP2, MSSGOP1, MSSGOP2	lbm	Mass of fluid in SG side inlet/outlet plena
22	Surge line	PLM	lbm	Fluid mass in surge line
23	Surge line	CLDP-602	in.	Collapsed liquid level in surge line
24	Surge line	UPSL	Btu	Fluid energy in surge line
25	RPV	MWRPV	lbm	Total fluid mass in reactor vessel

TABLE 5.5.3-1 (Continued)
OSU TEST ANALYSIS STANDARD PLOT PACKAGE FOR SUBSECTION 5.5.3
LONG-TERM TRANSIENT

Plot No.	Component	Variables	Units	Description
26	RPV	DCM	lbm	Fluid mass in downcomer
27	RPV	LDP01DC	in.	Collapsed liquid level in downcomer compared to various reference elevations
28	RPV	MW03RPV	lbm	Fluid mass in core region
29	RPV	LDP03RPV	in.	Collapsed liquid level in core
30	RPV	RPVAVDF2		Core exit void fraction
31	RPV	RPVAQOU2		Core exit quality
32	RPV	LDP06RPV	in.	Collapsed liquid level in the upper plenum
33	RPV	MW08RPV	lbm	Fluid mass in the upper head
34	RPV	RPVASL2	in.	Level of Tsat line
35	RPV	RPVAPab2, RPVPWR	kW	Heated rod power above and below Tsat level and total
36	RPV	RPVASOU2	lbm/sec.	Core steam generation rate
37	RPV	RPVALIN2	lbm/sec.	Calculated core flow
38	RPV	HTMXRPV, ST08RPV	°F	Maximum clad temperature, saturation temperature and delta
39	Hot leg	MWHL1, MWHL2	lbm	Water mass in hot legs
40	Hot leg	MVHL1, MVHL2	lbm	Vapor mass in hot legs
41	Cold leg	CL1WMS, CL2WMS, CL3WMS, CL4WMS	lbm	Water mass in cold legs
42	Cold leg	CL1VMS, CL2VMS, CL3VMS, CL4VMS	lbm	Vapor mass in cold legs
43	ADS and break	BRKSTIR, ADS13TIR, ADS41TIR, ADS42TIR	lbm	Total discharged mass for ADS 1-3, ADS-4, and break
44	ADS and break	ADS13TLR, ADS41TLR, ADS42TLR	lbm/sec.	Liquid flow out ADS 1-3 and ADS-4
45	ADS and break	BRKSTLR	lbm/sec.	Liquid flow and total flow out of break
46	Mass balance	TOTMASS	lbm	Total system mass inventory
47	Mass balance	PRIMMASS, PRIMASS2	lbm	Measured primary system inventory and valve from mass balances
48	Mass balance	MERROR	lbm	Mass balance error
49	Mass balance	MIN, MOUT SRCMASS	lbm	Integrated mass flow in and out of primary system and source mass
50	Energy balance	Various	Btu	Component of energy balance
51	ADS-4	ADS41TLR, ADS42TLR	lbm/sec.	Oscillations in ADS-4 liquid flow
52	Surge line	CLDP-602	in.	Oscillations in surgeline level
53	RPV	CPT-107	psia	Oscillations in upper head pressure

TABLE 5.5.3-1 (Continued)
OSU TEST ANALYSIS STANDARD PLOT PACKAGE FOR SUBSECTION 5.5.3
LONG-TERM TRANSIENT

Plot No.	Component	Variables	Units	Description
54	RPV	CLDP-113	in.	Oscillations in upper plenum level
55	RPV	LDP03RPV	in.	Oscillations in core level
56	RPV	LDP01DC	in.	Oscillations in downcomer level

THE FIGURES LISTED IN TABLE 5.5.3-1
ARE NOT INCLUDED IN THIS NONPROPRIETARY DOCUMENT

5.6 Analysis of Matrix Test SB12

Matrix Test SB12 (OSU Test U0112) simulated a DEG DVI SBLOCA with LTC and without the operation of the nonsafety-related systems. Reactor-side break flow was piped to the break separator. All other connections to the break separator were isolated by using blind inserts in the piping source. The CMT and accumulator-side break flow were aligned directly to the sump rather than a separator. Before break initiation, the break separator and primary sump were isolated from the break sources by two break valves.

The analysis of Matrix Test SB12 is divided into three subsections, as follows:

- Facility performance is discussed in Subsection 5.6.1. It provides a brief outline of the response of the test facility; further details are available in the Final Data Report.[1]

- The short-term transient for SB12 encompassed the start of the simulation up to [ ]^{a,b,c} seconds. This period included blowdown, natural circulation, ADS, and initial IRWST stages of the transient.

- The analysis of the long-term transient for SB12 encompassed the time frame from [ ]^{a,b,c} seconds to the end of the test. This phase of the transient included IRWST injection and covered the transition to sump injection. The long-term transient actually started at IRWST injection, which is discussed as part of the short-term transient. Between the end of the short-term transient and [ ]^{a,b,c} seconds, the system remained relatively inactive.

The discussion of the short- and long-term phase of the transient focuses on important thermal-hydraulic phenomena identified in the PIRT (Table 1.3-1). The mass and energy balance results are key indicators of the quality of the analysis on which this discussion is based. These are discussed in detail in Subsections 6.2.2 and 6.2.3.

5.6.1 Facility Performance

The performance of the OSU test facility during Matrix Test SB12 in reference to the five transient phases is outlined in the following:

- Blowdown
- Natural circulation
- ADS
- IRWST injection
- Sump injection

The overall performance of the facility during the transient is shown in Figures 5.6.1-1 to 5.6.1-4. Figure 5.6.1-1 shows the pressurizer pressure throughout the test with various phases and operating components delineated on the figure. The time scale was reduced for clarity since there were only small changes in system pressure during the long-term phase of the transient. Figure 5.6.1-2 shows the DVI-2 flow and its composition from the various sources at each time in the transient. Figure 5.6.1-3 shows the calculated core steam generation rate throughout the test, and Figure 5.6.1-4 shows the variation in average measured core outlet temperature and peak clad temperature relative to the core outlet saturation temperature.

Figures 5.6.1-1 and 5.6.1-2 show that there was a continuous flow of cool water to the core from the passive safety systems throughout the transient. Once initiated, the ADS depressurized the primary system, which enhanced the CMT-2 and ACC-2 injection flow rates. Ultimately, opening of the ADS-4 valves reduced the system pressure to start gravity-driven IRWST injection. The operation of the passive injection systems overlapped so that as one source of water drained, the next became operable to continue the cooling process. The level of steam generation in the core and the average measured core outlet fluid temperatures and maximum clad temperatures are shown in Figures 5.6.1-3 and 5.6.1-4. These figures show that there was sufficient cooling flow to prevent excessive core heating, and the core remained covered. The core remained subcooled for large periods of the transient and when steam production occurred, the rate of generation remained well below the rate at which water was delivered to the core.

5.6.1.1 Blowdown Phase

The blowdown phase began at time zero when the break was initiated and continued until the primary system pressure was in equilibrium with the secondary-side pressure at about [ ]^{a,b,c} seconds. Break flow from the CMT-1/ACC-1 side of the break started immediately when the break valves opened and was directed into the primary sump. Immediately following the opening of the break, the primary system pressure fell to the end of the blowdown phase. Both the liquid and steam flow from the break separator increased from the time of the break valve opening until about [ ]^{a,b,c} seconds. During this phase of the transient, cooling flow was provided from CMT-2, which remained in the recirculation mode, and heat was removed from the primary system via the SGs and break. The

pressurizer and surge line completely drained at [ ]^{a,b,c} and [ ]^{a,b,c} seconds, respectively. The large break flow created a rapid depressurization and level decrease in the RCS.

5.6.1.2 Natural Circulation Phase

In this LOCA simulation, the single- and two-phase natural circulation phase was marked by a slow reduction in system pressure, due to mass flow out the break. The liquid level in the downcomer fell below the elevation of the DVI line (break elevation), which resulted in the reduced break flow. After [ ]^{a,b,c} seconds, the liquid and steam break flows decreased dramatically. During this phase of the transient, the SG tubes drained by about [ ]^{a,b,c} seconds and at this time, heat removal from the primary system continued via the PRHR and the break. The steam in the SG tubes became superheated and remained so until the end of the transient. Due to the break, flow decreased in the RCS, the cold legs emptied, and the downcomer annulus liquid level was at the bottom of the DVI line. In response to voiding in CL-1, CMT-2 transitioned to draindown mode at [ ]^{a,b,c} seconds. The falling CMT-1 level reached the ADS low-level setpoint at [ ]^{a,b,c} seconds. The natural circulation phase of the transient continued to [ ]^{a,b,c} seconds when the ADS-1 valve opened.

5.6.1.3 Automatic Depressurization System Phase

ADS-1 actuation was followed by ADS-2 and ADS-3 actuation [ ]^{a,b,c} and [ ]^{a,b,c} seconds later, respectively. After the initiation of ADS, ACC-2 injection began at [ ]^{a,b,c} seconds. The influx of cold water, combined with increased venting via the break and ADS, led to a rapid depressurization of the primary system. The RCS inventory decreased and the minimum RPV inventory of [ ]^{a,b,c} lbm was indicated at about [ ]^{a,b,c} seconds. No temperature excursions were recorded as a result of the core reaching its minimum level.

Actuation of ADS-2 caused a refill of the pressurizer as water and steam flowed out of the ADS. The pressurizer gradually drained by [ ]^{a,b,c} seconds. [ ]^{a,b,c} seconds after the CMT-1 low-level setpoint occurred, when the primary system pressure had reached the level of [ ]^{a,b,c} psig, actuation of ADS-4 at [ ]^{a,b,c} seconds completed depressurization to a level that allowed IRWST injection at [ ]^{a,b,c} seconds via DVI-2. IRWST injection continued for the remainder of the test. The rate of RCS depressurization changed very little as a result of ADS-4 actuation; the large break dominated the primary system depressurization.

During the ACC-2 injection, increased resistance reduced flow out of CMT-2. As ACC-2 drained, CMT-2 flow resumed. ACC-2 was completely drained at [ ]^{a,b,c} seconds. The measured break flow significantly decreased due to the low liquid level in the downcomer, and the combined CMT-2 and ACC-2 injection was sufficient to start increasing the primary system inventory.

5.6.1.4 In-Containment Refueling Water Storage Tank Injection

IRWST injection was the transition from the short- to long-term phase of the transient. The initial phase of IRWST injection involved an increase in flow through DVI-2 (until about [ ]^{a,b,c} seconds), which was followed by a gradual flow reduction after [ ]^{a,b,c} seconds as the driving head between the IRWST and the RCS fell due to the reduced IRWST water level. The simultaneous occurrence of IRWST injection initiation and CMT-2 flow increase after ADS-4 actuation increased the inventory in the RCS and kept the bottom of the core subcooled. By the end of the test, about [ ]^{a,b,c} percent of the core was subcooled. Steam generation rate in the core decreased throughout the SB12 short-term transient.

The liquid levels in both the primary sump and the break separator continuously increased after about [ ]^{a,b,c} seconds, with the primary sump level about 5-in. higher than the level in the break separator. The primary sump overflowed into the secondary sump at [ ]^{a,b,c} seconds.

When the water level in the primary sump increased above the level of the break separator penetration into the sump, the break separator loop seal flow reversed at about [ ]^{a,b,c} seconds. The break flow decreased and reversed at about [ ]^{a,b,c} seconds, when the water level in the break separator reached the elevation of the break line penetration into the break separator. The flow through the ADS-4 increased with the break flow reversal.

5.6.1.5 Sump Injection

Injection from the primary sump via the check valves around the main sump injection valves began when the level in the IRWST was low enough to allow flow. This injection caused a reduction in the flow rate from the IRWST. When the IRWST level fell to [ ]^{a,b,c} in., the main sump injection valves opened at [ ]^{a,b,c} seconds. The primary sump-2 injection flowed to the reactor about [ ]^{a,b,c} seconds after the sump valves opened; however, reverse primary sump-1 injection flow was observed when the sump valves opened. The primary sump-1 injection line sustained backflow from the IRWST to the primary sump for the remainder of the test as the level in the tanks equalized.

TABLE 5.6.1-1 OSU TEST ANALYSIS PLOT PACKAGE FOR SUBSECTION 5.6.1				
Plot No.	**Component**	**Variables**	**Units**	**Description**
1	Pressurizer	CPT-604	psia	System pressure and event history
2	Water injection	WWTDVI1+WWTDVI2, WOUTACC1+WOUTACC2, WWTIRWI1+WWTIRWI2 WWTSMPIT	lbm/sec.	Total of CMT, accumulator, IRWST, and sump injection flows
3	Reactor vessel	RPVASOU2	lbm/sec.	Steam generation in reactor vessel
4	Reactor vessel	T08RPV, HTMXRPV, TSAT	°F	Reactor vessel outlet temperature, maximum clad temperature and fuel exit saturation temperature

THE FIGURES LISTED IN TABLE 5.6.1-1
ARE NOT INCLUDED IN THIS NONPROPRIETARY DOCUMENT

5.6.2 Short-Term Transient

For the DEG break of a DVI line, Matrix Test SB12, the short-term transient encompassed the time frame up to [ ]^{a,b,c} seconds. As shown in Figure 5.6.2-1, this period included the full depressurization of the RPV through the break and all four stages of the ADS, together with CMT and accumulator injection plus the initial stages of IRWST injection. The variation in mass, energy, pressure, and temperature throughout this stage of the transient are illustrated in the plot package outlined in Table 5.6.2-1. The plots concentrate on the primary system, including the accumulators, CMTs, IRWST, primary sump, and flow from the primary system via the ADS, break, and IRWST overflow.

There were two principal parameters of interest for the short-term transient:

- Adequate flow must be maintained from the passive systems to the reactor vessel.
- Adequate flow into the core must be maintained to ensure that decay heat was removed from the simulated fuel rods without a temperature excursion.

These parameters are addressed in the following discussion.

5.6.2.1 Maintenance of Core Cooling

Mass Injected to the Primary System

Figures 5.6.2-5 and 5.6.2-6 show the combined effect of the injection flow for the short-term phase of the transient. Separate plots of the individual contributions to the total flow can be located by consulting the plot package index given in Table 5.6.2-1. Note that the flow measurements for the outflow from CMTs were temporarily out-of-range for this test.

Figure 5.6.2-6 shows how the CMT-2, ACC-2, and IRWST supplied a continuous flow of cool water to the core. During the first [ ]^{a,b,c} seconds, cooling flow was provided by the CMT-2. The rate of flow from the CMT-2 increased after it transitioned to draindown mode at [ ]^{a,b,c} seconds. ACC-2 injection initiated at [ ]^{a,b,c} seconds, caused a temporary reduction in CMT-2 flow, but led to an overall increase in flow to the core to a peak value of about [ ]^{a,b,c} lbm/sec. Following the end of accumulator injection, the CMT-2 again provided cooling flow in combination with the IRWST injection flow.

Reactor Pressure Vessel and Downcomer Behavior

The effect of the water flow on the average measured core inlet/outlet temperatures and heater rod temperatures during the short-term phase of the transient is shown in Figures 5.6.2-3 and 5.6.2-57. CMT-2 flow was not sufficient to keep the core subcooled; shortly after the break valves were opened

(at about [ ]^{a,b,c} seconds), the decreasing saturation temperature reached the core outlet temperature. After this time, the core outlet temperature followed the saturation temperature until about [ ]^{a,b,c} seconds. When the collapsed level in the downcomer fell to the elevation of the DVI line at about [ ]^{a,b,c} seconds, steam was most likely vented out through the break, even though none was detected by the break steam flow meter. At the same time, ADS-1 actuated, and shortly afterward, ACC-2 injection occurred. ADS-1 and ACC-2 resulted in rapid primary system depressurization. After [ ]^{a,b,c} seconds, the influx of water from the IRWST and CMT-2 injection became sufficient to subcool the lower part of the core.

Figure 5.6.2-57 shows that there were no significant excursions in heater rod temperatures throughout the short-term transient; therefore, sufficient core inventory and flow was maintained through this phase of the transient to remove the simulated decay heat generation. For significant portions of the transient, a two-phase mixture was present in the core and upper plenum regions, with core boiling kept at a low level. The following discussion tracks the variation in water level and mass throughout the RPV and downcomer.

The mass and level for the core region are shown in Figures 5.6.2-44 and 5.6.2-45. The collapsed liquid level in the core indicates that the heater rods remained covered with a single- or two-phase mixture. The minimum core inventory of about [ ]^{a,b,c} lbm occurred about [ ]^{a,b,c} seconds into the transient. Figure 5.6.2-45 shows that the collapsed liquid level fell [ ]^{a,b,c} in. below the top of the core during this phase of the transient. The average void fraction of the core two-phase mixture may be estimated by dividing the measured core collapsed liquid level by the [ ]^{a,b,c} in. heated rod length. In this test, the minimum collapsed liquid level corresponded to a core void fraction of [ ].^{a,b,c} By about [ ]^{a,b,c} seconds, the IRWST injection reduced core boiling (Figure 5.6.2-55) to a low level.

The collapsed liquid level in the upper plenum region and the associated fluid mass are shown in Figures 5.6.2-49 and 5.6.2-48. After the break, the region of the upper plenum spanned by the LDP cell fully drained and remained so until IRWST injection supplied sufficient inventory to initiate a refill of the region after [ ]^{a,b,c} seconds. The upper plenum collapsed level stayed below the hot-leg elevation by the end of the short-term transient.

Figures 5.6.2-50 and 5.6.2-51 show that the upper head lost inventory later than the upper plenum. At about [ ]^{a,b,c} seconds, the upper head was drained to the upper support plate elevation until approximately [ ]^{a,b,c} seconds. The reduction in upper plenum and upper head inventory contributed to the reduction in overall RPV inventory.

The mass of fluid and collapsed liquid level in the RPV downcomer are shown in Figures 5.6.2-41 and 5.6.2-42. The downcomer collapsed liquid level fell to the DVI line elevation at [ ]^{a,b,c} seconds and to the top of the heater rods at [ ]^{a,b,c} seconds. The minimum downcomer inventory of [ ]^{a,b,c} lbm was indicated at [ ]^{a,b,c} seconds when the collapsed liquid level dropped 13-in. below the top of the heater rods. ACC-2 injection and IRWST inflow partly restored water inventory in the downcomer, and the collapsed liquid level increased to the elevation of the DVI line at about [ ]^{a,b,c} seconds.

5.6.2.3 Energy Transport from the Primary System

Following the break, energy was deposited in the primary system fluid by the heater rods to simulate decay heat and the primary system metal as it cooled down. Some fluid energy was lost to ambient and out the break. Energy must be removed from the primary system to prevent excessive fluid and heater rod temperature excursions. The AP600 is designed to remove heat by a combination of the SGs, PRHR, and the ADS.

Steam Generator and Passive Residual Heat Removal Heat Transfer

During normal operation, most of the primary system heat was removed via the SGs; however, once the coolant pumps tripped, the reduced system flow decreased primary-to-secondary-side heat transfer. The SGs were only available as heat sinks until the time when the primary system pressure dropped to that of the secondary side; afterward, the secondary side became a potential heat source for the primary side. The PRHR is designed to remove heat from the primary system via natural circulation once the safety signal opens the PRHR isolation valve. The PRHR continue to remove energy after the SGs are thermally isolated until ADS actuates, creating a path for the removal of energy from the primary system.

Figures 5.6.2-33 and 5.6.2-4 show the SG primary- and secondary-side pressure together with the PRHR integrated heat transfer, as represented by the IRWST fluid energy after allowing for the contribution from ADS 1-3 inflow. The SGs were a potential sink for primary system heat while the SG primary-side pressure was above that of the secondary side, that is, before [ ]^{a,b,c} seconds. PRHR heat removal began [ ]^{a,b,c} seconds into the test. The PRHR was responsible for all the IRWST heatup until ADS-1 actuation. The PRHR heat transfer reduced significantly after [ ]^{a,b,c} seconds. During the active phase, the PRHR transferred heat to the IRWST at an average rate of approximately [ ]^{a,b,c} Btu/sec., as calculated from the IRWST fluid energy increase.

Energy Transport via the Break and Automatic Depressurization System

The mass flow rate from the primary system via the break is shown in Figures 5.6.2-67 and 5.6.2-68. As shown in these figures, liquid flow was detected by the flow measuring devices for the short-term transient. The liquid flow reached its maximum flow rate of [ ]^{a,b,c} lbm/sec. at about [ ]^{a,b,c} seconds and then rapidly decreased. When ADS-1 actuated, the primary system depressurized to around [ ]^{a,b,c} psia (Figure 5.6.2-1). After the initiation of ADS-1, liquid flow through the break ceased at about [ ]^{a,b,c} seconds (most likely replaced by steam flow) due to the fluid level in the downcomer dropping below the elevation of the DVI line. The smaller liquid flow rate (about [ ]^{a,b,c} lbm/sec.) resumed through the break at about [ ]^{a,b,c} seconds and continued until the end of the short-term phase. ADS 1-3 rapidly depressurized the system and at [ ]^{a,b,c} seconds, ADS-4 initiated and the primary system continued to depressurize to BAMS header pressure.

By the end of the short-term transient ([ ]^{a,b,c} seconds), there was flow out of the two ADS-4 valves (most likely two-phase flow) and through the break (Figures 5.6.2-64, 5.6.2-63).

Integrated mass flow from the primary system via the ADS and the break is shown in Figure 5.6.2-62, and the corresponding integrated energy flow is shown in Figure 5.6.2-69. The total system inventory plot given in Figure 5.6.2-70 indicates that about [ ]^{a,b,c} lbm of inventory was gained during the short-term transient. The energy balance is shown in Figure 5.6.2-74.

TABLE 5.6.2-1
OSU TEST ANALYSIS STANDARD PLOT PACKAGE FOR SUBSECTION 5.6.2

Plot No.	Component	Variables	Units	Description
1	Pressurizer	CPT-604	psia	System pressure
2	RPV	RPVPWR	kW	Core power
3	RPV	T01RPV, T08RPV, ST08RPV	°F	Core inlet/outlet temperature, saturation temperature
4	Steam generator	CPT-201, CPT-204, CPT-301, CPT-302	psia	Primary and secondary pressures in SG
5	DVI-1	WWTDVIL1, WWTIRWI1, WOUTACC1, WWTIRWI3	lbm/sec.	Individual components and total flow in DVI-1
6	DVI-2	WWTDVIL2, WWTIRWI2, WOUTACC2, WWTIRWI4	lbm/sec.	Individual components and total flow in DVI-2
7	CMT	AMCMT1B, AMCMT2B	lbm	Fluid mass in CMTs (excludes balance lines)
8	CMT	CLDP-502, CLDP-507	in.	Collapsed liquid level in CMTs
9	CMT	MIWDVIL1, MIWDVIL2	lbm	Integrated mass out of CMTs
10	CMT	WWTDVIL1, WWTDVIL2	lbm/sec.	Flow out of CMTs
11	CMT	WOUTCLB1, WOUTCLB2	lbm/sec.	Flow into CMTs
12	CMT	CLDP-509, CLDP510	in.	Level CL-CMT balance lines
13	CMT	UCMT1, UCMT2	Btu	Fluid energy in CMTs
14	IRWST	IRWST	lbm	Mass of fluid in IRWST
15	IRWST	CLDP-701	in.	Collapsed liquid level in IRWST
16	IRWST	WWTIRWI1, WWTIRWI2	lbm/sec.	Flow from IRWST to DVI lines
17	IRWST	IRWSTOR	lbm/sec.	Overflow from IRWST to sump
18	IRWST	ADS13TMR	lbm/sec.	Total ADS flow into IRWST
19	IRWST	ADS13TIR, MIIRWI1, MIIRWI2, MIIRWIO	lbm	Integrated mass out of IRWST
20	IRWST	UIRWST	Btu	Fluid energy in IRWST
21	PRHR	CLDP-802	in.	Collapsed liquid level in PRHR HX

TABLE 5.6.2-1 (Continued) OSU TEST ANALYSIS STANDARD PLOT PACKAGE FOR SUBSECTION 5.6.2				
Plot No.	**Component**	**Variables**	**Units**	**Description**
22	PRHR	WWOTPRHR	lbm/sec.	Measured outlet flow from PRHR tube
23	Accumulator	AMACC1, AMACC2	lbm	Mass of fluid in accumulators
24	Accumulator	CLDP-401, CLDP-402	in.	Collapsed liquid level in accumulators
25	Accumulator	WOUTACC1, WOUTACC2	lbm/sec.	Flow from accumulators
26	Accumulator	MOUTACC1, MOUTACC2	lbm	Integrated mass out of accumulators
27	Accumulator	UACC1, UACC2	Btu	Fluid energy in accumulators
28	Primary sump	AMPSMP	lbm	Primary sump fluid mass
29	Primary sump	CLDP-901	in.	Primary sump level
30	Primary sump	UPSMP	Btu	Primary sump fluid energy
31	Steam generator	MSSGIP1, MSSGIP2, MSSGOP1, MSSGOP2	lbm	Mass of fluid in SG primary side inlet/outlet plena
32	Steam generator	MSSGHT1, MSSGHT2, MSSGCT1, MSSGCT2	lbm	Mass of fluid in SG primary side hot and cold tubes
33	Steam generator/PRHR	CPT-201, CPT-301, QPRHRI	psia & Btu	SG1 pressure and PRHR integrated heat output
34	Pressurizer	PZM	lbm	Fluid mass in pressurizer
35	Pressurizer	CLDP-601	in.	Collapsed liquid level in pressurizer
36	Pressurizer	UPZ	Btu	Fluid energy in pressurizer
37	Surge line	PLM	lbm	Fluid mass in surge line
38	Surge line	CLDP-602	in.	Collapsed liquid level in surge line
39	Surge line	UPSL	Btu	Fluid energy in surge line
40	RPV	MWRPV	lbm	Total fluid mass in reactor vessel
41	RPV	DCM	lbm	Fluid mass in downcomer
42	RPV	LDP01DC	in.	Collapsed liquid level in downcomer compared to various reference elevations
43	RPV	MW01RPV	lbm	Fluid mass in lower plenum
44	RPV	MW03RPV	lbm	Fluid mass in core region
45	RPV	LDP03RPV	in.	Collapsed liquid level in core
46	RPV	RPVXVFO		Core exit void fraction
47	RPV	RPVXRQO		Core exit quality
48	RPV	MW06RPV	lbm	Fluid mass in the upper plenum
49	RPV	LDP06RPV	in.	Collapsed liquid level in the upper plenum
50	RPV	MW08RPV	lbm	Fluid mass in the upper head
51	RPV	LDP08RPV	in.	Collapsed liquid level in the upper head

TABLE 5.6.2-1 (Continued)
OSU TEST ANALYSIS STANDARD PLOT PACKAGE FOR SUBSECTION 5.6.2

Plot No.	Component	Variables	Units	Description
52	RPV	URPV	Btu	Total fluid energy in reactor vessel
53	RPV	RPVXE, RPVASL2	in.	Level of Tsat line
54	RPV	RPVPab, RPVAPbl, RPVPWR	kW	Heater rod power above and below Tsat level and total
55	RPV	RPVRXV, RPVASOU2	lbm/sec.	Core steam generation rate
56	RPV	RPVALIN2	lbm/sec.	Calculated core flow
57	RPV	HTMXRPV, ST08RPV	°F	Maximum clad temperature and saturation temperature
58	Hot leg	MWHL1, MWHL2	lbm	Water mass in hot legs
59	Hot leg	MVHL1, MVHL2	lbm	Vapor mass in hot legs
60	Cold leg	CL1WMS, CL2WMS, CL3WMS, CL4WMS	lbm	Water mass in cold legs
61	Cold leg	CL1VMS, CL2VMS, CL3VMS, CL4VMS	lbm	Vapor mass in cold legs
62	ADS and break	BRKSTIR, ADS13TIR, ADS41TIR, ADS42TIR	lbm	Total discharged mass for ADS 1-3, ADS-4s, and break
63	ADS and break	BRKTIVF, AD13TIVF, AD41TIVF, AD42TIVF	lbm	Total integrated vapor flow for ADS and break
64	ADS and break	BRKTILF, AD13TILF, AD41TILF, AD42TILF	lbm	Total integrated liquid flow for ADS and break
65	ADS and break	ADS13SVR, ADS41SVR, ADS42SVR	lbm/sec.	Vapor flow out ADS 1-3 and ADS-4
66	ADS and break	ADS13SLR, ADS41SLR, ADS42SLR	lbm/sec.	Liquid flow out ADS 1-3 and ADS-4
67	ADS and break	BRKSSVR	lbm/sec.	Vapor flow out of break
68	ADS and break	BRKSSLR	lbm/sec.	Liquid flow out of break
69	ADS and break	BRKSPEI, ADS13EI, ADS41EI, ADS42EI	Btu	Integrated fluid energy for ADS 1-3, ADS-4, and break
70	Mass balance	TOTMASS	lbm	Total system mass inventory
71	Mass balance	PRIMMASS, PRIMASS2	lbm	Measured primary system inventory and value from mass balance
72	Mass balance	MERROR	lbm	Mass balance error
73	Mass balance	MIN, MOUT SRCMASS	lbm	Integrated mass flow in and out of primary system and source mass
74	Energy balance	Various	Btu	Components of energy balance

THE FIGURES LISTED IN TABLE 5.6.2-1
ARE NOT INCLUDED IN THIS NONPROPRIETARY DOCUMENT

5.6.3 Long-Term Transient

The long-term transient started after initiation of IRWST injection, covered the transition from IRWST to sump injection, and provided information on the LTC response of the AP600 plant. For the DEG DVI break, Matrix Test SB12, the long-term transient analyzed extends from [ ]^{a,b,c} seconds to the end of the test around [ ]^{a,b,c} seconds. The behavior of the test facility during this period of the transient is discussed in this subsection using the plot package detailed in Table 5.6.3-1. This analysis concentrates on the components of the primary system that remained active during the LTC phase, that is, the RPV, the hot legs, ADS-4, the sumps, and the IRWST.

During the long-term transient, the main thermal-hydraulic phenomena of interest were the maintenance of core cooling and the removal of energy from the primary system.

5.6.3.1 Maintenance of Core Cooling

Mass Injected into Primary System

Total DVI line flow, CMT flow, and IRWST flows are shown in Figures 5.6.3-6 and 5.6.3-7, and the flow from the primary sump is shown in Figure 5.6.3-19. Throughout the long-term transient, there was no contribution to the DVI flow from the CMTs as the CMTs were drained.

During the IRWST injection phase of the transient, IRWST-2 flow proceeded at a gradually declining rate. At [ ]^{a,b,c} seconds, flow from primary sump-2 began through the check valves, around the main injection valves, reducing IRWST-2 flow. The IRWST flow rate was maintained through DVI-2 decreasing from [ ]^{a,b,c} lbm at [ ]^{a,b,c} seconds to [ ]^{a,b,c} lbm/sec. at the end of the transient. At [ ]^{a,b,c} seconds, the primary sump injection valves opened and primary sump injection flow (about [ ]^{a,b,c} lbm/sec. started at [ ]^{a,b,c} seconds, slightly decreasing the IRWST flow in line-2. The net result was that an injection flow rate of [ ]^{a,b,c} lbm/sec. was maintained through DVI-2.

Reactor Pressure Vessel and Downcomer Response

The effect of the water inflow on the average measured downcomer fluid temperatures, core inlet, and core outlet temperatures, and heater rod temperatures during the long-term phase of the transient is shown in Figures 5.6.3-4, 5.6.3-5, and 5.6.3-38. Figure 5.6.3-4 shows that there was an increase in average downcomer fluid temperatures during the long-term transient. By the end of the test, this average temperature was about [ ]^{a,b,c} °F below the saturation temperature for the primary system. Figure 5.6.3-5 shows that the core remained near saturation throughout the long-term transient. As shown in Figures 5.6.3-34 to 5.6.3-36, the DVI line flow method described in Section 4.11 indicates that a small level of boiling was maintained throughout the long-term transient. Nevertheless, the level of boiling was small and showed that the inflow from IRWST-2 was sufficient to cool the core effectively.

Figure 5.6.3-38 shows that there were no significant excursions in heater rod temperatures throughout the long-term transient; therefore, sufficient core inventory and flow were maintained through this phase of the transient to remove decay heat. The following discussion tracks the variation in water level and mass throughout the RPV and downcomer.

The mass and level for the core region are shown in Figures 5.6.3-28 and 5.6.3-29. The collapsed liquid level in the core indicated that the heater rods were always covered with a single- or two-phase mixture. During the long-term transient, the collapsed liquid level remained below the top of the core until it reached the top of the core at the end of the transient. The impact of hot water injected from IRWST-2 as well as reversed break flow on the system temperatures is shown in Figures 5.6.3-4 and 5.6.3-5 as a small increase in fluid temperature in the downcomer and at the core inlet. The hot water also led to an increase in the calculated steam generation rate as shown in Figure 5.6.3-36 and a corresponding fall in the level at which the core reached saturation temperature (Figure 5.6.3-34).

The collapsed liquid level in the upper plenum region is shown in Figure 5.6.3-32. This figure indicates that the collapsed liquid level increased during this period, from the elevation of the DVI line at [ ]^{a,b,c} seconds; after the break flow was reversed at about [ ]^{a,b,c} seconds, the collapsed liquid level gradually increased above the hot-leg elevation.

The mass of water in the RPV is shown in Figure 5.6.3-25. After an initial decline, the RPV water mass settled at an average value of [ ]^{a,b,c} lbm until the break flow was reversed, after which time the RPV water inventory gradually increased to [ ]^{a,b,c} lbm ([ ]^{a,b,c} percent of the initial RPV liquid mass) by the end of the transient.

The mass of fluid and collapsed liquid level in the RPV downcomer are shown in Figures 5.6.3-26 and 5.6.3-27. The collapsed liquid level remained at the elevation of the DVI line until about [ ]^{a,b,c} seconds, when due to the reversed break flow, the level raised above the hot-leg elevation. The sump injection had no noticeable effect on the levels in the RPV and downcomer.

5.6.3.2 Energy Transport from the Primary System

During the long-term transient, energy continued to be deposited in the primary system from the heater rods and metal. The SGs remained inactive throughout this phase of the transient. The small PRHR flow continued until about [ ]^{a,b,c} seconds. The principal patin for energy out of the primary system was via the ADS-4 valves.

Integrated mass flow from the primary system via the ADS and the break is shown in Figure 5.6.3-43. During the LTC phase of the transient, the only significant energy outflow was through the ADS-4 valves. When the break flow was reversed after [ ]^{a,b,c} seconds, the outflow through ADS-4 increased to maintain the primary system inventory almost constant. This is confirmed by Figures 5.6.3-44 and 5.6.3-45, which show the flow through the ADS and the break. Throughout the

LTC, significant inflow was provided by IRWST-2 injection. During the sump injection phase of the transient (about [ ]^{a,b,c} second duration), outflow through the ADS-4 valves continued.

Figure 5.6.3-36 shows the calculated steam generation rate, as determined by the DVI line flow method discussed in Section 4.11. During this phase of the transient, steam generation decreased.

Figure 5.6.3-50 shows all the components to the system energy balance. The calculated steam generation rate, mass flow, and energy balance are affected by the break flow after it was reversed.

TABLE 5.6.3-1
OSU TEST ANALYSIS STANDARD PLOT PACKAGE FOR SUBSECTION 5.6.3
LONG-TERM TRANSIENT

Plot No.	Component	Variables	Units	Description
1	RPV	RPVPWR	kW	Core power
2	Primary sump	TSMPI1, TSMPI2	°F	Sump injection line temperatures
3	DVI	TDVIL1, TDVIL2	°F	DVI line temperatures
4	RPV	T01DC, T02DC, T03DC, ST01DC	°F	Water and saturation temperatures in downcomer
5	RPV	T01RPV, T08RPV, ST08RPV	°F	Core inlet/outlet temperature, saturation temperature
6	DVI-1	WWTDVIL1, WWTIRWI1, WWTIRWI3	lbm/sec.	Individual components and total flow in DVI-1
7	DVI-2	WWTDVIL2, WWTIRWI2, WWTIRWI4	lbm/sec.	Individual components and total flow in DVI-2
8	CMT	CLDP-502, CLDP-507	in.	Collapsed liquid level in CMTs
9	CMT	CLDP-509, CLDP510	in.	Level CL-CMT balance lines
10	IRWST	IRWST	lbm	Mass of fluid in IRWST
11	IRWST	CLDP-701	in.	Collapsed liquid level in IRWST
12	IRWST	UIRWST	Btu	Fluid energy in IRWST
13	Primary sump	AMPSMP	lbm	Primary sump fluid mass
14	Primary sump	CLDP-901	in.	Primary sump level
15	Primary sump	UPSMP	Btu	Primary sump fluid energy
16	Secondary sump	AMSSMP	lbm	Secondary sump fluid mass
17	Secondary sump	CLDP-902	in.	Secondary sump level
18	Secondary sump	USSMP	Btu	Secondary sump fluid energy
19	Primary sump	WSTSMPET, WWTSMPIT	lbm/sec.	Primary sump steam and liquid injection rate
20	Primary sump	MISMPI1, MISMPI2, MISMPIT, MIIRWT	lbm	Integrated primary sump and IRWST flows
21	SG	MSSGIP1, MSSGIP2, MSSGOP1, MSSGOP2	lbm	Mass of fluid in SG side inlet/outlet plena
22	Surge line	PLM	lbm	Fluid mass in surge line
23	Surge line	CLDP-602	in.	Collapsed liquid level in surge line
24	Surge line	UPSL	Btu	Fluid energy in surge line
25	RPV	MWRPV	lbm	Total fluid mass in reactor vessel

TABLE 5.6.3-1 (Continued)
OSU TEST ANALYSIS STANDARD PLOT PACKAGE FOR SUBSECTION 5.6.3
LONG-TERM TRANSIENT

Plot No.	Component	Variables	Units	Description
26	RPV	DCM	lbm	Fluid mass in downcomer
27	RPV	LDP01DC	in.	Collapsed liquid level in downcomer compared to various reference elevations
28	RPV	MW03RPV	lbm	Fluid mass in core region
29	RPV	LDP03RPV	in.	Collapsed liquid level in core
30	RPV	RPVRXVFO		Core exit void fraction
31	RPV	RPVRXQO		Core exit quality
32	RPV	LDP06RPV	in.	Collapsed liquid level in the upper plenum
33	RPV	MW08RPV	lbm	Fluid mass in the upper head
34	RPV	RPVASL	in.	Level of Tsat line
35	RPV	RPVAPab, RPVPWR	kW	Heater rod power above and below Tsat level and total
36	RPV	RPVASOUT	lbm/sec.	Core steam generation rate
37	RPV	RPVTMRI	lbm/sec.	Calculated core flow
38	RPV	HTMXRPV, ST08RPV	°F	Maximum clad temperature, saturation temperature and delta
39	Hot leg	MWHL1, MWHL2	lbm	Water mass in hot legs
40	Hot leg	MVHL1, MVHL2	lbm	Vapor mass in hot legs
41	Cold leg	CL1WMS, CL2WMS, CL3WMS, CL4WMS	lbm	Water mass in cold legs
42	Cold leg	CL1VMS, CL2VMS, CL3VMS, CL4VMS	lbm	Vapor mass in cold legs
43	ADS and break	BRKSTIR, ADS13TIR, ADS41TIR, ADS42TIR	lbm	Total discharged mass for ADS 1-3, ADS-4, and break
44	ADS and break	ADS13TLR, ADS41TLR, ADS42TLR	lbm/sec.	Liquid flow out ADS 1-3 and ADS-4
45	ADS and break	BRKSTLR	lbm/sec.	Liquid flow and total flow out of break
46	Mass balance	TOTMASS	lbm	Total system mass inventory
47	Mass balance	PRIMMASS, PRIMASS2	lbm	Measured primary system inventory and valve from mass balances
48	Mass balance	MERROR	lbm	Mass balance error
49	Mass balance	MIN, MOUT SRCMASS	lbm	Integrated mass flow in and out of primary system and source mass
50	Energy balance	Various	Btu	Component of energy balance

THE FIGURES LISTED IN TABLE 5.6.3-1
ARE NOT INCLUDED IN THIS NONPROPRIETARY DOCUMENT

5.7 Analysis of Matrix Test SB13

Matrix Test SB13 (OSU Test U0113) simulated a 2-in. break of DVI-1 SBLOCA with LTC and without the operation of the nonsafety-related systems. To simulate a 2-in. break of DVI-1, piping was installed from the DVI line to the break separator. The piping from the break separator connected to the DVI line via two break valves. One break valve isolated the break nozzle and separator inlet from the common injection line of CMT-1 and ACC-1. The other break valve isolated the common break nozzle and the inlet to the break separator from the portion of the DVI line, which connected to the reactor.

The analysis of Matrix Test SB13 is divided into three sections as follows:

- Facility performance is discussed in Subsection 5.7.1. It provides a brief outline of the response of the test facility; further details are available in the Final Data Report.[1]

- The short-term transient for SB13 encompassed the start of the simulation up to [ ]^{a,b,c} seconds. This period included blowdown, ADS, and initial IRWST stages of the transient.

- The analysis of the long-term transient for SB13 encompassed the time frame from [ ]^{a,b,c} seconds to the end of the test. This phase of the transient included IRWST injection and covered the transition to sump injection. The long-term transient actually started at IRWST injection, which is discussed as part of the short-term transient. Between the end of the short-term transient and [ ]^{a,b,c} seconds, the system remained relatively inactive with the exception of the CMT and pressurizer refill. At [ ]^{a,b,c} seconds, CMT-2 began to refill and CMT-1 followed [ ]^{a,b,c} seconds later. The CMT refill phenomena is discussed further in Subsection 6.1.1 and the discussion of the long-term transient provided here begins at [ ]^{a,b,c} seconds.

The discussion of the short- and long-term phase of the transient focuses on important thermal-hydraulic phenomena identified in the PIRT (Table 1.3-1). The mass and energy balance results are key indicators of the quality of the analysis on which this discussion is based. These are discussed in detail in Subsections 6.2.2 and 6.2.3.

5.7.1 Facility Performance

The performance of the OSU test facility during Matrix Test SB13 in reference to the four transient phases is outlined in the following:

- Blowdown
- ADS
- IRWST injection
- Sump injection

The overall performance of the facility during the transient is shown in Figures 5.7.1-1 to 5.7.1-4. Figure 5.7.1-1 shows the pressurizer pressure throughout the test with various phases and operating components delineated on the figure. The time scale was reduced for clarity since there were only small changes in system pressure during the long-term phase of the transient. Figure 5.7.1-2 shows the total DVI line flow and its composition from the various sources at each time in the transient. Figure 5.7.1-3 shows the calculated core steam generation rate throughout the test, and Figure 5.7.1-4 shows the variation in average measured core outlet temperature and heater rod temperature relative to the core outlet saturation temperature.

Figures 5.7.1-1 and 5.7.1-2 show that there was a continuous flow of water to the core from the passive safety-related systems throughout the transient. Once initiated, the ADS lines rapidly depressurized the primary system, which enhanced the CMT and accumulator injection flow rates. Ultimately, the opening of ADS-4 valves sufficiently reduced the system pressure to start gravity-driven IRWST injection. Operation of the passive injection systems overlapped so that as one source of water drained, the next became operable to continue the cooling process. The level of steam generation in the core and the response of the average measured core outlet fluid temperatures and maximum clad temperatures are shown in Figures 5.7.1-3 and 5.7.1-4. These figures show that there was sufficient cooling flow to prevent excessive core heating, and the core remained covered. The core remained subcooled for large periods of the transient and when steam production occurred, the rate of generation remained well below the rate at which water was delivered to the core.

5.7.1.1 Blowdown Phase

The blowdown phase began at time zero when the break was initiated and continued until the primary system pressure was in equilibrium with the secondary-side pressure at around [ ]^{a,b,c} seconds. Immediately following the opening of the break, the primary system pressure fell gradually until about [ ]^{a,b,c} seconds when core power started to reduce. During this phase of the transient, cooling flow was provided from CMT-2, which remained in the recirculation mode, and heat was removed from the primary system via the SGs. The pressurizer and surge line completely drained at [ ]^{a,b,c} and [ ]^{a,b,c} seconds, respectively.

When core power started to reduce at about [ ]^{a,b,c} seconds and CMT-2 transitioned to the injection mode of operation (at [ ]^{a,b,c} seconds) the primary system pressure nearly stabilized at about [ ]^{a,b,c} psia until the end of the blowdown phase. During this time, the SG tubes drained by about [ ]^{a,b,c} seconds and at this time, heat removal from the primary system continued via the PRHR. The steam in the SG tubes became superheated and remained so until the end of the transient.

In response to voiding in CL-3, CMT-1 transitioned to draindown mode at [ ]^{a,b,c} seconds, and the falling CMT level reached the ADS low-level setpoint at [ ]^{a,b,c} seconds. The blowdown phase of the transient continued to [ ]^{a,b,c} seconds when the primary- and secondary-side pressures equalized and the ADS-1 valve opened.

5.7.1.2 Natural Circulation Phase

There is no natural recirculation phase in Test SB13 since the primary and secondary-side pressures equalized at the time ADS-1 initiated.

5.7.1.3 Automatic Depressurization System Phase

ADS-1 actuation was followed by ADS-2 and ADS-3 actuation [ ]^{a,b,c} and [ ]^{a,b,c} seconds later, respectively. Accumulator injection began shortly after initiation of the ADS. The influx of cold water combined with increased venting via the ADS led to a rapid depressurization of the primary system. Actuation of ADS-4 at [ ]^{a,b,c} seconds completed depressurization to a level that allowed IRWST injection at [ ]^{a,b,c} seconds via DVI-1 and [ ]^{a,b,c} seconds via DVI-2. During accumulator injection, increased flow path resistance reduced flow out of the CMTs. As the accumulators drained, CMT flow resumed. The accumulators were fully drained at [ ]^{a,b,c} seconds, before IRWST commenced. CMT-1 and CMT-2 fully drained at [ ]^{a,b,c} and [ ],^{a,b,c} respectively.

The minimum RPV inventory of [ ]^{a,b,c} lbm was observed at [ ]^{a,b,c} seconds, shortly after ADS-3 actuation. The transfer from CMT-2 to IRWST-2 injection was indicated by a low RPV inventory of about [ ]^{a,b,c} lbm before IRWST-2 injection started.

Actuation of ADS-1 rapidly refilled the pressurizer as water and steam flowed out of the ADS. The pressurizer gradually drained by [ ]^{a,b,c} seconds.

5.7.1.4 In-Containment Refueling Water Storage Tank Injection

IRWST injection was the transition from the short- to long-term phase of the transient. The initial phase of IRWST-2 injection involved an increase in flow through DVI-2, which was followed by a gradual flow reduction as the driving head between the IRWST and the RCS fell due to the reduced IRWST water level. IRWST-2 injection flow started at [ ]^{a,b,c} seconds, about at the same time the CMT-2 emptied. Between [ ]^{a,b,c} and [ ]^{a,b,c} seconds, the only cooling available to the core was via IRWST-2 injection.

When maximum IRWST-2 flow was established, the influx of water from the IRWST was sufficient to keep the core subcooled from [ ]^{a,b,c} seconds. The steam generation rate increased after [ ]^{a,b,c} seconds from minimum steam generation rate of about [ ]^{a,b,c} lbm/sec. with a decreasing IRWST-2 injection rate and stabilized at [ ]^{a,b,c} lbm/sec. after [ ]^{a,b,c} seconds. After [ ]^{a,b,c} seconds, temperature at the top of the core followed the saturation temperature for primary system pressure.

After reflooding, the level of both CMTs stayed essentially constant for several thousand seconds. As the level in the IRWST decreased, the backpressure in each DVI line decreased and was low enough at approximately [ ]^{a,b,c} seconds for CMT-1 to start injecting to the break. CMT-2 started injecting to the vessel at about [ ]^{a,b,c} seconds. The injection flow from the CMTs was oscillating between approximately [ ]^{a,b,c} seconds. At about [ ]^{a,b,c} seconds flow from the break separator to the primary sump was reversed as indicated by flow meter FMM-905. Shortly after that the break flow was reversed as indicated by both decreasing integral break flow (see Figure 5.7.3-43) and break liquid flow (Figure 5.7.3-45).

5.7.1.5 Sump Injection

Injection from the primary sump via the check valves around the main sump injection valves began at about [ ]^{a,b,c} seconds when the level in the IRWST was low enough to allow flow. This caused a reduction in the flow rate from the IRWST-2. When the IRWST level fell to [ ]^{a,b,c} in., the main sump injection valves opened and the sump injection flow rate increased. This increase occurred at [ ]^{a,b,c} seconds and the driving head from the sump was sufficient for flow from the sump to the IRWST on the DVI line.

TABLE 5.7.1-1
OSU TEST ANALYSIS PLOT PACKAGE FOR SUBSECTION 5.7.1

Plot No.	Component	Variables	Units	Description
1	Pressurizer	CPT-604	psia	System pressure and event history
2	Water injection	WWTDVI1+WWTDVI2, WOUTACC1+WOUTACC2, WWTIRWI1+WWTIRWI2, WWTSMPIT	lbm/sec.	Total of CMT, accumulator, IRWST, and sump injection flows
3	Reactor vessel	RPVASOU2	lbm/sec.	Steam generation in reactor vessel
4	Reactor vessel	T08RPV, HTMXRPV, TSAT	°F	Reactor vessel outlet temperature, maximum clad temperature and fuel exit saturation temperature

THE FIGURES LISTED IN TABLE 5.7.1-1
ARE NOT INCLUDED IN THIS NONPROPRIETARY DOCUMENT

5.7.2 Short-Term Transient

For the 2-in. DVI line break, Matrix Test SB13, the short-term transient encompassed the time frame up to [ ]^{a,b,c} seconds. As shown in Figure 5.7.1-1, this period included the full depressurization of the facility through all four stages of the ADS, together with CMT and accumulator injection plus the initial stages of IRWST injection. Variations in mass, energy, pressure, and temperature throughout this stage of the transient are illustrated in the plot package outlined in Table 5.7.2-1. The plots concentrate on the primary system, including the accumulators, CMTs, IRWST, primary sump and flow from the primary system via the ADS, break, and IRWST overflow.

There were two principal parameters of interest for the short-term transient:

- Adequate flow from the passive systems to the reactor vessel must be maintained.
- Adequate flow into the core must be maintained to ensure that decay heat was removed from the simulated fuel rods, without a temperature excursion.

These parameters are addressed in the following discussion.

5.7.2.1 Maintenance of Core Cooling

Mass Injected to the Primary System

Figures 5.7.2-5 and 5.7.2-6 show the combined effect of the injection flows for the short-term phase of the transient. Separate plots of the individual contributions to the total flow can be located by consulting the plot package index given in Table 5.7.2-1.

Figure 5.7.2-6 shows how the CMT-2, ACC-2 and IRWST-2 supply a continuous flow of cooling water to the core. During the first [ ]^{a,b,c} seconds, cooling flow was provided by CMT-2. The rate of flow from CMT-2 increased from zero to [ ]^{a,b,c} lbm/sec. at [ ]^{a,b,c} seconds after ADS-1 actuated and ACC-2 injection started. ACC-2 injection resulted in a decrease in the CMT-2 flow but led to an overall increase in flow to the core to a peak value of [ ]^{a,b,c} lbm/sec. Following the end of accumulator injection, CMT-2 again provided cooling flow until it drained. The only period in which there was relatively little cooling flow was at about [ ]^{a,b,c} seconds when the CMT-2 drained and IRWST injection started.

Reactor Pressure Vessel and Downcomer Behavior

The effect of water flow on the average measured core inlet/outlet temperatures and heater rod temperatures during the short-term phase of the transient is shown in Figures 5.7.2-3 and 5.7.2-57. The combined CMT-2 and ACC-2 flow was sufficient to keep the bottom of the core subcooled from

about [ ]^{a,b,c} seconds. The core outlet temperature remained at the saturation level throughout the short-term transient until the influx of water from the IRWST-2 was sufficient to subcool the core.

Figure 5.7.2-57 shows that there were no significant excursions in heater rod temperatures throughout the short-term transient; therefore, sufficient core inventory and flow was maintained through this phase of the transient to remove the simulated decay heat. For significant portions of the transient, a two-phase mixture was present in the core and upper plenum regions, with core boiling kept at a low level. The following discussion tracks the variation in water level and mass throughout the reactor vessel and downcomer.

The mass and level within the core region are shown in Figures 5.7.2-44 and 5.7.2-45. The collapsed liquid level in the core indicates that the heater rods remained covered with a single- or two-phase mixture. The minimum core inventory of [ ]^{a,b,c} lbm occurred at [ ]^{a,b,c} seconds into the transient after ADS-3 actuated. Figure 5.7.2-45 shows that the collapsed liquid level dropped [ ]^{a,b,c} in. below the top of the heater rods during this phase of the transient. The average void fraction of the core two-phase mixture may be estimated by dividing the measured core collapsed liquid level by the [ ]^{a,b,c} in. heated rod length. In this test, the minimum collapsed liquid level corresponded to a core void fraction of [ ].^{a,b,c} After this time, core inventory increased due to injection from ACC-2 and CMT-2 and decreasing flow leaving the primary system through ADS 1-3 and the break. By the end of the short-term transient, IRWST-2 injection reduced core boiling (Figure 5.7.2-55) and the core was nearly water-solid.

The collapsed liquid level in the upper plenum region and the associated fluid mass are shown in Figures 5.7.2-49 and 5.7.2-48. The collapsed liquid level in the upper plenum span of LDP-113 decreased immediately after the break and fell to a minimum level (a few inches) between ADS-4 actuation and IRWST-2 injection (before the end of the accumulator injection). Then, IRWST-2 injection supplied sufficient inventory to initiate a refill. The upper plenum collapsed liquid level increased up to the elevation of the cold leg by the end of the short-term transient.

Figures 5.7.2-50 and 5.7.2-51 show that the upper head also lost inventory after the break valves opened and was almost drained by [ ]^{a,b,c} seconds. The upper head was refilled (collapsed liquid level at about 6 in.) at [ ]^{a,b,c} seconds when the pressurizer started to drain after refill and the IRWST-2 injection flow was close to maximum.

The reduction in upper plenum and upper head inventory was responsible for the reduction in overall RPV inventory until the IRWST injection started (Figure 5.7.2-40).

The mass of fluid and collapsed liquid level in the RPV downcomer are shown in Figures 5.7.2-41 and 5.7.2-42. The downcomer remained water-solid until about [ ]^{a,b,c} seconds, when the collapsed liquid level fell to the elevation of the cold legs, reaching the lowest level at about [ ]^{a,b,c} seconds (5 in. below the elevation of the top of heater rods). Then, the collapsed level increased almost to the elevation of the cold legs by the end of the short-term transient.

5.7.2.2 Energy Transport from the Primary System

Following the break, the heater rods deposited energy in the primary system fluid to simulate decay heat and the primary system metal as it cooled down. Some fluid energy was lost to the ambient and out of the break. Energy must be removed from the primary system to prevent excessive fluid and heater rod temperature excursions. In the AP600 plant, heat removal is designed to be achieved by a combination of the SGs and the PRHR plus the ADS.

Steam Generator and Passive Residual Heat Removal Heat Transfer

During normal operation, most of the primary system heat was removed via the SGs; however, once the coolant pumps tripped, reduced system flow caused a reduction in primary-to secondary-side heat transfer. The SGs were only available as heat sinks until the primary system pressure dropped to that of the secondary side, the two sides were then in thermal equilibrium. After that, the secondary side became a potential heat source for the primary side.

The PRHR is designed to remove heat from the primary system once the signal opens the isolation valve. The PRHR will continue to remove energy after the SGs are thermally isolated until ADS actuates. Once the ADS is actuated, ADS 1-3 becomes the predominant path for the removal of energy from the primary system.

Figure 5.7.2-33 shows the SG primary- and secondary-side pressure (together with the PRHR integrated heat transfer as represented by the IRWST fluid energy after allowing for the contribution from ADS 1-3 inflow).

PRHR heat removal began [ ]^{a,b,c} seconds into the test and the PRHR was responsible for all the IRWST heat-up until ADS-1 activation; the PRHR heat transfer then was reduced. The PRHR outlet flow ceased at about [ ]^{a,b,c} seconds. During the active phase, the PRHR transferred heat to the IRWST at an average rate of [ ]^{a,b,c} Btu/sec.

Energy Transport via the Break and Automatic Depressurization System

The mass flow rate from the primary system via the break is shown in Figures 5.7.2-67 and 5.7.2-68. The short-term transient liquid flow was calculated. During the first [ ]^{a,b,c} seconds following the break, [ ]^{a,b,c} lbm of fluid flowed out of the primary system via the break at an average rate of approximately [ ]^{a,b,c} lbm/sec., consisting of liquid ([ ]^{a,b,c} lbm) and steam ([ ]^{a,b,c} lbm). During this period, the primary system depressurized to around [ ]^{a,b,c} psia (Figure 5.2.2-1). With the initiation of ADS 1-3 and accumulator injection, steam flow through the break ceased and was replaced by steam and liquid flow through the ADS 1-3 valves. Between [ ]^{a,b,c} and [ ]^{a,b,c} seconds, ADS 1-3 caused the system to rapidly depressurize to about [ ]^{a,b,c} psia and at [ ]^{a,b,c} seconds, ADS-4 was initiated and the primary system continued to depressurize to BAMS header pressure.

The initiation of the ADS reduced the flow through the break. During ADS 1-3 depressurization, steam and liquid flow through the ADS 1-3 valves occurred at a rate of [ ]^{a,b,c} lbm/sec. ([ ]^{a,b,c} seconds). Flow through the ADS 1-3 continued at a declining rate until about [ ]^{a,b,c} seconds when the flow through ADS 1-3 terminated and was replaced by flow through the lower resistance ADS-4 paths. By the end of the short-term transient ([ ]^{a,b,c} seconds), water was flowing out of the two ADS-4 valves at approximately [ ]^{a,b,c} lbm/sec. (Figure 5.7.2-64).

Integrated mass flow from the primary system via the ADS and the break is shown in Figure 5.7.2-62, and the corresponding integrated energy flow is shown in Figure 5.7.2-63. The total system inventory plot given in Figure 5.7.2-70 indicates that up to [ ]^{a,b,c} lbm of inventory left the system during the short-term transient. Components of the energy balance are shown in Figure 5.7.2-74.

TABLE 5.7.2-1
OSU TEST ANALYSIS STANDARD PLOT PACKAGE FOR SUBSECTION 5.7.2

Plot No.	Component	Variables	Units	Description
1	Pressurizer	CPT-604	psia	System pressure
2	RPV	RPVPWR	kW	Core power
3	RPV	T01RPV, T08RPV, ST08RPV	°F	Core inlet/outlet temperature, saturation temperature
4	SG	CPT-201, CPT-204, CPT-301, CPT-302	psia	Primary and secondary pressures in SG
5	DVI-1	WWTDVIL1, WWTIRWI1, WOUTACC1, WWTIRWI3	lbm/sec.	Individual components and total flow in DVI-1
6	DVI-2	WWTDVIL2, WWTIRWI2, WOUTACC2, WWTIRWI4	lbm/sec.	Individual components and total flow in DVI-2
7	CMT	AMCMT1B, AMCMT2B	lbm	Fluid mass in CMTs (excludes balance lines)
8	CMT	CLDP-502, CLDP-507	in.	Collapsed liquid level in CMTs
9	CMT	MIWDVIL1, MIWDVIL2	lbm	Integrated mass out of CMTs
10	CMT	WWTDVIL1, WWTDVIL2	lbm/sec.	Flow out of CMTs
11	CMT	WOUTCLB1, WOUTCLB2	lbm/sec.	Flow into CMTs
12	CMT	CLDP-509, CLDP510	in.	Level CL-CMT balance lines
13	CMT	UCMT1, UCMT2	Btu	Fluid energy in CMTs
14	IRWST	IRWST	lbm	Mass of fluid in IRWST
15	IRWST	CLDP-701	in.	Collapsed liquid level in IRWST
16	IRWST	WWTIRWI1, WWTIRWI2	lbm/sec.	Flow from IRWST to DVI lines
17	IRWST	IRWSTOR	lbm/sec.	Overflow from IRWST to sump
18	IRWST	ADS13TMR	lbm/sec.	Total ADS flow into IRWST
19	IRWST	ADS13TIR, MIIRWI1, MIIRWI2, MIIRWIO	lbm	Integrated mass out of IRWST
20	IRWST	UIRWST	Btu	Fluid energy in IRWST
21	PRHR	CLDP-802	in.	Collapsed liquid level in PRHR HX

TABLE 5.7.2-1 (Continued) OSU TEST ANALYSIS STANDARD PLOT PACKAGE FOR SUBSECTION 5.7.2				
Plot No.	**Component**	**Variables**	**Units**	**Description**
22	PRHR	WWOTPRHR	lbm/sec.	Measured outlet flow from PRHR tube
23	Accumulator	AMACC1, AMACC2	lbm	Mass of fluid in accumulators
24	Accumulator	CLDP-401, CLDP-402	in.	Collapsed liquid level in accumulators
25	Accumulator	WOUTACC1, WOUTACC2	lbm/sec.	Flow from accumulators
26	Accumulator	MOUTACC1, MOUTACC2	lbm	Integrated mass out of accumulators
27	Accumulator	UACC1, UACC2	Btu	Fluid energy in accumulators
28	Primary sump	AMPSMP	lbm	Primary sump fluid mass
29	Primary sump	CLDP-901	in.	Primary sump level
30	Primary sump	UPSMP	Btu	Primary sump fluid energy
31	SG	MSSGIP1, MSSGIP2, MSSGOP1, MSSGOP2	lbm	Mass of fluid in SG primary side inlet/outlet plena
32	SG	MSSGHT1, MSSGHT2, MSSGCT1, MSSGCT2	lbm	Mass of fluid in SG primary side hot and cold tubes
33	SG/PRHR	CPT-201, CPT-301, QPRHRI	psia & Btu	SG1 pressure and PRHR integrated heat output
34	Pressurizer	PZM	lbm	Fluid mass in pressurizer
35	Pressurizer	CLDP-601	in.	Collapsed liquid level in pressurizer
36	Pressurizer	UPZ	Btu	Fluid energy in pressurizer
37	Surge line	PLM	lbm	Fluid mass in surge line
38	Surge line	CLDP-602	in.	Collapsed liquid level in surge line
39	Surge line	UPSL	Btu	Fluid energy in surge line
40	RPV	MWRPV	lbm	Total fluid mass in reactor vessel
41	RPV	DCM	lbm	Fluid mass in downcomer
42	RPV	LDP01DC	in.	Collapsed liquid level in downcomer compared to various reference elevations
43	RPV	MW01RPV	lbm	Fluid mass in lower plenum
44	RPV	MW03RPV	lbm	Fluid mass in core region
45	RPV	LDP03RPV	in.	Collapsed liquid level in core
46	RPV	RPVAVDF2		Core exit void fraction
47	RPV	RPVAQOU2		Core exit quality
48	RPV	MW06RPV	lbm	Fluid mass in the upper plenum
49	RPV	LDP06RPV	in.	Collapsed liquid level in the upper plenum
50	RPV	MW08RPV	lbm	Fluid mass in the upper head
51	RPV	LDP08RPV	in.	Collapsed liquid level in the upper head

TABLE 5.7.2-1 (Continued) OSU TEST ANALYSIS STANDARD PLOT PACKAGE FOR SUBSECTION 5.7.2				
Plot No.	**Component**	**Variables**	**Units**	**Description**
52	RPV	URPV	Btu	Total fluid energy in reactor vessel
53	RPV	RPVXE, RPVASL2	in.	Level of Tsat line
54	RPV	RPVPab, RPVAPab2, RPVPWR	kW	Heater rod power above and below Tsat level and total
55	RPV	RPVRXV, RPVASOU2	lbm/sec.	Core steam generation rate
56	RPV	RPVALIN2	lbm/sec.	Calculated core flow
57	RPV	HTMXRPV, ST08RPV	°F	Maximum clad temperature and saturation temperature
58	Hot leg	MWHL1, MWHL2	lbm	Water mass in hot legs
59	Hot leg	MVHL1, MVHL2	lbm	Vapor mass in hot legs
60	Cold leg	CL1WMS, CL2WMS, CL3WMS, CL4WMS	lbm	Water mass in cold legs
61	Cold leg	CL1VMS, CL2VMS, CL3VMS, CL4VMS	lbm	Vapor mass in cold legs
62	ADS and break	BRKSTIR, ADS13TIR, ADS41TIR, ADS42TIR	lbm	Total discharged mass for ADS 1-3, ADS-4s, and break
63	ADS and break	BRKTIVF, AD13TIVF, AD41TIVF, AD42TIVF	lbm	Total integrated vapor flow for ADS and break
64	ADS and break	BRKTILF, AD13TILF, AD41TILF, AD42TILF	lbm	Total integrated liquid flow for ADS and break
65	ADS and break	ADS13SVR, ADS41SVR, ADS42SVR	lbm/sec.	Vapor flow out ADS 1-3 and ADS-4
66	ADS and break	ADS13SLR, ADS41SLR, ADS42SLR	lbm/sec.	Liquid flow out ADS 1-3 and ADS-4
67	ADS and break	BRKSSVR	lbm/sec.	Vapor flow out of break
68	ADS and break	BRKSSLR	lbm/sec.	Liquid flow out of break
69	ADS and break	BRKSPEI, ADS13EI, ADS41EI, ADS42EI	Btu	Integrated fluid energy for ADS 1-3, ADS-4, and break
70	Mass balance	TOTMASS	lbm	Total system mass inventory
71	Mass balance	PRIMMASS, PRIMASS2	lbm	Measured primary system inventory and value from mass balance
72	Mass balance	MERROR	lbm	Mass balance error
73	Mass balance	MIN, MOUT SRCMASS	lbm	Integrated mass flow in and out of primary system and source mass
74	Energy balance	Various	Btu	Components of energy balance

THE FIGURES LISTED IN TABLE 5.7.2-1
ARE NOT INCLUDED IN THIS NONPROPRIETARY DOCUMENT

5.7.3 Long-Term Transient

The long-term transient started with initiation of IRWST injection, covered the transition from IRWST to sump injection, and provided information on the LTC response of the AP600 plant with sump injection. For the 2-in. DVI line break, Matrix Test SB13, the long-term transient phase began at [ ]^{a,b,c} seconds and continued to the end of the test at about [ ]^{a,b,c} seconds. The behavior of the test facility during this period of the transient is discussed in this subsection using the plot package detailed in Table 5.7.3-1. This analysis concentrates on the components of the primary system that remained active during the LTC phase, that is, the RPV, the hot legs, ADS-4, the sumps, and the IRWST.

During the long-term transient, the main thermal-hydraulic phenomena of interest were maintenance of core cooling and removal of energy from the primary system.

5.7.3.1 Maintenance of Core Cooling

Mass Injected into Primary System

Total DVI line flow, CMT flow, and IRWST flows are shown in Figures 5.7.3-6 and 5.7.3-7, and the flow from the primary sump is shown in Figure 5.7.3-19. From around [ ]^{a,b,c} seconds, there was a contribution to the DVI flow from CMT-2 as CMT-2 reached post-refill draindown.

Prior to sump injection, during the IRWST injection phase of the transient, IRWST flow proceeded at a gradually declining rate. At [ ]^{a,b,c} seconds, flow from the primary sump began through the check valves around the main injection valves, resulting in further reduction in IRWST-2 flow. From [ ]^{a,b,c} seconds to the end of the transient, a near-steady flow rate of [ ]^{a,b,c} lbm/sec. was maintained through DVI-2. At [ ]^{a,b,c} seconds, the main sump injection valves opened, resulting in a reversal of flow through IRWST injection line-1 and an increase in IRWST flow in line-2. The net result was that the injection flow rate in DVI-2 gradually decreased from [ ]^{a,b,c} lbm/sec. at [ ]^{a,b,c} seconds to [ ]^{a,b,c} lbm/sec. at the end of the transient.

Reactor Pressure Vessel and Downcomer Response

The effect of water inflow on the average measured downcomer fluid temperatures, core inlet and core outlet temperatures, and heater rod temperatures during the long-term phase of the transient is shown in Figures 5.7.3-4, 5.7.3-5, and 5.7.3-38. Figure 5.7.3-4 shows that there is a general increase in average downcomer fluid temperatures during the long-term transient. By the end of the test, some temperature stratification was observed in the downcomer. The temperature in the bottom of the downcomer was [ ]^{a,b,c} °F below saturation. Figure 5.7.3-5 shows that the core remained saturated for the entire long-term transient. Figures 5.7.3-34 to 5.7.3-36, show that the DVI line flow method discussed in Section 4.11 indicates that a small level of boiling was maintained until the end of the

transient. Nevertheless, the level of boiling was small and showed that the inflow from the IRWST and sumps was sufficient to subcool the RPV.

Figure 5.7.3-38 shows that there were no significant excursions in heater rod temperatures throughout the long-term transient; therefore, sufficient core inventory and flow was maintained throughout this phase of the transient to remove the decay heat generated. The following discussion tracks the variation in water level and mass throughout the reactor vessel and downcomer.

The mass and level for the core region are shown in Figures 5.7.3-28 and 5.7.3-29. The collapsed liquid level in the core indicated that the heater rods were always covered with a single- or two-phase mixture. During the later stages of the transient, the collapsed liquid level remained just below the top of the heater rods, and the core void fraction was [ ].[a,b,c] The fall in core inventory was a result of the influx of hot water from the primary sump as it flowed through the check valves. The impact of this hot water on the system temperatures is shown in Figures 5.7.3-4 and 5.7.3-5 as a sudden increase in fluid temperature in the downcomer and at the core inlet. The hot water also led to an increase in the calculated steam generation rate, as shown in Figure 5.7.3-36, and a corresponding fall in the level at which the core reached saturation temperature (Figure 5.7.3-34).

The collapsed liquid level in the upper plenum region is shown in Figure 5.7.3-32. This figure indicates that during the period before sump injection began, the collapsed liquid level initially fell and then remained at the elevation of the hot legs. Following the influx of hot water from the sumps, the level dropped to the elevation of the top of the DVI injection lines where it remained for the rest of the transient. This level corresponds to a void fraction of [ ][a,b,c] in the upper plenum.

The mass of water in the RPV is shown in Figure 5.7.3-25. After an initial decline, the reactor vessel water mass settled at an average value of [ ][a,b,c] lbm until sump injection started when it gradually fell to [ ][a,b,c] lbm, which is [ ][a,b,c] percent of the initial vessel water inventory, and remained at this level to the end of the transient. Oscillations in vessel inventory occurred as shown in Figures 5.7.3-51 through 5.7.3-56. These oscillations and possible mechanisms for their production are discussed in Subsection 6.1.3.

The mass of fluid and collapsed liquid level in the RPV downcomer are shown in Figures 5.7.3-26 and 5.7.3-27. The collapsed liquid level fell below the elevation of the cold legs after CMT-2 injection at about [ ][a,b,c] seconds for the entire long-term transient. The sump injection had little effect on water level in the downcomer.

5.7.3.2 Energy Transport from the Primary System

During the long-term transient, energy continued to be deposited in the primary system from the heater rods, metal, and fluid flowing from the primary sump. The SGs and PRHR remained inactive throughout this phase of the transient and the principal path for energy out of the primary system was via the ADS-4 valves.

Integrated mass flow from of the primary system via the ADS and the break is shown in Figures 5.7.3-43. During the LTC phase of the transient, the only significant outflow is through the ADS-4 valves. This is confirmed by Figures 5.7.3-44 and 5.7.3-45, which show flow through the ADS and the break. During the sump injection phase of the transient, outflow was indicated as liquid going through the ADS-4 valves. Water flowed through each of the valves at an average rate of [ ]^{a,b,c} lbm/sec.

Figure 5.7.3-36 shows the calculated steam generation rate as determined by the DVI line flow method. During the sump injection phase of the transient, steam was generated at about [ ]^{a,b,c} lbm/sec., indicate little or no flow from the steam vortex meters out of the ADS-4 valves. Steam left the primary circuit by this route as shown by the following.

- Figure 5.7.3-46 shows total measured system fluid inventory. During this phase of the transient after the start of primary sump injection (from [ ]^{a,b,c} seconds, that is, when core steam generation was most significant, the total system inventory fell by over [ ]^{a,b,c} lbm. This amount corresponds to a steam flow rate of [ ]^{a,b,c} lbm/sec., which would not have been detected by the vortex meters.

- Examination of the fluid thermocouples on the outlet of the ADS-4 valves indicates that temperatures remained at or above saturation temperature following the start of sump injection.

Furthermore, as discussed in Subsection 6.1.3, it was not possible for all the steam generated in the core to flow from the upper head to the downcomer via the bypass holes. It can therefore be concluded that steam was leaving the primary system via ADS-4. Figure 5.7.3-50 shows all the components to the system energy balance. Further discussion of steam loss from the primary circuit is provided in the mass and energy balance discussions of Section 6.2.

TABLE 5.7.3-1
OSU TEST ANALYSIS STANDARD PLOT PACKAGE FOR SUBSECTION 5.7.3
LONG-TERM TRANSIENT

Plot No.	Component	Variables	Units	Description
1	RPV	RPVPWR	kW	Core power
2	Primary sump	TSMPI1, TSMPI2	°F	Sump injection line temperatures
3	DVI	TDVIL1, TDVIL2	°F	DVI line temperatures
4	RPV	T01DC, T02DC, T03DC, ST01DC	°F	Water and saturation temperatures in downcomer
5	RPV	T01RPV, T08RPV, ST08RPV	°F	Core inlet/outlet temperature, saturation temperature
6	DVI-1	WWTDVIL1, WWTIRWI1, WWTIRWI3	lbm/sec.	Individual components and total flow in DVI-1
7	DVI-2	WWTDVIL2, WWTIRWI2, WWTIRWI4	lbm/sec.	Individual components and total flow in DVI-2
8	CMT	CLDP-502, CLDP-507	in.	Collapsed liquid level in CMTs
9	CMT	CLDP-509, CLDP510	in.	Level CL-CMT balance lines
10	IRWST	IRWST	lbm	Mass of fluid in IRWST
11	IRWST	CLDP-701	in.	Collapsed liquid level in IRWST
12	IRWST	UIRWST	Btu	Fluid energy in IRWST
13	Primary sump	AMPSMP	lbm	Primary sump fluid mass
14	Primary sump	CLDP-901	in.	Primary sump level
15	Primary sump	UPSMP	Btu	Primary sump fluid energy
16	Secondary sump	AMSSMP	lbm	Secondary sump fluid mass
17	Secondary sump	CLDP-902	in.	Secondary sump level
18	Secondary sump	USSMP	Btu	Secondary sump fluid energy
19	Primary sump	WSTSMPET, WWTSMPIT	lbm/sec.	Primary sump steam and liquid injection rate
20	Primary sump	MISMPI1, MISMPI2, MISMPIT, MIIRWT	lbm	Integrated primary sump and IRWST flows
21	SG	MSSGIP1, MSSGIP2, MSSGOP1, MSSGOP2	lbm	Mass of fluid in SG side inlet/outlet plena
22	Surge line	PLM	lbm	Fluid mass in surge line
23	Surge line	CLDP-602	in.	Collapsed liquid level in surge line
24	Surge line	UPSL	Btu	Fluid energy in surge line
25	RPV	MWRPV	lbm	Total fluid mass in reactor vessel

TABLE 5.7.3-1 (Continued)
OSU TEST ANALYSIS STANDARD PLOT PACKAGE FOR SUBSECTION 5.7.3
LONG-TERM TRANSIENT

Plot No.	Component	Variables	Units	Description
26	RPV	DCM	lbm	Fluid mass in downcomer
27	RPV	LDP01DC	in.	Collapsed liquid level in downcomer compared to various reference elevations
28	RPV	MW03RPV	lbm	Fluid mass in core region
29	RPV	LDP03RPV	in.	Collapsed liquid level in core
30	RPV	RPVAVDF2		Core exit void fraction
31	RPV	RPVAQOU2		Core exit quality
32	RPV	LDP06RPV	in.	Collapsed liquid level in the upper plenum
33	RPV	MW08RPV	lbm	Fluid mass in the upper head
34	RPV	RPVASL2	in.	Level of Tsat line
35	RPV	RPVAPab2, RPVPWR	kW	Heater rod power above and below Tsat level and total
36	RPV	RPVASOU2	lbm/sec.	Core steam generation rate
37	RPV	RPVALIN2	lbm/sec.	Calculated core flow
38	RPV	HTMXRPV, ST08RPV	°F	Maximum clad temperature, saturation temperature and delta
39	Hot leg	MWHL1, MWHL2	lbm	Water mass in hot legs
40	Hot leg	MVHL1, MVHL2	lbm	Vapor mass in hot legs
41	Cold leg	CL1WMS, CL2WMS, CL3WMS, CL4WMS	lbm	Water mass in cold legs
42	Cold leg	CL1VMS, CL2VMS, CL3VMS, CL4VMS	lbm	Vapor mass in cold legs
43	ADS and break	BRKSTIR, ADS13TIR, ADS41TIR, ADS42TIR	lbm	Total discharged mass for ADS 1-3, ADS-4, and break
44	ADS and break	ADS13TLR, ADS41TLR, ADS42TLR	lbm/sec.	Liquid flow out ADS 1-3 and ADS-4
45	ADS and break	BRKSTLR	lbm/sec.	Liquid flow and total flow out of break
46	Mass balance	TOTMASS	lbm	Total system mass inventory
47	Mass balance	PRIMMASS, PRIMASS2	lbm	Measured primary system inventory and valve from mass balances
48	Mass balance	MERROR	lbm	Mass balance error
49	Mass balance	MIN, MOUT SRCMASS	lbm	Integrated mass flow in and out of primary system and source mass
50	Energy balance	Various	Btu	Component of energy balance
51	ADS-4	ADS41TLR, ADS42TLR	lbm/sec.	Oscillations in ADS-4 liquid flow
52	Surge line	CLDP-602	in.	Oscillations in surgeline level
53	RPV	CPT-107	psia	Oscillations in upper head pressure

TABLE 5.7.3-1 (Continued) OSU TEST ANALYSIS STANDARD PLOT PACKAGE FOR SUBSECTION 5.7.3 LONG-TERM TRANSIENT				
Plot No.	**Component**	**Variables**	**Units**	**Description**
54	RPV	CLDP-113	in.	Oscillations in upper plenum level
55	RPV	LDP03RPV	in.	Oscillations in core level
56	RPV	LDP01DC	in.	Oscillations in downcomer level

THE FIGURES LISTED IN TABLE 5.7.3-1
ARE NOT INCLUDED IN THIS NONPROPRIETARY DOCUMENT

5.8 Analysis of Matrix Test SB14

Matrix Test SB14 (OSU Test U0014) simulated a no-break LOCA event with inadvertent actuation of the ADS and progressing to LTC, without operation of the nonsafety-related systems. In this event, ADS-1 opened to initiate the transient, while other safety-related systems activated in response to the passive safeguards actuation signals received. The simulated single failure was one of the ADS-4 lines.

The analysis of Matrix Test SB14 is divided into three sections as follows:

- Facility performance is given in Subsection 5.8.1 and it provides a brief outline of the response of the test facility. Further details are available in the Final Data Report.[1]

- The short-term transient for SB14 encompassed the start of the simulation up to [ ]^{a,b,c} seconds. This period includes the initial blowdown through the ADS and initial IRWST injection stages of the transient.

- The long-term transient for SB14 encompassed the time frame from [ ]^{a,b,c} seconds to the end of the test. This phase of the transient included the IRWST injection and covered the transition to sump injection. The long-term transient actually started at IRWST injection, which is discussed as part of the short-term transient. Between the end of the short-term transient and [ ]^{a,b,c} seconds, the system remained relatively inactive with the exception of the CMT refill. At [ ]^{a,b,c} seconds and [ ]^{a,b,c} seconds, respectively, CMT-1 and CMT-2 began to refill. The CMT-2 level instrument LDP-502 was unavailable during this test because the channel was used to initiate the transient. ADS actuation occurs when either CMT reaches the low-level setpoint. The operator induced a low-level signal from CMT-2 via LDP-502 to initiate SB14; the sum of CMT-2 level instruments LDP-504, LDP-506, and LDP-508 was therefore utilized to determine the CMT-2 level. Since CMT refill phenomena are discussed further in Section 6.1.1, the discussion of the long-term transient begins at [ ]^{a,b,c} seconds.

The discussion of the short- and long-term phases of the transient focuses on important thermal-hydraulic phenomena identified in the PIRT (Table 1.3-1). The mass and energy balance results are key indicators of the quality of the analysis on which this discussion is based. These are discussed in detail in Subsections 6.2.2 and 6.2.3.

5.8.1 Facility Performance

The performance of the OSU test facility during Matrix Test SB14 is outlined in reference to the five transient phases as follows:

- Blowdown
- Natural circulation
- ADS
- IRWST injection
- Sump injection

The overall performance of the facility during the transient is shown in Figures 5.8.1-1 to 5.8.1-4. Figure 5.8.1-1 shows the pressurizer pressure throughout the test with various phases and operating components. The time scale was reduced for clarity since there were only small changes in system pressure during the long-term phase of the transient. Figure 5.8.1-2 shows the total DVI line flow and its composition from the various sources at each time in the transient. Figure 5.8.1-3 shows the calculated core steam generation rate throughout the test, and Figure 5.8.1-4 shows the variation in average measured core outlet temperature and peak clad temperature relative to the core outlet saturation temperature.

Figures 5.8.1-1 and 5.8.1-2 show that there was a continuous flow of cooling water to the core from the passive safety-related systems throughout the transient. Once initiated, the ADS rapidly depressurized the primary system, and thereby enhanced CMT and accumulator injection flow rates. Ultimately, the ADS-4 vent path sufficiently reduced the system pressure to allow gravity-driven IRWST injection. The passive injection systems overlapped and as one source of water drained, the next became available to continue the cooling process. The level of steam generation in the core and the response of the average measured core outlet fluid temperatures and maximum clad temperatures are shown in Figures 5.8.1-3 and 5.8.1-4. These figures show that the cooling flow was sufficient to prevent excessive core heating, and the core remained covered. The core remained subcooled for large periods of the transient and when steam production did occur, the rate of generation remained below the rate at which water was delivered to the core.

5.8.1.1 Blowdown Phase

This event did not exhibit a blowdown phase as the break cases did; it began at time zero when ADS-1 was initiated, as though from a spurious actuation signal. The primary system pressure reached equilibrium with the secondary-side pressure at about [ ]^{a,b,c} seconds. Immediately after the ADS-1 valves opened, primary system pressure decreased as a vent path was established. During this phase, heat was removed from the primary system via the SGs until pressure equilibrium was reached with the secondary side. The pressurizer and surge line received flow from the primary loop to feed the open ADS valves throughout the initial phase of this event.

5.8.1.2 Natural Circulation Phase

In this simulation, the single- and two-phase natural circulation phase was insignificant since there was a large reduction in system pressure due to open ADS flow paths, compared to the more stable pressure observed in SB01. During this phase of the transient, the SG tubes all drained around [ ]^{a,b,c} seconds. At that time, heat removal from the primary system continued via the ADS outflow and to a lesser extent, the PRHR. Steam in the SG tubes became superheated and remained so until the end of the transient. In response to voiding in CL-3, CMT-1 transitioned to draindown mode before [ ]^{a,b,c} seconds elapsed.

5.8.1.3 Automatic Depressurization System Phase

Actuation of ADS-1 was followed by ADS-2 and ADS-3 actuation [ ]^{a,b,c} and [ ]^{a,b,c} seconds later, respectively. Accumulator injection began after all paths of ADS 1-3 were open. The influx of cold water combined with venting via the ADS produced rapid depressurization of the primary system. Actuation of ADS-4 at about [ ]^{a,b,c} seconds completed depressurization and resulted in IRWST injection at about [ ]^{a,b,c} seconds via DVI-1 and DVI-2. During accumulator injection, increased flow path resistance reduced flow out of the CMTs. CMT flow resumed again as the accumulators drained. The accumulators had fully drained before [ ]^{a,b,c} seconds of the transient elapsed, and the CMT-1 and CMT-2 levels showed that the tanks had drained completely at about [ ]^{a,b,c} seconds, shortly after IRWST injection began. Minimum RPV mass inventory of [ ]^{a,b,c} lbm occurred at about [ ]^{a,b,c} seconds into the transient.

Actuation of ADS-1 caused a rapid refill of the pressurizer as water and steam flowed out of the ADS. The pressurizer gradually drained by [ ]^{a,b,c} seconds.

5.8.1.4 In-Containment Refueling Water Storage Tank Injection

The start of IRWST injection is the transition from the short- to long-term phase of the transient. The initial phase of IRWST injection involved an increase in flow through the two DVI lines, which was followed by a gradual reduction in flow as the driving head between the IRWST and the RCS fell with the reducing IRWST water level. Once maximum flow was established, the influx of water from the IRWST was sufficient to keep the core subcooled from [ ]^{a,b,c} seconds to the end of the short-term transient. No RPV pressure/level oscillations were observed in the SB14 transient.

5.8.1.5 Sump Injection

Injection from the primary sump via the check valves around the main sump injection valves began at [ ]^{a,b,c} seconds when the level in the IRWST was low enough to allow that flow. This caused a reduction in the flow rate from the IRWST. When the IRWST level fell to [ ]^{a,b,c} in., the main sump injection valves opened and the sump injection flow rate increased at [ ]^{a,b,c} seconds via DVI-1. DVI-2 flow from the IRWST decreased to zero when the main sump valves opened;

thereafter, DVI-2 flow from the IRWST increased to approximately [ ]^{a,b,c} lbm/sec., the [ ]^{a,b,c} second value. This flow corresponded to the flow into the IRWST in DVI-1, which indicated that any additional decrease in IRWST inventory was small.

TABLE 5.8.1-1
OSU TEST ANALYSIS PLOT PACKAGE FOR SUBSECTION 5.8.1

Plot No.	Component	Variables	Units	Description
1	Pressurizer	CPT-604	psia	System pressure and event history
2	Water injection	WWTDVI1+WWTDVI2, WOUTACC1+WOUTACC2, WWTIRWI1+WWTIRWI2, WWTSMPIT	lbm/sec.	Total of CMT, accumulator, IRWST, and sump injection flows
3	Reactor vessel	RPVASOUT	lbm/sec.	Steam generation in reactor vessel
4	Reactor vessel	T08RPV, HTMXRPV, TSAT	°F	Reactor vessel outlet temperature, maximum clad temperature and fuel exit saturation temperature

THE FIGURES LISTED IN TABLE 5.8.1-1
ARE NOT INCLUDED IN THIS NONPROPRIETARY DOCUMENT

5.8.2 Short-Term Transient

For the inadvertent ADS actuation event, Matrix Test SB14, the short-term transient encompassed the time frame up to [ ]^{a,b,c} seconds. As shown in Figure 5.8.1-1, this period included full depressurization of the facility through all four stages of the ADS, together with CMT and accumulator injection plus the initial stages of IRWST injection. The variation in mass, energy, pressure and temperature throughout this stage of the transient are illustrated in the plot package outlined in Table 5.8.2-1. The plots concentrate on the primary system, including the accumulators, CMTs, IRWST, the primary sump, and flows from the primary system via the ADS, break, and IRWST overflow.

For the short-term transient there were two principal parameters to be examined:

- Adequate flow must be maintained from the passive systems to the reactor vessel.
- Adequate flow into the core must be maintained to ensure decay heat removal from the simulated fuel rods, without a temperature excursion.

These parameters are addressed in the following discussion.

5.8.2.1 Maintenance of Core Cooling

Mass Injected into the Primary System

Figures 5.8.2-5 and 5.8.2-6 show the combined injection flows for the short-term phase of the transient. Separate plots of the individual contributions to the total flow are presented in the plot package index given in Table 5.8.2-1. It should be noted that for this test, the CMT-2 values for level, mass, and fluid energy are obtained by summing the three narrow range level instrument readings because the wide range instrument LDP-502 had been used to initiate the event.

Figures 5.8.2-5 and 5.8.2-6 show how the CMTs, accumulators and IRWST supply a continuous flow of cool water to the core. During the first [ ]^{a,b,c} seconds, cooling flow was supplied by the CMTs. The rate of flow from the CMTs gradually increased to a steady value slightly above [ ]^{a,b,c} lbm/sec. during the initial [ ]^{a,b,c} seconds, then it fell in response to the start of accumulator injection, which temporarily shut off CMT flow. Following the end of accumulator injection, the CMTs again supplied cooling flow until they become fully drained. The only period in which there was minimal cooling flow was during [ ]^{a,b,c} seconds at the conclusion of CMT draining and the start of IRWST injection.

Reactor Pressure Vessel and Downcomer Behavior

The effect of water flow on the average measured core inlet/outlet temperatures and peak clad temperatures during the short-term phase of the transient is shown in Figures 5.8.2-3 and 5.8.2-57.

The core outlet temperature remained lower in the short-term transient than in the SBLOCA simulations because much of the initial hot RPV mass inventory was swept out of the open ADS valves quickly and replaced by cold passive safety system liquid. With no safety injection water lost to the break location, all passive safety-related system water was available to subcool the vessel.

Figure 5.8.2-57 shows that there were no significant excursions in heated rod temperatures throughout the short-term transient; therefore, sufficient core inventory and flow were maintained throughout this phase of the transient to remove the decay heat generated. For significant portions of the transient, a two-phase mixture was present in the core and upper plenum regions due to the high rate of RPV depressurization; however, the amount of core boiling was kept at a low level. The following discussion explains the variation in water level and mass throughout the reactor vessel and downcomer.

The mass and level for the core region are shown in Figures 5.8.2-44 and 5.8.2-45. The collapsed liquid level in the core indicated that the core voided rapidly when the ADS 1-3 valve opening sequence was in progress. With this two-phase mixture, the minimum core inventory of [ ]^{a,b,c} lbm occurred at [ ]^{a,b,c} seconds into the transient, before accumulator injection was more than one-third complete. As shown in Figure 5.8.2-45, the collapsed liquid level dropped to almost the midpoint of the heated rod length during this phase of the transient. The average void fraction of the core two-phase mixture may be estimated by dividing the measured core collapsed liquid level by the [ ]^{a,b,c} in. heated rod length. In this test, the minimum collapsed liquid level corresponds to a core void fraction that approached [ ].^{a,b,c} By the end of the short-term transient, the effect of further accumulator, CMT, and IRWST injection ended all core boiling (see Figure 5.8.2-55), and the core was again water solid.

The collapsed liquid level in the upper plenum region and the associated fluid mass are shown in Figures 5.8.2-49 and 5.8.2-48. During the period before accumulator injection, the upper plenum level decreased below the [ ]^{a,b,c} in. elevation and out of the LDP range. The start of accumulator injection provided the liquid necessary to quickly raise the collapsed upper plenum liquid level back to the elevation of the hot legs and above. Following the end of the accumulator injection, the upper plenum level decreased once again, but remained within the region spanned by the LDP until IRWST injection supplied inventory to initiate a refill. The upper plenum contained a two-phase mixture level at the minimum mass inventory point at the time of accumulator injection since the core outlet quality never exceeded a value of [ ].^{a,b,c} The upper plenum was again water-solid by the end of the short-term transient.

Figures 5.8.2-50 and 5.8.2-51 show that the upper head lost inventory rapidly during the initial [ ]^{a,b,c} seconds of the transient, partially refilled, then drained completely after accumulator injection ceased. This refilling behavior is the opposite of what is typical of a continuous strong mass flow through the open ADS 1-3 valves. The influx of cooler accumulator water produced a significant amount of condensation in the RPV downcomer, which drew liquid from the upper plenum into the upper head region. Once the accumulator was empty, injection flow decreased since it was provided

solely by CMT draindown. Downcomer condensation was no longer adequate to hold liquid any longer in the RPV upper head, which in turn drained its water into the RPV upper plenum. When the RPV mass increased due to continuous IRWST injection, upper head inventory was replenished again by downcomer condensation as occurred during accumulator injection (Figure 5.8.2-40) even as the core inventory increased (Figure 5.8.2-44).

The mass of fluid and collapsed liquid level in the RPV downcomer are shown in Figures 5.8.2-41 and 5.8.2-42. The downcomer level fell rapidly upon ADS-1 actuation to a minimum value, then recovered after accumulator injection. The downcomer level only fell to the [ ]^{a,b,c} in. elevation at [ ]^{a,b,c} seconds, implying that the upper plenum minimum level equaled about [ ]^{a,b,c} in., further confirming that the core remained covered during this portion of the test. Later in the transient, the downcomer refilled to the hot-leg and cold-leg piping elevations during IRWST injection.

5.8.2.2 Energy Transport from the Primary System

Following ADS initiation, energy was deposited in the primary system fluid by the heater rods simulating decay heat and by the primary system metal as it cooled down. Since fluid energy was lost to the ambient, energy must be removed from the primary system to prevent excessive fluid and heater rod temperature excursions. The AP600 is designed to remove heat by a combination of the SGs, the PRHR, and the ADS.

Steam Generator and Passive Residual Heat Removal Heat Transfer

During normal operation, most of the primary system heat was removed via the SGs; however, once the coolant pumps tripped, reduced system flow reduced primary- to secondary-side heat transfer. The SGs were only available as heat sinks until the primary system pressure dropped to that of the secondary side. The PRHR is designed to remove heat from the primary system once the safety signal opens the PRHR isolation valve. In test SB14 the PRHR continued to remove energy after the SGs were thermally isolated. Due to actuation of the ADS at time zero in this event, the ADS valve venting quickly became the preferred path for removal of energy from the primary system.

Figure 5.8.2-33 shows the SG pressure equalization together with the PRHR integrated heat transfer, as represented by the IRWST fluid energy after allowing for the contribution from the ADS 1-3 inflow. Heat was transferred to the secondary side of the SGs for only the first [ ]^{a,b,c} seconds of the transient, and the SG tubes drained by [ ]^{a,b,c} seconds. PRHR heat removal began after the isolation valve opened [ ]^{a,b,c} seconds into the test. The PRHR was responsible for only a portion of the IRWST heat-up during this transient due to ADS-1 activation at time zero. As shown in Figure 5.8.2-21, the PRHR drained completely at about [ ]^{a,b,c} seconds into the transient. Figure 5.8.2-22 can be disregarded after [ ]^{a,b,c} seconds since FMM-802 and -804 instruments were inoperable.

Energy Transport via the Break and Automatic Depressurization System

There was no flow of mass out of the primary system via any simulated break in test SB14, so Figures 5.8.2-67 and 5.8.2-68 are irrelevant. Initiation of ADS 1-3 provided a programmed, increasing mass release path with no other release path available until ADS-4 was activated based on the CMT low-low level signal. The initiation of ADS stages 1, 2 and 3 caused the system to depressurize rapidly. At [ ]^{a,b,c} seconds, ADS-4 initiated, and the primary system continued to depressurize to containment pressure.

During the inadvertent ADS actuation transient, steam and liquid flowed through the ADS 1-3 valves at peak rates which approached [ ] and [ ]^{a,b,c} lbm/sec, respectively, as shown on Figures 5.8.2-65 and 66. Flow through the ADS continued at a reduced rate thereafter, increased as the accumulators emptied, then diminished once again. After [ ]^{a,b,c} seconds, flow through ADS 1-3 was negligible for the rest of the short-term transient and was replaced by flow through the lower-resistance ADS-4 paths. By the end of the short-term transient, water was flowing out of the two ADS-4 valves at approximately [ ]^{a,b,c} lbm/sec. (Figure 5.8.2-64).

Integrated mass flow out of the primary system via the ADS is shown in Figure 5.8.2-62, and the corresponding integrated energy flow is shown in Figure 5.8.2-69. The total system inventory plot (Figure 5.9.2-70) indicates that a net mass increase of [ ]^{a,b,c} lbm occurred during the short-term transient. The energy balance components are presented in Figure 5.8.2-74.

TABLE 5.8.2-1 OSU TEST ANALYSIS STANDARD PLOT PACKAGE FOR SUBSECTION 5.8.2				
Plot No.	**Component**	**Variables**	**Units**	**Description**
1	Pressurizer	CPT-604	psia	System pressure
2	RPV	RPVPWR	kW	Core power
3	RPV	T01RPV, T08RPV, ST08RPV	°F	Core inlet/outlet temperature, saturation temperature
4	SG	CPT-201, CPT-204, CPT-301, CPT-302	psia	Primary and secondary pressures in SG
5	DVI-1	WWTDVIL1, WWTIRWI1, WOUTACC1, WWTIRWI3	lbm/sec.	Individual components and total flow in DVI-1
6	DVI-2	WWTDVIL2, WWTIRWI2, WOUTACC2, WWTIRWI4	lbm/sec.	Individual components and total flow in DVI-2
7	CMT	AMCMT1B, AMCMT2B	lbm	Fluid mass in CMTs (excludes balance lines)
8	CMT	CLDP-502, CLDP-507	in.	Collapsed liquid level in CMTs
9	CMT	MIWDVIL1, MIWDVIL2	lbm	Integrated mass out of CMTs
10	CMT	WWTDVIL1, WWTDVIL2	lbm/sec.	Flow out of CMTs
11	CMT	WOUTCLB1, WOUTCLB2	lbm/sec.	Flow into CMTs
12	CMT	CLDP-509, CLDP510	in.	Level CL-CMT balance lines
13	CMT	UCMT1, UCMT2	Btu	Fluid energy in CMTs
14	IRWST	IRWST	lbm	Mass of fluid in IRWST
15	IRWST	CLDP-701	in.	Collapsed liquid level in IRWST
16	IRWST	WWTIRWI1, WWTIRWI2	lbm/sec.	Flow from IRWST to DVI lines
17	IRWST	IRWSTOR	lbm/sec.	Overflow from IRWST to sump
18	IRWST	ADS13TMR	lbm/sec.	Total ADS flow into IRWST
19	IRWST	ADS13TIR, MIIRWI1, MIIRWI2, MIIRWIO	lbm	Integrated mass out of IRWST
20	IRWST	UIRWST	Btu	Fluid energy in IRWST
21	PRHR	CLDP-802	in.	Collapsed liquid level in PRHR HX

TABLE 5.8.2-1 (Continued)
OSU TEST ANALYSIS STANDARD PLOT PACKAGE FOR SUBSECTION 5.8.2

Plot No.	Component	Variables	Units	Description
22	PRHR	WWOTPRHR	lbm/sec.	Measured outlet flow from PRHR tube
23	Accumulator	AMACC1, AMACC2	lbm	Mass of fluid in accumulators
24	Accumulator	CLDP-401, CLDP-402	in.	Collapsed liquid level in accumulators
25	Accumulator	WOUTACC1, WOUTACC2	lbm/sec.	Flow from accumulators
26	Accumulator	MOUTACC1, MOUTACC2	lbm	Integrated mass out of accumulators
27	Accumulator	UACC1, UACC2	Btu	Fluid energy in accumulators
28	Primary sump	AMPSMP	lbm	Primary sump fluid mass
29	Primary sump	CLDP-901	in.	Primary sump level
30	Primary sump	UPSMP	Btu	Primary sump fluid energy
31	SG	MSSGIP1, MSSGIP2, MSSGOP1, MSSGOP2	lbm	Mass of fluid in SG primary side inlet/outlet plena
32	SG	MSSGHT1, MSSGHT2, MSSGCT1, MSSGCT2	lbm	Mass of fluid in SG primary side hot and cold tubes
33	SG/PRHR	CPT-201, CPT-301, QPRHRI	psia & Btu	SG1 pressure and PRHR integrated heat output
34	Pressurizer	PZM	lbm	Fluid mass in pressurizer
35	Pressurizer	CLDP-601	in.	Collapsed liquid level in pressurizer
36	Pressurizer	UPZ	Btu	Fluid energy in pressurizer
37	Surge line	PLM	lbm	Fluid mass in surge line
38	Surge line	CLDP-602	in.	Collapsed liquid level in surge line
39	Surge line	UPSL	Btu	Fluid energy in surge line
40	RPV	MWPRV	lbm	Total fluid mass in reactor vessel
41	RPV	DCM	lbm	Fluid mass in downcomer
42	RPV	LDP01DC	in.	Collapsed liquid level in downcomer compared to various reference elevations
43	RPV	MW01RPV	lbm	Fluid mass in lower plenum
44	RPV	MW03RPV	lbm	Fluid mass in core region
45	RPV	LDP03RPV	in.	Collapsed liquid level in core
46	RPV	RPVAVDF		Core exit void fraction
47	RPV	RPVAQOUT		Core exit quality
48	RPV	MW06RPV	lbm	Fluid mass in the upper plenum
49	RPV	LDP06RPV	in.	Collapsed liquid level in the upper plenum
50	RPV	MW08RPV	lbm	Fluid mass in the upper head
51	RPV	LDP08RPV	in.	Collapsed liquid level in the upper head

TABLE 5.8.2-1 (Continued) OSU TEST ANALYSIS STANDARD PLOT PACKAGE FOR SUBSECTION 5.8.2				
Plot No.	**Component**	**Variables**	**Units**	**Description**
52	RPV	URPV	Btu	Total fluid energy in reactor vessel
53	RPV	RPVXE, RPVASL	in.	Level of Tsat line
54	RPV	RPVPab, RPVAPab, RPVPWR	kW	Heated rod power above and below Tsat level and total
55	RPV	RPVRXV, RPVASOUT	lbm/sec.	Core steam generation rate
56	RPV	RPVALIN	lbm/sec.	Calculated core flow
57	RPV	HTMXRPV, ST08RPV	°F	Maximum clad temperature and saturation temperature
58	Hot leg	MWHL1, MWHL2	lbm	Water mass in hot legs
59	Hot leg	MVHL1, MVHL2	lbm	Vapor mass in hot legs
60	Cold leg	CL1WMS, CL2WMS, CL3WMS, CL4WMS	lbm	Water mass in cold legs
61	Cold leg	CL1VMS, CL2VMS, CL3VMS, CL4VMS	lbm	Vapor mass in cold legs
62	ADS and break	BRKSTIR, ADS13TIR, ADS41TIR, ADS42TIR	lbm	Total discharged mass for ADS 1-3, ADS-4s, and break
63	ADS and break	BRKTIVF, AD13TIVF, AD41TIVF, AD42TIVF	lbm	Total integrated vapor flow for ADS and break
64	ADS and break	BRKTILF, AD13TILF, AD41TILF, AD42TILF	lbm	Total integrated liquid flow for ADS and break
65	ADS and break	ADS13SVR, ADS41SVR, ADS42SVR	lbm/sec.	Vapor flow out ADS 1-3 and ADS-4
66	ADS and break	ADS13SLR, ADS41SLR, ADS42SLR	lbm/sec.	Liquid flow out ADS 1-3 and ADS-4
67	ADS and break	BRKSVLR	lbm/sec.	Vapor flow out of break
68	ADS and break	BRKSSLR	lbm/sec.	Liquid flow out of break
69	ADS and break	BRKSPEI, ADS13EI, ADS41EI, ADS42EI	Btu	Integrated fluid energy for ADS 1-3, ADS-4, and break
70	Mass balance	TOTMASS	lbm	Total system mass inventory
71	Mass balance	PRIMMASS, PRIMASS2	lbm	Measured primary system inventory and value from mass balance
72	Mass balance	MERROR	lbm	Mass balance error
73	Mass balance	MIN, MOUT SRCMASS	lbm	Integrated mass flow in and out of primary system and source mass
74	Energy balance	Various	Btu	Components of energy balance

THE FIGURES LISTED IN TABLE 5.8.2-1
ARE NOT INCLUDED IN THIS NONPROPRIETARY DOCUMENT

5.8.3 Long-Term Transient

The long-term transient started with the initiation of IRWST injection, covered the transition from IRWST to sump injection, and provided information on the LTC response of the AP600 with sump injection. For the inadvertent ADS actuation case, Matrix Test SB14, the long-term transient phase encompassed the time frame of [ ]^{a,b,c} seconds to the end of the test, around [ ]^{a,b,c} seconds. The behavior of the test facility during this period of the transient is discussed in this subsection using the plot package detailed in Table 5.8.3-1. The analysis concentrates on the components of the primary system that remained active during the LTC phase, that is the RPV, the hot legs, ADS-4, the sumps and the IRWST.

During the long-term transient, thermal-hydraulic phenomena of interest were:

- Maintenance of core cooling and removal of energy from the primary system.
- Level and pressure oscillations observed during test SB01 and other long-term transients that did not occur during SB14.

5.8.3.1 Maintenance of Core Cooling

Mass Injected into Primary System

The total DVI line flow, CMT flow, and IRWST flows are shown in Figures 5.8.3-6 and 5.8.3-7. Flow from the primary sump is shown in Figure 5.8.3-19.

During the pre-sump injection phase of the long-term transient, the IRWST flow proceeded continuously at a diminishing rate. At [ ]^{a,b,c} seconds, flow from the primary sump started through the check valves around the main injection valves further reducing IRWST flow. From [ ]^{a,b,c} seconds to the end of the transient, a nearly steady flow rate of [ ]^{a,b,c} lbm/sec. was maintained through each DVI line. At [ ]^{a,b,c} seconds, the main sump injection valves opened. This resulted in a reversal of flow through the IRWST injection line-1, while the flow in IRWST line-2 remained relatively constant. The net injection flow rate from the IRWST during sump injection was about [ ]^{a,b,c} lbm/sec. through both DVI lines.

Reactor Pressure Vessel and Downcomer Response

The effect of water inflow on the average measured downcomer fluid, core inlet and core outlet, and peak clad temperatures during the long-term phase of the transient is shown in Figures 5.8.3-4, 5.8.3-5, and 5.8.3-38. Figure 5.8.3-4 shows that there was a gradual increase in average downcomer fluid temperatures during the long-term transient once the sump began injecting. By the end of the test, the average core inlet temperature reached a value of [ ]^{a,b,c} below saturation. Figure 5.8.3-5 shows that the core remained at or near saturation for the entire long-term transient after [ ]^{a,b,c}

seconds. Figures 5.8.3-34 to 5.8.3-36 show that the DVI line flow method discussed in Subsection 4.11 indicated that a small level of boiling was maintained after [ ]^{a,b,c} seconds into the transient. Nevertheless, the level of boiling was small, and the test showed that the inflow from the IRWST and sumps was sufficient.

Figure 5.8.3-38 shows that there are no significant excursions in heater rod temperatures throughout the long-term transient. Therefore, sufficient core inventory and flow was maintained through this phase of the transient to remove the decay heat generated. For significant portions of the transient, a two-phase mixture was present in the core and upper plenum regions. The following discussion explains the variation in water level and mass throughout the reactor vessel and downcomer.

The mass and level for the core region are shown in Figures 5.8.3-28 and 5.8.3-29. The collapsed liquid level in the core indicates that the heated rods were always covered with a single- or two-phase mixture. During the later stages of the transient, the collapsed level remained just below the top of the heated rods and the core void fraction was about [ ].^{a,b,c} The fall in core inventory was a result of the influx of hot water from the primary sump as it flowed through the check valves. The impact of this hot water on the system temperatures is shown in Figures 5.8.3-4 and 5.8.3-5 as a sudden increase in fluid temperature in the downcomer and at the core inlet. The hotter water also led to an increase in the calculated steam generation rate shown in Figure 5.8.3-36 and a corresponding fall in the level at which the core reached saturation temperature (Figure 5.8.3-34).

The mass of water in the reactor pressure vessel is shown in Figure 5.8.3-25. After an initial decline, the reactor vessel water mass settled at an average value of 450 lbm until sump injection started, when it gradually fell to [ ]^{a,b,c} lbm, which is more than [ ]^{a,b,c} percent of the initial vessel water inventory.

The collapsed liquid level in the upper plenum region is shown in Figure 5.8.3-32. This figure shows that the collapsed liquid level initially fell, yet remained above the mid-level of the hot legs during the period before sump injection. Following a surge in level at the initial influx of hot water from the sumps, the level dropped first to the hot leg mid-elevation and then to the top of the DVI injection lines where it remained for the remainder of the transient. This corresponds to a void fraction of [ ].^{a,b,c}

The mass of fluid and collapsed liquid level in the RPV downcomer are shown in Figures 5.8.3-26 and 5.8.3-27. The collapsed liquid level remained above the DVI lines for the entire long-term transient. The start of sump injection reduced the level, but this was not enough to uncover the DVI lines. SB14 did not exhibit the RPV level/pressure oscillations observed in several of the other OSU small break LOCA tests.

5.8.3.2 Energy Transport from the Primary System

During the long-term transient, energy continued to be deposited in the primary system from the heater rods, the metal, and the fluid flowing from the primary sump. The SGs and PRHR remained inactive throughout this phase of the transient; the only paths out of the primary system were via the ADS 1-3 and ADS-4 ADS valves.

Integrated mass flow out of the primary system via the ADS is shown in Figure 5.8.3-43. By the end of the transient simulation, over [ ]^{a,b,c} lbm of water flowed out of the primary system. During the long-term cooling phase of the transient, the most significant outflow was through the ADS-4 valves, as confirmed by Figure 5.8.3-44, which depicts the flows through the ADS. During the sump injection phase of the transient, outflow was primarily in the form of liquid out of the ADS-4 valves; water flowed through each of the valves at an average rate of [ ]^{a,b,c} lbm/sec. In addition, there was some small mass flow out of the open ADS 1-3 valves.

Figure 5.8.3-36 shows the calculated steam generation rate determined using the DVI line flow method. During the sump injection phase of the transient, steam was generated at over [ ]^{a,b,c} lbm/sec., but there was no evidence from the vortex meters for steam flow out of the ADS-4 valves. However, there is evidence that steam was leaving the primary system by this route:

- Figure 5.8.3-46 shows the measured, total system fluid inventory. During this phase of the transient, the interval after the start of primary sump injection is when core steam generation is most significant, and the total system inventory fell by about [ ]^{a,b,c} lbm. This corresponds to a steam flow rate of [ ]^{a,b,c} lbm/sec, which would not have been detected by the vortex meters.

- Examination of the fluid thermocouples on the outlet of the ADS-4 valves indicates that the thermocouples remained at or above saturation temperature following the start of sump injection.

It was not possible for all the steam generated in the core to flow from the upper head to the downcomer via the bypass holes (Subsection 6.1.3). Therefore, steam did leave the primary system via the ADS-4. Figure 5.8.3-50 shows the components of the system energy balance. Further discussion of steam loss from the primary system is provided in the mass and energy balance discussions of Subsection 6.2.2 and 6.2.3.

TABLE 5.8.3-1
OSU TEST ANALYSIS STANDARD PLOT PACKAGE FOR SUBSECTION 5.8.3
LONG-TERM TRANSIENT

Plot No.	Component	Variables	Units	Description
1	RPV	RPVPWR	kW	Core power
2	Primary sump	TSMPI1, TSMPI2	°F	Sump injection line temperatures
3	DVI	TDVIL1, TDVIL2	°F	DVI line temperatures
4	RPV	T01DC, T02DC, T03DC, ST01DC	°F	Water and saturation temperatures in downcomer
5	RPV	T01RPV, T08RPV, ST08RPV	°F	Core inlet/outlet temperature, saturation temperature
6	DVI-1	WWTDVIL1, WWTIRWI1, WWTIRWI3	lbm/sec.	Individual components and total flow in DVI-1
7	DVI-2	WWTDVIL2, WWTIRWI2, WWTIRWI4	lbm/sec.	Individual components and total flow in DVI-2
8	CMT	CLDP-502, CLDP-507	in.	Collapsed liquid level in CMTs
9	CMT	CLDP-509, CLDP510	in.	Level CL-CMT balance lines
10	IRWST	IRWST	lbm	Mass of fluid in IRWST
11	IRWST	CLDP-701	in.	Collapsed liquid level in IRWST
12	IRWST	UIRWST	Btu	Fluid energy in IRWST
13	Primary sump	AMPSMP	lbm	Primary sump fluid mass
14	Primary sump	CLDP-901	in.	Primary sump level
15	Primary sump	UPSMP	Btu	Primary sump fluid energy
16	Secondary sump	AMSSMP	lbm	Secondary sump fluid mass
17	Secondary sump	CLDP-902	in.	Secondary sump level
18	Secondary sump	USSMP	Btu	Secondary sump fluid energy
19	Primary sump	WSTSMPET, WWTSMPIT	lbm/sec.	Primary sump steam and liquid injection rate
20	Primary sump	MISMPI1, MISMPI2, MISMPIT, MIIRWT	lbm	Integrated primary sump and IRWST flows
21	SG	MSSGIP1, MSSGIP2, MSSGOP1, MSSGOP2	lbm	Mass of fluid in SG side inlet/outlet plena
22	Surge line	PLM	lbm	Fluid mass in surge line
23	Surge line	CLDP-602	in.	Collapsed liquid level in surge line
24	Surge line	UPSL	Btu	Fluid energy in surge line
25	RPV	MWRPV	lbm	Total fluid mass in reactor vessel

TABLE 5.8.3-1 (Continued)
OSU TEST ANALYSIS STANDARD PLOT PACKAGE FOR SUBSECTION 5.8.3
LONG-TERM TRANSIENT

Plot No.	Component	Variables	Units	Description
26	RPV	DCM	lbm	Fluid mass in downcomer
27	RPV	LDP01DC	in.	Collapsed liquid level in downcomer compared to various reference elevations
28	RPV	MW03RPV	lbm	Fluid mass in core region
29	RPV	LDP03RPV	in.	Collapsed liquid level in core
30	RPV	RPVAVDF		Core exit void fraction
31	RPV	RPVAQOUT		Core exit quality
32	RPV	LDP06RPV	in.	Collapsed liquid level in the upper plenum
33	RPV	MW08RPV	lbm	Fluid mass in the upper head
34	RPV	RPVASL	in.	Level of Tsat line
35	RPV	RPVAPab, RPVPWR	kW	Heated rod power above and below Tsat level and total
36	RPV	RPVASOUT	lbm/sec.	Core steam generation rate
37	RPV	RPVALIN	lbm/sec.	Calculated core flow
38	RPV	HTMXRPV, ST08RPV	°F	Maximum clad temperature, saturation temperature and delta
39	Hot leg	MWHL1, MWHL2	lbm	Water mass in hot legs
40	Hot leg	MVHL1, MVHL2	lbm	Vapor mass in hot legs
41	Cold leg	CL1WMS, CL2WMS, CL3WMS, CL4WMS	lbm	Water mass in cold legs
42	Cold leg	CL1VMS, CL2VMS, CL3VMS, CL4VMS	lbm	Vapor mass in cold legs
43	ADS and break	BRKSTIR, ADS13TIR, ADS41TIR, ADS42TIR	lbm	Total discharged mass for ADS 1-3, ADS-4, and break
44	ADS and break	ADS13TLR, ADS41TLR, ADS42TLR	lbm/sec.	Liquid flow out ADS 1-3 and ADS-4
45	ADS and break	BRKSTLR	lbm/sec.	Liquid flow and total flow out of break
46	Mass balance	TOTMASS	lbm	Total system mass inventory
47	Mass balance	PRIMMASS, PRIMASS2	lbm	Measured primary system inventory and valve from mass balances
48	Mass balance	MERROR	lbm	Mass balance error
49	Mass balance	MIN, MOUT SRCMASS	lbm	Integrated mass flow in and out of primary system and source mass
50	Energy balance	Various	Btu	Component of energy balance

THE FIGURES LISTED IN TABLE 5.8.3-1
ARE NOT INCLUDED IN THIS NONPROPRIETARY DOCUMENT

5.9 Analysis of Matrix Test SB15

Matrix test SB15 (OSU Test U0015) simulated a 2-in. hot-leg break LOCA with LTC and without the operation of the nonsafety-related systems. The break was at the bottom of HL-2 and except for the break location, this test was identical to SB01, including the simulated failure of one of the ADS-4 lines.

Analysis of Matrix Test SB15 is divided into three sections as follows:

- Facility performance is discussed in Subsection 5.9.1. It provides a brief outline of the response of the test facility; further details are available in the Final Data Report.[1]

- The short-term transient for SB15 encompassed the start of the simulation up to [ ]^{a,b,c} seconds. This period includes blowdown, natural circulation, ADS and initial IRWST stages of the transient.

- Analysis of the long-term transient, SB15, encompassed the time frame from [ ]^{a,b,c} seconds to the end of the test. This phase of the transient concluded with the IRWST injection phase to the initiation of sump injection. The long-term transient actually started at IRWST injection, which is discussed as part of the short-term transient. Between the end of the short-term transient to [ ]^{a,b,c} seconds, the system remained relatively inactive with the exception of the CMT refill. At [ ]^{a,b,c} seconds, CMT-1 began to refill and CMT-2 followed [ ]^{a,b,c} seconds later. CMT refill phenomena is discussed further in Section 6.1.1 and the discussion of the long-term transient provided here begins at [ ]^{a,b,c} seconds.

The discussion of the short- and long-term phase of the transient focuses on important thermal-hydraulic phenomena identified in the PIRT (Table 1.3-1). The mass and energy balance results are key indicators of the quality of the analysis on which this discussion is based. These are discussed in detail in Subsections 6.2.2 and 6.2.3.

5.9.1 Facility Performance

The performance of the OSU test facility during Matrix Test SB15 in reference to the five transient phases is outlined in the following :

- Blowdown
- Natural circulation
- ADS
- IRWST injection
- Sump injection

The overall performance of the facility during the transient is shown in Figures 5.9.1-1 to 5.9.1-4. Figure 5.9.1-1 shows the pressurizer pressure throughout the test with various phases and operating components. The time scale was reduced for clarity since there were only small changes in system pressure during the long-term phase of the transient. Figure 5.9.1-2 shows the total DVI line flow and its composition from the various sources at each time in the transient. Figure 5.9.1-3 shows the calculated core steam generation rate throughout the test and Figure 5.9.1-4, the variation in core outlet temperature and peak clad temperature relative to the core outlet saturation temperature.

Figures 5.9.1-1 and 5.9.1-2 show that there was a continuous flow of cool water to the core from the passive safety systems throughout the transient. Once initiated, the ADS lines rapidly depressurized the primary system, which enhanced the CMT and accumulator injection flow rates. Ultimately, the ADS-4 valves sufficiently reduced the circuit pressure to start gravity-driven IRWST injection. The passive injection systems overlapped so that as one source of water drained, the next was available to continue the cooling process. The level of steam generation in the core and the response of the core outlet fluid temperatures and maximum clad temperatures are shown in Figures 5.9.1-3 and 5.9.1-4. These figures show that the cooling flow prevented any excessive core heating. The core remained subcooled for large periods of the transient and when steam production occurred, the rate of generation remained well below the rate at which water was delivered to the core.

5.9.1.1 Blowdown Phase

The blowdown phase began at time zero when the break was initiated and continued until the primary circuit pressure was nearly in equilibrium with the secondary-side pressure at around [ ]^{a,b,c} seconds. Immediately following the opening of the break, primary circuit pressure decreased as the small hot-leg break removed the energy being added from the core. Pressure fell gradually until the end of the blowdown phase. During this phase of the transient, cooling flow was provided from the two CMTs, which remained in the recirculation mode until around [ ]^{a,b,c} seconds. Heat was removed from the primary circuit via the PRHR and the SGs. The pressurizer and surge line completely drained at [ ]^{a,b,c} and [ ]^{a,b,c} seconds, respectively.

5.9.1.2 Natural Circulation Phase

In this LOCA simulation, the single- and two-phase natural circulation phase was marked by a gradual reduction in system pressure rather than by the more stable pressure observed in SB01. During this phase of the transient, the SG tubes all drained by about [ ]^{a,b,c} seconds and at that time, heat removal from the primary circuit continued via the PRHR. The steam in the SG tubes became superheated and remained so until the end of the transient. In response to voiding in CL-3, CMT-1 transitioned to draindown mode at [ ]^{a,b,c} seconds, and the falling CMT level reached the ADS low-level setpoint at [ ]^{a,b,c} seconds. The natural circulation phase of the transient continued to [ ]^{a,b,c} seconds when the ADS-1 valve opened.

5.9.1.3 Automatic Depressurization Phase

ADS-1 actuation was followed by ADS-2 and ADS-3 actuation at [ ]^{a,b,c} and [ ]^{a,b,c} seconds respectively. Accumulation injection began with initiation of the ADS. The influx of cold water combined with increased venting via the ADS led to a rapid depressurization of the primary circuit. Actuation of ADS-4 at [ ]^{a,b,c} seconds completed depressurization to a level that initiated IRWST injection at [ ]^{a,b,c} seconds via DVI-2 and [ ]^{a,b,c} seconds via DVI-1. During accumulator injection, increased circuit resistance reduced flow out of the CMTs. CMT flow resumed as the accumulators drained. The accumulators were fully drained [ ]^{a,b,c} seconds before IRWST injection began. The CMTs did not fully drain until [ ]^{a,b,c} and [ ]^{a,b,c} seconds after the start of IRWST injection. The transfer from CMT accumulator to IRWST injection was indicated by the minimum RPV inventory of [ ]^{a,b,c} lbm at [ ]^{a,b,c} seconds.

Actuation of ADS-1 rapidly refilled the pressurizer as water and steam flowed out of the ADS. The pressurizer gradually drained by [ ]^{a,b,c} seconds.

5.9.1.4 In-Containment Refueling Water Storage Tank Injection

IRWST injection signals the transition from the short- to long-term phase of the transient. The initial phase of IRWST injection involved an increase in flow through the two DVI lines, which was followed by a gradual flow reduction as the driving head between the IRWST and the RCS fell due to the reduced IRWST water level. Once maximum flow was established, the inflow of water from the IRWST was sufficient to keep the core subcooled from about [ ]^{a,b,c} seconds. Steam was subsequently generated in the core for the remainder of the transient. Following the restart of core steam generation, IRWST injection between [ ]^{a,b,c} seconds, was indicated by oscillations in delivery from the refilled CMT, and in pressure and level oscillations throughout the primary system. These oscillations were also observed in the ADS-4 liquid flow rates.

5.9.1.5 Sump Injection

Injection from the primary sump via the check valves around the main sump injection valves began at [ ]^{a,b,c} seconds when the level in the IRWST was low enough to allow flow. This reduced the flow rate from the IRWST. Since the test was terminated [ ]^{a,b,c} seconds beyond this point, no further analysis is provided of sump injection during long-term cooling in Test SB15.

TABLE 5.9.1-1
OSU TEST ANALYSIS PLOT PACKAGE FOR SUBSECTION 5.9.1

Plot No.	Component	Variables	Units	Description
1	Pressurizer	CPT-604	psia	System pressure and event history
2	Water injection	WWTDVI1+WWTDVI2, WOUTACC1+WOUTACC2, WWTIRWI1+WWTIRWI2, WWTSMPIT	lbm/sec.	Total of CMT, accumulator, IRWST, and sump injection flows
3	Reactor vessel	RPVASOUT	lbm/sec.	Steam generation in reactor vessel
4	Reactor vessel	T08RPV, HTMXRPV, TSAT	°F	Reactor vessel outlet temperature, maximum clad temperature 2 fuel exit saturation temperature

THE FIGURES LISTED IN TABLE 5.9.1-1
ARE NOT INCLUDED IN THIS NONPROPRIETARY DOCUMENT

5.9.2 Short-Term Transient

For the 2-inch hot-leg break, Matrix Test SB15, the short-term transient encompassed the time frame up to [ ]^{a,b,c} seconds. As shown in Figure 5.9.1-1, this period included full depressurization of the facility through all four stages of the ADS together with CMT and accumulator injection plus the initial stages of IRWST injection. Variations in mass, energy, pressure, and temperature throughout this stage of the transient are illustrated in the plot package outlined in Table 5.9.2-1. The plots concentrate on the primary system, including the accumulators, CMTs, IRWST, primary sump, and flows from the primary system via the ADS, break, and IRWST overflow.

For the short-term transient there were two principal concerns:

- Adequate flow from the passive systems to the reactor vessel must be maintained.
- Adequate flow into the core must be maintained to ensure that decay heat was removed from the simulated fuel rods without a temperature excursion.

These concerns are addressed in the following discussion.

5.9.2.1 Maintenance of Core Cooling

Mass Injected to the Primary System

Figures 5.9.2-5 and 5.9.2-6 show the combined effect of the injection flows for the short-term phase of the transient. Separate plots of the individual contributions to the total flow can be located by consulting the plot package index given in Table 5.9.2-1.

Figures 5.9.2-5 and 5.9.2-6 show how the CMTs, accumulators and IRWST supply an almost continuous flow of cool water to the core. During the first [ ]^{a,b,c} seconds, cooling flow was provided by the CMTs. The rate of flow from the CMTs gradually reduced from a maximum value of [ ]^{a,b,c} lbm/sec. as the driving head fell in response to the CMT water heat-up until ADS-1 initiation. Rapid accumulator injection temporarily reduced CMT flow, but led to an overall increase in flow to the core to a peak value of [ ]^{a,b,c} lbm/sec. in DVI-2. Following the end of accumulator injection, the CMTs again provided cooling flow until drained. The only period in which there was relatively little cooling flow was during the initial CMT recirculation period at the start of the transient.

Reactor Pressure Vessel and Downcomer Behavior

The effect of the water flow on core inlet/outlet temperatures and peak clad temperatures during the short-term phase of the transient is shown in Figures 5.9.2-3 and 5.9.2-57. The combined CMT and accumulator flow was sufficient to keep the core completely subcooled between [ ]^{a,b,c} seconds. The core outlet temperature then remained at the saturation level until about [ ]^{a,b,c}

seconds when the inflow of water from the IRWST became sufficient to again subcool the core. The core then remained subcooled until the end of the short-term transient.

Figure 5.9.2-57 shows that there were no significant excursions in heated rod temperatures throughout the short-term transient; therefore, sufficient core inventory and flow was maintained through this phase of the transient to remove the decay heat generated. For significant portions of the transient, a two-phase mixture was present in the core and upper plenum regions, although core boiling was kept at a low level. The following discussion tracks the variation in water level and mass throughout the reactor vessel and downcomer.

The mass and level for the core region are shown in Figures 5.9.2-44 and 5.9.2-45. The collapsed liquid level in the core indicates that the heated rods remained covered with a single- or two-phase mixture. The transient minimum core inventory of [ ]^{a,b,c} lbm occurred at about [ ]^{a,b,c} seconds into the transient, and is greater than the initial steady-state mass inventory. Figure 5.9.2-45 shows that the collapsed liquid level dropped to [ ]^{a,b,c} in. below the top of the heated rod length during the second boil-off period in this phase of the transient. This corresponds to a core void fraction of [ ].^{a,b,c} By the end of the short-term transient, the effect of IRWST injection ended all core boiling (Figure 5.9.2-55), and the core was again water-solid.

The collapsed liquid level in the upper plenum region and the associated fluid mass are shown in Figures 5.9.2-49 and 5.9.2-48. These figures show that at the time of minimum core mass inventory, the upper plenum collapsed level remained above the hot-leg centerline. The end of accumulator injection coincided with the start of a fall in collapsed liquid level to the minimum elevation observed in SB15. Following the start of IRWST injection, the upper plenum collapsed level increased. The upper plenum was again almost water-solid by the end of the short-term transient.

Figures 5.9.2-50 and 5.9.2-51 show that the upper head also gained inventory at the time when accumulator injection began. This behavior was the result of condensation from the large influx of cool accumulator water. Accumulator injection coincided with ADS-1 initiation. The flow of water and steam through the ADS rapidly refilled the pressurizer, which then removed water from the RPV. The loss of mass to the ADS valves and to the hot-leg break was responsible for minimizing the increase in overall RPV inventory during accumulator injection (Figure 5.9.2-40) as the core inventory also increased (Figure 5.9.2-44).

The mass of fluid and collapsed liquid level in the RPV downcomer are shown in Figures 5.9.2-41 and 5.9.2-42. The downcomer collapsed level remained at about the cold-leg elevation until ADS-1 actuation, when the level fell to the bottom of the DVI line piping. The downcomer level refilled to the top of the hot legs during accumulator injection, then fell back to just above the DVI line entry point, where it remained until IRWST injection once again raised the level to the hot legs.

5.9.2.3 Energy Transport from the Primary System

Following the break, energy was deposited in the primary circuit fluid by the heater rods to simulate decay heat and the primary circuit metal as it cooled down. Some fluid energy was lost to the ambient and out of the break. Excess energy must be removed from the primary system to prevent excessive fluid and heater rod temperature excursions. The AP600 plant is designed to remove heat by a combination of the SGs and the PRHR and ADS.

Steam Generator and Passive Residual Heat Removal Heat Transfer

During normal operation, most of the primary system heat was removed via the SGs; however, once the coolant pumps tripped, the reduced circuit flow decreased primary to secondary-side heat transfer. The SGs were only available as heat sinks until the primary system pressure dropped to that of the secondary side, then the two sides were in thermal equilibrium. The PRHR is designed to remove heat from the primary system once the safety signal opens the isolation valve. The PRHR continued to remove energy after the SGs were thermally isolated until ADS actuated. Once the ADS is actuated, it became the predominant path for the removal of energy from the primary circuit.

Figure 5.9.2-33 shows the SG pressure equalization together with the PRHR integrated heat transfer as represented by the IRWST fluid energy after allowing for the contribution from ADS 1-3 inflow. Heat was transferred to the secondary side of the SGs for only the first [ ]^{a,b,c} seconds of the transient. PRHR heat removal began [ ]^{a,b,c} seconds into the test. The PRHR was responsible for all the IRWST heat-up until ADS-1 activation, after which the PRHR heat transfer reduced significantly. During the active phase, the PRHR transferred heat to the IRWST at an average rate of [ ]^{a,b,c} Btu/sec.

Energy Transport via the Break and Automatic Depressurization System

The mass flow rate from the primary system via the break is shown in Figures 5.9.2-67 and 5.9.2-68. As seen from these figures, liquid flow was detected by the flow meters for a short-term transient. During the first [ ]^{a,b,c} seconds following the break, [ ]^{a,b,c} lbm of water flowed out of the primary circuit via the break at an average rate of approximately [ ]^{a,b,c} lbm/sec. During this period, the primary circuit depressurized to around [ ]^{a,b,c} psi (Figure 5.9.2-1). With initiation of ADS 1-3, vapor flow through the break ceased, but liquid flow continued well into the long-term cooling phase. Liquid and vapor flow through the ADS 1-3 valves began immediately upon actuation and continued until around [ ]^{a,b,c} seconds. By [ ]^{a,b,c} seconds, the time of ADS-4 activation, ADS 1-3 caused the circuit to depressurize rapidly to about [ ]^{a,b,c} psia. When ADS-4 was initiated, the primary circuit continued to depressurize to containment pressure.

The initiation of the ADS 1-3 did not terminate the liquid flow through the break because the break is located at the bottom of the hot leg, upstream of the ADS 1-3 valves. The break flow became completely liquid flow because the RPV mass was adequate to continuously cover the hot-leg break

elevation. The ADS 1-3 valves pass vapor and liquid at peak flow rates of about [ ]^{a,b,c} lbm/sec., respectively. Flow through ADS 1-3 continued at a declining rate until about [ ]^{a,b,c} seconds when it was almost completely terminated and replaced by flow through the lower resistance ADS-4 paths. By the end of the short-term transient, water was flowing out of the two ADS-4 valves at approximately [ ]^{a,b,c} lbm/sec. (see Figure 5.9.2-64); water was also flowing out of the break at about [ ] lbm/sec.

The integrated mass flow from the primary system via the ADS and the break is shown in Figures 5.9.2-62, and the corresponding integrated energy flow is shown in Figure 5.9.2-69. The total system inventory plot given in Figure 5.9.2-70 indicates that up to [ ]^{a,b,c} lbm of inventory was lost at the limiting point in time during the short-term transient. The lost inventory was steam, none of which had been detected on the flow meters; thus, this is not included in the energy balance shown in Figure 5.9.2-74.

TABLE 5.9.2-1 OSU TEST ANALYSIS STANDARD PLOT PACKAGE FOR SUBSECTION 5.9.2				
Plot No.	**Component**	**Variables**	**Units**	**Description**
1	Pressurizer	CPT-604	psia	System pressure
2	RV	RPVPWR	kW	Core power
3	RV	T01RPV, T08RPV, ST08RPV	°F	Core inlet/outlet temperature, saturation temperature
4	SG	CPT-201, CPT-204, CPT-301, CPT-302	psia	Primary and secondary pressures in SG
5	DVI-1	WWTDVIL1, WWTIRWI1, WOUTACC1, WWTIRWI3	lbm/sec.	Individual components and total flow in DVI-1
6	DVI-2	WWTDVIL2, WWTIRWI2, WOUTACC2, WWTIRWI4	lbm/sec.	Individual components and total flow in DVI-2
7	CMT	AMCMT1B, AMCMT2B	lbm	Fluid mass in CMTs (excludes balance lines)
8	CMT	CLDP-502, CLDP-507	in.	Collapsed liquid level in CMTs
9	CMT	MIWDVIL1, MIWDVIL2	lbm	Integrated mass out of CMTs
10	CMT	WWTDVIL1, WWTDVIL2	lbm/sec.	Flow out of CMTs
11	CMT	WOUTCLB1, WOUTCLB2	lbm/sec.	Flow into CMTs
12	CMT	CLDP-509, CLDP510	in.	Level CL-CMT balance lines
13	CMT	UCMT1, UCMT2	Btu	Fluid energy in CMTs
14	IRWST	IRWST	lbm	Mass of fluid in IRWST
15	IRWST	CLDP-701	in.	Collapsed liquid level in IRWST
16	IRWST	WWTIRWI1, WWTIRWI2	lbm/sec.	Flow from IRWST to DVI lines
17	IRWST	IRWSTOR	lbm/sec.	Overflow from IRWST to sump
18	IRWST	ADS13TMR	lbm/sec.	Total ADS flow into IRWST
19	IRWST	ADS13TIR, MIIRWI1, MIIRWI2, MIIRWIO	lbm	Integrated mass out of IRWST
20	IRWST	UIRWST	Btu	Fluid energy in IRWST
21	PRHR	CLDP-802	in.	Collapsed liquid level in PRHR HX

TABLE 5.9.2-1 (Continued)
OSU TEST ANALYSIS STANDARD PLOT PACKAGE FOR SUBSECTION 5.9.2

Plot No.	Component	Variables	Units	Description
22	PRHR	WWOTPRHR	lbm/sec.	Measured outlet flow from PRHR tube
23	Accumulator	AMACC1, AMACC2	lbm	Mass of fluid in accumulators
24	Accumulator	CLDP-401, CLDP-402	in.	Collapsed liquid level in accumulators
25	Accumulator	WOUTACC1, WOUTACC2	lbm/sec.	Flow from accumulators
26	Accumulator	MOUTACC1, MOUTACC2	lbm	Integrated mass out of accumulators
27	Accumulator	UACC1, UACC2	Btu	Fluid energy in accumulators
28	Primary sump	AMPSMP	lbm	Primary sump fluid mass
29	Primary sump	CLDP-901	in.	Primary sump level
30	Primary sump	UPSMP	Btu	Primary sump fluid energy
31	SG	MSSGIP1, MSSGIP2, MSSGOP1, MSSGOP2	lbm	Mass of fluid in SG primary side inlet/outlet plena
32	SG	MSSGHT1, MSSGHT2, MSSGCT1, MSSGCT2	lbm	Mass of fluid in SG primary side hot and cold tubes
33	SG/PRHR	CPT-201, CPT-301, QPRHRI	psia & Btu	SG1 pressure and PRHR integrated heat output
34	Pressurizer	PZM	lbm	Fluid mass in pressurizer
35	Pressurizer	CLDP-601	in.	Collapsed liquid level in pressurizer
36	Pressurizer	UPZ	Btu	Fluid energy in pressurizer
37	Surge line	PLM	lbm	Fluid mass in surge line
38	Surge line	CLDP-602	in.	Collapsed liquid level in surge line
39	Surge line	UPSL	Btu	Fluid energy in surge line
40	RV	MWRPV	lbm	Total fluid mass in reactor vessel
41	RV	DCM	lbm	Fluid mass in downcomer
42	RV	LDP01DC	in.	Collapsed liquid level in downcomer compared to various reference elevations
43	RV	MW01RPV	lbm	Fluid mass in lower plenum
44	RV	MW03RPV	lbm	Fluid mass in core region
45	RV	LDP03RPV	in.	Collapsed liquid level in core
46	RV	RPVAVDF		Core exit void fraction
47	RV	RPVAQOUT		Core exit quality
48	RV	MW06RPV	lbm	Fluid mass in the upper plenum
49	RV	LDP06RPV	in.	Collapsed liquid level in the upper plenum
50	RV	MW08RPV	lbm	Fluid mass in the upper head
51	RV	LDP08RPV	in.	Collapsed liquid level in the upper head

TABLE 5.9.2-1 (Continued)
OSU TEST ANALYSIS STANDARD PLOT PACKAGE FOR SUBSECTION 5.9.2

Plot No.	Component	Variables	Units	Description
52	RV	URPV	Btu	Total fluid energy in reactor vessel
53	RV	RPVXE, RPVASL	in.	Level of Tsat line
54	RV	RPVPab, RPVAPab, RPVPWR	kW	Heated rod power above and below Tsat level and total
55	RV	RPVRXV, RPVASOUT	lbm/sec.	Core steam generation rate
56	RV	RPVALIN	lbm/sec.	Calculated core flow
57	RV	HTMXRPV, ST08RPV	°F	Maximum clad temperature and saturation temperature
58	Hot leg	MWHL1, MWHL2	lbm	Water mass in hot legs
59	Hot leg	MVHL1, MVHL2	lbm	Vapor mass in hot legs
60	Cold leg	CL1WMS, CL2WMS, CL3WMS, CL4WMS	lbm	Water mass in cold legs
61	Cold leg	CL1VMS, CL2VMS, CL3VMS, CL4VMS	lbm	Vapor mass in cold legs
62	ADS and break	BRKSTIR, ADS13TIR, ADS41TIR, ADS42TIR	lbm	Total discharged mass for ADS 1-3, ADS-4s, and break
63	ADS and break	BRKTIVF, AD13TIVF, AD41TIVF, AD42TIVF	lbm	Total integrated vapor flow for ADS and break
64	ADS and break	BRKTILF, AD13TILF, AD41TILF, AD42TILF	lbm	Total integrated liquid flow for ADS and break
65	ADS and break	ADS13SVR, ADS41SVR, ADS42SVR	lbm/sec.	Vapor flow out ADS 1-3 and ADS-4
66	ADS and break	ADS13SLR, ADS41SLR, ADS42SLR	lbm/sec.	Liquid flow out ADS 1-3 and ADS-4
67	ADS and break	BRKSSVR	lbm/sec.	Vapor flow out of break
68	ADS and break	BRKSSLR	lbm/sec.	Liquid flow out of break
69	ADS and break	BRKSPEI, ADS13EI, ADS41EI, ADS42EI	Btu	Integrated fluid energy for ADS 1-3, ADS-4, and break
70	Mass balance	TOTMASS	lbm	Total system mass inventory
71	Mass balance	PRIMMASS, PRIMASS2	lbm	Measured primary system inventory and value from mass balance
72	Mass balance	MERROR	lbm	Mass balance error
73	Mass balance	MIN, MOUT SRCMASS	lbm	Integrated mass flow in and out of primary system and source mass
74	Energy balance	Various	Btu	Components of energy balance

THE FIGURES LISTED IN TABLE 5.9.2-1
ARE NOT INCLUDED IN THIS NONPROPRIETARY DOCUMENT

5.9.3 Long-Term Transient

The long-term transient started with initiation of IRWST injection, covered the transition from IRWST to sump injection, and provided information on the LTC response of the AP600 plant. For the 2-inch hot-leg break, Matrix Test SB15, the long-term transient analyzed runs from [ ]^{a,b,c} seconds to the end of the test at near [ ]^{a,b,c} seconds. The behavior of the test facility during this period of the transient is discussed in this subsection using the plot package detailed in Table 5.9.3-1. This analysis concentrates on the components of the primary system that remained active during the LTC phase, that is, the RPV, the hot legs, ADS-4, the sumps, and the IRWST.

During the long-term transient, the main thermal-hydraulic phenomena of interest were:

- Maintenance of core cooling and removal of energy from the primary circuit.
- Level oscillations (from [ ]^{a,b,c} seconds there were system wide level and pressure oscillations, which are discussed further in Subsection 6.1.3)

5.9.3.1 Maintenance of Core Cooling

Mass Injected into Primary System

Total DVI line flow, CMT flow, and IRWST flows are shown in Figures 5.9.3-6 and 5.9.3-7, and flow from the primary sump is shown in Figure 5.9.3-19. From around [ ]^{a,b,c} seconds, there was a contribution to the DVI flow from the CMTs as the CMTs reached post-refill draindown.

During the pre-sump injection phase of the transient, IRWST flow proceeded at a gradually declining rate with the effect of the primary system oscillations superimposed. At [ ]^{a,b,c} seconds, flow from the primary sump began through the check valves around the main injection valves resulting briefly in a further reduction in IRWST flow.

Reactor Pressure Vessel and Downcomer Response

The effect of the water inflow on the downcomer fluid temperatures, core inlet and core outlet temperatures, and peak clad temperatures during the long-term phase of the transient is shown in Figures 5.9.3-4, 5.9.3-5, and 5.9.3-38. Figure 5.9.3-4 shows that there was general increase in average downcomer fluid temperatures during the long-term transient. By the end of the CMT injection phase, this average temperature reached a value about [ ]^{a,b,c} °F below saturation. It decreased fairly rapidly thereafter as the colder IRWST was the sole water source, then increased once again as sump liquid entered the RPV via the check valve flow path. Figure 5.9.3-5 implies that the core remained subcooled for the entire long-term transient. However, as shown in Figures 5.9.3-34 to 5.9.3-36, the DVI Line method indicates that a small level of boiling was maintained after [ ]^{a,b,c} seconds into

the transient. Nevertheless, the level of boiling was small and showed that the inflow from the IRWST was sufficient.

Figure 5.9.3-38 shows that there were no significant excursions in heated rod temperatures throughout the long-term transient; therefore, sufficient core inventory and flow was maintained through this phase of the transient to remove the decay heat generated. For significant portions of the transient, a two-phase mixture was present in the core and upper plenum regions. The following discussion tracks the variation in water level and mass throughout the reactor vessel and downcomer.

The mass and level for the core region are shown in Figures 5.9.3-28 and 5.9.3-29. The collapsed liquid level in the core indicated that the heated rods were always covered with a single- or two-phase mixture. During the later stages of the transient, the collapsed liquid level remained above the top of the heated rods. Flow through the check valves of the hot water from the sump is shown in Figures 5.9.3-4 and 5.9.3-5 as a sudden increase in fluid temperature in the downcomer and at the core inlet. The hot water also led to an increase in the calculated steam generation rate, as shown in Figure 5.9.3-36.

The collapsed liquid level in the upper plenum region is shown in Figure 5.9.3-32. The figure indicates that the collapsed liquid level initially fell but then remained at the top of the hot legs during the period before sump injection began. Following the influx of relatively hot water from the sumps, the test was terminated at [ ]^{a,b,c} seconds.

The mass of water in the RPV is shown in Figure 5.9.3-25. After an initial decline, the reactor vessel water mass settled at an average value of [ ]^{a,b,c} lbm until the refilled CMTs emptied, when it gradually rose to [ ]^{a,b,c} lbm, which is more than [ ]^{a,b,c} percent of the initial vessel water inventory. From [ ]^{a,b,c} seconds, oscillations in vessel inventory were observed. For SB15, these oscillations are comparable in magnitude to those observed in SB01. Figures 5.9.3-51 to 5.9.3-56 illustrate these oscillations using plots on a restricted time frame from [ ]^{a,b,c} seconds. These oscillations are observed in primary system measurements from the upper plenum to to the ADS-4 flows. The oscillations have a period [ ].^{a,b,c} These oscillations and possible mechanisms for their production are discussed further in Subsection 6.1.3.

The mass of fluid and collapsed liquid level in the RPV downcomer are shown in Figures 5.9.3-26 and 5.9.3-27. The collapsed liquid level remained above the cold legs for the entire long-term transient up until the time at which the CMTs were empty.

5.9.3.2 Energy Transport from the Primary System

During the long-term transient, energy continued to be deposited in the primary system from the heated rods, metal, and fluid flowing from the primary sump. The SGs and PRHR remained inactive

throughout this phase of the transient and the principal paths for energy removal from the primary system were via the hot leg break and via the ADS-4 valves.

Integrated mass flow from the primary system via the ADS and the break is shown in Figure 5.9.3-43. Significant amounts of flow left the primary circuit through both the ADS-4 valves and the hot-leg break during the LTC phase of the transient. This is confirmed by Figures 5.9.3-44 to 5.9.3-45, which show the flows through the ADS and break.

Figure 5.9.3-36 shows the calculated steam generation rate as determined by the DVI line flow method. During the IRWST injection phase of the transient, steam was generated at [ ]^{a,b,c} lbm/sec. Steam left the primary circuit by the ADS-4 route, as evidenced by the following:

- The ADS 4-2 vapor flow rate showed periods of significant positive flow.
- Examination of the fluid thermocouples on the outlet of the ADS-4 valves indicates that temperatures remained at or above saturation.

Furthermore, it was not possible for all the steam generated in the core to flow from the upper head to the downcomer via the bypass holes (Subsection 6.1.3). Therefore steam left the primary system via ADS-4. Figure 5.9.3-50 shows all the components to the system energy balance; any contribution from steam leaving via the ADS-4 valves is not included in this figure. Further discussion of steam loss from the primary circuit is provided in the mass and energy balance discussions of Section 6.2.

TABLE 5.9.3-1
OSU TEST ANALYSIS STANDARD PLOT PACKAGE FOR SUBSECTION 5.9.3
LONG-TERM TRANSIENT

Plot No.	Component	Variables	Units	Description
1	RV	RPVPWR	kW	Core power
2	Primary sump	TSMPI1, TSMPI2	°F	Sump injection line temperatures
3	DVI	TDVIL1, TDVIL2	°F	DVI line temperatures
4	RPV	T01DC, T02DC, T03DC, ST01DC	°F	Water and saturation temperatures in downcomer
5	RPV	T01RPV, T08RPV, ST08RPV	°F	Core inlet/outlet temperature, saturation temperature
6	DVI-1	WWTDVIL1, WWTIRWI1, WWTIRWI3	lbm/sec.	Individual components and total flow in DVI-1
7	DVI-2	WWTDVIL2, WWTIRWI2, WWTIRWI4	lbm/sec.	Individual components and total flow in DVI-2
8	CMT	CLDP-502, CLDP-507	in.	Collapsed liquid level in CMTs
9	CMT	CLDP-509, CLDP510	in.	Level CL-CMT balance lines
10	IRWST	IRWST	lbm	Mass of fluid in IRWST
11	IRWST	CLDP-701	in.	Collapsed liquid level in IRWST
12	IRWST	UIRWST	Btu	Fluid energy in IRWST
13	Primary sump	AMPSMP	lbm	Primary sump fluid mass
14	Primary sump	CLDP-901	in.	Primary sump level
15	Primary sump	UPSMP	Btu	Primary sump fluid energy
16	Secondary sump	AMSSMP	lbm	Secondary sump fluid mass
17	Secondary sump	CLDP-902	in.	Secondary sump level
18	Secondary sump	USSMP	Btu	Secondary sump fluid energy
19	Primary sump	WSTSMPET, WWTSMPIT	lbm/sec.	Primary sump steam and liquid injection rate
20	Primary sump	MISMPI1, MISMPI2, MISMPIT, MIIRWT	lbm	Integrated primary sump and IRWST flows
21	SG	MSSGIP1, MSSGIP2, MSSGOP1, MSSGOP2	lbm	Mass of fluid in SG side inlet/outlet plena
22	Surge line	PLM	lbm	Fluid mass in surge line
23	Surge line	CLDP-602	in.	Collapsed liquid level in surge line
24	Surge line	UPSL	Btu	Fluid energy in surge line
25	RV	MWRPV	lbm	Total fluid mass in reactor vessel

TABLE 5.9.3-1 (Continued)
OSU TEST ANALYSIS STANDARD PLOT PACKAGE FOR SUBSECTION 5.9.3
LONG-TERM TRANSIENT

Plot No.	Component	Variables	Units	Description
26	RV	DCM	lbm	Fluid mass in downcomer
27	RV	LDP01DC	in.	Collapsed liquid level in downcomer compared to various reference elevations
28	RV	MW03RPV	lbm	Fluid mass in core region
29	RV	LDP03RPV	in.	Collapsed liquid level in core
30	RV	RPVAVDF		Core exit void fraction
31	RV	RPVAQOUT		Core exit quality
32	RV	LDP06RPV	in.	Collapsed liquid level in the upper plenum
33	RV	MW08RPV	lbm	Fluid mass in the upper head
34	RV	RPVASL	in.	Level of Tsat line
35	RV	RPVAPab, RPVPWR	kW	Heated rod power above and below Tsat level and total
36	RV	RPVASOUT	lbm/sec.	Core steam generation rate
37	RV	RPVALIN	lbm/sec.	Calculated core flow
38	RV	HTMXRPV, ST08RPV	°F	Maximum clad temperature, saturation temperature and delta
39	Hot leg	MWHL1, MWHL2	lbm	Water mass in hot legs
40	Hot leg	MVHL1, MVHL2	lbm	Vapor mass in hot legs
41	Cold leg	CL1WMS, CL2WMS, CL3WMS, CL4WMS	lbm	Water mass in cold legs
42	Cold leg	CL1VMS, CL2VMS, CL3VMS, CL4VMS	lbm	Vapor mass in cold legs
43	ADS and break	BRKSTIR, ADS13TIR, ADS41TIR, ADS42TIR	lbm	Total discharged mass for ADS 1-3, ADS-4, and break
44	ADS and break	ADS13TLR, ADS41TLR, ADS42TLR	lbm/sec.	Liquid flow out ADS 1-3 and ADS-4
45	ADS and break	BRKSTLR	lbm/sec.	Liquid flow and total flow out of break
46	Mass balance	TOTMASS	lbm	Total system mass inventory
47	Mass balance	PRIMMASS, PRIMASS2	lbm	Measured primary system inventory and valve from mass balances
48	Mass balance	MERROR	lbm	Mass balance error
49	Mass balance	MIN, MOUT SRCMASS	lbm	Integrated mass flow in and out of primary system and source mass
50	Energy balance	Various	Btu	Component of energy balance
51	ADS-4	ADS41TLR, ADS42TLR	lbm/sec.	Oscillations in ADS-4 liquid flow
52	Surge line	CLDP-602	in.	Oscillations in surgeline level
53	RV	CPT-107	psia	Oscillations in upper head pressure

TABLE 5.9.3-1 (Continued)
OSU TEST ANALYSIS STANDARD PLOT PACKAGE FOR SUBSECTION 5.9.3
LONG-TERM TRANSIENT

Plot No.	Component	Variables	Units	Description
54	RV	CLDP-113	in.	Oscillations in upper plenum level
55	RV	LDP03RPV	in.	Oscillations in core level
56	RV	LDP01DC	in.	Oscillations in downcomer level

THE FIGURES LISTED IN TABLE 5.9.3-1
ARE NOT INCLUDED IN THIS NONPROPRIETARY DOCUMENT

5.10 Analysis of Matrix Test SB19

Matrix Test SB19 (OSU Test U0019) simulated a 2-in. break LOCA with LTC and without the operation of the nonsafety-related systems. By automatically controlling the BAMS header pressure, the effect of containment backpressure was simulated. The break was located at the bottom of CL-3 and except for the simulation of backpressure, this test was similar to SB01, including the simulated failure of one of the ADS-4 lines. Changes to the OSU facility between SB01 and SB19 are identified in the Final Data Report.[1]

The analysis of Matrix Test SB19 is divided into three sections, as follows:

- Facility performance is discussed in Subsection 5.10.1. It provides a brief outline of the response of the test facility; further details are available in the Final Data Report.[1]

- The short-term transient for SB19 encompassed the start of the simulation up to [ ]^{a,b,c} seconds. This period includes blowdown, natural circulation, ADS, and initial IRWST stages of the transient. For this test, the CMT refill occurred during the short-term transient. At [ ]^{a,b,c} seconds, CMT-1 began to refill, and CMT-2 followed [ ]^{a,b,c} seconds later. This CMT refill phenomena is discussed further in Subsection 6.1.1 and is excluded from this discussion of the short-term transient.

- The analysis of the long-term transient for SB19 encompassed the time frame from [ ]^{a,b,c} seconds to the end of the test. This phase of the transient included IRWST injection and covered the transition to sump injection. The long-term transient actually started with IRWST injection, which is discussed as part of the short-term transient. Between the end of the short-term transient and [ ]^{a,b,c} seconds, the system remained relatively inactive, so this discussion begins at [ ]^{a,b,c} seconds.

The discussion of the short- and long-term phase of the transient focuses on important thermal-hydraulic phenomena identified in the PIRT (Table 1.3-1). The mass and energy balance results are key indicators of the quality of the analysis on which this discussion is based. These are discussed in detail in Subsections 6.2.2 and 6.2.3.

5.10.1 Facility Performance

The performance of the OSU test facility during Matrix Test SB19 in reference to the five transient phases is outlined in the following:

- Blowdown
- Natural circulation
- ADS
- IRWST injection
- Sump injection

The overall performance of the facility during the transient is shown in Figures 5.10.1-1 to 5.10.1-4. Figure 5.10.1-1 shows the pressurizer pressure throughout the test with various phases and operating components delineated on the figure. The time scale was reduced for clarity since there were only small changes in system pressure during the long-term phase of the transient. Figure 5.10.1-2 shows the total DVI line flow and its composition from the various sources at each time in the transient. Figure 5.10.1-3 shows the calculated core steam generation rate throughout the test, and Figure 5.10.1-4 shows the variation in average measured core outlet temperature and peak clad temperature relative to the core outlet saturation temperature.

Figures 5.10.1-1 and 5.10.1-2 show that there was a continuous flow of water to the core from the passive safety-related systems throughout the transient. Once initiated, the ADS lines rapidly depressurized the primary system, which enhanced the CMT and accumulator injection flow rates. Ultimately, the ADS-4 valves sufficiently reduced the system pressure to start gravity-driven IRWST injection. The passive injection systems overlapped so that as one source of water drained, the next was available to continue the cooling process. The level of steam generation in the core and the response of the average measured core outlet fluid temperatures and maximum clad temperatures are shown in Figures 5.10.1-3 and 5.10.1-4. These figures show that the cooling flow prevented core heatup, and the core remained covered. The core remained subcooled for large periods of the transient and when steam production occurred, the rate of generation remained well below the rate at which water was delivered to the core.

5.10.1.1 Blowdown Phase

The blowdown phase began at time zero when the break was initiated and continued until the primary system pressure was in equilibrium with the secondary-side pressure at around [ ]^{a,b,c} seconds. Immediately following the opening of the break, the primary system pressure fell gradually to the end of the blowdown phase. During this phase of the transient, cooling flow was provided from the two CMTs, which remained in the recirculation mode, and heat was removed from the primary system via the SGs.

5.10.1.2 Natural Circulation Phase

In this LOCA simulation, the single- and two-phase natural circulation phase was initially marked by a (Figure 5.10.1-1) short period of stable system pressure, followed by a gradual reduction after [ ]^{a,b,c} seconds when the primary system pressure fell below that of the secondary side. During this phase of the transient, the SG tubes drained by about [ ]^{a,b,c} seconds and at this time, heat removal from the primary system continued via the PRHR. The pressurizer and surge line completely drained at [ ]^{a,b,c} and [ ]^{a,b,c} seconds, respectively. In response to voiding in CL-3, CMT-1 transitioned to draindown mode at [ ]^{a,b,c} seconds, and the falling CMT level reached the ADS low-level setpoint at [ ]^{a,b,c} seconds. As shown in Figure 5.10.1-2, a low level of accumulator flow began at [ ]^{a,b,c} seconds. The natural circulation phase of the transient continued to [ ]^{a,b,c} seconds when the ADS-1 valve opened.

5.10.1.3 Automatic Depressurization System Phase

ADS-1 actuation was followed by ADS-2 and ADS-3 [ ]^{a,b,c} and [ ]^{a,b,c} seconds later. With initiation of the ADS, accumulator injection increased. The influx of cold water combined with increased venting via the ADS led to a rapid depressurization of the primary system. Actuation of ADS-4 at [ ]^{a,b,c} seconds completed depressurization to a level that allowed IRWST injection at [ ]^{a,b,c} seconds via both DVI lines. During the rapid accumulator injection, increased flow path system resistance reduced flow out of the CMTs. CMT flow resumed as the accumulators drained. The accumulators were fully drained [ ]^{a,b,c} seconds before IRWST injection began. The CMTs did not fully drain during the short-term transient. Flow from the CMTs ceased following the start of IRWST injection. The transfer from CMT/accumulator to IRWST injection was indicated by the minimum RPV inventory of [ ]^{a,b,c} lbm at [ ]^{a,b,c} seconds. This minimum inventory coincided with the refill of CMT-1. Another slightly higher minimum was observed at [ ]^{a,b,c} seconds when CMT-2 refilled.

Actuation of ADS-2 rapidly refilled the pressurizer as water and steam flowed out of the ADS. The pressurizer gradually drained by [ ]^{a,b,c} seconds.

5.10.1.4 In-Containment Refueling Water Storage Tank Injection

IRWST injection signals the transition from the short- to long-term phase of the transient. The initial phase of IRWST injection involved an increase in flow through the two DVI lines, which was followed by a gradual flow reduction as the driving head between the IRWST and the RCS fell due to the reduced IRWST water level. Once maximum flow was established, the influx of water from the IRWST was sufficient to keep the core subcooled from [ ]^{a,b,c} seconds (Figure 5.10.1-4). Steam was subsequently generated in the core for the remainder of the transient (Figure 5.10,1-3). Following the restart of core steam generation, IRWST injection between [ ]^{a,b,c} seconds, was marked by oscillations in pressure and level throughout the primary system. These oscillations were also observed in the ADS-4 liquid flow rates.

5.10.1.5 Sump Injection

When the IRWST level fell to [ ]^{a,b,c} in., the main sump injection valves opened and the sump injection flow started (Figure 5.10.1-2). Sump flow began at [ ]^{a,b,c} seconds, and the driving head from the sump was sufficient for flow to the IRWST on DVI-1. On DVI-2, there was a corresponding increase in the flow out of the IRWST, which indicated that there was no significant increase in IRWST inventory. Note that there was no flow through the check valves around the main sump injection valves before the main valves opened for this test.

TABLE 5.10.1-1
OSU TEST ANALYSIS PLOT PACKAGE FOR SUBSECTION 5.10.1

Plot No.	Component	Variables	Units	Description
1	Pressurizer	CPT-604	psia	System pressure and event history
2	Water injection	WWTDVI1+WWTDVI2, WOUTACC1+WOUTACC2, WWTIRWI1+WWTIRWI2, WWTSMPIT	lbm/sec.	Total of CMT, accumulator, IRWST, and sump injection flows
3	Reactor vessel	RPVASOU2	lbm/sec.	Steam generation in reactor vessel
4	Reactor vessel	T08RPV, HTMXRPV, TSAT	°F	Reactor vessel outlet temperature, maximum clad temperature and fuel exit saturation temperature

THE FIGURES LISTED IN TABLE 5.10.1-1
ARE NOT INCLUDED IN THIS NONPROPRIETARY DOCUMENT

5.10.2 Short-Term Transient

For the 2-in. cold-leg break with simulated containment backpressure, Matrix Test SB19, the short-term transient encompassed the time frame up to [ ]^{a,b,c} seconds. As shown in Figure 5.10.1-1, this period included the full depressurization of the facility through all four stages of the ADS, together with CMT and accumulator injection plus the initial stages of IRWST injection. The variations in mass, energy, pressure, and temperature throughout this stage of the transient are illustrated in the plot package outlined in Table 5.10.2-1. The plots concentrate on the primary system, including the accumulators, CMTs, IRWST, primary sump, and flows from the primary system via the ADS, break, and IRWST overflow.

There were two principal parameters to be examined for the short-term transient:

- Adequate flow must be maintained from the passive systems to the reactor vessel.
- Adequate flow into the core must be maintained to ensure that decay heat was removed from the simulated fuel rods without a temperature excursion.

These parameters are addressed in the following discussion.

5.10.2.1 Maintenance of Core Cooling

Mass Injected to the Primary System

Figures 5.10.2-6 and 5.10.2-7 show the combined effect of the injection flows for the short-term phase of the transient. Separate plots of the individual contributions to the total flow can be located by consulting the plot package index given in Table 5.10.2-1.

Figures 5.10.2-5 and 5.10.2-6 show how the CMTs, accumulators, and IRWST supplied a continuous flow of water to the core. During the first [ ]^{a,b,c} seconds, cooling flow was provided by the CMTs, which was then supplemented by flow from both accumulators. The rate of flow from the CMTs had an initial value of [ ]^{a,b,c} lbm/sec., which increased to [ ]^{a,b,c} lbm/sec. when draindown commenced. As the driving head fell in response to the CMT water heat-up and draindown, the flow rate gradually decreased until ADS-1 initiation, which resulted in an increase in accumulator flow. Rapid accumulator injection temporarily reduced CMT flow, but led to an overall increase in flow to the core to a peak value of [ ]^{a,b,c} lbm/sec. Following the end of accumulator injection, the CMTs again provided cooling flow until backpressure from IRWST injection ended the CMT draindown. Since IRWST injection began before the CMTs had fully drained, there was no period of the short-term transient when the passive safety systems failed to provide flow to the RPV.

Reactor Pressure Vessel and Downcomer Behavior

The effect of water flow on the average measured core inlet/outlet temperatures and peak clad temperatures during the short-term phase of the transient is shown in Figures 5.10.2-3 and 5.10.2-57. The core outlet temperature first reached saturation at [ ]^{a,b,c} seconds and remained at the saturation level until [ ]^{a,b,c} seconds when the rapid accumulator injection subcooled the core. The combined CMT and accumulator flow was sufficient to keep the core completely subcooled up to [ ]^{a,b,c} seconds. The core outlet temperature then remained at the saturation level for about [ ]^{a,b,c} seconds until the influx of water from the IRWST was sufficient to subcool the core again. The core then remained subcooled until the end of the short-term transient, with the exception of a short period during the reflood of CMT-2.

Figure 5.10.2-57 shows that there were no significant excursions in heater rod temperatures throughout the short-term transient; therefore, sufficient core inventory and flow was maintained through this phase of the transient to remove the decay heat generated. For significant portions of the transient, a two-phase mixture was present in the core and upper plenum regions, with core boiling kept at a low level.

The following discussion tracks the variation in water level and mass throughout the reactor vessel and downcomer. The mass and level for the core region are shown in Figures 5.10.2-44 and 5.10.2-45. The collapsed liquid level in the core indicates that the heater rods remained covered with a single- or two-phase mixture. The minimum core inventory of [ ]^{a,b,c} lbm occurred at [ ]^{a,b,c} seconds into the transient before accumulator injection began. Figure 5.10.2-45 shows that the collapsed liquid level dropped to [ ]^{a,b,c} in. below the top of the heater rod length during this phase of the transient. The average void fraction of the core two-phase mixture may be estimated by dividing the measured core collapsed liquid level by the [ ]^{a,b,c} in. heated rod length. In this test, the minimum collapsed liquid level corresponded to a core void fraction of [ ].^{a,b,c} During the period before IRWST flow was fully established, the core void fraction reached a maximum of [ ].^{a,b,c} By the end of the short-term transient, the effect of IRWST injection ended all core boiling (Figure 5.10.2-55), and the core was again water-solid.

The collapsed liquid level in the upper plenum region covered by LDP-113 and the associated fluid mass are shown in Figures 5.10.2-49 and 5.10.2-48. During the period before accumulator injection, the upper plenum gradually drained to the DVI line elevation. The start of accumulator injection caused an increase in collapsed liquid level to the elevation of the cold legs. Following the end of accumulator injection, the region of the upper plenum spanned by the LDP cell fully drained by [ ]^{a,b,c} seconds and remained drained until IRWST injection supplied sufficient inventory to initiate a refill. A further draining and refill of the upper plenum coincided with the reflood of CMT-2. The upper plenum was again water-solid by the end of the short-term transient.

Figures 5.10.2-50 and 5.10.2-51 show that the upper head variations were similar to those observed for the upper plenum. The upper head gradually drained before the onset of accumulator injection, which

caused an increase in upper head inventory. The upper head was fully drained by [ ]^{a,b,c} seconds. IRWST injection was sufficient to resupply a level in the upper head, and at the end of the short-term transient, a level below the elevation of the by-pass holes was maintained.

The mass of fluid and collapsed liquid level in the RPV downcomer are shown in Figures 5.10.2-41 and 5.10.2-42. The downcomer level fell to the middle of the cold-leg piping by [ ]^{a,b,c} seconds, where it remained for [ ]^{a,b,c} seconds. Before the start of accumulator injection, the downcomer level fell further but remained at or above the middle of the cold legs. As a result, there was a level of water in the cold legs for most of the short-term transient.

5.10.2.2 Energy Transport from the Primary System

Following the break, energy was deposited by the heater rods in the primary system fluid to simulate decay heat and by the primary system metal as it cooled down. Some fluid energy was lost to ambient and out of the break. Excess energy must be removed from the primary system to prevent excessive fluid and heater rod temperature excursions. The AP600 plant is designed to remove heat by a combination of the SGs and the PRHR plus the ADS.

Steam Generator and Passive Residual Heat Removal Heat Transfer

During normal operation, most of the primary system heat was removed via the SGs; however, once the RCPs tripped, the reduced system flow decreased primary- to secondary-side heat transfer. The SGs were only available as heat sinks until the time when the primary system pressure dropped to that of the secondary side; afterward, the two sides were in thermal equilibrium while the primary system had water in the SG tubes. The PRHR is designed to remove heat from the primary system once the S signal opens the isolation valve. The PRHR continues to remove energy after the SGs were thermally isolated until ADS actuated. Once ADS actuated, it became the predominant path for the removal of energy from the primary system.

Figure 5.10.2-33 shows the SG primary- and secondary-side pressure together with the PRHR integrated heat transfer, as represented by the IRWST fluid energy after allowing for the contribution from ADS 1-3 inflow. The SGs were potential sinks for primary system heat while the primary-side pressure was above that of the secondary side, that is, before [ ]^{a,b,c} seconds and before the SG tubes drained. PRHR heat removal began [ ]^{a,b,c} seconds into the test. The PRHR was responsible for all the IRWST heat-up until ADS-1 activation, after which the PRHR heat transfer reduced significantly. During the active phase, the PRHR transferred heat to the IRWST at an average rate of [ ]^{a,b,c} Btu/sec.

Energy Transport via the Break and Automatic Depressurization System

The mass flow rate from the primary system via the break is shown in Figures 5.10.2-67 and 5.10.2-68. As shown in these figures, steam and liquid flow were detected by the flow measuring

devices for the short-term transient. With initiation of ADS 1-3, steam flow through the break ceased, although liquid flow continued as a level in the cold legs was maintained. This liquid flow was supplemented by steam and liquid flow through the ADS 1-3 valves. Between [ ]^{a,b,c} and [ ]^{a,b,c} seconds, ADS 1-3 caused the system to rapidly depressurize and at [ ]^{a,b,c} seconds, ADS-4 was initiated and the primary system continued to the BAMS header pressure.

Flow through the ADS continued until [ ]^{a,b,c} seconds when the flow through the ADS 1-3 terminated and was replaced by flow through the lower resistance ADS-4 paths. By the end of the short-term transient, water was flowing out of the two ADS-4 valves at approximately [ ]^{a,b,c} lbm/sec. (Figure 5.10.2-64).

The integrated mass flow from the primary system via the ADS and the break is shown in Figure 5.10.2-62, and the corresponding integrated energy flow is shown in Figure 5.10.2-69. The total system inventory plot given in Figure 5.10.2-70 indicates that [ ]^{a,b,c} lbm of inventory was gained during the short-term transient. Components of the energy balance are shown in Figure 5.10.2-74.

TABLE 5.10.2-1 OSU TEST ANALYSIS STANDARD PLOT PACKAGE FOR SUBSECTION 5.10.2				
Plot No.	**Component**	**Variables**	**Units**	**Description**
1	Pressurizer	CPT-604	psia	System pressure
2	RPV	RPVPWR	kW	Core power
3	RPV	T01RPV, T08RPV, ST08RPV	°F	Core inlet/outlet temperature, saturation temperature
4	SG	CPT-201, CPT-204, CPT-301, CPT-302	psia	Primary and secondary pressures in SG
5	DVI-1	WWTDVIL1, WWTIRWI1, WOUTACC1, WWTIRWI3	lbm/sec.	Individual components and total flow in DVI-1
6	DVI-2	WWTDVIL2, WWTIRWI2, WOUTACC2, WWTIRWI4	lbm/sec.	Individual components and total flow in DVI-2
7	CMT	AMCMT1B, AMCMT2B	lbm	Fluid mass in CMTs (excludes balance lines)
8	CMT	CLDP-502, CLDP-507	in.	Collapsed liquid level in CMTs
9	CMT	MIWDVIL1, MIWDVIL2	lbm	Integrated mass out of CMTs
10	CMT	WWTDVIL1, WWTDVIL2	lbm/sec.	Flow out of CMTs
11	CMT	WOUTCLB1, WOUTCLB2	lbm/sec.	Flow into CMTs
12	CMT	CLDP-509, CLDP510	in.	Level CL-CMT balance lines
13	CMT	UCMT1, UCMT2	Btu	Fluid energy in CMTs
14	IRWST	IRWST	lbm	Mass of fluid in IRWST
15	IRWST	CLDP-701	in.	Collapsed liquid level in IRWST
16	IRWST	WWTIRWI1, WWTIRWI2	lbm/sec.	Flow from IRWST to DVI lines
17	IRWST	IRWSTOR	lbm/sec.	Overflow from IRWST to sump
18	IRWST	ADS13TMR	lbm/sec.	Total ADS flow into IRWST
19	IRWST	ADS13TIR, MIIRWI1, MIIRWI2, MIIRWIO	lbm	Integrated mass out of IRWST
20	IRWST	UIRWST	Btu	Fluid energy in IRWST
21	PRHR	CLDP-802	in.	Collapsed liquid level in PRHR HX

TABLE 5.10.2-1 (Continued)
OSU TEST ANALYSIS STANDARD PLOT PACKAGE FOR SUBSECTION 5.10.2

Plot No.	Component	Variables	Units	Description
22	PRHR	WWOTPRHR	lbm/sec.	Measured outlet flow from PRHR tube
23	Accumulator	AMACC1, AMACC2	lbm	Mass of fluid in accumulators
24	Accumulator	CLDP-401, CLDP-402	in.	Collapsed liquid level in accumulators
25	Accumulator	WOUTACC1, WOUTACC2	lbm/sec.	Flow from accumulators
26	Accumulator	MOUTACC1, MOUTACC2	lbm	Integrated mass out of accumulators
27	Accumulator	UACC1, UACC2	Btu	Fluid energy in accumulators
28	Primary sump	AMPSMP	lbm	Primary sump fluid mass
29	Primary sump	CLDP-901	in.	Primary sump level
30	Primary sump	UPSMP	Btu	Primary sump fluid energy
31	SG	MSSGIP1, MSSGIP2, MSSGOP1, MSSGOP2	lbm	Mass of fluid in SG primary side inlet/outlet plena
32	SG	MSSGHT1, MSSGHT2, MSSGCT1, MSSGCT2	lbm	Mass of fluid in SG primary side hot and cold tubes
33	SG/PRHR	CPT-201, CPT-301, QPRHRI	psia & Btu	SG1 pressure and PRHR integrated heat output
34	Pressurizer	PZM	lbm	Fluid mass in pressurizer
35	Pressurizer	CLDP-601	in.	Collapsed liquid level in pressurizer
36	Pressurizer	UPZ	Btu	Fluid energy in pressurizer
37	Surge line	PLM	lbm	Fluid mass in surge line
38	Surge line	CLDP-602	in.	Collapsed liquid level in surge line
39	Surge line	UPSL	Btu	Fluid energy in surge line
40	RPV	MWRPV	lbm	Total fluid mass in reactor vessel
41	RPV	DCM	lbm	Fluid mass in downcomer
42	RPV	LDP01DC	in.	Collapsed liquid level in downcomer compared to various reference elevations
43	RPV	MW01RPV	lbm	Fluid mass in lower plenum
44	RPV	MW03RPV	lbm	Fluid mass in core region
45	RPV	LDP03RPV	in.	Collapsed liquid level in core
46	RPV	RPVAVDF2		Core exit void fraction
47	RPV	RPVAQOU2		Core exit quality
48	RPV	MW06RPV	lbm	Fluid mass in the upper plenum
49	RPV	LDP06RPV	in.	Collapsed liquid level in the upper plenum
50	RPV	MW08RPV	lbm	Fluid mass in the upper head
51	RPV	LDP08RPV	in.	Collapsed liquid level in the upper head

TABLE 5.10.2-1 (Continued)
OSU TEST ANALYSIS STANDARD PLOT PACKAGE FOR SUBSECTION 5.10.2

Plot No.	Component	Variables	Units	Description
52	RPV	URPV	Btu	Total fluid energy in reactor vessel
53	RPV	RPVXE, RPVASL2	in.	Level of Tsat line
54	RPV	RPVPab, RPVAPab2, RPVPWR	kW	Heated rod power above and below Tsat level and total
55	RPV	RPVRXV, RPVASOU2	lbm/sec.	Core steam generation rate
56	RPV	RPVALIN2	lbm/sec.	Calculated core flow
57	RPV	HTMXRPV, ST08RPV	°F	Maximum clad temperature and saturation temperature
58	Hot leg	MWHL1, MWHL2	lbm	Water mass in hot legs
59	Hot leg	MVHL1, MVHL2	lbm	Vapor mass in hot legs
60	Cold leg	CL1WMS, CL2WMS, CL3WMS, CL4WMS	lbm	Water mass in cold legs
61	Cold leg	CL1VMS, CL2VMS, CL3VMS, CL4VMS	lbm	Vapor mass in cold legs
62	ADS and break	BRKSTIR, ADS13TIR, ADS41TIR, ADS42TIR	lbm	Total discharged mass for ADS 1-3, ADS-4s, and break
63	ADS and break	BRKTIVF, AD13TIVF, AD41TIVF, AD42TIVF	lbm	Total integrated vapor flow for ADS and break
64	ADS and break	BRKTILF, AD13TILF, AD41TILF, AD42TILF	lbm	Total integrated liquid flow for ADS and break
65	ADS and break	ADS13SVR, ADS41SVR, ADS42SVR	lbm/sec.	Vapor flow out ADS 1-3 and ADS-4
66	ADS and break	ADS13SLR, ADS41SLR, ADS42SLR	lbm/sec.	Liquid flow out ADS 1-3 and ADS-4
67	ADS and break	BRKSSVR	lbm/sec.	Vapor flow out of break
68	ADS and break	BRKSSLR	lbm/sec.	Liquid flow out of break
69	ADS and break	BRKSPEI, ADS13EI, ADS41EI, ADS42EI	Btu	Integrated fluid energy for ADS 1-3, ADS-4, and break
70	Mass balance	TOTMASS	lbm	Total system mass inventory
71	Mass balance	PRIMMASS, PRIMASS2	lbm	Measured primary system inventory and value from mass balance
72	Mass balance	MERROR	lbm	Mass balance error
73	Mass balance	MIN, MOUT SRCMASS	lbm	Integrated mass flow in and out of primary system and source mass
74	Energy balance	Various	Btu	Components of energy balance

THE FIGURES LISTED IN TABLE 5.10.2-1
ARE NOT INCLUDED IN THIS NONPROPRIETARY DOCUMENT

5.10.3 Long-Term Transient

The long-term transient started with initiation of IRWST injection, covered the transition from IRWST to sump injection, and provided information on the LTC response of the AP600 plant. For the 2-in. cold-leg break with simulated containment backpressure, Matrix Test SB19, the long-term transient analyzed ran from [ ]^{a,b,c} seconds to the end of the test around [ ]^{a,b,c} seconds. The behavior of the test facility during this period of the transient is discussed in this subsection using the plot package detailed in Table 5.10.3-1. This analysis concentrates on the components of the primary system that remained active during the LTC phase, that is, the RPV, the hot legs, ADS-4, the sumps, and the IRWST.

For the long-term transient, thermal-hydraulic phenomena of interest were:

- Maintenance of core cooling and removal of energy from the primary system.
- Level oscillations (from [ ]^{a,b,c} seconds there were system wide level and pressure oscillations, which are discussed further in Subsection 6.1.3).

5.10.3.1 Maintenance of Core Cooling

Mass Injected into Primary System

Total DVI line flow, CMT flow, and IRWST flows are shown in Figures 5.10.3-6 and 5.10.3-7, and the flow from the primary sump is shown in Figure 5.10.3-19. From around [ ]^{a,b,c} seconds, there was a contribution to the DVI flow from the CMTs as the CMTs reached post-refill draindown.

During the pre-sump injection phase of the transient, IRWST flow proceeded at a gradually declining rate with the effect of the primary system oscillations superimposed. At [ ]^{a,b,c} seconds, the main sump injection valves opened, resulting in a reversal of flow through IRWST injection line-1 and an increase in IRWST flow in line-2. The net result was that an injection flow rate of [ ]^{a,b,c} lbm/sec. was maintained through DVI-1 and -2, respectively.

Reactor Pressure Vessel and Downcomer Response

The effect of the water inflow on the average measured downcomer fluid temperatures, core inlet and core outlet temperatures, and heater rod temperatures during the long-term phase of the transient is shown in Figures 5.10.3-4, 5.10.3-5, and 5.10.3-38. Figure 5.10.3-4 shows that there was a general increase in average downcomer fluid temperatures during the long-term transient. By the end of the test, this average temperature was [ ]^{a,b,c} °F below saturation. Figure 5.10.3-5 shows that the core was above saturation temperature for most of the long-term transient. Figures 5.10.3-34 to 5.10.3-36 show that the DVI line flow method discussed in Section 4.11 indicates that a small level of core

boiling was maintained after [ ]^{a,b,c} seconds into the transient. Nevertheless, the level of boiling was small and showed that the inflow from the IRWST and sumps was sufficient to maintain cooling.

Figure 5.10.3-38 shows that there were no significant excursions in heater rod temperatures throughout the long-term transient; therefore, sufficient core inventory and flow was maintained through this phase of the transient to remove the decay heat generated. For significant portions of the transient, a two-phase mixture was present in the core and upper plenum regions.

The following discussion tracks the variation in water level and mass throughout the reactor vessel and downcomer. The mass and level for the core region are shown in Figures 5.10.3-28 and 5.10.3-29. The collapsed liquid level in the core indicated that the heater rods, were always covered with a single- or two-phase mixture. During the later stages of the transient, the collapsed liquid level fell just below the top of the heater rods, and the maximum core void fraction was [ ].^{a,b,c} The fall in core inventory was a result of the influx of hot water from the primary sump as it flowed through the check valves. The impact of this hot water on the system temperatures is shown in Figures 5.10.3-4 and 5.10.3-5 as a sudden increase in fluid temperature in the downcomer and at the core inlet. The hot water also led to an increase in the calculated steam generation rate, as shown in Figure 5.10.3-36, and a corresponding fall in the level at which the core reached saturation temperature (Figure 5.10.3-34).

The collapsed liquid level in the upper plenum region covered by LDP-113, is shown in Figure 5.10.3-32. The figures indicate that during the period before sump injection began, the collapsed liquid level initially fell and then remained at the top of the hot legs. Following the influx of relatively hot water from the sumps, the level dropped to the bottom of the hot legs, where it remained for the rest of the transient. This level corresponded to a void fraction of [ ].^{a,b,c}

The mass of water in the reactor pressure vessel is shown in Figure 5.10.3-25. After an initial decline, the reactor vessel water mass settled at an average value of [ ]^{a,b,c} lbm until the time sump injection started when it fell to [ ]^{a,b,c} lbm, which is [ ]^{a,b,c} percent of the initial vessel water inventory. From [ ]^{a,b,c} seconds, oscillations in vessel inventory were observed. Figures 5.10.3-51 to 5.10.3-56 illustrate these oscillations using plots on a restricted time frame from [ ]^{a,b,c} seconds. These oscillations are observed in primary system measurements from the upper plenum to the ADS-4 flows. The oscillations occurred for [ ]^{a,b,c} seconds. The oscillations in the ADS flow lagged behind those in the upper head pressure by around [ ]^{a,b,c} seconds. These oscillations and possible mechanisms for their production are discussed further in Subsection 6.1.3.

The mass of fluid and collapsed liquid level in the RPV downcomer are shown in Figures 5.10.3-26 and 5.10.3-27. The collapsed liquid level remained above the mid-elevation of the cold legs until [ ]^{a,b,c} seconds. At this time the level fell below the cold legs and subsequently, the start of sump injection reduced the level to the DVI line elevation before it recovered to the hot legs. The downcomer level remained at this level for the rest of the transient.

5.10.3.2 Energy Transport from the Primary System

During the long-term transient, energy continued to be deposited in the primary system from the heated rods, metal, and fluid flowing from the primary sump. The SGs and PRHR remained inactive throughout this phase of the transient, and the principle path for energy out of the primary system was via the ADS-4 valves.

Integrated mass flow from the primary system via the ADS and the break is shown in Figure 5.10.3-43. During the LTC phase of the transient until nearly [ ]^{a,b,c} seconds, there is significant outflow through the break and ADS-4 valves. This is confirmed by Figures 5.10.3-44 to 5.10.3-45, which show flow through the ADS and break. At [ ]^{a,b,c} seconds, flow through the break ceased as the cold legs drained. From [ ]^{a,b,c} seconds, there is reverse flow through the break as indicated by the reducing integral given in Figure 5.10.3-43. During the sump injection phase of the transient, measured outflow is in the form of liquid out of the ADS-4 valves. Water flowed through each of these valves at an average rate of [ ]^{a,b,c} lbm/sec.

Figure 5.10.3-36 shows the calculated steam generation rate, as determined by the DVI line flow method. During the sump injection phase of the transient, steam was generated at over [ ]^{a,b,c} lbm/sec., although the steam vortex meters indicate little or no flow out of the ADS-4 valves. The following two indications show that steam is leaving the primary system by this route:

- Figure 5.10.3-46 shows total measured system fluid inventory. During this phase of the transient after the start of primary sump injection, that is, when core steam generation was most significant, the total system inventory fell by about [ ]^{a,b,c} lbm. This amount corresponds to a steam flow rate of [ ]^{a,b,c} lbm/sec., which would not have been detected by the vortex meters.

- Examination of the fluid thermocouples on the outlet of the ADS-4 valves indicates that temperatures remained at or above saturation temperature following the start of sump injection.

It was not possible for all the steam generated in the core to flow from the upper head to the downcomer via the bypass holes (Subsection 6.1.3). Therefore, steam was leaving the primary system via ADS-4. Figure 5.10.3-50 shows all the components to the system energy balance. Further discussion of steam loss from the primary system is provided in the mass and energy balance discussions of Section 6.2.

TABLE 5.10.3-1
OSU TEST ANALYSIS STANDARD PLOT PACKAGE FOR SUBSECTION 5.10.3
LONG-TERM TRANSIENT

Plot No.	Component	Variables	Units	Description
1	RPV	RPVPWR	kW	Core power
2	Primary sump	TSMPI1, TSMPI2	°F	Sump injection line temperatures
3	DVI	TDVIL1, TDVIL2	°F	DVI line temperatures
4	RPV	T01DC, T02DC, T03DC, ST01DC	°F	Water and saturation temperatures in downcomer
5	RPV	T01RPV, T08RPV, ST08RPV	°F	Core inlet/outlet temperature, saturation temperature
6	DVI-1	WWTDVIL1, WWTIRWI1, WWTIRWI3	lbm/sec.	Individual components and total flow in DVI-1
7	DVI-2	WWTDVIL2, WWTIRWI2, WWTIRWI4	lbm/sec.	Individual components and total flow in DVI-2
8	CMT	CLDP-502, CLDP-507	in.	Collapsed liquid level in CMTs
9	CMT	CLDP-509, CLDP510	in.	Level CL-CMT balance lines
10	IRWST	IRWST	lbm	Mass of fluid in IRWST
11	IRWST	CLDP-701	in.	Collapsed liquid level in IRWST
12	IRWST	UIRWST	Btu	Fluid energy in IRWST
13	Primary sump	AMPSMP	lbm	Primary sump fluid mass
14	Primary sump	CLDP-901	in.	Primary sump level
15	Primary sump	UPSMP	Btu	Primary sump fluid energy
16	Secondary sump	AMSSMP	lbm	Secondary sump fluid mass
17	Secondary sump	CLDP-902	in.	Secondary sump level
18	Secondary sump	USSMP	Btu	Secondary sump fluid energy
19	Primary sump	WSTSMPET, WWTSMPIT	lbm/sec.	Primary sump steam and liquid injection rate
20	Primary sump	MISMPI1, MISMPI2, MISMPIT, MIIRWT	lbm	Integrated primary sump and IRWST flows
21	SG	MSSGIP1, MSSGIP2, MSSGOP1, MSSGOP2	lbm	Mass of fluid in SG side inlet/outlet plena
22	Surge line	PLM	lbm	Fluid mass in surge line
23	Surge line	CLDP-602	in.	Collapsed liquid level in surge line
24	Surge line	UPSL	Btu	Fluid energy in surge line
25	RPV	MWRPV	lbm	Total fluid mass in reactor vessel

TABLE 5.10.3-1 (Continued)
OSU TEST ANALYSIS STANDARD PLOT PACKAGE FOR SUBSECTION 5.10.3
LONG-TERM TRANSIENT

Plot No.	Component	Variables	Units	Description
26	RPV	DCM	lbm	Fluid mass in downcomer
27	RPV	LDP01DC	in.	Collapsed liquid level in downcomer compared to various reference elevations
28	RPV	MW03RPV	lbm	Fluid mass in core region
29	RPV	LDP03RPV	in.	Collapsed liquid level in core
30	RPV	RPVAVDF2		Core exit void fraction
31	RPV	RPVAQOU2		Core exit quality
32	RPV	LDP06RPV	in.	Collapsed liquid level in the upper plenum
33	RPV	MW08RPV	lbm	Fluid mass in the upper head
34	RPV	RPVASL2	in.	Level of Tsat line
35	RPV	RPVAPab2, RPVPWR	kW	Heated rod power above and below Tsat level and total
36	RPV	RPVASOU2	lbm/sec.	Core steam generation rate
37	RPV	RPVALIN2	lbm/sec.	Calculated core flow
38	RPV	HTMXRPV, ST08RPV	°F	Maximum clad temperature, saturation temperature and delta
39	Hot leg	MWHL1, MWHL2	lbm	Water mass in hot legs
40	Hot leg	MVHL1, MVHL2	lbm	Vapor mass in hot legs
41	Cold leg	CL1WMS, CL2WMS, CL3WMS, CL4WMS	lbm	Water mass in cold legs
42	Cold leg	CL1VMS, CL2VMS, CL3VMS, CL4VMS	lbm	Vapor mass in cold legs
43	ADS and break	BRKSTIR, ADS13TIR, ADS41TIR, ADS42TiR	lbm	Total discharged mass for ADS 1-3, ADS-4, and break
44	ADS and break	ADS13TLR, ADS41TLR, ADS42TLR	lbm/sec.	Liquid flow out ADS 1-3 and ADS-4
45	ADS and break	BRKSTLR	lbm/sec.	Liquid flow and total flow out of break
46	Mass balance	TOTMASS	lbm	Total system mass inventory
47	Mass balance	PRIMMASS, PRIMASS2	lbm	Measured primary system inventory and valve from mass balances
48	Mass balance	MERROR	lbm	Mass balance error
49	Mass balance	MIN, MOUT SRCMASS	lbm	Integrated mass flow in and out of primary system and source mass
50	Energy balance	Various	Btu	Component of energy balance
51	ADS-4	ADS41TLR, ADS42TLR	lbm/sec.	Oscillations in ADS-4 liquid flow
52	Surge line	CLDP-602	in.	Oscillations in surgeline level
53	RPV	CPT-107	psia	Oscillations in upper head pressure

TABLE 5.10.3-1 (Continued)
OSU TEST ANALYSIS STANDARD PLOT PACKAGE FOR SUBSECTION 5.10.3
LONG-TERM TRANSIENT

Plot No.	Component	Variables	Units	Description
54	RPV	CLDP-113	in.	Oscillations in upper plenum level
55	RPV	LDP03RPV	in.	Oscillations in core level
56	RPV	LDP01DC	in.	Oscillations in downcomer level

THE FIGURES LISTED IN TABLE 5.10.3-1
ARE NOT INCLUDED IN THIS NONPROPRIETARY DOCUMENT

5.11 Analysis of Matrix Test SB21

Matrix Test SB21 (OSU Test U0021) simulated a double 4-in. cold-leg break LOCA with LTC and without the operation of the nonsafety-related systems. The breaks were located on the top and bottom of CL-3 and except for the break size, this test was similar to SB01, including the simulated failure of one of the ADS-4 lines. Changes to the OSU facility since the performance of SB01 are noted in the Final Data Report.[1]

The analysis of Matrix Test SB21 is divided into three sections as follows:

- The facility performance is discussed in Subsection 5.11.1, which provides a brief outline of the response of the test facility; further details are available in the Final Data Report.[1]

- The short-term transient for SB21 encompassed the start of the simulation up to [ ]^{a,b,c} seconds. This period included the blowdown, natural circulation, ADS, and initial IRWST stages of the transient.

- The analysis of the long-term transient for SB21 encompassed the time frame from [ ]^{a,b,c} seconds to the end of the test. This phase of the transient includes IRWST injection and covered the transition to sump injection. The long-term transient actually started with IRWST injection, which is discussed as part of the short-term transient. Between the end of the short-term transient and [ ]^{a,b,c} seconds, the system remained relatively inactive with the exception of the CMT refill. At [ ]^{a,b,c} seconds, CMT-1 began to refill, and CMT-2 followed [ ]^{a,b,c} seconds later. CMT refill phenomena is discussed further in Subsection 6.1.1, and the discussion of the long-term transient provided here begins at [ ]^{a,b,c} seconds.

The discussion of the short- and long-term phase of the transient focuses on important thermal-hydraulic phenomena identified in the PIRT (Table 1.3-1). The mass and energy balance results are key indicators of the quality of the analysis on which this discussion is based. These are discussed in detail in Subsections 6.2.2 and 6.2.3.

5.11.1 Facility Performance

The performance of the OSU test facility during Matrix Test SB21 in reference to the five transient phases is outlined in the following :

- Blowdown
- Natural circulation
- ADS
- IRWST injection
- Sump injection

The overall performance of the facility during the transient is shown in Figures 5.11.1-1 to 5.11.1-4. Figure 5.11.1-1 shows the pressurizer pressure throughout the test with various phases and operating components delineated on the figure. The time scale was reduced for clarity since there were only small changes in system pressure during the long-term phase of the transient. Figure 5.11.1-2 shows the total DVI line flow and its composition from the various sources at each time in the transient. Figure 5.11.1-3 shows the calculated core steam generation rate throughout the test, and Figure 5.11.1-4 shows the variation in average measured core outlet temperature and peak clad temperature relative to the core outlet saturation temperature.

Figures 5.11.1-1 and 5.11.1-2 show that there was a continuous flow of water to the core from the passive safety-related systems throughout the transient. Once initiated, the ADS lines rapidly depressurized the primary system, which enhanced the CMT and accumulator injection flow rates. Ultimately, the ADS-4 valves sufficiently reduced the system pressure to start gravity-driven IRWST injection. The passive injection systems overlapped so that as one source of water drained, the next was available to continue the cooling process. The level of steam generation in the core and the response of the average measured core outlet fluid temperatures and maximum clad temperatures are shown in Figures 5.11.1-3 and 5.11.1-4. These figures show that the cooling flow prevented core heatup and the core remained covered. The core remained subcooled for large periods of the transient and when steam production occurred, the rate of generation remained well below the rate at which water was delivered to the core.

5.11.1.1 Blowdown Phase

The blowdown phase began at time zero when the break was initiated and continued until the primary system pressure was in equilibrium with the secondary-side pressure at about [ ]^{a,b,c} seconds. During this phase of the transient, cooling flow was provided from the two CMTs, which remained in

recirculation. Heat was removed from the primary system via the SGs. The pressurizer and surge line completely drained at [ ]^{a,b,c} and [ ]^{a,b,c} seconds, respectively.

5.11.1.2 Natural Circulation Phase

After a brief period of stability, the single- and two-phase natural circulation phase was marked by a (Figure 5.11.1-1) gradual reduction in system pressure in this LOCA simulation, rather than by the more stable pressure observed in SB01. During this phase of the transient, the SG tubes drained by about [ ]^{a,b,c} seconds and at this time, heat removal from the primary system continued via the PRHR. In response to voiding in CL-3, CMT-1 transitioned to draindown mode at [ ]^{a,b,c} seconds before the end of the blowdown phase, and the falling CMT level reached the ADS low-level setpoint at [ ]^{a,b,c} seconds. CMT-2 recirculation flow ceased at [ ]^{a,b,c} seconds, which was after CMT-1, but the ADS low level setpoint was reached before CMT-1 at [ ]^{a,b,c} seconds. At [ ]^{a,b,c} seconds, the accumulators began (Figure 5.11.1-2) to inject at a steady rate of over [ ]^{a,b,c} lbm/sec. without affecting the CMT outflow. The natural circulation draindown phase of the transient continued to [ ]^{a,b,c} seconds when the ADS-1 valve opened. The minimum RPV inventory was estimated as [ ]^{a,b,c} lbm at around [ ]^{a,b,c} seconds. This is an overestimate of the actual mass present by up to [ ]^{a,b,c} lbm because LDP-313 spanning the upper plenum was inoperable during SB21.

5.11.1.3 Automatic Depressurization System Phase

ADS-1 actuation was followed by ADS-2 and ADS-3 [ ]^{a,b,c} and [ ]^{a,b,c} seconds later. With initiation of the ADS, a rapid phase of accumulator injection began. The influx of cold water combined with increased venting via the ADS led to a rapid depressurization of the primary system. Actuation of ADS-4 at [ ]^{a,b,c} seconds completed depressurization to a level that allowed IRWST injection at [ ]^{a,b,c} seconds via DVI-2 and [ ]^{a,b,c} seconds via DVI-1. During the rapid accumulator injection, increased flow path resistance reduced flow out of the CMTs. CMT flow resumed as the accumulators drained. The accumulators were fully drained [ ]^{a,b,c} seconds before IRWST injection began. Because of the relative elevation heads, CMT flow essentially ceased [ ]^{a,b,c} seconds after the start of IRWST injection, before the CMTs were fully drained.

Actuation of ADS-2 rapidly refilled the pressurizer as water and steam flowed out of the ADS. The pressurizer gradually drained by [ ]^{a,b,c} seconds.

Note that following the actuation of ADS-1 in Test SB21, a series of irregular oscillations discussed in the Final Data Report [1] were observed in pressure, level, flow, and temperature readings. These continued until around [ ]^{a,b,c} seconds when the CMT-1 balance line was refilling and were believed to have resulted from continued low level irregular flow through the SG tubes.

5.11.1.4 In-Containment Refueling Water Storage Tank Injection

IRWST injection signals the transition from the short- to long-term phase of the transient. The initial phase of IRWST injection involved an increase in flow through the two DVI lines, which was followed by a gradual flow reduction as the driving head between the IRWST and the RCS fell due to the reduced IRWST water level. Once maximum flow was established, the influx of water from the IRWST was sufficient to keep the core subcooled until [ ]^{a,b,c} seconds (Figure 5.11.1-4). Steam was subsequently (Figure 5.11.1-3) generated in the core for the remainder of the transient. The period of IRWST injection between [ ]^{a,b,c} seconds was marked by oscillations in pressure and level throughout the primary system. These oscillations were also observed in the ADS-4 liquid flow rates.

5.11.1.5 Sump Injection

When the IRWST level fell to [ ]^{a,b,c} in., the main sump injection valves opened and the sump injection flow started (Figure 5.11.1-2). Sump flow began at [ ]^{a,b,c} seconds and the driving head from the sump was sufficient for flow to the IRWST on DVI-1. On DVI-2, there was a corresponding increase in the flow out of the IRWST, which indicated that there was no significant increase in IRWST inventory until later in the transient. Note that there was no flow through the check valves around the main sump injection valve before those valves opened for this test.

TABLE 5.11.1-1
OSU TEST ANALYSIS PLOT PACKAGE FOR SUBSECTION 5.11.1

Plot No.	Component	Variables	Units	Description
1	Pressurizer	CPT-604	psia	System pressure and event history
2	Water injection	WWTDVI1+WWTDVI2, WOUTACC1+WOUTACC2, WWTIRWI1+WWTIRWI2, WWTSMPIT	lbm/sec.	Total of CMT, accumulator, IRWST, and sump injection flows
3	Reactor vessel	RPVASOU2	lbm/sec.	Steam generation in reactor vessel
4	Reactor vessel	T08RPV, HTMXRPV, TSAT	°F	Reactor vessel outlet temperature, maximum clad temperature and fuel exit saturation temperature

THE FIGURES LISTED IN TABLE 5.11.1-1
ARE NOT INCLUDED IN THIS NONPROPRIETARY DOCUMENT

5.11.2 Short-Term Transient

For the largest cold-leg break LOCA simulation, Matrix Test SB21, the short-term transient encompassed the time frame up to [ ]^{a,b,c} seconds. As shown in Figure 5.11.1-1, this period included the full depressurization of the facility through all four stages of the ADS, together with CMT and accumulator injection plus the initial stages of IRWST injection. The variations in mass, energy, pressure, and temperature throughout this stage of the transient are illustrated in the plot package outlined in Table 5.11.2-1. The plots concentrate on the primary system, including the accumulators, CMTs, IRWST, primary sump, and flows from the primary system via the ADS, break, and IRWST overflow.

There were two principal parameters to be examined for the short-term transient:

- Adequate flow must be maintained from the passive systems to the reactor vessel.
- Adequate flow into the core must be maintained to ensure that decay heat was removed from the simulated fuel rods without a temperature excursion.

These parameters are addressed in the following discussion.

5.11.2.1 Maintenance of Core Cooling

Mass Injected into the Primary System

Figures 5.11.2-6 and 5.11.2-7 show the combined effect of the injection flows for the short-term phase of the transient. Separate plots of the individual contributions to the total flow can be located by consulting the plot package index given in Table 5.11.2-1.

Figures 5.11.2-5 and 5.11.2-6 show how the CMTs, accumulators, and IRWST supply a continuous flow of water to the core. During the first [ ]^{a,b,c} seconds, cooling flow was provided by the CMTs, which was then supplemented by flow from both accumulators. The rate of flow from the CMTs gradually reduced from an initial value of [ ]^{a,b,c} lbm/sec. as the driving head fell in response to the CMT water heat-up and draindown until [ ]^{a,b,c} seconds when the depressurization following ADS-1 initiation generated rapid accumulator injection. The rapid accumulator flow temporarily stopped CMT flow, but led to an overall increase in flow to the core to a peak value of [ ]^{a,b,c} lbm/sec. Following the end of accumulator injection, the CMTs again provided cooling flow until the flow from IRWST injection ended CMT draindown. Since IRWST injection began before the CMTs had fully drained, there was no period of the short-term transient when the passive safety systems failed to provide flow to the RPV.

Reactor Pressure Vessel and Downcomer Behavior

The effect of the water flow on the average measured core inlet/outlet temperatures and peak clad temperatures during the short-term phase of the transient is shown in Figures 5.11.2-3 and 5.11.2-57. The core outlet temperature reached the saturation point at [ ]^{a,b,c} seconds and remained at the saturation level until the end of the short-term transient.

Figure 5.11.2-57 shows that there were no significant excursions in heater rod temperatures throughout the short-term transient; therefore, sufficient core inventory and flow was maintained through this phase of the transient to remove the decay heat generated. For significant portions of the transient, a two-phase mixture was present in the core and upper plenum regions, with core boiling kept at a low level.

The following discussion tracks the variation in water level and mass throughout the reactor vessel and downcomer. The mass and level for the core region are shown in Figures 5.11.2-44 and 5.11.2-45. The collapsed liquid level in the core indicates that the heater rods remained covered with a single- or two-phase mixture throughout the short-term transient. The minimum core inventory of [ ]^{a,b,c} lbm occurred at [ ]^{a,b,c} seconds into the transient before accumulator injection began. Figure 5.11.2-45 shows that the collapsed liquid level dropped to [ ]^{a,b,c} in. below the top of the heated rod length during this phase of the transient. The average void fraction of the core two-phase mixture may be estimated by dividing the measured core collapsed liquid level by the [ ]^{a,b,c} in. heated rod length. In this test, the minimum collapsed liquid level corresponded to a core void fraction of [ ].^{a,b,c} By the end of the short-term transient, the effect of IRWST injection ended all core boiling (Figure 5.11.2-55), and the core was again water-solid.

The collapsed liquid level in the upper plenum region and the associated fluid mass are shown in Figures 5.11.2-49 and 5.11.2-48. The LDP spanning the upper plenum (LDP-113) was inoperable for all of the transients and indicated that the upper plenum remained full of water. This resulted in an overestimation of the minimum vessel water inventory of up to [ ]^{a,b,c} lbm. The precise error depends on how full the upper plenum was at the time.

Figures 5.11.2-50 and 5.11.2-51 show that the upper head drained rapidly during SB21. The upper head remained essentially drained for the entire short-term transient.

The mass of fluid and collapsed liquid level in the RPV downcomer are shown in Figures 5.11.2-41 and 5.11.2-42. The downcomer collapsed liquid level fell to the bottom of the cold-leg piping during the first [ ]^{a,b,c} seconds. IRWST injection maintained the collapsed liquid level at the center of the cold legs. Cold-leg refill began at around [ ]^{a,b,c} seconds. Following ADS-1 actuation, there were irregular oscillations in the downcomer level, which probably resulted from continued flow through the SG tubes.

5.11.2.2 Energy Transport from the Primary System

Following the break, energy was deposited by the heater rods in the primary circuit fluid to simulate decay heat and by the primary circuit metal as it cooled down. Some fluid energy was lost to the ambient and out of the break. The energy must be removed from the primary system to prevent excessive fluid and heater rod temperature excursions. The AP600 plant is designed to remove heat by a combination of the SGs and the PRHR plus the ADS.

Steam Generator and Passive Residual Heat Removal Heat Transfer

During normal operation, most of the primary system heat was removed via the SGs; however, once the RCPs tripped, the reduced system flow decreased primary- to secondary-side heat transfer. The SGs were only available as heat sinks until the primary system pressure dropped to that of the secondary side; afterward, the two sides were in thermal equilibrium. The PRHR is designed to remove heat from the primary system once the S signal opens the isolation valve. The PRHR continues to remove energy after the SGs are thermally isolated until ADS actuates. Once ADS actuates, it becomes the predominant path for the removal of energy from the primary system.

Figure 5.11.2-33 shows the SG primary- and secondary-side pressure together with the PRHR integrated heat transfer, as represented by the IRWST fluid energy after allowing for the contribution from ADS 1-3 inflow. The SGs were potential sinks for primary system heat, while the primary-side pressure was above that of the secondary side, that is, before [ ]^{a,b,c} seconds. PRHR heat removal began [ ]^{a,b,c} seconds into the test, and the PRHR was responsible for all the IRWST heat-up until ADS-1 activation. Following actuation of the ADS, PRHR heat transfer continued for [ ]^{a,b,c} seconds. This was different from the behavior observed in the smaller break cases, as discussed in Subsection 7.1.2. During the active phase, the PRHR transferred heat to the IRWST at an average rate of [ ]^{a,b,c} Btu/sec.

Energy Transport via the Break and Automatic Depressurization System

The mass flow rate from the primary system via the break is shown in Figures 5.11.2-67 and 5.11.2-68. During the first [ ]^{a,b,c} seconds following the break, nearly [ ]^{a,b,c} lbm of water appeared to flow out of the primary system via the break (Figure 5.11.2-62). Figure 5.11.2-71 shows that there was no evidence of such a dramatic loss of primary system inventory from the mass balance. The apparent mass flow resulted from the indicated increase in break separator inventory, caused by a rise in pressure above the fluid in response to the opening of the break. The first [ ]^{a,b,c} seconds should therefore be ignored in reference to mass loss from the break. At [ ]^{a,b,c} seconds, the operator (as instructed) isolated the 8-in. vent line as the volumetric steam flow rate dropped below the [ ]^{a,b,c} cfm level. This caused a small increase in break separator pressure, which increased the steam and liquid flow at this time.

Following the initiation of ADS 1-3, flow through the break continued and was augmented by steam and liquid flow through the ADS 1-3 valves. Between [ ]^{a,b,c} and [ ]^{a,b,c} seconds, ADS 1-3 rapidly depressurized the system and at [ ]^{a,b,c} seconds, ADS-4 was initiated and the primary system continued to depressurize to the BAMS header pressure.

Beyond [ ]^{a,b,c} seconds, there was continued flow through the break as cold-leg refill was occurring. Flow through the ADS continued at a declining rate until [ ]^{a,b,c} seconds when flow through ADS 1-3 terminated and was replaced by flow through the lower resistance ADS-4 paths for the rest of the short-term transient.

Integrated mass flow from the primary system via the ADS and the break is shown in Figure 5.11.2-62, and the corresponding integrated energy flow is shown in Figure 5.11.2-69. The total system inventory plot given in Figure 5.11.2-70 indicates that only [ ]^{a,b,c} lbm of inventory left the system during the short-term transient. Components of the energy balance are shown in Figure 5.11.2-74.

TABLE 5.11.2-1
OSU TEST ANALYSIS STANDARD PLOT PACKAGE FOR SUBSECTION 5.11.2

Plot No.	Component	Variables	Units	Description
1	Pressurizer	CPT-604	psia	System pressure
2	RPV	RPVPWR	kW	Core power
3	RPV	T01RPV, T08RPV, ST08RPV	°F	Core inlet/outlet temperature, saturation temperature
4	SG	CPT-201, CPT-204, CPT-301, CPT-302	psia	Primary and secondary pressures in SG
5	DVI-1	WWTDVIL1, WWTIRWI1, WOUTACC1, WWTIRWI3	lbm/sec.	Individual components and total flow in DVI-1
6	DVI-2	WWTDVIL2, WWTIRWI2, WOUTACC2, WWTIRWI4	lbm/sec.	Individual components and total flow in DVI-2
7	CMT	AMCMT1B, AMCMT2B	lbm	Fluid mass in CMTs (excludes balance lines)
8	CMT	CLDP-502, CLDP-507	in.	Collapsed liquid level in CMTs
9	CMT	MIWDVIL1, MIWDVIL2	lbm	Integrated mass out of CMTs
10	CMT	WWTDVIL1, WWTDVIL2	lbm/sec.	Flow out of CMTs
11	CMT	WOUTCLB1, WOUTCLB2	lbm/sec.	Flow into CMTs
12	CMT	CLDP-509, CLDP510	in.	Level CL-CMT balance lines
13	CMT	UCMT1, UCMT2	Btu	Fluid energy in CMTs
14	IRWST	IRWST	lbm	Mass of fluid in IRWST
15	IRWST	CLDP-701	in.	Collapsed liquid level in IRWST
16	IRWST	WWTIRWI1, WWTIRWI2	lbm/sec.	Flow from IRWST to DVI lines
17	IRWST	IRWSTOR	lbm/sec.	Overflow from IRWST to sump
18	IRWST	ADS13TMR	lbm/sec.	Total ADS flow into IRWST
19	IRWST	ADS13TIR, MIIRWI1, MIIRWI2, MIIRWIO	lbm	Integrated mass out of IRWST
20	IRWST	UIRWST	Btu	Fluid energy in IRWST
21	PRHR	CLDP-802	in.	Collapsed liquid level in PRHR HX

TABLE 5.11.2-1 (Continued)
OSU TEST ANALYSIS STANDARD PLOT PACKAGE FOR SUBSECTION 5.11.2

Plot No.	Component	Variables	Units	Description
22	PRHR	WWOTPRHR	lbm/sec.	Measured outlet flow from PRHR tube
23	Accumulator	AMACC1, AMACC2	lbm	Mass of fluid in accumulators
24	Accumulator	CLDP-401, CLDP-402	in.	Collapsed liquid level in accumulators
25	Accumulator	WOUTACC1, WOUTACC2	lbm/sec.	Flow from accumulators
26	Accumulator	MOUTACC1, MOUTACC2	lbm	Integrated mass out of accumulators
27	Accumulator	UACC1, UACC2	Btu	Fluid energy in accumulators
28	Primary sump	AMPSMP	lbm	Primary sump fluid mass
29	Primary sump	CLDP-901	in.	Primary sump level
30	Primary sump	UPSMP	Btu	Primary sump fluid energy
31	SG	MSSGIP1, MSSGIP2, MSSGOP1, MSSGOP2	lbm	Mass of fluid in SG primary side inlet/outlet plena
32	SG	MSSGHT1, MSSGHT2, MSSGCT1, MSSGCT2	lbm	Mass of fluid in SG primary side hot and cold tubes
33	SG/PRHR	CPT-201, CPT-301, QPRHRI	psia & Btu	SG1 pressure and PRHR integrated heat output
34	Pressurizer	PZM	lbm	Fluid mass in pressurizer
35	Pressurizer	CLDP-601	in.	Collapsed liquid level in pressurizer
36	Pressurizer	UPZ	Btu	Fluid energy in pressurizer
37	Surge line	PLM	lbm	Fluid mass in surge line
38	Surge line	CLDP-602	in.	Collapsed liquid level in surge line
39	Surge line	UPSL	Btu	Fluid energy in surge line
40	RPV	MWRPV	lbm	Total fluid mass in reactor vessel
41	RPV	DCM	lbm	Fluid mass in downcomer
42	RPV	LDP01DC	in.	Collapsed liquid level in downcomer compared to various reference elevations
43	RPV	MW01RPV	lbm	Fluid mass in lower plenum
44	RPV	MW03RPV	lbm	Fluid mass in core region
45	RPV	LDP03RPV	in.	Collapsed liquid level in core
46	RPV	RPVAVDF2		Core exit void fraction
47	RPV	RPVAQOU2		Core exit quality
48	RPV	MW06RPV	lbm	Fluid mass in the upper plenum
49	RPV	LDP06RPV	in.	Collapsed liquid level in the upper plenum
50	RPV	MW08RPV	lbm	Fluid mass in the upper head
51	RPV	LDP08RPV	in.	Collapsed liquid level in the upper head

TABLE 5.11.2-1 (Continued)
OSU TEST ANALYSIS STANDARD PLOT PACKAGE FOR SUBSECTION 5.11.2

Plot No.	Component	Variables	Units	Description
52	RPV	URPV	Btu	Total fluid energy in reactor vessel
53	RPV	RPVXE, RPVASL2	ft	Level of Tsat line
54	RPV	RPVPab, RPVAPab2, RPVPWR	kW	Heated rod power above and below Tsat level and total
55	RPV	RPVRXV, RPVASOU2	lbm/sec.	Core steam generation rate
56	RPV	RPVALIN2	lbm/sec.	Calculated core flow
57	RPV	HTMXRPV, ST08RPV	°F	Maximum clad temperature and saturation temperature
58	Hot leg	MWHL1, MWHL2	lbm	Water mass in hot legs
59	Hot leg	MVHL1, MVHL2	lbm	Vapor mass in hot legs
60	Cold leg	CL1WMS, CL2WMS, CL3WMS, CL4WMS	lbm	Water mass in cold legs
61	Cold leg	CL1VMS, CL2VMS, CL3VMS, CL4VMS	lbm	Vapor mass in cold legs
62	ADS and break	BRKSTIR, ADS13TIR, ADS41TIR, ADS42TIR	lbm	Total discharged mass for ADS 1-3, ADS-4s, and break
63	ADS and break	BRKTIVF, AD13TIVF, AD41TIVF, AD42TIVF	lbm	Total integrated vapor flow for ADS and break
64	ADS and break	BRKTILF, AD13TILF, AD41TILF, AD42TILF	lbm	Total integrated liquid flow for ADS and break
65	ADS and break	ADS13SVR, ADS41SVR, ADS42SVR	lbm/sec.	Vapor flow out ADS 1-3 and ADS-4
66	ADS and break	ADS13SLR, ADS41SLR, ADS42SLR	lbm/sec.	Liquid flow out ADS 1-3 and ADS-4
67	ADS and break	BRKSSVR	lbm/sec.	Vapor flow out of break
68	ADS and break	BRKSSLR	lbm/sec.	Liquid flow out of break
69	ADS and break	BRKSPEI, ADS13EI, ADS41EI, ADS42EI	Btu	Integrated fluid energy for ADS 1-3, ADS-4, and break
70	Mass balance	TOTMASS	lbm	Total system mass inventory
71	Mass balance	PRIMMASS, PRIMASS2	lbm	Measured primary system inventory and value from mass balance
72	Mass balance	MERROR	lbm	Mass balance error
73	Mass balance	MIN, MOUT SRCMASS	lbm	Integrated mass flow in and out of primary system and source mass
74	Energy balance	Various	Btu	Components of energy balance

THE FIGURES LISTED IN TABLE 5.11.2-1
ARE NOT INCLUDED IN THIS NONPROPRIETARY DOCUMENT

5.11.3 Long-Term Transient

The long-term transient started with initiation of IRWST injection, covered the transition from IRWST to sump injection, and provided information on the LTC response of the AP600 plant. For the large cold-leg break, Matrix Test SB21, the long-term transient analyzed runs from [ ]^{a,b,c} seconds to the end of the test around [ ]^{a,b,c} seconds. The behavior of the test facility during this period of the transient is discussed in this subsection using the plot package detailed in Table 5.11.3-1. This analysis concentrates on the components of the primary system that remained active during the LTC phase, that is, the RPV, the hot legs, ADS-4, the sumps, and the IRWST.

During the long-term transient, the main thermal-hydraulic phenomena of interest were:

- Maintenance of core cooling and removal of energy from the primary system.
- Level oscillations (from [ ]^{a,b,c} seconds there were system wide level and pressure oscillations, which are discussed further in Subsection 6.1.3).

5.11.3.1 Maintenance of Core Cooling

Mass Injected into Primary System

Total DVI line flow, CMT flow, and IRWST flows are shown in Figures 5.11.3-6 and 5.11.3-7, and the flow from the primary sump is shown in Figure 5.11.3-19. From around [ ]^{a,b,c} seconds, there was a contribution to the DVI flow from the CMTs as the CMTs reached post-refill draindown.

During the pre-sump injection phase of the transient, IRWST flow proceeded at a gradually declining rate with the effect of the primary system oscillations superimposed. At [ ]^{a,b,c} seconds, flow from the primary sump began through the main injection valves, which opened as the IRWST reached the low-low level setpoint. This resulted in a reversal of flow through IRWST injection line-1 and an increase in IRWST flow in line-2. The net result was that an injection flow rate of [ ]^{a,b,c} lbm/sec. was maintained through both DVI lines.

Reactor Pressure Vessel and Downcomer Response

The effect of the water inflow on the downcomer fluid temperatures, core inlet and core outlet temperatures, and heater rod temperatures during the long-term phase of the transient is shown in Figures 5.11.3-4, 5.11.3-5, and 5.11.3-38. Figure 5.11.3-4 shows that there was a general increase in average downcomer fluid temperatures during the long-term transient. By the end of the test, this average temperature reached an equilibrium [ ]a,b,c °F below saturation. Figure 5.11.3-5 shows that the core outlet temperature remained at or above saturation for most of the long-term transient. Figures 5.11.3-34 to 5.11.3-36 show that the DVI line flow method described in Section 4.11 indicates

that a small level of boiling was maintained after [ ]^{a,b,c} seconds into the transient. Nevertheless, the level of boiling was small and showed that the inflow from the IRWST and sumps was sufficient to maintain cooling.

Figure 5.11.3-38 shows that there were no significant excursions in heater rod temperatures throughout the long-term transient; therefore, sufficient core inventory and flow was maintained through this phase of the transient to remove the decay heat generated. For significant portions of the transient, a two-phase mixture was present in the core and upper plenum regions.

The following discussion tracks the variation in water level and mass throughout the reactor vessel and downcomer. The mass and level for the core region are shown in Figures 5.11.3-28 and 5.11.3-29. The collapsed liquid level in the core indicated that the heater rods were always covered with a single- or two-phase mixture. During the later stages of the transient (beyond [ ]^{a,b,c} seconds), the collapsed liquid level remained just below the top of the heater rods, and the core void fraction was [ ].^{a,b,c} There was a reduction in the core collapsed liquid level following the start of sump injection as the DVI flow settled at a new value. There is, however, no impact on primary system fluid temperatures in this test since the sump water was relatively cold (Figures 5.11.3-4 and 5.11.3-5). During sump injection, the calculated steam generation rate was at a maximum of about [ ]^{a,b,c} lbm/sec. (Figure 5.11.3-3).

The collapsed liquid level in the upper plenum region is shown in Figure 5.11.3-32. For this test, the LDP for the upper plenum (LDP-113) was inoperable; thus, variations in upper plenum mass and level were not tracked. Figure 5.11.3-33 shows the mass of water in the upper head, which remained below [ ]^{a,b,c} lbm until the end of the test.

The mass of water in the reactor pressure vessel is shown in Figure 5.11.3-25. For the entire long-term transient, the reactor vessel water mass remained at an average value of [ ]^{a,b,c} lbm, which is [ ]^{a,b,c} percent of the initial vessel water inventory. From [ ]^{a,b,c} seconds, oscillations in vessel inventory were observed. Figures 5.11.3-51 to 5.11.3-56 illustrate these oscillations using plots on a restricted time frame from [ ]^{a,b,c} seconds. These oscillations are observed in primary system measurements from the upper plenum to the ADS-4 flows. The oscillations in the ADS flow lagged behind those in the upper head pressure. These oscillations and possible mechanisms for their production are discussed further in Subsection 6.1.3.

The mass of fluid and collapsed liquid level in the RPV downcomer is shown in Figures 5.11.3-26 and 5.11.3-27. The collapsed liquid level remained above the cold legs until [ ]^{a,b,c} seconds, then decreased to the center of the hot legs. This occurred at about the same time CMT-1 completed draindown and the cold legs drained (see Figure 5.10.3-41). There was no effect on downcomer level resulting from the start of sump injection.

5.11.3.2 Energy Transport from the Primary System

During the long-term transient, energy continued to be deposited in the primary system from the heated rods, metal, and fluid flowing from the primary sump. The SGs and PRHR remained inactive throughout this phase of the transient, and the primary path for energy out of the primary system was via the ADS-4 valves.

Integrated mass flow from the primary system via the ADS and the break is shown in Figure 5.11.3-43. During the LTC phase of the transient, the only significant outflow is through the ADS-4 valves and, until [ ]^{a,b,c} seconds, the break. This is confirmed in Figures 5.11.3-44 and 5.11.3-45, which show flow through the ADS and break. After [ ]^{a,b,c} seconds, there was reverse flow through the break, as indicated by the reducing integrated flow shown in Figure 5.11.3-43. During the sump injection phase of the transient, the only measured flow was liquid out of the ADS-4 valves. By the end of the test, water flowed through these valves at a combined average rate of [ ]^{a,b,c} lbm/sec.

Figure 5.11.3-36 shows the calculated steam generation rate, as determined by the DVI line flow method. During the sump injection phase of the transient, steam was generated around [ ]^{a,b,c} lbm/sec., although the steam vortex meters indicate little or no flow out of the ADS-4 valves. The following two indications show that steam is leaving the primary system by this route:

- Figure 5.11.3-46 shows total measured system fluid inventory. During this phase of the transient after the start of primary sump injection (from [ ]^{a,b,c} seconds), that is, when core steam generation was most significant, the total system inventory fell by about [ ]^{a,b,c} lbm. This amount corresponds to a steam flow rate of [ ]^{a,b,c} lbm/sec., which would not have been detected by the vortex meters.

- Examination of the fluid thermocouples on the outlet of the ADS-4 valves indicates that temperatures remained at or above saturation temperature following the start of sump injection.

It was not possible for all the steam generated in the core to flow from the upper head to the downcomer via the bypass holes (Subsection 6.1.3). It can therefore be concluded that steam was leaving the primary system via ADS-4. Figure 5.11.3-50 shows all the components to the system energy balance. Further discussion of steam loss from the primary system is provided in the mass and energy balance discussions of Section 6.2.

TABLE 5.11.3-1
OSU TEST ANALYSIS STANDARD PLOT PACKAGE FOR SUBSECTION 5.11.3
LONG-TERM TRANSIENT

Plot No.	Component	Variables	Units	Description
1	RPV	RPVPWR	kW	Core power
2	Primary sump	TSMPI1, TSMPI2	°F	Sump injection line temperatures
3	DVI	TDVIL1, TDVIL2	°F	DVI line temperatures
4	RPV	T01DC, T02DC, T03DC, ST01DC	°F	Water and saturation temperatures in downcomer
5	RPV	T01RPV, T08RPV, ST08RPV	°F	Core inlet/outlet temperature, saturation temperature
6	DVI-1	WWTDVIL1, WWTIRWI1, WWTIRWI3	lbm/sec.	Individual components and total flow in DVI-1
7	DVI-2	WWTDVIL2, WWTIRWI2, WWTIRWI4	lbm/sec.	Individual components and total flow in DVI-2
8	CMT	CLDP-502, CLDP-507	in.	Collapsed liquid level in CMTs
9	CMT	CLDP-509, CLDP510	in.	Level CL-CMT balance lines
10	IRWST	IRWST	lbm	Mass of fluid in IRWST
11	IRWST	CLDP-701	in.	Collapsed liquid level in IRWST
12	IRWST	UIRWST	Btu	Fluid energy in IRWST
13	Primary sump	AMPSMP	lbm	Primary sump fluid mass
14	Primary sump	CLDP-901	in.	Primary sump level
15	Primary sump	UPSMP	Btu	Primary sump fluid energy
16	Secondary sump	AMSSMP	lbm	Secondary sump fluid mass
17	Secondary sump	CLDP-902	in.	Secondary sump level
18	Secondary sump	USSMP	Btu	Secondary sump fluid energy
19	Primary sump	WSTSMPET, WWTSMPIT	lbm/sec.	Primary sump steam and liquid injection rate
20	Primary sump	MISMPI1, MISMPI2, MISMPIT, MIIRWT	lbm	Integrated primary sump and IRWST flows
21	SG	MSSGIP1, MSSGIP2, MSSGOP1, MSSGOP2	lbm	Mass of fluid in SG side inlet/outlet plena
22	Surge line	PLM	lbm	Fluid mass in surge line
23	Surge line	CLDP-602	in.	Collapsed liquid level in surge line
24	Surge line	UPSL	Btu	Fluid energy in surge line
25	RPV	MWRPV	lbm	Total fluid mass in reactor vessel

TABLE 5.11.3-1 (Continued)
OSU TEST ANALYSIS STANDARD PLOT PACKAGE FOR SUBSECTION 5.11.3
LONG-TERM TRANSIENT

Plot No.	Component	Variables	Units	Description
26	RPV	DCM	lbm	Fluid mass in downcomer
27	RPV	LDP01DC	in.	Collapsed liquid level in downcomer compared to various reference elevations
28	RPV	MW03RPV	lbm	Fluid mass in core region
29	RPV	LDP03RPV	in.	Collapsed liquid level in core
30	RPV	RPVAVDF2		Core exit void fraction
31	RPV	RPVAQOU2		Core exit quality
32	RPV	LDP0[illegible]PV	in.	Collapsed liquid level in the upper plenum
33	RPV	MW08[illegible]PV	lbm	Fluid mass in the upper head
34	RPV	RPVASL2	in.	Level of Tsat line
35	RPV	RPVAPab2, RPVPWR	kW	Heated rod power above and below Tsat level and total
36	RPV	RPVASOU2	lbm/sec.	Core steam generation rate
37	RPV	RPVALIN2	lbm/sec.	Calculated core flow
38	RPV	HTMXRPV, ST08RPV	°F	Maximum clad temperature, saturation temperature and delta
39	Hot leg	MWHL1, MWHL2	lbm	Water mass in hot legs
40	Hot leg	MVHL1, MVHL2	lbm	Vapor mass in hot legs
41	Cold leg	CL1WMS, CL2WMS, CL3WMS, CL4WMS	lbm	Water mass in cold legs
42	Cold leg	CL1VMS, CL2VMS, CL3VMS, CL4VMS	lbm	Vapor mass in cold legs
43	ADS and break	BRKSTIR, ADS13TIR, ADS41TIR, ADS42TIR	lbm	Total discharged mass for ADS 1-3, ADS-4, and break
44	ADS and break	ADS13TLR, ADS41TLR, ADS42TLR	lbm/sec.	Liquid flow out ADS 1-3 and ADS-4
45	ADS and break	BRKSTLR	lbm/sec.	Liquid flow and total flow out of break
46	Mass balance	TOTMASS	lbm	Total system mass inventory
47	Mass balance	PRIMMASS, PRIMASS2	lbm	Measured primary system inventory and valve from mass balances
48	Mass balance	MERROR	lbm	Mass balance error
49	Mass balance	MIN, MOUT SRCMASS	lbm	Integrated mass flow in and out of primary system and source mass
50	Energy balance	Various	Btu	Component of energy balance
51	ADS-4	ADS41TLR, ADS42TLR	lbm/sec.	Oscillations in ADS-4 liquid flow
52	Surge line	CLDP-602	in.	Oscillations in surgeline level
53	RPV	CPT-107	psia	Oscillations in upper head pressure

TABLE 5.11.3-1 (Continued)
OSU TEST ANALYSIS STANDARD PLOT PACKAGE FOR SUBSECTION 5.11.3
LONG-TERM TRANSIENT

Plot No.	Component	Variables	Units	Description
54	RPV	CLDP-113	in.	Oscillations in upper plenum level
55	RPV	LDP03RPV	in.	Oscillations in core level
56	RPV	LDP01DC	in.	Oscillations in downcomer level

THE FIGURES LISTED IN TABLE 5.11.3-1
ARE NOT INCLUDED IN THIS NONPROPRIETARY DOCUMENT

5.12 Analysis of Matrix Test SB23

Matrix Test SB23 (OSU Test U0023) simulated an 0.5-in. break LOCA with LTC and without the operation of the nonsafety-related systems. The break was located at the bottom of CL-3 and except for the break size, this test was identical to SB01, including the simulated failure of one of the ADS-4 lines. As noted in Section 1.5, the original scaling methodology used indicates that the selected OSU break area was larger than necessary for a true simulation of a 0.5-in. break. However, the results are acceptable to validate codes since the calculations account for this variation when predicting test results.

The analysis of Matrix Test SB23 is divided into three sections, as follows:

- The facility performance is discussed in Subsection 5.12.1. It provides a brief outline of the response of the test facility; further details are available in the Final Data Report.[1]

- The short-term transient for SB23 encompassed the start of the simulation up to [ ]^{a,b,c} seconds. This period includes the blowdown, natural circulation, ADS, and initial IRWST stages of the transient.

- The analysis of the long-term transient for SB23 encompassed the time frame from [ ]^{a,b,c} seconds to the end of the test. This phase of the transient includes IRWST injection and covered the transition to sump injection. The long-term transient actually started with IRWST injection, which is discussed as part of the short-term transient. Between the end of the short-term transient and [ ]^{a,b,c} seconds, the system remained relatively inactive with the exception of the CMT refill. At [ ]^{a,b,c} seconds, CMT-1 began to refill, and CMT-2 followed [ ]^{a,b,c} seconds later. CMT refill phenomena is discussed further in Subsection 6.1.1, so the discussion of the long-term transient presented begins at [ ]^{a,b,c} seconds.

The discussion of the short- and long-term phase of the transient focuses on important thermal-hydraulic phenomena identified in the PIRT (Table 1.3-1). The mass and energy balance results are key indicators of the quality of the analysis on which this discussion is based. These are discussed in detail in Subsections 6.2.2 and 6.2.3.

5.12.1 Facility Performance

The performance of the OSU test facility during Matrix Test SB23 in reference to the five transient phases is outlined in the following:

- Blowdown
- Natural circulation
- ADS
- IRWST injection
- Sump injection

The overall performance of the facility during the transient is shown in Figures 5.12.1-1 to 5.12.1-4. Figure 5.12.1-1 shows the pressurizer pressure throughout the test with the various phases and operating components delineated on the figure. The time scale was reduced for clarity since there were only small changes in system pressure during the long-term phase of the transient. Figure 5.12.1-2 shows the total DVI line flow and its composition from the various sources at each time in the transient. Figure 5.12.1-3 shows the calculated core steam generation rate throughout the test, and Figure 5.12.1-4 shows the variation in average measured core outlet temperature and peak clad temperature relative to the core outlet saturation temperature.

Figures 5.12.1-1 and 5.12.1-2 show that there was an almost continuous flow of water to the core from the passive safety-related systems throughout the transient. Once initiated, the ADS lines rapidly depressurized the primary system, which enhanced the CMT and accumulator injection flow rates. Ultimately, the ADS-4 valves sufficiently reduced the system pressure to start gravity-driven IRWST injection. The passive injection systems overlapped so that as one source of water drained, the next was available to continue the cooling process. The level of steam generation in the core and the response of the average measured core outlet fluid temperatures and maximum clad temperatures are shown in Figures 5.12.1-3 and 5.12.1-4. These figures show that the cooling flow prevented core heatup, and the core remained covered. The core remained subcooled for large periods of the transient and when steam production occurred, the rate of generation remained well below the rate at which water was delivered to the core.

5.12.1.1 Blowdown Phase

The blowdown phase began at time zero when the break was initiated and continued until the primary system pressure was in equilibrium with the secondary-side pressure at around [ ]^{a,b,c} seconds (Figure 5.12.1-1). Immediately following the opening of the break, the primary system pressure increased since the small break was incapable of removing the energy being added from the core

heater rods. This caused the pressure relief valves to open. After the valves closed, the system pressure fell gradually almost to the end of the blowdown phase. During this phase of the transient, cooling flow was provided from the two CMTs, which remained in the recirculation mode, and heat was removed from the primary system via the SGs. The pressurizer and surge line completely drained at [ ]^{a,b,c} and [ ]^{a,b,c} seconds respectively.

5.12.1.2 Natural Circulation Phase

In this LOCA simulation, the single- and two-phase natural circulation phase was marked by a gradual reduction in system pressure rather than by the more stable pressure observed in SB01. During this phase of the transient, the SG tubes drained by about [ ]^{a,b,c} seconds and at this time, heat removal from the primary system continued via the PRHR. The steam in the SG tubes became superheated and remained so until the end of the transient. In response to voiding in CL-3, CMT-1 transitioned to draindown mode at [ ]^{a,b,c} seconds, and the falling CMT level reached the ADS low-level setpoint at [ ]^{a,b,c} seconds. The natural circulation phase of the transient continued to [ ]^{a,b,c} seconds when the ADS-1 valve opened.

5.12.1.3 Automatic Depressurization System Phase

ADS-1 actuation was followed by ADS-2 and ADS-3 [ ]^{a,b,c} and [ ]^{a,b,c} seconds later. With the initiation of the ADS, accumulator injection began (Figure 5.12.1-2). The influx of cold water combined with increased venting via the ADS led to a rapid depressurization of the primary system. Actuation of ADS-4 at [ ]^{a,b,c} seconds completed depressurization to a level that allowed IRWST injection at [ ]^{a,b,c} seconds via DVI-2 and [ ]^{a,b,c} seconds via DVI-1. During accumulator injection, increased system flow path resistance reduced flow out of the CMTs. CMT flow resumed as the accumulators drained. The accumulators were fully drained [ ]^{a,b,c} seconds before IRWST injection began. The CMTs did not fully drain until [ ]^{a,b,c} and [ ]^{a,b,c} seconds after the start of IRWST injection. The transfer from CMT/accumulator to IRWST injection was indicated by the minimum RPV inventory of [ ]^{a,b,c} lbm at [ ]^{a,b,c} seconds.

Actuation of ADS-1 rapidly refilled the pressurizer as water and steam flowed out of the ADS. The pressurizer gradually drained by [ ]^{a,b,c} seconds.

5.12.1.4 In-Containment Refueling Water Storage Injection

IRWST injection signals the transition from the short- to long-term phase of the transient. The initial phase of IRWST injection involved an increase in flow through the two DVI lines, which was followed by a gradual flow reduction as the driving head between the IRWST and the RCS fell due to

the reduced IRWST water level. Once maximum flow was established, the influx of water from the IRWST was sufficient to keep the core subcooled from [ ]^{a,b,c} seconds (Figure 5.12.1-4). Steam was subsequently generated in the core for the remainder of the transient (Figure 5.12.1-3). Following the restart of core steam generation, IRWST injection between [ ]^{a,b,c} seconds, was marked by oscillations in pressure and level throughout the primary system. These oscillations were also observed in the ADS-4 liquid flow rates.

5.12.1.5 Sump Injection

Injection from the primary sump via the check valves around the main sump injection valves began at [ ]^{a,b,c} seconds when the level in the IRWST was low enough to allow flow. This reduced the flow rate from the IRWST. When the IRWST level fell to [ ]^{a,b,c} in., the main sump injection valves opened and the sump injection flow rate increased (Figure 5.12.1-2). This increase occurred at [ ]^{a,b,c} seconds and the driving head from the sump was sufficient for flow to the IRWST on DVI-1. On DVI-2, there was a corresponding increase in the flow out of the IRWST, which meant that there was only a small initial increase in IRWST inventory.

TABLE 5.12.1-1
OSU TEST ANALYSIS PLOT PACKAGE FOR SUBSECTION 5.12.1

Plot No.	Component	Variables	Units	Description
1	Pressurizer	CPT-604	psia	System pressure and event history
2	Water injection	WWTDVI1+WWTDVI2, WOUTACC1+WOUTACC2, WWTIRWI1+WWTIRWI2, WWTSMPIT	lbm/sec.	Total of CMT, accumulator, IRWST, and sump injection flows
3	Reactor vessel	RPVASOU2	lbm/sec.	Steam generation in reactor vessel
4	Reactor vessel	T08RPV, HTMXRPV, TSAT	°F	Reactor vessel outlet temperature, maximum clad temperature and fuel exit saturation temperature

THE FIGURES LISTED IN TABLE 5.12.1-1
ARE NOT INCLUDED IN THIS NONPROPRIETARY DOCUMENT

5.12.2 Short-Term Transient

For the 0.5-in. cold-leg break, Matrix Test SB23, the short-term transient encompassed the time frame up to [ ]^{a,b,c} seconds. As shown in Figure 5.12.1-1, this period included the full depressurization of the facility through all four stages of the ADS, together with CMT and accumulator injection plus the initial stages of IRWST injection. The variations in mass, energy, pressure, and temperature throughout this stage of the transient are illustrated in the plot package outlined in Table 5.12.2-1. The plots concentrate on the primary system, including the accumulators, CMTs, IRWST, primary sump, and flows from the primary system via the ADS, break, and IRWST overflow.

For the short-term transient there were two principal parameters to examine:

- Adequate flow must be maintained from the passive systems to the reactor vessel.
- Adequate flow into the core must be maintained to ensure that decay heat was removed from the simulated fuel rods without a temperature excursion.

These parameters are addressed in the following discussion.

5.12.2.1 Maintenance of Core Cooling

Mass Injected to the Primary System

Figures 5.12.2-6 and 5.12.2-7 show the combined effect of the injection flows for the short-term phase of the transient. Separate plots of the individual contributions to the total flow can be located by consulting the plot package index given in Table 5.12.2-1. Note that the flow measurements for the outflow from ACC-1 were incorrect for this test. Due to the similarity in the level behavior for the two accumulators, (Figure 5.12.2-24) ACC-2 outflows have been used for ACC-1 in the mass balance calculations and in the flow figures. The level calculations confirm the flow rates.

Figures 5.12.2-5 and 5.12.2-6 show how the CMTs, accumulators, and IRWST combined to supply an almost continuous flow of water to the core. During the first [ ]^{a,b,c} seconds, cooling flow was provided by the CMTs. The rate of flow from the CMTs gradually reduced from an initial value of [ ]^{a,b,c} lbm/sec. as the driving head fell in response to the CMT water heat-up and draindown until ADS-1 initiation, which resulted in an increase in CMT flow. Rapid accumulator injection temporarily reduced CMT flow, but led to an overall increase in flow to the core to a peak value of [ ]^{a,b,c} lbm/sec. Following the end of accumulator injection, the CMTs again provided cooling flow until they drained. The only period in which there was relatively little cooling flow was for [ ]^{a,b,c} seconds between CMT draining and the start of IRWST injection.

Reactor Pressure Vessel and Downcomer Behavior

The effect of water flow on the average measured core inlet/outlet temperatures and peak clad temperatures during the short-term phase of the transient is shown in Figures 5.12.2-3 and 5.12.2-57. The combined CMT and accumulator flow was sufficient to keep the core completely subcooled up to [ ]^{a,b,c} seconds. The core outlet temperature then remained at the saturation level for about [ ]^{a,b,c} seconds until the influx of water from the IRWST was sufficient to subcool the core again. The core remained subcooled until the end of the short-term transient.

Figure 5.12.2-57 shows that there were no significant excursions in heater rod temperatures throughout the short-term transient; therefore, sufficient core inventory and flow was maintained through this phase of the transient to remove the decay heat generated. For significant portions of the transient, a two-phase mixture was present in the core and upper plenum regions, with core boiling kept at a low level.

The following discussion tracks the variation in water level and mass throughout the reactor vessel and downcomer. The mass and level for the core region are shown in Figures 5.12.2-44 and 5.12.2-45. The collapsed liquid level in the core indicated that the heater rods remained covered with a single- or two-phase mixture throughout the short-term transient. The minimum core inventory of [ ]^{a,b,c} lbm occurred at [ ]^{a,b,c} seconds into the transient before IRWST injection was fully established. Figure 5.12.2-45 shows that the collapsed liquid level dropped to [ ]^{a,b,c} in. below the top of the heated rod length during this phase of the transient. The average void fraction of the core two-phase mixture may be estimated by dividing the measured core collapsed liquid level by the [ ]^{a,b,c} in. heated rod length. In this test, the minimum collapsed liquid level corresponded to a core void fraction of [ ].^{a,b,c} By the end of the short-term transient, the effect of IRWST injection ended all core boiling (Figure 5.12.2-55), and the core was again water-solid.

The collapsed liquid level in the upper plenum region covered by LDP-113 and the associated fluid mass are shown in Figures 5.12.2-49 and 5.12.2-48. During the period before accumulator injection, the upper plenum was water-solid. The start of accumulator injection coincided with a fall in collapsed liquid level to the elevation of the cold legs. Following the end of accumulator injection, the region of the upper plenum spanned by the LDP cell fully drained and remained drained until IRWST injection supplied sufficient inventory to initiate a refill. The upper plenum was again water-solid by the end of the short-term transient.

Figures 5.12.2-50 and 5.12.2-51 show that the upper head also lost inventory at the time when accumulator injection began. This behavior is the opposite of what might be expected as a result of the influx of cooler accumulator water. Accumulator injection coincided with ADS-1 initiation. The flow of water and steam through the ADS rapidly refilled the pressurizer, which removed water from the RPV. The reduction in upper plenum and upper head inventory reduced the overall RPV inventory during accumulator injection (Figure 5.12.2-40) even though the core inventory increased (Figure 5.12.2-44).

The mass of fluid and collapsed liquid level in the RPV downcomer are shown in Figures 5.12.2-41 and 5.12.2-42. The downcomer remained water-solid until ADS-1 actuation when the level fell to the bottom of the cold-leg piping, where it remained until IRWST injection once again raised the level above the cold legs, and cold leg refill began.

5.12.2.2 Energy Transport from the Primary System

Following the break, energy was deposited by the heater rods in the primary system fluid to simulate decay heat and by the primary system metal as it cooled down. Some fluid energy was lost to ambient and out of the break. Excess energy must be removed from the primary system to prevent excessive fluid and heater rod temperature excursions. The AP600 plant is designed to remove heat by a combination of the SGs and the PRHR plus the ADS.

Steam Generator and Passive Residual Heat Removal Heat Transfer

During normal operation, most of the primary system heat was removed via the SGs; however, once the RCPs tripped, the reduced system flow decreased primary- to secondary-side heat transfer. The SGs were only available as heat sinks until the time when the primary system pressure dropped to that of the secondary side; afterward, the two sides were in thermal equilibrium. The PRHR is designed to remove heat from the primary system once the S signal opens the isolation valve. The PRHR continues to remove energy after the SGs are thermally isolated until ADS actuates. Once ADS actuates, it becomes the predominant path for the removal of energy from the primary system.

Figure 5.12.2-33 shows the SG primary- and secondary-side pressure together with the PRHR integrated heat transfer, as represented by the IRWST fluid energy after allowing for the contribution from ADS 1-3 inflow. The SGs were potential sinks for primary system heat, while the primary-side pressure was above that of the secondary side, that is, before [ ]^{a,b,c} seconds. PRHR heat removal began [ ]^{a,b,c} seconds into the test. The PRHR was responsible for all the IRWST heat-up until ADS-1 activation, after which the PRHR heat transfer reduced significantly. During the active phase, the PRHR transferred heat to the IRWST at an average rate of [ ]^{a,b,c} Btu/sec.

Energy Transport via the Break and Automatic Depressurization System

The mass flow rate from the primary system via the break is shown in Figures 5.12.2-67 and 5.12.2-68. As shown in these figures, liquid flow was detected by the flow measuring devices for the short-term transient. During the first [ ]^{a,b,c} seconds following the break, [ ]^{a,b,c} lbm of water flowed out of the primary system via the break at an average rate of approximately [ ]^{a,b,c} lbm/sec. During this period, the primary system depressurized to around [ ]^{a,b,c} psi (Figure 5.12.2-1). With the initiation of ADS 1-3, flow through the break stopped and was replaced by steam and liquid flow through the ADS 1-3 valves. Between [ ]^{a,b,c} and [ ]^{a,b,c} seconds, ADS 1-3 caused the system to depressurize rapidly and at [ ]^{a,b,c} seconds, ADS-4 was initiated and the primary system continued to depressurize to the BAMS heater pressure.

Initiation of the ADS terminated the flow through the break. During ADS 1-3 depressurization, break flow was replaced by steam and liquid flow through the ADS 1-3 valves at a peak rate of over [ ]^{a,b,c} lbm/sec. Flow through the ADS continued at a declining rate until [ ]^{a,b,c} seconds when the flow through the ADS 1-3 terminated and was replaced by flow through the lower resistance ADS-4 paths. By the end of the short-term transient, water was flowing out of the two ADS-4 valves at approximately [ ]^{a,b,c} lbm/sec. (Figure 5.12.2-64).

The integrated mass flow from the primary system via the ADS and the break is shown in Figure 5.12.2-62, and the corresponding integrated energy flow is shown in Figure 5.12.2-69. The inventory plot given in Figure 5.12.2-70 indicates that there was little or no steam flow out of the primary system during the short-term transient. Components of the energy balance are shown in Figure 5.12.2-74.

TABLE 5.12.2-1
OSU TEST ANALYSIS STANDARD PLOT PACKAGE FOR SUBSECTION 5.12.2

Plot No.	Component	Variables	Units	Description
1	Pressurizer	CPT-604	psia	System pressure
2	RPV	RPVPWR	kW	Core power
3	RPV	T01RPV, T08RPV, ST08RPV	°F	Core inlet/outlet temperature, saturation temperature
4	SG	CPT-201, CPT-204, CPT-301, CPT-302	psia	Primary and secondary pressures in SG
5	DVI-1	WWTDVIL1, WWTIRWI1, WOUTACC1, WWTIRWI3	lbm/sec.	Individual components and total flow in DVI-1
6	DVI-2	WWTDVIL2, WWTIRWI2, WOUTACC2, WWTIRWI4	lbm/sec.	Individual components and total flow in DVI-2
7	CMT	AMCMT1B, AMCMT2B	lbm	Fluid mass in CMTs (excludes balance lines)
8	CMT	CLDP-502, CLDP-507	in.	Collapsed liquid level in CMTs
9	CMT	MIWDVIL1, MIWDVIL2	lbm	Integrated mass out of CMTs
10	CMT	WWTDVIL1, WWTDVIL2	lbm/sec.	Flow out of CMTs
11	CMT	WOUTCLB1, WOUTCLB2	lbm/sec.	Flow into CMTs
12	CMT	CLDP-509, CLDP510	in.	Level CL-CMT balance lines
13	CMT	UCMT1, UCMT2	Btu	Fluid energy in CMTs
14	IRWST	IRWST	lbm	Mass of fluid in IRWST
15	IRWST	CLDP-701	in.	Collapsed liquid level in IRWST
16	IRWST	WWTIRWI1, WWTIRWI2	lbm/sec.	Flow from IRWST to DVI lines
17	IRWST	IRWSTOR	lbm/sec.	Overflow from IRWST to sump
18	IRWST	ADS13TMR	lbm/sec.	Total ADS flow into IRWST
19	IRWST	ADS13TIR, MIIRWI1, MIIRWI2, MIIRWIO	lbm	Integrated mass out of IRWST
20	IRWST	UIRWST	Btu	Fluid energy in IRWST
21	PRHR	CLDP-802	in.	Collapsed liquid level in PRHR HX

TABLE 5.12.2-1 (Continued) OSU TEST ANALYSIS STANDARD PLOT PACKAGE FOR SUBSECTION 5.12.2				
Plot No.	**Component**	**Variables**	**Units**	**Description**
22	PRHR	WWOTPRHR	lbm/sec.	Measured outlet flow from PRHR tube
23	Accumulator	AMACC1, AMACC2	lbm	Mass of fluid in accumulators
24	Accumulator	CLDP-401, CLDP-402	in.	Collapsed liquid level in accumulators
25	Accumulator	WOUTACC1, WOUTACC2	lbm/sec.	Flow from accumulators
26	Accumulator	MOUTACC1, MOUTACC2	lbm	Integrated mass out of accumulators
27	Accumulator	UACC1, UACC2	Btu	Fluid energy in accumulators
28	Primary sump	AMPSMP	lbm	Primary sump fluid mass
29	Primary sump	CLDP-901	in.	Primary sump level
30	Primary sump	UPSMP	Btu	Primary sump fluid energy
31	SG	MSSGIP1, MSSGIP2, MSSGOP1, MSSGOP2	lbm	Mass of fluid in SG primary side inlet/outlet plena
32	SG	MSSGHT1, MSSGHT2, MSSGCT1, MSSGCT2	lbm	Mass of fluid in SG primary side hot and cold tubes
33	SG/PRHR	CPT-201, CPT-301, QPRHRI	psia & Btu	SG1 pressure and PRHR integrated heat output
34	Pressurizer	PZM	lbm	Fluid mass in pressurizer
35	Pressurizer	CLDP-601	in.	Collapsed liquid level in pressurizer
36	Pressurizer	UPZ	Btu	Fluid energy in pressurizer
37	Surge line	PLM	lbm	Fluid mass in surge line
38	Surge line	CLDP-602	in.	Collapsed liquid level in surge line
39	Surge line	UPSL	Btu	Fluid energy in surge line
40	RPV	MWRPV	lbm	Total fluid mass in reactor vessel
41	RPV	DCM	lbm	Fluid mass in downcomer
42	RPV	LDP01DC	in.	Collapsed liquid level in downcomer compared to various reference elevations
43	RPV	MW01RPV	lbm	Fluid mass in lower plenum
44	RPV	MW03RPV	lbm	Fluid mass in core region
45	RPV	LDP03RPV	in.	Collapsed liquid level in core
46	RPV	RPVAVDF2		Core exit void fraction
47	RPV	RPVAQOU2		Core exit quality
48	RPV	MW06RPV	lbm	Fluid mass in the upper plenum
49	RPV	LDP06RPV	in.	Collapsed liquid level in the upper plenum
50	RPV	MW08RPV	lbm	Fluid mass in the upper head
51	RPV	LDP08RPV	in.	Collapsed liquid level in the upper head

TABLE 5.12.2-1 (Continued)
OSU TEST ANALYSIS STANDARD PLOT PACKAGE FOR SUBSECTION 5.12.2

Plot No.	Component	Variables	Units	Description
52	RPV	URPV	Btu	Total fluid energy in reactor vessel
53	RPV	RPVXE, RPVASL2	in.	Level of Tsat line
54	RPV	RPVPab, RPVAPab2, RPVPWR	kW	Heated rod power above and below Tsat level and total
55	RPV	RPVRXV, RPVASOU2	lbm/sec.	Core steam generation rate
56	RPV	RPVALIN2	lbm/sec.	Calculated core flow
57	RPV	HTMXRPV, ST08RPV	°F	Maximum clad temperature and saturation temperature
58	Hot leg	MWHL1, MWHL2	lbm	Water mass in hot legs
59	Hot leg	MVHL1, MVHL2	lbm	Vapor mass in hot legs
60	Cold leg	CL1WMS, CL2WMS, CL3WMS, CL4WMS	lbm	Water mass in cold legs
61	Cold leg	CL1VMS, CL2VMS, CL3VMS, CL4VMS	lbm	Vapor mass in cold legs
62	ADS and break	BRKSTIR, ADS13TIR, ADS41TIR, ADS42TIR	lbm	Total discharged mass for ADS 1-3, ADS-4s, and break
63	ADS and break	BRKTIVF, AD13TIVF, AD41TIVF, AD42TIVF	lbm	Total integrated vapor flow for ADS and break
64	ADS and break	BRKTILF, AD13TILF, AD41TILF, AD42TILF	lbm	Total integrated liquid flow for ADS and break
65	ADS and break	ADS13SVR, ADS41SVR, ADS42SVR	lbm/sec.	Vapor flow out ADS 1-3 and ADS-4
66	ADS and break	ADS13SLR, ADS41SLR, ADS42SLR	lbm/sec.	Liquid flow out ADS 1-3 and ADS-4
67	ADS and break	BRKSSVR	lbm/sec.	Vapor flow out of break
68	ADS and break	BRKSSLR	lbm/sec.	Liquid flow out of break
69	ADS and break	BRKSPEI, ADS13EI, ADS41EI, ADS42EI	Btu	Integrated fluid energy for ADS 1-3, ADS-4, and break
70	Mass balance	TOTMASS	lbm	Total system mass inventory
71	Mass balance	PRIMMASS, PRIMASS2	lbm	Measured primary system inventory and value from mass balance
72	Mass balance	MERROR	lbm	Mass balance error
73	Mass balance	MIN, MOUT SRCMASS	lbm	Integrated mass flow in and out of primary system and source mass
74	Energy balance	Various	Btu	Components of energy balance

THE FIGURES LISTED IN TABLE 5.12.2-1
ARE NOT INCLUDED IN THIS NONPROPRIETARY DOCUMENT

5.12.3 Long-Term Transient

The long-term transient started with initiation of IRWST injection, covered the transition from IRWST to sump injection, and provided information on the LTC response of the AP600 plant. For the 0.5-in. cold-leg break, Matrix Test SB23, the long-term transient analyzed ran from [ ]^{a,b,c} seconds to the end of the test around [ ]^{a,b,c} seconds. The behavior of the test facility during this period of the transient is discussed in this subsection using the plot package detailed in Table 5.12.3-1. This analysis concentrates on the components of the primary system that remained active during the LTC phase, that is, the RPV, the hot legs, ADS-4, the sumps, and the IRWST.

For the long-term transient, thermal-hydraulic phenomena of interest were:

- Maintenance of core cooling and removal of energy from the primary system.
- Level oscillations (from [ ]^{a,b,c} seconds; there were system wide level and pressure oscillations, which are discussed further in Subsection 6.1.3).

5.12.3.1 Maintenance of Core Cooling

Mass Injected into Primary System

Total DVI line flow, CMT flow, and IRWST flows are shown in Figures 5.12.3-6 and 5.12.3-7, and the flow from the primary sump is shown in Figure 5.12.3-19. From around [ ]^{a,b,c} seconds, there was a contribution to the DVI flow from the CMTs as the CMTs reached post-refill draindown.

During the pre-sump injection phase of the transient, IRWST flow proceeded at a gradually declining rate with the effect of the primary system oscillations superimposed. At [ ]^{a,b,c} seconds, flow from the primary sump began through the check valves around the main injection valves, further reducing IRWST flow. From [ ]^{a,b,c} seconds to the end of the transient, a nearly steady flow rate of [ ]^{a,b,c} lbm/sec. was maintained through each DVI line. At [ ]^{a,b,c} seconds, the main sump injection valves opened, reversing flow through IRWST injection line-1 and increasing IRWST flow in line-2. The net result was that an injection flow rate of [ ]^{a,b,c} lbm/sec. was maintained through both DVI lines.

Reactor Pressure Vessel and Downcomer Response

The effect of the water inflow on the average measured downcomer fluid temperatures, core inlet and core outlet temperatures, and heater rod temperatures during the long-term phase of the transient is shown in Figures 5.12.3-4, 5.12.3-5, and 5.12.3-38. Figure 5.12.3-4 shows that there is a general increase in average downcomer fluid temperatures during the long-term transient. By the end of the test, this average temperature reached an equilibrium of [ ]^{a,b,c} °F below saturation. Figure 5.12.3-5

implies that the core remained at or near saturation for all of the long-term transient after [ ]^{a,b,c} seconds. However, Figures 5.12.3-34 to 5.12.3-36 show that the DVI line flow method described in Section 4.11 indicates that a small level of boiling was maintained after [ ]^{a,b,c} seconds into the transient. Nevertheless, the level of boiling was small and showed that the inflow from the IRWST and sumps was sufficient to maintain cooling.

Figure 5.12.3-38 shows that there were no significant excursions in heater rod temperatures throughout the long-term transient; therefore, sufficient core inventory and flow was maintained through this phase of the transient to remove the decay heat generated. For significant portions of the transient, a two-phase mixture was present in the core and upper plenum regions.

The following discussion tracks the variation in water level and mass throughout the reactor vessel and downcomer. The mass and level for the core region are shown in Figures 5.12.3-28 and 5.12.3-29. The collapsed liquid level in the core indicated that the heater rods were always covered with a single- or two-phase mixture. During the later stages of the transient, the collapsed liquid level remained just below the top of the heater rods, and the core void fraction was [ ].^{a,b,c} The fall in core inventory was a result of the influx of hot water from the primary sump as it flowed through the check valves. The impact of this hot water on the system temperatures is shown in Figures 5.12.3-4 and 5.12.3-5 as a sudden increase in fluid temperature in the downcomer and at the core inlet. The hot water also led to an increase in the calculated steam generation rate, as shown in Figure 5.12.3-36, and a corresponding fall in the level at which the core reached saturation temperature (Figure 5.12.3-34).

The collapsed liquid level in the upper plenum region covered by LDP-113 is shown in Figure 5.12.3-32. The figures indicate that during the period before sump injection began, the collapsed liquid level initially fell and then remained at the top of the hot legs. Following the influx of hot water from the sumps, the level dropped first to the hot-leg mid-elevation and then to the top of the DVI injection lines, where it remained for the remainder of the transient. This level corresponded to a void fraction of [ ].^{a,b,c}

The mass of water in the reactor pressure vessel is shown in Figure 5.12.3-25. After an initial decline, the reactor vessel water mass settled at an average value of [ ]^{a,b,c} lbm until the time sump injection started when it gradually fell to [ ]^{a,b,c} lbm, which is [ ]^{a,b,c} percent of the initial vessel water inventory. From [ ]^{a,b,c} seconds, oscillations in vessel inventory were observed although, these oscillations are not as marked for SB23 as those observed in SB01. Figures 5.12.3-51 to 5.12.3-56 illustrate these oscillations using plots on a restricted time frame from [ ]^{a,b,c} seconds. These oscillations are observed in primary system measurements from the upper plenum to the ADS-4 flows. The oscillations occurred for [ ]^{a,b,c} seconds. The oscillations in the ADS flow lagged behind those in the upper head pressure by around [ ]^{a,b,c} seconds. These oscillations and possible mechanisms for their production are discussed further in Subsection 6.1.3.

The mass of fluid and collapsed liquid level in the RPV downcomer are shown in Figures 5.12.3-26 and 5.12.3-27. The collapsed liquid level remained above the cold legs for the entire long-term

transient. The start of sump injection reduced the level, but this was not sufficient to uncover the cold legs.

5.12.3.2 Energy Transport from the Primary System

During the long-term transient, energy continued to be deposited in the primary system from the heated rods, metal, and fluid flowing from the primary sump. The SGs and PRHR remained inactive throughout this phase of the transient and the primary path for energy out of the primary system was via the ADS-4 valves.

Integrated mass flow from the primary system via the ADS and the break is shown in Figure 5.12.3-43. During the LTC phase of the transient, the only significant outflow is through the ADS-4 valves. This is confirmed by Figures 5.12.3-44 to 5.12.3-45, which show flow through the ADS and break. During the sump injection phase of the transient, measured outflow is in the form of liquid out of the ADS-4 valves. Water flowed through each of the valves at an average rate of [ ]^{a,b,c} lbm/sec.

Figure 5.12.3-36 shows the calculated steam generation rate, as determined by the DVI line flow method. During the sump injection phase of the transient, steam was generated at over [ ]^{a,b,c} lbm/sec., although the steam vortex meters indicate little or no flow out of the ADS-4 valves. The following two indications show that steam is leaving the primary system by this route:

- Figure 5.12.3-46 shows total measured system fluid inventory. During this phase of the transient after the start of primary sump injection, that is, when core steam generation was most significant, the total system inventory fell by about [ ]^{a,b,c} lbm. This amount corresponds to a steam flow rate of [ ]^{a,b,c} lbm/sec., which would not have been detected by the vortex meters.

- Examination of the fluid thermocouples on the outlet of the ADS-4 valves indicates that temperatures remained at or above saturation temperature following the start of sump injection.

It was not possible for all the steam generated in the core to flow from the upper head to the downcomer via the bypass holes (Subsection 6.1.3). Therefore, steam was leaving the primary system via ADS-4. Figure 5.12.3-50 shows all the components to the system energy balance. Further discussion of steam loss from the primary system is provided in the mass and energy balance discussions of Section 6.2.

TABLE 5.12.3-1
OSU TEST ANALYSIS STANDARD PLOT PACKAGE FOR SUBSECTION 5.12.3
LONG-TERM TRANSIENT

Plot No.	Component	Variables	Units	Description
1	RPV	RPVPWR	kW	Core power
2	Primary sump	TSMPI1, TSMPI2	°F	Sump injection line temperatures
3	DVI	TDVIL1, TDVIL2	°F	DVI line temperatures
4	RPV	T01DC, T02DC, T03DC, ST01DC	°F	Water and saturation temperatures in downcomer
5	RPV	T01RPV, T08RPV, ST08RPV	°F	Core inlet/outlet temperature, saturation temperature
6	DVI-1	WWTDVIL1, WWTIRWI1, WWTIRWI3	lbm/sec.	Individual components and total flow in DVI-1
7	DVI-2	WWTDVIL2, WWTIRWI2, WWTIRWI4	lbm/sec.	Individual components and total flow in DVI-2
8	CMT	CLDP-502, CLDP-507	in.	Collapsed liquid level in CMTs
9	CMT	CLDP-509, CLDP510	in.	Level CL-CMT balance lines
10	IRWST	IRWST	lbm	Mass of fluid in IRWST
11	IRWST	CLDP-701	in.	Collapsed liquid level in IRWST
12	IRWST	UIRWST	Btu	Fluid energy in IRWST
13	Primary sump	AMPSMP	lbm	Primary sump fluid mass
14	Primary sump	CLDP-901	in.	Primary sump level
15	Primary sump	UPSMP	Btu	Primary sump fluid energy
16	Secondary sump	AMSSMP	lbm	Secondary sump fluid mass
17	Secondary sump	CLDP-902	in.	Secondary sump level
18	Secondary sump	USSMP	Btu	Secondary sump fluid energy
19	Primary sump	WSTSMPET, WWTSMPIT	lbm/sec.	Primary sump steam and liquid injection rate
20	Primary sump	MISMPI1, MISMPI2, MISMPIT, MIIRWT	lbm	Integrated primary sump and IRWST flows
21	SG	MSSGIP1, MSSGIP2, MSSGOP1, MSSGOP2	lbm	Mass of fluid in SG side inlet/outlet plena
22	Surge line	PLM	lbm	Fluid mass in surge line
23	Surge line	CLDP-602	in.	Collapsed liquid level in surge line
24	Surge line	UPSL	Btu	Fluid energy in surge line
25	RPV	MWRPV	lbm	Total fluid mass in reactor vessel

TABLE 5.12.3-1 (Continued)
OSU TEST ANALYSIS STANDARD PLOT PACKAGE FOR SUBSECTION 5.12.3
LONG-TERM TRANSIENT

Plot No.	Component	Variables	Units	Description
26	RPV	DCM	lbm	Fluid mass in downcomer
27	RPV	LDP01DC	in.	Collapsed liquid level in downcomer compared to various reference elevations
28	RPV	MW03RPV	lbm	Fluid mass in core region
29	RPV	LDP03RPV	in.	Collapsed liquid level in core
30	RPV	RPVAVDF2		Core exit void fraction
31	RPV	RPVAQOU2		Core exit quality
32	RPV	LDP06RPV	in.	Collapsed liquid level in the upper plenum
33	RPV	MW08RPV	lbm	Fluid mass in the upper head
34	RPV	RPVASL2	ft.	Level of Tsat line
35	RPV	RPVAPab2, RPVPWR	kW	Heated rod power above and below Tsat level and total
36	RPV	RPVASOU2	lbm/sec.	Core steam generation rate
37	RPV	RPVALIN2	lbm/sec.	Calculated core flow
38	RPV	HTMXRPV, ST08RPV	°F	Maximum clad temperature, saturation temperature and delta
39	Hot leg	MWHL1, MWHL2	lbm	Water mass in hot legs
40	Hot leg	MVHL1, MVHL2	lbm	Vapor mass in hot legs
41	Cold leg	CL1WMS, CL2WMS, CL3WMS, CL4WMS	lbm	Water mass in cold legs
42	Cold leg	CL1VMS, CL2VMS, CL3VMS, CL4VMS	lbm	Vapor mass in cold legs
43	ADS and break	BRKSTIR, ADS13TIR, ADS41TIR, ADS42TIR	lbm	Total discharged mass for ADS 1-3, ADS-4, and break
44	ADS and break	ADS13TLR, ADS41TLR, ADS42TLR	lbm/sec.	Liquid flow out ADS 1-3 and ADS-4
45	ADS and break	BRKSTLR	lbm/sec.	Liquid flow and total flow out of break
46	Mass balance	TOTMASS	lbm	Total system mass inventory
47	Mass balance	PRIMMASS, PRIMASS2	lbm	Measured primary system inventory and valve from mass balances
48	Mass balance	MERROR	lbm	Mass balance error
49	Mass balance	MIN, MOUT SRCMASS	lbm	Integrated mass flow in and out of primary system and source mass
50	Energy balance	Various	Btu	Component of energy balance
51	ADS-4	ADS41TLR, ADS42TLR	lbm/sec.	Oscillations in ADS-4 liquid flow
52	Surge line	CLDP-602	in.	Oscillations in surgeline level
53	RPV	CPT-107	psia	Oscillations in upper head pressure

TABLE 5.12.3-1 (Continued)
OSU TEST ANALYSIS STANDARD PLOT PACKAGE FOR SUBSECTION 5.12.3
LONG-TERM TRANSIENT

Plot No.	Component	Variables	Units	Description
54	RPV	CLDP-113	in.	Oscillations in upper plenum level
55	RPV	LDP03RPV	in.	Oscillations in core level
56	RPV	LDP01DC	in.	Oscillations in downcomer level

THE FIGURES LISTED IN TABLE 5.12.3-1
ARE NOT INCLUDED IN THIS NONPROPRIETARY DOCUMENT

6.0 TEST FACILITY PERFORMANCE

This section discusses the following test analysis issues common to the matrix testing performed at Oregon State University (OSU):

- Observed thermal-hydraulic behavior, including the phenomena associated with core makeup tank (CMT) refill and oscillation in the reactor
- Passive residual heat removal (PRHR) performance
- Results of the mass and energy balance
- Effects of nitrogen dispersal from accumulator injection

6.1 Observed Thermal-Hydraulic Phenomena

The following thermal-hydraulic phenomena, observed during the matrix test program and identified in the OSU Final Data Report[1] are evaluated:

- CMT refill, which appeared to be the result of condensation in the CMT after initial injection and draindown
- PRHR performance
- Causes of pressure and liquid level oscillations in the reactor
- Effects of accumulator nitrogen

6.1.1 Core Makeup Tank Refill Response

Upon initiation of CMT draindown, incoming steam from the reactor coolant system (RCS) via the cold-leg balance line heated the CMT inside wall surface. Figure 6.1.1-1 represents the average fluid and through-thickness metal temperatures and inside surface heat flux for one metal segment in the upper head of CMT-1 based on Matrix Test SB18; Figure 6.1.1-2 represents the same parameters for CMT-2. Given the sign convention used in the OSU data analysis code, the negative heat flux represents heat flow into the metal CMT walls from fluid in the enclosed volume.

Following initial draindown, the CMTs and respective cold-leg balance lines contained steam and, possibly, some quantity of noncondensable gas. The back pressure from the IRWST flow caused the CMT check valve to close and remain closed such that the CMT tank was isolated from the DVI line. As the uninsulated CMTs continued to transfer heat to the environment, steam condensed in the CMTs, resulting in a decrease in CMT pressure relative to primary system pressure. At this time, both the cold leg and the cold-leg balance line connection at the top of the CMT were liquid solid. As the condensation continued, the decrease in CMT pressure resulted in an increase in the cold-leg balance line level (Figure 6.1.1-3). When the cold-leg balance line completely refilled, water entered the CMT through the inlet diffuser, resulting in rapid condensation of steam in the CMT and a corresponding rapid additional decrease in CMT pressure (Figure 6.1.1-4). The sudden decrease in pressure resulted in a quick refill of the CMT through the balance line (Figure 6.1.1-5).

Refill of subcooled fluid resulting in a CMT condensation/depressurization event is reflected in the reactor vessel mass (Figure 6.1.1-6). The event is also reflected in the cold-leg water levels (Figure 6.1.1-7).

The CMT refill event continued until the cold legs uncovered in the reactor vessel downcomer. Figure 6.1.1-8 shows that the end of the refill event correlates to the downcomer level and, additionally, that this level corresponds to the top of the cold-leg nozzles located at about the 71-in. elevation. The system water inventory, available prior to uncovering the cold legs, was sufficient to refill the CMT to about two-thirds full: therefore, the CMT refill event was terminated prior to the entire CMT refilling.

CMT refill, drawing fluid from the cold leg, also caused a rapid decrease in the measured CMT internal fluid temperatures which caused local fluid temperatures to fall below local CMT metal temperatures. This resulted in the heat transfer process reversing itself as seen by the sign change of the heat flux from negative to positive; heat flowed from the now heated CMT walls into the adjacent subcooled liquid. The CMT metal temperatures are seen to rapidly decrease as energy stored in the metal previously heated by steam was now transferred into the adjacent liquid in the CMT.

The phenomena that drive the CMT refill response are identical for both CMTs and whichever CMT refills first appears to be random. However, once the refill event was initiated in a particular CMT, the accompanying decrease in system fluid levels precluded the event from taking place in the

remaining CMT until the first refill event terminated and the system fluid levels were restored by IRWST injection. This characteristic is illustrated in Figure 6.1.1-9, which shows that the CMT-1 balance line level was depressed as a result of CMT-2 refill. Immediately, following recovery of the downcomer level, the CL-3/CMT-1 balance line began to refill; as soon as the balance line level recovered to completely full, the CMT-1 refill event was initiated.

This refill phenomenon generally occurred in all tests where the cold-leg balance line was intact. Additional discussion and comparison of the CMT refill phenomenon is given in Subsection 7.2.2.

The 1/4 scale of the OSU test facility contributes to the facility's ability to refill. The decrease in CMT pressure, which lifted the liquid up and filled the cold-leg balance line, was only about [ ]^{a,b,c} psi (Figure 6.1.1-3). This corresponds to an absolute CMT pressure of about [ ]^{a,b,c} psia in the OSU test. In comparison, the pressure decrease in the AP600 would have to be about [ ]^{a,b,c} psi. Since the reactor system is nearly at containment pressure, about [ ]^{a,b,c} psia for a SBLOCA during this period, the CMTs would have to be at an absolute pressure of about [ ]^{a,b,c} psia. Other factors that could influence the potential for, as well as the timing of, a CMT refill include: energy stored in the CMT metal, heat loss to the environment, and presence of noncondensables in the CMT.

While it is possible that CMT refill could occur in the AP600, and evidence of the CMT balance line beginning to refill was observed in SPES-2,[3] the ease with which the CMTs refilled in the OSU test is believed to be a result of a scaling distortion. Therefore, refill of the CMTs would be less likely to occur in the AP600 than in the OSU test.

TABLE 6.1.1-1 OSU TEST ANALYSIS PLOT PACKAGE FOR SUBSECTION 6.1.1				
Plot No.	**Component**	**Variables**	**Units**	**Description**
1	CMT	–	°F Btu/sec.	CMT-1 Average fluid and through-thickness metal temperatures and upper head heat flux
2	CMT	–	°F Btu/sec.	CMT-2 Average fluid and through-thickness metal temperatures and upper head heat flux
3	CMT	–	psia in.	Effect of CMT pressure on balance line level
4	CMT	–	lbm/sec. psia	Effect of flow from CMT balance line on CMT pressure
5	CMT	–	psia in.	CMT Refill - response to CMT pressure decrease
6	CMT	–	in. lbm	Effect of CMT refill on RPV mass
7	CMT	–	in.	Effect of CMT refill on cold-leg level
8	CMT	–	in.	Effect of CMT refill on downcomer level
9	CMT	–	in.	Effect of CMT refill on balance line and downcomer levels

THE FIGURES LISTED IN TABLE 6.1.1-1
ARE NOT INCLUDED IN THIS NONPROPRIETARY DOCUMENT

6.1.2 Passive Residual Heat Removal System Performance

The passive residual heat removal (PRHR) system is designed to remove core decay heat in the event that the active safety-related systems are not available. The PRHR heat exchanger (HX) is located inside the in-containment refueling water storage tank (IRWST). It consists of a series of C-tubes, each end connected to an inlet and outlet header, which are connected to the hot leg (inlet) and pump suction (outlet), respectively. The inlet header enters the IRWST slightly below the water surface and the outlet header exits the tank near the bottom. At normal operating conditions, the PRHR is isolated from the primary system. In the event of an accident, the isolation valves are opened and natural circulation flow is established, driven by the density difference between the hot fluid entering the PRHR and the cold fluid exiting the PRHR. Heat is transferred from the tubes to the IRWST water by either subcooled boiling or free convection.

This section describes the heat transfer characteristics of the OSU representation o. the PRHR/IRWST. Also included is a discussion of the PRHR heat removal from the primary system and the interaction between the PRHR and other heat removal mechanisms, including the energy out of the break, the heat transfer through the steam generators, and the automatic depressurization system (ADS). The calculations presented in this section were performed for Test SB18. However, the conclusions are valid and describe the PRHR performance in all of the LOCA tests based on calculations for these other matrix tests. The heat transfer from the PRHR tubes to the IRWST can be calculated by either of the following two methods:

- Inferred from the increase in the internal energy of the IRWST water
- Heat transfer calculations from the external tube walls to the IRWST water

Passive Residual Heat Removal System Performance Inferred from the In-Containment Refueling Water Storage Tank Energy Increase

The most accurate method for determining the heat transfer from the PRHR tubes to the IRWST is to infer the heat transfer by observing the increase in the internal energy of the IRWST water. The PRHR is the sole source of energy input into the IRWST until actuation of the ADS 1-3. After this time, the PRHR heat transfer is determined by:

$$Q_{PRHR} = (dU/dt)_{IRWST} - Q_{ADS13} \qquad 6.1.2\text{-}1$$

where:

Q_{PRHR}	=	Heat transferred from the PRHR, Btu/sec.
$(dU/dt)_{IRWST}$	=	Time rate of change of the IRWST water energy, Btu/sec.
Q_{ADS13}	=	Heat transferred from the ADS stage 1-3 flow, Btu/sec.

Equation 6.1.2-1 can be integrated:

$$\int Q_{PRHR} dt = (U - Uo)_{IRWST} - \int Q_{ADS13} dt \qquad 6.1.2\text{-}2$$

The water temperature in the IRWST was measured at axial locations. By associating a volume with each of these measurements, a total fluid internal energy was calculated for each time step. The difference between this value and the internal energy of the tank at the start of the test is used in Equation 6.1.2-2 to determine the total PRHR energy transferred until actuation of ADS 1-3. No evaporative heat loss from the IRWST was considered in this calculation, as the IRWST is highly subcooled during the period of interest (<1000 sec). The results of these calculations for Matrix Test SB18 are shown in Figures 6.1.2-1 to 6.1.2-3.

Passive Residual Heat Removal System Performance Determined from the External Tube Heat Transfer

The PRHR heat exchanger consists of 88 tubes in a C-tube arrangement. Two of the tubes, the longest (the top tube in the inlet tube bundle), and the shortest (the bottom tube in the inlet tube bundle) have been instrumented. The tubes are fed from a common header; flow in the long and short tubes may be different depending on conditions in the header. Four thermocouples are located on each instrumented tube to determine the tube external wall temperature at the center of the horizontal inlet tube, one-fourth of the way down the vertical tube, three-fourths of the way down the vertical tube, and at the center of the horizontal outlet tube. The temperatures in the IRWST are determined at twelve axial locations from the bottom to the top of the tank. These instruments are summarized in Table 6.1.2-1.

Heat transfer calculations were performed for both tubes at the four thermocouple locations. One-half of the tubes (44) were assumed to behave as short tubes, while the remainder were assumed to behave as long tubes. Previous studies of the PRHR performance[3] indicate that the condensation of a high temperature two-phase mixture inside the inlet portion of the tubes results in high heat fluxes, which promote subcooled boiling on the external tube surface. However, the tube wall temperatures at the PRHR inlet for OSU[1] indicate that the boiling did not occur for any of the tests. This is due to the lower primary system pressure in OSU, which reduces the energy of the flow into the PRHR relative to the SPES tests which were performed at full pressure. Consequently, the external heat transfer in the PRHR at OSU is characterized solely by free convection for all test conditions.

Horizontal Tube Heat Transfer

The heat transfer coefficient is calculated using the free convection correlation for horizontal tubes from Holman:[19]

$$h = k/d \; 0.53 \; (GrPr)^{1/4} \qquad 6.1.2\text{-}3$$

where:

k	=	Liquid thermal conductivity in the tank, Btu/sec.-ft.-°F
d	=	Tube outer diameter, ft.
Pr	=	Liquid Prandtl number
Gr	=	Liquid Grashof number given by

$$Gr = g\beta (T_w - T_{bulk}) d^3 / \nu^2 \qquad 6.1.2\text{-}4$$

where:

g	=	Gravitational constant, ft./sec.^{2}
ν	=	Liquid kinematic viscosity, ft.^{2}/sec.
T_w	=	Wall temperature of the tube section, °F
T_{bulk}	=	IRWST water temperature in the vicinity of the tube, °F
β	=	Volumetric expansion coefficient given by

$$\beta = (\rho_{bulk} - \rho_w) / [\rho_w (T_w - T_{bulk})] \qquad 6.1.2\text{-}5$$

where:

ρ_{bulk}	=	Liquid density evaluated at the bulk tank temperature, lbm/ft.^{3}
ρ_w	=	Liquid density evaluated at the wall temperature, lbm/ft.^{3}

Finally, the heat transfer from the tube section is given by:

$$Q_{seg} = hL_{seg}\pi d (T_w - T_{bulk}) N_{tubes} \qquad 6.1.2\text{-}6$$

where:

L_{seg}	=	Length of the tube segment, ft.
N_{tubes}	=	Number of tubes represented in the calculation

Vertical Tube Heat Transfer

The heat transfer rate in the vertical segment was evaluated in the same way except that the free convection correlation for vertical cylinders was used. The free convection heat transfer coefficient is given by Holman[19] as:

$$h = k\ 0.13 [g\beta (T_w - T_{bulk}) Pr / \nu^2]^{1/3} \qquad 6.1.2\text{-}7$$

The heat transfer from the vertical tube sections is given by equation 6.1.2-6.

External Tube Heat Transfer Results

The results of this study are presented in plots that are shown in Table 6.1.2-3. The heat transfer rate as calculated for the long tubes is shown in Figure 6.1.2-1. This figure shows that during the period of steady operation, nearly [ ]^{abc} percent of the total heat transfer occurred in the inlet horizontal section, while [ ]^{abc} percent occurred in the vertical section, and [ ]^{abc} percent occurred in the outlet horizontal section. These results are due to the high heat flux associated with the two-phase mixture condensing in the inlet tube, and are consistent with observation from the SPES tests.(3) The heat transfer rate remained essentially constant at [ ]^{a,b,c} Btu/sec once natural circulation flow had been established until the initiation of ADS 1-3 at approximately [ ]^{abc} seconds.

The heat transfer for the short tubes is shown in Figure 6.1.2-2. The heat transfer rate was much lower for the short tubes than for the long tubes during the most significant period of PRHR operation (up until ADS actuation). This is due to density stratification in the inlet header, which preferentially feeds two-phase mixture to the top (long) tubes, and single-phase liquid to the bottom (short) tubes. This is verified by the inlet plenum differential pressure cell, which indicates that the plenum drains at ADS actuation. During the pre-ADS period, the heat transfer was equally split between the inlet, vertical, and outlet tube segments.

Figure 6.1.2-2 also shows that the short tube heat transfer increases after ADS actuation. This is due to the draining of the PRHR header to the point where only the tubes at the bottom of the bundle continue to receive flow.

Figure 6.1.2-3 shows a heat balance on the IRWST and includes the integrated heat transfer from all the PRHR tubes, the integrated heat flow into the IRWST from the ADS 1-3, and the change in the IRWST internal energy relative to the beginning of the test. Also shown is the energy removed from the primary system by flow out the 2-in. break. This figure shows good correlation between external tube heat transfer calculation and the IRWST internal energy calculation for times up to the initiation of ADS 1-3 at [ ]^{abc} sec. After this time, the PRHR continues to transfer heat at a reduced rate until initiation of ADS-4 at [ ]^{abc} seconds, when the PRHR heat transfer ceases.

During the early stages of a SBLOCA, the primary system sensible heat and the reactor decay heat are removed by the flow of steam and water out of the break, heat transfer in the SGs from the primary to the secondary side, and heat transfer in the PRHR. As was observed in both the OSU and SPES tests, the SG heat transfer is significantly reduced after the secondary-side is isolated and the primary side flow transitions to natural circulation and ends when the primary side pressure reaches the secondary side pressure. The two sides are then in thermal equilibrium, and the steam generator tubes are drained. At this time, the primary heat removal paths become the break and the PRHR. In the case of the 2-in. break, flow out of the break accounts for six times as much energy removal as the PRHR. These results indicate that the PRHR is far more effective at removing energy from the primary system

in non-LOCA events such as the steam generator tube rupture (SGTR), where the primary system pressure and inventory remain high.

The results observed for SB-18 were typical of all the LOCA tests.

TABLE 6.1.2-1 INSTRUMENTATION FOR CALCULATING THE PRHR/IRWST HEAT BALANCE	
Description	**Instrumentation Tag**
PRHR Short Tube Wall - Inlet Temperature	TW-807
PRHR Short Tube Wall - Vertical Temperature	TW-805, TW-804
PRHR Short Tube Wall - Outlet Temperature	TW-802
PRHR Long Tube Wall - Inlet Temperature	TW-808
PRHR Long Tube Wall - Vertical Temperature	TW-806, TW-803
PRHR Long Tube Wall - Outlet Temperature	TW-801
IRWST Temperatures	TF-701, TF-702, TF-703, TF-704, TF-705, TF-706, TF-707, TF-708, TF-709, TF-710, TF-711, TF-712
IRWST Pressure	PT-701
IRWST Water Level	LDP-701

TABLE 6.1.2-2 KEY PARAMETERS FOR CALCULATING THE PRHR/IRWST HEAT BALANCE	
Description	**Value**
PRHR Short Tube - Inlet/Outlet Length	18.26 in.
PRHR Short Tube - Vertical Length	43.93 in.
PRHR Long Tube - Inlet/Outlet Length	25.01 in.
PRHR Long Tube - Vertical Length	57.43 in.
Tube Outer Diameter	0.375 in.
Number of Long Tubes	44
Number of Short Tubes	44

TABLE 6.1.2-3 OSU TEST ANALYSIS PLOT PACKAGE FOR SECTION 6.1.2	
Plot No.	**Description**
1	Breakdown of Heat Transfer for Long Tubes, SB18
2	Breakdown of Heat Transfer for Short Tubes, SB18
3	Integrated Energy from PRHR and IRWST Heat-up for SB18

THE FIGURES LISTED IN TABLE 6.1.2-3
ARE NOT INCLUDED IN THIS NONPROPRIETARY DOCUMENT

6.1.3 Flow Oscillations During Long-Term Cooling

Cyclic flow, pressure, level, and temperature oscillations were observed in about 65 percent of the OSU tests. These oscillations occurred during the latter stage of the IRWST injection phase of SBLOCA simulations. Several possible causes of these oscillations, evaluation of test data, and the extrapolated effect in the AP600 plant are identified in this section. The most likely cause of the oscillations is also presented in detail.

6.1.3.1 Introduction

The flow paths in the reactor vessel during IRWST injection are schematically illustrated in Figure 6.1.3-1. Liquid from the IRWST entered the downcomer through the two DVI lines, which are located 180 degrees apart, flowed down through the downcomer and up through the core, where heat addition from the electrical heater rods generated steam. A two-phase water/steam mixture exited the core. Liquid (and possibly some steam) was released from the reactor vessel through the hot legs and ADS-4 lines, which are open during this portion of the test. Steam was separated from the liquid in the upper head and flowed into the downcomer through a series of ten small holes in the downcomer top plate. This steam condensed on the surface of the cooler water in the downcomer.

The key features of the oscillations are summarized in Table 6.1.3-1. The oscillations exhibit several common characteristics:

- The oscillations begin after net steam was generated in the core during IRWST injection.
- The oscillations were regular with a period between 110 and 135 seconds.
- The oscillations started gradually and end gradually (Figure 6.1.3-2).

For all the tests, the measured upper plenum collapsed liquid level oscillated around the top of the hot leg nozzles, and in all tests the measured downcomer collapsed liquid level covered the cold-leg nozzles.

The difference in the oscillation start and stop time and the oscillation period is related to the break size and location. These two parameters affect the amount of the steam generated in the core and eventually, the amount of steam condensed in the downcomer.

Five mechanisms have been postulated to explain these oscillations. Each hypothesis is described in detail in Subsection 6.1.3.2. A detailed analysis of the oscillations for SB01, the reference transient, is presented in Subsection 6.1.3.3. The oscillations observed in the other tests are also briefly discussed in Subsection 6.1.3.3 in comparison with the reference transient SB01.

6.1.3.2 Proposed Hypotheses

Flow oscillations were observed to occur during FLECHT-SET gravity-feed reflood tests[18] and have been analyzed. The oscillations were found to be natural oscillations, which are U-tube (manometer) oscillations due to the gravity force alone, with an oscillation period of three seconds. The vessel in the OSU test is shorter than that in the FLECHT-SET test. Since the period of natural oscillation is proportional to the height of the vessel, the period of natural oscillations in the OSU test is shorter than the three second period observed in the FLECHT-SET test. However, the observed oscillation period in the OSU test was [ ]^{a,b,c} seconds. Therefore, the oscillations in the OSU test are not natural oscillations, but are forced oscillations due to force induced by the steam generation and condensation.

In the OSU test, the driving force of the oscillations was determined to be the steam generated in the vessel, which caused the pressure in the vessel to increase. To have oscillations with repetitive cycles, this pressure build-up in the vessel was relieved by venting the steam. The possible vent paths are: (a) through the hot legs and the ADS-4 lines, (b) through the upper head bypass holes and the cold legs, and (c) through the upper head bypass holes with condensation at the top of the downcomer, with the injected DVI line flow as shown in Figure 6.1.3-1.

Five candidate hypotheses for the oscillations observed during LTC were investigated and are described and evaluated in this section. The candidate hypotheses are:

1. Level fluctuations in the upper plenum opened and closed the steam vent path at the hot-leg nozzle. Level fluctuations were driven by pressure changes resulting from alternately covering and uncovering the hot-leg nozzle. No condensation occurs in the downcomer.

2. Slug flow in ADS-4 lines caused pressure surges when the steam slugs discharged into the separator by changing the two-phase flow regime and pressure drop in these lines.

3. The observed pressure fluctuations were driven by changes in condensation rates for steam flowing from the upper head and condensing in the downcomer.

4. The observed pressure and level fluctuations were due to alternately covering and uncovering of the hot-leg nozzle and steam condensation in the downcomer.

5. The observed pressure and level fluctuations were due to alternately covering and uncovering of the upper head bypass holes.

The following sections describe assessment of the data and will show only Hypothesis 4 can be the probable cause of the oscillations.

6.1.3.2.1 Hypothesis 1: Fluctuating Level About the Hot-Leg Nozzle

This hypothesis holds that steam pressure in the reactor head increased because all the steam generated in the core was not released when the two-phase flow vented through the ADS-4 lines. As pressure in the reactor vessel head increased, the level in the reactor vessel upper plenum decreased until the hot-leg nozzle became uncovered by the two-phase mixture. When the nozzle became uncovered, steam was vented from the upper plenum and reactor head through the hot leg to ADS-4. As steam was vented, pressure in the reactor head decreased and the mixture level in the upper plenum rose until the hot-leg nozzle was covered. Without considering condensation in the downcomer, when the hot-leg nozzle became covered again, pressure again began to rise. This cycle continued to repeat until the fluid level in the upper plenum decreased below the hot leg so that steam was continuously vented through the ADS-4 lines. When steam could flow through the hot leg and ADS-4 lines without restriction, steam was not available to accumulate in the reactor head, and the pressure increase/level decrease fluctuations halted.

Figures 6.1.3-2 shows the collapsed levels in the upper plenum for Matrix Tests SB01 and SB18. For this particular level instrument, the relative position of the hot-leg nozzle is:

Top of hot leg	[ ]^{a,b,c} in.
Centerline of hot leg	[ ]^{a,b,c} in.
Bottom of hot leg	[ ]^{a,b,c} in.

The average collapsed level did not decrease until about [ ]^{a,b,c} seconds after the oscillations stopped. Therefore, the hot-leg steam venting path did not change significantly when the oscillations stopped.

Based on a pressure change of [ ]^{a,b,c} psi in the upper head and the calculated core steam generation rate ([ ]^{a,b,c} lb/sec.), it would require only a net accumulation of [ ]^{a,b,c} percent of the steam generated to provide this pressure rise in [ ]^{a,b,c} seconds (one-half the period, i.e., the time during a cycle when the pressure was increasing). The net steam accumulation in the reactor head was the difference between the steam generated less the steam vented through the ADS-4 lines and the steam flowing into the downcomer. It is more likely that this steam accumulation was a large fraction of the steam production based on the flow analysis of the ADS-4 line which is discussed later. A larger rate of steam accumulation would result in a much smaller period for the oscillations than that which was observed.

This hypothesis considers only the level fluctuation about the hot-leg nozzle without considering the steam condensation in the downcomer. The resulting pressure rise would be very fast and the oscillation period would be very short, which is not consistent with the observed oscillation period. Therefore, this hypothesis is not a probable cause of the flow oscillation.

6.1.3.2.2 Hypothesis 2: Slug Flow in ADS-4 Lines

This hypothesis holds that oscillations could be produced if slug flow was induced in the ADS-4 lines. When alternate slugs of vapor and liquid discharge into the separator, pressure pulses could be generated that would be propagated through the system.

To investigate this hypothesis, several approaches were used. First, the flow regimes in the hot legs and ADS-4 lines were estimated using a flow pattern map (Figure 6.1.3-3) published by Baker.[15] Based on the measured liquid flow from the ADS-4 separators, the calculated steam flow through the ADS-4 lines (calculated from the total steam generated in the core less the steam flow to the downcomer which was calculated from the pressure difference across the flow holes in the downcomer top), and the flow areas of the piping, flow in the [ ]^{a,b,c}-in. diameter hot leg and [ ]^{a,b,c}-in. diameter ADS-4 line were in the stratified and slug regime, respectively (Figure 6.1.3-3). The calculated transport time through the hot leg and ADS-4 line based on an average volume for the steam/liquid mixture, is about [ ]^{a,b,c} seconds.

Several analyses were performed to determine the flow characteristics in the ADS-4 lines during the long-term oscillations. These analyses are discussed below.

Steam flow measured downstream of ADS-4 steam/water separator is shown in Figure 6.1.3-4. Figure 6.1.3-4 shows that, before [ ]^{a,b,c} seconds, there was steam flow in the line. Between [ ]^{a,b,c} and [ ]^{a,b,c} seconds, there was no measured steam flow in the ADS-4 line because the core did not generate steam. After [ ]^{a,b,c} seconds, the core did generate steam; however, Figure 6.1.3-4 shows that the steam flow rate in the ADS-4 line was very small, except for a few spikes with very short durations that may have been slugs of steam. Figure 6.1.3-5 shows that a spike of steam flow occurred at [ ]^{a,b,c} seconds. The magnitude of the spike was smaller than one half of the peak flow rate in Figure 6.1.3-4. That is, the steam flow meter used to measure steam flow in the ADS-4 line was sensitive enough to indicate the steam flow from the vessel. Since the magnitude of steam flow is only indicative because the vortex flow meter for the ADS-4 is overranged, it is possible that some slugs of steam have been undetected. However, the data analyses for transport time confirm that steam flow was intermittent and small, so that transport time was unaffected.

The transport time of fluid in the ADS-4 line, computed by assuming that flow was single-phase liquid, agreed with the time lag between the flow oscillations in the vessel and downstream of the ADS-4 steam/water separator. The oscillation is a marker that can be used to trace fluid. That is, the time lag between flow oscillations in the vessel and downstream of the ADS-4 steam/water separators should be equal to the transport time of the fluid between these two locations. Since the vessel flow rate has been computed for steam but not for liquid, the steam flow rate will be used for the vessel, while the liquid flow rate will be used for the ADS-4 line in the oscillation time-lag calculation. Figure 6.1.3-19 shows the oscillation of steam flow in the vessel, and Figure 6.1.3-18 shows the oscillation of liquid flow of ADS-4. The time lag between the oscillations was about [ ]^{a,b,c} seconds. Conversely, assuming that flow in the ADS-4 line and the hot leg were single-phase liquid and that the

fluid was travelling at the measured average flow rate of [ ]^{a,b,c} lbm/sec., the transport time is calculated to be [ ]^{a,b,c} seconds. This transport time is about the same as the observed time lag between the two oscillations which was about [ ]^{a,b,c} seconds. This suggests that the hot leg flow was primarily single-phase liquid.

Further evidence of this is that the level measurement (LDP-112) at the inner barrel wall above the core plate and the fluid temperature (TF-170) indicated this region was liquid-solid with an annular liquid region above the upper core plate. Therefore, this liquid is more likely to flow into the hot leg and the ADS-4 line.

The above discussion suggests that the hot-leg flow contained primarily liquid and that an occasional vapor bubble flowed down the hot-leg and out of the ADS-4 valve.

Slug Flow

- It is extremely unlikely that the slugs of steam in the two ADS-4 lines would be exactly synchronized so that the period would be as regular as observed.

- The measured time lags for the ADS-4 oscillations agreed with the calculated time lag for single-phase liquid flow.

- Two-phase flow pressure variations would be random and would occur at a shorter period than the observed [ ]^{a,b,c} seconds.

Liquid Flow

- If the flow through the ADS-4 lines were completely liquid, there would be no pressure pulses because of vapor/liquid slugs. In this case, the observed flow oscillations would have originated from pressure pulses driven by another source.

As a result of the above analysis, this hypothesis is not thought to be a probable mechanism for the observed oscillation.

6.1.3.2.3 Hypothesis 3: Downcomer Condensation/Fluctuations

Under this hypothesis, a large fraction of the steam in the upper head was postulated to have flowed through the ten holes ([ ]^{a,b,c}-in. diameter) in the top of the downcomer and condensed on the surface of the coolant in the downcomer. Steam flow into the downcomer has been estimated by the three following methods:

- Pressure drop measurement (DP-130) across the downcomer top plate (i.e., across the flow holes)

- Heat balance based on the temperature rise of flow through the downcomer

- Total steam generation assuming there was no steam flow through the ADS-4 line (based on previous discussion of transport analysis of flow in the ADS-4 line)

The results of these methods provide a range of estimated steam flow into the downcomer as summarized below:

Method	Steam Flow to Downcomer (lb/sec.)
Pressure drop across downcomer top	[ ]^{a,b,c}
Heat balance	[ ]^{a,b,c}
Core heat generation	[ ]^{a,b,c}

During IRWST injection, the temperature of the injection flow into the downcomer slowly increased with time (Figure 6.1.3-9) because the water in the IRWST had been heated first by operation of the PRHR and, as the test progressed, by steam released through the ADS 1-3 lines. Steam production in the core started at about [ ]^{a,b,c} seconds (Figure 6.1.3-11). The existing superheated steam bubble in the upper head gradually cooled by heat loss through the reactor head. When steam produced in the core mixed with superheated steam in the upper head, the steam temperature in the upper head began to decline. The start of this temperature reduction, which occurred at about [ ]^{a,b,c} seconds, indicated the initiation of steam production in the core.

Oscillations were observed to begin about [ ]^{a,b,c} seconds after the initiation of steam production in the simulated core. Therefore, the initiating event for the oscillations was not simply the onset of boiling in the simulated core. However, the temperature difference between liquid (TF-167) (Figure 6.1.3-9) and steam downcomer vapor space decreased about [ ]^{a,b,c} percent during the period from the initiation of steam production and the start of the oscillations. Oscillations began when the temperature of the downcomer liquid became so high that not all the steam flowing from the upper plenum to the downcomer could be condensed. The pressure then increased in the downcomer causing flow from the upper head to decrease. Since steam continued to be generated, pressure in the upper head increased, raising flow through the ADS-4 line and decreasing IRWST injection. Increased flow in the ADS-4 line reduced steam pressure which decreased steam flow to the downcomer. The level changes in the downcomer, because of these pressure changes also caused some mixing of liquid at the steam/liquid interface, and enhanced the condensation rate. The enhanced condensation tended to further reduce pressure in the downcomer and upper head. As the steam-downcomer liquid interface increased in temperature from the collecting condensate, the condensation rate decreased below the rate of steam flowing into the downcomer, and pressure began to rise again. This cycle was repeated, producing the observed oscillations.

It is possible that a layer of saturated liquid formed on the liquid interface causing condensation to stop completely. If so, the increase in steam saturation temperature resulting from the pressure increase, and mixing from the level change would tend to initiate condensation again. This process would result in the observed oscillating behavior.

The oscillations ceased when the level in the downcomer decreased sufficiently that the cold leg was uncovered, and steam could be released through the cold leg instead of increasing pressure in the downcomer vapor volume and reactor upper head. Since the level changes required to release steam through the cold leg were too small to be determined from the level measurement, the presence of steam in the CMTs was used to indicate initial release of steam through the cold leg. Figure 6.1.3-8 shows a rise in CMT temperature slightly before the oscillations stopped, supports the uncovering of the cold leg as the termination mechanism for the oscillations. The uncovering of the cold-leg nozzles is also supported by evidence that the thermocouples at the top of the cold-leg nozzles reached saturation temperature, which indicated the presence of steam at the top of the cold legs.

The downcomer condensation model is supported by the following observations:

- Both the start and the end of the oscillations were gradual. This is consistent with the slow increase in IRWST temperature at the onset of the oscillations and the gradual decrease in downcomer liquid level at the end of the oscillations.

- The oscillations were regular and smooth, which would result from changes in a process, such as condensation, where a very small driving temperature exists.

- Oscillations stopped when steam was vented through the cold leg to the CMT (and also through the break).

- The level and pressure oscillations were 180 degrees out of phase.

- The heat balance indicated that up to [ ]^{a,b,c} lbm/sec. of steam was condensed in the downcomer.

- The estimated average condensation heat transfer coefficient for [ ]^{a,b,c} lb/sec. of steam flow was about [ ]^{a,b,c} Btu/hr., ft.^{2}, °F, which is consistent with values for condensation of steam. This was a bounding estimate using the downcomer liquid temperature (TF-167), which is lower than the temperature of the liquid at the interface.

This hypothesis was considered a valid mechanism in the Revision 0 of this report.[20] Based on further investigations this hypothesis, which considers only the downcomer condensation alone, is not considered a probable mechanism for the observed oscillations, although downcomer condensation is thought to be an important factor contributing to the oscillations.

6.1.3.2.4 Hypothesis 4: Covering and Uncovering of Hot Leg with Downcomer Condensation

To facilitate the explanation of this hypothesis for the flow oscillations, the idealized behaviors of the flow variables are schematically shown in Figure 6.1.3-7. Figure 6.1.3-7(a) shows the mixture level, L, in the upper plenum, where the top of the hot leg, nozzle L_{HL}, is labeled. Figure 6.1.3-7(b) shows the total flow rate out of the hot leg, $\dot{m}_{HL}$. Figure 6.1.3-7(c) shows the steam generation rate from the core, $\dot{m}_v$. Figure 6.1.3-7(d) shows the pressure in the upper plenum. Figure 6.1.3-7(e) shows the sum of the injection flow rate from two DVI lines, $\dot{m}_{inj}$. Note that when the pressure in the vessel is low, the pressure difference between the IRWST and the vessel is larger, resulting in a larger DVI injection flow rate. The large injection rate in turn causes the steam generation rate to be low. Thus, $\dot{m}_v$ oscillates in phase with the pressure, P, while $\dot{m}_{inj}$ oscillates out of phase with P and $\dot{m}_v$.

Consider that initially the mixture level was at the hot-leg level so that the steam can vent through the hot leg. Hence, the pressure in the vessel was at a low value (point A in Figure 6.1.3-7(d). Because of low pressure in the vessel, the injection flow rate was high, and the steam generation rate and the hot-leg flow rate were low. As a result, $\dot{m}_{inj}$ is larger than $\dot{m}_{HL}$ and the mixture level moved up. As the mixture level moved above the hot-leg level, the steam cannot be vented through the hot leg. Therefore, the pressure increased and the injection rate decreased. As the injection rate decreased, the steam generation rate increased, which further caused the pressure to increase. The increase of the pressure forced more fluid to go out of the hot leg and thus increased the hot leg flow rate, $\dot{m}_{HL}$. When the hot-leg flow rate became equal to the injection flow rate (point B) and continued to increase, the mixture level started to decrease. When the mixture level decreased below the top of the hot leg (point C in Figure 6.1.3-7(a), the steam vented through the hot leg and the pressure dropped from point C to point D. As the pressure drops, the injection rate, $\dot{m}_{inj}$, increased and the hot-leg flow rate, $\dot{m}_{HL}$, decreased so that $\dot{m}_{inj}$ became larger than $\dot{m}_{HL}$. As a result, the mixture level increased. When the mixture level increased past the top of the hot leg (point E), the hot leg is covered and the steam cannot leave the hot leg. Therefore, the pressure increased again and the cycle repeats.

Note that in a real case, the pressure, P, does not drop instantaneously when the hot leg is uncovered (point C to point D in Figure 6.1.3-7(d), rather it decreases gradually as shown by the dashed line in the Figure 6.1.3-7(d). Other variables, $\dot{m}_{HL}$, $\dot{m}_v$, and $\dot{m}_{inj}$, also do not change abruptly, these variables change gradually as indicated by the dashed lines in Figures 6.1.3-7(b), (c), and (e). Also note that when the hot leg is covered, only a small amount of generated steam is available to pressurize the vessel. Most of the steam goes through the upper head bypass holes to the top of the downcomer and is condensed there.

Detailed calculations and comparisons with the data are given in Subsection 6.1.3.3. In comparing the level data, keep in mind that the data represents the collapsed liquid level, not the two phase mixture level, since the mixture level was not measured. The collapsed liquid level is generally lower than the

mixture level. The calculations show that the high hot-leg flow rate, $\dot{m}_{HL}$, during the hot leg covering period is single-phase liquid flow. Since the hot-leg flow rate is not measured, the liquid flow rate downstream of the ADS-4 steam/water separator is used, which has a time lag of about [ ]^{a,b,c} seconds due to transportation time from the entrance to the hot leg to the downstream location of the ADS-4 steam/water separator.

6.1.3.2.5 Hypothesis 5: Covering and Uncovering of Upper Head Bypass Holes

When the mixture level is always above the hot-leg nozzle so that the hot-leg nozzle is never uncovered, Hypothesis 4 does not apply. In this case, flow oscillations may be due to the alternate, covering and uncovering of the upper head bypass holes.

Initially, the mixture level is above the top of the upper head bypass holes. Since the bubbles can only move upward, the bubbles cannot go to the bypass holes. Therefore, only water will go to the bypass holes, that is, the bypass holes are covered with water. With the water covering the bypass holes, the steam cannot go through the bypass holes easily. Therefore, the pressure in the vessel increases. As the pressure increases, the DVI injection rate, $\dot{m}_{inj}$, decreases and the hot-leg flow rate, $\dot{m}_{HL}$, increases. The decrease $\dot{m}_{inj}$ in turn causes the steam generation rate to increase, which causes the pressure to further increase. When $\dot{m}_{HL}$ becomes larger than $\dot{m}_{inj}$, the mixture level drops. As the mixture level drops, the bypass holes are uncovered. As the bypass holes are uncovered, the pressure drops. The decrease in the pressure causes the injection rate to increase and the hot-leg flow rate to decrease. The increase of the injection rate in turn causes the steam generation rate to decrease, which causes the pressure to further decrease. As the injection rate becomes larger than the hot-leg flow rate, the mixture level rises. When the mixture level rises above the top of the bypass holes, the bypass holes are covered with water and the steam cannot go through the bypass holes easily. Therefore, the pressure increases. Then, the flow conditions return to the initial state and the cycle repeats.

When the bypass holes are covered, pressurization of the upper head is very fast because of the high steam flow rate in comparison with the small upper head volume as discussed in Subsection 6.1.3.3. High pressure will cause the mixture level in the upper head to drop quickly, which will cause the bypass holes to be covered in a short time. As a result, the predicted oscillation period is much shorter than the observed oscillation period. Thus, this hypothesis is not a probable cause for the observed flow oscillations.

6.1.3.3 Examination of the Test Data to Evaluate the Postulated Oscillation Mechanism

As discussed in Section 6.1.3, flow, pressure, level and temperature oscillations have been observed in most of the OSU tests. Hypothesis 4, described in Subsection 6.1.3.2, is the one consistent with all the tests. The oscillation process is described in detail for Test SB01, which is the reference transient. The other tests are discussed briefly because of similarities with Test SB01.

6.1.3.3.1 Oscillations in Test SB01

During IRWST injection, the temperature of the injection flow into the downcomer slowly increases (Figure 6.1.3-9). The injection flow rate also decreases because the IRWST liquid level decreases (Figure 6.1.3-10). At about [ ]^{a,b,c} seconds, steam production in the core starts (Figure 6.1.3-11) and the upper plenum collapsed liquid level starts to drop (Figure 6.1.3-12). A small amount of steam generated in the core accumulated in the upper plenum, but most of it was discharged from the upper head through the bypass holes into the downcomer where it condensed with the cold water. The ADS-4 high flow rate and subcooled temperature (Figure 6.1.3-13 and 6.1.3-14) indicate that during this time period (from 8000 to [ ]^{a,b,c} seconds), the discharge is essentially pure liquid. At about [ ]^{a,b,c} seconds, the upper plenum collapsed liquid level reaches the top level of the hot-leg nozzles (Figure 6.1.3-12) and steam starts to a discharge through the ADS-4 valves (Figure 6.1.3-13) and the oscillations start.

In the following, one period of oscillation corresponding to the time interval from [ ]^{a,b,c} to [ ]^{a,b,c} seconds, starting when the upper plenum collapsed liquid level is at its minimum, is analyzed.

Conditions at [ ]^{a,b,c} seconds (Figures 6.1.3-15 to 6.1.3-19) are:

- Upper plenum collapsed liquid level = [ ]^{a,b,c} in.
- Upper plenum pressure = [ ]^{a,b,c} psia
- Total injection flow rate is = [ ]^{a,b,c} lbm/sec.
- Total ADS-4 discharge = [ ]^{a,b,c} lbm/sec.
- Steam generation in the core = [ ]^{a,b,c} lbm/sec.

The hot-leg nozzle is partially uncovered and steam is discharged easily through ADS-4. The pressure decreases consistently as injection increases and steam generation decreases as a result of increased injection. At about [ ]^{a,b,c} seconds, the ADS-4 discharge starts to decrease when the pressure in the upper plenum is at [ ]^{a,b,c} psia. At [ ]^{a,b,c} seconds, injection from the DVIs is higher than the discharge from ADS-4 and steam provided by the core reaches its minimum value ([ ]^{a,b,c} lbm/sec.); thus, the level in the upper plenum recovers. At about [ ]^{a,b,c} seconds, the upper plenum collapsed liquid level reaches its maximum ([ ]^{a,b,c} in.) and completely covers the hot-leg nozzles. The steam flow rate to ADS-4 is prevented and the steam generated is preferentially discharged into the upper head.

The pressure in the upper plenum and upper head, which reaches its minimum ([ ]^{a,b,c} psia) at about [ ]^{a,b,c} seconds starts to increase as a consequence of the reduction of the steam flow to ADS-4. The increase of upper plenum pressure is responsible for the decrease of the injection rate and as a result, steam generation rate increases. The generated steam flows into the upper head and is discharged into the downcomer where it condenses with the cold liquid. Steam flow from the upper

head to the downcomer is driven by the pressure difference between the upper head and downcomer (Figure 6.1.3-20).

The upper head pressure oscillation amplitude is [ ]^{a,b,c} psi. Pressurization of the upper head/plenum is due to the difference between the steam generation rate in the core and the condensation rate in the downcomer when the hot-leg and cold-leg nozzles are covered. It takes only a small amount of steam accumulation to pressurize the upper head/plenum. The upper head/plenum is pressurized when the downcomer cannot condense all the generated steam. When the cold leg is uncovered, the generated steam flows through the cold legs, then the upper head/plenum cannot be pressurized and the oscillations stop.

At about [ ]^{a,b,c} seconds, the pressure reaches [ ]^{a,b,c} psia. The pressure in the upper plenum is higher than the gravity head of the liquid column in the ADS-4 line ([ ]^{a,b,c} psia). The upper plenum and hot leg liquid is pushed into the ADS-4 lines. This is consistent with a sharp increase in the ADS-4 discharge as soon as the liquid reaches the ADS valves after a short time lag.

The upper plenum collapsed liquid level then uncovers the hot-leg nozzles again and reaches its minimum at about [ ]^{a,b,c} seconds. Steam provided by the core is again vented to the ADS-4 lines and the upper plenum pressure starts to decrease; injection increases and the cycle is repeated.

The period of oscillation is about [ ]^{a,b,c} seconds and is consistent with a global mass balance, where periodically the water injected ([ ]^{a,b,c} lbm) is at first accumulated in the upper plenum, hot legs, surge line and SGs inlet plenums, then is rapidly discharged through the ADS-4 valves. This is consistent with the upper plenum collapsed liquid level being out of phase with the ADS-4 mass flow rate.

At about [ ]^{a,b,c} seconds, the injection temperature has been increased and the injection flow rate has slowly decreased. The average steam generation rate in the core increased slightly. At this time, the thermocouples at the top of the cold-leg nozzles have reached saturation temperature (Figure 6.1.3-6), which indicates the presence of steam at the top of the cold legs. Therefore, the cold-leg nozzle was uncovered and steam was vented from the downcomer to the cold legs preventing the upper head/plenum from pressurization. Consequently, the flow oscillations stopped.

6.1.3.3.1.1 The Quasi-steady State Before Oscillations Start

A quasi-steady state is established before the oscillations occur (at [ ]^{a,b,c} seconds). Cold water is provided by injection, no steam is generated and warmer water is discharged by the ADS-4 valves and the break. At this time, both cold-leg and hot-leg nozzles are covered.

The upper plenum pressure which is able to maintain this quasi-steady state (Figure 6.1.3-21) can be calculated as follows:

The measured total injection rate $\dot{m}_{inj}$ is the sum of two DVI flow rates, $\dot{m}_{DVI-1}$ and $\dot{m}_{DVI-2}$:

$$\dot{m}_{inj} = \dot{m}_{DVI-1} + \dot{m}_{DVI-2} = [\quad\quad\quad\quad\quad\quad]^{a,b,c} \text{ lbm/sec.} \qquad 6.1.3\text{-}1$$

The measured total discharge flow rate $\dot{m}_{discharge}$ is the sum of the flow rates from ADS 4-1, ADS 4-2 and break $\dot{m}_{ADS,\,4-1}$, $\dot{m}_{ADS,\,4-2}$, and $\dot{m}_{break}$, respectively:

$$\dot{m}_{discharge} = \dot{m}_{ADS,\,4-1} + \dot{m}_{ADS,\,4-2} + \dot{m}_{Break} = [\quad\quad\quad\quad\quad\quad]^{a,b,c} \text{ lbm/sec.} \qquad 6.1.3\text{-}2$$

Note that the fluid discharged is subcooled liquid and no steam is generated at this time.

From these quantities, the pressure drops across the ADS-4 valves can be evaluated in the following.

The measured mass flow rate $\dot{m}$ in ADS 4-1 is [ ]^{a,b,c} lbm/sec. ([ ]^{a,b,c} kg/sec.). Thus from the ADS 4-1 orifice diameter ([ ]^{a,b,c} mm) and the liquid density ρ, the velocity V inside the orifice can be evaluated:

$$\text{Orifice flow area} = A = [\quad\quad\quad\quad]^{a,b,c} \qquad 6.1.3\text{-}3$$

$$V = \dot{m}/(\rho A) = [\quad\quad\quad\quad\quad\quad]^{a,b,c} \text{ m/sec.} \qquad 6.1.3\text{-}4$$

The differential pressure, $\Delta P_{ADS,4-1}$, across the valve ADS 4-1 is then evaluated from the orifice K factor. The orifice K factor is evaluated from Idelchick Manual[24] and is equal to 1.1.

$$\Delta P_{ADS,\,4-1} = K\rho V^2/2 = [\quad]^{a,b,c} \text{ psia} \qquad 6.1.3\text{-}5$$

For ADS 4-2, the measured mass flow rate is 0.8 lbm/sec. (0.363 kg/sec.) and the discharge flow area A is double [ ]^{a,b,c}. The velocity, V, is then:

$$V = \dot{m}/(\rho A) = [\quad\quad\quad\quad\quad\quad]^{a,b,c} \text{ m/sec.} \qquad 6.1.3\text{-}6$$

and the differential pressure, $\Delta P_{ADS,4-2}$, across the valve ADS 4-2 is:

$$\Delta P_{ADS,4-2} = K\rho V^2/2 = (\text{with } K=[\quad]^{a,b,c}) = [\quad]^{a,b,c} \text{ psia} \qquad 6.1.3\text{-}7$$

The average differential pressure, $\Delta P_{ADS,4}$, of ADS 4-1 and ADS 4-2 is then:

$$\Delta P_{ADS,4} = [\quad]^{a,b,c} \text{ psia} \qquad 6.1.3\text{-}8$$

The upper plenum pressure at the hot-leg nozzle elevation can be evaluated assuming that the distributed pressure drops are negligible.

The gravity head ΔP_g of the ADS line (full of liquid) is: ($h = [\quad]^{a,b,c}$ m)

$$\Delta P_g = \rho\, g\, h = [\quad]^{a,b,c} \text{ psia} \qquad 6.1.3\text{-}9$$

The collapsed liquid level in the upper plenum is $[\ ]^{a,b,c}$ in. above the hot-leg elevation which corresponds to a gravity head, $\Delta P_{g,up}$, of $[\quad]^{a,b,c}$ psia. Thus, the pressure of the upper plenum in the steam volume is:

$$P_{UP} = P_{atm} + \Delta P_{ADS,4} + \Delta P_g - \Delta P_{g,UP} = [\quad]^{a,b,c} \text{ psia} \qquad 6.1.3\text{-}10$$

where P_{atm} is the atmospherical pressure. The oscillations start some time after steam is generated in the core.

6.1.3.3.1.2 Steam Generation and the Onset of the Oscillations

The oscillations start at $[\quad]^{a,b,c}$ seconds and the steam generated by the core ($\dot{m}_v$) is:

$$\dot{m}_v = [\quad]^{a,b,c} \text{ lbm/sec.} \qquad 6.1.3\text{-}11$$

After about $[\quad]^{a,b,c}$ seconds, the generated steam oscillates between $[\quad]^{a,b,c}$ and $[\quad]^{a,b,c}$ lbm/sec.with an average value of about $[\quad]^{a,b,c}$ lbm/sec.

When the collapsed liquid level in the upper plenum covers the hot-leg nozzles and the ADS-4 steam flow is essentially prevented, the steam flows into the upper head and from the upper head to the downcomer where it condenses with the subcooled IRWST injection. When the hot-leg nozzles are uncovered, the steam generated is vented through the ADS-4 valves.

The oscillation of the steam generation rate is a result of the injection flow rate oscillation. When the hot-leg nozzles are covered and the upper plenum is pressurizing, injection is decreasing, and consistently the steam generation rate is increasing. The steam generation rate reaches its maximum just before the hot-leg nozzles are uncovered, then as steam is released through ADS-4 and the pressure decreases, injection increases and consequently, steam generation rate decreases.

In conclusion, the steam generation rate is out of phase with the injection flow rate because core power is constant. The maximum injection rate ([ ]^{a,b,c} lbm/sec.) corresponds to the minimum steam generation rate ([ ]^{a,b,c} lbm/sec.) and the minimum injection rate ([ ]^{a,b,c} lbm/sec.) corresponds the maximum steam generation rate ([ ]^{a,b,c} lbm/sec.).

The oscillation phenomena is subdivided into the following phases:

- Downcomer steam condensation when hot leg is covered [ ]^{a,b,c} seconds
- Upper head pressurization and upper plenum draining [ ]^{a,b,c} seconds
- Upper head depressurization [ ]^{a,b,c} seconds
- Upper plenum level recovery [ ]^{a,b,c} seconds

These phases are described in the following.

6.1.3.3.1.3 Steam Condensation

The steam condenses and the saturated condensate liquid layer collects at the top of the downcomer liquid level. As the thickness of the condensate increases, the condensation rate decreases. After while, if mixing does not occur, condensation stops because the saturated layer thickens and the steam-liquid interface becomes insulated from the subcooled water. Only conduction through the condensate layer cools the interface, but the conduction process becomes less and less effective as the condensate layer develops.

The condensation rate can be calculated by the following basic equation where the mixing effect into the downcomer is considered negligible. Assuming no-mixing occurs at the interface, the condensation rate can be evaluated based on the conduction of the liquid across the interface layer as the only significant heat transfer resistance:

The interfacial heat exchange coefficient, h, is:

$$h = k_f / d \qquad 6.1.3\text{-}12$$

where:

k_f = liquid conductivity
d = condensate layer thickness

The condensate layer thickness is related to the steam flow $\dot{m}_v$ with the equation:

$$d = \dot{m}_v t/(\rho_f A) \qquad 6.1.3\text{-}13$$

where:

ρ_ℓ	=	Liquid density
A	=	Downcomer flow area = steam-liquid interface area = [ ]^{a,b,c} ft.^{2}
t	=	Time (assuming d = 0 at t=0)

The basic equation of heat transfer notes:

heat exchange at the interface = steam condensation rate

$$h\ A\ \Delta T = \dot{m}_v h_{fg} \qquad 6.1.3\text{-}14$$

$\dot{m}_v$ is obtained from the previous three equations (6.1.3-12), 6.1.3-13), and (6.1.3-14):

$$\dot{m}_v = (k_\ell \rho_\ell A^2 \Delta T / h_{fg})^{0.5} / t^{0.5} \qquad 6.1.3\text{-}15$$

Pressure = [ ]^{a,b,c} psia gives:

k_ℓ	=	[ ]^{a,b,c} Btu/ft. hr.°F	6.1.3-16
ρ_ℓ	=	[ ]^{a,b,c} lbm/ft.^{3}	6.1.3-17
h_{fg}	=	[ ]^{a,b,c} Btu/lbm	6.1.3-18

$$\Delta T = T_{sat} - T_{inj} = 212 - [\ ]^{a,b,c} = [\ ]^{a,b,c}\ °F \qquad 6.1.3\text{-}19$$

Thus:

$$\dot{m}_v = [\ ]^{a,b,c} / t^{0.5} \qquad 6.1.3\text{-}20$$

t = [ ]^{a,b,c} sec.	$\dot{m}_v$ = [ ]^{a,b,c} lbm/sec.	6.1.3-21
t = [ ]^{a,b,c} sec.	$\dot{m}_v$ = [ ]^{a,b,c} lbm/sec.	6.1.3-22
t = [ ]^{a,b,c} sec.	$\dot{m}_v$ = [ ]^{a,b,c} lbm/sec.	6.1.3-23
t = [ ]^{a,b,c} sec.	$\dot{m}_v$ = [ ]^{a,b,c} lbm/sec.	6.1.3-24

From these calculations, the interfacial heat transfer in the downcomer condenses all the steam generated in the core during the first [ ]^{a,b,c} seconds. At [ ]^{a,b,c} seconds, the condensation capability is reduced by a factor [ ]^{a,b,c} and only [ ]^{a,b,c} percent of the steam generated is condensed. In the test, the hot-leg nozzles are covered (the upper plenum collapsed liquid level is greater than 11 in.) for about [ ]^{a,b,c} seconds.

Considering the integral over [ ]^{a,b,c} seconds:

$$\int_0^{[40]^{a,b,c}} \dot{m}_v dt \qquad 6.1.3\text{-}25$$

The average flow rate, $\bar{\dot{m}}$ is:

$$\bar{\dot{m}}_v = [\quad]^{a,b,c} \text{ lbm/sec.} \qquad 6.1.3\text{-}26$$

This is only about [ ]^{a,b,c} percent of the steam generated in the same time period.

The observed upper head, downcomer and upper plenum pressurization ([ ]^{a,b,c} psia) in the same time period is due to about [ ]^{a,b,c} lbm of accumulated steam at constant volume. During pressurization, the steam volume in the upper plenum expands to about [ ]^{a,b,c} ft. and this corresponds to an accumulation of [ ]^{a,b,c} lbms. The total accumulation is [ ]^{a,b,c} lbm, which corresponds to an average mass flow rate in the same time period of [ ]^{a,b,c} lb/sec., which is only [ ]^{a,b,c} percent of the steam generation rate. It is concluded that mixing occurring in the downcomer increases the steam condensation rate by at least a factor of [ ]^{a,b,c}.

The mixing effect reduces the layer thickness and presumably during the time period ([ ]^{a,b,c} seconds) when the hot-leg nozzles are covered, all the steam generated is condensed. This implies that the average layer thickness during these [ ]^{a,b,c} seconds is:

$$d = k_f A\ \Delta T/(\dot{m}_v h_{fg}) = [\quad]^{a,b,c} = [\quad]^{a,b,c} \text{ ft.} = [\quad]^{a,b,c} \text{ in.} \qquad 6.1.3\text{-}27$$

Assuming that all condensate is collected at the top without any mixing, the layer thickness should have been:

$$d = \dot{m}_v t/(\rho_f A) = [\quad]^{a,b,c} \text{ in.} \qquad 6.1.3\text{-}28$$

After [ ]^{a,b,c} seconds, the layer thickness is high enough (also with the mixing) to shut off the condensation. The imbalance between steam generated and condensed pressurizes the downcomer, upper head and upper plenum.

6.1.3.3.1.4 Upper Head pressurization and Upper Plenum draining

The upper plenum draining follows the upper head pressurization. The water accumulated in upper head, hot-leg, SG plenums and pressurizer surge line is discharged out of the system through the ADS 4-1 and 4-2.

In the actual test, there is a complex feedback between the upper plenum pressurization, the upper plenum level and the steam generation. The upper head pressure increases because of the steam provided by the core. As the pressure increases, the upper plenum level decreases which means that a larger volume is available for the steam expansion. Conversely as the pressure increases, injection decreases and as a result, the steam generation rate increases. Thus, more steam is provided to the upper head during pressurization. The steam volume provided by the core is much greater than the new steam volume available as a consequence of the upper plenum draining. The result is that the pressure in the upper head increases during the upper plenum draining.

In order to evaluate the maximum flow rate from the upper plenum to the ADS-4 an instantaneous pressurization without the upper plenum level decreasing, followed by the upper plenum draining at constant pressure is assured. When the pressure in the upper plenum reaches [ ]^{a,b,c} psia and the upper plenum collapsed liquid level at [ ]^{a,b,c} in.:

$$\Delta P_g(\text{upper plenum from } [\ ]^{a,b,c} \text{ in. to } [\ ]^{a,b,c} \text{ in.}) = [\ ]^{a,b,c} \text{ psia} \qquad 6.1.3\text{-}29$$

$$(\text{Pressure upstream of ADS 4-1 or ADS 4-2 valves}) = [\ ]^{a,b,c} + [\ ]^{a,b,c} - 1.12 = [\ ]^{a,b,c} \text{ psia} \qquad 6.1.3\text{-}30$$

This means that the differential pressure across the ADS-4 valves is:

$$\Delta P_{ADS,4} = [\ ]^{a,b,c} - 14.7 = [\ ]^{a,b,c} \text{ psia} \qquad 6.1.3\text{-}31$$

From this value, the mass flow rates $\dot{m}_{ADS,\,4\text{-}1}$ and $\dot{m}_{ADS,\,4\text{-}2}$ can be evaluated with the assumption that until the hot-leg nozzles are uncovered, no steam is discharged by the ADS-4 valves. In this case, the ADS-4 valves and lines pressure drops are single-phase liquid:

The new ADS 4-1 and ADS 4-2 mass flow rate are evaluated using the previously (old) calculated values for the quasi-steady state before the oscillations start:

$$\dot{m}_{ADS,\,4\text{-}1} = [(\Delta P_{new}/\Delta P_{old})\dot{m}^2_{old}]^{0.5} = [\ ]^{0.5}]^{a,b,c} = 0.9 \text{ lbm/sec.} \qquad 6.1.3\text{-}32$$

$$\dot{m}_{ADS,\,4\text{-}2} = [(\Delta P_{new}/\Delta P_{old})\dot{m}^2_{old}]^{0.5} = [\ ]^{0.5}] = 1.5 \text{ lbm/sec.} \qquad 6.1.3\text{-}33$$

The total discharge is [ ]^{a,b,c} lbm/sec. This value is very close to the maximum measured value. With this flow rate, the ADS-4 valves discharge [ ]^{a,b,c} lbm of liquid in about [ ]^{a,b,c} seconds. The [ ]^{a,b,c} lbm is the mass accumulated in the system in one period of oscillation (measured value): [ ]^{a,b,c} lbm is in the upper plenum, [ ]^{a,b,c} lbm in the pressurizer surge line, [ ]^{a,b,c} in the SG plenums and [ ]^{a,b,c} lbm in the hot legs.

In the test, the ADS-4 total flow rate is about [ ]^{a,b,c} lbm/sec. for about [ ]^{a,b,c} seconds, then it decreases to [ ]^{a,b,c} in about [ ]^{a,b,c} seconds. An average of [ ]^{a,b,c} lbm is discharged in [ ]^{a,b,c} seconds. Note that the ADS-4 maximum flow rate occurs about [ ]^{a,b,c} seconds later than when the upper plenum starts to drain. This is the transportation time from the upper plenum to the ADS-4 valve as evaluated in Subsection 6.1.3.2.

In the test, the upper plenum pressure can be considered constant only during the first [ ]^{a,b,c} seconds of ADS-4 discharge, but then the pressure decreases because the hot-leg nozzles uncover and steam is vented with the liquid through the ADS-4 valves.

Thus, after the first [ ]^{a,b,c} seconds of ADS-4 high flow rate (pure-liquid) discharge, the two-phase contribution to the ADS-4 pressure drops evaluation also has to be considered. In order to quantify this contribution, it is assumed that during the ADS-4 discharge, all the steam provided by the core ($\dot{m}_v$ = [ ]^{a,b,c} lbm/sec.) was discharged together with the liquid.

For example, the ADS 4-1 calculation is iterative:

$$\dot{m}_v = [\quad]^{a,b,c} \text{ lbm/sec.} \qquad 6.1.3\text{-}34$$

The total mass flowrate, $\dot{m}_{tot}$, is the sum of steam flowrate, $\dot{m}_v$, and liquid flowrate $\dot{m}_l$;

$$\dot{m}_{tot} = \dot{m}_v + \dot{m}_l \qquad 6.1.3\text{-}35$$

By definition the quality, x, is:

$$X = \dot{m}_v/\dot{m}_{tot} \qquad 6.1.3\text{-}36$$

$$\text{Assume } \dot{m}_l = [\ ]^{a,b,c} \text{ lbm/sec.} \qquad 6.1.3\text{-}37$$

$$\text{Quality} = X = [\qquad\qquad]^{a,b,c}\% \qquad 6.1.3\text{-}38$$

The two-phase ADS-4 valves pressure drops (across the orifice), $\Delta P_{2\phi}$, are evaluated utilizing the formula:

$$\Delta P_{2\phi} = \Delta P_{1\phi,\ell}\, \phi_f^2 \qquad 6.1.3\text{-}39$$

where $\Delta P_{1\phi,\ell}$ is the single-phase liquid pressure drop considering all fluid to be liquid and ϕ_f^2 is the two phase pressure drop multiplier evaluated with the Griffith correlation[22] as:

$$\phi_f^2 = 1 + CX(\rho_\ell / \rho_g) \qquad 6.1.3\text{-}40$$

The constant C for orifices is 0.8

$$\rho_\ell/\rho_g = 1575 \quad \text{at P=15 psia} \qquad 6.1.3\text{-}41$$

where ρ_ℓ is the liquid density and ρ_g is the vapor density.

$$\phi_f^2 = 37.8 \text{ at P=15 psia and X=[ ]}^{a,b,c} \% \qquad 6.1.3\text{-}42$$

The single phase differential pressure across the valve is evaluated by rationing the previously calculated pressure drop ΔP_{old} (=[ ]^{a,b,c} psia) corresponding to a liquid flow rate $\dot{m}_{old}$ of [ ]^{a,b,c} lbm/sec.

$$\Delta P_{1\phi,\ell} = (\dot{m}_{new} / \dot{m}_{old})^2 \Delta P_{old} = [\quad]^{a,b,c} \text{ psia} \qquad 6.1.3\text{-}43$$

where:

$$\dot{m}_{new} \equiv \dot{m}_{tot}$$

Therefore, from equation (6.1.3-39)

$$\Delta P_{2\phi} = [\quad]^{a,b,c} (37.8) = [\quad]^{a,b,c} \text{ psia} \qquad 6.1.3\text{-}44$$

which is too large. Thus, the estimated [ ]^{a,b,c} lbm/sec. is not compatible with the available pressure drop.

Assume $\dot{m}_\ell$ = [ ]^{a,b,c} lbm/sec. 6.1.3-45

$$\dot{m}_{tot} = [\quad]^{a,b,c} \qquad 6.1.3\text{-}46$$

$$\Delta P_{1\phi,\ell} = [\quad]^{a,b,c} \text{ psia} \qquad 6.1.3\text{-}47$$

$$X = [\quad]^{a,b,c}\%, \quad P = [\quad]^{a,b,c} \text{ psia} \implies \phi_f^2 = [\quad]^{a,b,c} \qquad 6.1.3\text{-}48$$

$$\Delta P_{2\phi} = [\quad]^{a,b,c} \text{ psi} \qquad 6.1.3\text{-}49$$

Assuming slip ratio = 1, the void fraction is evaluated as follows:

$$\text{(Density ratio } \rho_v/\rho_\ell) = R = [\quad]^{a,b,c} \text{ at } [\quad]^{a,b,c} \text{ psia} \qquad 6.1.3\text{-}50$$

By definition, the void fraction, α, is:

$$\alpha = 1/[\quad] = 1 / [\quad]^{a,b,c})/[\quad]^{a,b,c})([\quad]^{a,b,c})] = [\quad]^{a,b,c} \qquad 6.1.3\text{-}51$$

Therefore the elevation pressure drop, ΔP_g, line is:

$$\Delta P_{g,\,line} = [\quad]^{a,b,c} \text{ psia} \qquad 6.1.3\text{-}52$$

and the pressure in the upper plenum P_{up} is:

$$P_{UP} = [\quad]^{a,b,c} \text{ psia} \qquad 6.1.3\text{-}53$$

which is the initially assumed pressure in the upper plenum. Thus, with the pressure drop available to discharge all the steam generated by the core ([ ]^{a,b,c} lb/sec.), the total flow from ADS-4 is limited below [ ]^{a,b,c} lbm/sec. Note that the assumption of slip ratio = 1.0 tends to underestimate the gravity head of the ADS line. Generally, it will be slip ratio >> 1.0 resulting in a lower void fraction in the ADS line and consequently a higher elevation pressure drops $\Delta P_{g,\,line}$. The ADS-line friction losses would tend to slightly increase, the total pressure drops, but these were not considered.

In conclusion, the presence of steam limits the ADS-4 flow rate and it can be inferred that during the high ADS-4 flow rate phase, only pure liquid can be discharged by the ADS-4 valves. The steam can be discharged only when the steam path to the ADS-4 valves is open as the hot-leg nozzles uncover. When this occurs, the liquid flow rate is very low.

6.1.3.3.1.5 Upper Head Depressurization (Low ADS-4 Mass Flow Rate Phase)

When the level in the upper plenum drops below 11 in., the hot-leg nozzles uncover and ADS 4-1 and 4-2 start to vent steam. The steam flow from the upper plenum to the downcomer reduces significantly.

In this case, the hot-leg and upper plenum pressure decrease to the minimum value:

$$\text{Pressure upstream ADS-4} = 14.7 + (\Delta P_{2\phi} \text{ in the ADS line}) \qquad 6.1.3\text{-}54$$

$\Delta P_{2\phi}$ in the ADS line is the sum of the pressure drops across the valve $\Delta P_{2\phi}$, valve and the pressure drops in the line $\Delta P_{2\phi}$, line.

$$\Delta P_{2\phi} = \Delta P_{2\phi,\ valve} + \Delta P_{2\phi,\ line} \qquad 6.1.3\text{-}55$$

$$\Delta P_{2\phi,\ valve} = \Delta P_{1\phi,\ \ell}\ \phi_g^2 \qquad 6.1.3\text{-}56$$

where:

ϕ_f^2 = Two-phase flow pressure drop multiplier

Two situations are considered:

a) Pure steam discharge

All steam generated in the core is discharged by the ADS-4 valves without entrainment of liquid from the hot legs.

$$\dot{m}_{tot} = \dot{m}_v = [\quad]^{a,b,c} \text{ lbm/sec.} \quad \text{and } X=[\quad]^{a,b,c}\% \qquad 6.1.3\text{-}57$$

$$\phi_f^2 = [\quad]^{a,b,c} \text{ at } X=100\%,\ P=15 \text{ psia} \qquad 6.1.3\text{-}58$$

The single phase differential pressure (liquid) across the valve, $\Delta P_{1\phi,\ \ell}$ is evaluated by rationing the previously calculated (old) value corresponding to a liquid mass flow rate of [ ]^{a,b,c} lbm/sec.:

$$\Delta p_{1\phi,\ \ell} = (\dot{m}_{new}/\dot{m}_{old})^2 \Delta P_{old} = [\qquad\qquad]^{a,b,c} \text{ psia} \qquad 6.1.3\text{-}59$$

when $\dot{m}_{new} = \dot{m}_{tot}$

$$\Delta P_{2\phi,\ valve} = \Delta P_{1\phi,\ \ell}\ \phi_f^2 = [\qquad\qquad]^{a,b,c} \text{ psia} \qquad 6.1.3\text{-}60$$

The pressure losses and the gravity head $\Delta P_{g,\ line}$ of the ADS line are negligible:

$$\Delta P_{2\phi,\ line} = \Delta P_{loss,\ line} + \Delta P_{g,\ line} = 0. \text{ (the line is pure steam)} \qquad 6.1.3\text{-}61$$

$$\Delta P_{2\phi} = [\quad]^{a,b,c} + 0.0 = [\quad]^{a,b,c} \text{ psia} \qquad 6.1.3\text{-}62$$

b) Quality [ ]^{a,b,c} percent discharge

The slip ratio can be assumed to be 1.0 to simplify the calculation:

$$\dot{m}_{tot} = \dot{m}_v + \dot{m}_\ell = \dot{m}_v/X = [\quad]^{a,b,c} = [\quad]^{a,b,c} \text{ lbm/sec.} \qquad 6.1.3\text{-}63$$

The single phase (liquid) differential pressure across the valve is:

$$\Delta P_{1\phi,\ \ell} = (\dot{m}_{new}/\dot{m}_{old})^2 \Delta P_{old} = [\quad]^{a,b,c} \text{ psia} \qquad 6.1.3\text{-}64$$

$$\phi_f^2 = [\quad]^{a,b,c} \text{ at } X = [\quad]^{a,b,c}\% \text{ and } P = [\quad]^{a,b,c} \text{ psia} \qquad 6.1.3\text{-}65$$

$$\Delta P_{2\phi,\ valve} = [\quad]^{a,b,c} \text{ psia} \qquad 6.1.3\text{-}66$$

The ADS line void fraction is evaluated assuming slip=1 from the equation:

$$\alpha = 1 / [\quad] \qquad 6.1.3\text{-}67$$

where ρ_g/ρ_ℓ is the density ratio which is [ ]^{a,b,c} at the atmospheric pressure:

$$\alpha = [\quad]\ ]^{a,b,c} \qquad 6.1.3\text{-}68$$

$$\Delta P_{2\phi,\ line} = \Delta P_{g,\ line} = [\quad]^{a,b,c} \qquad 6.1.3\text{-}69$$

$$\Delta P_{2\phi} = [\quad]^{a,b,c} \text{ psia} \qquad 6.1.3\text{-}70$$

Finally, the upper plenum pressure oscillation minimum in the two situations is evaluated:

$$\text{In case (a)} \quad P_{up} = 14.7 + [\quad]^{a,b,c} = [\quad]^{a,b,c} \text{ psia} \qquad 6.1.3\text{-}71$$

$$\text{In case (b)} \quad P_{up} = 14.7 + [\quad]^{a,b,c} = [\quad]^{a,b,c} \text{ psia} \qquad 6.1.3\text{-}72$$

The oscillation amplitude (the maximum pressure is [ ]^{a,b,c} psia) is then:

(a) $P_{up,\,max} - P_{up,\,min}$ = [ ]^{a,b,c} psia 6.1.3-73

(b) $P_{up,\,max} - P_{up,\,min}$ = [ ]^{a,b,c} psia 6.1.3-74

The measured minimum pressure is about [ ]^{a,b,c} psia and the pressure oscillation amplitude is about [ ]^{a,b,c} psia. This is consistent with the calculated value if the quality is about [ ]^{a,b,c} percent. In this case, the ADS 4-1 flow rate is [ ]^{a,b,c} lbm/sec. and ADS-4-2 is estimated to be about [ ]^{a,b,c} lbm/sec. The total ADS-4 flow is about [ ]^{a,b,c}, which is less than the average injection ([ ]^{a,b,c} lbm/sec.). The imbalance in flow results in the level recovery.

6.1.3.3.1 Upper Plenum Level Recovery (End of One Cycle)

As the upper plenum pressure and level oscillate, the total injection oscillates as well. The amplitude can be considered small (+/- [ ]^{a,b,c} percent of the mean value) and the injection can be considered fairly constant in comparison with the discharge.

The average injection is about [ ]^{a,b,c} lbm/sec. To recover the [ ]^{a,b,c} lbm discharged during the upper plenum draining phase requires [ ]^{a,b,c} seconds, which is the measured oscillation period.

As soon as the hot leg nozzles are recovered, the generated steam again flows into the upper head. Meanwhile, the condensate layer in the downcomer is mixed sufficiently for the interface to be subcooled again. Condensation occurs again and the cycle is repeated.

6.1.3.3.2 Oscillations in the Other Tests

Oscillations in tests: SB06, SB09, SB10, SB12, SB13, SB14, SB15, SB18, SB19, SB21 and SB23 are included in the following discussion.

These tests are grouped into subsets, which show strong similarities in the oscillation characteristics. The following subdivision also emphasizes the break location. This grouping shows that the oscillation parameters are more strongly related to the break location than to the break size.

With Figure 6.1.3-22 as the starting point for each test, the following set of seven plots is presented:

1. Total DVIs injection mass flowrate (DVI-1 + DVI-2)

2. DVI nozzles liquid temperature (injection temperature)

3. Liquid temperature in the downcomer at the elevation of the hot leg nozzles

4. Total ADS-4 mass flowrate (ADS 4-1 plus ADS 4-2)

5. Core steam generation rate

6. Upper plenum collapsed liquid level

7. Upper head pressure

6.1.3.3.2.1 Subset 1 - SB18, SB19, SB23, SB06, SB21 - Cold-Leg Break

Test SB18 (Figures 6.1.3-71 to 6.1.3-77) was a 2-in. cold-leg break (a duplicate of SB01); SB19 (Figures 6.1.3-78 to 6.1.3-84) was a 2-in. cold-leg break with a backpressure; SB23 (Figures 6.1.3-94 to 6.1.3-100) was a 0.5-in. cold-leg break, SB06 (Figures 6.1.3-22 to 6.1.3-28) was a 4-in. cold-leg break and SB21 (Figures 6.1.-85 to 6.1.3-93) was a double 4-in. cold-leg break.

In SB18, steam generation started at about [ ]^{a,b,c} seconds and the oscillations started at about [ ]^{a,b,c} seconds when the steam generation reached [ ]^{a,b,c} lbm/sec. which is consistent with the calculated steam generation at the start of the oscillations in Test SB01. The average oscillation period in the time interval [ ]^{a,b,c} seconds was about [ ]^{a,b,c} seconds. In Test SB01, the oscillation period was higher (about [ ]^{a,b,c} seconds) and this is consistent with a [ ]^{a,b,c} °F lower, top downcomer temperature measured in SB01. The lower the temperature in the downcomer, the higher the condensation rate and the longer it takes to develop a saturated condensate liquid layer, which stops condensation and starts the pressurization of the upper head.

The oscillations in Test SB19 are very similar to the ones in SB18. Steam generation started at about the same time ([ ]^{a,b,c} seconds) and the oscillations started at about [ ]^{a,b,c} seconds when the steam generation reached about [ ]^{a,b,c} lbm/sec. The temperature at the top of the downcomer was very close to SB18. The average oscillation period, in the time interval [ ]^{a,b,c} seconds is [ ]^{a,b,c} seconds, was very close to the value of SB18.

In Test SB23, steam generation started at about [ ]^{a,b,c} seconds and the oscillations started at about [ ]^{a,b,c} seconds when the steam generation reached [ ]^{a,b,c} lbm/sec. The oscillations are not as well defined as in SB18 and in the time interval [ ]^{a,b,c} seconds, the average period is about [ ]^{a,b,c} seconds.

In Test SB06, the calculated core steam generation rate RPVASOU2 is presented instead of RPVASOUT. RPVASOU2 considers the net core flow (the difference between the total DVI flow and the DVI to Cold-leg break bypass flow). In SB06, the DVI to break by-pass flow is higher and consequently, the core flow rate was lower during the IRWST injection. In this case, the predicted core steam generation rate after [ ]^{a,b,c} seconds was about [ ]^{a,b,c} lbm/sec. As a result, the oscillations started very early in the transient at about [ ]^{a,b,c} seconds. The average oscillation period is [ ]^{a,b,c} seconds, which is shorter than in SB01.

In Test SB21, the oscillations started at about 7200 seconds with an oscillation period of about [ ]^{a,b,c} seconds. In SB21 the upper plenum collapsed liquid level (CLDP-113 in Figure 6.1.3-91) is not operable and the total vessel collapsed liquid level (CLDP-127 in Figure 6.1.3-90) is utilized instead. However the vessel collapsed liquid level does not represent the true collapsed liquid level, because of the presence of the lower core plate, the upper core plate and the upper support plate, which introduce significant pressure drops. Therefore the collapsed liquid level overestimates the vessel level.

6.1.3.3.2.2 Subset 2 - SB12, SB13 - Direct Vessel Injection Line Breaks

Tests SB12 and SB13 (Figures 6.1.3-43 to 6.1.3-56) are the DVI breaks (DEG and 2-in., respectively). No oscillations were observed in the DEG DVI (SB12) as a result of the break location and size. The break kept a low inventory of mass in the system and the upper plenum collapsed liquid level was always below the top of the hot-leg nozzles so that the steam core always vented to ADS-4. The mechanism for oscillation cannot occur if the upper plenum level is lower and steam vents out of the hot leg. Steam generation starts at about [ ]^{a,b,c} seconds, and is vented through ADS-4 . The upper head pressurization does not occur.

In the 2-in. DVI break (SB13), steam generation occurs through the entire transient. The oscillations start at about [ ]^{a,b,c} seconds when the steam generation rate is [ ]^{a,b,c} lbm/sec. The fact that steam generation is higher is a consequence of the partially lost injection flow though the break in DVI since the lower the injection, the higher the steam generation rate. The average period of oscillation in the time period between [ ]^{a,b,c} and [ ]^{a,b,c} seconds is [ ]^{a,b,c} seconds.

6.1.3.3.2.3 Subset 3 - SB15 - Hot-Leg Break

Test SB15 (Figures 6.1.3-64 to 6.1.3-70) was a 2-in. hot-leg break. Steam generation started at about [ ]^{a,b,c} seconds and the oscillations started at about [ ]^{a,b,c} seconds when the steam generation rate was about [ ]^{a,b,c} lbm/sec. The average period of oscillation was [ ]^{a,b,c} seconds in the time interval [ ]^{a,b,c} seconds, and the period is reducing during the transient: between [ ] seconds is [ ]^{a,b,c} seconds and between [ ]^{a,b,c} seconds the period is [ ]^{a,b,c} seconds. The reason that the oscillation period is smaller in SB15 than in the other tests is because there is an additional flow path through the hot-leg break so the hot-leg nozzle can uncover faster than in the other tests.

6.1.3.3.2.4 Subset 4 - SB09, SB10 - Cold Leg/Core Makeup Tank Balance Line Break

Tests SB09 and SB10 (Figures 6.1.3-23 to 6.1.3-42) were the 2-in. cold-leg balance line break and DEG cold-leg balance line break. The system response was very similar during the oscillations. Steam started to generate at about [ ]^{a,b,c} seconds in SB09 and [ ]^{a,b,c} seconds in SB10. The oscillations started at about [ ]^{a,b,c} seconds in SB09 and [ ]^{a,b,c} seconds in SB10 when the steam generation rate was [ ]^{a,b,c} lbm/sec. The average oscillation period is [ ]^{a,b,c} seconds in

SB09 and [ ]^{a,b,c} seconds in SB10. The steam generation rate at the onset of the oscillations was higher in Tests SB09 and SB10 ([ ]^{a,b,c} lbm/sec.) than for the tests of group 1 ([ ]^{a,b,c} lbm/sec., SB18, SB19, and SB23). The difference is that the tests in group-1 are bottom cold-leg breaks while the tests of group-4 are top cold-leg breaks. In this case, some steam was vented by the break, and downcomer pressurization was delayed. In both cases, the downcomer collapsed liquid level was around the top of the cold-leg nozzles in both SB09 and SB10: since a break is at the top of the cold leg, some steam was collected at the top of the cold leg and was discharged by the break in both SB09 and SB10.

6.1.3.3.2.5 Subset 5 - SB14 - Inadvertent ADS opening

In this transient (Figures 6.1.3-57 to 6.1.3-63), the observed oscillations time interval was very short and includes only [ ]^{a,b,c} cycles. There was not time enough to establish a clean periodic behavior as shown in the other tests. This transient was on the borderline of the conditions required to establish the oscillations.

Steam generation started at about [ ]^{a,b,c} seconds. At about [ ]^{a,b,c} seconds, steam generation reached [ ]^{a,b,c} lbm/sec. and just before [ ]^{a,b,c} seconds, the oscillations started. The injection temperature was higher than in the other transients because the IRWST was warmed-up for a longer time by the ADS 1-2-3 discharge. The liquid temperature at the top of the downcomer was higher, thus the condensation in the downcomer was reduced and as a result, the oscillation time period which is driven by the downcomer condensation lasted for a shorter period of time. At about [ ]^{a,b,c} seconds, the downcomer top reached saturation and the collapsed liquid level in the downcomer dropped below the cold-leg nozzles elevation and the oscillations ceased.

6.1.3.4 Expected Effect in AP600 Facility

The oscillations observed in the OSU AP600 scaled test facility during IRWST injection may also occur in the AP600 facility. Timing of the initiation and termination of these oscillations may be different in the AP600 plant than was observed in the tests, and will depend on the following factors:

- Temperature and flow rate from the IRWST, as it affects the condensation rate of steam flowing to the downcomer compared to the production rate in the core
- Hydraulic flow characteristics of the steam path from the upper head to the downcomer, which determine the steam flow rate
- Liquid level in the downcomer relative to the cold leg, which will determine when the oscillations begin

Since the pressures in AP600 plant and the OSU AP600 scaled test facility will be close to atmospheric pressure during IRWST injection, there is no pressure scaling necessary for the condensation process.

The oscillation period in the AP600 plant can be estimated as follows. The oscillation period, τ, is proportional to the time that is required to remove the mass, M, from the system in order to uncover the hot leg. That is:

$$\tau \propto \frac{M}{\dot{m}} \qquad 6.1.3\text{-}75$$

where m is the flow rate for removing the mass. The flow rate can be expressed as:

$$\Delta P = \frac{K\dot{m}^2}{2g_c\rho A^2} \quad \text{or} \quad \dot{m} = A\sqrt{\frac{2g_c\rho\Delta P}{K}} \qquad 6.1.3\text{-}76$$

where:

K	=	loss coefficient*
$\dot{m}$	=	mass flow rate, lbm/sec.
ρ	=	density, lbm/ft.^{3}
A	=	area, ft.^{2}
ΔP	=	pressure drop, psi

Mass can be expressed as $M = V\rho$, where V is the volume of the fluid to be removed and ρ is the fluid density. Substituting equation 6.1.3-76 in 6.1.3-75 gives:

$$\begin{aligned} \tau &\propto \frac{M}{A}\sqrt{\frac{K}{2g_c\rho\Delta P}} \\ &\propto V\frac{\rho}{A}\sqrt{\frac{K}{2g_c\rho\Delta P}} \\ &\propto L\rho\sqrt{\frac{K}{2g_c\rho\Delta P}} \end{aligned} \qquad 6.1.3\text{-}77$$

where L = V/A is the geometric length. Since the pressure in both the AP600 and OSU tests will be close to atmospheric pressure, density is the same in both cases. Therefore, equation 6.1.3-77 can be written as:

$$\tau \propto L \sqrt{\frac{K}{\Delta P}} \qquad 6.1.3\text{-}78$$

The pressure drop ΔP is the difference between the atmospheric pressure (exit of the ADS-4 line) and the pressure in the vessel. The pressure in the vessel is proportional to the steam generation rate and is inversely proportional to the steam volume in the upper plenum and upper head, V_{upper}. Furthermore, the steam generation rate is proportional to the power, assuming that the core inlet temperature and the velocity are the same for the AP600 plant and OSU tests. That is:

$$\Delta P \propto \frac{\text{Steam Generation Rate}}{V_{upper}} \propto \frac{\text{Power}}{V_{upper}} \qquad 6.1.3\text{-}79$$

where V_{upper} is the volume of the upper head/plenum.

The scalings of the OSU tests are as follows:

Parameter	Scaling Ratio
K	[ ]^{a,b,c}
L	[ ]^{a,b,c}
power	[ ]^{a,b,c}
V_{upper}	[ ]^{a,b,c}

Therefore, from equation 6.1.3-79

$$\Delta P_{AP600} = \left[\quad \right]^{a,b,c} \Delta P_{test} \approx \left[\quad \right]^{a,b,c} \Delta P_{test} \qquad 6.1.3\text{-}80$$

and from equation 6.1.3-80

$$\tau_{AP600} = \left[\quad \right]^{a,b,c} = [\ ]^{a,b,c} \tau_{test} \qquad 6.1.3\text{-}81$$

That is, the oscillation periods in the AP600 will be 5.7 times longer than those in the OSU tests, i.e., about [ ]^{a,b,c} minutes, relatively slow and stable.

The oscillations will not become unstable in the AP600, because the pressure in the vessel cannot increase beyond the value where the hot leg becomes uncovered and the level oscillation amplitude is limited by the distance between the hot leg and the highest elevation the mixture level can attain. Furthermore, since the oscillations are the forced oscillations with oscillation period of order of 100 seconds, which is much larger than natural oscillation period of order of 2 seconds, the oscillations will not be amplified by the resonance. The core remains covered during the oscillations for the following reasons. When the mixture level drops below the hot leg, steam vents through the hot leg and the vessel depressurizes. As the vessel depressurizes, the DVI injection rate increases and the hot-leg flow rate decreases. When the injection rate becomes larger than the hot-leg flow rate, the mixture level in the upper plenum rises and the hot leg will be covered. Therefore, the mixture level oscillates around the hot leg and keeps the cold leg covered during the oscillations.

6.1.3.5 Conclusions

Pressure, level and flow rate periodic oscillations have been observed in several OSU test during the last period of the IRWST injection phase. Five mechanisms have been postulated to explain the oscillation process and are reported in Subsection 6.1.3.2. The fourth mechanism is consistent with all the tests. In Mechanism 4, the onset of the oscillations requires the following plant conditions:

1. Steam generation in the core

2. Steam condensation in downcomer

3. Upper plenum liquid level covering the hot-leg nozzle

4. Downcomer liquid level covering the cold-leg nozzles.

As soon as the oscillations are established, the driving force is the plugging and unplugging of the steam vent path, which is typically ADS-4. In this process, the liquid mass injected in the system, is at first accumulated when the steam vent path to the ADS-4 is open, then discharged when the steam vent path is closed. The product of the oscillation amplitude (in terms of mass) and oscillation frequency is equal to the injection flow rate. The greater the steam condensation in the downcomer condensation, the lower the frequency and the higher the amplitude.

The SB01 oscillations have been analyzed in detail and the postulated Mechanism 4 is supported by the calculations. All other tests have been analyzed briefly in comparison with the reference transient SB01. The oscillation period is about [ ]^{a,b,c} seconds in all the tests with the exception of SB01 where it is [ ]^{a,b,c} seconds and SB15 where it is [ ]^{a,b,c} seconds. The steam generation rate at the onset of the oscillations is about [ ]^{a,b,c} lbm/sec. for most of the tests (SB01, SB14, SB15, SB18

and SB23). In SB19, it is lower ([ ]^{a,b,c} lbm/sec.) due to the break backpressure, which is holding the pressure in the downcomer while in SB09 and SB10 it is higher ([ ]^{a,b,c} lbm/sec.) because some steam is vented through the break at the top of the cold leg and this is reducing the pressure in downcomer. In SB13, a very high value ([ ]^{a,b,c} lbm/sec.) of steam generation rate is evaluated before the onset of the oscillations. This can be explained only if some steam is vented by the break in the DVI line or from the CMTs through the balance but there is no evidence of this in the SB13 data.

TABLE 6.1.3-1
SUMMARY OF FLOW OSCILLATION DATA

Test No.	Break Type	Oscil. Start Time (sec.)	Oscil. End Time (sec.)	Core Steam Generation at Start Time (lbm/sec.)	IRWST Level at Start Time (in.)	IRWST Level at End Time (in.)	Oscil. Period (sec.)
SB01	2-in. CL	9400	13000	0.03	37	22	135
SB06	4-in. CL	2200	10700	0.06	75	20	111
SB09	2-in. CL/CMT Balance Line	10200	13000	0.05	33	23	125
SB10	DEG CL/CMT Balance Line	10000	12600	0.05	32	23	119
SB12	DEG DVI Line (No Oscillations)	N/A	N/A	N/A	N/A	N/A	N/A
SB13	2-in. DVI Line	7600	9600	0.08	44	35	117
SB14	Inadvertent ADS Opening	8000	8300	0.03	42	38	N/A (1)
SB15	2-in. HL	10000	12600	0.05	32	24	111
SB18	2-in. CL	8800	13200	0.03	40	23	120
SB19	2-in. CL with Backpressure	8500	12600	0.02	38	23	114
SB21	4-in Bottom & 4-in. Top CL	6200	9500	0.0 (2)	38	22	133
SB23	0.5-in. CL	9600	12000	0.03	46	36	120

Note 1 - For SB14 oscillations due to hypothesis 4 occurred only in two cycles as is evident from Figure 6.1.3-62 which shows the hot leg was uncovered twice at 7975 seconds and at 8065 seconds.

Note 2 - The steam generation rate is higher than zero, because there is uncertainty in calculating the steam generation rate due to the uncertainty in computing the core inlet flow.

TABLE 6.1.3-2 OSU TEST ANALYSIS PLOT PACKAGE FOR SECTION 6.1.3				
Plot No.	**Component**	**Variables**	**Units**	**Description**
1	RV	N/A	N/A	Reactor vessel/flow paths
2	RV	CLDP-113	in.	Compensated level, reactor vessel upper plenum SB01
3	ADS-4 Lines	N/A	N/A	Flow pattern map
4	ADS 4-2	ADS42VR FVM-602	lbm/sec. CFM	Steam flow in ADS-4-2, SB18
5	ADS 4-2	ADS42VR FVM-602	lbm/sec. CFM	Steam flow in ADS-4-2, SB18, expanded scale
6	RV	SC-105 SC-101 SC-106 SC-102	°F	Fluid Temperature at the top of the cold leg nozzles - SB01
7	N/A	N/A	N/A	Schematics of the idealized flow parameter behavior during flow oscillations in OSU test
8	CMT	TF-524 TF-528 TF-540 TF-542	°F	Top CMT-2 Temperature SB01
9	DVIs	TF-115 TF-114	°F	DVI nozzles and DC fluid temperature - SB01
10	DVIs	WWTIRWI3 WWTIRWI4	lbm/sec.	DVIs Injection flowrates SB01
11	RV	RPVASOUT	lbm/sec.	Steam generation rate SB01
12	RV	CLDP-113	in.	Upper Plenum collapsed liquid level SB01
13	ADS-4	ADS41TMR ADS42TMR	in.	ADS stage 4 total mass flowrate - SB01
14	ADS-4 Lines	TF-609	°F	ADS 4-1 Line temperature SB01
15	RV	PT-107	psig	Upper Plenum pressure SB01 (time window)
16	RV	CLDP-113	in.	Upper Plenum collapsed liquid level (time window) - SB01
17	DVIs	WWTIRWI3+ WWTIRWI4	lbm/sec.	Total Injection flowrate (time window) SB01

TABLE 6.1.3-2 (Continued) OSU TEST ANALYSIS PLOT PACKAGE FOR SECTION 6.1.3				
Plot No.	**Component**	**Variables**	**Units**	**Description**
18	ADS-4	ADS41TMR+ ADS42TMR	lbm/sec.	Total ADS-4 mass flowrate (time window) SB01
19	RV	RPVASOUT	lbm/sec.	Steam generation rate (time window) SB01
20	RV	DP-130	in-H_20	DP across UH bypass holes (time window)SB01
21	N/A	N/A	N/A	Scheme of the quasi-steady state before the oscillations begin
22	DVIs	WWTIRWI3 WWTIRWI4	lbm/sec.	Injection flowrates (time window) SB06
23	DVIs	TF-115 TF-114	°F	DVI nozzles temperature (time window) SB06
24	RV	TF-167	°F	Downcomer fluid temp. at the top (time window) SB06
25	ADS 4	ADS41TMR+ ADS42TMR	lbm/sec.	Total ADS-4 mass flowrate (time window) SB06
26	RV	RPVASOU2	lbm/sec.	Steam generation rate (time window) SB06
27	RV	CLDP-113	in.	Upper Plenum collapsed liquid level (time window) SB06
28	RV	PT-107	psig	Upper Head pressure (time window) SB06
29	DVIs	WWTIRWI3 WWTIRWI4	lbm/sec.	Injection flowrates (time window) SB09
30	DVIs	TF-115 TF-114	°F	DVI nozzles temperature (time window) SB09
31	RV	TF-167	°F	Downcomer fluid temp. at the top (time window) SB09
32	ADS 4	ADS41TMR+ ADS42TMR	lbm/sec.	Total ADS-4 mass flowrate (time window) SB09
33	RV	RPVASOUT	lbm/sec.	Steam generation rate (time window) SB09
34	RV	CLDP-113	in.	Upper Plenum collapsed liquid level (time window) SB09
35	RV	PT-107	psig	Upper Head pressure (time window) SB09
36	DVIs	WWTIRWI3 WWTIRWI4	lbm/sec.	Injection flowrates (time window) SB10

TABLE 6.1.3-2 (Continued) OSU TEST ANALYSIS PLOT PACKAGE FOR SECTION 6.1.3				
Plot No.	**Component**	**Variables**	**Units**	**Description**
37	DVIs	TF-115 TF-114	°F	DVI nozzles temperature (time window) SB10
38	RV	TF-167	°F	Downcomer fluid temp. at the top (time window) SB10
39	ADS 4	ADS41TMR+ ADS42TMR	lbm/sec.	Total ADS-4 mass flowrate (time window) SB10
40	RV	RPVASOUT	lbm/sec.	Steam generation rate (time window) SB10
41	RV	CLDP-113	in.	Upper Plenum collapsed liquid level (time window) SB10
42	RV	PT-107	psig	Upper Head pressure (time window) SB10
43	DVIs	WWTIRWI3 WWTIRWI4	lbm/sec.	Injection flowrates (time window) SB12
44	DVIs	TF-115 TF-114	°F	DVI nozzles temperature (time window) SB12
45	RV	TF-167	°F	Downcomer fluid temp. at the top (time window) SB12
46	ADS 4	ADS41TMR+ ADS42TMR	lbm/sec.	Total ADS-4 mass flowrate (time window) SB12
47	RV	RPVASOUT	lbm/sec.	Steam generation rate (time window) SB12
48	RV	CLDP-113	in.	Upper Plenum collapsed liquid level (time window) SB12
49	RV	PT-107	psig	Upper Head pressure (time window) SB12
50	DVIs	WWTIRWI3 WWTIRWI4	lbm/sec.	Injection flowrates (time window) SB13
51	DVIs	TF-115 TF-114	°F	DVI nozzles temperature (time window) SB13
52	RV	TF-167	°F	Downcomer fluid temp. at the top (time window) SB13
53	ADS 4	ADS41TMR+ ADS42TMR	lbm/sec.	Total ADS-4 mass flowrate (time window) SB13
54	RV	RPVASOUT	lbm/sec.	Steam generation rate (time window) SB13
55	RV	CLDP-113	in.	Upper Plenum collapsed liquid level (time window) SB13

TABLE 6.1.3-2 (Continued) OSU TEST ANALYSIS PLOT PACKAGE FOR SECTION 6.1.3				
Plot No.	**Component**	**Variables**	**Units**	**Description**
56	RV	PT-107	psig	Upper Head pressure (time window) SB13
57	DVIs	WWTIRWI3 WWTIRWI4	lbm/sec.	Injection flowrates (time window) SB14
58	DVIs	TF-115 TF-114	°F	DVI nozzles temperature (time window) SB14
59	RV	TF-167	°F	Downcomer fluid temp. at the top (time window) SB14
60	ADS 4	ADS41TMR+ ADS42TMR	lbm/sec.	Total ADS-4 mass flowrate (time window) SB14
61	RV	RPVASOUT	lbm/sec.	Steam generation rate (time window) SB14
62	RV	CLDP-113	in.	Upper Plenum collapsed liquid level (time window) SB14
63	RV	PT-107	psig	Upper Head pressure (time window) SB14
64	DVIs	WWTIRWI3 WWTIRWI4	lbm/sec.	Injection flowrates (time window) SB15
65	DVIs	TF-115 TF-114	°F	DVI nozzles temperature (time window) SB15
66	RV	TF-167	°F	Downcomer fluid temp. at the top (time window) SB15
67	ADS 4	ADS41TMR+ ADS42TMR	lbm/sec.	Total ADS-4 mass flowrate (time window) SB15
68	RV	RPVASOUT	lbm/sec.	Steam generation rate (time window) SB15
69	RV	CLDP-113	in.	Upper Plenum collapsed liquid level (time window) SB15
70	RV	PT-107	psig	Upper Head pressure (time window) SB15
71	DVIs	WWTIRWI3 WWTIRWI4	lbm/sec.	Injection flowrates (time window) SB18
72	DVIs	TF-115 TF-114	°F	DVI nozzles temperature (time window) SB18
73	RV	TF-167	°F	Downcomer fluid temp. at the top (time window) SB18
74	ADS 4	ADS41TMR+ ADS42TMR	lbm/sec.	Total ADS-4 mass flowrate (time window) SB18

TABLE 6.1.3-2 (Continued) OSU TEST ANALYSIS PLOT PACKAGE FOR SECTION 6.1.3				
Plot No.	**Component**	**Variables**	**Units**	**Description**
75	RV	RPVASOUT	lbm/sec.	Steam generation rate (time window) SB18
76	RV	CLDP-113	in.	Upper Plenum collapsed liquid level (time window) SB18
77	RV	PT-107	psig	Upper Head pressure (time window) SB18
78	DVIs	WWTIRWI3 WWTIRWI4	lbm/sec.	Injection flowrates (time window) SB19
79	DVIs	TF-115 TF-114	°F	DVI nozzles temperature (time window) SB19
80	RV	TF-167	°F	Downcomer fluid temp. at the top (time window) SB19
81	ADS 4	ADS41TMR+ ADS42TMR	lbm/sec.	Total ADS-4 mass flowrate (time window) SB19
82	RV	RPVASOUT	lbm/sec.	Steam generation rate (time window) SB19
83	RV	CLDP-113	in.	Upper Plenum collapsed liquid level (time window) SB19
84	RV	PT-107	psig	Upper Head pressure (time window) SB19
85	DVIs	WWTIRWI3 WWTIRWI4	lbm/sec.	Injection flowrates (time window) SB21
86	DVIs	TF-115 TF-114	°F	DVI nozzles temperature (time window) SB21
87	RV	TF-167	°F	Downcomer fluid temp. at the top (time window) SB21
88	ADS 4	ADS41TMR+ ADS42TMR	lbm/sec.	Total ADS-4 mass flowrate (time window) SB21
89	RV	RPVASOUT	lbm/sec.	Steam generation rate (time window) SB21
90	RV	CLDP-127	in.	Total Vessel collapsed liquid level (time window) SB21 (note 1)
91	RV	CLDP-113	in.	Upper Plenum collapsed liquid level (time window) SB21
93	BREAK Line	BRKSTMR	lbm/sec.	Break Mass Flowrate time window) SB21
94	DVIs	WWTIRWI3 WWTIRWI4	lbm/sec.	Injection flowrates (time window) SB23

TABLE 6.1.3-2 (Continued) OSU TEST ANALYSIS PLOT PACKAGE FOR SECTION 6.1.3				
Plot No.	**Component**	**Variables**	**Units**	**Description**
95	DVIs	TF-115 TF-114	°F	DVI nozzles temperature (time window) SB23
96	RV	TF-167	°F	Downcomer fluid temp. at the top (time window) SB23
97	ADS 4	ADS41TMR+ ADS42TMR	lbm/sec.	Total ADS-4 mass flowrate (time window) SB23
98	RV	RPVASOUT	lbm/sec.	Steam generation rate (time window) SB23
99	RV	CLDP-113	in.	Upper Plenum collapsed liquid level (time window) SB23
100	RV	PT-107	psig	Upper Head pressure (time window) SB23

Note 1 - Figure 6.1.3-90, SB21 vessel collapsed liquid level (CLDP-127) does not represent the true collapsed liquid level, because of the presence of the lower core plate, the upper core plate and the upper support plate, which introduce significant pressure drops. Therefore the collapsed liquid level overestimates the vessel level.

FIGURES 6.1.3-1, 6.1.3-3, 6.1.3-7 AND 6.1.3-21 ARE NOT PROPRIETARY

THE REMAINING FIGURES LISTED IN TABLE 6.1.3-2 ARE PROPRIETARY, AND ARE NOT INCLUDED IN THIS NONPROPRIETARY DOCUMENT

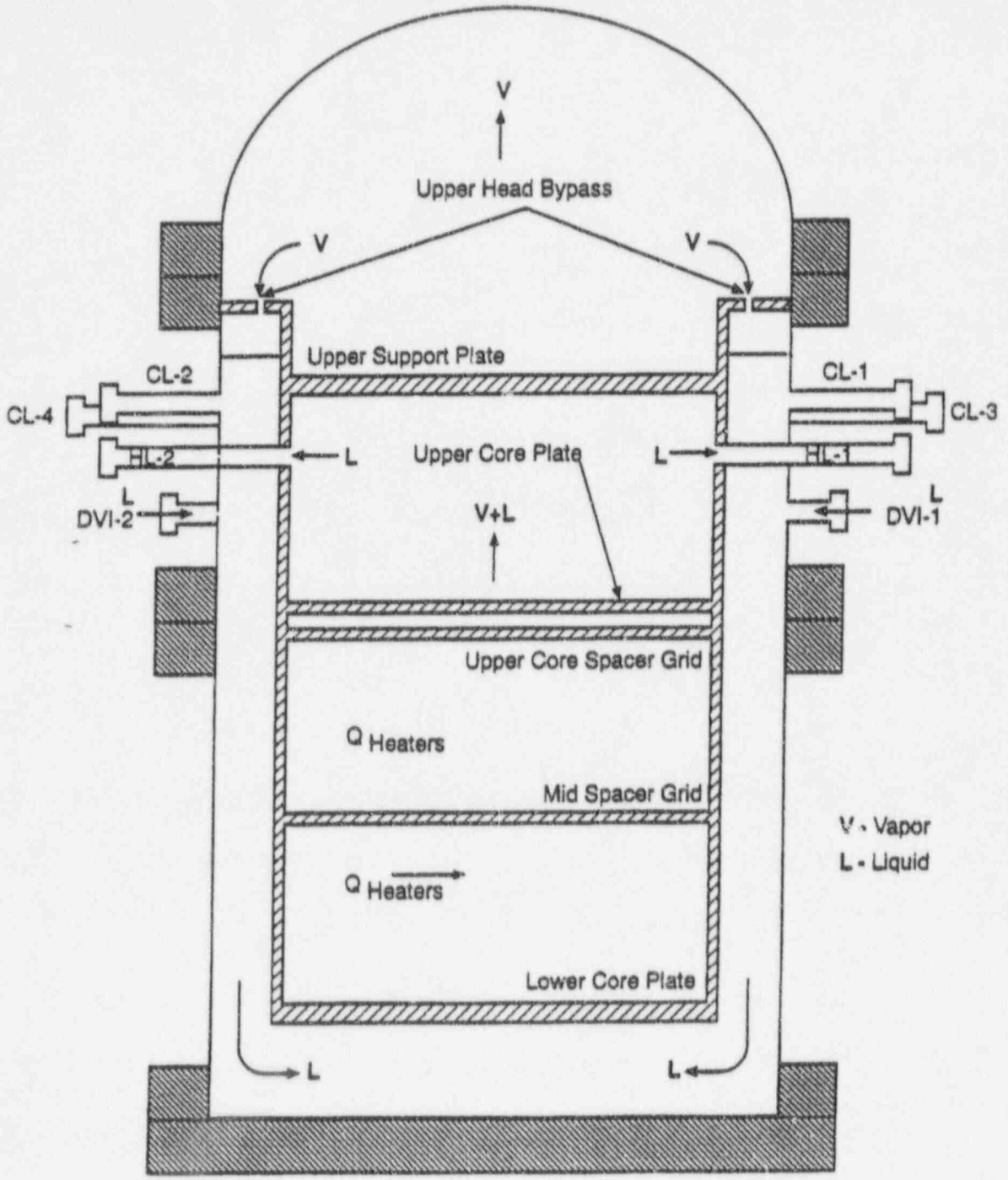

Figure 6.1.3-1 Reactor Flow Paths During IRWST Injection

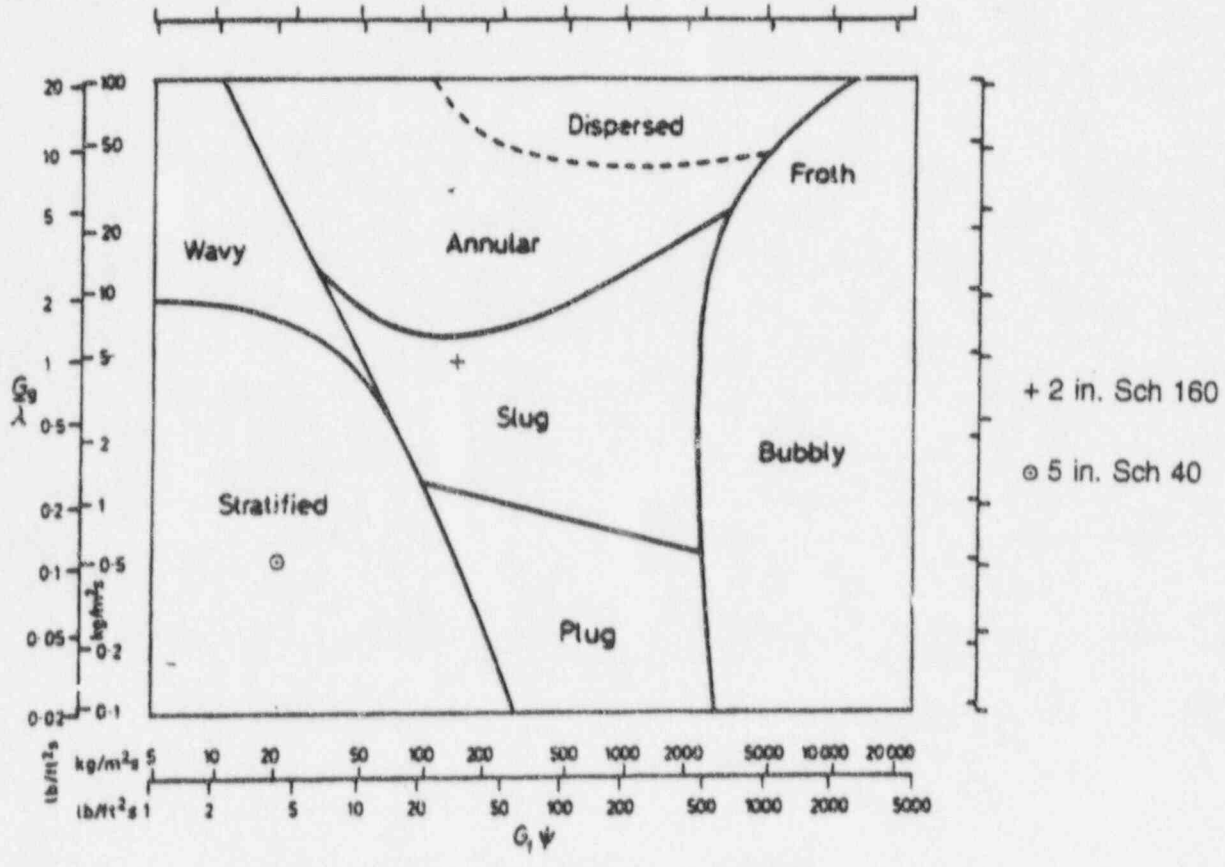

Flow pattern map for horizontal flow (Baker 1954).

Figure 6.1.3-3 Flow Regimes in ADS-4 Lines Matrix Test SB18

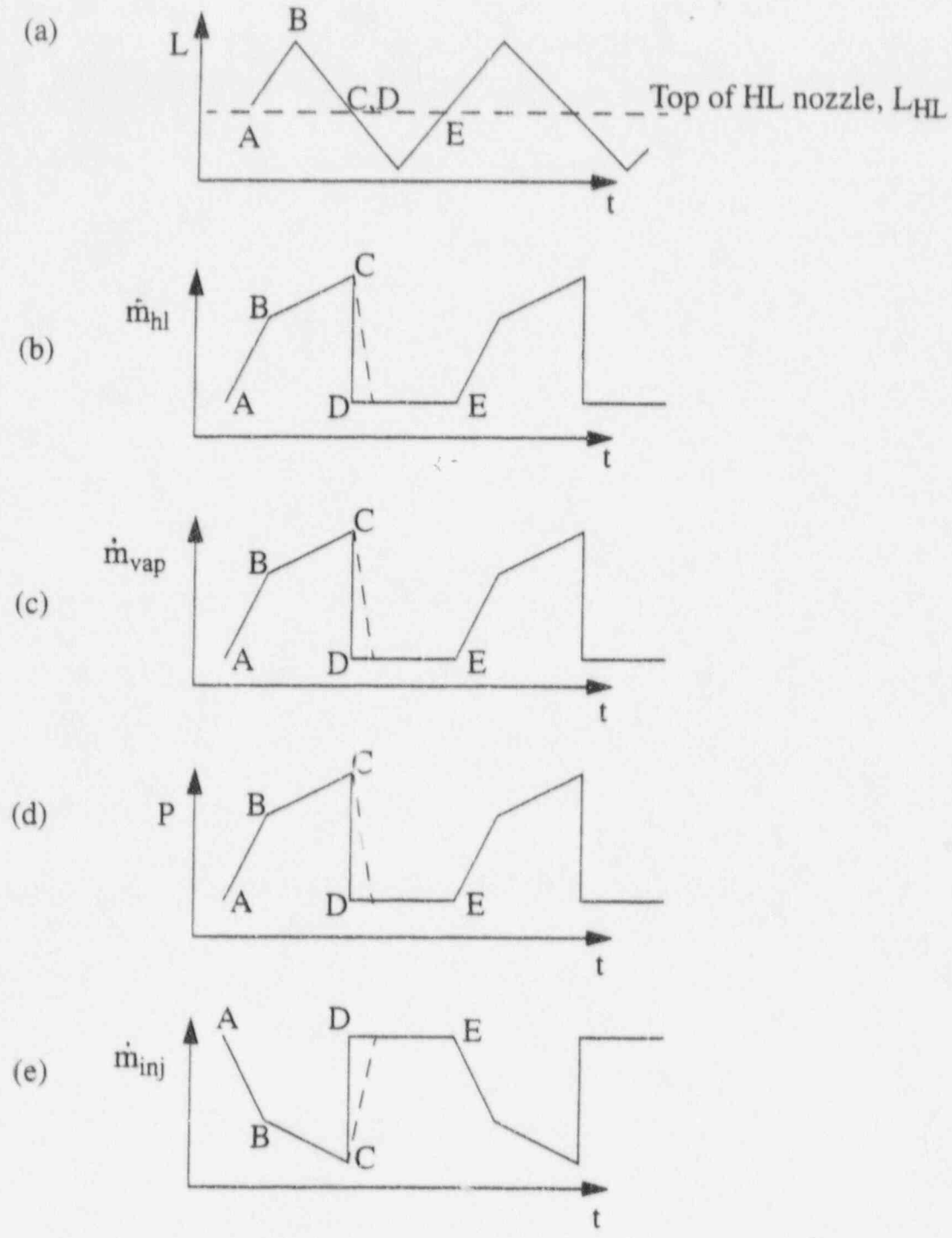

Figure 6.1.3-7 - Schematics of the idealized flow parameters behaviours during the flow oscillations in OSU tests.

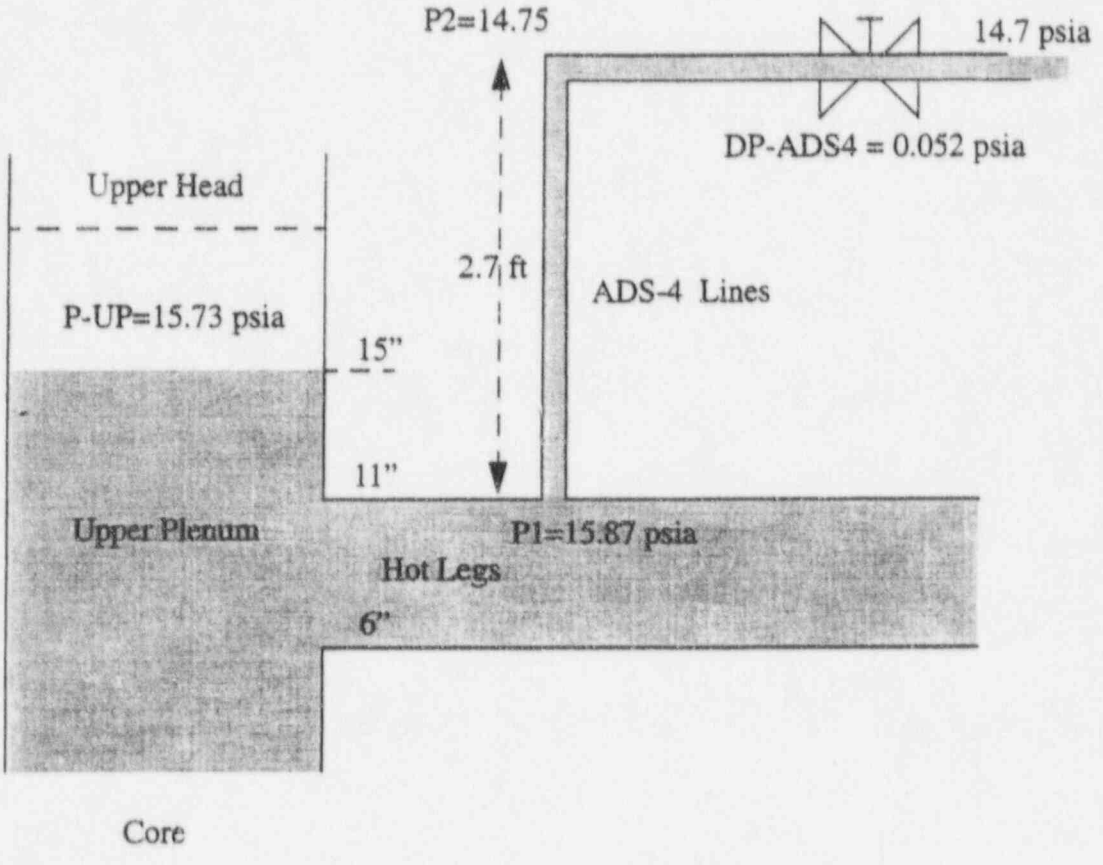

Figure 6.1.3-21 - Quasi-steady state before the oscillations start.

6.1.4 Effects of Accumulator Nitrogen

The following discussion describes the movement of nitrogen from the accumulators into and out of the primary system of the OSU test facility during Test SB01. Accumulator nitrogen is discharged into the DVI lines, and could possibly either remain in the primary system or exit through the break and/or the ADS.

Each of the two accumulators was pre-charged with approximately [ ]^{a,b,c} lbm of nitrogen at approximately [ ]^{a,b,c} psia (Table 6.1.4-1). When the primary system pressure decreased below the accumulator gas pressure, the water stored in the accumulator was injected into the primary system. When the water was totally ejected, the nitrogen gas volume continued to expand, injecting approximately [ ]^{a,b,c} lbm of nitrogen from each accumulator into the primary system; this is equivalent to approximately [ ]^{a,b,c} ft.^{3} of nitrogen at standard conditions and approximately [ ]^{a,b,c} ft.^{3} at the point where the nitrogen is injected into the system for each accumulator. Most of the nitrogen was released immediately following accumulator draindown, but some nitrogen continued to be released as the system depressurized.

Plots describing the propagation of nitrogen are summarized in Table 6.1.4-2.

Review of the pressure curve for Test SB01 showed that there was a change in slope at [ ]^{a,b,c} seconds for ACC-1 and at [ ]^{a,b,c} seconds for ACC-2 (Figure 6.1.4-1). The change in the rate of pressure decrease indicated that nitrogen injection began, this was confirmed by changes in discharge temperatures TF-401 and TF-402 (Figure 6.1.4-1). The change in pressure occurred when the accumulator pressures reached approximately [ ]^{a,b,c} psia, which was the equivalent pressure for the nitrogen volume expanded to the full accumulator size. The pressure in both accumulators continued to decrease as system pressure decreased. Small changes occurred in the accumulator discharge temperature as the nitrogen was released.

The nitrogen was initially released into the downcomer from the DVI lines. The collapsed level in the downcomer just prior to nitrogen injection was between the DVI and the cold leg (Figure 6.1.4-2), with the cold legs effectively drained (Figure 6.1.4-3). Nitrogen was then released into the downcomer where it most likely bubbled out of the liquid to the top of the downcomer. No positive pressure differential existed across the downcomer flow holes that connect to the upper plenum; therefore, nitrogen flow into the upper plenum or head was unlikely. Collapsed level indications in the downcomer showed the level at about [ ]^{a,b,c} in. and the level of the DVI lines was [ ]^{a,b,c} in. Review of the cold-leg water volume indicated that the cold leg was essentially empty between [ ]^{a,b,c} seconds. Therefore, nitrogen could distribute into the test facility cold legs. The indicated flow of liquid and vapor through the break separator after nitrogen injection was essentially zero; however, if the flow rates were below the minimum measurable flow rate for the flow meter in the break vapor exhaust, small nitrogen gas flow rates may not have been measured. Thus, some nitrogen may have exited through the cold-leg break without being measured.

For this test, the SG tubes effectively drained after [ ]^{a,b,c} seconds, and the fluid on the primary side became superheated at the secondary-side saturation temperature, thereby preventing natural convection flow in the primary system. This assures that steam or nitrogen flow into the hot legs and the reactor vessel through the cold legs is insignificant.

The CMT balance lines appeared to be partially filled for times greater than [ ]^{a,b,c} seconds (Figure 6.1.4-4). Temperatures in the CMT vapor space generally remained above the saturation temperature of the CMT pressure over the first [ ]^{a,b,c} seconds (Figure 6.1.4-5), and thus provided no indication of a nitrogen partial pressure. If there were a partial pressure of nitrogen present, the saturation temperature for the water vapor would be reduced from that corresponding to the total pressure of the CMT.

Nitrogen can enter the reactor upper head through the flow holes between the downcomer and the reactor head. But as indicated previously, the differential pressure did not show any evidence of flow from the downcomer into the reactor head. In addition, the temperatures in the upper plenum and upper head stayed at superheated steam values and, as in the CMT, offer no evidence of the presence of any nitrogen. The quantity of nitrogen (approximately [ ]^{a,b,c} ft.^{3} at [ ]^{a,b,c} psia from each accumulator) represents approximately [ ]^{a,b,c} ft. in height of the reactor vessel. The reactor levels do show a combined level decrease of approximately [ ]^{a,b,c} in. between [ ]^{a,b,c} seconds (sum of the changes in the three collapsed levels, core, upper plenum, and upper head, Figures 6.1.4-6, 6.1.4-7, and 6.1.4-8). In general, the collapsed level in the upper plenum (Figure 6.1.4-7) remained above the level of the hot leg until after [ ]^{a,b,c} seconds so that access of nitrogen to the hot leg would be restricted to times greater than [ ]^{a,b,c} seconds.

If nitrogen enters the hot leg, it could flow through the pressurizer to the ADS, flow into the PRHR or exit ADS-4. It is likely that any nitrogen entering the hot leg would either be trapped in the PRHR or exit through ADS-4.

The PRHR flow ceases prior to accumulator nitrogen injection, so there is no conclusive evidence to indicate that nitrogen contributes to the PRHR shutdown.

There are no discernable effects of nitrogen during the LTC portion of the test.

Evaluation of the other LOCA tests yielded similar indications of nitrogen behavior as were observed in Test SB01. Thus, the release of accumulator nitrogen gas had little, if any effect on the tests evaluated.

TABLE 6.1.4-1 SUMMARY OF ACCUMULATOR BEHAVIOR FOR TEST SB01		
	[	a,b,c]
Initial Pressure		
Initial Temperature		
Inventory Water		
Inventory Nitrogen		
Start Discharge		
Final Pressure		
Final Temperature		
Final Inventory Water		
Final Inventory Nitrogen		
Mass Nitrogen Discharged	]	

TABLE 6.1.4-2 OSU TEST ANALYSIS PLOT PACKAGE FOR SUBSECTION 6.1.4	
Plot No.	**Description**
1	Accumulator Pressure and Temperature, SB01
2	Downcomer Level, SB01
3	Cold Leg Liquid Mass, SB01
4	CMT Cold Leg Balance Line Level, SB01
5	CMT Temperatures, SB01
6	Core Liquid Level, SB01
7	Upper Plenum Liquid Level, SB01
8	Upper Head Liquid Level, SB01

THE FIGURES LISTED IN TABLE 6.1.4-2
ARE NOT INCLUDED IN THIS NONPROPRIETARY DOCUMENT

6.2 Data Evaluation

The data evaluation presented in this section considers the energy input to the system by the core simulation, the overall system fluid mass balance, and the overall energy balance.

6.2.1 Core Energy

Two general methods for evaluating core energy and steam production are defined in Section 4.11. The effectiveness of these methods is evaluated in this section for a range of test conditions. To provide additional insight into the reliability of these methods, a simplified DVI flow method is also included.

The three methods are:

1. Tsat Method

   The saturation line is determined by finding the intersection between axial curves of local saturation temperature and fluid temperature. Steam production is then determined from the power above the saturation line.

2. DVI Flow Method

   An enthalpy rise calculation, based on core power, lower plenum temperature, and liquid flow rate into the core, is used to determine core outlet mixture enthalpy, steam production, and the saturation line. This method approximates liquid flow rate into the core using the combination of metered DVI and break flows. This flow rate is calculated as:

$$\dot{M}_{CORE} = \dot{M}_{DVI} - \dot{M}_{BRKSEP} \qquad (6.2.1\text{-}1)$$

   For the tests investigated in this section, the break separator is connected to the cold leg. Therefore, this approach uses the appropriate approximation for flow to the core. For tests with hot-leg breaks and tests without breaks, break flow from the cold leg and the break flow in the above equation are zero.

   This method neglects the rate of mass change in the lower plenum and downcomer. The general applicability and limitations of this assumption are investigated in this section.

3. Simplified DVI Flow Method

   This method simplifies the DVI flow method by including only DVI line flow. Liquid flow into the core is approximated as:

$$\dot{M}_{CORE} \approx \dot{M}_{DVI} \qquad (6.2.1\text{-}2)$$

   For the tests investigated in this section, this method generally overestimates flow to the core since it excludes the break flow. For tests with hot-leg breaks and tests without breaks, this method is the same as the DVI flow method. These results are included to provide insight into the sensitivity to flow rate for the DVI flow method.

Section 4.11 identifies issues dealing with data uncertainty and limitations of the calculational methods. This section investigates these and other issues and demonstrates the viability of the chosen methods. Key uncertainties and limitations discussed include:

- Uncertainty in the measurement of core pressure at low pressures, which is investigated in Subsection 6.2.1.2

- Mass effects, the use of metered flow as an approximation of flow into the core and the importance of mass changes in the lower plenum and downcomer, which are investigated in Subsection 6.2.1.3

Plots are provided in this section to compare the various methods and identify key issues. To enhance usability for this intended purpose, all plots in this section are post-analysis smoothed using the algorithms and constants of Section 4.20. This smoothing has the effect of eliminating the very high frequency oscillations (noise) while keeping the general plot shape and amplitude required to support the comparisons of this section.

6.2.1.1 Matrix Test Results

A range of cold-leg breaks and two other break locations were selected:

- Test SB23, 0.5-in. cold-leg break
- Test SB01, 2-in. cold-leg break
- Test SB06, 4-in. cold-leg break
- Test SB13, 2-in. DVI line break
- Test SB09, 2-in. CMT cold-leg balance line break

Figures 6.2.1-1 through 6.2.1-20 provide plots of smoothed results for the above tests and include:

- Calculated core steam production based on each of the three methods
- Calculated saturation line based on each of the three methods
- Core inlet flow for the two DVI methods
- Comparison of the measured core outlet temperature to the predicted temperature for the DVI flow method. Measured temperatures T08RPV and T09RFV are just below and above the top of the core, respectively.

Results for SB23 are provided in Figures 6.2.1-1 through 6.2.1-4. The three methods are consistent in the prediction of zero steam production for the period bounding [ ]^{a,b,c} seconds. The expected problems in predicting steam production at the start of the test, which are due to the large flows, depressurization, and draining of components, are evident for the three methods. After [ ]^{a,b,c} seconds, and during LTC, the DVI line flow methods predict greater steam production than the Tsat method. The small difference in the two DVI methods during LTC is due to the small difference in core inlet flow resulting from the small break area and minimal break flow. The saturation lines are consistent with the steam production plots. The DVI flow method generally predicts core outlet temperature within [ ]^{a,b,c} °F. The spikes in calculated core outlet temperatures are attributed to downward spikes in the calculated core inlet flow. These spikes are the result of the core inlet flow approximation and are discussed in Subsection 6.2.1.3.

Results for SB01 are provided in Figures 6.2.1-5 through 6.2.1-8. The observations for SB23 generally also apply to this test. Spikes in the calculated core outlet temperature were not observed. The rise in calculated core outlet temperature at [ ]^{a,b,c} seconds for the DVI flow method suggests that the start of calculated steam production is somewhat early.

Results for SB06 are provided in Figures 6.2.1-9 through 6.2.1-12. This test had the largest break area evaluated in this subsection. Thus, trends noted for the simplified DVI flow method for tests SB23 and SB01 would reasonably be expected to differ from this test. The DVI flow method and the Tsat method are consistent for SB06; the DVI flow method predicts greater core steam production, and both methods predict steam production for essentially the entire test. The DVI flow method predicts the fluid temperature at the core outlet for most of the test to within approximately [ ]^{a,b,c} °F. As noted for SB23, the spikes in core outlet temperature are the result of the core inlet flow approximation. The simplified DVI flow method underpredicts steam production in this case because the large break flow is not considered.

Results for SB13 are provided in Figures 6.2.1-13 through 6.2.1-16. Results for the three methods are generally consistent with the exception of calculated steam production at [ ]^{a,b,c} seconds; the Tsat method predicts no steam production while the DVI methods do. The large difference in the DVI flow method calculated core outlet temperature and measured temperatures is inconsistent with results for the other tests discussed in this section. This difference is attributed to pressure uncertainties and is discussed in detail in Subsection 6.2.1.2.

Results for SB09 are provided in Figures 6.2.1-17 through 6.2.1-20. The three methods are consistent in the prediction of zero steam production for the period bounding [ ]^{a,b,c} seconds, which is consistent with measured core outlet temperatures, which are generally below [ ]^{a,b,c}°F during this period. The break is located in the CMT cold-leg balance line, which is above the top of the core. As a result, the core is effectively cooled during the period around [ ]^{a,b,c} seconds. The small spike at [ ]^{a,b,c} seconds in steam production predicted by the Tsat method is consistent with the spike in measured core outlet temperature. The DVI methods do not predict this spike, a result which is attributed to the core inlet flow approximation. After [ ]^{a,b,c} seconds and during the LTC, the two DVI flow methods predict greater steam production than the Tsat method. The small difference in the two DVI methods is due to the break location and small break flow.

6.2.1.2 Core Pressure Uncertainty

Two pressure measurements are provided, one located at the top and one located at the bottom of the reactor vessel. The measurement uncertainty for the pressure instruments, PT-107 and PT-108, is ±3.7 psi.[1] The corresponding pressure difference uncertainty is ±7.4 psi. As discussed in Section 4.11, the measured pressures should differ by approximately 2 psi to 3 psi due to water column effects. Given the uncertainty, pressure differences of from –5.4 psi to 10.4 psi would be expected. Pressure differences during LTC were found to generally fall within the expected range and vary from test to test.

The consequence of this pressure uncertainty on calculated core steam production is observed in the changes in water properties and the saturation temperature. An example of the impacts of a possible range of water properties is shown in Table 6.2.1-1 for 18 psia, which is representative of LTC conditions. As shown in the table, changes in density and enthalpy are relatively minor. The saturation temperature change is approximately 6°F for a 2 psi pressure change.

The accuracy of the DVI line flow method is dependent on the uncertainty in an enthalpy rise calculation. The influence of pressure on enthalpy over the expected uncertainty range is limited. Thus, this method would be expected to be relatively insensitive to the pressure uncertainty.

The accuracy of the Tsat method is dependent on the uncertainty in the saturation line calculation. Given the lower power levels during LTC, no appreciable superheating occurs. As a result, a 6°F error in predicted saturation temperature can shift the saturation line. An overprediction could result in the conclusion that the saturation temperature was never reached and zero steam was produced. An underprediction could result in a significant overprediction in steam production. The Tsat method is particularly sensitive to this error during LTC because of the combination of low pressure and low power.

The effects of the pressure uncertainty are shown for Test SB13 in Figures 6.2.1-21 through 6.2.1-24. Figure 6.2.1-21 shows the difference between pressure taps PT-107 and PT-108. As shown in the figure, the pressure difference is within the expected uncertainty range during LTC. Figures 6.2.1-22

and 6.2.1-23 provide comparisons of calculated steam production based on these two pressure taps. As shown in Figure 6.2.1-22, the effect on the Tsat method was significant during LTC. As shown in Figure 6.2.1-23, the effect on the DVI line flow method was limited (~[ ]^{a,b,c} lbm/sec.). The measured core outlet temperature is compared to the calculated temperature per the DVI flow method in Figure 6.2.1-24. The effect of pressure measurement uncertainty is evident in the calculated temperatures, which are low using PT-107 and high using PT-108.

The use of the Tsat method for LTC is not recommended because of its sensitivity to the uncertainty in measured pressure. The use of the DVI flow method is recommended for LTC for the prediction of steam production. The calculated core outlet temperature is provided to demonstrate closure for the DVI flow method and is not used for other purposes in this report.

Results provided elsewhere in this report are based on a test by test selection of PT-107 or PT-108. The pressure tap selection criterion is the consistency of calculated steam production between the Tsat and DVI flow methods during LTC.

6.2.1.3 Mass Effects

Section 4 provides flow rates based on two calculational methods: (1) flow calculated from flow meter data, and (2) inferred flow calculated from mass balances and rates of change in stored mass. Flow-meter based flow is generally stable. The inferred flow is typically noisy, since small variations in tank levels result in small changes in stored mass and extremely large calculated rates of change in stored mass. The smoothing algorithm and smoothing constants of Section 4.20 are effective in eliminating most of the noise effects.

The overall structure of the data analysis program provides the option to use data smoothing on raw data prior to analysis, and on calculated results after running the analysis program. The program is structured to process all calculations for a given time step and then proceed to the next time step, because of the large volume of data. The data smoothing algorithm of Section 4.20 requires the simultaneous availability of all data. As a result, data smoothing is limited to: (1) smoothing prior to the analysis program calculations, and (2) post-analysis smoothing. All smoothed plots provided in this subsection are post-analysis smoothed using the algorithms and constants of Section 4.20.

The Tsat method for calculating core steam production does not employ flow into the core and, therefore, is unaffected by the flow rate issues.

The DVI line flow method is based on flow into the core, and requires a relatively stable flow. Large, very high frequency oscillations (noise) in calculated flow around the actual value can cause computational problems. Even though the analysis program includes logic to prevent aborts due to potential problems such as large negative flow, large oscillations can make the results unusable. To ensure reliable results for the DVI line flow method, inferred flows were not used.

The DVI line flow method is based on two metered flows: (1) the DVI line, which is a combination of individual meters or two overall line meters, and (2) the break separator flowmeter. DVI line flow meters measure DVI flow to the downcomer. The break separator flow meter measures flow to the primary sump from the break separator tank. Thus, the flow meter does not provide a direct measure of break flow leaving the primary system. The use of the combination of DVI line flow to the downcomer and break separator flow to the sump as an approximation to the flow from the lower plenum to the core requires several assumptions, which include:

- The draining of primary system components, such as the cold legs and SGs, is neglected. This affects the early part of the transient, which limits use of the DVI flow method during this period.

- Mass effects of the reactor vessel lower plenum. The rate of change of mass in the lower plenum is neglected. Since the lower plenum remains water-solid throughout the tests, the mass effects are assumed to be insignificant.

- Mass effects of the downcomer. The rate of change of mass in the downcomer is neglected.

- Mass effects of the break separator tank and vapor flow through the break separator vapor flow meter. The rate of change of mass in the break separator is neglected.

The importance of the downcomer and break separator mass effects is examined graphically. The potential impacts can be investigated by comparing metered flow to the flow with these effects considered.

The importance of including the downcomer mass effects is shown in Figure 6.2.1-25, which compares smoothed plots of the DVI line flow into the downcomer to flow from the downcomer to the lower plenum for Matrix Test SB01. (For the purpose of showing mass effects, downcomer to lower plenum flow is taken as the DVI line flow less the rate of change in downcomer mass.) A smoothed plot of downcomer level is shown in Figure 6.2.1-26 for this test. As evident in these plots, DVI line flow into the downcomer is a good approximation for downcomer flow into the lower plenum for periods when level changes in the downcomer are limited or moderate.

The importance of including break separator tank mass effects is shown in Figure 6.2.1-27, which compares the smoothed plots for metered flow (from the break separator to the primary sump) to the inferred break flow leaving the primary system for Matrix Test SB01. A smoothed plot of the break separator level is shown in Figure 6.2.1-28 for this test. As evidenced by the plots, the metered flow is generally a good proxy for the inferred break flow.

For some brief periods, the mass effects may have noticeable error. These can be identified by periods of sudden changes in core steam production and the saturation line. As shown for Test SB23 in Figures 6.2.1-1 and 6.2.1-2, short duration spikes in core steam production and saturation line occur at

[ ]^{a,b,c} seconds. Both spikes are attributed to rapid level changes in the break separator tank. While these two spikes are due to mass effects, it should be noted that other specific spikes may be due to mass effects or represent actual variations in core steam production.

6.2.1.4 Core Energy Results

The DVI line flow method provides good results across the range of tests investigated. Pressure uncertainties were found to have only a minor effect on calculated steam production. Pressure uncertainties did, however, influence the ability to demonstrate closure by comparing calculated and measured core outlet temperature. The DVI line flow method depends on the accuracy of excluding draining of the primary system and rapid tank level changes. As a result, this method is generally applicable after the initial draining of the primary system; the other exception to the applicability is for short durations due to flow spikes associated with rapid changes in tank levels.

The Tsat method was found to be sensitive to the pressure uncertainties and is not recommended for use during LTC due to low test pressures. Consistency between this method and the DVI line flow method was established by showing that they produce similar results during early IRWST injection, which supports the validity of the DVI line flow method.

The similarity of results for the DVI line flow method and simplified DVI line flow method, with the exception of Test SB06, demonstrates the relative robustness of the DVI line flow method. (Because of the large break area, SB06 results differ significantly.) Thus, this similarity also supports the validity of the DVI line flow method.

TABLE 6.2.1-1 SATURATED WATER PROPERTIES				
Property	**Value at 16 psia**	**Value at 18 psia**	**Value at 20 psia**	**Difference Relative to 18 psia**
Liquid Enthalpy, Btu/lbm	184.5	190.7	196.3	+2.9% −3.2%
Vapor Enthalpy, Btu/lbm	1152.1	1154.3	1156.3	+0.2% −0.2%
Saturation Temperature, °F	216.3	222.4	228.0	+5.6°F −6.1°F

TABLE 6.2.1-2
OSU TEST ANALYSIS PLOT PACKAGE FOR SUBSECTION 6.2.1

Plot Number	Component	Variables	Units	Description
1	Reactor Vessel	RPVRXV RPVASOU2 RPVASOUT	lbm/sec.	Core Steam Production for Test SB23: for Tsat Method for DVI Flow Method for Simplified DVI Flow Method
2	Reactor Vessel	RPVXE RPVASL2 RPVASL	in.	Saturation Line for Test SB23: for Tsat Method for DVI Flow Method for Simplified DVI Flow Method
3	Reactor Vessel	RPVALIN2 RPVALIN	lbm/sec.	Core Inlet Flow for Test SB23: for DVI Flow Method for Simplified DVI Flow Method
4	Reactor Vessel	RPVATOU2 T08RPV T09RPV	°F	Fluid Temperatures for Test SB23: Core Outlet Temp. for DVI Flow Method Measured Temp. Just Below Top of Core Measured Temp. Just Above Top of Core
5	Reactor Vessel	RPVRXV RPVASOU2 RPVASOUT	lbm/sec.	Core Steam Production for Test SB01: for Tsat Method for DVI Flow Method for Simplified DVI Flow Method
6	Reactor Vessel	RPVXE RPVASL2 RPVASL	in.	Saturation Line for Test SB01: for Tsat Method for DVI Flow Method for Simplified DVI Flow Method
7	Reactor Vessel	RPVALIN2 RPVALIN	lbm/sec.	Core Inlet Flow for Test SB01: for DVI Flow Method for Simplified DVI Flow Method
8	Reactor Vessel	RPVATOU2 T08RPV T09RPV	°F	Fluid Temperatures for Test SB01: Core Outlet Temp. for DVI Flow Method Measured Temp. Just Below Top of Core Measured Temp. Just Above Top of Core
9	Reactor Vessel	RPVRXV RPVASOU2 RPVASOUT	lbm/sec.	Core Steam Production for Test SB06: for Tsat Method for DVI Flow Method for Simplified DVI Flow Method
10	Reactor Vessel	RPVXE RPVASL2 RPVASL	in.	Saturation Line for Test SB06: for Tsat Method for DVI Flow Method for Simplified DVI Flow Method

TABLE 6.2.1-2 (Continued)
OSU TEST ANALYSIS PLOT PACKAGE FOR SUBSECTION 6.2.1

Plot Number	Component	Variables	Units	Description
11	Reactor Vessel	RPVALIN2 RPVALIN	lbm/sec.	Core Inlet Flow for Test SB06: for DVI Flow Method for Simplified DVI Flow Method
12	Reactor Vessel	RPVATOU2 T08RPV T09RPV	°F	Fluid Temperatures for Test SB06: Core Outlet Temp. for DVI Flow Method Measured Temp. Just Below Top of Core Measured Temp. Just Above Top of Core
13	Reactor Vessel	RPVRXV RPVASOU2 RPVASOUT	lbm/sec.	Core Steam Production for Test SB13: for Tsat Method for DVI Flow Method for Simplified DVI Flow Method
14	Reactor Vessel	RPVXE RPVASL2 RPVASL	in.	Saturation Line for Test SB13: for Tsat Method for DVI Flow Method for Simplified DVI Flow Method
15	Reactor Vessel	RPVALIN2 RPVALIN	lbm/sec.	Core Inlet Flow for Test SB13: for DVI Flow Method for Simplified DVI Flow Method
16	Reactor Vessel	RPVATOU2 T08RPV T09RPV	°F	Fluid Temperatures for Test SB13: Core Outlet Temp. for DVI Flow Method Measured Temp. Just Below Top of Core Measured Temp. Just Above Top of Core
17	Reactor Vessel	RPVRXV RPVASOU2 RPVASOUT	lbm/sec.	Core Steam Production for Test SB09: for Tsat Method for DVI Flow Method for Simplified DVI Flow Method
18	Reactor Vessel	RPVXE RPVASL2 RPVASL	in.	Saturation Line for Test SB09: for Tsat Method for DVI Flow Method for Simplified DVI Flow Method
19	Reactor Vessel	RPVALIN2 RPVALIN	lbm/sec.	Core Inlet Flow for Test SB09: for DVI Flow Method for Simplified DVI Flow Method
20	Reactor Vessel	RPVATOU2 T08RPV T09RPV	°F	Fluid Temperatures for Test SB09: Core Outlet Temp. for DVI Flow Method Measured Temp. Just Below Top of Core Measured Temp. Just Above Top of Core
21	Reactor Vessel	PT-108 PT-107 PT-108 - PT-107	psi	Pressures for Test SB13: Pressure at Bottom of Vessel Pressure at Top of Vessel Pressure Difference

TABLE 6.2.1-2 (Continued)
OSU TEST ANALYSIS PLOT PACKAGE FOR SUBSECTION 6.2.1

Plot Number	Component	Variables	Units	Description
22	Reactor Vessel	RPVRXV RPVRXV	lbm/sec.	Core Steam Production for Test SB13: for Tsat Method using PT-107 for Tsat Method using PT-108
23	Reactor Vessel	RPVASOU2 RPVASOU2	lbm/sec.	Core Steam Production for Test SB13: for DVI Flow Method using PT-107 for DVI Flow Method using PT-108
24	Reactor Vessel	 RPVTOU2 RPVTOU2 T08RPV T09RPV	°F	Fluid Temperatures for Test SB13: At Core Outlet, DVI Flow Method w/PT-107 At Core Outlet, DVI Flow Method w/PT-108 Measured Temp. Just Below Top of Core Measured Temp. Just Above Top of Core
25	Downcomer	 RPVTMRI RPVMRI	lbm/sec.	Flow Rates for Test SB01: DVI Flow DVI Flow + Downcomer Mass Effects
26	Downcomer	LDP01DC	in.	Downcomer Level for Test SB01
27	Break Separator	 BRKSMPF3 BRKSTMR	lbm/sec.	Break Separator Flow Rates for Test SB01: Metered Flow to Primary Sump Break Flow = Metered Flow + Mass Effects
28	Break Separator	CLDP-905	in.	Break Separator Level for Test SB01

THE FIGURES LISTED IN TABLE 6.2.1-2
ARE NOT INCLUDED IN THIS NONPROPRIETARY DOCUMENT

6.2.2 Mass Balance

Figures 6.2.2-1 to 6.2.2-12 reproduce the total system mass inventory for all the OSU tests discussed in Section 5. These and the other figures discussed in this section are listed in Table 6.2.2-1. The total inventory includes all the large volumes (including the BAMS separator tanks), but excludes the secondary side of the SGs. The features of the total system inventory results for Test SB01 are discussed in Subsection 6.2.2.1. Many of these features are common to all the tests, exceptions are noted in Subsection 6.2.2.2. Finally, in Subsections 6.2.2.3 and 6.2.2.4, the estimated steam losses are compared to the integrated steam flow for the short-term transient, and the core steam generation rate for the long-term transient, to demonstrate mass balance closure.

6.2.2.1 System Inventory for Test SB01

The system mass inventory results for Test SB01 are given in Figure 6.2.2-1. The initial mass of the system is calculated to be [ ]^{a,b,c} lbs. The variations in mass inventory throughout the transient exhibit the following features:

Initial Mass Increase – Immediately following the opening of the break, there was a sharp dip and then an immediate rise in the total system mass inventory. The sharp dip is seen throughout the mass measurements, but is most obvious in the BAMS separator tanks, which accounts for the majority of the apparent observed mass loss. This dip was a result of the pressure response to the opening of the break. The subsequent increase in inventory is a result of the continued response to the opening of the break and level adjustments in the primary circuit as the pumps are shut off.

Mass Decrease During Pre-sump Injection Phase – Following the initial increase in mass inventory, there was a second reduction in inventory before the onset of primary sump injection. The mass reduction was associated with the steam leaving the primary system via the break. Although there was provision for this steam to be accounted for by additions to the primary sump, this was not done during the OSU tests because at that time, the detected steam loss was believed to be very low. Instead, the vapor flow was allowed to vent to atmosphere. For SB01, the system inventory showed the reduction in mass was [ ]^{a,b,c} lbm and it occurred during the first [ ]^{a,b,c} seconds of the transient. The value indicated from the mass inventory is consistent with the [ ]^{a,b,c} lbm of steam that was measured flowing through the break, as discussed in Subsection 5.1.2.

Mass Variations During Pre-sump Injection Phase – Following the mass decrease, lengthy variations were observed. The system mass inventory calculations included all of the major components, but neglected some of the connecting pipework. As the transient progressed, water flowed into and out of the major components as the system pipework drained and refilled in response to the operation of the passive safety systems. In addition, events such as opening of the ADS valves caused further adjustments in level measurements due to the pressure variations induced in the BAMS.

A Mass Inventory Peak at the Start of Sump Injection – This peak arises at the time when the primary sump overflows to the secondary sump. It occurs as the sump and BAMS measurements adjust to the new equilibrium.

Mass Decrease During Sump Injection – Following the sump peak, there was a gradual reduction in system mass inventory until the end of the test. For Test SB01 approximately [ ]^{a,b,c} lbm of mass was unaccountable during the last [ ]^{a,b,c} seconds of the transient. This mass decrease represents the steam that flowed out of the system to atmosphere during the long-term transient which was not detected by the vortex meters. However, as will be discussed below, there is evidence that steam was leaving the system at a very low flow rate, via the ADS-4 valves for the entire sump injection phase of the transient.

Mass Inventory Dips During Long-Term Cooling – There were marked dips of approximately [ ]^{a,b,c} lbm in primary system inventory throughout the long-term cooling phase of the transient, as shown in Figure 6.2.2-13. These dips resulted from equivalent changes in the measured primary sump mass. Examination of the mass results from the primary sump load cells indicates that there were no such short-term variations in mass. This conclusion is supported by the fact that there were no changes in outflow from the primary sump associated with these dips. Figure 6.2.2-13 also shows that associated with each dip, there is a small increase in pressure above the primary sump water surface. This increase caused an apparent reduction in measured level and hence calculated mass. It is believed that the small pressure change was associated with water condensing in the sump vent line causing a backpressure to buildup until it was large enough to sweep the water through the check valve.

6.2.2.2 Mass Balance for Other Tests: Variations from Behavior Exhibited by Test SB01

Tests SB09, SB10, and SB13 (Figures 6.2.2-4, 6.2.2-5, and 6.2.2-7) exhibit essentially the same features as SB01. Variations from the behavior of test SB01 are outlined below.

Test SB18 (Figure 6.2.2-2) results did not continue into the sump injection phase of the transient as a rack of instruments was lost when the DAS prematurely shutdown and thus, no reduction in inventory was observed during the long-term transient. There was no marked increase in system inventory immediately following the opening of the break. By the time of sump injection, there had been an increase in inventory, rather than the decrease observed in SB01. The integrated break steam flow indicated that [ ]^{a,b,c} lbm of steam left the primary system via the break during the first [ ]^{a,b,c} seconds of the transient. This loss can be seen as a reduction in the mass inventory curve between [ ]^{a,b,c} seconds.

Test SB06 (Figure 6.2.2-3) did not continue into the sump injection phase of the transient. The initial inventory increase was [ ]^{a,b,c} lbm. This was followed by a reduction of around [ ]^{a,b,c} lbm before the onset of mass variations, but by the time of sump injection, there had been no overall inventory decrease. The integrated break steam flow confirms that [ ]^{a,b,c} lbm of steam left the primary system via the break during the first [ ]^{a,b,c} seconds of the transient.

Test SB12 (Figure 6.2.2-6) did not display many of the features noted for SB01. There was a marked overall increase in inventory during the test and many dips as a result of primary sump mass variations. There was no measurement for any steam leaving the primary system. However, as noted below, the fluid thermocouples on the outlet of the ADS-4 valves did reach saturation temperature indicating that steam may have been leaving by this route for most of the transient. Furthermore, the downcomer level was generally low enough for steam to leave the primary system via the break.

Test SB14 (Figure 6.2.2-8) exhibited a [ ]^{a,b,c} lbm increase in inventory during the pre-sump injection phase of the transient. There was no evidence from the inventory plot for steam leaving the primary system, but the ADS flow indicates that [ ]^{a,b,c} lbm of steam left the primary system via the ADS break path during the first [ ]^{a,b,c} seconds of the transient.

Test SB15 (Figure 6.2.2-9) did not continue very long after the start of sump injection and thus, the mass inventory did not show reduction during this phase.

Test SB19 (Figure 6.2.2-10) showed a [ ]^{a,b,c} lbm rise in system inventory in the first [ ]^{a,b,c} seconds. The sump dips and pre-sump peak were not obvious for this test.

Test SB21 (Figure 6.2.2-11) did not exhibit a marked peak at the start of sump injection.

Test SB23 (Figure 6.2.2-12) did not show any significant steam loss during the pre-sump injection phase. No steam flow was measured by the vortex meters during this phase of the transient for this smallest break case which implies all the break flow was liquid.

6.2.2.3 Steam Flow During Pre-Sump Injection Phase

For most break sizes, the initial flow through the break was composed of steam and water. The break steam flow will fall markedly when ADS-1 actuates and provides a less restrictive path out of the primary system. Subsequently, additional steam flow may occur through the ADS-4 valves. Table 6.2.2-2 includes a quantification of the steam flow estimated from the mass inventory results presented in Figures 6.2.2-1 to 6.2.2-12. This estimate is based on the size of the observed mass reduction following the initial inventory increase. For comparison, measured integrated steam break flow is also presented, and there is, in general, good agreement between the two figures.

6.2.2.4 Steam Flow via Automatic Depressurization System-4 Valves During Long-Term Transient

During the sump injection phase of all the LOCA simulations, the rod bundle energy balance indicates that steam must be exiting the core. During this phase of the transient, there is a marked reduction in total system inventory, which may represent the amount of steam that left the system during this phase of the test. The energy balance discussion presented in Subsection 6.2.3 also concludes that a considerable quantity of steam may have left the system during this phase of the test.

In all the tests, the vortex meters on the ADS-4 and break separators did not detect any steam flow during the long-term cooling phase of the transient, that is, during ADS-4 and IRWST/sump injection stages. The reduction in system inventory during the sump injection phase can be used to estimate the rate at which steam was flowing out of the primary system. The results of these estimates are given in Table 6.2.2-2. These rates have been determined by assuming a linear reduction in inventory after the mass inventory peak which occurred at the start of sump injection, until the end of the transient. The maximum estimated steam flow rate is [ ]^{a,b,c} lbm/sec. At normal atmospheric conditions, this maximum rate corresponds to a volumetric flow rate of [ ]^{a,b,c} cfm. The 6-in. vortex meters have a minimum recommended flow rate of approximately [ ]^{a,b,c} cfm, although the meter will detect lower flow rates. Since all the steam leaving the primary system is measured by a sump 6-in. vortex meter in the exhaust piping exiting the test building, the maximum estimated steam flow rate is below the minimum recommended flow rate and may not be detected.

Also presented in Table 6.2.2-2 is the rate of core steam production, together with the inferred rate of steam flow out of the primary system. If the two mass rates are correct, then the inferred mass loss and core steam generation rate is balanced between [ ]^{a,b,c} lbm/sec. or between [ ]^{a,b,c} percent of the steam produced must have remained within the primary system most likely due to condensation in the downcomer region. That is, the rate of steam generation is such that if it was assumed that all of the steam generated left the primary system, the steam loss would exceed the mass balance error. It should be noted, however, that in tests where reverse flow through the break occurs, the calculated DVI line flow is an underestimate of the true value and thus, the steam generation rate predicted for such cases is too high.

Although the vortex meters did not measure any steam flow, the instrumentation did show evidence of steam leaving the primary system via the ADS-4 valves.

- Intermittent flow spikes were observed in the ADS-4 flow meters. Although these spikes were below the minimum recommended flow, it was indicative of continued flow.

- Figure 6.2.2-14 to 6.2.2-25 show the temperature readings on the fluid thermocouples located downstream of the ADS-4 vortex meters for all tests described in Section 5. These figures indicate that for the entire sump injection phase, the fluid temperatures were at or above the saturation temperature. It can therefore be concluded that for this period of the transient, steam was flowing out of the primary system via the ADS-4 valves.

It should be noted that for the larger breaks (SB06, SB12 and SB21), there are indications that steam was leaving via the ADS-4 valves for the entire transient after the ADS-4 valves opened. For smaller breaks, the fluid thermocouples reached saturation [ ]^{a,b,c} seconds before there were clear indications of steam loss from the inventory measurements. There were also indications of steam leaving via the ADS-4 shortly after its initial actuation, until the steam generation in the core was

quenched by the IRWST injection. There were therefore indications that more steam left the primary system through the ADS-4 valves than can be inferred from the inventory results. Furthermore, the rod bundle energy balance also indicated that steam should be leaving the primary system.

TABLE 6.2.2-1 OSU TEST ANALYSIS PLOT PACKAGE FOR SUBSECTION 6.2.2				
Plot Number	**Component**	**Variables**	**Units**	**Description**
1	System Inventory	TOTMASS	lbm	System mass for SB01
2	System Inventory	TOTMASS	lbm	System mass for SB18
3	System Inventory	TOTMASS	lbm	System mass for SB06
4	System Inventory	TOTMASS	lbm	System mass for SB09
5	System Inventory	TOTMASS	lbm	System mass for SB10
6	System Inventory	TOTMASS	lbm	System mass for SB12
7	System Inventory	TOTMASS	lbm	System mass for SB13
8	System Inventory	TOTMASS	lbm	System mass for SB14
9	System Inventory	TOTMASS	lbm	System mass for SB15
10	System Inventory	TOTMASS	lbm	System mass for SB19
11	System Inventory	TOTMASS	lbm	System mass for SB21
12	System Inventory	TOTMASS	lbm	System mass for SB23
13	Primary Sump	AMPSMP, PT-901	lbm & psig	Mass and pressure for SB01
14	BAMS	TF-622, TF-623	°F	Fluid temperatures in outlet pipe to ADS-4 valves for SB01
15	BAMS	TF-622, TF-623	°F	Fluid temperatures in outlet pipe to ADS-4 valves for SB18
16	BAMS	TF-622, TF-623	°F	Fluid temperatures in outlet pipe to ADS-4 valves for SB06
17	BAMS	TF-622, TF-623	°F	Fluid temperatures in outlet pipe to ADS-4 valves for SB09
18	BAMS	TF-622, TF-623	°F	Fluid temperatures in outlet pipe to ADS-4 valves for SB10
19	BAMS	TF-622, TF-623	°F	Fluid temperatures in outlet pipe to ADS-4 valves for SB12

TABLE 6.2.2-1 (continued)
OSU TEST ANALYSIS PLOT PACKAGE FOR SUBSECTION 6.2.2

Plot Number	Component	Variables	Units	Description
20	BAMS	TF-622, TF-623	°F	Fluid temperatures in outlet pipe to ADS-4 valves for SB13
21	BAMS	TF-622, TF-623	°F	Fluid temperatures in outlet pipe to ADS-4 valves for SB14
22	BAMS	TF-622, TF-623	°F	Fluid temperatures in outlet pipe to ADS-4 valves for SB15
23	BAMS	TF-622, TF-623	°F	Fluid temperatures in outlet pipe to ADS-4 valves for SB19
24	BAMS	TF-622, TF-623	°F	Fluid temperatures in outlet pipe to ADS-4 valves for SB21
25	BAMS	TF-622, TF-623	°F	Fluid temperatures in outlet pipe to ADS-4 valves for SB23

TABLE 6.2.2-2
STEAM FLOW DURING SHORT- AND LONG-TERM TRANSIENTS

Test	Short-Term Transient		Long-Term Transient		
	Inferred Mass Loss (lbm)	Measured Mass Loss (lbm)	Inferred Mass Loss (lbm)	Inferred Mass Loss Rate (lbm/sec.)	Core Steam Generation Rate (lbm/sec.)
SB01	350	330	700 to 800	0.05	0.09 to 0.1
SB18	400	300	N/A	N/A	N/A
SB06	200	205	N/A	N/A	N/A
SB09	300 to 400	350	350	0.05	0.08 to 0.09
SB10	500 to 900	600	900	0.06	0.09
SB12	Unknown	250	N/A	N/A	0.05 to 0.2
SB13	400 to 600	120	450	0.04	0.11
SB14	Unknown	370	400	0.05	0.1
SB15	300	400	N/A	N/A	0.04 to 0.06
SB19	300 to 400	300	500	0.08	0.08 to 0.09
SB21	<500	270	500	0.06	0.09
SB23	None	None	600	0.08	0.08 to 0.11

THE FIGURES LISTED IN TABLE 6.2.2-1
ARE NOT INCLUDED IN THIS NONPROPRIETARY DOCUMENT

6.2.3 Overall Energy Balance

An overall energy inventory was performed to provide insight into the OSU test results. The system energy inventory is determined by considering the OSU facility (primary system, CMTs, accumulators, IRWST, sumps, PRHR, and separators) as a control volume. The energy balance deficit on this control volume is defined as:

$$U_{deficit} = U_{rods} - U_{st\text{-}ex} - U_{amb} - U_{sg} + \Delta U_{fluid} + \Delta U_{met} \qquad 6.2.3\text{-}1$$

where:

$U_{deficit}$ = Deficit in the overall energy balance
U_{rods} = Integrated power in the heated rods
$U_{st\text{-}ex}$ = Energy of the steam exhausted from the control volume
U_{amb} = Integrated heat loss to the ambient
U_{sg} = Integrated heat transfer in the SGs
ΔU_{fluid} = Change in the energy of the fluid in the control volume
ΔU_{met} = Change in the energy of the metal in the control volume

There are several assumptions necessary to calculate the components of the energy balance. These include:

- Energy transfer in the SGs is inferred from the change in the fluid energy on the secondary side. Energy transfer is assumed to stop after the primary- and secondary-side pressures equalize.

  This assumption results in a small energy transfer rate due to the isolation of the secondary side and the loss of flow on the primary side. The total integrated energy is small for all of the LOCA tests.

- The total fluid energy at the start of the tests neglects a small amount of fluid due to the exclusion of several small diameter piping runs.

  A small amount of liquid is initially omitted from the mass inventory from various piping runs, which are not modeled. This results in an amount of energy equal to the neglected mass times the saturated liquid enthalpy at operating conditions. It is expected that a small fraction of energy is not accounted for by the energy balance and is included in the overall error when these pipes are discharged into the primary system.

- The ambient losses are calculated assuming a uniform insulation thickness around insulated components.

The actual condition of the insulation is expected to be somewhat less than uniform, which would account fo. nigher than calculated ambient losses.

- Uncertainties associated with measurements.

  The deficiencies in the data from uncertainties in the instrumentation are accumulated throughout the test. They affect the overall energy balance and are included in the overall mass and energy deficit.

  The largest source of deficit in the energy balance is expected from the steam exhaust flow meters, which operate for large periods of time at steam flow rates estimated to be below the minimum recommended flow rate. It is believed that the lack of measured steam exhaust flow over the LTC phase of the transient accounts for the majority of the calculated deficit in the energy balance.

The energy balance plot showing the individual components of Equation 6.2.3-1 are reproduced from Section 5 in Figures 6.2.3-1 to 6.2.3-24, along with the energy balance deficit for each test. These plots are summarized in Table 6.2.3-1. A detailed discussion of the energy balance for test SB01 follows including variations in the behavior exhibited in SB01 for each of the tests.

6.2.3.1 System Energy Inventory for SB01

Test SB01 was the 2-in. cold-leg break. The components of the energy balance for SB01 are shown in Figure 6.2.3-1, and the deficit in the energy balance is shown in Figure 6.2.3-2. These results are presented in the following features.

Pre-IRWST Injection Phase (up to [ ]^{a,b,c} seconds) showed a drop in the fluid and metal energy immediately following the opening of the break. This drop was compensated for by an increase in the energy exhausted in the form of steam out of the break and integrated decay heat. There were smaller contributions from the SG heat transfer and the heat losses to the environment. The large increase in the energy balance deficit is believed to be caused by undetected steam exhausted from the break and ADS-4.

Post-IRWST Injection Phase ([ ]^{a,b,c} seconds) showed an increase in the fluid energy due to the heat-up of the IRWST and sump water. This increase almost matches the rate of increase of the integrated rod power. During this period, there was no steam generation in the core. The deficit in the energy balance remained nearly constant during this phase, exhibiting a peak caused by the thermal lag of metal in the control volume.

Pre-Sump Injection Phase ([ ]^{a,b,c} seconds) showed a steady increase in the fluid energy as the IRWST and sump continued to heat. The rate of increase in the fluid heat-up was less than the rate of increase of the integrated rod power, resulting in an increasing deficit. During this time, steam

was generated again in the core. The deficit was most likely caused by undetected steam exhausted from ADS-4. In addition, sump energy is calculated using three axial thermocouples. Uncertainty in this calculation could account for a portion of the error later in the test.

Long-Term Cooling Sump Injection Phase ([ ]^{a,b,c} seconds to end of test) showed that the rate of increase in the fluid energy decreased as the entire inventory neared saturation temperature. This increased the core steam generation, which remained constant until the end of the test. Therefore, the ADS-4 steam flow was expected to increase, and the corresponding deficit in the energy balance was a result of the inability of the vortex flow meters to detect the low steam flows.

The mass inventory showed a discrepancy of [ ]^{a,b,c} lbm up to the time of sump injection. Assuming that this quantity is unmeasured steam, the contribution to the energy balance deficit is approximately [ ]^{a,b,c} Btu, or nearly one-half of the total deficit. The remaining deficit was probably due to an underpredicted heat loss to the ambient and through the SGs.

After sump injection, the unmeasured steam resulted in a [ ]^{a,b,c} lbm deficit in the mass balance. This corresponds to an energy balance error of approximately [ ]^{a,b,c} Btu, which is nearly two-thirds of the total deficit. The remaining deficit was most likely caused by the ambient losses and other components of the energy balance.

Near closure can be reached on the energy balance by assuming that all the steam generated in the core was exhausted from the primary system.

6.2.3.2 System Energy Inventory for Other Tests

Test SB18 duplicated the 2-in. cold-leg break. This test was terminated at approximately [ ]^{a,b,c} seconds at the start of sump injection. The components of the energy balance are shown in Figure 6.2.3-3, and the deficit is shown in Figure 6.2.3-4. Both of these figures show results that are nearly identical to SB01 up to the point of sump injection.

Test SB06 was a 4-in. cold-leg break. This test was terminated at approximately [ ]^{a,b,c} seconds at the start of sump injection. The components of the energy balance are shown in Figure 6.2.3-5, and the deficit is shown in Figure 6.2.3-6. As in SB01, the exhausted steam from the break and ADS-4 are not accounted for after [ ]^{a,b,c} seconds into the test. This coupled with the underpredicted ambient losses, resulted in an energy balance deficit of nearly [ ]^{a,b,c} Btu. From [ ]^{a,b,c} seconds, the core steam generation was reduced, and the fluid energy increased at nearly the same rate as the integrated rod power. The energy balance deficit during this period remained fairly constant. After [ ]^{a,b,c} seconds, the core resumed steaming and the mass deficit increased, most likely due to additional steam exhausted through ADS-4 but undetected by the steam vortex meters. Overall, the energy balance was better for SB06 than for SB01.

Test SB09 was a 2-in. cold-leg balance line break. This test ran to completion and included the sump injection phase. The components of the energy balance are shown in Figure 6.2.3-7, and the deficit is shown in Figure 6.2.3-8. This test follows the same pattern as SB01 in that the measured steam exhausted from the break and ADS-4 ended after about [ ]^{a,b,c} seconds. After this time, the fluid energy increased as was observed in SB01 until the fluid approached saturation temperature. The deficit exhibited the characteristic increase during the first [ ]^{a,b,c} seconds to about [ ]^{a,b,c} Btu, most likely as a result of the undetected exhaust steam and the ambient heat loss. The error remained essentially constant when no steam was generated in the core ([ ]^{a,b,c} seconds). After [ ]^{a,b,c} seconds, the deficit again likely increased to the same magnitude as the SB01 error deficit to undetected steam that left the break and ADS-4.

Test SB10 was a double-ended guillotine cold-leg-to-CMT balance line break. The components of the energy balance are shown in Figure 6.2.3-9, and the deficit is shown in Figure 6.2.3-10. Due to the location of the break, less steam exhaust was observed for this test than for SB01. Other than this difference, the energy balance and overall deficit are similar to SB01.

Test SB12 was a double-ended guillotine DVI line break. This test was terminated before the start of sump injection. The components of the energy balance are shown in Figure 6.2.3-11, and the deficit is shown in Figure 6.2.3-12. Due to the larger break size, the primary system blowdown occurred over a shorter time than was observed in SB01. Consequently, the time that fluid in the control volume reached minimum energy and began to gain energy was much quicker than in SB01 ([ ]^{a,b,c} seconds vs. [ ]^{a,b,c} seconds). The resulting deficit in the energy balance increased continually since the core steam generation continued throughout IRWST injection.

Test SB13 was a 2-in. DVI line break. The components of the energy balance are shown in Figure 6.2.3-13, and the deficit is shown in Figure 6.2.3-14. Due to the location of the break, the integrated steam exhaust energy was less than one-half of that observed in SB01. The core steam generation occurred until about [ ]^{a,b,c} seconds. The fraction of this steam, which likely exhausted through ADS-4, was not detected by the vortex flow meters; thus, the energy balance deficit increased until core steaming ceased. The deficit remained essentially constant until the core again produced steam (about [ ]^{a,b,c} seconds), and increased at a constant rate until the end of the test.

Test SB14 was an inadvertent ADS with no break. The components of the energy balance are shown in Figure 6.2.3-15, and the deficit is shown in Figure 6.2.3-16. Fluid energy increase closely paralleled the integrated rod power up to the point of sump injection ([ ]^{a,b,c} seconds). The steam exhausted from ADS-4 was not detected during the initial period of core steaming ([ ]^{a,b,c} seconds) and resulted in an accumulated energy balance error of about [ ]^{a,b,c} Btu. During the IRWST injection period (up to about [ ]^{a,b,c} seconds), core steam generation ceased, and the deficit remained nearly constant. After this time, the core again produced steam, and the deficit was likely due to the undetected steam exhausted from ADS-4.

Test SB15 was a 2-in. hot-leg break that was terminated before the start of sump injection. The components of the energy balance are shown in Figure 6.2.3-17, and the deficit is shown in Figure 6.2.3-18. In this test, the steam exhaust energy caused by the break was much higher ([ ]^{a,b,c} Btu vs. [ ]^{a,b,c} Btu) than that observed in the cold-leg break. Thus, a higher portion of the primary system energy was removed by the break as opposed to the ADS. Because of this, the deficit in the overall energy balance was somewhat less for the hot-leg break ([ ]^{a,b,c} Btu vs. [ ]^{a,b,c} Btu) up to the point where the core steam generation ceased because of IRWST injection (approximately [ ]^{a,b,c} seconds). The core resumed steam generation at approximately [ ]^{a,b,c} seconds, at which time the deficit increased due to undetected steam exhaust.

Test SB19 was a 2-in. cold-leg break that simulated containment backpressure. The components of the energy balance are shown in Figure 6.2.3-19, and the deficit is shown in Figure 6.2.3-20. Backpressure allowed the primary system energy to reach a higher level consistent with the higher saturation pressure. Thus, less energy was lost out of ADS-4, and the overall energy balance deficit was lower than SB01.

Test SB21 was a 4-in. cold-leg break. The components of the energy balance are shown in Figure 6.2.3-21, and the deficit is shown in Figure 6.2.3-22. The large break resulted in a sharp drop in the fluid energy as the primary system depressurized. Steam generation in the core started at ADS-4 actuation (approximately [ ]^{a,b,c} seconds), and continued throughout IRWST injection. Thus, the integrated steam exhaust energy exiting ADS-4, which was not detected, was probably much greater than SB01. This was confirmed by the deficit in the energy balance, which was significantly higher than in SB01.

Test SB23 was a 0.5-in. cold-leg break. The components of the energy balance are shown in Figure 6.2.3-23, and the deficit is shown in Figure 6.2.3-24. As a result of the small break, steam exhausted from the break was too low to be detected by the vortex flow meter. Thus, the energy balance deficit was significantly higher during the break phase than that calculated for SB01. After sump injection began, the rate of increase of the energy imbalance was similar to SB01.

Energy balances were calculated for all the tests reported herein. The results of each test indicated that it was not possible to account for the total system energy inventory, however, the deficit is attributable in part to the mass of steam that leaves the control volume via the ADS-4 and exits to atmosphere in the facility (Subsection 6.2.2), and to uncertainties in the facility heat losses. Each test has been examined and the deficits in the energy balance have been explained.

TABLE 6.2.3-1 OSU TEST ANALYSIS PLOT PACKAGE FOR SUBSECTION 6.2.3				
Plot No.	**Component**	**Variables**	**Units**	**Description**
1	Energy Balance	POWERINT,SGU, METU, TOTU, EXHAUSTU, AMBU	Btu	Energy Balance Components for SB01
2	Energy Balance	UERROR	Btu	Deficit in Energy Balance for SB01
3	Energy Balance	POWERINT, SGU, METU, TOTU, EXHAUSTU, AMBU	Btu	Energy Balance Components for SB18
4	Energy Balance	UERROR	Btu	Deficit in Energy Balance for SB18
5	Energy Balance	POWERINT, SGU, METU, TOTU, EXHAUSTU, AMBU	Btu	Energy Balance Components for SB06
6	Energy Balance	UERROR	Btu	Deficit in Energy Balance for SB06
7	Energy Balance	POWERINT, SGU, METU, TOTU, EXHAUSTU, AMBU	Btu	Energy Balance Components for SB09
8	Energy Balance	UERROR	Btu	Deficit in Energy Balance for SB09
9	Energy Balance	POWERINT, SGU, METU, TOTU, EXHAUSTU, AMBU	Btu	Energy Balance Components for SB10
10	Energy Balance	UERROR	Btu	Deficit in Energy Balance for SB10
11	Energy Balance	POWERINT, SGU, METU, TOTU, EXHAUSTU, AMBU	Btu	Energy Balance Components for SB12

TABLE 6.2.3-1 (Continued)
OSU TEST ANALYSIS PLOT PACKAGE FOR SUBSECTION 6.2.3

Plot No.	Component	Variables	Units	Description
12	Energy Balance	UERROR	Btu	Deficit in Energy Balance for SB12
13	Energy Balance	POWERINT, SGU, METU, TOTU, EXHAUSTU, AMBU	Btu	Energy Balance Components for SB13
14	Energy Balance	UERROR	Btu	Deficit in Energy Balance for SB13
15	Energy Balance	POWERINT, SGU, METU, TOTU, EXHAUSTU, AMBU	Btu	Energy Balance Components for SB14
16	Energy Balance	UERROR	Btu	Deficit in Energy Balance for SB14
17	Energy Balance	POWERINT, SGU, METU, TOTU, EXHAUSTU, AMBU	Btu	Energy Balance Components for SB15
18	Energy Balance	UERROR	Btu	Deficit in Energy Balance for SB15
19	Energy Balance	POWERINT, SGU, METU, TOTU, EXHAUSTU, AMBU	Btu	Energy Balance Components for SB19
20	Energy Balance	UERROR	Btu	Deficit in Energy Balance for SB19
21	Energy Balance	POWERINT, SGU, METU, TOTU, EXHAUSTU, AMBU	Btu	Energy Balance Components for SB21
22	Energy Balance	UERROR	Btu	Deficit in Energy Balance for SB21
23	Energy Balance	POWERINT, SGU, METU, TOTU, EXHAUSTU, AMBU	Btu	Energy Balance Components for SB23
24	Energy Balance	UERROR	Btu	Deficit in Energy Balance for SB23

THE FIGURES LISTED IN TABLE 6.2.3-1
ARE NOT INCLUDED IN THIS NONPROPRIETARY DOCUMENT

7.0 SYSTEM ANALYSIS FOR SMALL-BREAK LOSS OF COOLANT ACCIDENTS AND LONG-TERM COOLING

The OSU test matrix provides a comprehensive spectrum of SBLOCA events to examine the thermal-hydraulic phenomena that occur in the AP600 when the passive safety-related systems are operating. The more significant tests have been analyzed in depth individually in Section 5 of this report, and phenomena that occurred during testing at the facility are discussed in Section 6 together with evaluations of the calculated mass and energy balances. In this section, comparisons between tests are made to further discuss the performance of the passive safety-related systems for simulated SBLOCAs.

Table 7-1 shows the sequence of events for the OSU tests analyzed herein; also included are minimum mass inventory information for the core and RPV, and primary system pressure at the time ADS-1 actuation occurred. Table 7-1 information is discussed in the sections which follow.

TABLE 7-1 CONTAINS PROPRIETARY INFORMATION
AND IS NOT INCLUDED IN THIS NONPROPRIETARY DOCUMENT

7.1 Variations in Break Size

The 2-in. break at the bottom of CL-3 is the base case (Test SB01) in the OSU test matrix. In all tests simulating design basis LOCA events, the passive safety systems successfully reduced the RPV pressure to containment pressure, and stable IRWST injection was achieved. Furthermore, LTC via sump injection was efficient in the tests which were carried out for that length of time.

Due to the low-pressure nature of the OSU facility, actuation of the passive safety-related systems based on pressurizer pressure, as would occur in a SBLOCA event for the AP600, was impractical. Consequently, CMT and PRHR isolation valves were opened automatically early in each test at about the same time. Likewise, the OSU primary system pumps were tripped early, independent of break size, and the reactor decay power profile was very similar in all cases. Therefore, CMT and PRHR system behavior is similar at the beginning of all the SBLOCA break transients. The effect of break size on individual component performance for selected tests is discussed in the following subsections.

7.1.1 Passive Residual Heat Removal Behavior

As was discussed in Subsection 6.1.2, during a LOCA, the PRHR is designed to remove reactor decay heat up to the time when the ADS is actuated. During this period, heat is transferred from the PRHR tubes to the IRWST water. The heat transfer rate and duration of operation are strong functions of the break size.

This section shows the effect of break size on the PRHR performance for a range of cold-leg break sizes, including:

- Test SB18, 2-in. break
- Test SB06, 4-in. break
- Test SB23, 0.5-in. break
- Test SB21, top and bottom 4-in. breaks

For these cases, the plots of the PRHR performance (from Section 5) were examined to determine the following:

- Average heat transfer from the PRHR to the IRWST
- Total integrated heat transfer up to the initiation of ADS
- Period of peak PRHR operation

The results are summarized in Table 7.1.1-1.

Each of the four tests showed a delay of approximately 100 seconds until the PRHR began to operate. This is because heat is preferentially removed via the steam generators until they are thermally isolated; heat is removed by the PRHR once an adequate natural circulation flow rate through the heat exchanger is established to replace the initial PRHR inventory with hot-leg fluid.

The integrated heat removal plots from Section 5 indicate that the PRHR transferred heat at a slightly higher rate during the large break size tests. This was due to rapidly decreasing primary system pressure which resulted in higher quality two-phase mixture entering the PRHR tubes. The average heat transfer rate was about the same for the break sizes greater than or equal to 2-in. The difference between the 2-in. break and the 0.5-in. break was more substantial, which indicates that the inlet flow to the PRHR was likely single-phase during the smaller break.

The duration of PRHR operation was strongly affected by break size, as ADS 1-3 initiation, which marks the end of PRHR peak operation, is determined by the rate of system depressurization and its corresponding effect on CMT draining. For the large break size tests, the PRHR operates at peak levels for about 100 seconds. For the 2-in. break, the PRHR operates for 150 seconds. For the 0.5-in. break, the PRHR operates for nearly 2200 seconds.

As the break size decreases, the PRHR more closely behaves as it would for non-LOCA cases (e.g., single-phase heat removal for an indeterminate period). Thus, the integrated heat removal is much higher for the 0.5-in. break than for larger breaks.

TABLE 7.1.1-1
PRHR BEHAVIOR FOR VARIOUS COLD-LEG BREAK SIZES

Test	t_{start} (sec.)	t_{stop} (sec.)	Q_{avg} (Btu/sec.)	$\int Qdt$ (Btu)
SB18, 2-in. CL break	[			] a,b,c
SB06, 4-in. CL break				
SB21, double 4-in. break				
SB23, 1/2-in. CL break				

7.1.2 Event Timing Discussions

Core Makeup Tank Recirculation and Draindown

Table 7-1 presents the timing of significant events in the OSU tests. This section provides an overview of important behavior and compares SB01 with the CL-3 breaks of different sizes.

The duration of the CMT recirculation flow phase is a direct function of break size. Larger breaks not only depressurize more rapidly than do smaller breaks at a given location, but they also deplete the primary system inventory faster. Since the full draining of the CMT depends upon draining its balance line, large breaks, which drained the balance line to feed the break early on, also drained the CMT(s) to the ADS-1 level actuation setpoint much earlier than did SB01. During the CMT recirculation period, the flow delivery from each CMT into the RPV is [ ]^{a,b,c} lbm/sec., independent of break size. During the CMT draining, this rate increased to a value in excess of [ ]^{a,b,c} lbm/sec. in SB01 and the other breaks as well. The drain rate decreased from its peak value due to the loss of static driving head as the CMT drained; it also was diminished by interaction with accumulator flow in the DVI line.

Accumulator

The larger breaks achieved accumulator injection long before the ADS valves opened; this was not the case for SB01. While accumulator injection did precede ADS actuation for some of the other 2-in. breaks, it was only for a short time interval. Since the start of full flow accumulator injection depended upon sufficiently depressurizing the primary system, it coincided closely with ADS 1-3 actuation for the 2-in. breaks. Also, the depressurization caused by the break flow enhanced the accumulator delivery to the point that it shut off all CMT delivery completely for a period during the larger breaks, which was not the case for SB01 or the other 2-in. breaks. Despite this difference, the total duration of accumulator injection did not vary greatly among the various break sizes at the cold-leg and DVI break locations, the exception being the 0.5-in. cold-leg break, Test SB23, exhibited a much longer accumulator injection period because the PRHR depressurized the primary system to the accumulator gas pressure long before the CMT level reached the ADS 1-3 actuation setpoint. As a result, the accumulator injected during this break at a minuscule rate for an extended period prior to ADS actuation. Once the ADS 1-3 sequence was underway, the rate of accumulator injection for the 0.5-in. break was very similar to the rate during the other cold-leg break sizes.

Automatic Depressurization System

The ADS valves are designed to provide a phased depressurization of the RPV to permit IRWST injection. Once the ADS 1-3 valves actuated, the valves became the primary mass release path in SB01, receiving almost all of the mass flow leaving the primary system. Upon actuation during SB01, the ADS-4 valves supplanted ADS 1-3 as the recipient of almost all mass flow out of the primary system; this situation continued until IRWST injection refilled the RPV and caused the broken cold leg

to spill water out the break. For the larger break sizes, the break continued to release mass for at least a portion of the time while ADS was active.

Pressurizer

The pressurizer level behavior reflected the ADS operation in SB01. The pressurizer drained as a result of the break, refilled to a level higher than the initial level as ADS 1-3 activated, then emptied again as ADS-4 became the preferred path for mass release. Although this general behavior occurred independent of break size, lower ADS 1-3 flow rates produced a lower peak pressurizer mass for the larger breaks than SB01 exhibited when it refilled.

Sump Injection

Even with the single failure of one ADS-4 flow path simulated, the ADS provided adequate venting of steam generated in the core to permit continuous injection from the IRWST as it drained, independent of break size. The pressure relieving capability of the ADS was sufficient to allow sump injection through the check valves in the tests prior to receipt of the IRWST LO-LO level signal, which opens the primary sump flow path isolation valve. IRWST draining was almost the same independent of break size (except for SB21). Sump injection began through the check valve path at about the same time for all breaks.

During sump injection, break size had little or no impact on system performance. This proved to be true even though the largest breaks (SB10, SB21) exhibited a high downcomer liquid level and liquid in the cold legs throughout the sump injection period. In contrast, the corresponding 2-in. breaks (SB09, SB01) had no liquid in the cold legs once sump injection was fully established together with a downcomer level below the cold-leg elevation. It appears that the break was large enough in SB10 and SB21 to maintain liquid level in the cold legs during sump injection. Nevertheless, during long-term sump injection, all of the aforementioned tests exhibited stable and similar core mass inventories of about [ ]^{a,b,c} lbm. The mass released via the ADS-4 valves was also very similar among tests of different break sizes at the same break location.

7.1.3 Downcomer Condensation Phenomena

The 0.5-in. break differed from the other breaks in terms of the impact of accumulator injection on RPV upper head behavior. In SB01 and other larger breaks, the upper head had drained to the extent that only a small fraction of the initial mass remained at the time at which accumulator injection coincided with ADS 1-3 operation. At this point, the accumulator injected into the downcomer at a sufficient rate to condense enough steam to induce inflow from the upper head through the bypass plate, which in turn caused liquid from the upper plenum to partially refill the upper head. The upper head later drained into the upper plenum at the conclusion of accumulator injection. However, the 0.5-in. break had drained only about [ ]^{a,b,c} percent of its initial inventory at the time of coincident accumulator/ADS 1-3 operation, so the upper head refill phenomenon could not occur in the same way. All break sizes exhibited another, later upper head refill due to downcomer condensation when IRWST injection was fully established and CMT delivery had ceased.

IRWST injection followed ADS-4 initiation in all tests analyzed. For the larger break sizes, the break itself provided a significant vent path for steam to augment the ADS paths in depressurizing the RPV. Therefore, the time interval between ADS-4 actuation and IRWST delivery is much smaller for the larger breaks than for SB01, the 2-in. breaks of DVI and balance line, and SB23. Condensation-induced oscillations occur in SB01 during the IRWST injection phase; these oscillations occur significantly earlier in the larger cold-leg break SB06 and SB21 transients but they exhibit a similar period (Subsection 6.1.3).

7.1.4 Break Flow and Flow Integrals

The break flow observed during the cold-leg break LOCA tests is made up of two distinct phases:

- Break flow initially consisted of blowdown of the initial RCS mass inventory, which occurred as the primary system depressurized during the initial blowdown and natural circulation phases of the transient. This flow started at the beginning of the test and continued until ADS actuated. The integrated flow during this phase exhibited a steep ramp, which transitions to a plateau phase when flow out the break ceases as the depressurization path switched to the ADS.

- After IRWST injection began, some of the DVI line flow was diverted out of the cold-leg break, which increased the flow spilling out the break.

Break flow during both phases was highly dependent on the break size. The purpose of this section is to show how break flow varied with the size of the cold-leg break. The following test results are used:

- Test SB01, 2-in. break (base case)
- Test SB06, 4-in. break
- Test SB21, top and bottom 4-in. breaks
- Test SB23, 0.5-in. break

Figure 7.1.4-1 shows integrated break flow for the four tests up to the point of sump injection. The blowdown portion of the curves shows that the total break flow is dependent on the break size. The integrated mass out of the break was about [ ]^{a,b,c} lbm for the 2-in. break, [ ]^{a,b,c} lbm for the 4-in. break, [ ]^{a,b,c} lbm for the double 4-in. break, and about [ ]^{a,b,c} lbm for the 0.5-in. break.

The duration of the break flow phase was short for the larger breaks (2-in. or greater), ending by approximately [ ]^{a,b,c} seconds. The duration of the break flow for the 0.5-in. break was nearly [ ]^{a,b,c} seconds due to its lower depressurization rate, which delayed actuation of the ADS.

The duration of the plateau phase between the end of the ADS period and the start of the IRWST injection period was also shorter for the larger breaks, lasting about [ ]^{a,b,c} seconds for the 4-in. breaks, and [ ]^{a,b,c} seconds for the 2-in. break. The plateau phase for the 0.5-in. break was nearly [ ]^{a,b,c} seconds.

For the IRWST draindown portion, the mass flow rate out of the break also increased with increasing break size. For the 2-in. break, the flow rate was about [ ]^{a,b,c} lbm/sec., while for the 4-in. break, the flow rate was nearly [ ]^{a,b,c} lbm/sec. For the double 4-in. break, the flow rate during IRWST draindown was [ ]^{a,b,c} lbm/sec. Finally, for the 0.5-in. break, the flow rate during draindown was [ ]^{a,b,c} lbm/sec.

Figure 7.1.4-2 shows the integrated energy for the four tests up to the point of sump injection. As was observed for the mass flow, the energy flow was highly dependent on the break size. The integrated energy increased rapidly, then leveled out after the initial blowdown and natural circulation phase. The energy increased once again after IRWST draindown actuated, when IRWST flow was diverted out of the broken cold leg.

Since none of these four OSU tests led to core uncovery, one criterion which may be used to assess the relative severity of breaks is to identify the minimum core inventory. The largest breaks (SB06 and SB21) exhibited lower minimum core mass values than SB01, as shown in Figure 7.1.4-3. SB06 and SB21 lost mass out of the break so rapidly that the minimum core mass inventories occurred at [ ]^{a,b,c} seconds and [ ]^{a,b,c} seconds, respectively; SB21, the larger of the two breaks, exhibited the lower minimum core mass inventory. The SB06 and SB21 minimum RPV mass inventories (Figure 7.1.4-4), occurred at [ ]^{a,b,c} and at [ ]^{a,b,c} seconds, respectively, when they were increased by accumulator injection flow. The minimum RPV mass inventory for the much smaller SB01 break did not occur until around the time at which [ ]^{a,b,c} began, and the SB01 core inventory was never lower than the steady-state inventory prior to break initiation. This is consistent with the general trend that the larger the break size at a given location, the lower the value of the minimum core and RPV mass inventories (Table 7-1).

Note that the minimum RPV mass inventory of SB21 is overstated in Table 7-1 by up to [ ]^{a,b,c} lbm (Subsection 5.11.1.2) due to an erroneous measurement of the upper plenum level.

TABLE 7.1.4-1
SUBSECTION 7.1.4 PLOT PACKAGE

Plot No.	Description
1	Integrated Break Flow vs. Break Size
2	Integrated Break Energy vs. Break Size
3	Minimum Core Mass Inventory vs. Simulated Break Flow Area
4	Minimum RPV Mass Inventory vs. Simulated Break Flow Area

THE FIGURES LISTED IN TABLE 7.1.4-1
ARE NOT INCLUDED IN THIS NONPROPRIETARY DOCUMENT

7.2 Variations in Break Location

The OSU test matrix included simulated LOCAs with the break located on the cold leg, the balance line, the DVI line, and the hot leg, and an inadvertent ADS actuation event. For tests with the same break size, changing the break location from cold leg to balance line showed little impact. The comparative behavior described in the previous section for SB01 versus SB06 and SB21, also holds true for SB09 compared to SB10, except that the times at which the minimum core and RPV mass inventories occurred during SB10 are approximately the same. The early initiation of ADS 1-3 due to the draining of CMT-1 during the double-ended DVI line break, SB12, produced a significantly different transient than SB06, which investigated the same break size located on the cold leg. SB13 showed the impact on the 2-in. equivalent diameter break of the accelerated draining of CMT-1 due to the DVI break location relative to SB01; SB13 was more severe than SB01 in terms of its minimum core and RPV mass inventories.

Plots of the minimum core and RPV mass inventories for all breaks are provided as indicated in Table 7.1.4-1. A review of these figures indicates that while break location did not have a strong effect on system behavior for three 2-in. break sizes, it had more influence on larger break sizes, and the DVI break location strongly affected both the double-ended DVI and 2-in. break cases. The double-ended DVI break (SB12) exhibited the minimum core mass inventory.

7.2.1 Event Timing/Phenomena

In this section, differences in important behaviors are identified among breaks of comparable size in different locations. Figures 7.1.4-3 and 7.1.4-4 show minimum mass inventory for breaks of the OSU spectrum.

Blowdown Phase

The break area of the double-ended balance line break, Matrix Test SB10, was approximately 200 percent larger than SB06 and 50 percent larger than SB21. In addition, the break deactivated one CMT during the initial injection phase of SB10. Given those facts, it might be anticipated that SB10 would show smaller minimum core and RPV mass inventories than SB06 and SB21. Note that the SB21 RPV minimum mass inventory is overstated in Figure 7.1.4-4 (Subsection 5.11.1.2) by possibly as much as 150 lbm. SB10 did exhibit a smaller minimum RPV mass inventory at an earlier time than SB06, which befits its size and location. However, the minimum core mass inventory of SB10 was greater than that of SB21; in both tests, accumulator flow provided the mass to the core to replenish core inventory from the minimum value.

The unique break configuration of SB21 provided the capability to vent steam through the top of the broken cold leg at the same time that liquid flowed out the bottom; as a result, the top break was uncovered early on, enabling primary system pressure to drop more rapidly in SB21 than in SB10. The lower SB21 pressure activated the accumulators earlier than in SB10 and caused the liquid in the core to flash, leading to a lower core minimum mass. The lower pressure of SB21 was accomplished during the first 100 seconds despite a significantly lower total break mass flow than in SB10 because the steam vent break flow path was present on top of the broken cold leg. In contrast with these break location effects among the larger breaks, the SB01 and SB09 core and RPV minimum mass inventory transients were very similar, indicating that the balance line location of SB09 had little impact.

Table 7-1 indicates that little difference existed during LTC among SB01 and the other 2-in. breaks.

Long-Term Cooling Phase

During LTC, SB10, which behaved like SB09, differed from SB21 in that SB21 initiated sump injection about [ ]^{a,b,c} seconds earlier; the smaller break size, SB21, initiated sump injection earlier than SB10 because it drained the IRWST faster. ADS 4-1 and ADS 4-2 liquid flow were much lower during IRWST injection in SB21 than in SB10. This suggests that steam generated in the core was more effectively vented via ADS-4, as was also indicated by the ADS outlet temperatures (Section 6.2-2). The RPV pressure was lower in SB21 than SB10, another indication that steam was generated in the core during SB10 at the same time that the upper plenum LDP cell indicated that the upper plenum was filled with liquid. The resulting higher RPV pressure in SB10 decreased the IRWST injection flow rate relative to SB21. Nevertheless, all of the tests cooled the core effectively and exhibited no core uncovering during both phases of LTC.

IRWST injection, which begins the LTC phase of the test transients, required the depressurization of the RPV to a value within a few psi of the atmospheric pressure. Neglecting SB19, in which the IRWST actuated early because a containment pressure of 8 psig was intentionally established as a boundary condition, IRWST injection initiation for 2-in. breaks at other locations corresponded closely to the SB01 result.

Moving the break location to the balance line caused almost no change in SB09 in the start of IRWST delivery through the DVI line connected to the CMT balance line unaffected by the broken balance line, relative to SB01. The 2-in. hot-leg break, SB15, has the additional hot-leg vent path of the break itself, and it initiated IRWST injection before SB01. In the 2-in. DVI line break, the CMT feeding the broken DVI line generated a LO-LO level signal several hundred seconds earlier than had occurred in SB01. Therefore, SB13 began ADS-4 operation and achieved IRWST injection several hundred seconds before SB01. The order in which IRWST injection began among SB13, SB15, and SB01 also proved to be the order in which sump injection initiated later during those 2-in. break transients.

Core and Reactor Pressure Vessel Inventory

Figure 7.1.4-3 shows the minimum core mass inventories for the 2-in. and 4-in. DVI line breaks (SB13 and SB12) are much less than for the cold-leg breaks of the same size. In comparing SB13 with SB01, the location of the break in the DVI line produced a mixed break flow of RPV and CMT water. The DVI-1 break flow had a lower enthalpy than did the cold-leg break flow in SB01, and the primary system repressurized by several psi between 150 and 300 seconds in SB13. With the SB13 DVI-1 break location, CMT-1 drained more rapidly than in SB01, and ADS 1-3 opened earlier in the transient. As the CMT-1 flow through the time of ADS actuation had largely passed through the break rather than into the RPV, the liquid in the RPV was at a higher enthalpy at the time of ADS actuation in SB13 than in SB01. Therefore, more liquid flashing took place in the core and RPV than was the case in SB01. The increase in mass lost due to flashing produced the lower minimum core mass in SB13 relative to SB01. SB13 exhibits a minimum RPV mass inventory which is not only below that of SB01, but also occurs a short time after ADS actuation, rather than near the start of IRWST injection. The behaviors observed later in SB13, after the accumulators replenished the RPV inventory from its minimum condition, were very similar to SB01, but they occurred somewhat earlier, which is consistent with the earlier SB13 ADS actuation.

The minimum core and RPV mass inventories of SB12 were less than those of SB06 for the same reason; enthalpies in the RPV at the time of ADS actuation were higher in SB12 because cool CMT-1 water was lost through the break. Their respective break locations caused SB14 and SB12 to not exhibit extended condensation-induced oscillations during LTC IRWST injection. SB14 lacked adequate condensation capability in the downcomer to sustain oscillations. As all of the initial primary system energy was deposited in the liquid of the IRWST prior to ADS-4 actuation, the IRWST in SB14 was much hotter than in the other tests and was close to saturation temperature, limiting the potential for condensation in the downcomer. The oscillations did not occur in SB12 because the large break at a location beneath the hot legs held the upper plenum level below the hot-leg elevation,

allowing ADS 1-4 to continuously vent steam. SB12 and SB14 stand in contrast to the other breaks, which exhibited these oscillations independent of break size. Refer to Subsection 6.1.3 for further discussion of the condensation-induced oscillations during IRWST injection.

7.2.2 Core Makeup Tank Drain/Refill Behavior

Refilling of the CMTs was commonly observed to occur in the OSU tests at times on the order of [ ]^{a,b,c} of seconds into IRWST injection. However, during SB19, the test performed with a simulated containment backpressure of [ ]^{a,b,c} psig, CMT refill began at about the time of [ ]^{a,b,c}.

The behavior of the CMT refill following initial draindown, and the mechanism driving this behavior, was discussed in Subsection 6.1.1. This section presents a discussion about the test conditions observed during CMT reflood.

Break Size Effects

Data from the four cold-leg break tests served as the basis for this comparison;

- Test SB23, 0.5-in. cold-leg break
- Test SB01, 2-in. cold-leg break
- Test SB06, 4-in. cold-leg break
- Test SB21, 4-in. top and bottom cold-leg breaks

The CMT-1 water level history for each of the preceding four tests is shown in Figure 7.2.2-1. From this figure, the following are observed;

- All four tests exhibited draindown and refill behavior.

- The 0.5-in. break took the longest time to drain and did not initiate refilling until much later in the transient than the larger breaks. The CMT also refilled to a much higher level for the 0.5-in. break than did the other break sizes.

- Both of the 4-in. break tests performed similarly with respect to time. The CMT did not drain to quite as low a level and refilled sooner and to a slightly higher level for the 4-in. top and bottom break than for the 4-in. bottom break.

- The draindown for the 2-in. break behaved similarly to that of the 4-in. breaks. However, the reflood, while occurring about [ ]^{a,b,c} seconds earlier in the transient and refilling to about 6-in. lower in the CMT, was similar to that of the 0.5-in. break.

Similar draindown and refill behavior is noted for CMT-2 in each of these tests, as shown in Figure 7.2.2-2.

Figures 7.2.2-3 through 7.2.2-6 show the time histories of the water level in CMT-1, the CL-3/CMT-1 balance line, and the downcomer, as well as the pressure in the CMT for each of the four tests

identified above. These plots support the reflood mechanism described in Subsection 6.1.1; that liquid from a filled cold-leg balance line spilled into the CMT, causing steam to condense and pressure to drop, resulting in more liquid being drawn into the CMT. The refilling process was observed to terminate when the CMT pressure reached approximately [ ]^{a,b,c} psia or the liquid level in the cold leg dropped below approximately [ ]^{a,b,c} inches.

Hot-Leg versus Cold-Leg Break

The liquid level history of CMT-1 for the hot-leg break simulation, Test SB15, was compared to that of the reference 2-in. cold-leg break, Test SB01, in Figure 7.2.2-7. The plot shows that the draindown behavior of both breaks was similar, with the hot-leg break refilling about [ ]^{a,b,c} seconds earlier than cold-leg break. Both transients resulted in the CMT being reflooded to about the same elevation. Comparing the history of the liquid level in CMT-1, CL-3/CMT-1 balance line, and the downcomer with the CMT-1 pressure history as shown in Figure 7.2.2-8, it is again noted that there was a pressure drop in the CMT consistent with high water levels in the downcomer and the balance line, so that after the pressure reached a minimum, the water level in CMT-1 was observed to begin increasing.

DVI Line Breaks

The CMT draindown and refill behavior was noted to be dependent upon the size of the DVI line break. As shown in Figure 7.2.2-9, for the 2-in. DVI line break, Test SB13, CMT-1 drained in a manner similar to that observed for Test SB01 and reflooded at about the same time, but to a level approximately [ ]^{a,b,c}-in. higher than was observed in Test SB01. For the 2-in. DVI line break, CMT-1 completed the second draindown by about [ ]^{a,b,c} seconds into the test, or about [ ]^{a,b,c} seconds before CMT-1 drained for the second time in the reference 2-in. cold-leg break test. For Test SB12, the double ended guillotine DVI line break, CMT-1 drained quickly and did not reflood during the test.

As shown in Figure 7.2.2-10, CMT-2 was observed to drain fastest for the double ended guillotine DVI line break (Test SB12), with Tests SB13 and SB01 exhibiting similar draindown behavior. Similar to the broken loop CMT-1, the intact loop CMT-2 did not refill in Test SB12. However, in Test SB13, CMT-2 exhibited a refill behavior similar to that observed in SB01, although delayed by about [ ]^{a,b,c} seconds. Also, for SB13, CMT-2 redrained much more quickly than it did in Test SB01, completing its second draindown by about [ ]^{a,b,c} seconds into the test.

Figure 7.2.2-11 shows that the liquid levels in both the downcomer and the cold-leg balance line were high at the time CMT-1 reflood initiated during Test SB13. As CMT-1 was observed to refill, the local pressure in the CMT remained low, about [ ]^{a,b,c} psia. However, for Test SB12, the double-ended guillotine (DEG) cold-leg balance line break, Figure 7.2.2-12 shows the water level in the cold-leg balance line was too low (about [ ]^{a,b,c} in.) throughout the test to be drawn into CMT-1 and the CMT did not refill.

This information, combined with the preceding observations for CMT-2 performance for both DVI line break tests, suggests that the mechanism for CMT reflood was water from the cold-leg balance line being drawn into the CMT, resulting in condensation that reduced the pressure causing additional water to be drawn into the CMT, resulting in refilling of the CMT as described in Subsection 6.1.1.

Cold-Leg Balance Line Breaks

As expected, the draindown and refill behavior of the CMTs was observed to be dependent upon their location with respect to the break location. As shown in Figure 7.2.2-13, the response of broken loop CMT-1 to a 2-in. cold-leg balance line break was similar to that of the reference 2-in. cold-leg break, although the initial draindown was delayed by about [ ]^{a,b,c} seconds, or until about [ ]^{a,b,c} seconds into the test. During SB01, CMT-1 refilled to an elevation of about [ ]^{a,b,c}-in., while in Test SB09, it was observed to not refill. For the DEG break, the CMT draindown was not started until about [ ]^{a,b,c} seconds after initiation of the test, and was a gradual process that continued until about [ ]^{a,b,c} seconds into the test; in Test SB10, CMT-1 was not observed to refill.

From Figure 7.2.2-14, however, CMT-2 was observed to reflood for all three tests with the reflood occurring earliest for the DEG cold-leg balance line break. The DEG cold-leg balance line break was also observed to refill and hold a water level that was about [ ]^{a,b,c}-in. greater than either of the other two breaks. It was also noted that, for both of the balance line breaks, the second draindown was completed at about the same time, which was about [ ]^{a,b,c} seconds before that for base case Test SB01.

From Figure 7.2.2-15, it was noted that the liquid level in the downcomer for Test SB09 remained high over the time period in which CMT refill might be expected; from approximately [ ]^{a,b,c} seconds. However, since the primary system break was in the CL-3/CMT-1 balance line, it could not fill and promote the reflooding of CMT-1. Similarly, the break in CL-3/CMT-1 balance line for Test SB10 precluded CMT reflood.

However, the intact cold-leg balance line did promote refill of CMT-2, Figure 7.2.2-16. The requisite conditions were present in both Tests SB09 and SB10 to support drawing of water from the cold-leg into CMT-2; high downcomer level (> [ ]^{a,b,c}-in. of water), high cold-leg balance line level, and low CMT pressure. These observations further support the mechanism of CMT reflood as described in Subsection 6.1.1.

Inadvertent Automatic Depressurization System

The inadvertent ADS event was noted to produce an initial draindown of CMT-1 that was similar to that observed in the reference 2-in. cold-leg break, Figure 7.2.2-17. The CMT refill occurred at about the same time in both tests, but was observed to result in only about [ ]^{a,b,c}-in. of water being drawn into the CMT compared to the approximately [ ]^{a,b,c}-in. for the reference test. Comparing water levels in the cold-leg balance line, the downcomer, and the CMT, Figure 7.2.2-18, it was noted that

the downcomer water level, and therefore, the cold-leg water level decreased below about [ ]^{a,b,c}-in. at about the time CMT-1 refilling was terminated. Also at that time, the CMT pressure recovered to a nominal value of about [ ]^{a,b,c} psia. Thus, although at a reduced pressure, the CMT could not draw fluid from the downcomer as its liquid level had dropped below the cold leg.

The level instrument for CMT-2 was not operable for Test SB14. However, data from channels LDP-504, LDP-506, and LDP-508, which collectively spanned the same elevation as the overall level measurement of LDP-502, indicated the CMT-2 refill behavior was similar to that of CMT-1; CMT-2 drained within about the first [ ]^{a,b,c} seconds of the test, refilling began at about [ ]^{a,b,c} seconds into the test with a maximum refill level of about [ ]^{a,b,c} inches of water reached at about [ ]^{a,b,c} seconds, and the second drain of the tank completed at about [ ]^{a,b,c} seconds into the test.

Containment Backpressure Effects

Containment backpressure, as simulated in Test SB19, was noted to have some affect on the CMT refill behavior compared to the behavior noted in reference Test SB01. Specifically, for Test SB19, both CMTs were observed to stop their initial draining before becoming completely empty, and refilled quickly (Figures 7.2.2.-19 and 7.2.2-20). This suggests the higher system pressure, and therefore, higher steam temperatures in the CMTs, promoted higher condensation rates on the inside surfaces of the CMTs early in Test SB19, which, in turn, resulted in lower CMT pressures relative to the cold leg earlier in the test. Combined with the earlier IRWST injection, also a consequence of increased containment backpressure, which provided for high downcomer water levels earlier than occurred in reference Test SB01, the low CMT pressures early in Test SB19 allowed the CMTs to draw water from the cold-leg balance lines earlier than was observed in reference Test SB01. Thus, the results of Test SB19 demonstrate that the early IRWST injection, promoted by the increased containment backpressure, provided for higher water levels in the downcomer and cold legs earlier than was observed in reference Test SB01.

Both CMTs were also observed to complete their second draindown by about [ ]^{a,b,c} seconds before the same event occurred in base case Test SB01. Comparing the liquid level in the downcomer and the cold-leg balance line for both CMT-1 and CMT-2, Figures 7.2.2-21 and 7.2.2-22 respectively, it is noted that the downcomer fluid level was above [ ]^{a,b,c} inches until the CMTs completed their second draindown. Also, as the CMTs approached complete draindown, the fluid level in the cold-leg balance lines dropped to about [ ]^{a,b,c}-in. and the CMT pressure increased. This suggests that the drop in water level in the downcomer and cold-leg precluded the inflow of water into the CMT, resulting in complete draining of the tank.

TABLE 7.2.2-1
OSU TEST ANALYSIS PLOT PACKAGE FOR SECTION 7.2.2
CMT DRAIN / REFILL BEHAVIOR

Plot No.	Component	Variables	Units	Description
1	CMT 1	CLDP-507	in.	CMT 1 water level for cold leg breaks;SB-23, -01, -06, -21
2	CMT 2	CLDP-502	in.	CMT 2 water level for cold leg breaks;SB-23, -01, -06, -21
3	CMT 1 CLBL Downcomer CMT 1	CLDP-507 CLDP-509 CLDP-140 PTPLCMT1	in. in. in. psia	CMT 1 water level, SB-23 CLBL water level, SB-23 Downcomer water level, SB-23 CMT 1 pressure, SB-23
4	CMT 1 CLBL Downcomer CMT 1	CLDP-507 CLDP-509 CLDP-140 PTPLCMT1	in. in. in. psia	CMT 1 water level, SB-01 CLBL water level, SB-01 Downcomer water level, SB-01 CMT 1 pressure, SB-01
5	CMT 1 CLBL Downcomer CMT 1	CLDP-507 CLDP-509 CLDP-140 PTPLCMT1	in. in. in. psia	CMT 1 water level, SB-06 CLBL water level, SB-206 Downcomer water level, SB-06 CMT 1 pressure, SB-06
6	CMT 1 CLBL Downcomer CMT 1	CLDP-507 CLDP-509 CLDP-140 PTPLCMT1	in. in. in. psia	CMT 1 water level, SB-21 CLBL water level, SB-21 Downcomer water level, SB-21 CMT 1 pressure, SB-21
7	CMT 1	CLDP-507	in.	CMT 1 water level for hot leg break; SB-01, -15
8	CMT 1 CLBL Downcomer CMT 1	CLDP-507 CLDP-509 CLDP-140 PTPLCMT1	in. in. in. psia	CMT 1 water level, SB-15 CLBL water level, SB-15 Downcomer water level, SB-15 CMT 1 pressure, SB-15
9	CMT 1	CLDP-507	in.	CMT 1 water level for DVI line breaks; SB-01, -13, -12
10	CMT 2	CLDP-502	in.	CMT 2 water level for DVI line breaks; SB-01, -13, -12

TABLE 7.2.2-1 (Continued)
OSU TEST ANALYSIS PLOT PACKAGE FOR SECTION 7.2.2
CMT DRAIN / REFILL BEHAVIOR

Plot No.	Component	Variables	Units	Description
11	CMT 1 CLBL Downcomer CMT 1	CLDP-507 CLDP-509 CLDP-140 PTPLCMT1	in. in. in. psia	CMT 1 water level, SB-13 CLBL water level, SB-13 Downcomer water level, SB-13 CMT 1 pressure, SB-13
12	CMT 1 CLBL Downcomer CMT 1	CLDP-507 CLDP-509 CLDP-140 PTPLCMT1	in. in. in. psia	CMT 1 water level, SB-12 CLBL water level, SB-12 Downcomer water level, SB-12 CMT 1 pressure, SB-12
13	CMT 1	CLDP-507	in.	CMT 1 water level for CLBL breaks; SB-01, -09, -10
14	CMT 1	CLDP-502	in.	CMT 2 water level for CLBL breaks; SB-01, -09, -10
15	CMT 1 CLBL Downcomer CMT 1	CLDP-507 CLDP-509 CLDP-140 PTPLCMT1	in. in. in. psia	CMT 1 water level, SB-09 CLBL water level, SB-09 Downcomer water level, SB-09 CMT 1 pressure, SB-09
16	CMT 2 CLBL Downcomer CMT 2	CLDP-502 CLDP-510 CLDP-140 PTPLCMT2	in. in. in. psia	CMT 2 water level, SB-09 CLBL water level, SB-09 Downcomer water level, SB-09 CMT 2 pressure, SB-09
17	CMT 1	CLDP-507	in.	CMT 1 water level for Inadvertant ADS; SB-01, -14
18	CMT 1 CLBL Downcomer CMT 1	CLDP-507 CLDP-509 CLDP-140 PTPLCMT1	in. in. in. psia	CMT 1 water level, SB-14 CLBL water level, SB-14 Downcomer water level, SB-14 CMT 1 pressure, SB-14
19	CMT 1	CLDP-507	in.	CMT 1 water level, Containment Backpressure; SB-01, -19
20	CMT 2	CLDP-502	in.	CMT 2 water level, Containment Backpressure; SB-01, -19

TABLE 7.2.2-1 (Continued)
OSU TEST ANALYSIS PLOT PACKAGE FOR SECTION 7.2.2
CMT DRAIN / REFILL BEHAVIOR

Plot No.	Component	Variables	Units	Description
21	CMT 1	CLDP-507	in.	CMT 1 water level, SB-19
	CLBL	CLDP-509	in.	CLBL water level, SB-19
	Downcomer	CLDP-140	in.	Downcomer water level, SB-19
	CMT 1	PTPLCMT1	psia	CMT 1 pressure, SB-19
22	CMT 2	CLDP-502	in.	CMT 1 water level, SB-19
	CLBL	CLDP-510	in.	CLBL water level, SB-19
	Downcomer	CLDP-140	in.	Downcomer water level, SB-19
	CMT 2	PTPLCMT2	psia	CMT 1 pressure, SB-19

THE FIGURES LISTED IN TABLE 7.2.2-1
ARE NOT INCLUDED IN THIS NONPROPRIETARY DOCUMENT

7.3 Closure on the Phenomena Identification Ranking Table for AP600 Small-Break Loss-of-Coolant Accident and Long-Term Cooling for the OSU Tests

The PIRT has been used to identify key thermal-hydraulic parameters of interest for the SBLOCA and LTC transient. The PIRT for AP600 is given in Table 1.3-1 for the SBLOCA and LTC events. High importance phenomena are indicated with an "H" in the table, and have been addressed in the OSU tests and are discussed below. The items which were marked "M" were also covered in the tests, but are not specifically addressed.

7.3.1 Initial Blowdown

The highly ranked phenomena for the initial blowdown phase include the critical flow at the break and the power in the rod bundle, both of which cause flow and mass redistribution within the primary system. The CMT begins to inject and recirculate during this time period.

In the blowdown phase of the transient, critical break flow and decay heat were directly measured, and the system mass inventory was calculated from level pressure drop cells on components in the system so that transient mass distribution with acceptable accuracy was obtained. The tests provide the necessary data to achieve closure on the "H" items.

7.3.2 Natural Circulation

In the natural circulation phase, system pressure is stabilized at the secondary-side pressure as the system drains through the break. The CMTs recirculate and begin to drain as the upper elevations of the primary system drain.

The natural circulation phase had the same items as in the blowdown phase ranked highly in the PIRT, but also included the hot-leg flow pattern, CMT balance line pressure drops, single- and two-phase flow into the CMT, and heat transfer from the PRHR. The only item not directly measured was the hot-leg flow pattern; however, the levels in the SG inlet plenum and RPV upper plenum, combined with calculated steam generation in the core, permitted assessment of the hot-leg behavior for this phase of the transient.

One key item not directly mentioned in the PIRT is the cold leg balance line draining. The draining behavior of the cold-leg balance line is the initiating event for the CMT draining and the resulting initiation of the ADS activation. While this was not specifically identified in the PIRT, the tests did provide instrumentation to identify this particular phenomenon.

7.3.3 Automatic Depressurization System

Once the ADS valves open, a mass redistribution occurs as a result of the blowdown through the ADS valves on the pressurizer, with mass accumulation occurring in the pressurizer.

The ADS blowdown period was characterized by a rapid depressurization of the primary system. Therefore, flow through ADS 1-3 and the pressure drop in the piping system are highly ranked items. ADS flow and the pressure drop across the system and ADS valves were directly measured. The rapid depressurization caused a redistribution of system mass inventory due to the flow path caused by opening the ADS valves on the top of the pressurizer. The accumulators also inject and refill portions of the primary system. The accumulator injection is an important parameter during this time period since the accumulator refills the primary system. The transient mass redistribution within the primary system was directly measured and was also calculated during this period of the transient for all components and major piping in the primary and safety-related systems.

7.3.4 IRWST Injection

Once the primary system has depressurized below the IRWST pressure head, the IRWST check valves open and IRWST injection begins.

The IRWST injection period was characterized by a near constant pressure, quasi-steady state condition in which the mass inventory in the RPV and primary system, which is highly ranked in the PIRT, was nearly constant with injection from the IRWST into the RPV and venting of flow through the hot legs and ADS-4. The decay heat, which is also ranked high, is also nearly constant during this time frame. Initially, as the injection flow from the IRWST was large with significant subcooling; the vapor generation in the core was suppressed, and liquid flow discharged out of the ADS-4 valves. The venting capacity of the ADS-4 valves results in a low pressure drop vent path out of the primary system. The ADS-4 valves are also highly ranked in the PIRT. As the IRWST drained and subcooling of the injection flow decreased, steam generation was calculated to occur in the simulated rod bundle so that a two-phase mixture was then vented out of the hot leg. The IRWST levels, flow and temperature were directly measured in the test and were used to calculate the mass inventories and energy distribution during this period.

7.3.5 Long-Term Cooling

As the IRWST drains, and its head becomes less than the sump elevation head, the flow will be initiated from the sump into the primary system.

The phenomena of importance for the LTC with sump injection phase are the same as the IRWST period except that the decay power and injection flowrate are lower. The lower injection flow with reduced inlet subcooling resulted in net steam generation within the core for this period. The PIRT identifies that the important phenomena during this period are the venting capacity of the ADS-4 valves and the DVI injection flow into the vessel, and the decay heat level.

The pump flow, levels, and DVI line flow were directly measured, and the transient mass inventories were calculated during this period. The flow rate out of ADS-4 was not able to be measured in the

tests due to the underranged vortex flow meters. However, the mass and energy balance on the rod bundle indicated the presence of steam, which is believed to have vented out the ADS-4 valves.

7.3.6 Other Phenomena Observed in the Tests

The phenomena identified as being important in the PIRT were directly measured or calculated from the data. However, five other important phenomena observed in the experiments were not identified in the PIRT. These include:

- Refilling of the CMT late in the transient
- Very regular oscillations in flow and pressure observed as the IRWST emptied and the transition to the sump flow occurred
- Thermal stratification in the cold legs
- Condensation induced pressure spike in the upper downcomer/RPV head region.
- Reverse flow into the IRWST at the initiation of sump injection.

Core Makeup Tank

The CMT refilling was due to the wall condensation which decreased the steam pressure in the CMT and induced flow up the CMT balance line to the tank. When the cold leg is voided, only steam will flow up the balance line to be condensed; which results in a small amount of mass being condensed in the CMT. When the cold leg is liquid-solid, the condensation can induce the liquid level to rise in the balance line to the top of the CMT, resulting in an overflow and more rapid condensation in the CMT tank, as discussed in Subsection 6.1.1. This situation can only occur when the primary system is essentially overfilled so that the cold legs are liquid-solid. Although this phenomenon was not identified in the PIRT, it does not have any significant effect on the core cooling as observed in the tests. Also, since the OSU facility is 1/4-scale in height and the pressures are full scale at this time in the test, this phenomenon occurs easily in the tests relative to the AP600 due to the full elevation of the cold-leg balance line. In either case, however, this phenomenon results in a mass redistribution from an overfilled system and core cooling is not impaired.

Oscillating Behavior

The second phenomenon observed in the tests was long stable period oscillations detected during the LTC phase of the transient at the end of IRWST injection and the transition to sump injection. A detailed explanation of these oscillations is provided in Subsection 6.1.3, and indicates that the oscillations were caused by the venting of steam which was generated in the core. The oscillations were well-behaved and exhibited a period of 100-160 seconds. Oscillation occurring in the vessel

resulted in oscillations of the DVI injection flow and are associated with the condensation in the downcomer and venting out the hot leg. While the DVI flow oscillated, the flow was always positive from the passive systems to the RPV so that core cooling was never impaired. These oscillations were also a result of the vessel being overfilled, so that the hot-leg or cold-leg vent paths were blocked such that the RPV pressure increased to vent steam out of the hot legs or cold legs. The phenomenon is very repeatable and does not challenge the core cooling since the mixture level is within the upper plenum. The oscillations observed in the OSU test facility could also occur in the AP600, since the system pressure is very low at this stage of the transient and large changes in steam volumes will occur which will require venting of the steam out of the hot legs or through the vessel upper head to downcomer vent paths to the cold legs. Again, the oscillations occurred because the vessel was in an overfilled state such that the system pressurized to force flow through the hot- and cold-leg vent paths. For SB12, a larger break test where the hot legs were not covered, the oscillations did not occur.

Thermal Stratification

Another phenomenon not included into the PIRT was the observed fluid thermal stratification in the cold legs, which contains the PRHR return lines. The stratification is an AP600 design issue, not a core cooling safety issue, since cooling is maintained with the observed stratification.

Steam Condensation Events

The rapid condensation phenomenon, which occurred in the top of the downcomer and RPV head was due to an isolated pocket of steam that rapidly condensed, and momentarily caused an upsurge of flow in the vessel. The issues on this phenomenon are again related to the mechanical design of the AP600. There are no core cooling concerns since this condensation behavior only occurred when the reactor vessel was adequately filled with water.

Reverse Flow into the In-containment Refueling Water Storage Tank

Another observation in the test, which is an AP600 design issue, is the reversal of flow in the IRWST-1 line that occurs when the sump valves open. This flow reversal occurs as a result of the balancing of the differential level between the sump and IRWST water levels and the lower resistance in the IRWST-1 line connected to the DVI line. Since the net flow into the core through the DVI-1 and DVI-2 lines is maintained, core cooling is maintained.

7.3.7 PIRT Conclusions

The items identified in the PIRT as highly ranked phenomena were effectively measured and quantified in the OSU Final Data Report[1] and in this report, so that computer code assessment can be made with the data.

Five new phenomena were observed in the tests which were not captured in the PIRT. Two of these phenomena have been analyzed and discussed in detail in this report, whereas, the other three phenomena, cold-leg stratification, rapid condensation in the upper downcomer, and flow reversal of the IRWST line, reflect potential AP600 design issues and will be addressed in the design.

The OSU PIRT proved useful for ordering the analysis of the data and of identifying and discussing the phenomena observed in the tests.

8.0 CONCLUSIONS

The Oregon State University (OSU) test facility was constructed specifically to investigate the AP600 passive system characteristics. The facility design models the detail of the AP600 geometry, including the primary system, pipe routings, layout for the passive safety systems and selected nonsafety-related systems. The OSU test matrix was designed to capture the thermal-hydraulic phenomena expected during a postulated AP600 SBLOCA and LTC transients. These phenomena were identified in the PIRT (Table 1.3-1). After detailed analysis of the test data, the passive safety systems were found to provide more than sufficient flow to maintain excellent core cooling. None of the design basis tests indicated a core uncovery.

A two-phase scaling methodology was used to design the OSU tests. This methodology preserved the phenomena of interest so that the expected response of the AP600 was modeled. Effects of the scaling comparisons were observed in the tests. For example, break sizes less than 2-inches in diameter used the mass flow basis for scaling, whereas a later revision to the break scaling indicated that an energy basis should have been used. As a result, the 1-in. and 0.5-in. cold-leg breaks are oversized relative to the AP600 and appear larger than originally planned. The data obtained is valid, however, the revised break scaling must be considered when comparing the OSU response to the SPES-2 tests or the AP600 plant. The other scaling issue observed was the refilling of the CMTs in the OSU facility due to the reduced-height scaling. This was not a problem for modeling the tests with computer codes, but the refilling may be nonprotypical because of the reduced-height scaling used in the test.

The PIRT was used to organize phenomena of interest and helped set priority in the test design, instrumentation, and data analysis. Key phenomena identified in the PIRT were fully analyzed in this report. The tests covered a wide range of SBLOCAs with different break sizes and locations so that phenomena of interest were captured in the tests performed. Most of the tests continued into LTC so that the transition from IRWST injection into long-term recirculation was captured in the tests. The associated analyses show that continuous, stable, core cooling was maintained for the tests indicating that the passive system provides adequate injection flow to maintain core cooling indefinitely.

There were also phenomena observed in the tests that were not addressed in the PIRT. One phenomenon, the CMT refilling, is related to test facility scaling, while the others are thermal-hydraulic phenomena that potentially could occur in the AP600 plant. Three of these identified phenomena, thermal stratification, rapid condensation, and flow reversal in the IRWST injection line are AP600 design issues that will be addressed in future design efforts. The fourth phenomena, oscillations during LTC were analyzed and hypotheses were developed to explain those oscillations. None of the new phenomena observed in the tests impaired the core's cooling ability or the ability of the passive safety injection systems to provide adequate flow for core cooling.

Since the OSU tests covered high-pressure blowdown as well as low-pressure, long-term cooling phenomena, test instrumentation was required to cover wide ranges. In the low pressure, long-term cooling period, some of the instrumentation, such as the steam flow vortex meters did not perform at

the low flow experienced during these time periods. However, redundant measurements which were designed into the system, compensated for most of the instrument limitations.

The low vapor flow measurements from the break location ADS-4, and ADS 1-3 for the post blowdown and long-term cooling periods indicated little or no steam flow. However, the detailed mass and energy analysis program indicated that the core produced a net steam flow during the transients, which was not measured leaving the system, due to the underranged vortex meters. Although the system mass and energy balances up to 800 seconds were achieved with good closure, balances beyond this time period were not accurate due to the lack of valid low flow steam measurements from the vortex meters. However, by assuming that the mass deficit calculated from the mass balance was steam exhaust that was not measured, and by including that steam energy in the energy balance, the energy balance was closer to closure.

While not having the low steam flow measurements hindered complete understanding of the tests; the system mass/energy balance analysis guided the data analysis so that this analysis along with the other instrumentation, provided a rational explanation for all the phenomena which occurred in the tests, including the unanticipated CMT refill and system oscillations.

The PIRT for the AP600 was validated by the OSU test program and the test results are sufficient for use in validation of the safety analysis codes used to analyze the AP600.